COO-2250-2
MITNE-148

ASSESSMENT OF THORIUM BLANKETS FOR FAST BREEDER REACTORS

by

P.J. Wood and M.J. Driscoll

July, 1973

Department of Nuclear Engineering
Massachusetts Institute of Technology
Cambridge, Massachusetts 02139

AEC Research and Development Report
UC-34 Physics
Contract AT(11-1)-2250
U.S. Atomic Energy Commission

MASSACHUSETTS INSTITUTE OF TECHNOLOGY

DEPARTMENT OF NUCLEAR ENGINEERING

Cambridge, Massachusetts

ASSESSMENT OF THORIUM BLANKETS FOR FAST BREEDER REACTORS

by

P. J. Wood and M. J. Driscoll

July, 1973

COO-2250-2

MITNE - 148

AEC Research and Development Report

UC-34 Physics

Contract AT(11-1) - 2250

U.S. Atomic Energy Commission

DISTRIBUTION

COO-2250-2 MITNE-148

AEC Research and Development Contract

AT(11-1)-2250

UC-34 Physics

1-3. U.S. Atomic Energy Commission, Headquarters
Division of Reactor Development and Technology
Reactor Physics Branch

4, 5. U.S. Atomic Energy Commission
Cambridge Office

6. Dr. Paul Greebler, Manager
Nuclear Energy Division
Breeder Reactor Department
General Electric Company
310 DeGuigne Drive
Sunnyvale, California 94086

7. Dr. Harry Morewitz, Manager
LMFBR Physics and Safety Projects
Atomics International
P.O. Box 309
Canoga Park, California 91305

8. Mr. Malcolm Dyos, Manager
Nuclear Development, LMFBR Project
Westinghouse Electric Corporation
Advanced Reactors Division
Waltz Mill Site
P.O. Box 158
Madison, Pennsylvania 15663

9. Dr. Robert Avery, Director
Reactor Physics Division
Argonne National Laboratory
9700 South Cass Avenue
Argonne, Illinois 60439

10. Dr. Charles A. Preskitt, Jr., Manager
Atomic and Nuclear Department
Gulf Radiation Technology
P.O. Box 608
San Diego, California 92112

ABSTRACT

An assessment of the neutronic, economic, and engineering aspects of the use of thorium in the radial and axial blankets of Liquid Metal Cooled Fast Breeder Reactors (LMFBR's) has been performed. While the breeding performance of a thorium blanketed system has been shown to be slightly inferior to that of a comparable uranium blanketed system in terms of fissile production rate, its economic performance is significantly superior, as evidenced by up to a 30% reduction in fuel cycle costs for a 1000 MW_e reactor arising from the added 1.6 million dollars in annual income. This superiority, which arises from the projected high value of the product U-233 relative to fissile Pu in thermal spectrum reactors, is expected to persist for approximately twenty years after LMFBR commercialization, and can, therefore, significantly enhance the incentive for rapid acceptance and introduction of the breeder into utility power systems.

Detailed cash flow analysis was shown to reduce to particularly simple expressions for the fuel cycle contribution to the total cost of power:

U-238 Blanketed System $\quad C = 0.02173\ P^{49} + 0.6203$

Th-232 Blanketed System $\quad C = 0.07613\ P^{49} - 0.04793\ P^{23} + 0.6648$

where

C = the fuel cycle contribution to the cost of power, mills/kw-hr,
P^{49} = the price of fissile Pu, \$/g, and
P^{23} = the price of U-233, \$/g.

In addition, a universal economic parameter was developed to characterize blanket performance under a wide range of economic environments. Both of the above developments will greatly reduce the amount of work required for future economic studies.

Experimental studies with thorium and uranium foils irradiated in the M.I.T. Blanket Test Facility, Blanket Mockup No. 4 were

performed to check the cross section data used in the remainder of the study, and to assign an uncertainty band to the fissile material production rate predictions.

Evaluation of the relevant physics parameters has shown that the reactor kinetics and dynamics characteristics (e.g., neutron lifetime, delayed neutron fraction, and Doppler reactivity coefficients) of the two systems are the same within calculational uncertainties, while the thorium blanketed system requires approximately 4% more core fissile material and 9% more control poison than a corresponding uranium blanketed system. Radial power gradients and blanket assembly average temporal power variations are somewhat greater for a thorium radial blanket. In-out shuffle blanket management has been shown to be the most desirable of those studies both from the economic (by a small margin) and from the thermal-hydraulic points of view.

It is concluded that LMFBR systems can be designed to accommodate uranium and thorium blankets on an interchangeable basis, and that the thorium blanket deserves strong consideration as the reference design concept for LMFBR systems.

ACKNOWLEDGMENTS

The work described in this report has been performed primarily by the principal author, P. J. Wood, who has submitted substantially the same report in partial fulfillment of the requirements for the Sc.D. degree at M.I.T.

Financial support from the U.S. Atomic Energy Commission under Contract AT(11-1)-2250 is gratefully acknowledged. The principal author also wishes to express gratitude for the financial support furnished him by the Westinghouse Electric Corporation, Power Systems, Advanced Reactor Division, and for the recommendation and encouragement of Dr. E.A. DeZubay, his supervisor at Westinghouse. Others at Westinghouse who have provided significant advice and guidance during this work include S. Ramchandran, G. H. Madden, R. K. Disney, R. B. Kidman, and R. W. Hardie.

The advice and assistance of A. Supple on the experimental work as well as the helpful suggestions of V. A. Miethe on computational problems are gratefully acknowledged.

Computer calculations were carried out at the M.I.T. Information Processing Center, and the Laboratory for Nuclear Science. Typing of this manuscript has been very ably handled by Mrs. Mary Bosco and Miss Linda Wildman.

Finally, the principal author wishes to thank his wife, Lee Woodruff Wood, whose patience and good humor have made life bearable during the most trying times prior to completion of this work.

TABLE OF CONTENTS

LIST OF FIGURES

LIST OF TABLES

Chapter 1

INTRODUCTION

1.1 FOREWORD

The primary objective of the Liquid Metal Cooled Fast Breeder Reactor (LMFBR) program, both in the U.S. and abroad, is to develop an environmentally benign source of power capable of meeting the growing demand for economical energy. The LMFBR is expected to meet this demand, in large part, through its ability to breed nuclear fuel. In the breeding process, fertile materials (e.g., U-238 or Th-232) are converted into fissile materials (e.g., Pu-239 or U-233) by neutron-induced transmutation. The primary effort in the LMFBR program is being directed toward developing the U-238/Pu-239 breeding cycle. The work presented here is concerned with the detailed evaluation (see sec. 1.3 for a specific prospectus) of a variation on this cycle, in which the core is fueled with a mixture of depleted uranium and fissile plutonium but in which the radial and axial blankets contain the fertile material thorium. The purpose of this chapter is to discuss why consideration should be given to thorium blankets in LMFBR's, and then to outline the work which will be presented in the remainder of the report.

1.2 THORIUM UTILIZATION

1.2.1 Systems Considered

Power production in a nuclear reactor affords an opportunity to convert non-fuel (fertile) material into fuel (fissile) material by using extra neutrons from the energy releasing fission reaction. Two main cycles have been proposed in which neutron capture in a fertile nuclide leads to generation of a fissile nuclide. These are the uranium/plutonium and the thorium/uranium cycles. The reactions involved in these cycles are shown below.

$$\text{(U/Pu):}\quad \text{U-238}(n,\gamma)\text{U-239} \xrightarrow[23.5\ \text{min}]{\beta^-} \text{Np-239} \xrightarrow[2.35\ \text{days}]{\beta^-} \text{Pu-239}$$

$$\text{Pu-239}(n,f)\ \text{fission products} + \text{neutrons} + \text{energy}$$

$$\text{(Th/U):}\quad \text{Th-232}(n,\gamma)\text{Th-233} \xrightarrow[21.1\ \text{min}]{\beta^-} \text{Pa-233} \xrightarrow[27.4\ \text{days}]{\beta^-} \text{U-233}$$

$$\text{U-233}(n,f)\ \text{fission products} + \text{neutrons} + \text{energy}$$

The LMFBR program in the U.S. has as its purpose development of a reactor system in which the U/Pu cycle is used to produce power as well as to generate more fissile plutonium than is consumed in power production.

Three systems in which thorium is used as a fertile material are, or until recently have been, under development in the United States:

1. The High Temperature Gas Cooled Reactor (HTGR), a converter reactor (i.e., less than one atom of fissile material is formed by fertile capture per fissile atom removed by neutron absorption).

2. The Light Water Breeder Reactor (LWBR), which likely would be operated most economically as a converter rather than as a breeder reactor.

3. The Molten Salt Breeder Reactor (MSBR), a system recently eliminated from the list of those being actively pursued by the USAEC.

It should be noted that all three systems which utilize the Th/U cycle operate with predominantly thermal neutron energy spectra. The reason for using the Th-232/U-233 cycle in high conversion ratio thermal spectrum reactors is that the number of fission neutrons produced per neutron absorbed (eta, η) is higher for U-233 than for any other common fissile isotope in a thermal spectrum (L1, D1). Eta values for various fissile materials are shown in Table 1.1 (D2).

TABLE 1.1

Eta Values for Major Fissile Species in Various Neutron Spectra

$$\overline{\eta_i} = \overline{\nu\sigma_f}/\overline{\sigma_a}$$

Nuclide	Standard Spectra				Typical Reactors	
	2200 M/S	Thermal (Maxwellian)	Epithermal (1/E)	Fast (Fission)	Thermal (LWR)	Fast
U-233	2.29	2.28	2.14	2.64	2.2	2.3→2.4
U-235	2.07	2.05	1.63	2.46	2.0	2.0→2.2
Pu-239	2.09	1.96	1.76	3.03	1.9	2.4→2.7

Thus it might be expected that U-233 would be superior as a fuel material to both U-235 and Pu-239 in thermal reactors. Unfortunately, however, U-233 does not occur in nature in any recoverable quantity.

Consequently, if U-233 is to be used as a fuel in thermal spectrum reactors, it must be produced by the neutron bombardment of Th-232. Because thermal spectrum reactors are unable to produce more fuel than they consume (with the possible exception of the LWBR or MSBR), an external source of U-233 must be developed to allow more efficient operation of this type of reactor. This need leads to the logical deduction that as long as sufficient plutonium (produced by Light Water Reactors, LWR's) exists to fuel LMFBR's, more efficient use might be made of LMFBR's if U-233 were produced by irradiation of thorium in their blankets. This suggestion has been made by a number of investigators (K1, L2, F1).

Several characteristics qualify thorium for consideration as a blanket material for LMFBR's. Two factors deserve mention at this point. First is the relative ability of thorium to utilize neutrons which leak from the core in the fertile to fissile conversion process. Table 1.2 shows a comparison of the microscopic capture cross sections for U-238 and Th-232. As shown, at all energies above about 50 eV, the capture cross section of thorium is greater than that of uranium. The second factor is an economic one. In a report issued by the USAEC (D3), curves showing anticipated fissile material values are presented for a number of mixes of fossil and nuclear power generating systems. For the case in which the total energy cost to U.S. consumers between now and the year 2020 was the lowest, the value of U-233 was significantly higher than that of Pu-239 for nearly every year after 1977. Figure 1.1 is a reproduction of the fissile isotope value history from that report. Recent developments in the LMFBR schedule have prompted speculation (L3) that the curve for fissile plutonium value should be shifted forward

TABLE 1.2

Comparison of Infinitely Dilute Capture Cross Sections (B1, N1)

Group	Upper Energy (eV)	σ_c (barns)		
		Th-232	U-238	Th-232/U-238
1	10.5×10^6	0.01	0.00	—
2	6.5×10^6	0.02	0.01	2.00
3	4.0×10^6	0.04	0.02	2.00
4	2.5×10^6	0.08	0.06	1.33
5	1.4×10^6	0.14	0.13	1.08
6	0.8×10^6	0.17	0.13	1.31
7	0.4×10^6	0.19	0.14	1.36
8	0.2×10^6	0.27	0.17	1.59
9	0.1×10^6	0.42	0.26	1.62
10	46.5×10^3	0.56	0.50	1.12
11	21.5×10^3	0.75	0.75	1.00
12	10.0×10^3	1.35	0.78	1.73
13	4.65×10^3	2.10	1.20	1.75
14	2.15×10^3	3.30	2.10	1.57
15	1.00×10^3	5.00	3.60	1.39
16	465	11.0	4.50	2.44
17	215	19.0	17.0	1.12
18	100	28.0	15.0	1.87
19	46.5	47.0	58.0	0.81
20	21.5	12.0	82.0	0.15
21	10.0	0.46	171.0	0.0027
22	4.65	0.67	0.54	1.24
23	2.15	0.99	0.47	2.11
24	1.0	1.45	0.58	2.50
25	0.465	2.11	0.90	2.34
26	Thermal	7.56	2.71	2.79

Fig. 1.1 Marginal Value of U-233 and Fissile Plutonium (D3)

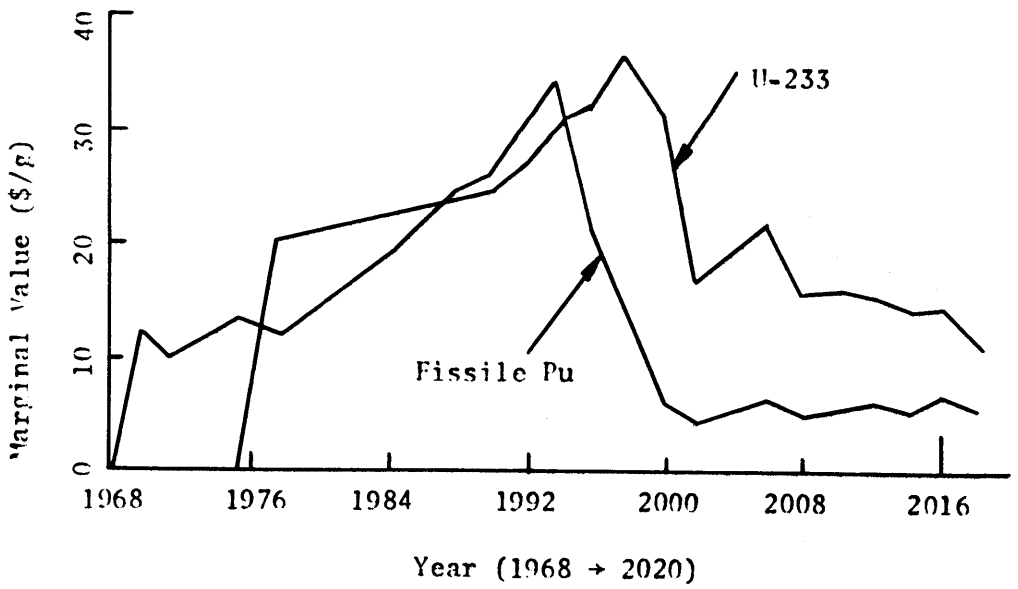

in time by approximately 10 years. This shift would assure the higher value of U-233 (relative to fissile plutonium) until after the year 2000. Another independent system study performed at Oak Ridge National Laboratory (K1) has shown that the expected value of U-233 is higher than that for fissile plutonium until about the year 1996. Figure 1.2 is a reproduction of the estimated fissile isotope values from that report.

Both Figs. 1.1 and 1.2 show that fissile isotope values will continue to rise until about the year 2000, and thereafter decline. This behavior has been attributed to the high value of plutonium in Fast Breeder Reactors (FBR's) coupled with the incentive to build this type of plant (K1). The decrease in fissile values can be traced to the production of excess plutonium in FBR's after they begin to produce a significant fraction of the nation's energy requirements. The high relative value of U-233 results from the economic attractiveness of High Temperature Gas Cooled Reactors (HTGR's) and the fact that U-233 is a fuel superior to fissile plutonium in HTGR's. It is apparent that if FBR's with thorium blankets were constructed in significant numbers, the shape of Figs. 1.1 and 1.2 would change. However, prior to about the year 2000, the number of FBR's would be expected to be sufficiently small that the general shape of these curves would be little affected by the use of thorium blankets.

Another obvious feature of Figs. 1.1 and 1.2 is that the value of U-233 is projected to exceed that of fissile plutonium even after the LMFBR begins to generate a significant fraction of the electric power produced in the U.S. This would indicate that thorium blankets on at least some of the operational LMFBR's would be economically advantageous for as many years into the future as these studies have

Fig. 1.2 U_3O_8 Price and Shadow Prices of Bred Fissile Materials (K1)

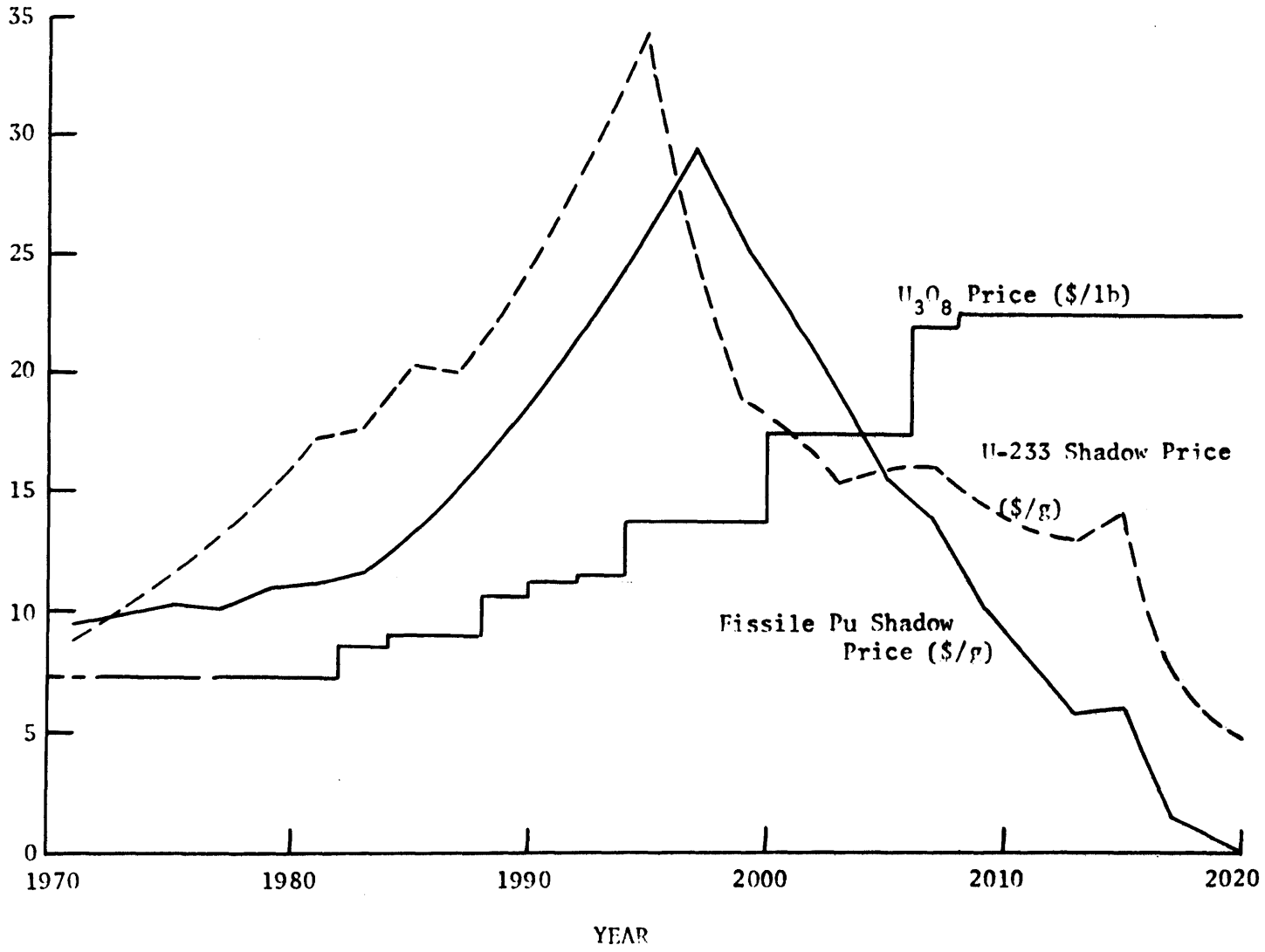

projected. To evaluate the market penetration of thorium blanketed LMFBR's, a detailed system study similar to those discussed above is required. This study is beyond the scope of the work to be presented here.

A more detailed review of relative fissile isotope values in various thermal spectrum reactors will be presented in section 5.2. It is sufficient here to say that in all studies in which the value of fissile plutonium has been compared to that of U-233 as fuel material for thermal spectrum reactors, U-233 always proves to be more valuable.

1.2.2 Previous Studies

A number of investigators have assessed the relative merits of the U-238/Pu-239 and the Th-232/U-233 breeding cycles for use in LMFBR's (A1, H1, L4, L5, O1, S1). In one of the earliest papers, that of Loewenstein and Okrent (L4), the conversion ratios in relatively small spherical cores were determined to be 1.2 to 1.4 for the thorium cycle compared to 1.4 to 1.7 for the uranium cycle. A later revision of that study (O1) using updated cross section data showed that the thorium cycle was even less attractive from the breeding ratio point of view.

Hankel et al. (H1) performed a scoping feasibility and economic evaluation of the Th-232/U-233 cycle for fast breeder reactors. This investigation concluded that the lowest doubling time and the lowest fuel cycle costs of the systems investigated were derived using a carbide fuel. Other important conclusions of Hankel's work derived from a comparison of the Th-232/U-233 FBR with a comparable FBR using the U-238/Pu-239 cycle were:

1. Higher core power densities were achieved for the U-238/Pu-239 reactor.
2. Lower system doubling times were achieved with the U-238/Pu-239 reactor.
3. Lower power generation costs were achieved with the U-238/Pu-239 reactor.
4. A negative sodium void coefficient was obtained for the Th-232/U-233 FBR while a positive coefficient was obtained for the U-238/Pu-239 system.
5. At least 50% more excess reactivity was required for a given burnup in the Th-232/U-233 system than in the U-238/Pu-239 reactor.

Other investigators such as Loewenstein (L5) and Allen (A1) have emphasized the safety advantages which can be attained by using thorium in the central region of large LMFBR's. This advantage was shown primarily to be associated with changing the sodium void coefficient from positive to negative by the use of thorium within the core.

A fairly detailed discussion of the potential safety-related problems of a Th-232/U-233 fueled FBR was presented by Sofer (S1) for a carbide fueled system. Among the problems pointed out were:

1. The increase in core reactivity following shutdown due to the decay of Pa-233 to U-233.
2. The smaller delayed neutron fraction in the U-233/Th-232 system (0.003 vs 0.004 for the Pu-239/U-238 system) resulting from the significantly smaller contribution to the total fission rate of the fertile Th-232.
3. More excess reactivity is required in the core because of the delay in fissile isotope formation following fertile capture. This delay is caused by the long half life (27.4 days) of Pa-233.

In all the studies of a pure Th-232/U-233 fuel cycle for an LMFBR, it was concluded that the increased core inventory required and the decreased breeding ratio compared to a similar U-238/Pu-239 fueled system made the thorium cycle economically unattractive for use in an LMFBR. The main motivation for pursuing studies of the thorium cycle for LMFBR's seemed to be the effect that it had in reducing a positive sodium void coefficient or, in some cases, making that coefficient negative.

A number of studies have been performed by Russian investigators analyzing the characteristics of mixed-fuel LMFBR systems (B2, L6, L7). Leipunskii et al. (L6) performed an optimization of an LMFBR in which thorium was the fertile material in the blanket, and a mixture of Pu-239, U-233, and U-238 was used in the core. He concluded that the conversion factor of a mixed-fuel, thorium-blanketed LMFBR could be optimized to be close to that for a U-238/Pu-239 system. His calculations also showed that the U-233 produced in the blanket regions was relatively free of U-232 contamination. U-232 is an undesirable contaminant because of the severe radiation shielding problem during fuel processing resulting from the buildup of the U-232 daughter product, Bi-212 (D1).

In an experimental study using the reactor BR-1, Batyrebekov et al. (B2) evaluated the breeding contribution of an infinitely thick thorium metal blanket. Multigroup calculations, which were shown to agree quite well with experimental predictions, indicated that the breeding ratio for a reactor with an infinitely thick thorium metal blanket would be approximately 20% less than that for the same reactor with an infinitely thick uranium metal blanket. This difference was attributed

to the difference between the fission rate in a uranium and a thorium blanket. No detailed information on absolute capture or fission rate distributions was presented in this report.

In a more recent study, Leipunskii (L7) analyzed a number of reactor configurations, all of which had thorium blankets. His study dealt primarily with the effect of isotopic composition of the core on safety, power flattening, and temporal variations in power distribution within the core. Again his most favorable case was one in which the core was composed of a mixture of U-238, U-233, and Pu-239. Leipunskii showed that providing an optimal distribution of fissile plutonium and U-233 in the core allowed achievement of a reduction in the core radial peak to average power density from ~1.8 to ~1.2. For our purposes the main conclusion to be drawn from Leipunskii's work is that a continuing interest is being shown by some factions in the Soviet Union in the use of thorium blankets for LMFBR's.

Recently a number of studies have been made (L2, L8, L9, W1) in which the use of crossed-progeny fuel cycle schemes was investigated. A crossed-progeny fuel cycle is one in which two or more nuclear reactor types, operating in the same energy economy, breed fissile material for interchange among these reactor types. A simple example would be an energy economy in which Light Water Reactors (LWR) burn natural uranium enriched with U-233 and convert the U-238 in natural uranium into Pu-239 for use as fuel in LMFBR's. The LMFBR's, in turn, use Th-232 as a blanket material to allow production of U-233 for use as fuel in LWR's. This sytem would be equally valid if HTGR's were substituted for the LWR's or operated in parallel with them.

Lang (L2, L8, L9) has performed a crossed-progeny fuel cycle analysis using LMFBR's and spectrum-hardened Pressurized Water Reactors (PWR). He evaluated the use of thorium in the blanket region of the low yield LMFBR proposed by Allis Chalmers in 1964. This reactor had an outer radial blanket as well as a blanket region in the center of the core. His analysis, which included the effect of blanket shuffling to minimize U-233 in-reactor residence time, led to the conclusion that the early demonstration of the U-233-producing blanket associated with an optimized LMFBR core design would tend to stay the early economic obsolescence of LWR's. Lang also concluded (L9) that the largest part of the economic savings associated with the use of crossed-progeny fueling would be realized in the first generation of oxide-fueled breeders, and that these savings could be sufficient to bring the power costs of early breeders in line with those of LWR's.

Wenzel (W1) performed a scoping economic study of the use of a thorium blanket in an LMFBR with a somewhat more optimally designed core than that used in Lang's analysis. His study considered the use of PWR's and LMFBR's in parallel. Two important conclusions were reached by Wenzel:

1. During various stages in the growth of the power economy, the fuel cycle costs of PWR's could be reduced by from 10% to 30%by the use of the crossed-progeny fuel cycle, while the cost of the LMFBR fuel cycle would be relatively unaffected.
2. The use of crossed-progeny fuel cycles could reduce some of the peak demand for separative work expected to occur during the 1980's.

1.3 OUTLINE OF THIS WORK

1.3.1 Preface

As discussed above, previous studies which have assessed the use of thorium as the fertile material in LMFBR blankets have confined themselves to scoping nuclear and safety calculations and overall system economic evaluation. This work is not intended to be an overall system study. Crossed-progeny fuel cycles using two or more reactor types will not be addressed as such. Rather this work will attempt to define the break-even point for the use of thorium rather than uranium as the fertile material in LMFBR blankets. In other words, given a price for Pu-239, this study will assess the minimum price which must be received for U-233 to make the breeding of U-233 in LMFBR blankets economically attractive.

It should be emphasized that the use of thorium blankets for LMFBR's is expected to be most economically attractive during the early years following LMFBR introduction. During this period there will be a plutonium glut and a shortage of U-233, both resulting from the large number of thermal spectrum (LWR and HTGR) reactors in use. In actual fact, use of thorium blankets in LMFBR's may contribute significantly to insuring the early acceptance of the LMFBR by the utility industry. The large reduction in LMFBR fuel cycle cost which this study will show can result from the use of thorium blankets may be sufficient to offset the higher capital costs expected for early LMFBR's. The early acceptance of the LMFBR may be crucial if, as some authors have suggested (R1), a huge gap between U.S. energy demand and energy sources is developing.

Questions other than the economics of thorium blanketed LMFBR's will be addressed in this study. One of the major objectives is to compare all design-related aspects of uranium and thorium blanketed systems to determine whether or not uranium and thorium blankets can be easily interchanged. Design-related questions will be addressed in Chapter 6 and summarized in section 6.5. Work leading to the final economic and system performance comparisons will be presented in five major categories:

1. Methods and Models (Chapter 2),
2. Experimental Verification of Methods (Chapter 3),
3. Burnup Calculations (Chapter 4),
4. Economic Analysis (Chapter 5),
5. System Performance Comparison (Chapter 6).

In the remainder of this section, the work to be presented in these five categories will be discussed. It should be noted that, because of the priority assigned to oxide fuel development in the U.S., only oxide cores and blankets will be evaluated. A recent study (Z1) of the use of metallic thorium-uranium mixtures as fuel for LWR's has shown that their conversion ratio and economic performance can be significantly improved over oxide fueled LWR's. This same effect would be expected for thorium metal blankets because of the higher number density of thorium achievable and the lower fabrication costs expected (Z1).

1.3.2 Methods and Models

Under the heading of Methods and Models (Chapter 2), details of the analytical techniques used in carrying out this study will be presented. This will include discussion of the reference geometry, cross section preparation, details of the burnup method used, and a brief description of the economics model. Wherever necessary, the implications of assumptions made on the final result will receive attention.

1.3.3 Experimental Verification of Methods

In Chapter 3 comparisons will be made between predicted and experimentally determined fission and capture rates for thorium and uranium foils irradiated in the M.I.T. Blanket Test Facility's Blanket Mockup Number 4. The purpose of this chapter is to determine how effective the cross sections developed using the techniques discussed in Chapter 2 are in predicting foil activities for a simulated LMFBR blanket. The major result of interest to this study developed in Chapter 3 will be a comparison of thorium and uranium capture rates in the blanket as derived from both the experiments and the analysis. The expected effect of this comparison on relative thorium and uranium blanket performance predictions will be included in the analysis of error presented at the end of Chapter 5.

1.3.4 Burnup Calculations

The methods presented in Chapter 2 will be applied in Chapter 4 to the burnup analysis of three standard LMFBR systems. The three systems include:

1. Depleted uranium/fissile plutonium core with depleted uranium blankets.

2. Depleted uranium/fissile plutonium core with thorium blankets.

3. Thorium/U-233 core with thorium blankets.

The primary emphasis in this chapter will be on a comparison between the first two systems listed above. Three types of blanket management will be considered: batch irradiation, zone scatter management, and in-out shuffle management. The material inventories developed in this chapter will be used in performing the economic analysis of Chapter 5.

1.3.5 Economic Analysis

The primary results and conclusions of this work will be developed in the economic analysis of Chapter 5. Fuel cycle cost contributions from the core, the axial blanket, and from the three rows of radial blanket will be generated for uranium and thorium blanketed systems using the material inventories developed in Chapter 4 for the three management schemes. Detailed economic analysis will then be made to define under what economic conditions thorium rather than uranium blankets should be considered for LMFBR's. After the initial economic analysis has been presented, a unified method to handle the effect of changes in the economic environment on optimum blanket irradiation time will be developed and verified. Finally, the effects of analytical uncertainties and blanket management on relative blanket economic performance will be summarized.

1.3.6 Comparison of System Performance

In the last major chapter (Chapter 6) a detailed comparison between the physical characteristics and system performance of uranium and thorium blanket systems will be made. The main topics to be covered in this chapter include comparison of axial blanket shielding performance, summary of the relative thermal performance of the two blankets, and discussion of the effect of blanket fertile material on physics characteristics related to system dynamic performance.

A significant portion of Chapter 6 will be devoted to evaluation and comparison of the thermal characteristics of the two blankets. Included under the general heading of thermal characteristics are such topics as fission, neutron, and gamma heating; power variations with burnup; and post shutdown heating rate in the blanket. System dynamics comparisons will include discussion of the effect of blanket type on the sodium void coefficient, the Doppler coefficient, the prompt neutron lifetime, and the power coefficient. In all comparisons, the idea of blanket interchangeability between thorium and uranium should be kept in mind. A summary of blanket interchangeability considerations will be presented in section 6.5.

In the final chapter (Chapter 7) the work presented throughout this report will be summarized.

Chapter 2

METHODS AND MODELS

2.1 INTRODUCTION

The overall objective of this study was to analyze the nuclear and economic performance of LMFBR systems in which both thorium and uranium are used as fertile blanket materials. To assure that as consistent as possible a comparison was made, the same cross sections, reactor physical dimensions, and analytical methods were used wherever possible in the analysis of the two systems. The purpose of this chapter is to review the input data and analytical methods, discussing where appropriate the effect of these factors on the final results. Topics to be presented in this chapter include:

1. Standard system geometry,
2. Cross section selection and preparation,
3. The cross section group collapse technique,
4. The burnup analysis,
5. The economic model.

The discussion here will be of a general nature, and detailed results will be presented in later chapters.

2.2 REFERENCE GEOMETRY

A detailed review of the information available on the expected design features of 1000-MW_e LMFBR's was performed by Brewer (B3). For the purpose of this study, the same reactor dimensions used in his work were selected as the standard system. Figure 2.1 shows the

Fig. 2.1 Elevation Schematic View of the Upper Right Quadrant of the Standard Reactor System

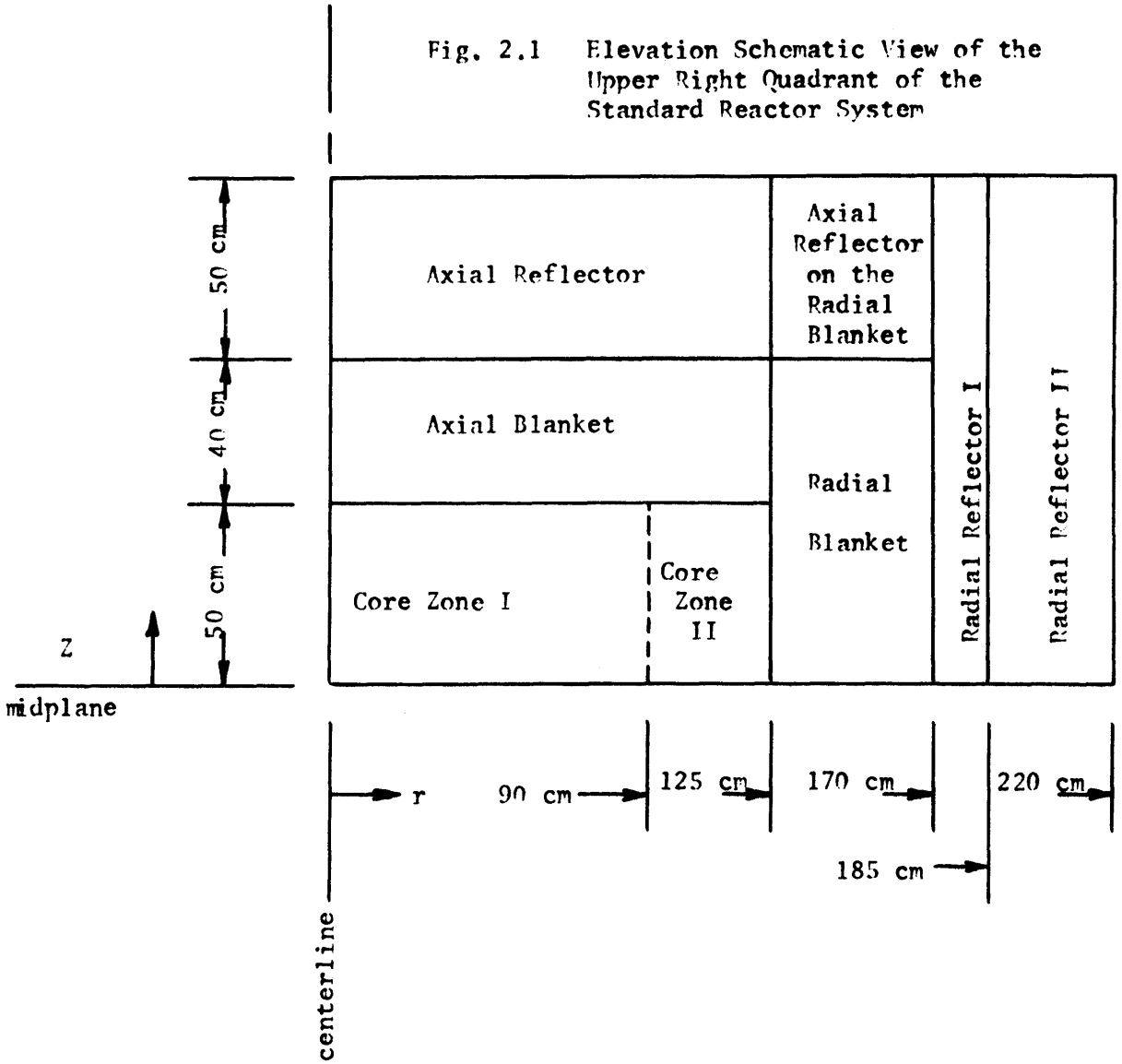

pertinent physical dimensions. The main features of this system are a two-zone, oxide-fueled core with the ratio of outer zone to inner zone enrichment equal to 17/11; a three-row, oxide-fueled radial blanket with one row of stainless steel and 35 cm of sodium serving as radial shielding; and a 40-cm-thick axial blanket with 50 cm of axial shielding. Table 2.1 summarizes the compositions of the various regions shown in Figure 2.1, and Table 2.2 summarizes the physical characteristics and dimensions.

TABLE 2.1 Standard Reactor Compositions

Region	Volume Fraction		
	Fuel	Sodium	Stainless Steel
Core Zone I	0.3	0.5	0.2
Core Zone II	0.3	0.5	0.2
Radial Blanket	0.5	0.3	0.2
Radial Reflector I	0.0	0.1	0.9
Radial Reflector II	0.0	1.0	0.0
Axial Blanket	0.3	0.5	0.2
Axial Reflector	0.0	0.5	0.5
Radial Blanket Axial Reflector	0.0	0.5	0.5

TABLE 2.2 Standard Reactor Physical Characteristics and Dimensions

Parameter	Dimension	Value
Core: Height	cm	100
Diameter	cm	250
Volume	liters	4906
Axial blanket thickness	cm	40
Radial blanket thickness	cm	45
Core power density	kW_T/liter	~500
Core zone I O.D.	cm	90
Core zone I volume	liters	2540
Core zone II O.D.	cm	125
Core zone II volume	liters	2366
Plant rated thermal power	MW_T	2560
Plant rated electrical power	MW_e	1000

To allow for fuel swelling during irradiation, designers are presently using oxide fuel in both the core and blankets which is less than 100% of theoretical density. In this study the approximate percent of theoretical density currently being considered for the Westinghouse demonstration plant design was used (D4). These values are reported in Table 2.3.

TABLE 2.3 Fuel Material Densities as Percent of Theoretical

Region	% of Theoretical Oxide Density
Core zone I	85
Core zone II	85
Radial blanket	95
Axial blanket	95

2.3 CROSS SECTION PREPARATION

To allow a consistent set of data to be used in the burnup analysis, all studies were performed using the modified Russian (ABBN) 26-group cross section set (B1, N1). (Cross sections not available in this set were derived from several other sources. See Appendix B for details.) Sections 2.3 and 2.4 of this report deal with the processing which was performed on these cross sections prior to the burnup analysis. The first step in the processing was to develop a set of resonance self-shielded cross sections using the code 1DX (H2, K2). The 1DX code generates resonance self-shielded cross sections, using as input a description of the system geometry, specification of all material number densities, and a tabulation of all necessary 26-group cross sections and resonance self-shielding factors from the modified ABBN

set. As used here, 1DX generated a 26-group set of resonance self-shielded cross sections (in the same energy format as the input data) for all the isotopes in each of the core and blanket regions. Table 2.4 shows the infinitely dilute U-238 capture cross section as well as the self-shielded cross sections for radial and axial blankets. Table 2.5 shows the same information for Th-232. These two tables show that the predicted capture rates in both U-238 and Th-232 are significantly affected when these isotopes appear in a region in high concentration.

2.4 PRELIMINARY PHYSICS ANALYSIS

In this section an evaluation will be made of the cross section group collapse technique and of the use of diffusion rather than transport theory in physics-depletion calculations. It will be shown that use of a 4-group set of region-collapsed cross sections is adequate to describe blanket burnup and breeding performance. Also the errors introduced by the use of diffusion rather than transport theory in analyzing the radial and axial blankets will be shown to be small.

2.4.1 Cross Section Group Collapse

To reduce the computational cost associated with the burnup analysis, the 26-group self-shielded cross sections were collapsed to four groups using the ANISN transport code (E1). The group structure used for the four energy groups was the same as for the 5-group set reported by Hinkelmann (H3), except that his bottom two groups were consolidated into one energy group. Table 2.6 shows a comparison of the collapsed group structure used in this work with that recommended by several other investigators. As shown, the collapsed group structure

TABLE 2.4 Comparison of Infinitely Dilute and Resonance Self-Shielded Capture Cross Sections for U-238

Group Number	Upper Energy (eV)	U-238 Capture Cross Section (barns)		
		Infinitely Dilute	Radial Blanket	Axial Blanket
1	10.5×10^6	0.0	0.0	0.0
2	6.5×10^6	0.01	0.01	0.01
3	4.0×10^6	0.02	0.02	0.02
4	2.5×10^6	0.06	0.06	0.06
5	1.4×10^6	0.13	0.13	0.13
6	0.8×10^6	0.13	0.13	0.13
7	0.4×10^6	0.14	0.14	0.14
8	0.2×10^6	0.17	0.17	0.17
9	0.1×10^6	0.26	0.26	0.26
10	46.5×10^3	0.50	0.4919	0.4941
11	21.5×10^3	0.75	0.7247	0.7351
12	10.0×10^3	0.78	0.7024	0.7264
13	4.65×10^3	1.20	0.9548	1.0583
14	2.15×10^3	2.10	1.0499	1.2244
15	1.00×10^3	3.60	1.2366	1.4380
16	465	4.50	0.9847	1.1845
17	215	17.0	1.4499	1.7257
18	100	15.0	0.9127	1.1000
19	46.5	58.0	2.0707	2.3998
20	21.5	82.0	3.0300	3.6230
21	10.0	171.0	8.2362	9.7168
22	4.65	0.54	0.54	0.54
23	2.15	0.47	0.47	0.47
24	1.0	0.58	0.58	0.58
25	0.465	0.90	0.90	0.90
26	Thermal	2.71	2.71	2.71

TABLE 2.5 Comparison of Infinitely Dilute and Resonance Self-Shielded Capture Cross Sections for Th-232

Group Number	Upper Energy (eV)	Th-232 Capture Cross Section (barns)		
		Infinitely Dilute	Radial Blanket	Axial Blanket
1	10.5×10^6	0.01	0.01	0.01
2	6.5×10^6	0.02	0.02	0.02
3	4.0×10^6	0.04	0.04	0.04
4	2.5×10^6	0.08	0.08	0.08
5	1.4×10^6	0.14	0.14	0.14
6	0.8×10^6	0.17	0.17	0.17
7	0.4×10^6	0.19	0.19	0.19
8	0.2×10^6	0.27	0.27	0.27
9	0.1×10^6	0.42	0.42	0.42
10	46.5×10^3	0.56	0.5537	0.5570
11	21.5×10^3	0.75	0.7124	0.7262
12	10.0×10^3	1.35	1.1898	1.2507
13	4.65×10^3	2.10	1.6370	1.8208
14	2.15×10^3	3.30	1.6283	1.9128
15	1.00×10^3	5.00	1.5802	1.9528
16	465	11.0	2.1909	2.6428
17	215	19.0	2.3505	2.8371
18	100	28.0	1.7115	2.0535
19	46.5	47.0	2.8619	3.4419
20	21.5	12.0	0.9136	1.1198
21	10.0	0.46	0.46	0.46
22	4.65	0.67	0.67	0.67
23	2.15	0.99	0.99	0.99
24	1.00	1.45	1.45	1.45
25	0.465	2.11	2.11	2.11
26	Thermal	7.56	7.56	7.56

TABLE 2.6 Comparison of Collapsed Group Structures

Group Number	Upper Neutron Energy (eV)			
	This Study	Hinkelmann (H3)	Hoover and Menley (H4)	Fuller (F2)
1	10.5×10^6	10.0×10^6	10.0×10^6	10.0×10^6
2	0.8×10^6	0.8×10^6	0.4979×10^6	1.35335×10^6
3	46.5×10^3	46.5×10^3	24.79×10^3	40.8677×10^3
4	1.0×10^3	1.0×10^3	3.355×10^3	1.2341×10^3
5		0.465×10^3		

is quite similar to that used by these other analysts. Hoover and Menley (H4) have made quantitative comparisons involving the collapse of a 13-group cross section set to 4 groups using region-dependent collapse spectra. Their results show that the largest error obtained in analyzing a GE 1000-MW_e advanced LMFBR design was approximately 0.2% in the radial blanket Pu-241 discharge mass. This error is acceptable for the type of overall fuel cycle analysis to be reported here.

To evaluate the effect of the ANISN cross section collapse from 26 to 4 neutron energy groups, a simple one-dimensional analysis was performed. First an ANISN problem was prepared using the 26-group resonance self-shielded cross sections from 1DX. The case analyzed was a radial geometry simulation of a two-zone core with a three-row radial blanket composed of depleted uranium. Next the same problem was analyzed using the region-collapsed 4-group cross section set generated from the 26-group case. The difference in the effective multiplication factor calculated in the two cases was approximately 0.5%, with the 4-group analysis predicting a higher k_{eff} than the 26-group case. Table 2.7 shows the ratio of the calculated U-238 fission

TABLE 2.7 Reaction Rate Prediction Ratios, 4-Group Analysis : 26-Group Analysis

Radial Distance from the Core Interface (cm)	U-238 Fission Rate	U-238 Capture Rate	Radial Blanket Row
0-5	1.0034	0.9850	1
5-10	0.9982	1.0096	1
10-15	1.0026	1.0309	1
15-20	0.9859	1.0192	2
20-25	1.0323	1.0347	2
25-30	1.0142	1.0500	2
30-35	1.0354	1.0364	3
35-40	1.0400	1.0519	3
40-45	1.0540	1.0707	3

and absorption rates in the radial blanket for the two cases. The ratios were obtained by dividing the predicted reaction rates from the 4-group case by those from the 26-group case. As shown in nearly all blanket regions, the predicted reaction rates are higher using the 4-group cross section set. In the row 1 radial blanket the predicted reaction rates are very nearly the same for the 4- and 26-group cases, while the discrepancy becomes larger in rows 2 and 3. This discrepancy arises because of the treatment of the transport cross section in the ANISN group collapse technique (F3, R3). Since the purpose of this work is to compare the performance of two systems – one with thorium blankets and one with uranium blankets – it is expected that the small error introduced by the ANISN group collapse technique will be normalized out when the final comparisons between the two systems are made. In accordance with this expectation, all analyses in this study have been performed for two completely comparable systems using the same

initial data and the same analytical methods.

2.4.2 Transport Theory vs Diffusion Theory

Because all of the burnup analyses on which this study is based have been performed using the diffusion theory code 2DB (L10), it was necessary to evaluate the accuracy of diffusion theory calculations against the more accurate transport theory approach for the assessment of external blanket neutronics. The ANISN (E1) code was again used in this evaluation because of its ability to perform both transport and diffusion theory calculations. A spherical reactor with characteristics shown in Table 2.8 was modeled using ANISN. This reactor was analyzed using the S_{16} angular quadrature approximation as well as the diffusion theory approximation. Angular quadrature weights and cosines for Gaussian quadrature with constant weight function were derived from Reference (K3). Table 2.9 shows the results of these analyses. As shown, both the fission and absorption rates in the core predicted using diffusion theory are very nearly the same as those derived from transport theory. However, the diffusion theory prediction of the U-238 fission rate in the blanket is significantly in error.

TABLE 2.8 Model Parameters for the Standard Spherical Reactor

Property	Units	Value
Core radius	cm	105
Blanket thickness	cm	40
Reflector thickness	cm	50
Blanket type	–	Axial U-238 (see Table 2.1)
Reflector type	–	Axial (see Table 2.1)

TABLE 2.9 Comparison Between Transport and Diffusion Theory Predictions of U-238 Reaction Rates

Interval Number*	Region	Reaction Rate Ratio (Diffusion/Transport) U-238 Fission	U-238 Absorption
1	Core I	1.002	1.002
2		1.001	1.001
3		1.001	1.001
4		1.001	1.001
5		1.001	1.001
6		1.001	1.001
7		1.001	1.001
8		1.000	1.000
9		1.000	1.000
10		1.000	1.000
11		1.000	0.999
12		1.000	0.999
13		1.000	0.999
14		0.999	0.999
15		0.999	0.998
16		0.998	0.998
17		0.998	0.998
18	Core II	0.994	0.998
19		0.991	0.998
20		0.974	0.998
21		0.979	1.002
22	Blanket I	1.120	1.010
23		1.089	1.009
24		1.049	1.011
25		0.990	1.010
26	Blanket II	0.943	1.010
27		0.888	1.008
28		0.834	1.008
29		0.800	1.007

*The interval inner and outer diameter (in centimeters) can be defined by the following relationships, where IN ≡ interval number:

I.D. = (IN-1) (5.0 cm)
O.D. = (IN) (5.0 cm)

This might be expected since U-238 fission is a threshold reaction ($E_{threshold} \cong 1.0$ MeV) and the transport calculation would better predict the behavior of high energy neutrons. As shown in Table 2.9, the absorption rate in U-238 is predicted correctly within about 1 percent by the diffusion theory calculation.

The conclusion that diffusion theory calculations overpredict the blanket fertile capture rate is the same as that reached by Rohan (R2). He also showed that the agreement between diffusion and transport theory in prediction of the effective multiplication factor was quite good.

For the purpose of this study, the absorption rate is much more important than the U-238 fission rate because we are primarily concerned with fissile isotope production in the blankets, and to a lesser degree concerned with the fission rate in the fertile isotope. It should be noted at this point that one would expect all threshold type reactions to be predicted inaccurately by the diffusion theory analysis, while reactions which have significant cross sections across the entire neutron energy range would be predicted much more accurately. The chief threshold reactions which will be of concern in this study are the following:

U-238 (n,f)
Th-232 (n,f)
Th-232 (n,2n) Th-231
U-233 (n,2n) U-232.

The first two of these are related to the energy release in the blanket regions (see sec. 6.3.2) while the last two are related to the production of the contaminant U-232 in thorium blankets (see sec. 2.5.3).

Except where noted in this report, all transport theory calculations were performed using an S_8 angular quadrature approximation. This was justified by Leung through comparisons of analytical predictions with experimental data (L11).

2.5 BURNUP ANALYSIS

2.5.1 Introduction

Burnup analyses were performed using cross sections which had been resonance self-shielded by 1DX and regionwise collapsed to four groups by ANISN. For this analysis the two-dimensional diffusion theory burnup code 2DB (L10) was used. The purpose of this section is to present the approximations made in the burnup analysis. This will be handled in two sections: the approach to dealing with reactivity swings is treated first, followed by a discussion of the assumptions governing the burnup and buildup of isotopes during irradiation.

Because of capacity requirements of the 2DB code, it was necessary to limit the sum of the number of cross section sets and the number of burnup regions to 99. Figure 2.2 shows the physical arrangement of the burnup zones for the 2DB analysis, and Table 2.10 shows the correspondence between burnup zones and regions in the reactor. It was desirable to use as large as possible a number of burnup zones in the radial and axial blankets because of the treatment given by 2DB to material number densities in a burnup zone during irradiation steps. In 2DB each burnup zone is considered a homogeneous mixture of material and remains so during irradiation. Consequently, each region in which definition of material inventory is desired as a function of time at power must be treated as a separate burnup zone. Figure 2.2 shows

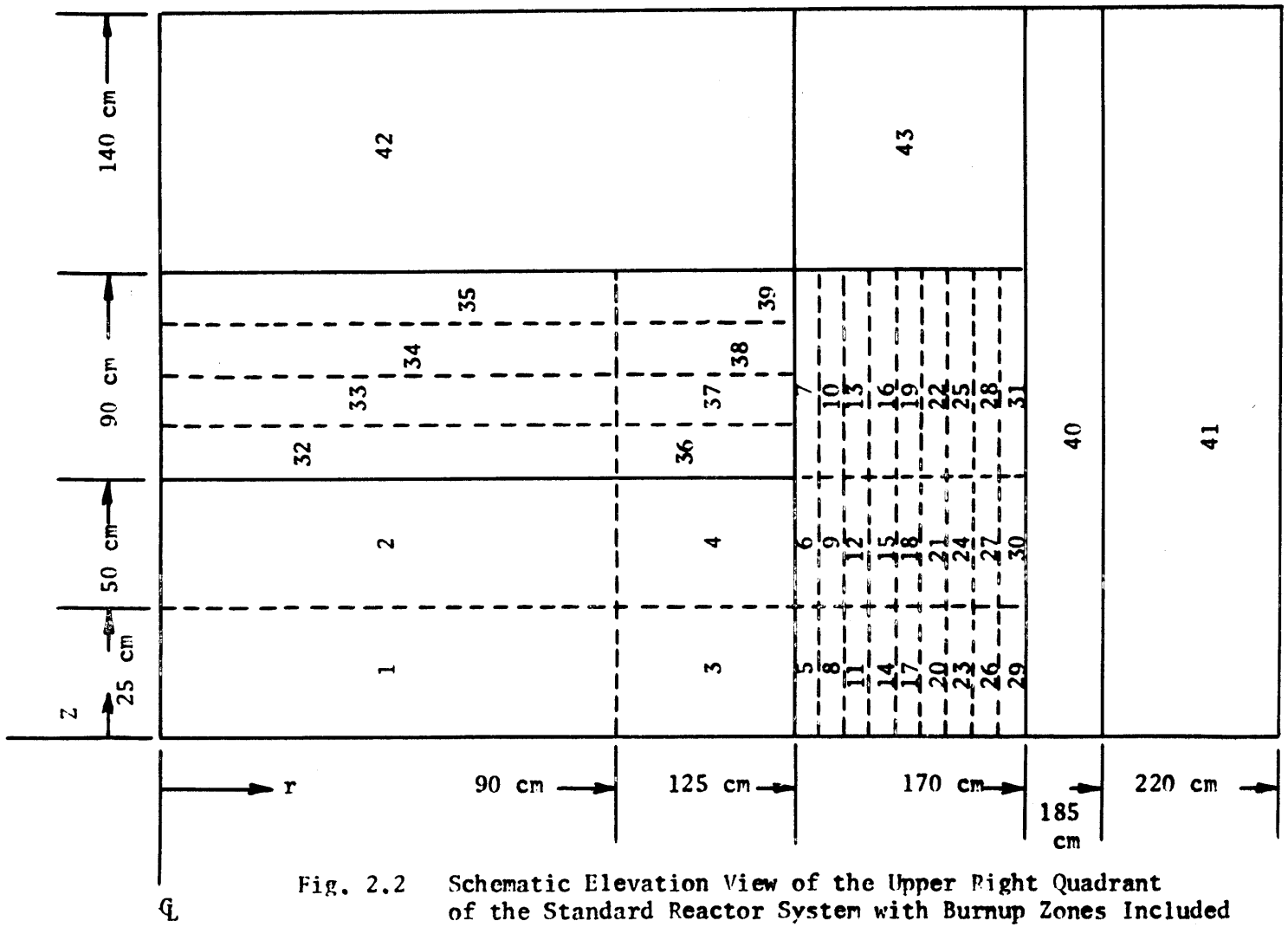

Fig. 2.2 Schematic Elevation View of the Upper Right Quadrant of the Standard Reactor System with Burnup Zones Included

TABLE 2.10 Summary of Burnup Region Types
(See Figure 2.2 and Tables 2.1 and 2.2 for further details.)

Burnup Zones	Region
1 and 2	Core zone I
3 and 4	Core zone II
5 → 13	Radial blanket row 1
14 → 22	Radial blanket row 2
23 → 31	Radial blanket row 3
32 → 39	Axial blanket
40	Stainless steel radial reflector I
41	Sodium radial reflector II
42	Core axial reflector
43	Radial blanket axial reflector

that, of the 43 burnup zones used in this analysis, only 4 were core zones, 27 were radial blanket zones, and 8 were axial blanket zones. The remaining 4 shielding zones were required only to allow definition of the different types of shielding material used in the standard reactor.

To reduce the number of cross section sets used in the burnup analyses, only the fertile isotope (i.e., U-238 or Th-232) cross sections were input by zone in the radial and axial blankets. All other materials were characterized by region: as core materials, radial blanket materials, axial blanket materials, radial reflector zones 1 and 2, or axial reflector materials. A summary of the regions for which collapsed cross sections were generated in these studies is presented in Table 2.11.

TABLE 2.11 Region-Collapsed Cross Sections Used in the Burnup Analysis
(X indicates that region-collapsed cross sections were used.)

Material	Core	Radial Blanket			Axial Blanket		Radial Reflector		Axial Reflector
		Row 1	Row 2	Row 3	Upper	Lower	Zone 1	Zone II	
Pu-239	X	X				X			
Pu-240	X	X				X			
Pu-241	X	X				X			
Pu-242	X	X				X			
U-235	X	X				X			
U-238	X	X	X	X	X	X			
O	X	X				X			
Fe	X	X				X	X		X
Cr	X	X				X	X		X
Ni	X	X				X	X		X
Na	X	X				X	X	X	X
Pu-239 F.P.*	X	X				X			
Th-232		X	X	X	X	X			
U-233		X				X			
U-233 F.P.*		X				X			
Pa-233		X				X			
B-10	X								

*F.P. indicates fission products from fission of named isotope.

2.5.2 Burnup Method

2.5.2.1 Reactivity Variations

The overall goal in defining a fuel management scheme is to minimize the total power cost. An earlier core and blanket optimization study (T1) has shown that this minimization is achieved in a design in which the following criteria are met:

1. Radial and axial power profiles are as flat as possible.
2. Burnup is maximized.
3. Initial critical mass is minimized.
4. Internal breeding ratio is maximized.

Conversely, the optimization study showed that if the design is varied until the power cost is minimized, the above constraints will be met by the resulting design. The other constraint on the operation of a plant to minimize the total power cost is that as high as possible a system availability be achieved. (It has been estimated that every day of reactor down-time for a 1000-MW_e reactor costs 10^5 dollars (T2).) This section will discuss the core management method used in the present study. One of the conclusions to be developed in this work is that the method chosen for core management will have little effect on the economic and breeding performances of the radial and axial blankets. The reason that so much detail on core management will be presented here is to verify and to extend the conclusions of Hirons and O'Dell (H5) that core management had little effect on blanket economics. The extension was required because their study included only k_{eff} variations of 3% whereas this study will use a core management scheme in which k_{eff} varies as much as 12% during a single batch core irradiation.

Figure 2.3.A shows a schematic of the unpoisoned reactivity variations during several refueling intervals. In actual operation, it is necessary to maintain the system effective multiplication factor, k_{eff}, at unity throughout the operating cycle. This is accomplished through the use of movable poison rods inserted into the reactor core. For the purposes of this study it was necessary to approximate the actual operating sequence of the reactor because the 2DB code does not have the capability for handling movable poison rods. The net effect of the approximations was that during any burnup interval the system k_{eff} varied about the "real" value of unity. Small variations in k_{eff} about unity have been shown by Hirons and O'Dell (H5) to have an insignificant effect on the results of economic analysis of an LMFBR core and blanket. Later in this work (see sec. 5.3.2) an evaluation of the impact of the core management method on blanket economics will be presented. In preview, it can be said that the core batch management replacement interval will be shown to have a small effect on predicted blanket economics.

2.5.2.2 Core Enrichment

For the purposes of this study, batch management of the reactor core was used. In other words, a core and axial blanket were loaded and assumed to remain in the reactor until the target average burnup of approximately 105,000 (T2) megawatt-days per metric ton of heavy metal (MWD/MTM) was reached. This section will discuss how core enrichment was decided upon, and the following section will discuss poison concentration.

The first assumption in selecting a core enrichment was that the 1000-MW_e LMFBR would be refueled only once per year. Hence the

Fig. 2.3 Schematic Diagrams of System Reactivity Variations

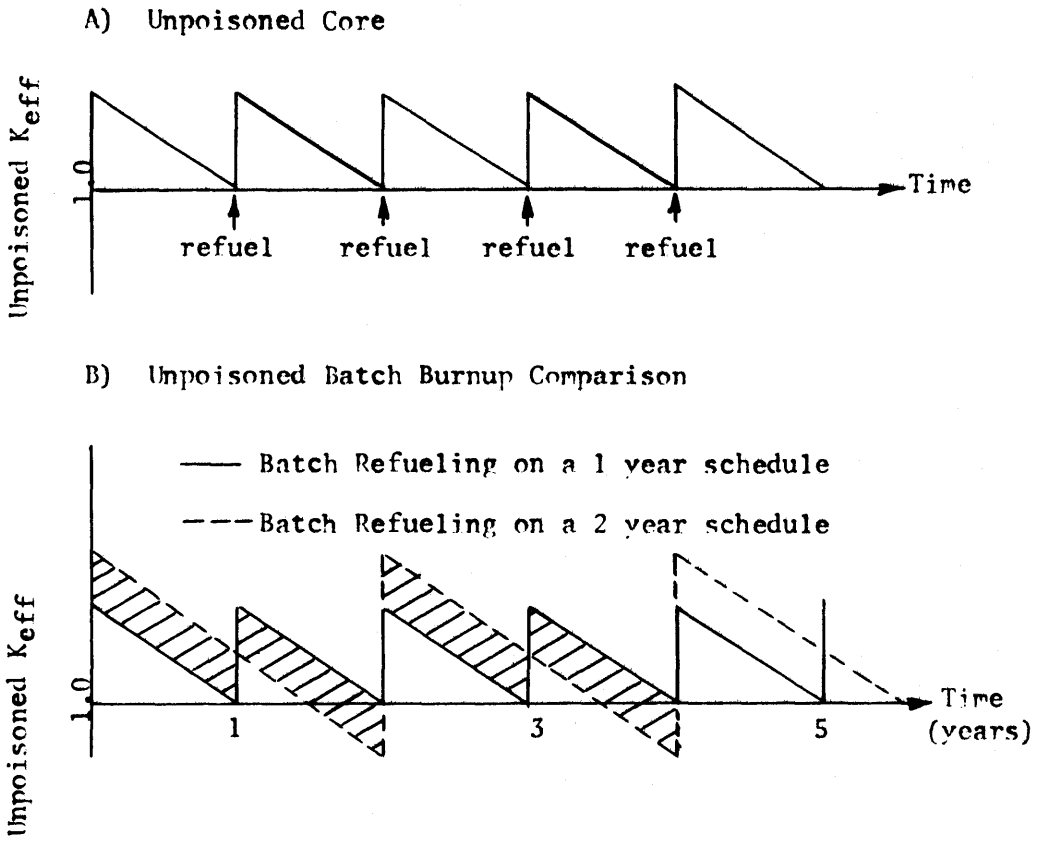

Fig. 2.3 (continued)

C) Poisoned and Unpoisoned Batch Burnup (1 year refueling)

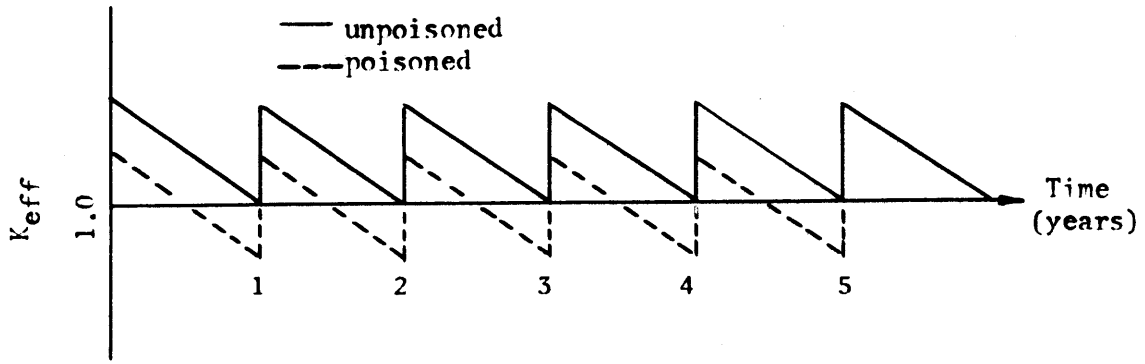

D) Poisoned and Unpoisoned Batch Burnup (2 year refueling)

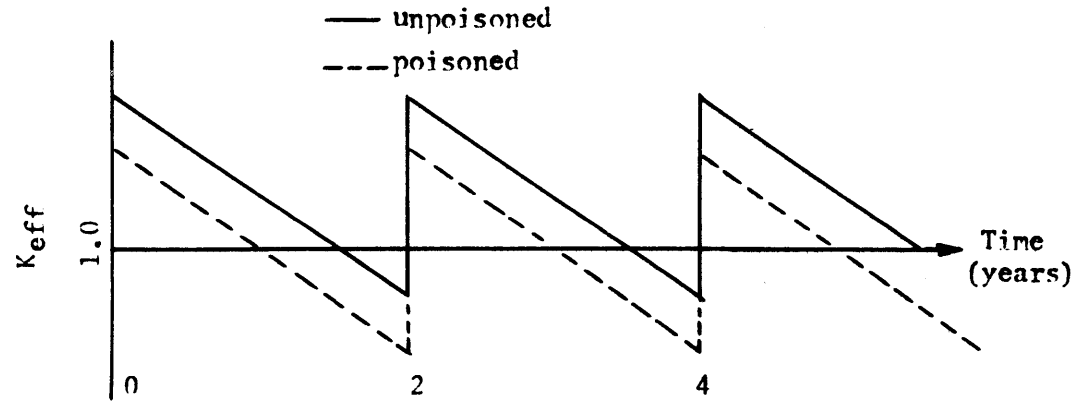

unpoisoned reactivity swing would be represented by Fig. 2.3.A with a refueling interval of one year. Next, a two-year batch burnup was selected as the reference for the analytical studies. This time was selected because a two-year batch burnup at 82% availability (600 full power days) resulted in an average core burnup of approximately the 105,000 MWD/MTM target. If it is next assumed that the system k_{eff} is proportional to the fissile loading (this assumption will be verified in sec. 4.2.1) and that the system k_{eff} varies linearly with burnup, a fissile loading can be defined which will make the two-year batch burnup consistent with two one-year batch irradiations. Figure 2.3.B shows the unpoisoned reactivity swing for two one-year batch burnups and for a consistent two-year batch burnup. Because of the last two assumptions above and the fact that the area of the cross-hatched region above the one-year batch curve equals the area below the one-year batch curve, it is apparent that the average fissile loading over a two-year period is the same for the two refueling patterns. If this objective is achieved, then the basis on which breeding ratios, doubling times, and economic analyses are evaluated for the two systems should be the same. An assessment of the effect of core management on blanket breeding performance will be made in section 4.3, and the economic effect will be treated in section 5.3.2.

2.5.2.3 Poison Concentration

In an attempt to account for the effect of control poison on breeding performance, boron-10 was added to the core and axial blanket. In this analysis, the B-10 was added without changing the inventory of other materials in the core and blanket. Although this treatment is physically

unrealistic, it allowed a first estimate of the effect of control poison on blanket performance to be made. The same technique was applied to both the thorium and the uranium blanket systems, so the results from the two analyses should be consistent. It should be noted that for analysis reported here, a system which was symmetric about the core midplane was assumed.

To proceed with this discussion, it is first necessary to derive the relative poison concentration in the core and axial blanket. The following observations and assumptions were made:

1) The safety system is composed of rods which are always in the ready position. That position was in the upper axial blanket with their lower ends at the interface between the axial blanket and the core.

2) The safety system has 50% more poison material than the control system.

3) The reference reactor refueling cycle is one refueling every year. During that year (300 days) the control rods are uniformly withdrawn from the fully inserted position to the fully withdrawn position.

4) The control system has sufficient worth (on a time average basis) to make the system k_{eff} equal to 1.0 after 150 days of operation.

5) For the reactor analyzed here (which was assumed symmetric about the center plane), it was assumed that the poison concentration in the axial blanket is half the poison concentration expected in the upper axial blanket.

6) The control rod was assumed to be 100 cm long, a length equivalent to the core height.

7) For the burnup analysis it was assumed that the poison is distributed uniformly throughout the core at the appropriate concentration and uniformly throughout the axial blanket at the (higher) appropriate concentration.

8) For the burnup analysis the poison concentration is the same throughout the life of the system.

Using the above assumptions, the poison (B-10) concentration in the axial blanket was determined to be 2.3 times the concentration in the core.

Figure 2.3.C is a schematic of the poisoned and unpoisoned reactivity variation for the yearly refueling cycle. As shown, sufficient poison was added to the system to require k_{eff} to pass through unity after 150 full power days. Given the assumption of linear variation of k_{eff} with burnup, the poison concentration selected to give a k_{eff} of unity halfway through the burnup cycle would be the time average poison concentration in the system. Because the goal of the two-year burnup analysis was to have the same time average isotope concentrations as the one-year batch refueling scheme, the poison concentration for the two-year batch burnup analysis was selected to correspond to the Δk for the first 150 days of batch burnup. Figure 2.3.D shows the poisoned and unpoisoned reactivity swing for the two-year batch burnup analysis. Detailed poison concentrations and fissile enrichments will be developed for the thorium and uranium blanket systems in section 4.2.3.

2.5.3 Materials Included in the Burnup

2.5.3.1 Introduction

In the burnup analysis performed by 2DB (L10), materials whose concentration changed as a function of irradiation time were specified together with the precursor isotope and the reaction which produced the isotope of interest. In this section, a discussion will presented of the reactions assumed to contribute to isotope buildup and depletion.

2.5.3.2 Fission Products

The following reactions were assumed to contribute to the fission product buildup in the core and blankets.

Pu-239 (n,f) Pu-239 FP
Pu-240 (n,f) Pu-239 FP
Pu-241 (n,f) Pu-239 FP
Pu-242 (n,f) Pu-239 FP
U-235 (n,f) Pu-239 FP
U-238 (n,f) Pu-239 FP
U-233 (n,f) U-233 FP
Th-232 (n,f) U-233 FP
Pa-233 (n,f) U-233 FP

Because only two sets of fission product cross sections were available, all fission reactions were assumed to produce fission products with the same nuclear characteristics as those from the fission of Pu-239 and U-233.

2.5.3.3 Fissile Isotope Buildup

The following reactions were assumed to contribute to the buildup of heavy isotopes.

Pu-239 (n, γ) Pu-240
Pu-240 (n, γ) Pu-241
Pu-241 (n, γ) Pu-242
U-238 (n, γ) Pu-239

Th-232 (n, γ) Pa-233
Pa-233 (Decay) U-233
Pa-233 (n, γ) U-234

As shown, the formation of the Np-239 intermediate following neutron capture in U-238 was neglected. Instead, neutron capture in U-238 was assumed to lead directly to the production of Pu-239. This assumption will produce a very slight overprediction in the formation rate of Pu-239, as a result of neglecting the neutron captures in Np-239. In the generation of U-233 from neutron capture in Th-232, however, the intermediate Pa-233 was assumed to be formed and to decay by beta decay to U-233. This assumption allows a realistic evaluation of the rate of formation of U-233 by accounting for the depletion of Pa-233 due to fission and neutron capture.

The assumptions involving immediate vs. delayed conversion of the fertile isotopes (U-238 and Th-232) are justified by the fact that the half lives of the intermediate species (Np-239 and Pa-233, respectively) are different by an order of magnitude (2.35 days for Np-239 and 27.4 days for Pa-233). The method used in treating fissile isotope buildup in the two systems will predict a very slightly better relative performance for the uranium blankets than for the thorium blankets.

2.5.3.4 U-232 Buildup

One of the difficulties associated with irradiating thorium in the reactor spectrum typical of fast reactors is that U-232 is formed along

with the fissile U-233. U-232 is considered a contaminant because it decays by alpha emission to form Th-228. This nuclide in turn decays in a long chain of α, β, and γ emitting isotopes which lead quickly to a high level of activity in freshly processed fuel containing a very small concentration of U-232 (D1, H1). The reactions considered in this burnup analysis which lead to the formation of U-232 include

Th-232(n,2n) Pa-231 (Threshold E = 6.34 MeV)
Pa-231(n,γ) U-232

and

U-233(n,2n) U-232 (Threshold E $\cong$ 6 MeV)

As shown, both reactions leading to the formation of U-232 are high energy threshold reactions. Earlier work (H1) has shown that 90% to 95% of the U-232 produced in a fast breeder reactor is from the first series of reactions. Both mechanisms were included in this work. As indicated above, the time associated with decay of intermediate isotopes was neglected as was the decay of the U-232. These assumptions will lead to a small overprediction in the amount of U-232 present in the blanket materials. This again makes the thorium blanket appear slightly more unfavorable than it actually is.

2.5.3.5 Poison Material

As discussed earlier, the B-10 poison concentration in the core and axial blanket was selected to be the time average concentration present in the system. For this reason, the depletion of B-10 was neglected in the burnup analysis, leading to a constant B-10 concentration throughout core and blanket life.

2.6 ECONOMICS MODEL

2.6.1 Model Characteristics

For the economic analysis performed in this work, the basic cash flow method and computer model (SPP1A) developed by Brewer (B3) were used. (See Appendix C for a brief discussion of this code.) All results quoted here were derived using accounting method A in which material purchase and fabrication charges were capitalized, reprocessing charges were considered as expensed costs, material credit was assumed to be a taxable revenue, and material purchase and fabrication were depreciated for tax purposes. Use of this method was suggested by Brewer (B4).

In adapting Brewer's computer model for use in this study, two changes were made. First, the model was revised to allow the use of material inventories predicted by 2DB rather than material inventories developed within the program using the semi-analytic depletion method (SAM) of Brewer. Second, provisions were made to accommodate all cost components associated with the thorium blanket including an economic penalty related to the presence of U-232 in the irradiated blanket. A listing of the modified program together with a description of the input variables and a sample problem is presented in Appendix C.

2.6.2 Penalty for U-232

The method used to account for the presence of the U-232 contaminant in the product U-233 (A2, U1) formed in the blankets involved a table of penalty factors. These U-232 penalty factors, shown in Table 2.12, were determined by the AEC (U1) to account for additional

TABLE 2.12 USAEC's U-232 Penalty Factors

Parts of U-232 Per Million Parts of Uranium	Deduction in Dollars Per Gram of Total Uranium
0	0.40
20	0.60
45	0.80
80	1.00
130	1.20
190	1.40
250	1.50
350	1.60
500	1.70
700	1.80
1000	1.90
1500›	2.00

costs of reprocessing and fabricating uranium enriched in U-233 and contaminated by U-232. Note that the penalty is given in terms of a deduction in dollars per gram of total uranium.

2.7 SUMMARY AND CONCLUSIONS

This chapter has presented discussions of the computational models and analytical methods used in this work. The potential errors associated with the use of diffusion theory rather than transport theory in analyzing the burnup characteristics of LMFBR blankets have been shown to be sufficiently small for present purposes. Errors arising from the regionwise cross section collapse performed by ANISN have been shown to be small and are expected to be normalized out when comparisons are made between thorium and uranium blankets which have been analyzed using the same input data and methods. The prediction of fissile buildup rates in the blankets has been shown to slightly favor overprediction of

the Pu-239 inventories in a uranium blanket, and to predict as accurately as possible the U-233 inventories in a thorium blanket. A method of handling the physics and economic effects of the U-232 contaminant in the thorium blanket has been shown to overestimate the negative impact of U-232 on blanket economics by slightly overpredicting the contaminant concentration in the product U-233.

The purpose of the next chapter is to further assess the reliability of this analysis by evaluating the key cross sections involved. This objective was attained by performing U-238 and Th-232 foil irradiations in the Blanket Test Facility using Blanket Mockup Number 4 as a host assembly. The experimentally determined ratio of capture and fission rates in the two foil materials will be compared to the analytically determined ratios. The effect of heterogeneous resonance self-shielding will also be evaluated for blanket rods made of uranium.

Chapter 3

EXPERIMENTAL EVALUATION

3.1 INTRODUCTION

In the previous chapter, the analytical techniques used in this work were presented. Despite the fact that these techniques, and the cross sections utilized therein, have been employed extensively by other investigators for fast reactor physics analysis (R5, A3), it was desirable to perform an experimental evaluation of the thorium and uranium cross sections using the M.I.T. Blanket Test Facility, Blanket Mockup Number 4. The purpose of these experiments was to compare the measured and calculated capture and fission rates for thorium and uranium foils irradiated in a neutron spectrum typical of the radial blanket of a demonstration LMFBR. The results of these experiments together with corresponding analytical predictions will be presented in this chapter. Because previous investigators (D9, F8, F9, F10, K8, L11, O2) have discussed in great detail both the design of the Blanket Test Facility and the experimental methods used in conjunction with that facility, only a brief presentation on those topics will be given here. Furthermore, the emphasis in this discussion will be on differences between the experiments presented here and those discussed by earlier investigators at M.I.T.

A brief discussion of the design and characteristics of Blanket Mockup No. 4 will appear in section 3.2. In section 3.3.2 the experimental procedures used and a discussion of the experimental

normalization factors will be presented. The normalized experimental results together with the corresponding analytical predictions will be discussed in section 3.3.3. In preview of the information to be presented in that section, it can be said that the experimental results indicate that the relative fission cross sections for uranium and thorium are reasonably well represented by the ABN-FTR-200 (N1) cross section set, and the relative values of the infinitely dilute capture cross sections of uranium and thorium have been fairly well characterized. However, the experiments have shown that the incorrect downscatter cross sections in the ABN-FTR-200 set predict too soft a spectrum, and that this soft spectrum leads to considerable discrepancies between predicted and experimentally determined uranium and thorium capture rates in the Blanket Mockup No. 4. The incorrect downscatter cross section will be shown, however, to have a small impact on the breeding performance of either thorium or uranium blankets, and hence a small effect on the comparative results presented elsewhere in this report.

3.2 DESCRIPTION OF BLANKET MOCKUP NO. 4

The purpose of Blanket Mockup No. 4 is to evaluate the nuclear performance of a three-row steel-reflected uranium oxide radial blanket driven by a core leakage spectrum typical of an LMFBR demonstration plant (Ref. D9, Chapter 8). To accomplish this, the three rows of blanket assemblies and the steel reflector previously utilized in Blanket Mockup No. 2 (L11), see Fig. 3.1, are driven by a modified converter assembly. The modified converter design (D9) consists of a 5-cm-thick graphite reflector and 10 rows of UO_2 fuel.

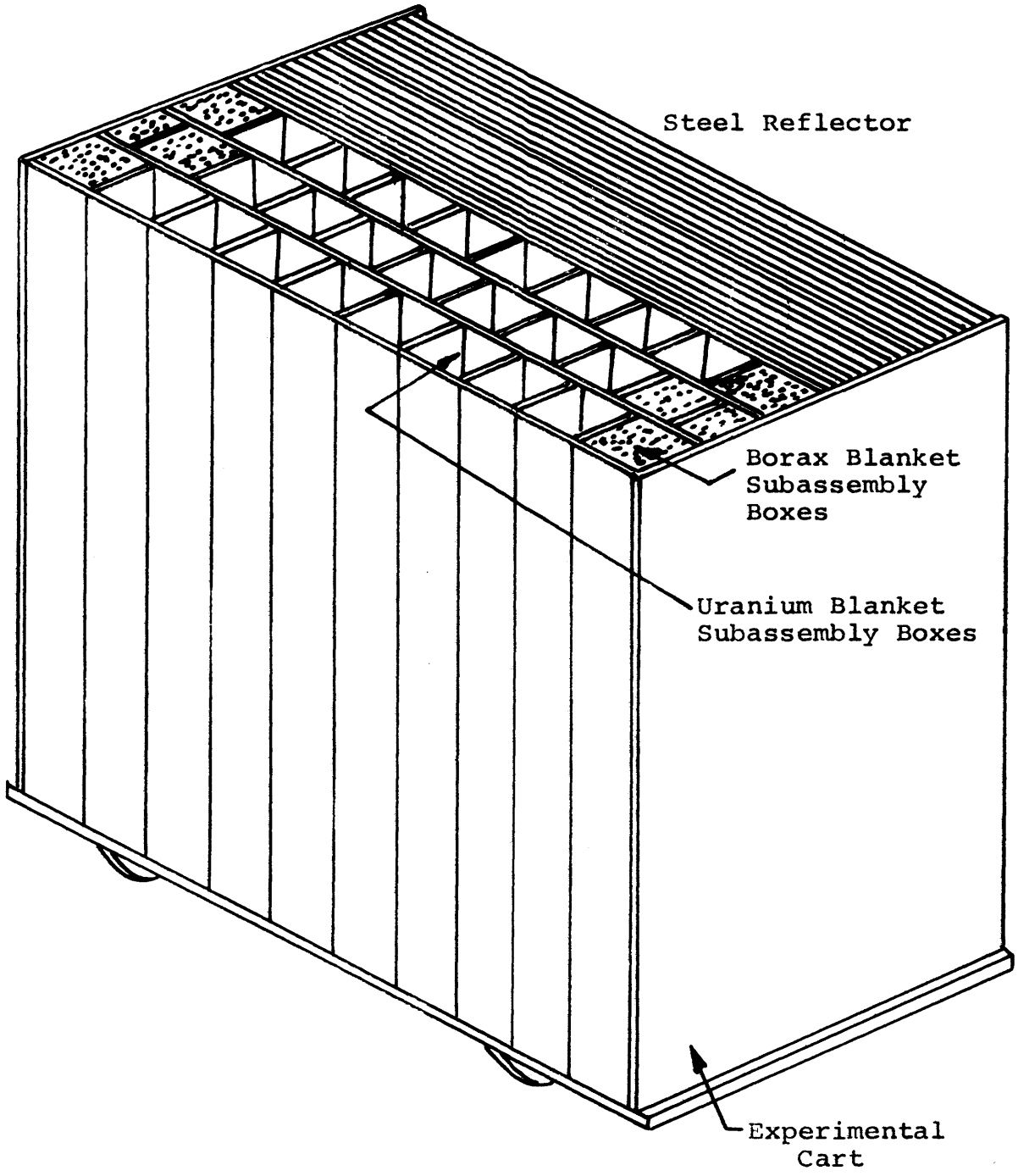

Fig. 3.1 Schematic View of Blanket Assembly No. 4

Sandwiched between the UO_2 fuel and the blanket subassemblies is a sheet of boral of thickness 0.317 cm.

The subassembly atom densities for Blanket No. 4 are given in Table 3.1. Also presented in that table, for purposes of comparison, are the atom densities in an "equivalent realistic blanket." As shown, good correspondence exists between the experimental blanket and a prototypic radial blanket.

TABLE 3.1 Homogenized Atom Densities in Blanket No. 4 (Atoms/barn-cm)

Nuclide	Blanket No. 4		Equivalent Realistic Blanket*	
U^{235}	0.000088		0.000016	
U^{238}	0.008108		0.008131	
O	0.016293		0.016293	
Na	0.008128		0.008128	
Cr	0.004064	0.017814	0.003728	0.017814
Fe	0.013750		0.012611	
Ni	0.000000		0.001475	
H	0.000073		0.000000	
C	0.000096		0.000082	

Nuclide	Steel Reflector
C	0.000590
Fe	0.084570

*Composed of 37.0 v/o depleted UO_2 (at 90% of the theoretical density), 20.7 v/o Type 316 stainless steel, 32.0 v/o sodium and 10.3 v/o void.

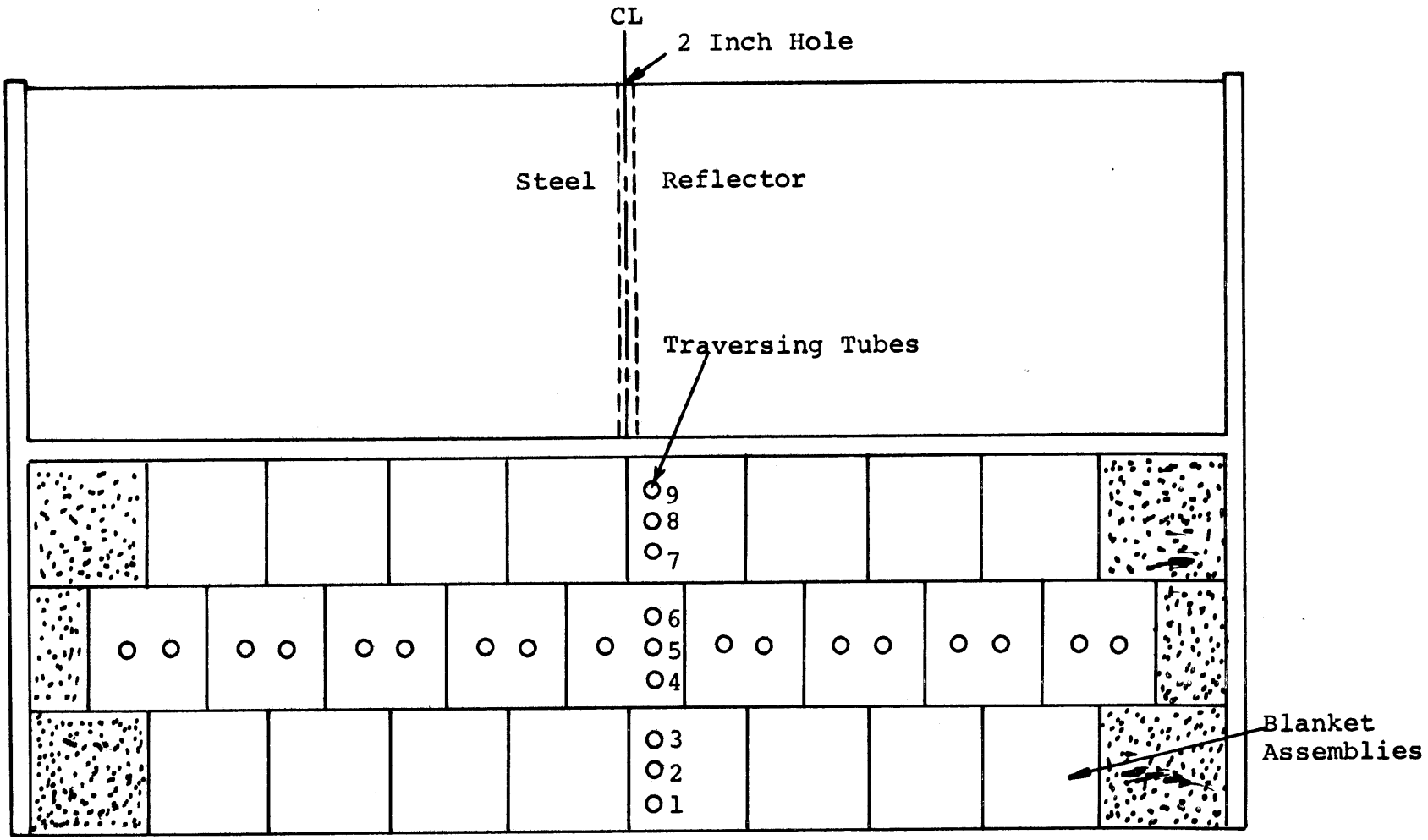

Fig. 3.2 Plan View of Blanket Assembly Showing
The Traversing Tube Positions

The configuration described above has been shown (D9) to model the leakage spectrum from ZPPR Assembly 2 (the ANL Demonstration Reactor Benchmark) quite well. Earlier experimental work (L11, D9, Chapter 4) has shown that a one-dimensional calculational model is valid for describing the nuclear performance of the Blanket Test Facility.

In section 3.3.3, results from experiments in which thorium and uranium foil material was irradiated in various positions in the Blanket Test Facility will be discussed. Figure 3.2 shows the positions in the facility which were used to perform these irradiations. Nine such positions were used. These positions are numbered from 1 (near the converter interface) to 9 (near the reflector interface). All irradiations in the blanket were performed with foils located at or within less than 2 inches of the axial midplane. At these positions the flux is sufficiently uniform spatially (L11, D9) that an insignificant difference in the foil activation rate will result for small vertical foil displacements from the midplane. Traverses in the blanket from the converter interface to the reflector interface will be the primary objective of the present discussion. These traverses will be referred to as radial traverses because of their similarity to a radial traverse in the blanket surrounding a cylindrical LMFBR core. In fact, the facility dimensions were selected so that there is almost exact one-to-one correspondence despite the fact that the BTF uses slab geometry (F8).

Two other small experimental facilities at the MITR were used to provide data for normalization of thorium and uranium foil traverses. One of these facilities (2CH1) provided a thermal neutron spectrum, while the other (6CH1) provided a spectrum very close to a fission

spectrum (L13). The use of these facilities in data normalization will be discussed in section 3.3.2. It should be noted that all three facilities used in these studies (the blanket, 2CH1, and 6CH1) are driven with neutrons from the MITR thermal column. Thus, variations in reactor power and disturbances from control rod motion have the same effect on the neutron flux in all three facilities. This greatly simplifies the foil normalization procedures described subsequently.

3.3 EXPERIMENTAL ASPECTS

3.3.1 Objectives

Because the major purpose of this report is to evaluate the breeding and economic characteristics of a thorium blanketed LMFBR relative to a uranium blanketed system, it was useful to attempt an experimental comparison of the nuclear characteristics of these two systems. The facility in which this comparison was made was the M.I.T. Blanket Test Facility, Blanket Mockup No. 4. This facility, described briefly in section 3.2, simulates the uranium radial blanket of an LMFBR demonstration reactor. The purpose of this section is to describe experiments in which uranium and thorium foils were irradiated at various positions in Blanket Mockup No. 4, and to discuss analytical results developed to evaluate the data from these experiments.

In section 3.3.2, a discussion of the counting technique and normalization procedure will be accompanied by an evaluation of the necessary experimental correction factors for the foil traverse data. In section 3.3.3, fission and capture rate data from the uranium and thorium foil

traverses will be compared to analytical predictions. Also discussed in section 3.3.3 will be a series of diagnostic experiments performed to illuminate the discrepancies between experimental results and analytical predictions. The conclusions to be developed in section 3.3.3 indicate that the use of the ABN-FTR-200 cross section set (N1), prepared for use with the ANISN code (E1) by a resonance self-shielding analysis performed using 1DX (H2), allows:

1. Reasonably accurate calculation of the relative fission rates in thorium and uranium foils irradiated in the test facility blanket,
2. Accurate calculation of the relative capture rates in thorium and uranium foils irradiated in the reflector, where uranium resonance self-shielding is not a factor,
3. Fairly accurate calculation of the relative capture rates in thorium, manganese and gold foils irradiated in the center of the blanket, but
4. Inexact calculation of the relative capture rates in uranium and thorium foils irradiated at the center of the blanket, where uranium resonance self-shielding is an important factor.

This final discrepancy has been traced, at least in part, to the 1/E weighting spectrum used in the development of the ABN-FTR-200 cross section set. Two techniques to correct the neutron scattering matrix in that set will be discussed in section 3.3.3.4.

3.3.2 Experimental Procedure

3.3.2.1 Counting Technique

The NaI well-type scintillation counting system described by Leung (L11, page 62) and Akalin (A5) was used to evaluate the activity of foils

irradiated in the blanket, the thermal facility, and the fission spectrum facility. The radioisotopes Co^{57}(γ @ 122 keV), Na^{22}(γ @ 511 keV), and Mn^{54}(γ @ 835 keV) were used to calibrate the counting system. A calibration was performed prior to counting each group of foils because of calibration drift which seemed to be related to variations in room temperature. (Over the several weeks period covered by the counting experiments, the room temperature varied between 64° F and 88° F, but was fairly constant during the counting of any series of foils.) Pertinent data on the foil materials irradiated in these experiments are presented in Table 3.2.

Because of the procedure used to normalize the experimental data (to be discussed in sec. 3.3.2.2), only very small correction factors were required to account for decay of the fission products and the Mn-55 capture product. For those data, small correction factors (from 0 to 8%) were required because of the large number of foils counted (usually 5 to 12 foils counted for 10 minutes each) and because of the short effective half life of the fission products (~3-1/2 hours) and of Mn-56 (2.58 hours). Corrections were made in all data analyzed for background count rate and to normalize out differences in foil weights.

3.3.2.2 Count Rate Normalization

The experimental technique used to evaluate the activity of all the foils counted in any particular batch at a single point in time was to count all foils twice, once forward and once in reverse, and then to average the two count rates for each foil. Thus, if a single batch

TABLE 3.2 Data Pertinent to Foil Counting

Parameter	FOIL MATERIAL			
	Thorium	Thorium	Uranium	Uranium
Reaction	$Th^{232}(n,f)$	$Th^{232}(n,\gamma)$	$U^{238}(n,f)$	$U^{238}(n,\gamma)$
Product nuclide	Fission products	Pa^{233}	Fission products	Np^{239}
Half life	~3.5 hours	27.4 days	~3.5 hours	2.35 days
E_γ peak (MeV)	$\geqslant$ 0.5 MeV	0.312	$\geqslant$ 0.5 MeV	0.106
E_γ detected (MeV)	0.72 $\rightarrow \infty$	0.224 $\rightarrow$ 0.384	0.72 $\rightarrow \infty$	0.086 $\rightarrow$ 0.172
Typical total counts accumulated (less background)	7,000	60,000	20,000	250,000
Counting time (minutes)	10	10	10	10
Irradiation time (hours)	4	4	4	4
Time prior to counting	4 hours	7 days	4 hours	24 hours

Continued

TABLE 3.2 Data Pertinent to Foil Counting (Concluded)

Parameter	FOIL MATERIAL	
	Au	Mn
Reaction	$Au^{197}(n, \gamma)$	$Mn^{55}(n, \gamma)$
Product nuclide	Au^{198}	Mn^{56}
Half life	64.8 hours	2.58 hours
E_γ peak (MeV)	0.412	0.845
E_γ detected (MeV)	0.318 → 0.600	0.707 → 0.968
Typical total counts accumulated (less background)	450,000	300,000
Counting time (minutes)	10	10
Irradiation time (hours)	4	4
Time prior to counting	24 hours	18 hours

contained three foils, they would be counted in the order 1,2,3,3,2,1. The average activity of a given foil counted at two points in time would then be a very good estimate of the count rate which would have been obtained had the foil been counted at the midpoint of the sequence. As mentioned in the previous section, the only foils which required that a correction factor be applied to the average count rates were thorium and uranium foils when they were being counted for their fission product activity, and the manganese foils when capture products were being counted. Even for these short half-life materials, the maximum correction factor was only about 8%.

Next we will discuss the procedure used to normalize the count rate obtained in one foil material to its appropriate value relative to another material. This normalization was required to correct for counter efficiency in counting gamma peaks of different energies. Since the foil material irradiated in the blanket, 2CH1 and 6CH1, was the same thickness for any particular foil, the normalization procedure corrected for gamma self-absorption. Uncertainties in the gamma yields per disintegration were also normalized out. For the purpose of this example, let us assume that weight- and background-corrected data have been generated for thorium and uranium capture products. A complete set of these data would include background- and weight-corrected count rates for both types of foils irradiated in various positions in the blanket and in the thermal spectrum facility (2CH1). To eliminate the errors associated with differences in the total fluence to which foils might be exposed, all the foils of any given material were irradiated at the same time, and counted at the same time.

(As mentioned earlier, the fact that all three facilities are driven by the same source of neutrons, the MITR thermal column, assures that the effect of variations in the driving flux will be cancelled out.) This would include all foils of a given material irradiated in the blanket, the thermal spectrum facility, and the fission spectrum facility. If the uranium capture rate data were chosen as the standard, then the following normalization would be performed on the thorium capture rate data:

$$C_{Th}^{N} = C_{Th}^{B}\left[\frac{C_{U}^{2CH1}}{C_{Th}^{2CH1}}\right]\left[\frac{\sigma_{C,Th}^{2CH1}}{\sigma_{C,U}^{2CH1}}\right] \qquad (3.1)$$

where

C_{Th}^{N} = the count rate of a thorium foil irradiated in the blanket, normalized to uranium foil count rate (cpm/mg),

C_{Th}^{B} = the background, weight, and self-shielding (see Eq. 3.4) corrected count rate of a thorium foil irradiated in the blanket (cpm/mg),

C_{U}^{2CH1} = the background, weight, and cadmium ratio (see Eq. 3.5) corrected count rate for a uranium foil irradiated simultaneously in the thermal spectrum facility (2CH1),

C_{Th}^{2CH1} = the background, weight, and cadmium ratio (see Eq. 3.5) corrected count rate for a thorium foil irradiated simultaneously in the thermal spectrum facility (2CH1),

$\sigma_{C,Th}^{2CH1}$ = the capture cross section for thorium in a thermal spectrum, and

$\sigma_{C,U}^{2CH1}$ = the capture cross section for uranium in a thermal spectrum.

This same normalization procedure was applied to the fission rate counting data by simply substituting the fission spectrum averaged cross sections (Z2) and the fission product count rates for foils irradiated in the fission spectrum facility (6CH1) where appropriate. The expressions used for this normalization are:

$$C_{Th}^{N} = C_{Th}^{B}\left[\frac{C_{U}^{6CH1}}{C_{Th}^{6CH1}}\right]\left[\frac{\bar{\sigma}_{f}^{Th}}{\bar{\sigma}_{f}^{U}}\right]N \tag{3.2}$$

$$N = \frac{\sum_{i} \sigma_{f,i}^{Th}\,\phi_{i}^{6CH1} \Big/ \sum_{i} \sigma_{f,i}^{U}\,\phi_{i}^{6CH1}}{\sum_{i} \sigma_{f,i}^{Th}\,\phi_{i}^{fission} \Big/ \sum_{i} \sigma_{f,i}^{U}\,\phi_{i}^{fission}} \tag{3.3}$$

where

C_{j}^{6CH1} = the background and weight corrected count rate for a foil of material j irradiated simultaneously in the fission spectrum facility,

$\bar{\sigma}_{f}^{j}$ = the fission spectrum average fission cross section for material, j,

N = the correction factor to account for the fact that 6CH1 is not a pure fission spectrum,

$\sigma_{f,i}^{j}$ = the fission cross section for material, j, in energy group i,

ϕ_{i}^{k} = the neutron flux in energy group i for the spectrum appropriate to spectrum, k.

The correction factor, N, defined in Eq. 3.3 was required because the neutron spectrum in the 6CH1 facility was not exactly a fission spectrum. Figure 3.3 shows a comparison between a fission spectrum and the calculated spectrum in 6CH1. As shown, the spectrum predicted using

Fig. 3.3 Comparison of ABBN Fission Spectrum With Calculated Spectrum in 6CH1

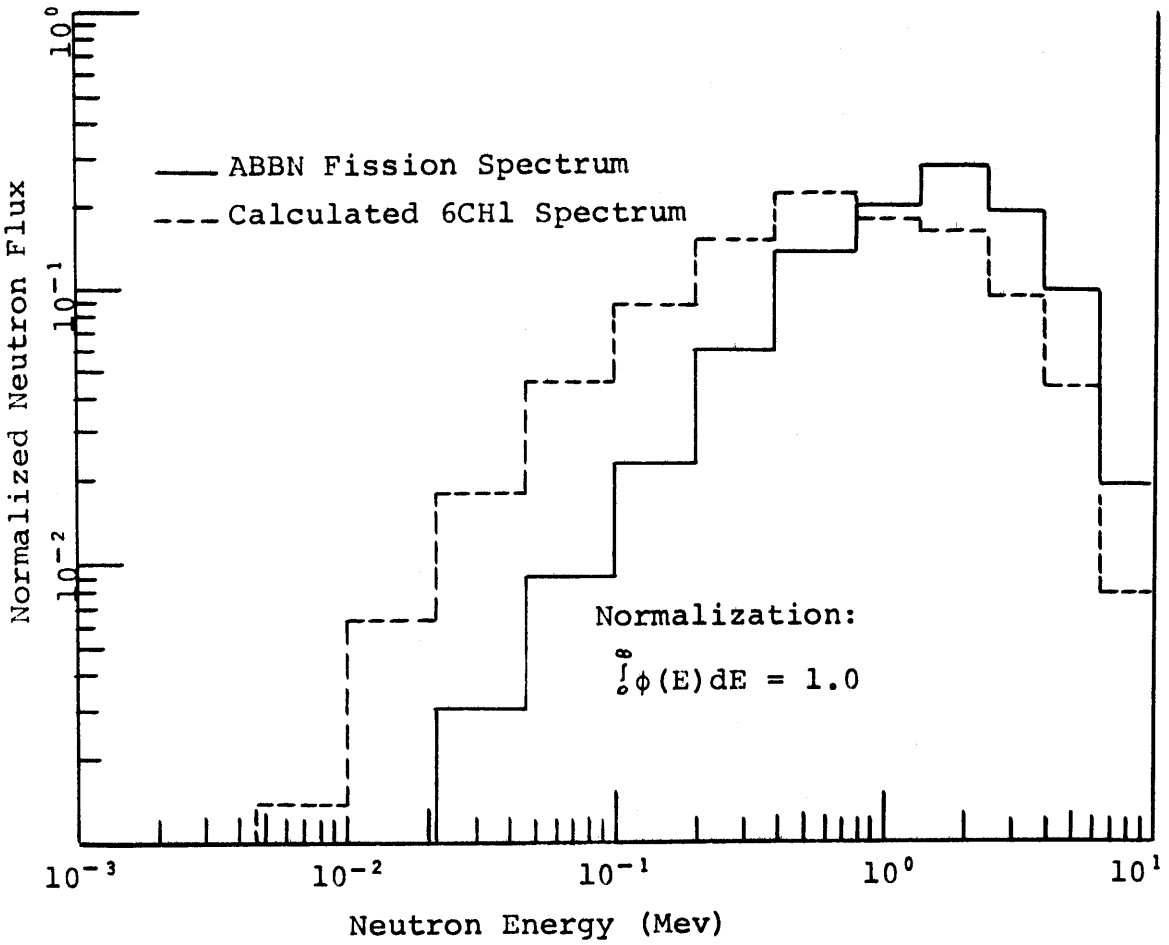

ANISN (E1) to analyze 6CH1 is somewhat softer than a fission spectrum. However, despite the fact that there appears to be a reasonable difference between the 6CH1 spectrum and a fission spectrum, the correction factor, N, in Eq. 3.3 was only 0.966. Consideration of Fig. 3.3 shows that reasonable agreement exists between the shapes of the predicted spectrum and the fission spectrum above about 1 MeV. This is in agreement with the experimental findings of Ho (H8).

The capture cross section data were obtained from an up-to-date tabulation of Maxwellian spectrum average capture cross sections provided by the Brookhaven National Laboratory (BNL) Cross Section Evaluation Group. Table 3.3 shows the fission and capture cross sections in a fission spectrum and in a Maxwellian thermal spectrum, respectively, for the materials of interest in this study. The thorium

TABLE 3.3 Cross Sections for Data Normalization

Isotope	BNL Maxwellian Average Capture Cross Section (barns)	Fission Spectrum Average Fission Cross Section (mb)
U-238	2.41607	310. (Z2)
Th-232	6.52828	71.9 (Z2)
Au-197	88.0026	0.0
Mn-55	11.7931	0.0

fission cross section in a fission spectrum recommended by Zijp (Z2), 71.9 mb, is in reasonably good agreement with the evaluated numbers developed by other investigators (V2) of 70.2 ± 13.5 mb. However, the experimental data of Fabry (V2) show that the thorium fission cross section in a fission spectrum may be somewhat higher, 82 ± 3 mb.

This same conclusion has been reached through experiments performed by Deen et al. (D11). This discrepancy has not yet been resolved. Davey (D5) has reviewed the literature on U-238 fission cross sections in a fission spectrum and derived a mean value of 309 mb. This is in good agreement with the value recommended by Zijp (Z2), 310 mb.

Before comparisons can be made between experimental data and analytical predictions of uranium and thorium capture and fission rates, several additional correction factors must be evaluated. These factors, which include foil self-shielding, uranium and thorium resonance overlap, and the non-thermal neutron contribution to foil activation in the thermal spectrum facility, will be discussed in the next section.

3.3.2.3 Sources of Experimental Error

Before final comparison between the experimental data and analytical predictions can be made, several correction factors must be evaluated and applied to the experimental data, including:

1. Foil self-shielding caused by finite foil thickness,
2. The epithermal neutron contribution to foil activation in the thermal spectrum facility,
3. Resonance overlap between thorium and uranium.

Resonance self-shielding in thorium foils was evaluated by irradiating two thorium foil packages of different thicknesses in the Blanket Mock-up No. 4 at the center of the blanket (position 5, see Fig. 3.2). The results of these foil irradiations were foil activities of 1534, and 1387 cpm/mg for foils of effective thickness 5 and 10 mils, respectively. The multiplicative factor applied to correct the count rate of a 5-mil-thick thorium foil to that appropriate for a foil of zero thickness was

then

$$F_T = \frac{C_5^{Th}}{C_{10}^{Th}} \tag{3.4}$$

where

F_T = the correction factor for foil thickness,

C_5^{Th} = the background corrected count rate from the 5-mil-thick foil (cpm/mg), and

C_{10}^{Th} = the background corrected count rate from the 10-mil-thick foil (cpm/mg).

Thus, activities of 5-mil-thick thorium foils irradiated in the blanket were corrected for self-shielding effects by multiplying by 1.11. Leung (L11 , Fig. 4.2) has shown that resonance self-shielding of Au, Mo, and U-238 foils in a somewhat softer spectrum test facility (Blanket Mockup No. 2) plays an insignificant role in the activation of those foils.

To correct the activities of the foils irradiated in the thermal spectrum facility (2CH1) to those characteristic of a pure thermal spectrum, experiments were performed in which bare and cadmium-covered foils were irradiated in 2CH1. The cadmium covers were sufficiently thick (> 20 mils) to assure that no thermal neutrons would penetrate them to cause foil activation. The results of these experiments are presented in the form of correction factors to be applied to bare foil data obtained in 2CH1 in Table 3.4. These correction factors were derived from the bare and cadmium-covered foil data using the expression:

$$F_{Cd} = \frac{C_B^j - C_{Cd}^j}{C_B^j} \qquad (3.5)$$

where

F_{Cd} = the correction factor for epithermal neutrons in the thermal facility (2CH1),

C_B^j = the background corrected count rate for a bare foil of material, j, in 2CH1 (cpm/mg), and

C_{Cd}^j = the background corrected count rate for a cadmium-covered foil of material, j, in 2CH1 (cpm/mg).

The factors were applied as multiplicative constants to the background corrected specific activities of foils irradiated in 2CH1.

TABLE 3.4 Correction Factors for Epithermal Neutron Activation in the Thermal Facility.

Foil	Correction Factor
U-238	0.811
Th-232	0.953
Au-197	0.982

Resonance overlap in mixtures of thorium and uranium oxides in a lead oxide diluent has been shown to contribute a small, less than 3%, decrease in thorium sample activities in a 1/E spectrum (F4). Nevertheless, it was decided to perform an experiment in which the existence of resonance overlap effects could be assessed. In this experiment, two thorium foils were irradiated in the steel reflector at a distance of

approximately five inches from the blanket interface. One of these foils was bare and the other was sandwiched between two 1/4-inch-thick pieces of uranium metal. These experiments showed that the bare foil achieved a specific activity (cpm/mg) approximately 4% greater than the foil in the uranium sandwich. Because this effect was so small and might be attributed to flux depression rather than resonance overlap between uranium and thorium, the resonance overlap effect was neglected in the normalization of thorium foil data.

Finally, two experiments were performed using 1/4-inch-diameter thorium and uranium foils which had been cut into two pieces: an outer annulus, and a 1/8-inch-diameter central disk. These two-piece foils were sandwiched between 1-1/2-inch-long pellets of the same material as the foil and irradiated in blanket position no. 5 (see Fig. 3.2). After irradiation the two pieces of the foils were counted separately for capture product activity, and and evaluation of the effect of heterogeneity on foil activities was made. These experiments showed that the central uranium disk achieved a specific activity (cpm/mg) of 10.3% less than the annular foil, while the central thorium disk achieved a specific activity of 11.7% less than the annular foil. These experiments are interesting because they show that the effect of heterogeneity on foil activity is nearly the same for a uranium foil and a uranium pin in a uranium blanket as for a thorium foil in a thorium pin in a uranium blanket. It should be noted, however, that the Dancoff effect is much different for a thorium pin in a uranium blanket than for a uranium pin in a

uranium blanket. Therefore this result leads to the expectation that the effect of heterogeneity for a thorium pin in a thorium blanket would be smaller than for a uranium pin in a uranium blanket.

Now that the experimental correction factors have been developed, we can proceed to a discussion of the experimental results and analytical predictions.

3.3.3 Experimental Results and Numerical Predictions

3.3.3.1 Introduction

In this section, foil traverse data taken with uranium foils irradiated both in-rod and ex-rod, as well as data taken with thorium foils irradiated ex-rod will be presented and compared with analytical predictions. The purpose of these comparisons is to evaluate how well the analytical methods to be used in Chapter 4 of this report can predict capture and fission rates for uranium and thorium in a typical uranium blanket spectrum. As will be shown, the experimental data and the analytical predictions for relative uranium and thorium capture rates are not in particularly good agreement. For this reason, both an analytical (sec. 3.3.3.4) and an experimental (sec. 3.3.3.5) evaluation of these discrepancies will be presented here. As will be shown later, the differences between analytical predictions and experimental data have been attributed to two sources: errors in the elastic downscatter cross sections in the ABN-FTR-200 cross section set (N1), and possible discrepancies in the uranium self-shielding formulation performed by the code 1DX (H2) using the same cross section set.

3.3.3.2 Analysis of Experimental Error

In general, the uncertainties shown in the tabulated results in this section are standard deviation from the mean (SDM) computed, where possible, from duplicate experiments. Many of the reported experiments, such as the thorium and uranium foil traverses in the blanket, were not repeated. In cases such as these, the indicated uncertainties have been computed by considering: counting statistics, foil weight uncertainties, and background corrections. In all cases, standard statistical techniques have been used in computing and combining uncertainties (P1, V3). Almost without exception, total count rates in excess of 10,000 counts were accumulated for each measurement; hence counting statistics have contributed only about ± 1% to the uncertainty.

3.3.3.3 Thorium and Uranium Foil Traverse Data

The uranium and thorium foil traverse data of interest in this section are presented in Table 3.5. These data have been corrected for foil self-shielding, foil weights, background, and have been normalized to the ex-rod uranium capture and fission data using epithermal (i.e., cadmium ratio) -corrected thermal spectrum capture activities (see Eq. 3.1), and fission spectrum fission product activities (Eq. 3.2), respectively. Thus the information in Table 3.5 represents the final form of the experimental data on relative fission and capture rates for thorium and uranium foils irradiated in a demonstration LMFBR uranium radial blanket.

TABLE 3.5 Results of Radial (Z) Reaction Rate Traverses

Distance from the Converter Interface (cm)	NORMALIZED REACTION RATES					
	$U^{238}(n,\gamma)$ (Ex-Rod)	$U^{238}(n,f)$ (Ex-Rod)	$U^{238}(n,\gamma)$ (In-Rod)	$U^{238}(n,f)$ (In-Rod)	$Th^{232}(n,\gamma)$ (Ex-Rod)	$Th^{232}(n,f)$ (Ex-Rod)
2.34	100,000 ± 121	10,000 ± 33	99,608 ± 162	10,317 ± 39	181,967 ± 919	2,635 ± 26
7.50	90,593 ± 114	6,388 ± 28	88,238 ± 151	6,684 ± 33	174,570 ± 909	1,670 ± 25
12.70	86,031 ± 115	4,126 ± 25	76,642 ± 142	4,466 ± 29	164,496 ± 895	1,081 ± 24
17.40	78,122 ± 111	2,747 ± 22	65,682 ± 133	3,079 ± 27	147,124 ± 878	787 ± 23
22.60	65,440 ± 100	1,887 ± 20	53,862 ± 124	2,140 ± 25	125,998 ± 858	518 ± 23
27.80	56,192 ± 96	1,350 ± 19	44,738 ± 116	1,566 ± 24	110,153 ± 836	380 ± 22
32.60	48,175 ± 88	942 ± 17	36,530 ± 109	1,196 ± 24	94,774 ± 813	347 ± 22
37.60	40,028 ± 82	675 ± 17	28,880 ± 102	896 ± 23	78,085 ± 790	193 ± 22
42.80	38,046 ± 81	490 ± 16	23,546 ± 94	600 ± 22	71,899 ± 756	121 ± 21

Comparisons can now be made between these data and fission and capture activities calculated using the ANISN code (E1) to analyze the M.I.T. Blanket Test Facility, Blanket Mockup No. 4. Cross sections for this analysis were developed using the 1DX code (H2) to generate self-shielded cross sections from the ABN-FTR-200 data set (N1). The calculated activities for thorium and uranium foils were normalized to the appropriate experimental activity (either capture or fission rate) for the uranium foil in blanket position 5 (see Fig. 3.2). Figure 3.4 is a comparison of the experimental and calculated fission rates for uranium and thorium foils irradiated (ex-rod) in a uranium blanket. As shown, the comparison between the experimental data and the predictions is relatively good. Small discrepancies between the calculated and experimental fission rates exist near the converter interface for the uranium foils and from mid-blanket to the reflector interface for the thorium foils. The fact that the experimental fission rates for thorium are somewhat higher than predicted is in agreement with the results of Deen et al. (D11) in which he showed approximately a 10% discrepancy between experimental and calculated fission rates in a Cf-252 fission spectrum. When the same comparison is made between thorium and uranium capture rates as determined by experimentation and analysis, much poorer agreement is obtained. Figure 3.5 shows this comparison. As shown, two discrepancies exist: the slope of the experimental capture rate traverse for the uranium foils is less steep than predicted, and, more significantly, the experimental thorium capture rates are considerably below the predicted capture rates. In other words, the numerical computations predict that the

Fig. 3.4 Comparison of Calculated and Experimental Fission Rates for Thorium and Uranium Foil Traverses in BTF 4, Cross Sections from ABBN-FTR-200 Set (11)

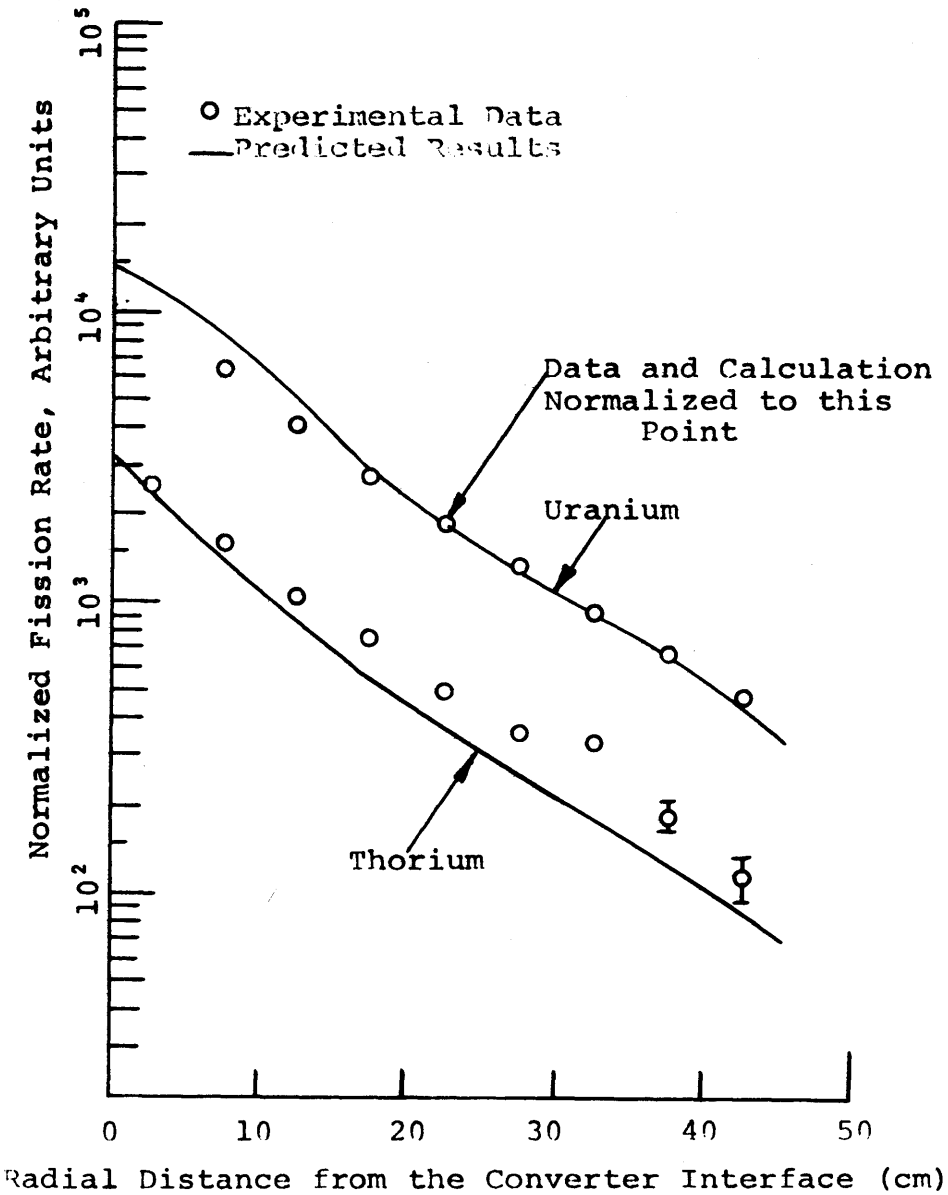

Fig. 3.5 Comparison of Experimental and Predicted Fertile Capture Rates of Thorium and Uranium Foils, Cross Sections Prepared using 1DX

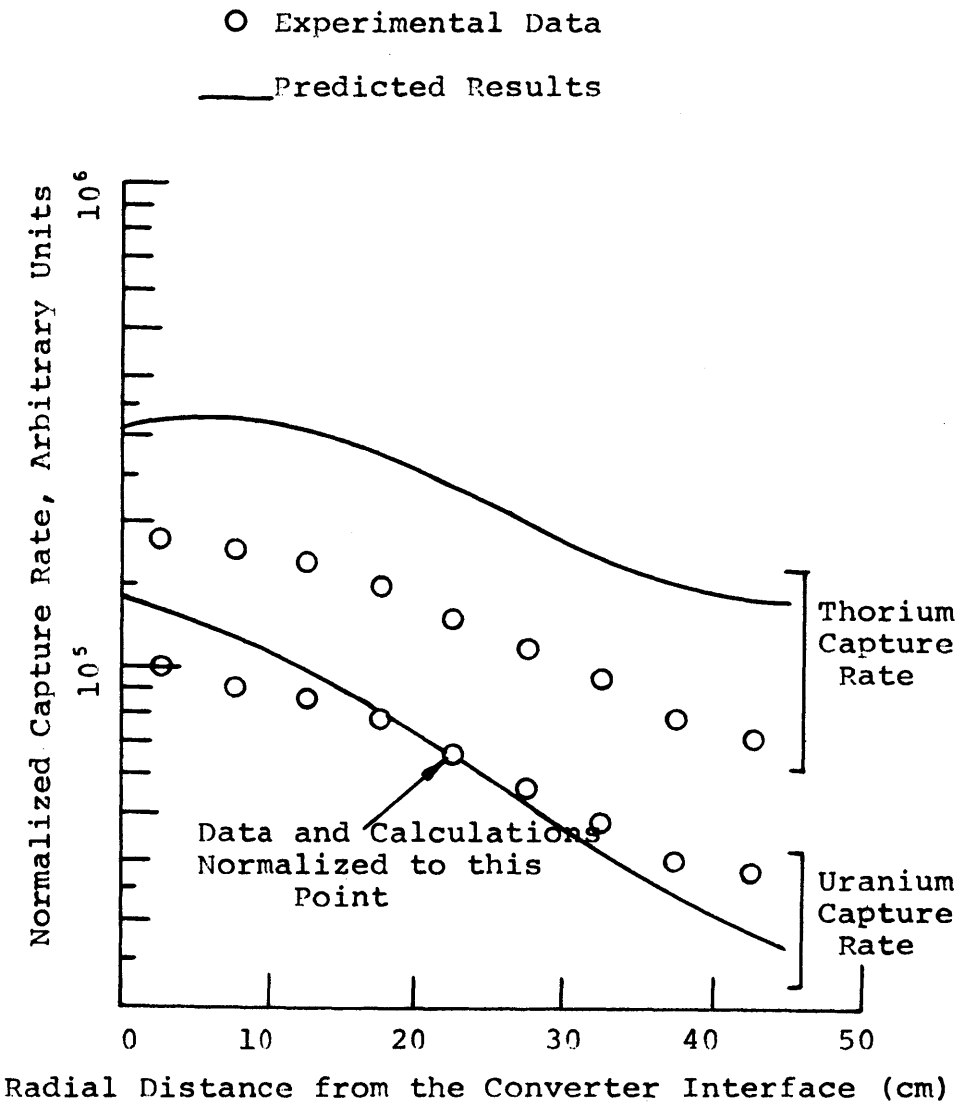

ratio of thorium to uranium capture rate in a uranium blanket is much higher than that observed experimentally. In the next two sections, analytical and experimental studies will be discussed to clarify the reasons for the difference between the experimentally determined and analytically predicted capture rate data shown in Fig. 3.5.

One additional set of data was taken in Blanket Mockup No. 4. In that experiment, 1/4-inch-diameter depleted (18 ppm U-235) uranium foils covered by thin (~1 mil) aluminum foils were irradiated inside 1/4-inch-diameter uranium metal rods. Data from these in-rod experiments were normalized to the uranium foil ex-rod data by multiplying the in-rod data (both capture and fission) by the ratio of the specific activities of uranium foils irradiated simultaneously in the thermal spectrum facility. Figure 3.6 shows a comparison between the in-rod and ex-rod fission rate in uranium foils irradiated in the blanket. Also shown in that figure is the predicted fission rate normalized to the midpoint of the ex-rod foil traverse. As shown, in-rod fission rate data follow very nearly the same shape as the ex-rod data, except that the in-rod data show somewhat higher fission rates. This is as expected because the fission reaction in U-238 is a threshold reaction, and the first-flight neutron flux (from a fission event) would tend to increase the fission rate for the foils irradiated in-rod (i.e., the well-known fast-effect of thermal reactor physics).

Figure 3.7 compares the in-rod and ex-rod capture rate data against the corresponding predictions. The two predicted curves were normalized to the capture rate expected outside a uranium rod at mid-blanket. As shown, the in-rod and ex-rod predictions are nearly parallel, while the experimental data show that the heterogeneous

Fig. 3.6 Comparison of Calculated and Experimental Fission Rates for Uranium Foils Irradiated Both In-Rod and Ex-Rod, ABBN-FTR-200 Cross Section Set Used (N1)

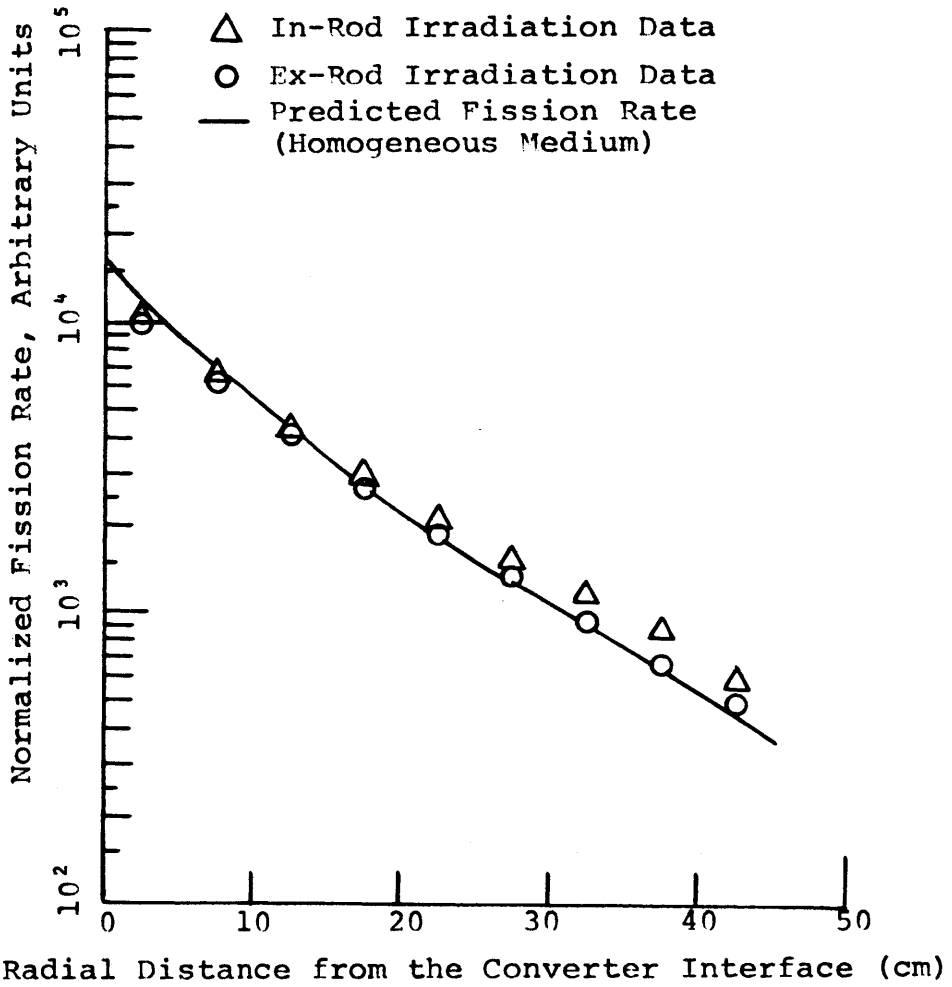

Fig. 3.7 Comparison of Predicted and Experimental Capture Rates for Uranium Foils Irradiated Both In-Rod and Ex-Rod, Cross Sections Generated using 1DX

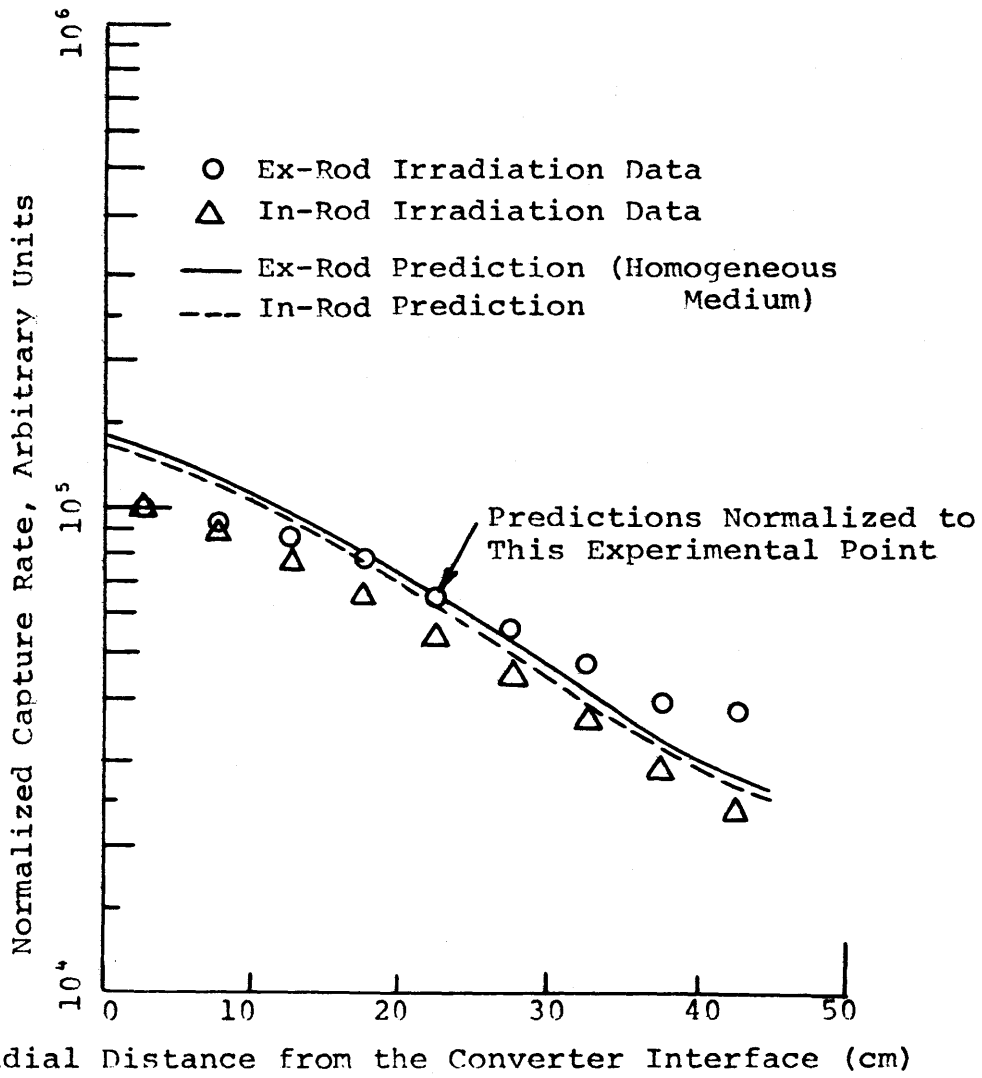

self-shielding effect increases as the neutron spectrum becomes softer at greater distances from the converter interface. This discrepancy is expected from the fact that the heterogeneity correction method used by 1DX (the Bell modification to the rational approximation [B12]) relies on a simple geometric factor, and no allowance is made for the decrease in self-shielding due to the decreased population of neighboring fuel rods near the iron reflector.

3.3.3.4 Modification of Elastic Downscatter Cross Section

In an attempt to understand the discrepancies between the analytical capture rate predictions and the experimentally observed capture rates, the integral distribution of fertile captures as a function of neutron energy was calculated for thorium in a thorium blanket, uranium in a uranium blanket, and thorium in a uranium blanket. Figure 3.8 shows these normalized distributions. As shown, the capture rate distributions for thorium foils in thorium blankets and uranium foils in uranium blankets are very nearly identical. Neutron capture at higher energies ($\geq$ 2 keV) contributes more to the total capture rate in thorium blankets than high energy captures in uranium blankets. On the other hand, thorium foil material irradiated in a uranium blanket receives a much larger contribution to its total capture rate from low energy neutrons than does a uranium foil in a uranium blanket. The differential capture rate distributions for the same three cases are shown in Fig. 3.9. This figure also shows the important role that low energy neutron capture plays in the activation of a thorium foil irradiated in a uranium blanket. This observation leads to the conclusion that if the analytical methods used to predict the capture rate distributions in

Fig. 3.8 Integral Neutron Capture Rates for Thorium and Uranium in Thorium and Uranium Radial Blankets

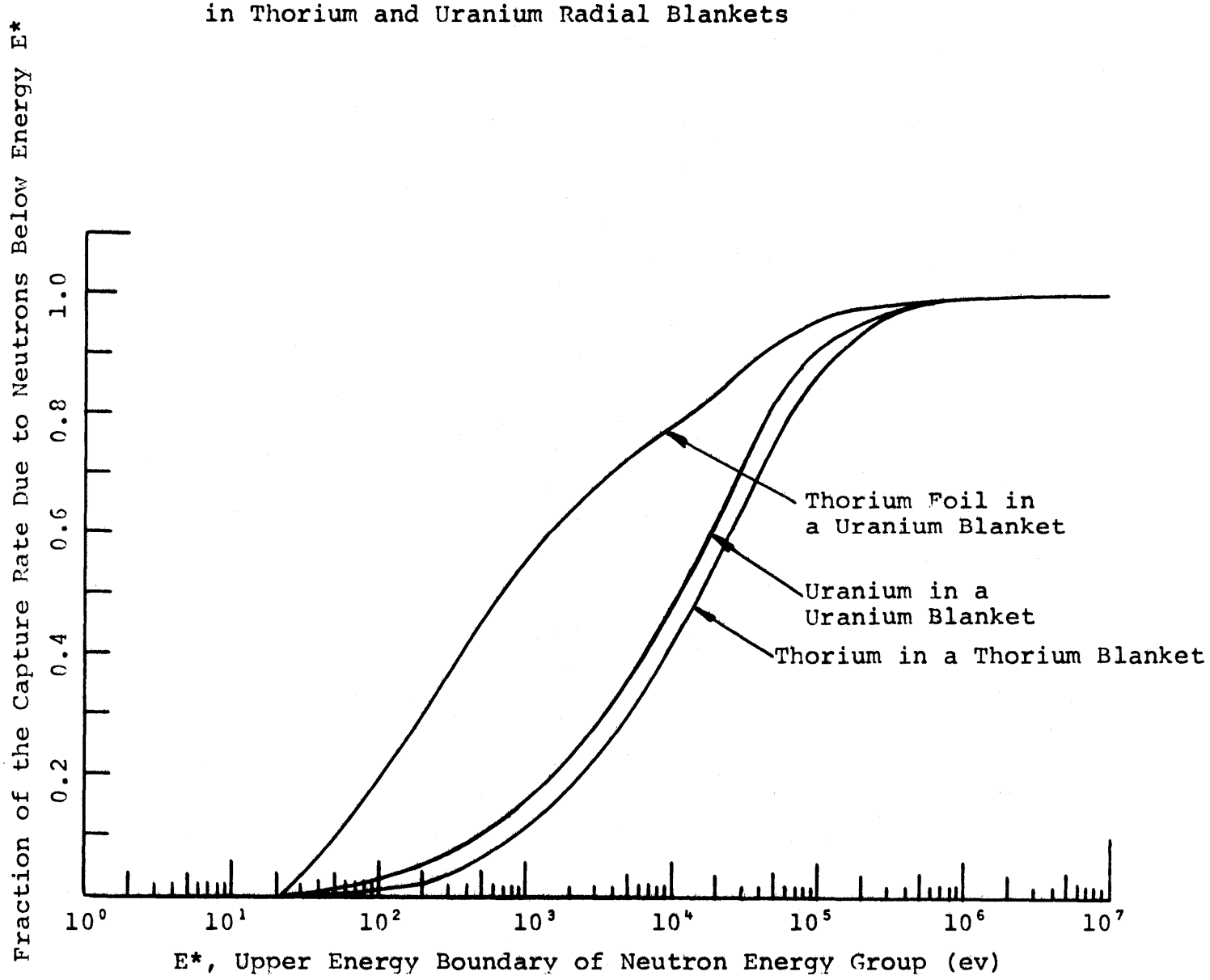

Fig. 3.9 Comparison of Differential Capture Rates in Radial Blanket

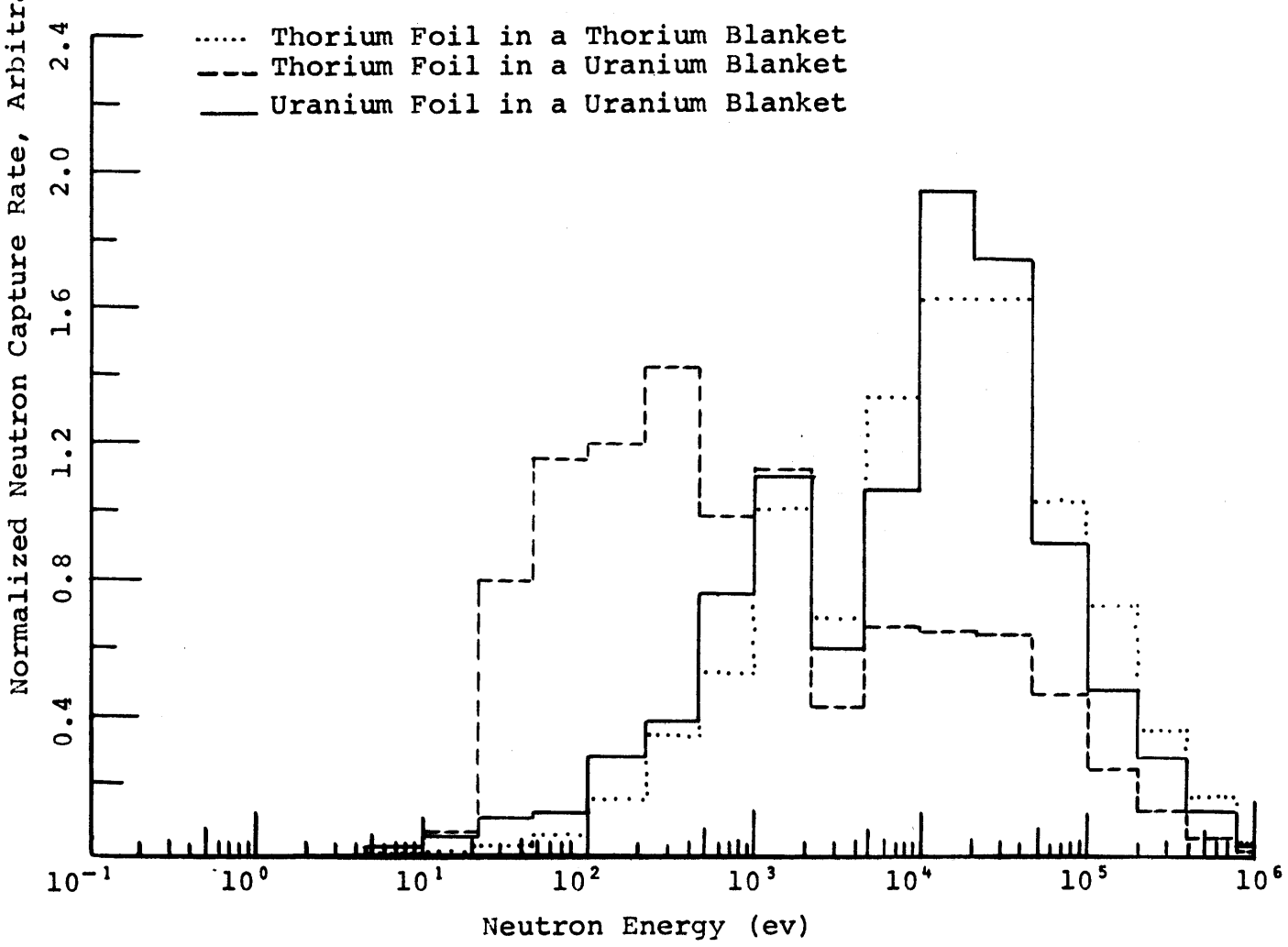

Fig. 3.5 produced a softer spectrum than existed, it would have a small effect on the predicted uranium capture rate, and a large impact on the predicted thorium foil capture rate. (This same conclusion was corroborated by arbitrarily reducing the neutron flux at all energies below 1 keV by 50%. This reduction had the effect of reducing the predicted uranium foil capture rate by about 9% while reducing the predicted thorium foil capture rate by about 25%.) In the analysis of Blanket Mockup No. 2, Leung (L11) concluded that the ABBN cross section set (B1) did apparently calculate a softer spectrum than was observed. He attributed this to the fact that in the development of the ABBN cross section set, the assumption was made that the flux per unit energy below 2.5 MeV was inversely proportional to neutron energy:

$$E\phi(E) = \phi(U) = \text{constant}. \tag{3.6}$$

To correct for this potential error, Leung presented a scheme in which the downscatter cross section could be modified based on the expected flux in the region of interest (L11, Appendix C). In Fig. 3.10, a comparison is made between the experimental data and the predicted capture rates using corrected downscatter cross sections, developed assuming that the flux per unit lethargy was proportional to the neutron energy, $\phi(U) \propto E$, which roughly approximates the functional dependence in the region of interest. A comparison between the curves generated assuming $\phi(U) \propto E$ and $\phi(U) = \text{constant}$ shows that about 45% of the discrepancy between thorium predicted and experimental capture rates has been eliminated through the use of a downscatter correction scheme.

Another approach which can be used to correct the 26-group cross section set to account for errors in the downscatter cross section

Fig. 3.10 Comparison of Experimental and Calculated Capture Rates in Thorium and Uranium, Fluxes Calculated using Modified Elastic Down-Scatter Cross Section Generated by Assuming $\phi(u) \propto E$

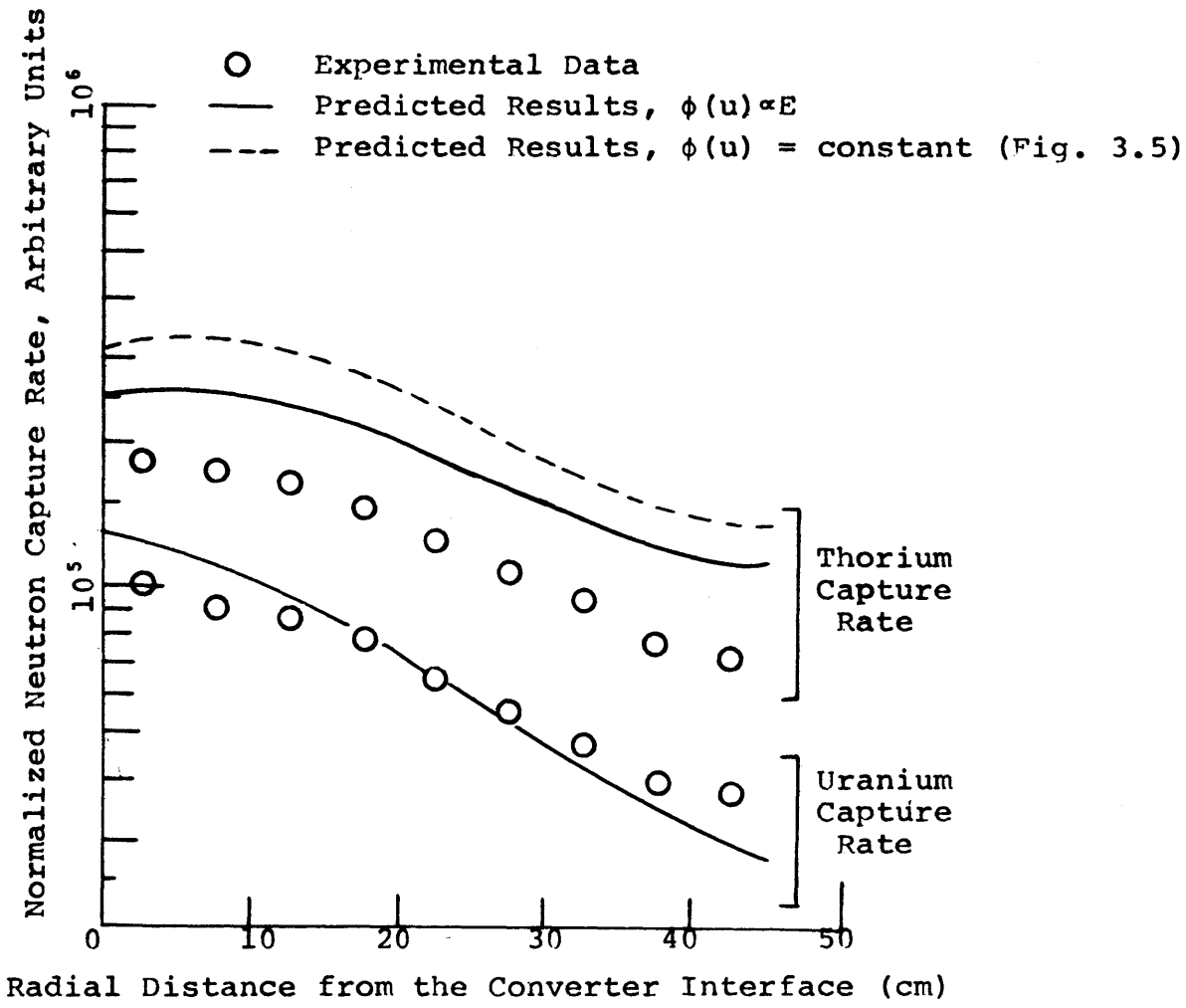

formulation is to decrease the lethargy width of the groups used in the calculation. This approach was implemented here by expanding each of the lower 16 energy groups (in which inelastic scattering is unimportant) into six groups each, giving a total of 106 energy groups. This was done by correcting the selfscatter and downscatter cross sections in the lower 16 groups of the 26-group cross section set used with ANISN by the following prescriptions:

Selfscatter

$$\sigma^{*}_{g\to g} = \sigma_{g\to g} + \sigma_{g-1\to g}(1-X) \tag{3.7}$$

Downscatter

$$\sigma^{*}_{g-1\to g} = X\sigma_{g-1\to g} \tag{3.8}$$

where

X is the new number of energy groups for each old group (i.e., six),

$\sigma_{i\to j}$ is the transfer cross section from group i to group j in the 26-group set,

and

$\sigma^{*}_{i\to j}$ is the transfer cross section from group i to group j in the 106-group set.

The only exception to the algorithm presented in Eqs. 3.7 and 3.8 was that the downscatter cross section from the unmodified wide group number 10 to the modified narrow group number 11 was kept the same as in the 26-group set. This was justified because, in the absence of inelastic scattering, a neutron gains, on the average, ξ lethargy units per collision, and the new narrow groups had lethargy widths greater than ξ for the lightest element in the blanket (other than the trace of

hydrogen). Figure 3.11 shows the comparison between the experimental capture rate data and the 106-group predictions. In that figure the predictions were normalized to the data point at the center of the uranium foil traverse. Because of the apparent good agreement in the shapes of the predicted and experimental thorium foil capture rate distributions and the fact that both the thorium and uranium foil predictions in Fig. 3.11 are high with respect to experimental data near the converter interface, the predictions were renormalized to the data point at the center of the thorium traverse. This new normalization of the 106-group predictions is shown in Fig. 3.12. As shown, excellent agreement is achieved between the thorium foil data and predictions, while the uranium foil predictions are reasonably good near the converter interface, but become significantly lower than the data at greater distances from the converter interface. In an attempt to resolve the discrepancies between predictions and experimental data, a series of diagnostic experiments will be discussed in the next section. Before leaving this section, however, a comparison will be made between the mid-blanket spectra as calculated using each of the three cross section sets discussed in this section. Figure 3.13 shows that comparison. As shown, the two modified cross section sets both predict somewhat harder neutron spectra than does the original 26-group cross section set. As discussed earlier, the harder predicted spectrum has the effect of reducing the predicted thorium foil (infinitely dilute) capture rate relative to that for uranium.

A clearer view of the differences among the three predicted spectra can be had by considering Figs. 3.14 and 3.15. In these figures the integral capture rate distributions for uranium and thorium foils

Fig. 3.11 Comparison of Calculated and Experimental Capture Rates in Thorium and Uranium Foils; Predictions were made using the 106 Group Modified ABBN Cross Section Set

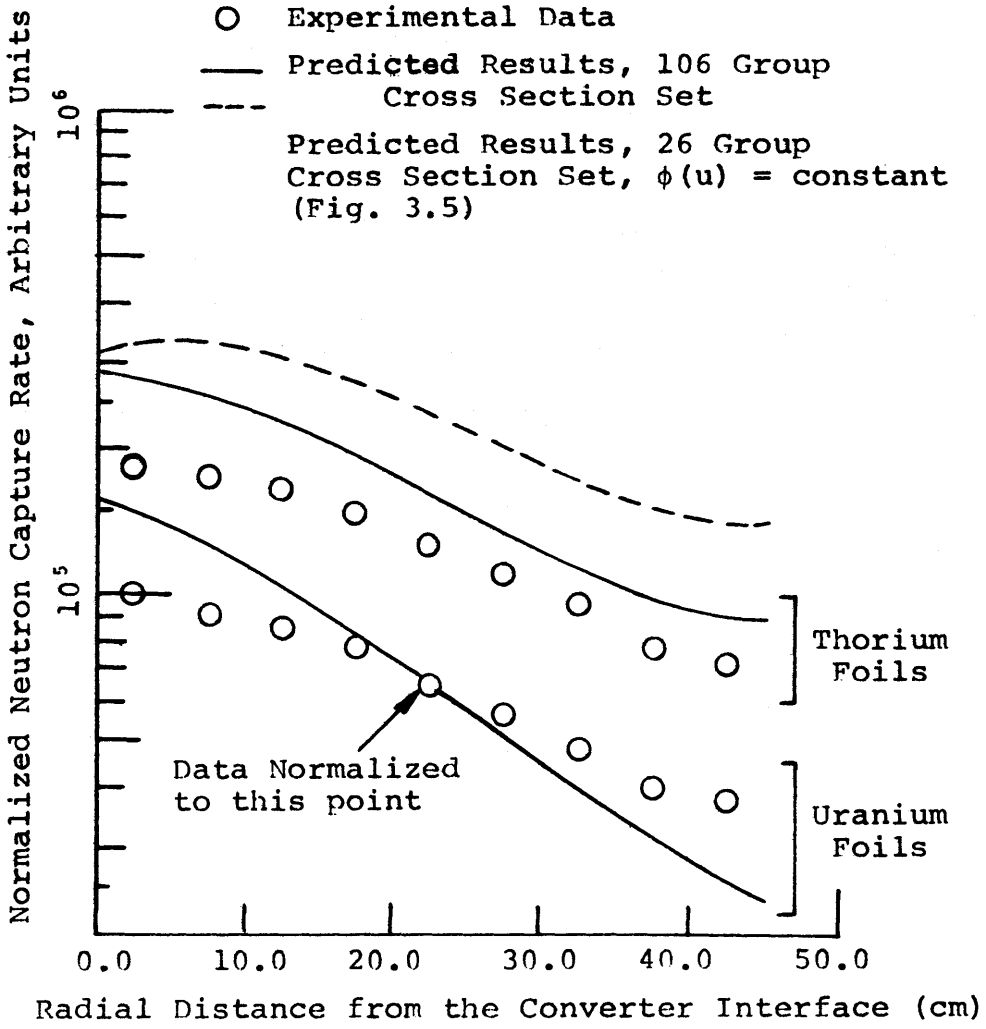

Fig. 3.12 Comparison of Experimental and Calculated Capture Rates in Thorium and Uranium Foils, Predictions Made using the 106 Group Modified ABBN Cross Section Set

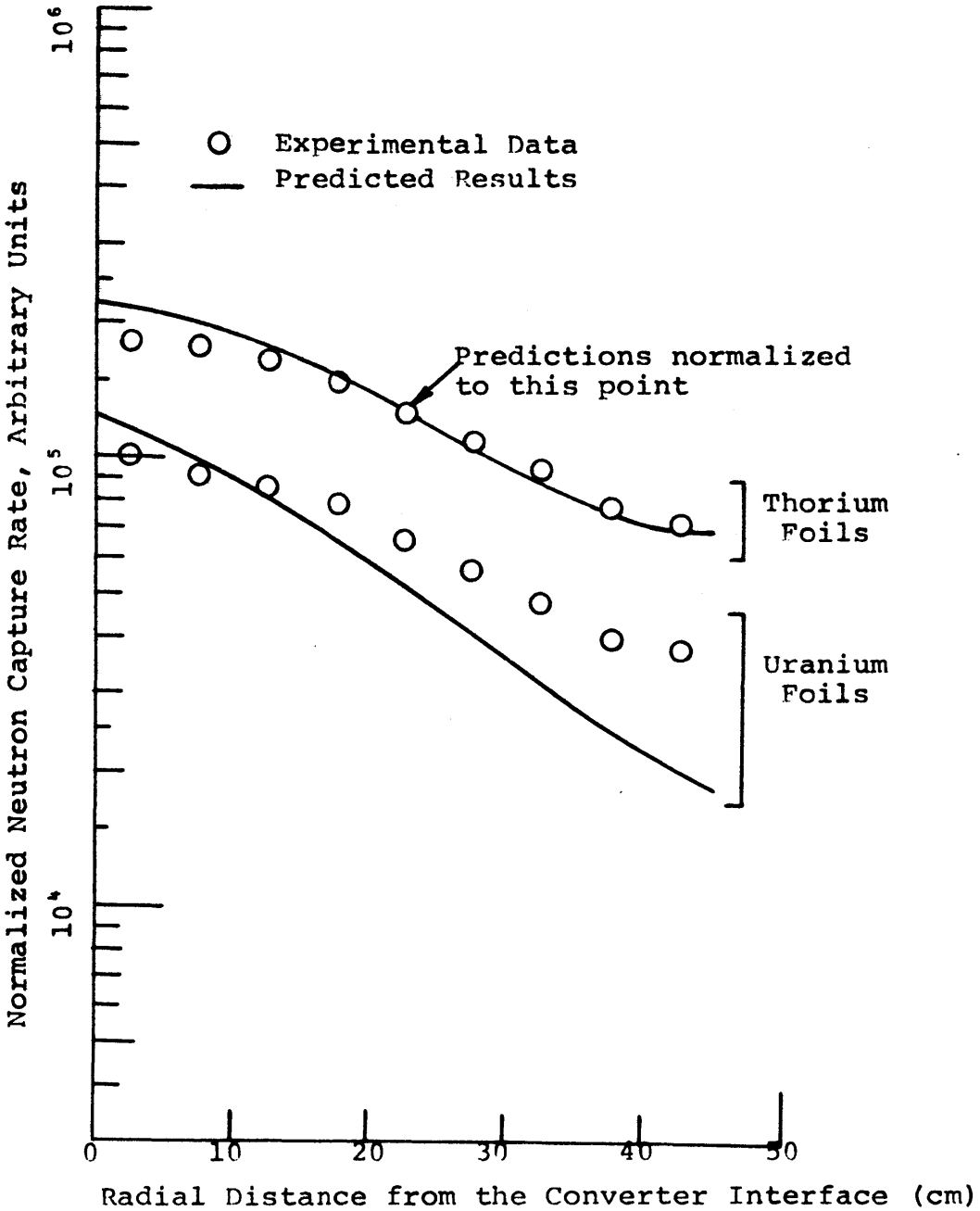

Fig. 3.13 Comparison of Calculated Mid-Blanket Neutron Spectra for Blanket Mock-Up Number 4

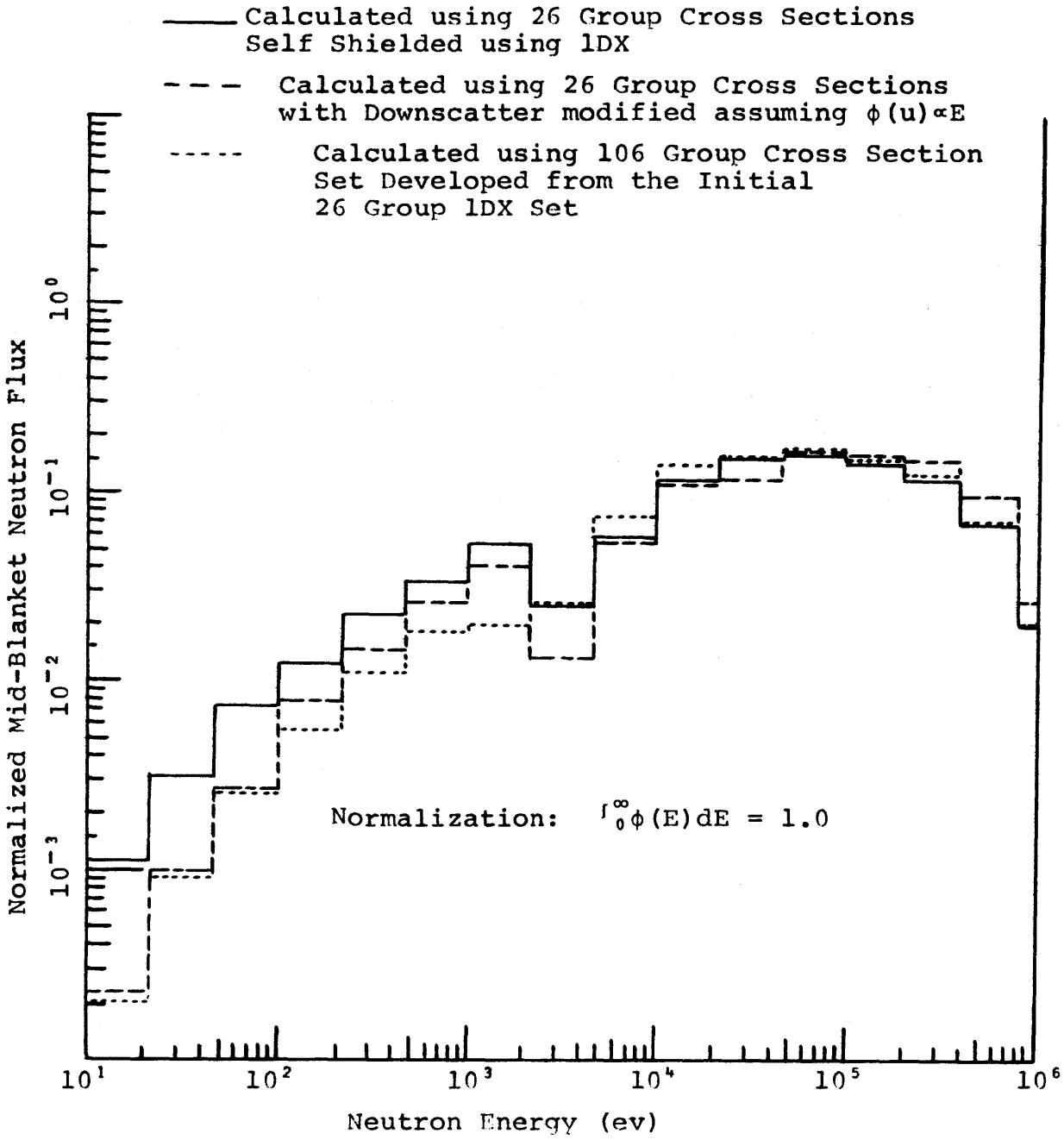

Fig. 3.14 Comparisons of Calculated Integral Uranium Capture Rate Distributions in Various Mid-Blanket Spectra

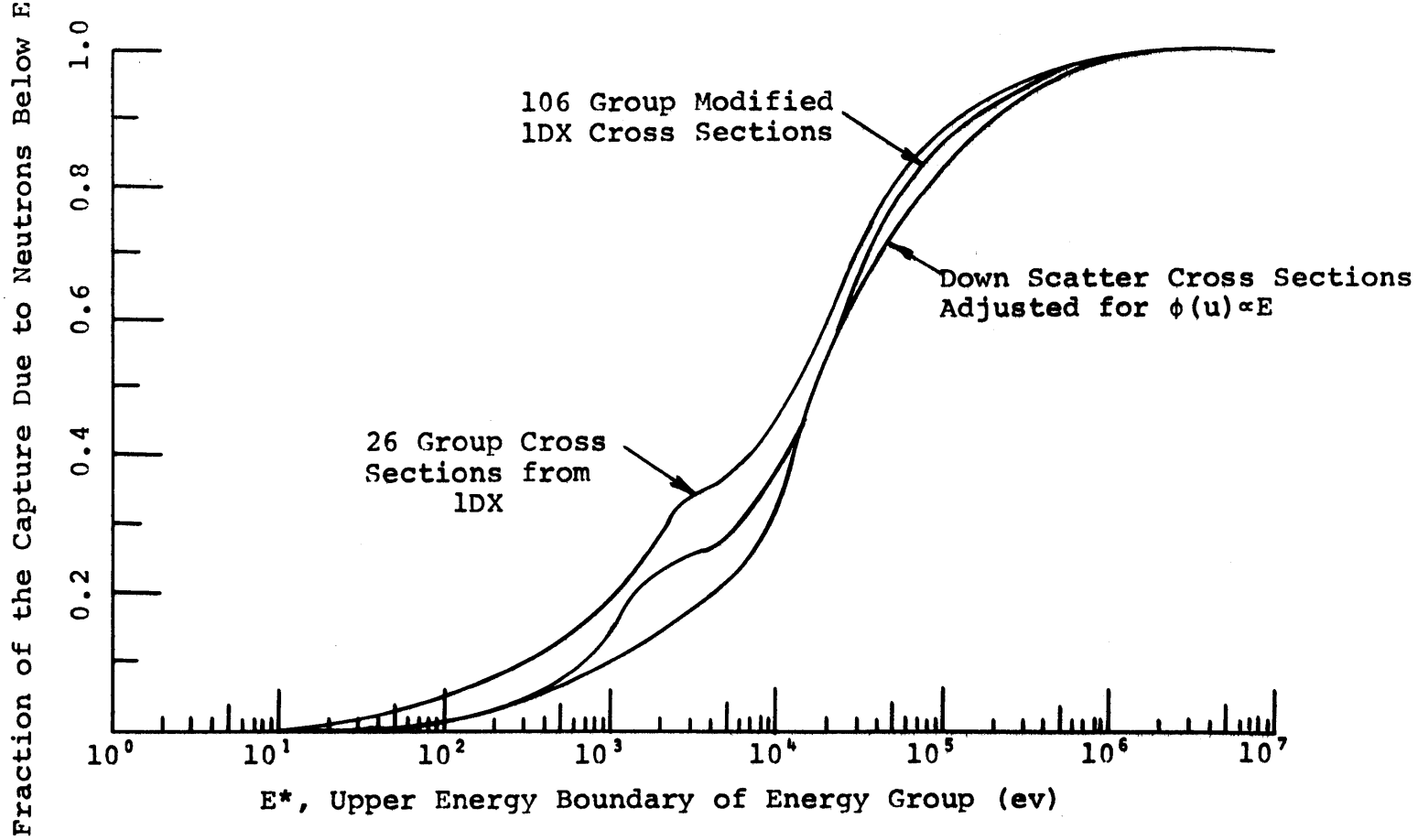

Fig. 3.15 Comparison of Calculated Integral Thorium Capture Rate Distributions in Various Mid-Blanket Spectra

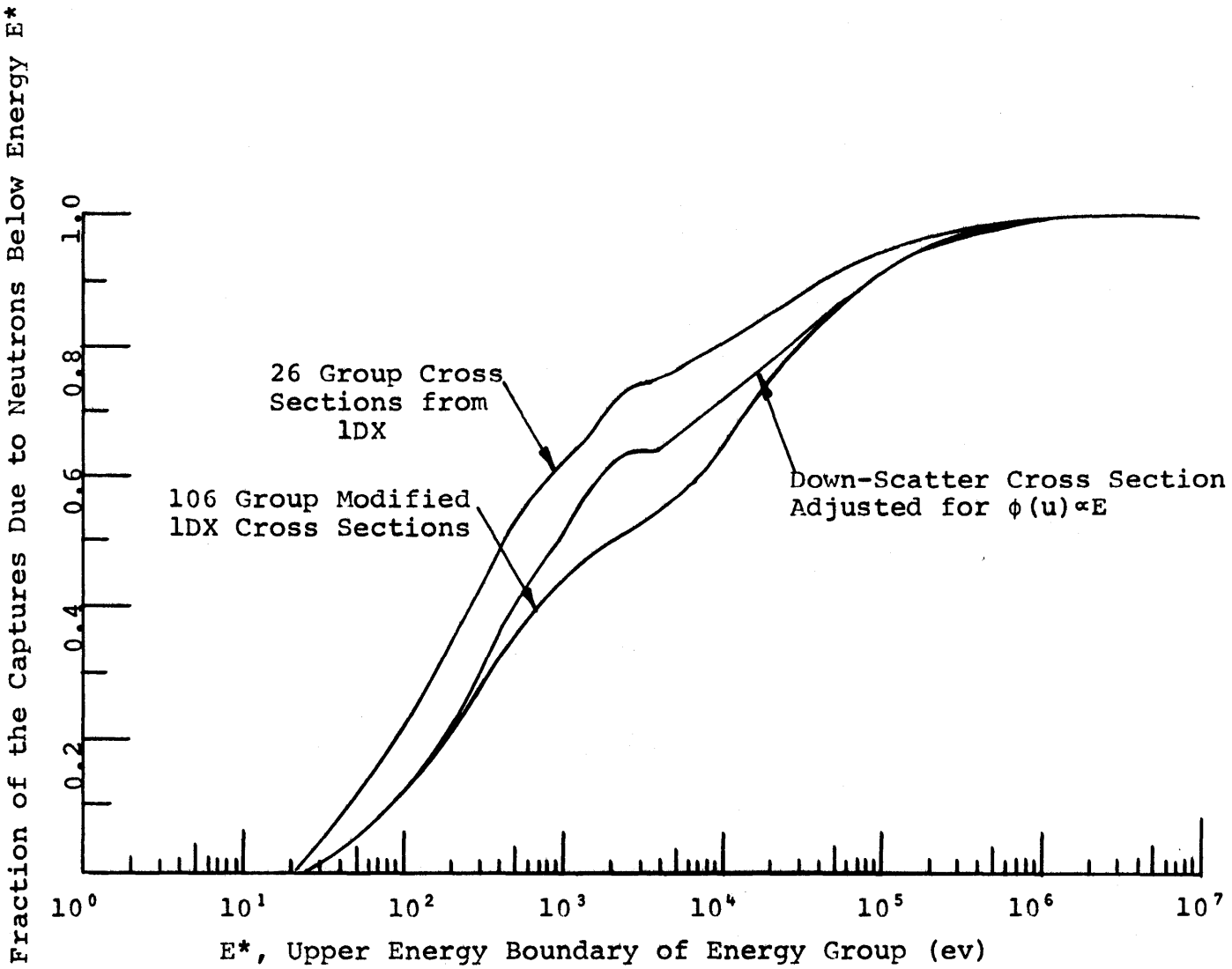

irradiated in a uranium blanket are shown for various predicted spectra. As shown, over the energy range where a significant fraction of fertile material neutron captures occur, the two modified cross section sets predict a lower integral activity than the original ABN-FTR-200, 1DX cross section set. This again confirms that the modified cross section sets produce a harder neutron spectrum when used to analyze the blanket. Later, total capture rate ratios for various foils of interest will be compared using fluxes determined by the three cross section sets. It should be mentioned that the effect of hardening the predicted spectrum on the fissile production rate in both the uranium and thorium blankets to be analyzed in Chapter 4 is a small net reduction, approximately 10% for the uranium blankets and somewhat less for the thorium blankets.

3.3.3.5 Diagnostic Experiments

As shown in Figs. 3.10 and 3.12, corrections made to the analysis of the experimental blanket data in the form of downscatter modification and an increase in the number of energy groups used in the analysis were successful in accounting for only part of the discrepancy between experimental results and analytical predictions. In this section a series of experiments will be discussed which attempted to clarify the source of the remaining observed discrepancy. Three types of experiments will be discussed:

1. Capture rate comparisons in the reflector, where both uranium and thorium foils can be characterized as infinitely dilute,
2. Capture rate comparisons among various foils (Th, U, Au, and Mn) in the middle of the blanket where only the uranium resonances were shielded,

3. Capture rate comparisons between U and Th foils in the fission spectrum facility where no resonance self-shielding existed for any of the foil materials.

The first diagnostic experiment to be discussed is the uranium and thorium foil irradiation in the reflector. The purpose of this experiment was to determine how effective the infinitely dilute uranium and thorium capture cross sections are at predicting relative neutron capture rates in a soft spectrum. (Figure 3.16 shows a comparison between calculated reflector and mid-blanket neutron spectra.) The only corrections made to the data from this experiment were background, foil weight, and experimentally determined foil self-shielding (determined using one- and two-foil packets of both materials, see Eq. 3.4). The foils for this experiment were located in the steel reflector approximately five inches from the blanket interface. At this distance the resonance flux depletion resulting from the large concentration of U-238 in the blanket was expected to be washed out by neutron scatter events. Before the experimental capture rate ratio was determined, the thorium foil activity was normalized to the uranium foil activity using capture rate data from the thermal spectrum facility, as in Eq. 3.1. Table 3.6 shows the results of these experiments together with predicted results using the reflector spectra calculated from the three cross section sets discussed earlier.

TABLE 3.6 Comparison of Thorium and Uranium Capture Rates in the Reflector

Conditions	Capture Rate Ratio (Th/U)
Experimental	0.784 ± 0.015
Flux calculated using 1DX cross sections	0.657
Flux calculated using modified 106-group cross section set	0.700
Flux calculated using cross sections with modified downscatter	0.681

Fig. 3.16 Comparison of Calculated Mid-Blanket and Steel Reflector Spectra Using the 106 Group Cross Section Set Developed from the 26 Group 1DX Generated Set

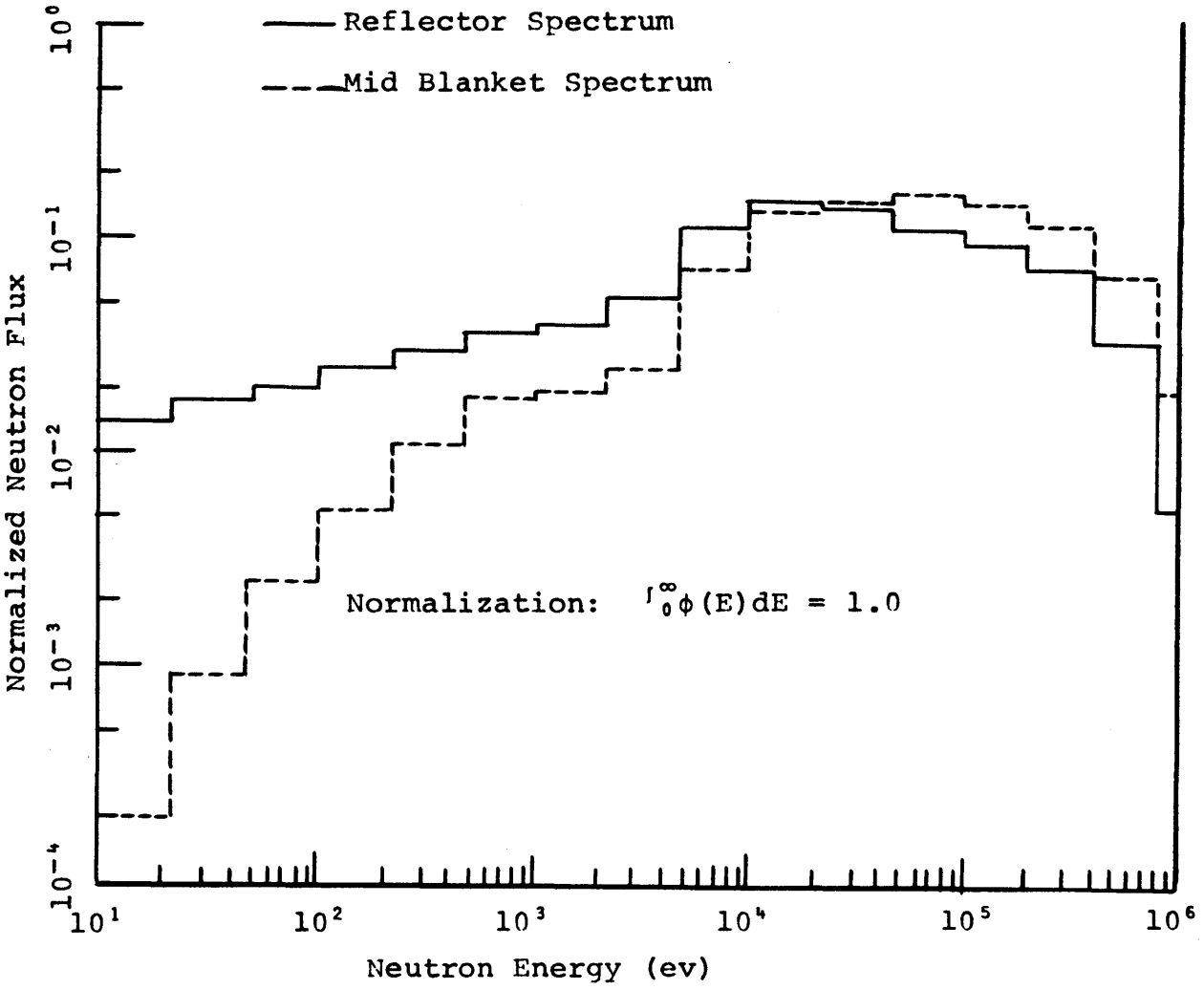

As shown in the table, all three cross section sets predicted lower ratios of thorium to uranium capture than was observed experimentally, by approximately 15%. This result implies that the spectrum-averaged infinitely dilute thorium capture cross section is actually greater (or correspondingly the effective infinitely dilute uranium cross section is less) than that predicted using various versions of the ABBN (B1) cross section set. The discrepancy between the experimental and calculated capture rates is not unrealistically large in light of the uncertainties in measured uranium and thorium cross sections in the resonance region (D10, S5). A 1966 survey (G5) showed that the uncertainties on both U-238 and Th-232 capture cross sections in the energy range from 100 eV to 100 keV was approximately ± 25%. The ABBN thorium cross sections were developed prior to that time, while the U-238 cross sections have been more recently updated in the ABN-FTR-200 set (N1). In a more recent evaluation (S5), differences in the U-238 capture cross section, as determined by investigators at Oak Ridge and at Gulf General Atomic, ranged from 2% to 41% over the energy range from 1 keV to 100 keV. A blanket spectrum-average difference between these two cross section sets was calculated to be approximately 12%.

In the next series of experiments, various foil materials (including U-238, Th-232, Au-197, and Mn-55) were irradiated in blanket position number 5 (see Fig. 3.2) while, simultaneously, similar foils were irradiated in the thermal spectrum facility. The purpose of these experiments was to provide data for comparison of the measured uranium and thorium capture rates with other secondary standards. Gold and manganese were chosen as secondary standards because both materials have fairly well characterized capture cross sections, and the

capture rate distribution versus energy for these materials is reasonably similar to that of thorium (see Fig. 3.17). (Figure 3.18 also compares the differential capture distributions for several foils in the mid-blanket spectrum.) The foils irradiated in blanket position 5 were corrected for background, foil self-shielding, and foil weight, and then normalized to either thorium or uranium foils using thermal spectrum irradiation data, through Eq. 3.1. Table 3.7 shows the results of these experiments together with predictions made using mid-blanket spectra generated with the three cross section sets discussed earlier. As shown, the use of the 106-group cross section set improved the agreement between the experimental and calculated capture rate ratios for all data considered, except for the ratio of thorium capture rate to gold capture rate. If the capture rate ratios predicted using the 106-group cross section set are assumed to be the most accurate of those presented in Table 3.7, then there appears to be a residual discrepancy of from 5% to 18% in the infinitely dilute thorium capture cross section when compared with manganese and gold. If this discrepancy exists, then the ABN-FTR-200 infinitely dilute thorium capture cross sections are somewhat larger than the experiments show they should be.

There is also an apparent discrepancy of from 17% to 22% in the self-shielded uranium capture cross section when compared with manganese and gold. If the predicted spectrum using the 106-group set were still too soft, this would explain the observed discrepancy. Two factors might contribute to make the calculated spectrum softer than that in the blanket. First, evidence exists (B13) that the inelastic scattering cross section for uranium in the present and past versions of the Evaluated Nuclear Data File overpredicts low energy inelastic scattering.

Fig. 3.17 Comparison of Integral Neutron Capture Rates for Various Foil Materials in Blanket Mockup Number 4, Fluxes from Down Scatter Corrected Cross Sections with $\phi(u) \propto E$

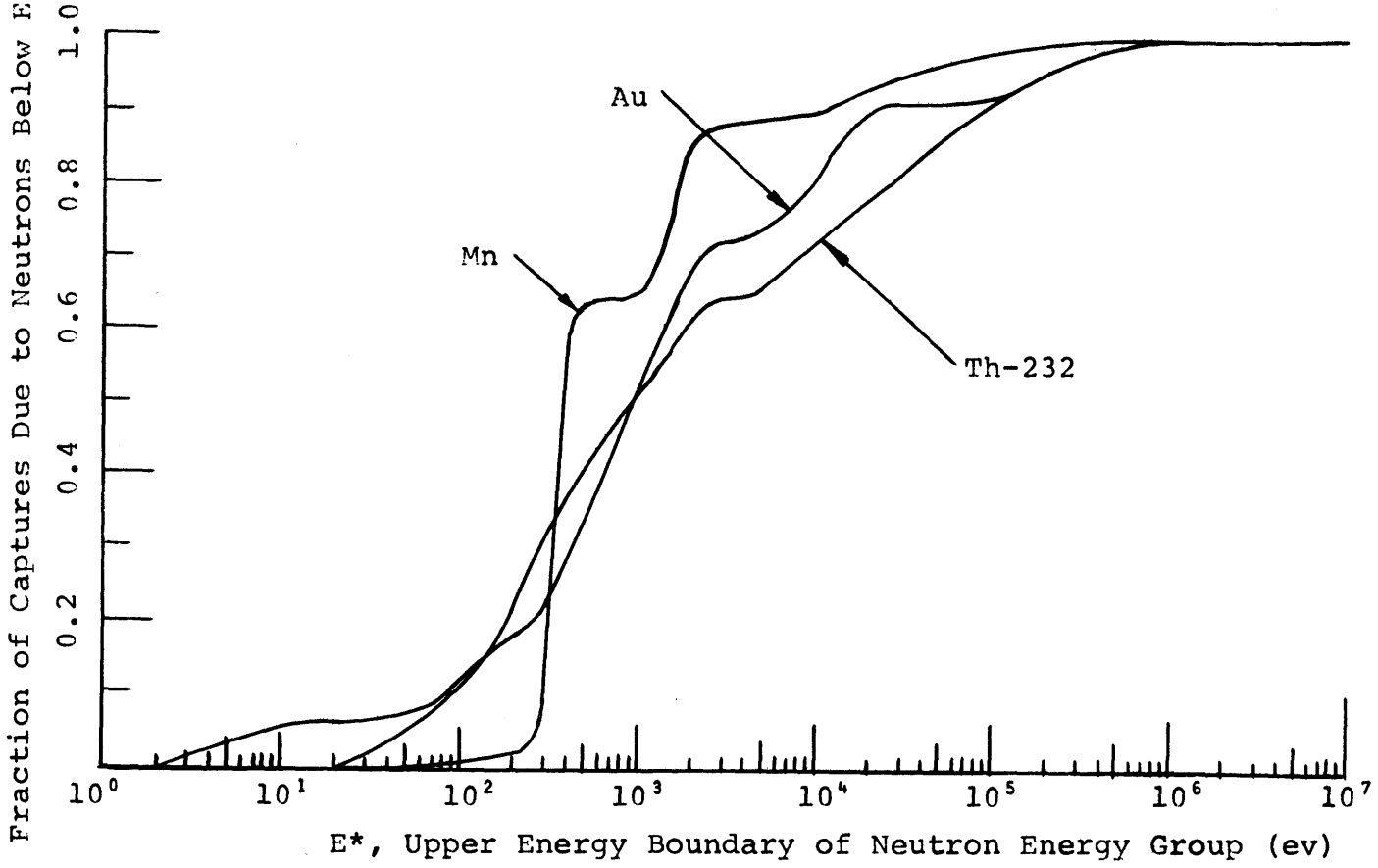

Fig. 3.18 Comparison of Energy Group Differential Capture Rates, Fluxes from 106 Group Cross Section Set Analysis, Mid-Blanket

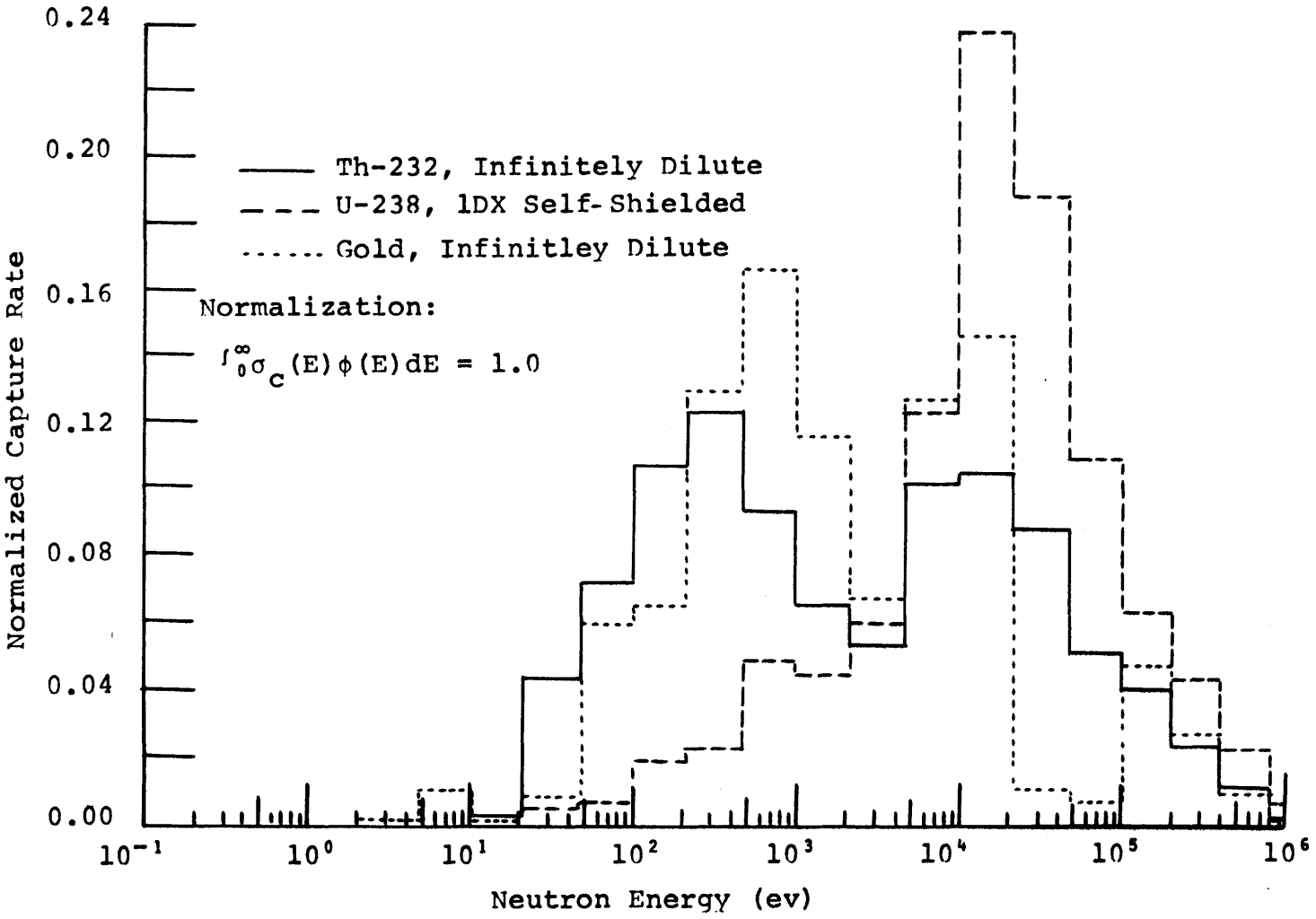

TABLE 3.7 Comparison of Mid-Blanket Foil Irradiation Data

Capture Rate Ratio	Experimental Ratio	Ratio of Calculated (Using Flux 2)* to Experimental	Calculated Capture Rate Ratios*		
			Using Flux 1	Using Flux 2	Using Flux 3
Th/U	1.823 ± 0.140	1.343	3.604	2.449	2.870
Th/Au	0.779 ± 0.028	1.182	0.824	0.921	0.831
Th/Mn	5.173 ± 0.436	1.052	4.665	5.440	4.519
U/Au	0.452 ± 0.016	0.832	0.229	0.376	0.290
U/Mn	2.838 ± 0.324	0.783	1.294	2.221	1.574

*Flux 1 was calculated using the 26-group cross section set developed from the ABN-FTR-200 set by the use of 1DX.

Flux 2 was calculated using the 106-group modified version of Flux 1.

Flux 3 was calculated using the 26-group downscatter corrected cross section set described by Leung (L11).

Second, if the less effective resonance self-shielding in uranium near the blanket-reflector interface were accounted for, more low energy uranium capture events would occur in that region, and the resulting spectrum could be harder. Counterbalancing these two effects is the observation by Yule (Y1) that calculated spectra in a depleted-uranium pile were brought in closer agreement with experimentally observed spectra by including a spectrum softening U-238(n,γ,n') reaction. Thus, it is apparent that much additional work on interface effects as well as uranium inelastic scattering is required before a definitive explanation of the differences between the calculated and experimentally observed capture rates can be given. It should, however, be noted that the increase in fertile capture rate near the blanket-reflector interface over that predicted will occur in both uranium and thorium blankets. This increase will also have a small effect on fissile production rate because most of the fissile production occurs nearer the core interface where the neutron flux is higher.

One final experiment will now be discussed. In that experiment uranium, thorium, gold, and manganese foils were irradiated in both the fission spectrum facility and the thermal spectrum facility. The purpose of this experiment was to compare capture rates for these foil materials in a spectrum similar to a fission spectrum (see Fig. 3.3). This was of interest because no resonance self-shielding exists in a fission spectrum. Table 3.8 summarizes the results from these experiments. This table shows that relatively good agreement was obtained, using the ANISN code to evaluate the 6CH1 spectrum, between the calculated and experimental capture rate ratios for thorium and uranium, while somewhat poorer agreement resulted when other capture

TABLE 3.8 Comparison of Calculated and Experimental Reaction Rate Ratios in a Spectrum Similar to a Fission Spectrum.

Ratio	Experimental	Calculated	Calculated/ Experimental
$(Th/U)_{capture}$	1.186 ± 0.187	1.324	1.116
$(Th/Au)_{capture}$	0.761 ± 0.017	1.144	1.503
$(Th/Mn)_{capture}$	11.97 ± 1.01	18.85	1.575
$(U/Au)_{capture}$	0.642 ± 0.102	0.864	1.346
$(U/Mn)_{capture}$	10.10 ± 1.80	14.24	1.410
$(Th/U)^{*}_{fission}$	0.109 ± 0.008	0.201	1.842

*This ratio is for fission rates in the 6CH1 facility, presented here for purposes of comparison. This ratio was developed assuming that the fission product yields for thorium and uranium are the same.

rates were compared. The predicted reaction rates in thorium and uranium are shown to be high relative to gold and manganese. In the only experiment which was repeated several times, that to compare thorium and uranium, a large SDM was obtained. This can be partially explained by the fact that spatial flux variations of as much as 20% exist inside the 6CH1 facility in which the foils were irradiated (L13). The large discrepancy between the experimental and calculated capture rate ratios involving other foil materials has not yet been explained. However, reference to Fig. 3.8 shows that a very small percentage of the total blanket capture rate occurs in the energy range where fission neutrons originate, so errors in the high energy capture cross section will have little effect on blanket performance.

3.4 RESULTS OF OTHER EXPERIMENTS

Several experiments are reported in the literature in which thorium was studied in fast spectrum facilities. Perhaps the most interesting of these experiments was one reported by Batyrbekov (B2) in which an effectively infinitely thick thorium metal blanket surrounding the BR-1 experimental fast reactor was investigated. Because of the small size of the driving reactor and the complete lack of moderating material in the metallic blanket, the blanket spectrum would be expected to be very hard. Therefore thorium resonance self-shielding was most likely not as significant as it would be in a typical LMFBR blanket. In any event, Batyrbekov used the 26-group ABBN cross section set to predict, quite accurately, the capture rate in thorium foils irradiated in the blanket.

Other investigators (A3) have determined the reactivity worth of samples of uranium and thorium metal in the Zero Energy Fast Reactor (FRO). They have also used the ABBN cross section set to evaluate the expected reactivity worth of the samples. Comparisons between calculated and experimentally determined reactivity worths were shown to be quite good for large samples of uranium metal, and less accurate for small samples (~300 g) of thorium and uranium metal. Both for thorium and for uranium the analysis predicted a somewhat larger reactivity worth than was observed. The overprediction was somewhat more severe for the uranium samples than for the thorium samples, leading to the conclusion that the ABBN cross section set predicts a larger relative value of $[\overline{\sigma}_a - \overline{\nu\sigma}_f]$ for uranium than for thorium. Carpenter (C1) also measured reactivity worths of various sized pieces of uranium and thorium metal and compared the measured worths to

calculated values. (He did not use the ABBN cross section set.) His data show that the reactivity worth of thorium was calculated to be significantly greater (~30%) than the measured reactivity worth, while the experimental uranium reactivity worths were measured to be about 40% greater than the calculated values.

From these data it can be qualitatively concluded that in a hard spectrum blanket, the ABBN cross section set can be used to characterize thorium metal capture rates fairly accurately, but that no comprehensive data are available to test the resonance self-shielding formulations in the ABBN set for a softer spectrum blanket typical of those considered in the analytical study presented in Chapter 4 of this report. The small sample reactivity data and analysis of Andersson (A3) have also shown that, relative to uranium, the spectrum-averaged thorium capture cross section is somewhat smaller than would be calculated using the ABBN cross section set. This observation is in qualitative agreement with the data from this study presented in Fig. 3.4 and Table 3.7.

3.5 SUMMARY AND CONCLUSIONS

In this chapter an experimental comparison has been made between the fission and capture rates in thorium and uranium foil material irradiated in a neutron spectrum typical of the radial blanket region surrounding a demonstration LMFBR. The facility in which these irradiations were performed is the M.I.T. Blanket Test Facility, Blanket Mockup No. 4. The capture and fission rates in the thorium were normalized to those for uranium through the use of normalization

foils irradiated in reasonably well characterized thermal and fission spectrum facilities. A comparison between the experimental data and analytical predictions made using the ANISN code (E1) with cross sections from the ABN-FTR-200 (N1) cross section set which were resonance self-shielded using the code 1DX (H2), showed that the relative uranium and thorium fission rates could be predicted fairly well, while the neutron capture rate in thorium was predicted to be too high relative to that for uranium. Evaluation of the discrepancies revealed that a significant fraction of the difference between the predicted and experimentally observed ratio of thorium to uranium capture rate could be attributed to an inexact development of the downscatter cross section in the initial cross section set (see Figs. 3.11 and 3.12). However, discrepancies in the shape of the capture rate distribution for uranium foils irradiated in Blanket Mockup No. 4 remained when the downscatter was more exactly treated by using a 106-group cross section set developed from the initial 26-group 1DX generated set. These discrepancies are quite likely related to the reduction in uranium resonance self-shielding expected near the reflector interface and the spectral hardening which will accompany this reduction. These two related phenomena would have the same effect (i.e., that of increasing the observed fertile capture rate near the reflector) on both uranium and thorium blankets. A series of diagnostic experiments using secondary standard foil materials showed the following:

1. The relative thorium and uranium capture rates in the reflector (where uranium self-shielding is not an important factor) were predicted reasonably accurately, with experimentally observed thorium data actually being somewhat higher, relative to uranium, than was predicted;

2. Neutron capture rates measured for thorium, uranium, gold, and manganese in the center of the blanket showed that the thorium capture rate, relative to those for gold and manganese, was predicted to be from 6% to 18% higher than observed; while uranium (self-shielded) capture rates were predicted to be about 20% less than observed relative to the same standards;
3. Although some discrepancies were observed, the relative capture rates for thorium and uranium foils irradiated in a spectrum similar to a fission spectrum were predicted accurately within experimental uncertainty.

The net result of the experiments and analyses reported in this chapter can be summarized in three points:

1. The 26-group ABN-FTR-200 cross section set with self-shielding analysis performed using the shield factor approach as implemented in the 1DX code predicts a spectrum which is significantly softer than that which exists in the blanket. This effect, however, has little impact on predictions of blanket breeding performance;
2. The infinitely dilute effective thorium capture cross section in the blanket may be as much as 6% to 18% lower than predicted in the ABN-FTR-200 cross section set. Again this discrepancy may only be in the low energy thorium capture cross section and have little impact on thorium blanket performance;
3. Self-shielded cross sections for uranium foil materials irradiated in the blanket appear to lead to an effective capture cross section which is approximately 20% less than that determined experimentally. This may be related to reflector interface effects and inexact spectrum predictions.

The effect of these experimentally based conclusions on the analytical work presented in this report will be discussed in section 5.6.4.

In preview, it can be said that the effect of a softer predicted spectrum, resulting from inexact treatment of the downscatter cross section in the ABN-FTR-200 set, on the net fissile production rate in both a uranium and a thorium blanket is small (approximately 10%). If this calculated spectral softening were taken into account, thorium blankets would show slightly improved breeding performance relative to uranium blankets. No firm conclusion can be made regarding the relative spectrum-averaged values of uranium and thorium capture cross sections in uranium and thorium blankets. However, it can be said that even if the unresolved resonance region ($\sim 10^4$ to ~10 eV) capture cross section for thorium in a thorium blanket were reduced by 20%, the fissile production rate would be decreased by less than 1%.

The work presented in this chapter appears to raise more questions about blanket performance predictions than it answers. To help clarify and resolve these questions, further work is required in at least three major areas. First, duplicate experiments should be performed in which uranium, thorium, gold, manganese, and molybdenum foil traverses are made in the blanket, and the results are consistently normalized using the thermal spectrum irradiation facility. Second, additional analytical effort is required in three areas: assessment of the validity of the shield-factor method of predicting blanket resonance self-shielded cross sections; improvement on the two methods used here to compensate for incorrect evaluation of the elastic downscatter cross section; and evaluation of the blanket-reflector interface effect on blanket fissile capture rate. Finally, a thorium blanket should be built and characterized to allow comparison of the experimentally

determined resonance self-shielding of thorium with that calculated using some appropriate cross section set. Until both uranium and thorium blankets have been experimentally characterized, no unequivocal assessment of the validity of the relative fissile inventories predicted later in this report can be made.

Chapter 4

BURNUP CALCULATIONS

4.1 INTRODUCTION

The purpose of this chapter is to apply the calculational procedures outlined in Chapter 2 to the analysis of three 1000-MW_e LMFBR systems. The three systems, all of which have the same physical dimensions as described in section 2.2, are

1. Standard Pu/U core with depleted uranium blankets,
2. Standard Pu/U core with thorium blankets,
3. Core composed of U-233/Th-232 with thorium blankets.

An attempt will be made here to show how the three systems were burned up in a consistent manner, thus allowing an economic comparison to be made in Chapter 5. The bulk of this chapter is concerned with a comparison between the first two systems tabulated above. At the end, a brief discussion of the U-233/Th-232 core and blanket system will be presented.

This chapter has been arranged so that the physics and burnup analyses are presented in the order in which they were performed. The first topic is the method used to select the core enrichment and poison concentration for the 600-day batch burnup steps. Next a discussion is presented of the batch burnup mode of managing the radial blanket. As a first refinement to the batch blanket management mode, zone scatter and in-out shuffle management are discussed. Finally, the physics and burnup performance of the U-233/Th-232 core and blanket system are presented.

4.2 INITIAL PHYSICS ANALYSIS

4.2.1 Effect of Fissile Loading on k_{eff}

To accomplish system burnup in the manner outlined in section 2.5, two correlations were necessary: the effect of core enrichment on system k_{eff}, and the effect of B-10 concentration on system k_{eff}. These two correlations together with a knowledge of the shape of the system k_{eff} vs. irradiation time were sufficient to define the required core enrichment and poison concentration. This section will be concerned with the effect of core fissile loading on system k_{eff}. To evaluate this effect, the 2DB program (L10) was used to perform snapshot physics calculations using various beginning-of-life (BOL) fissile inventories in the core.

For the purpose of this work, the isotopic composition of the plutonium used in the reactor core was chosen to be that associated with an equilibrium LMFBR fuel cycle (D6). Table 4.1 shows the equilibrium LMFBR plutonium isotopic concentrations used in this study together with the isotopic composition used by other investigators. As shown,

TABLE 4.1 Plutonium Isotopic Concentrations

Isotope	Equilibrium LMFBR Composition (D6)	LWR Discharge Composition (K1)	LWR Discharge Composition (G1)
Pu-239	0.630	0.60	0.57
Pu-240	0.273	0.24	0.26
Pu-241	0.059	0.12	0.13
Pu-242	0.038	0.04	0.04

the plutonium produced by LMFBR's is expected to be cleaner (i.e., to have a smaller fraction of higher isotopes) than that produced by light water reactors (LWR's). If LWR discharge plutonium had been used in this study, it would have had the effect of reducing slightly the enrichment of fissile plutonium required in the core. This would have resulted because of the superior nuclear properties of Pu-241 in a fast reactor environment. For example, the one-group core spectrum collapsed cross section set presented by Driscoll (D6) shows that $[\overline{\nu\sigma}_f - \overline{\sigma}_a]$ for Pu-239 is 3.397 while that for Pu-241 is 5.326. Thus, doubling times calculated from this burnup analysis will be somewhat longer than those calculated from analyses done using LWR discharge plutonium.

Using the non-fuel isotope number densities shown in Table 4.2, the blanket compositions shown in Table 4.3, and several assumed fissile enrichments, it was possible to use 2DB snapshot physics calculations to develop a graphical relationship between changes in core fissile loading and the corresponding changes in system k_{eff}. Figures 4.1 and 4.2 show these relationships. Figure 4.1 is for a depleted (i.e., 0.2% U-235) uranium blanket system while Fig. 4.2 is for a thorium blanket system. As discussed in section 2.2, the ratio of the fissile enrichment in core zone I to that in core zone II was maintained constant at 11/17 for all parametric variations. Core fissile material number densities at the beginning-of-life (BOL) will be developed in section 4.2.3. In that section it will be shown that use of thorium blankets requires 1.04 times the fissile loading needed for a uranium blanketed system.

TABLE 4.2 Non-Fuel Number Densities

Material	Material Number Density (atoms/barn-cm)			
	Core	Axial Blanket	Radial Blanket	Radial Reflector I
Iron	0.01213	0.01213	0.01213	0.05459
Chromium	0.00312	0.00312	0.00312	0.01404
Nickel	0.00195	0.00195	0.00195	0.008775
Sodium	0.01096	0.01096	0.006576	0.002192

Material	Material Number Density (atoms/barn-cm)		
	Radial Reflector II	Axial Reflector	Axial Reflector on the Radial Blanket
Iron	0.0	0.03033	0.03033
Chromium	0.0	0.0078	0.0078
Nickel	0.0	0.004875	0.004875
Sodium	0.02192	0.01096	0.01096

TABLE 4.3 Blanket Material Number Densities

Material	Material Number Density (atoms/barn-cm)			
	Uranium Radial Blanket	Uranium Axial Blanket	Thorium Radial Blanket	Thorium Axial Blanket
Oxygen	0.02326	0.01395	0.02170	0.01302
U-238	0.01161	0.006963	0.0	0.0
U-235	2.326×10^{-5}	1.395×10^{-5}	0.0	0.0
Th-232	0.0	0.0	0.01085	0.006509

Fig. 4.1 The Effect of Core Fissile Loading on System Effective Multiplication Factor, Uranium Blanket System

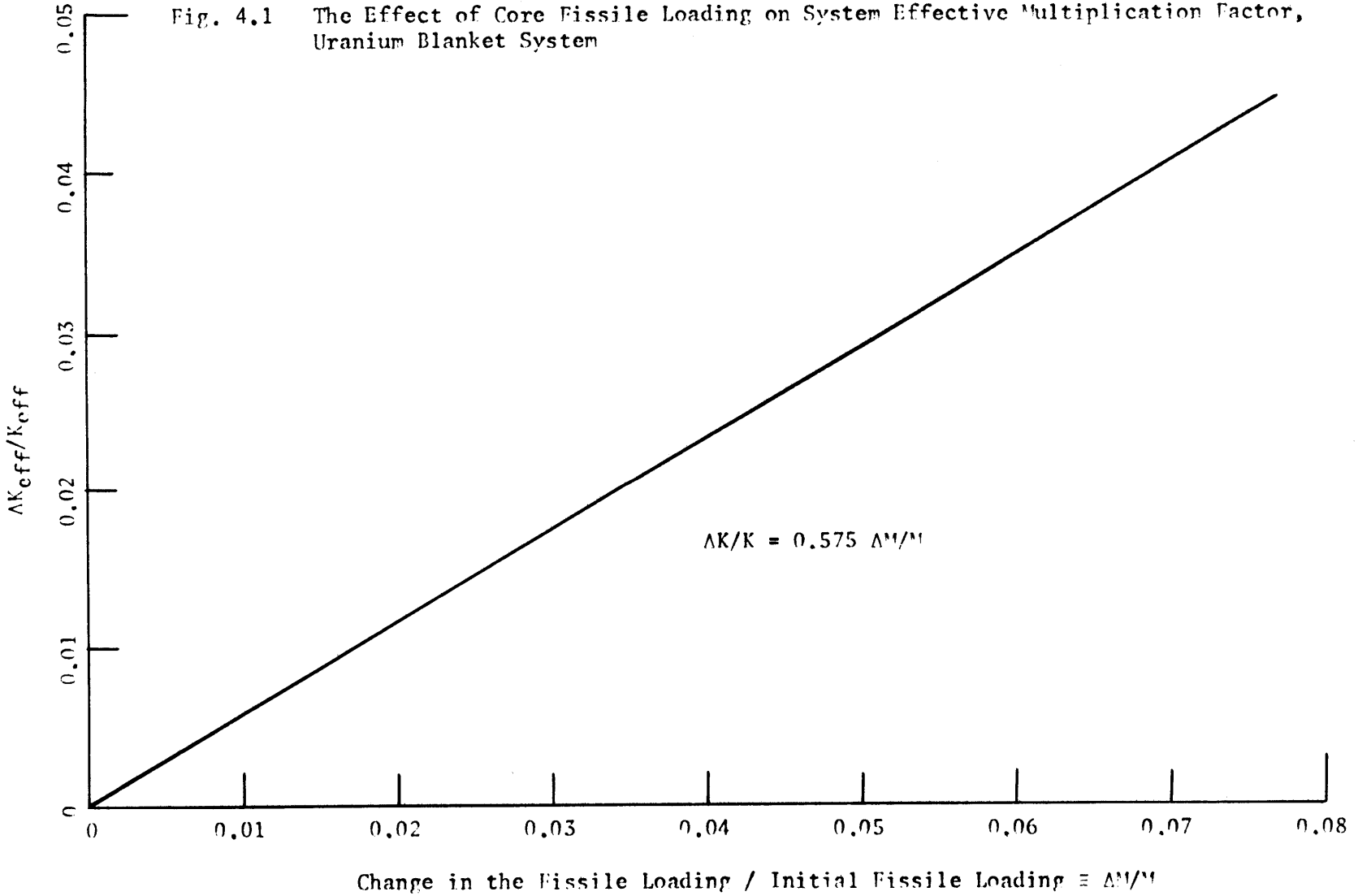

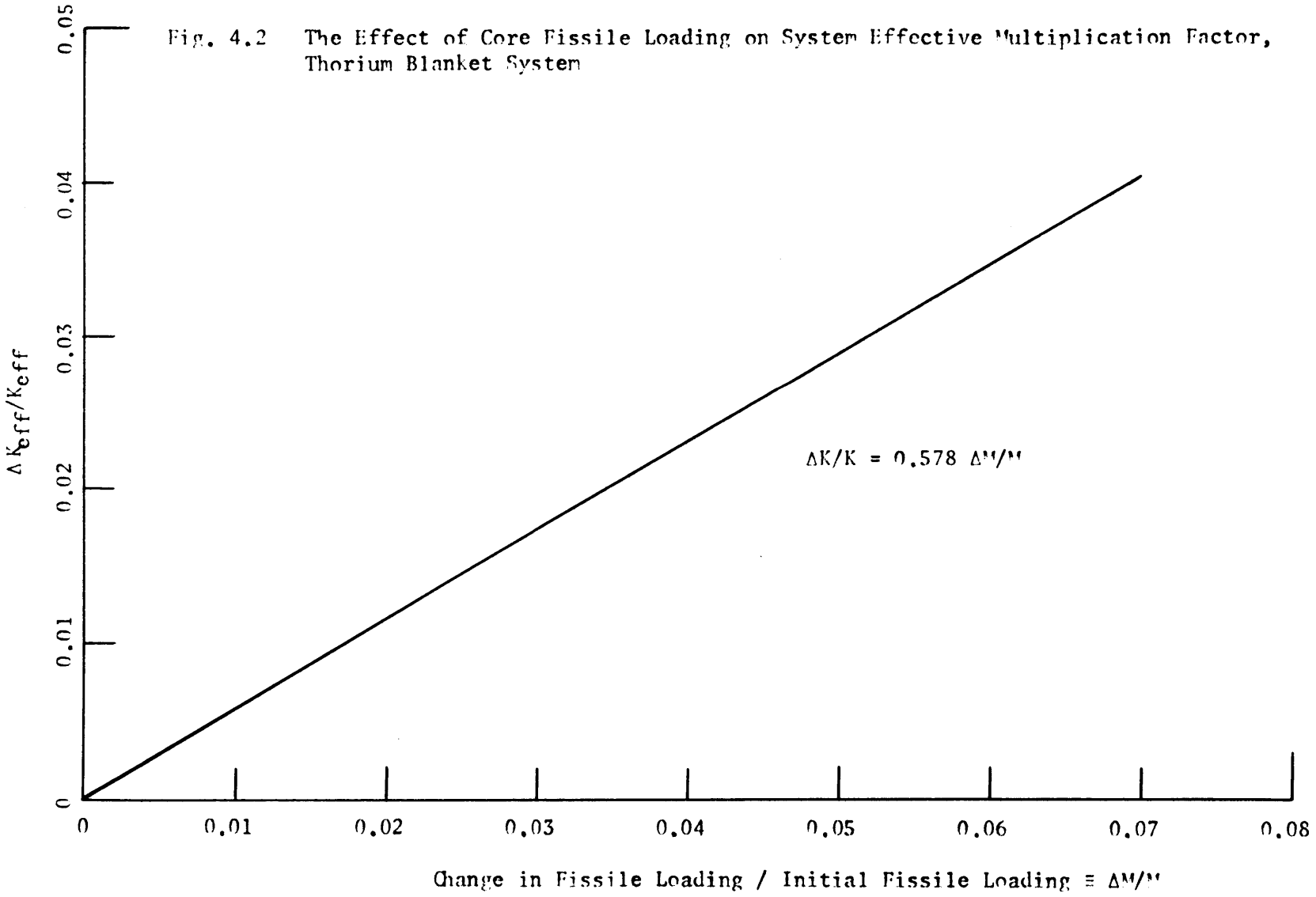

Fig. 4.2 The Effect of Core Fissile Loading on System Effective Multiplication Factor, Thorium Blanket System

4.2.2 Effect of Poison Concentration on k_{eff}

The other parameter which must be specified so that the burnup may be performed as outlined in section 2.5.2 is the poison concentration in the core and axial blanket. To allow this quantity to be specified, it was necessary to evaluate the effect of boron-10 concentration on system effective multiplication factor, k_{eff}. This was again achieved using 2DB to perform several snapshot physics calculations in which the B-10 concentration in the core was varied. In all cases, the ratio of the B-10 number density in the core to the number density in the axial blanket was 1.0:2.3 as specified in section 2.5.2.3. Figures 4.3 and 4.4 show the effect of core poison concentration on system k_{eff}. The next section will show how these curves were used to evaluate the core B-10 concentration for the burnup analysis.

4.2.3 Initial Core and Blanket Loadings

The purpose of this section is to show how the relationships presented in the previous two sections were used in selecting the core and blanket isotope concentrations at the beginning-of-life. The first information necessary to specify the fissile material and control poison loadings was data on the behavior of the system effective multiplication factor with burnup. To obtain this information, initial estimates of the required core inventory and poison concentrations were made, and the two systems (uranium and thorium blankets) were burned up for a full core cycle of 600 full power days. Figures 4.5 and 4.6 show the effect of irradiation on system k_{eff}. Two features are apparent from these curves: first, the fissile enrichment required (as defined in sec. 2.5.2)

Fig. 4.3 The Effect of Core Poison Concentration on K_{eff}
U-238 Blanket System

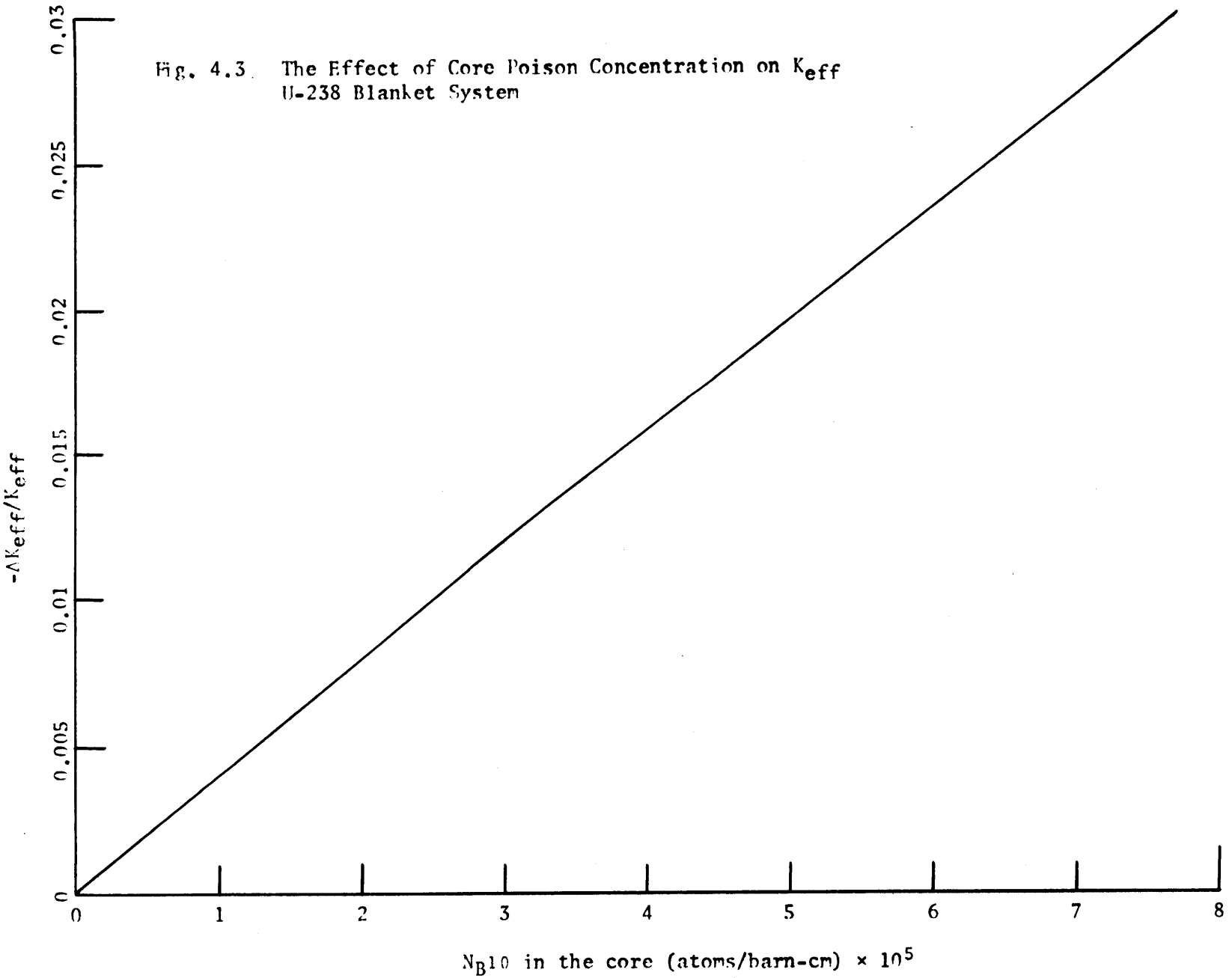

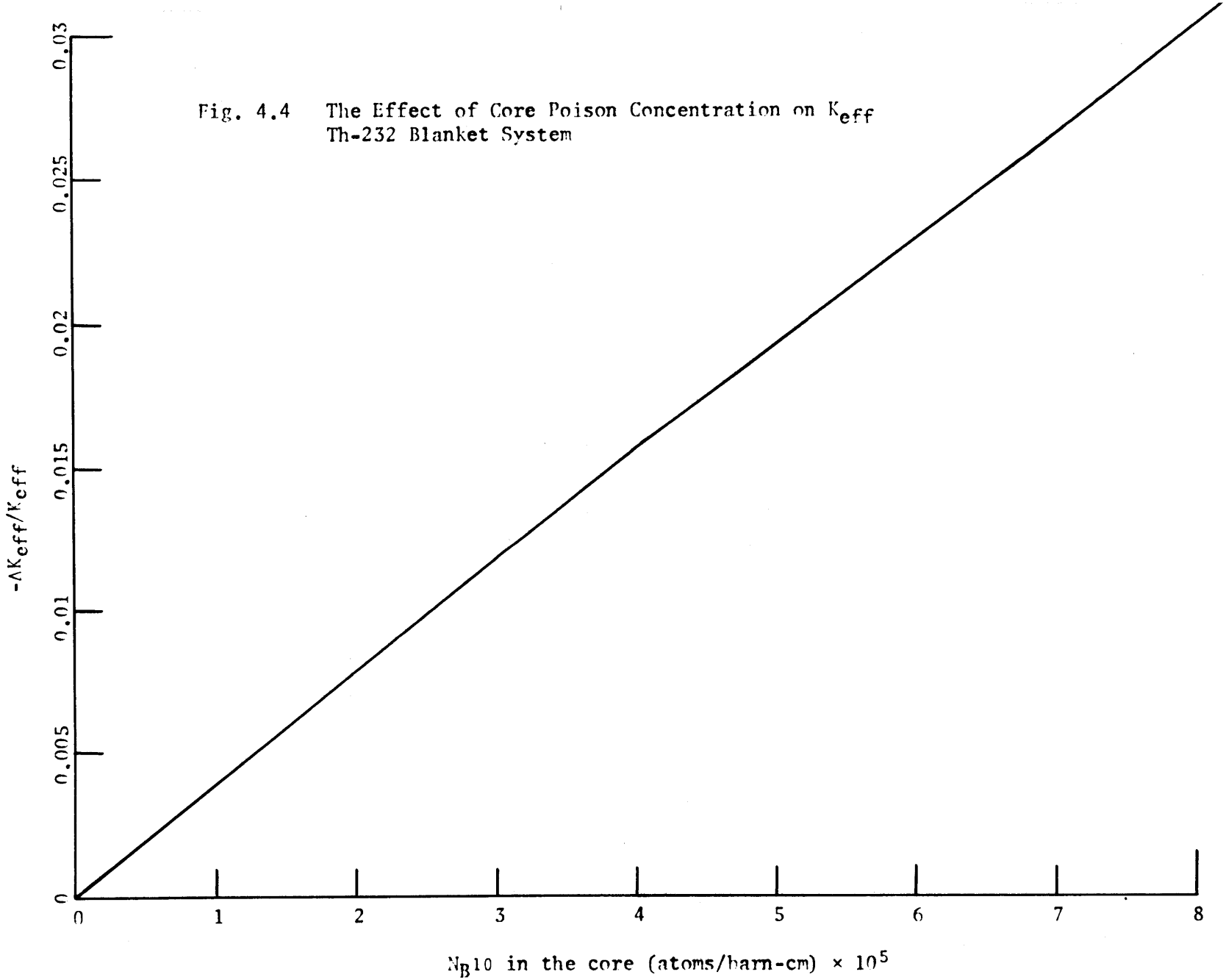

Fig. 4.4 The Effect of Core Poison Concentration on K_{eff} Th-232 Blanket System

Fig. 4.5 The Effect of Irradiation on System Effective Multiplication Factor, Uranium Blanket System

N_{B10} = 5.0×10^{-5} atoms/barn-cm in the core

Fissile Enrichment: Core Zone I = 12.27%
Core Zone II = 18.97%

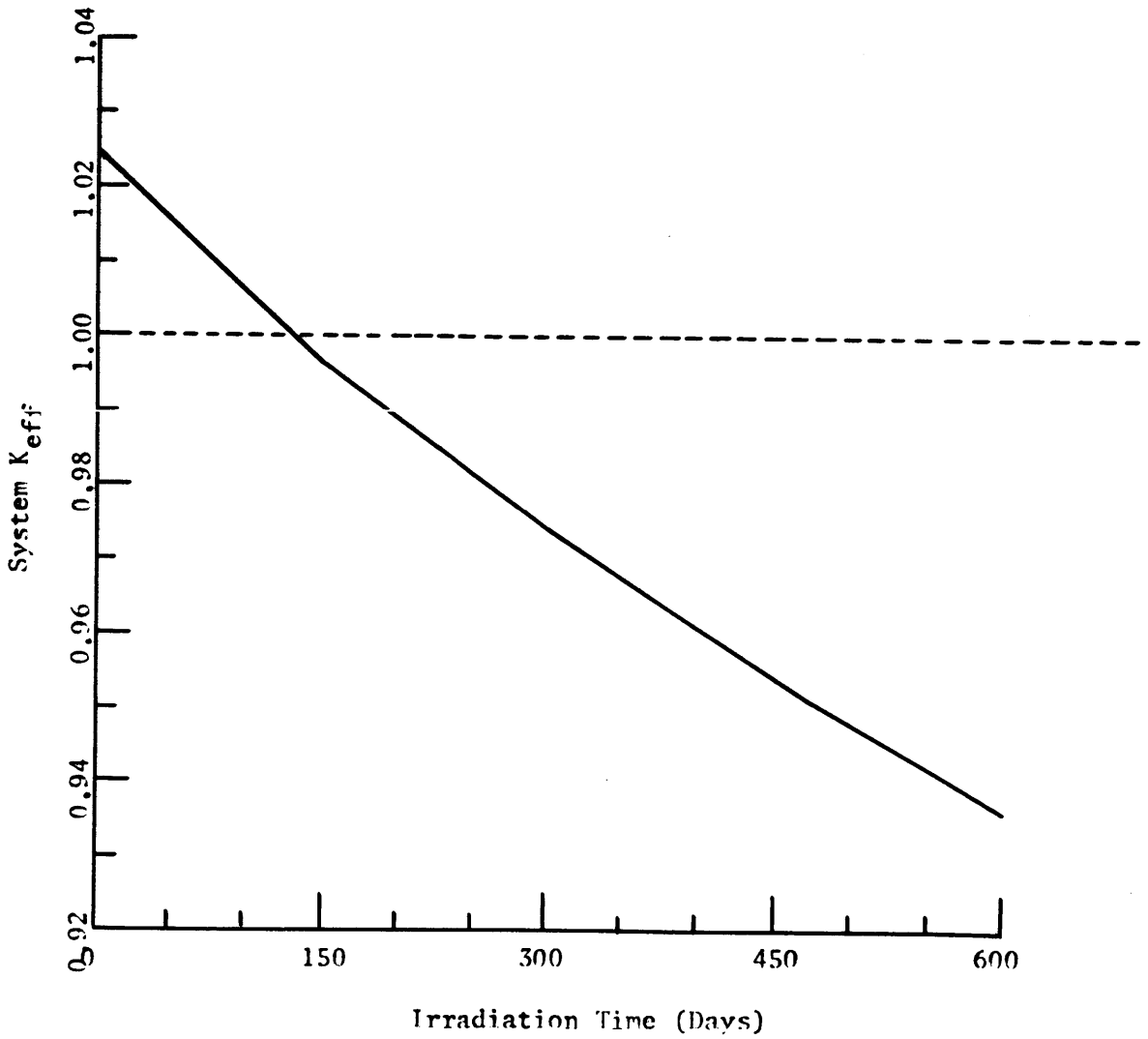

Fig. 4.6 The Effect of Irradiation on System Effective Multiplication Factor, Thorium Blanket System

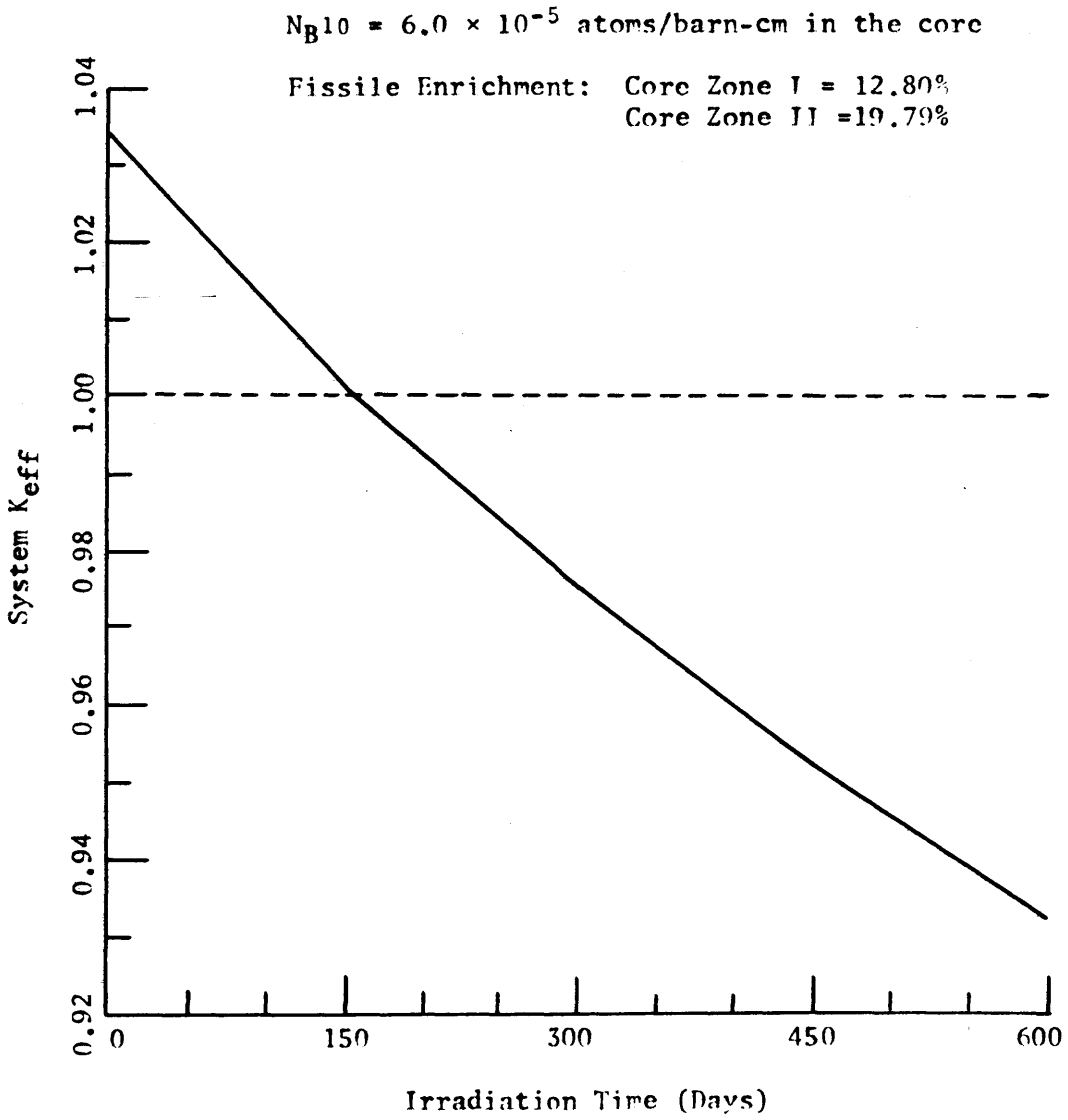

was underestimated in both cases; second, the plot of system k_{eff} vs. irradiation time is not exactly a straight line.

The procedure used in selecting core enrichment and poison concentration was to provide sufficient enrichment to allow the unpoisoned system k_{eff} to pass through 1.0 after 450 days of irradiation, and to provide sufficient poison concentration to reduce the initial system k_{eff} by the Δk associated with the first 150 days of irradiation. The results of using these guidelines to select fissile and poison concentrations from Figs. 4.1 through 4.4 are shown in Table 4.4 for a uranium blanketed system and in Table 4.5 for a thorium blanketed system.

TABLE 4.4 Beginning of Life Fissile and Poison Concentrations, Uranium Blanketed System

Blanket Type	Isotope	Isotope Number Densities (atoms/barn-cm)		
		Core Zone I	Core Zone II	Axial Blanket
Uranium	Pu-239	0.0007296	0.001127	0.0
Uranium	Pu-240	0.0003162	0.0004886	0.0
Uranium	Pu-241	0.00006833	0.0001056	0.0
Uranium	Pu-242	0.000044	0.00006801	0.0
Uranium	U-238	0.005074	0.004444	0.006963
Uranium	U-235	0.00001017	0.00000890	0.00001395
Uranium	Oxygen	0.01248	0.01248	0.01395
Uranium	B-10	0.000067	0.000067	0.000154

TABLE 4.5 Beginning of Life Fissile and Poison Concentrations, Thorium Blanketed System

Blanket Type	Isotope	Isotope Number Density (atoms/barn-cm)		
		Core Zone I	Core Zone II	Axial Blanket
Thorium	Pu-239	0.0007591	0.001173	0.0
Thorium	Pu-240	0.0003290	0.0005084	0.0
Thorium	Pu-241	0.00007109	0.0001099	0.0
Thorium	Pu-242	0.00004578	0.00007076	0.0
Thorium	U-238	0.005027	0.004372	0.0
Thorium	U-235	0.00001007	0.00000876	0.0
Thorium	Th-232	0.0	0.0	0.006509
Thorium	Oxygen	0.01248	0.01248	0.01302
Thorium	B-10	0.000084	0.000084	0.000193

The required enrichments for the two systems are shown in Table 4.6. As shown, the required fissile enrichment for a system with a thorium blanket is approximately a factor of 1.04 greater than for a system with a uranium blanket. This difference in required core fissile inventory can be attributed to two effects. The first is the difference in beginning-of-life fission rate between a uranium and a thorium

TABLE 4.6 Required Core Fissile Enrichments

Blanket Type	Fissile Enrichment (%)	
	Core Zone I	Core Zone II
Uranium	12.78	19.75
Thorium	13.30	20.55

blanket, and the second is the difference in blanket reflective properties. Both of these effects will be evaluated in the next section.

4.2.4 One-Group Albedo Analysis

4.2.4.1 Introduction

The purpose of this section is to evaluate the effect of fission rate and blanket reflective properties on system k_{eff}. The motivation for this is to shed light on why the thorium blanketed system requires a higher core fissile loading than the uranium blanketed system. Both of these effects can be characterized by using a simple one-group albedo analysis of the blankets. This section will be divided into three parts. First, an expression will be developed to show the effect of blanket albedo on system k_{eff}; second, the relative reflective properties of a number of possible blanket compositions will be compared; and third, an evaluation of the effect of blanket fission rate on system k_{eff} will be made. In all this work, the one-group core spectrum collapsed cross sections presented by Driscoll (D6) will be used. The fact that the spectrum in the blanket is softer than that in the core has been ignored. Hence the results presented here are to be interpreted only in a relative sense.

The albedo evaluation has been performed here both including and excluding the effect of fissions in the blanket on effective albedo. This distinction has been made to allow separation of the effects of blanket reflective properties and fission contributions to the effective albedo. The separation of the two effects is justified because fission neutrons have a different spectrum than reflected neutrons, and have a higher worth in the core. Thus, when the fission contribution to effective

albedo is included by defining the denominator in the diffusion length equation as $[\Sigma_a - \nu\Sigma_f]$ rather than simply as Σ_a, two counterbalancing effects occur. First, the fission contribution is underestimated because of the high worth of fission neutrons, and, second, the fission contribution is overestimated because the blanket spectral softening tends to increase Σ_a while decreasing $\nu\Sigma_f$ at greater distances from the core interface. Thus, qualitatively, the one-group albedo analysis presented here is adequate if both Th and U have similar fission spectra and similar fission cross section spectral dependence. This is not a bad first order assumption.

4.2.4.2 Effect of Albedo on k_{eff}

To show the effect of blanket albedo on system effective multiplication factor, consider first the geometric buckling of a spherical reactor. This buckling can be written as

$$B^2 = [\pi/R+S]^2 \qquad (4.1)$$

where R is the radius of the spherical core,

S is the reflector savings.

To allow the reflector savings to be related to the blanket albedo coefficient, assume that the blanket region can be approximated as a slab reflector. The expression for the albedo of a slab reflector can be written as (G2):

$$\beta = \frac{1 - (2D_R/L_R) \coth (a/L_R)}{1 + (2D_R/L_R) \coth (a/L_R)} \qquad (4.2)$$

where β is the blanket albedo,

D_R is diffusion coefficient in the reflector,

L_R is the diffusion length in the reflector,

a is the reflector thickness.

Next the reflector savings can be expressed as (G3):

$$S = (D_C/D_R)L_R \tanh (a/L_R) \tag{4.3}$$

where D_C is the diffusion coefficient in the core.

Manipulating Eq. 4.3 and combining the results with Eq. 4.2 gives:

$$\beta = \frac{1 - 2D_C/S}{1 + 2D_C/S} \tag{4.4}$$

Rearranging Eq. 4.4 yields an expression for the reflector savings which can be substituted into Eq. 4.1 for the buckling. This results in the following expression:

$$B^2 = \left[\frac{(1-\beta)\pi}{R(1-\beta)+2D_C(1+\beta)}\right]^2 \tag{4.5}$$

The effective multiplication factor for the system of interest must now be written:

$$k_{eff} = \frac{\nu\Sigma_f}{\Sigma_a + D_C B^2} \tag{4.6}$$

Substitution of Eq. 4.5 into Eq. 4.6 produces the expression of interest:

$$k_{eff} = \frac{\nu\Sigma_f}{\Sigma_a + D_C\left[\frac{(1-\beta)\pi}{R(1-\beta)+2D_C(1+\beta)}\right]^2} \tag{4.7}$$

If a one-zone spherical reactor with the same core volume, enrichment, and material volume fractions as the one-zone cylindrical reactor of Brewer (Ref. B3, Fig. 4.2) is selected, the following set of parameters can be calculated using the one-group cross section set (D6):

$$\nu\Sigma_f = 0.005899 \text{ cm}^{-1}$$
$$\Sigma_a = 0.004552 \text{ cm}^{-1}$$
$$D_C = 1.7167 \text{ cm}$$
$$R = 105.43 \text{ cm.}$$

For a typical radial blanket albedo of 0.7, the effective multiplication factor is calculated to be 1.0462. Using Eq. 4.7, one can evaluate k_{eff} for a number of β's. By taking differences between closely spaced pairs of k_{eff} and β values, a graphical relationship can be developed between changes in the reflector albedo (β) and corresponding changes in the system effective multiplication factor (k_{eff}). Figure 4.7 shows this relationship. As shown, for a typical blanket albedo coefficient 0.7, approximately a 6% change in β is required to produce a 1% change in k_{eff}. As the albedo increases, the effective multiplication factor becomes more sensitive to changes in β.

4.2.4.3 Blanket Reflective Properties

The objective of this section is to show the effect of changes in core reflector material on the reflector albedo. Equation 4.2 together with the one-group set of fast reactor cross sections was used to evaluate the albedo for a number of core reflectors. In this analysis, the reflector diffusion length (L_R) was defined as

$$L_R^2 = D_R/\Sigma_a .$$

Fig. 4.7 The Effect of Reflector (Blanket) Albedo Coefficient (β) on the System Effective Multiplication Factor (K_{eff})

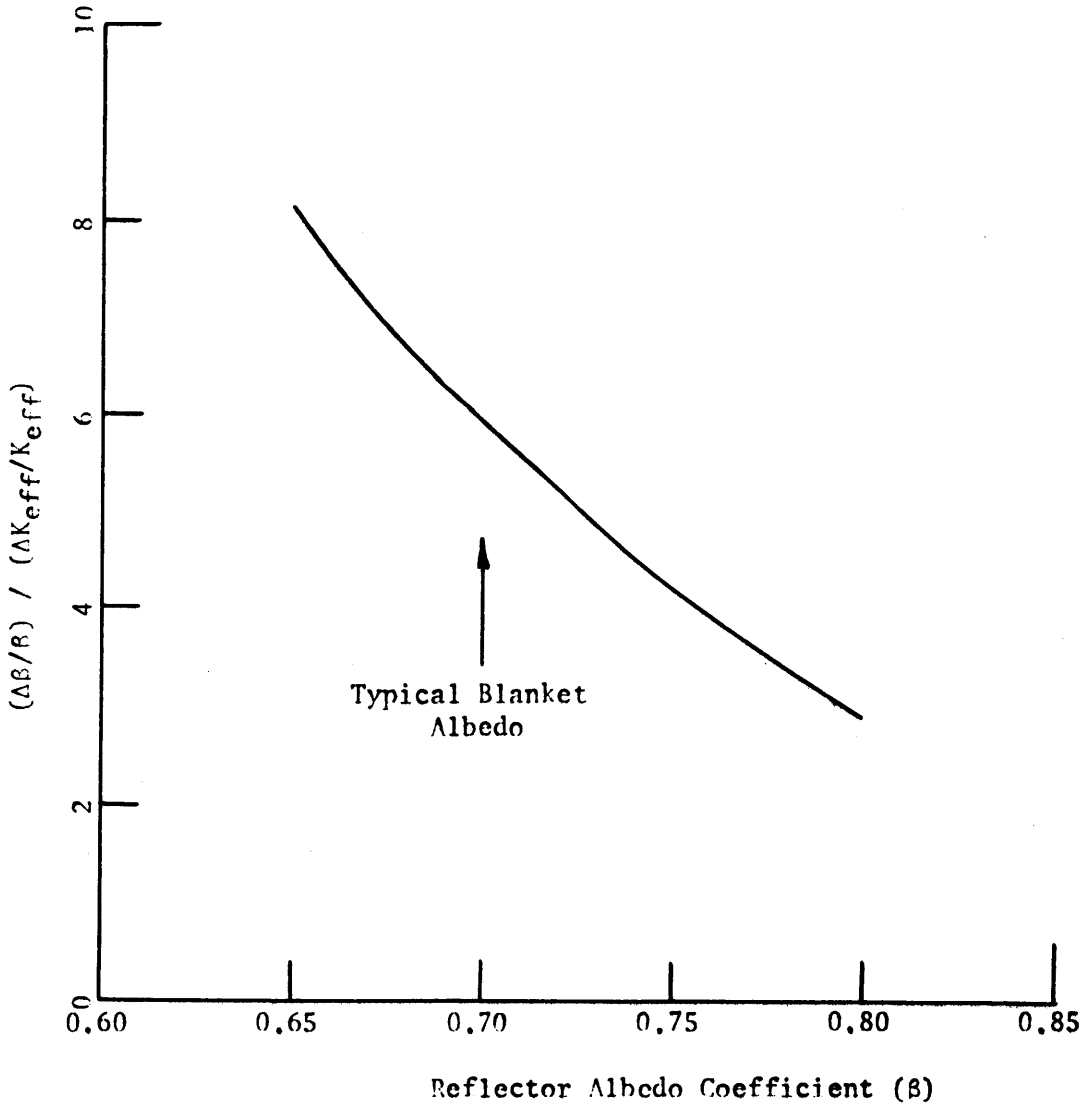

This definition neglects the contribution of blanket fissions to the effective albedo. This effect will be evaluated in the next section.

Table 4.7 lists the albedo coefficient for a number of core reflectors of thickness 45 cm. As shown, BeO or beryllium pins are the most effective reflectors of the materials listed. Because the radial blanket contributes a significant economic benefit to the performance of an LMFBR, most designers are using blankets composed of fertile material rather than core reflectors. The albedo coefficients of typical U-238 and Th-232 radial blankets are shown to be much lower than other non-breeding reflectors. Also shown in the table is the fact that the thorium radial blanket is somewhat less effective as a core reflector than a uranium radial blanket. If, however, the thorium oxide in the radial blanket were diluted with 50% zirconium oxide, the modified thorium blanket would be a better core reflector than the unmodified uranium blanket. Because dilution of the thorium blanket would significantly reduce the fissile breeding capability of the blanket, the use of blanket diluents was ruled out.

4.2.4.4 Blanket Reflective Performance

In an attempt to explain the observed 4% increase in core critical loading required when a thorium blanket is substituted for a uranium blanket, both blanket reflective and fission characteristics will be considered here. To allow an estimate of the effect of beginning-of-life fission rate in the blanket on required core fissile loading, the diffusion length (L_R) was redefined as

$$L_R^2 = D_R/(\Sigma_a - \nu\Sigma_f) .$$

TABLE 4.7 Comparison of Albedo Coefficients for Various Core Reflectors

Reflector Material	One-Group Albedo (β) for a Thickness of 45 cm
Clad BeO pins	0.891
Clad beryllium pins	0.882
Clad ZO_2 pins	0.869
Clad VO pins	0.867
Clad NiO pins	0.864
Clad graphite pins	0.862
80% stainless steel, 20% sodium	0.860
Clad TiO pins	0.859
80% vanadium, 20% sodium	0.851
80% inconel, 20% sodium	0.849
80% zirconium, 20% sodium	0.848
80% nickel, 20% sodium	0.845
80% titanium, 20% sodium	0.815
U-238 blanket (50% ZrO_2)	0.783
Th-232 blanket (50% ZrO_2)	0.770
U-238 blanket (radial)	0.722
Th-232 blanket (radial)	0.700
Sodium	0.691

With the diffusion length defined in this manner, it is possible to calculate a blanket albedo which takes into account the effect of relative fission rate in the two blankets. Table 4.8 lists the blanket albedo coefficients calculated with and without the fission rate correction.

TABLE 4.8 Radial Blanket Albedo Comparison

	One-Group Albedo (β)	
Blanket Type	Initial	Fission Rate Corrected
U-238 Radial	0.722	0.764
Th-232 Radial	0.700	0.705

As shown, the fission rate correction factor increases the effective albedo of the uranium blanket relative to that of the thorium blanket. This would be expected because of the factor of five differences between the fission cross sections of U-238 and Th-232.

By using the relationships developed in section 4.2.1 between core fissile loading and system k_{eff} together with the information in Fig. 4.7 and in Table 4.8, it is possible to estimate the difference in the required critical loading for the uranium and thorium blanket systems. It will be assumed here that the differences between the uranium and thorium radial blankets have the same effect on required core fissile loading as the differences between uranium and thorium axial blankets. It will also be assumed that the only factors necessitating a larger core fissile loading for a thorium blanket system than for a uranium blanket system are blanket reflective properties and blanket fission rate differences. (This is not strictly true since the two systems burn up

differently.) Under these assumptions, the thorium blanket system would be expected to require a 4.2% larger core fissile loading than a similar uranium blanket system. This is in good agreement with the 4.0% difference determined using the detailed procedures described in section 4.2.3. The slight overprediction of the relative core inventories can be justified in light of the fact that the one-group fission cross sections used in this analysis were collapsed over a typical core spectrum. Because the blanket spectrum is softer than that in the core, and because both uranium and thorium fissions are high energy threshold events, it would be expected that the fission rate correction to the albedo coefficient would be smaller than predicted in this analysis. Also, the capture cross section would be expected to be larger for the same reason. Thus the actual difference in albedo coefficients between the two blanket systems would be smaller, and the extra core enrichment required for the thorium blanket system would be smaller than the 4.2% predicted above. The assumption that the effective albedos of the axial and radial blankets contribute equally to differences in core fissile loadings is also a potential source of error.

4.3 EVALUATION OF CORE MANAGEMENT

In an attempt to evaluate the effect of core management on blanket performance, a series of preliminary burnup cases were analyzed using 2DB. These analyses were performed on a standard Pu/U core with thorium radial and axial blankets. The comparisons presented in this section are between two cases in which the core was managed differently. In the first case (here referred to as the batch case) the core, axial,and radial blankets were burned up together for 600 full power days.

In the second case (here referred to as the managed case) the core, axial, and radial blankets were all loaded together and irradiated for 300 full power days. After 300 days of irradiation, the core was replaced while the axial and radial blanket irradiation was continued. This system was then irradiated for 300 additional full power days. The initial core enrichments and poison concentrations are specified in Table 4.9.

TABLE 4.9 Initial Fissile Enrichments and Poison Concentrations for the Trial Core Management

Core Management	Fissile Enrichment		Initial B-10 Concentration	
	Core Zone I	Core Zone II	Core	Axial Blanket
Batch	12.30	19.00	4.0×10^{-5}	9.2×10^{-5}
Managed	12.30	19.00	4.0×10^{-5}	9.2×10^{-5}

These burnup cases are different from those to be discussed later in this chapter in that the B-10 poison was allowed to be depleted here whereas the poison concentration was kept constant in later cases.

Figure 4.8 shows the system k_{eff} as a function of full power days of irradiation for the two cases. As shown, a significant difference exists between the two cases. If core management has a measurable effect on blanket performance, then it should be exaggerated in this comparison. Figure 4.9 shows the total radial and axial blanket fissile inventories for the batch irradiation case. To emphasize the differences in fissile inventory in the blankets for the two cases being compared, Fig. 4.10 shows the percent difference in inventories as functions

Fig. 4.8 The Effect of Core Management Scheme on K_{eff}

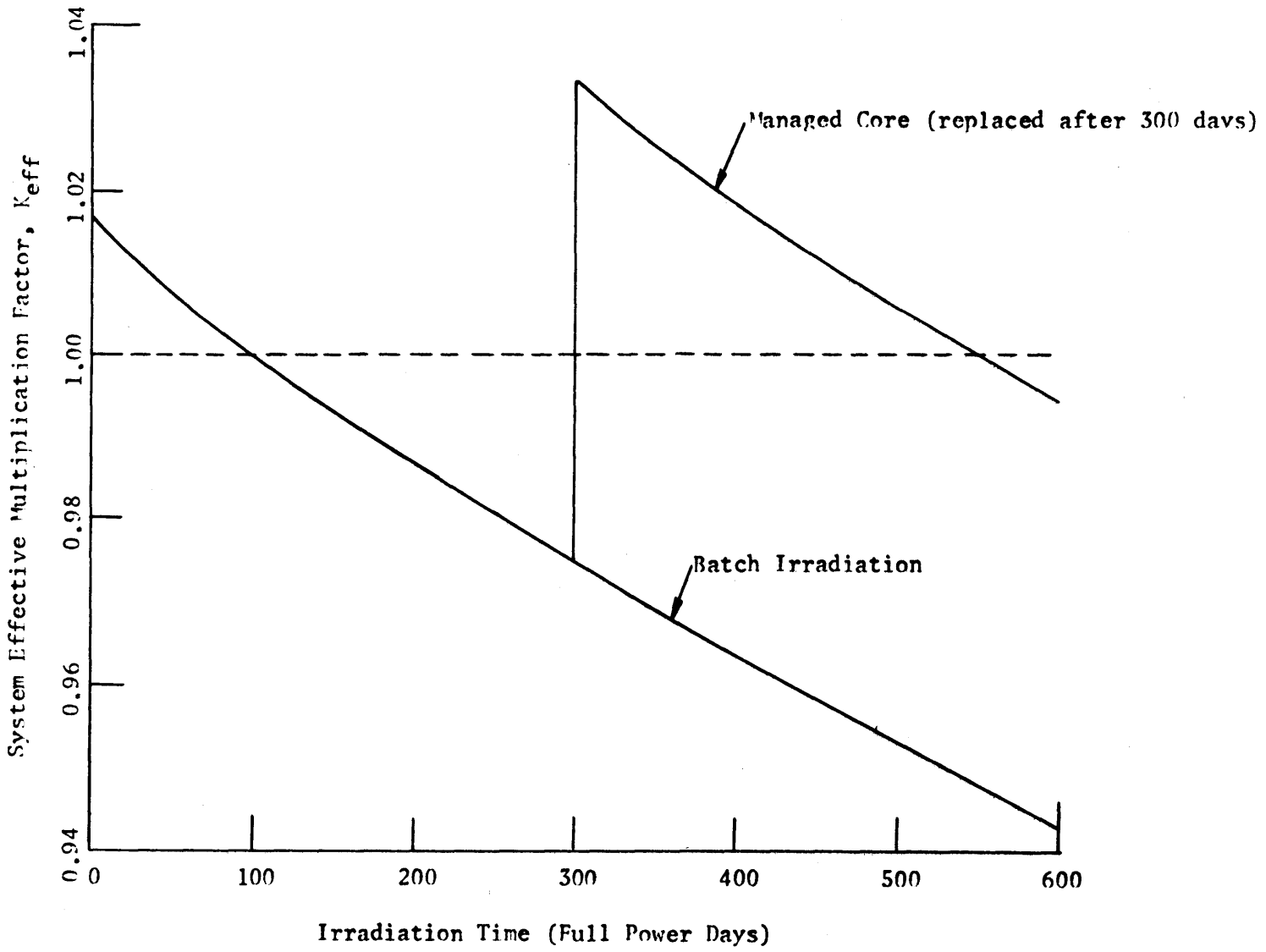

Fig. 4.9 Radial and Axial Blanket Fissile Inventories for a Batch Managed Core

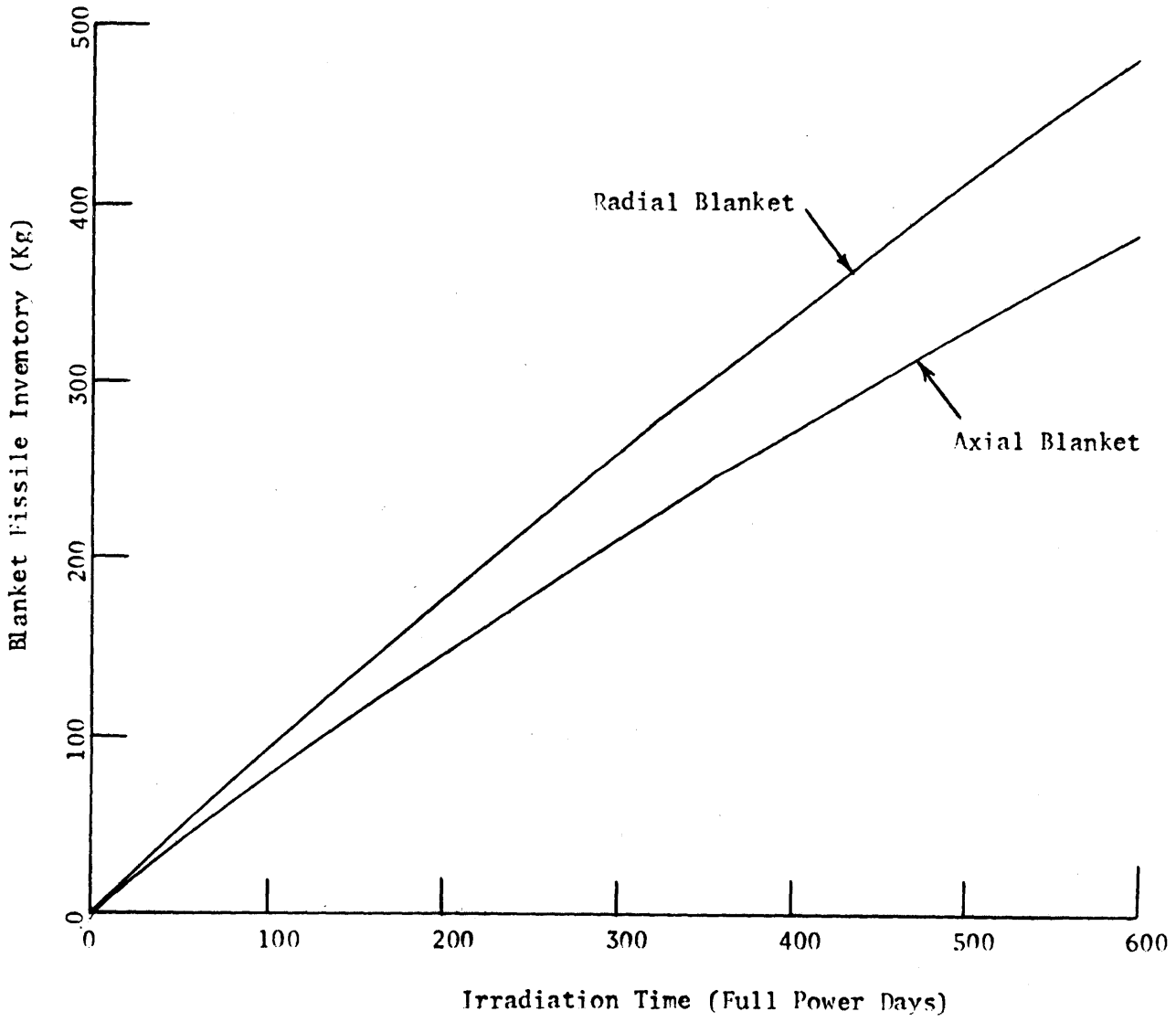

Fig. 4.10 The Effect of Core Management Scheme on Blanket Fissile Inventories

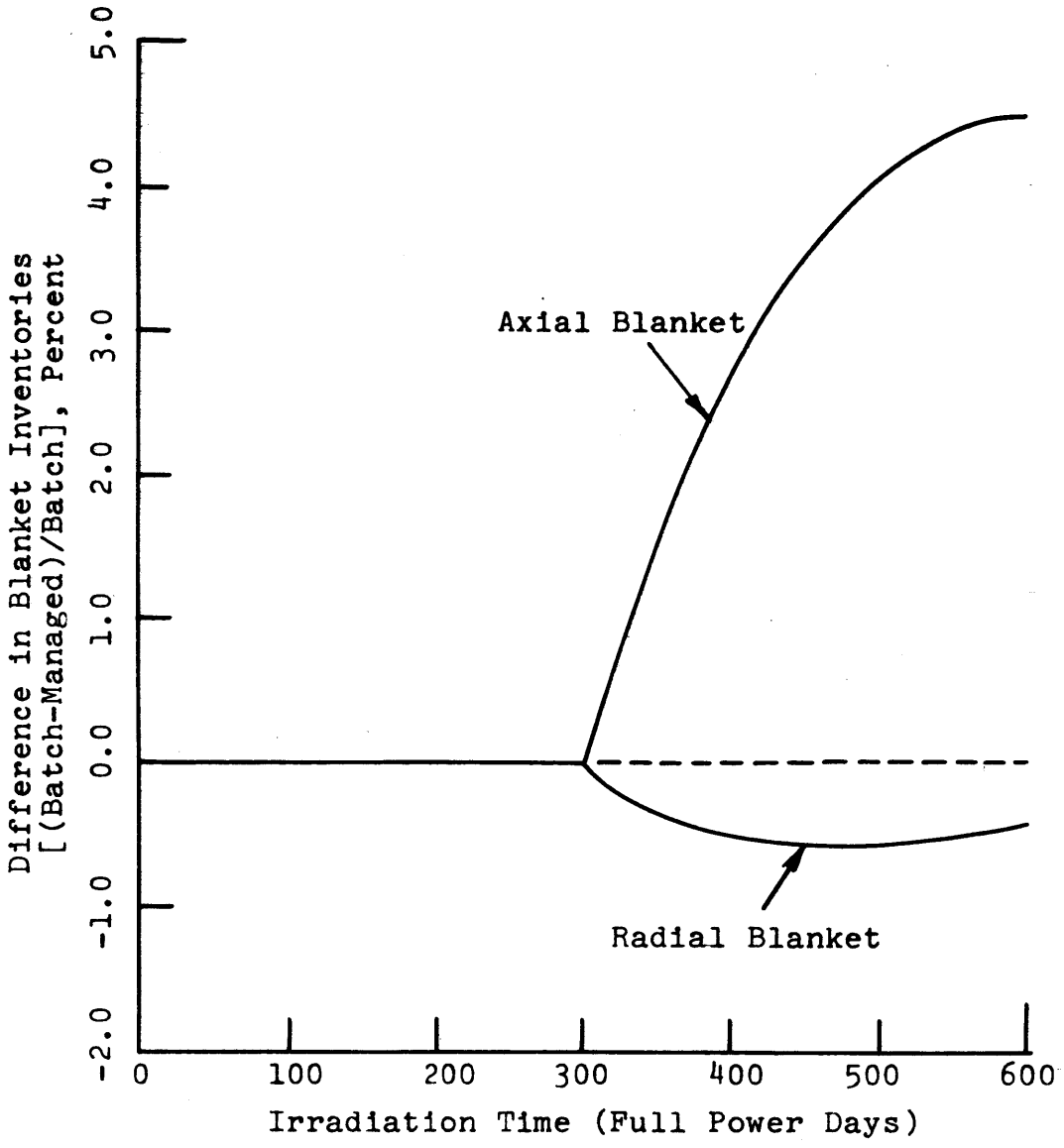

of irradiation time for the radial and axial blankets. As shown, the difference in the radial blanket inventories between the two cases is quite small (less than 0.6%). The percentage difference peaks at approximately 450 days and then decreases toward zero. On the other hand, the differences between the two cases in the axial blanket are quite pronounced, approaching 4.5% after 600 days. It should be noted that in the burnup analysis reported in the remainder of this chapter, the core and axial blanket are assumed to be replaced simultaneously as would be done in an operating reactor. Thus the blanket fissile inventories have been shown to be insensitive to core management schemes, and the axial blanket fissile inventories, although somewhat more sensitive, are unlikely to be affected strongly by core management schemes because the core and axial blanket are necessarily managed together. The effect of management scheme on blanket economic performance is the subject of section 5.3.2, where it will be shown that the effect of various batch core reload times on blanket economic performance is small.

4.4 BLANKET BATCH BURNUP

4.4.1 Introduction

After the beginning-of-life (BOL) core enrichments and poison concentrations had been defined, it was possible to perform consistent burnup analyses on the two systems (uranium and thorium blankets) of interest. As discussed earlier, the core and axial blanket management scheme consisted of performing a batch irradiation until the core average burnup limit (approximately 105,000 MWD/MTM, or 600 full

power days) was reached, then replacing the entire core and axial blanket with assemblies characteristic of BOL conditions. Three different blanket management schemes were used. In the first scheme, referred to here as batch irradiation or burnup, the radial blanket was simply batch-irradiated through several core and axial blanket replacement cycles. The results obtained from this mode of operation will be discussed in this section. In the second scheme, referred to here as zone scatter management, the radial blanket was batch-irradiated until the radial blanket row 1 reached its economic optimum. At this time, to be defined in Chapter 5, the row 1 radial blanket was replaced by unirradiated blanket material and the batch irradiation was continued. The results obtained using this scheme will be discussed in section 4.5.

The third scheme considered was in-out shuffle management. In this scheme new radial blanket assemblies were loaded in row 1 nearest the core and moved outward to the adjacent row in successive refueling intervals. Fully irradiated assemblies were then removed from row 3 for reprocessing.

4.4.2 Comparison of Blankets

4.4.2.1 System k_{eff}

The method used to define the core enrichments and poison concentrations has been discussed earlier (see sec. 2.5.2). The objective of defining these concentrations consistently was to allow intercomparison between the uranium and thorium blanket systems. As evidence of the consistency of the burnup method, consider Fig. 4.11. In this figure the system effective multiplication factors for both uranium and thorium

Fig. 4.11 The Effect of Burnup Time on System K_{eff}
(Refueling every 600 days)

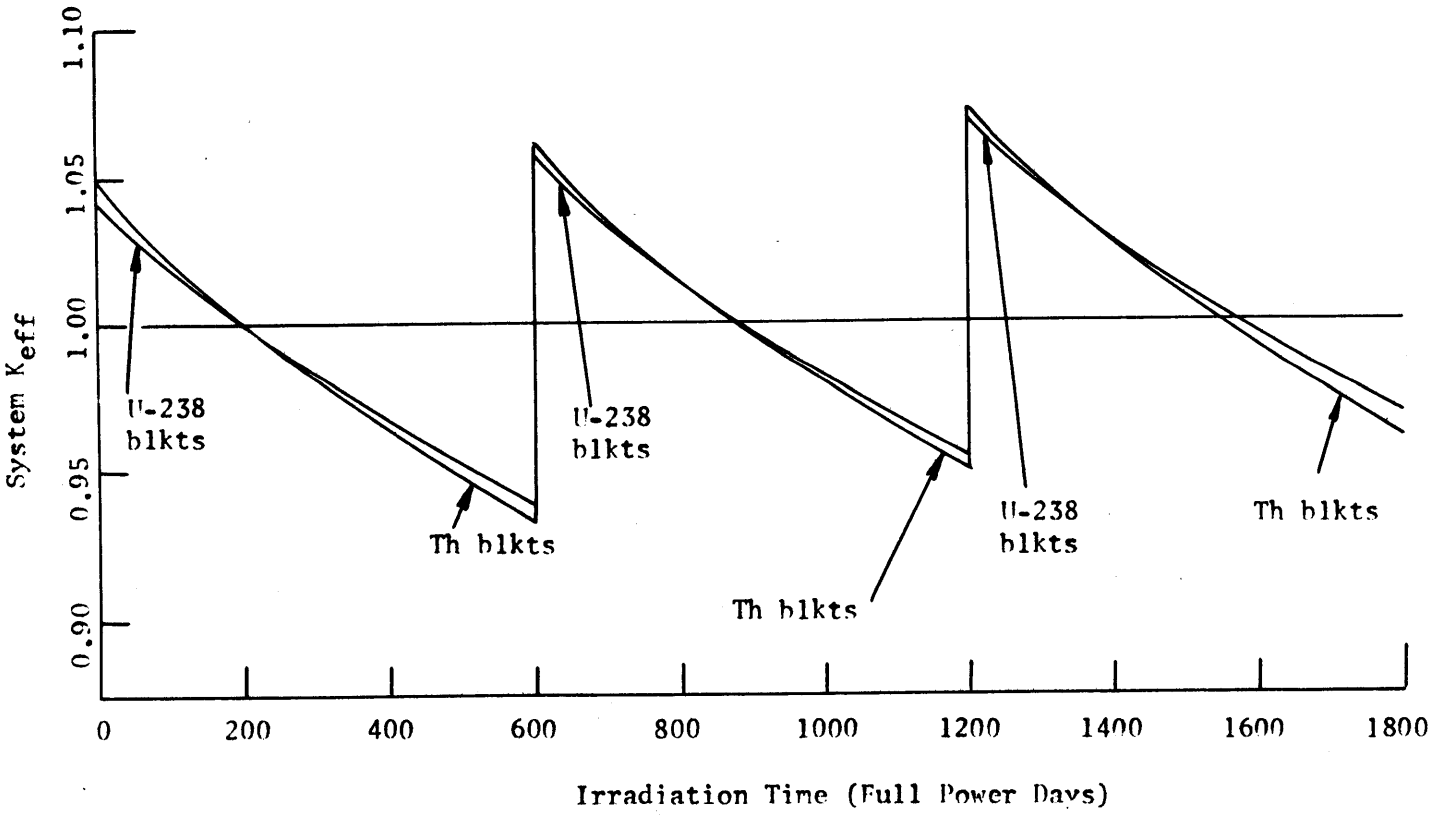

blanket systems have been plotted as functions of irradiation time. As shown, the two systems were burned up in as nearly consistent as possible a manner. With this prelude, consideration can now be given to blanket breeding characteristics.

4.4.2.2 Breeding Performance

As a measure of the breeding performance of the blankets, consider the fissile inventory produced. Figures 4.12 and 4.13 show this quantity for uranium and thorium radial blankets. As shown, the total fissile inventory produced in the radial blanket decreases markedly as the distance from the core interface increases. The three rows of radial blanket referred to in these figures are annular regions of radial width 15 cm. Another interesting feature to observe is that the inventory curves for row 1 are concave downward while those for row 2 are nearly linear, and those for row 3 are slightly concave upward. These differences in shape can be attributed to changes in blanket cross sections as the flux hardens and to variations in the blanket flux. These variations will be discussed in more detail in section 4.4.3, but it should be mentioned here that the qualitative shape of the inventory curves for all three rows would be the same if the semi-analytic depletion model proposed by Brewer were used to predict the blanket inventory changes.

Figures 4.14 and 4.15 show comparisons of radial blanket row 1 performance for the uranium and thorium blankets. As shown, when fissile inventory is plotted against irradiation time, the performance of the uranium radial blanket row 1 is superior to that of the same region in the thorium radial blanket. However, when blanket enrichment is plotted as the ordinate of the curves (Fig. 4.15), the thorium blanket

Fig. 4.12 Uranium Radial Blanket Fissile Inventories, Batch Irradiation

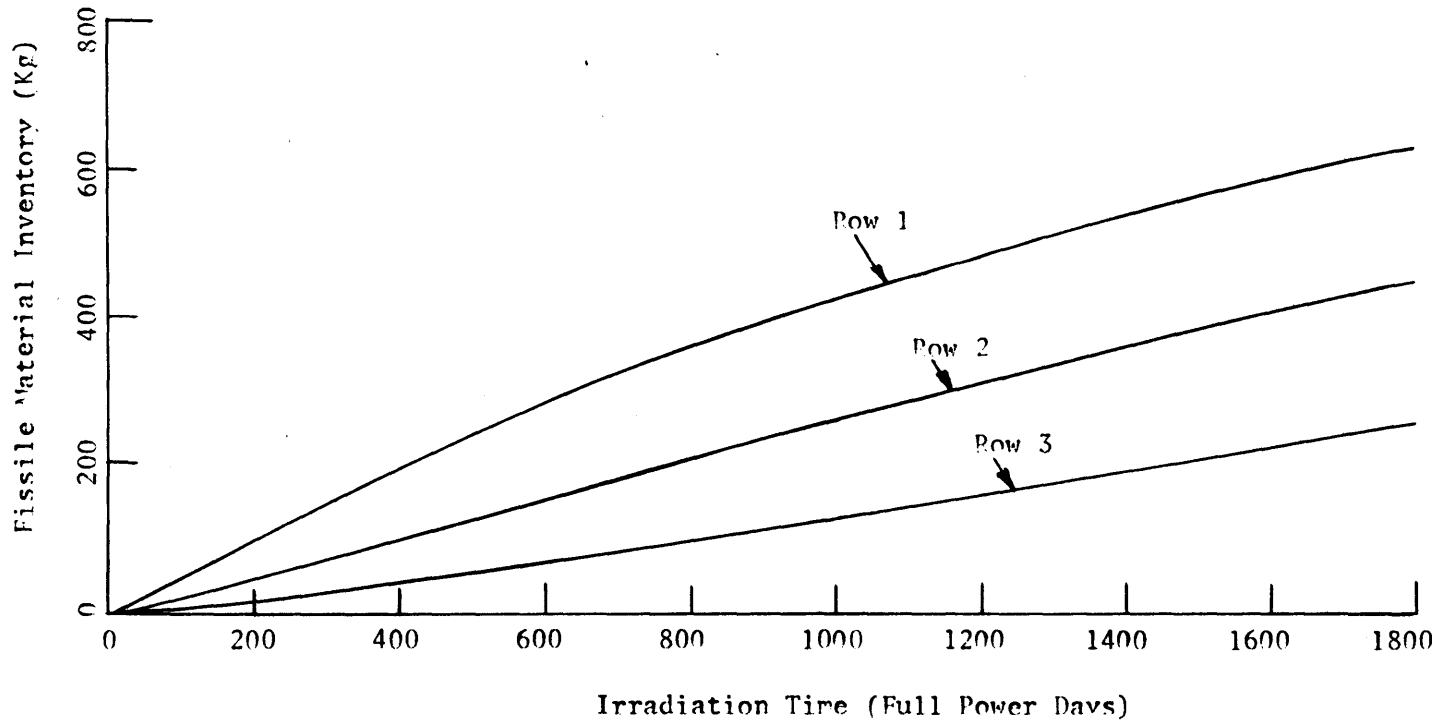

Fig. 4.13 Thorium Radial Blanket Fissile Inventories, Batch Irradiation

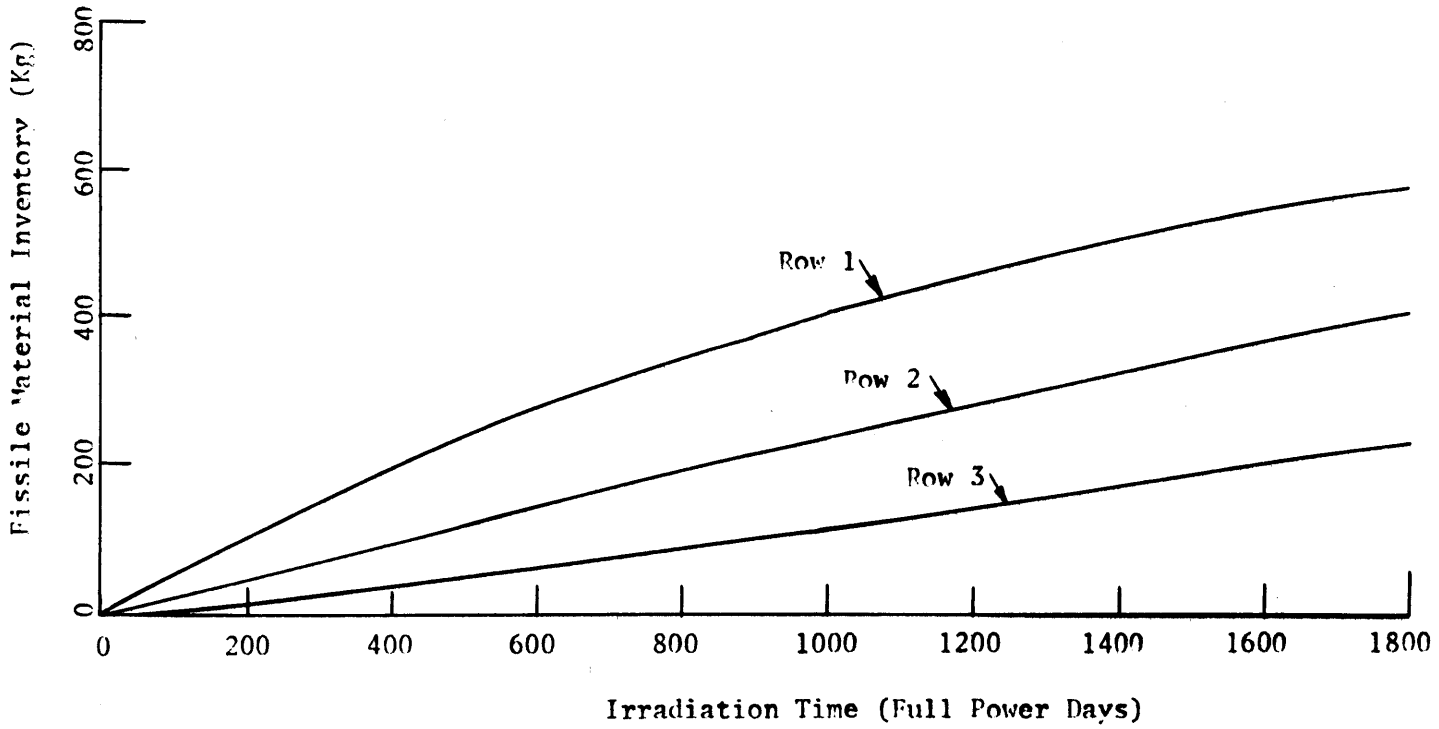

Fig. 4.14 Comparison of the Breeding Performance (Inventory) of Row 1 Radial Blanket under Batch Irradiation Conditions

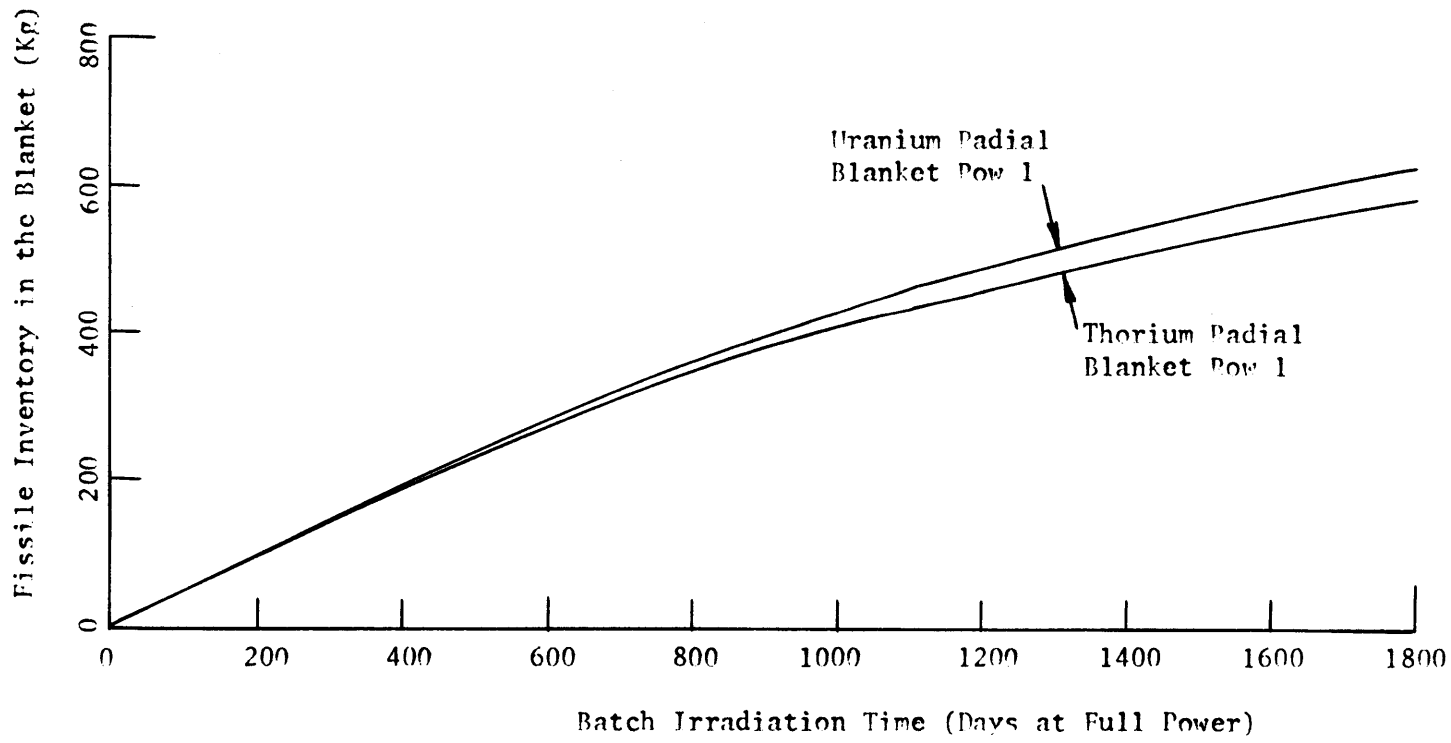

Fig. 4.15 Comparison of the Breeding Performance of Row 1 Radial Blanket Under Batch Irradiation Conditions

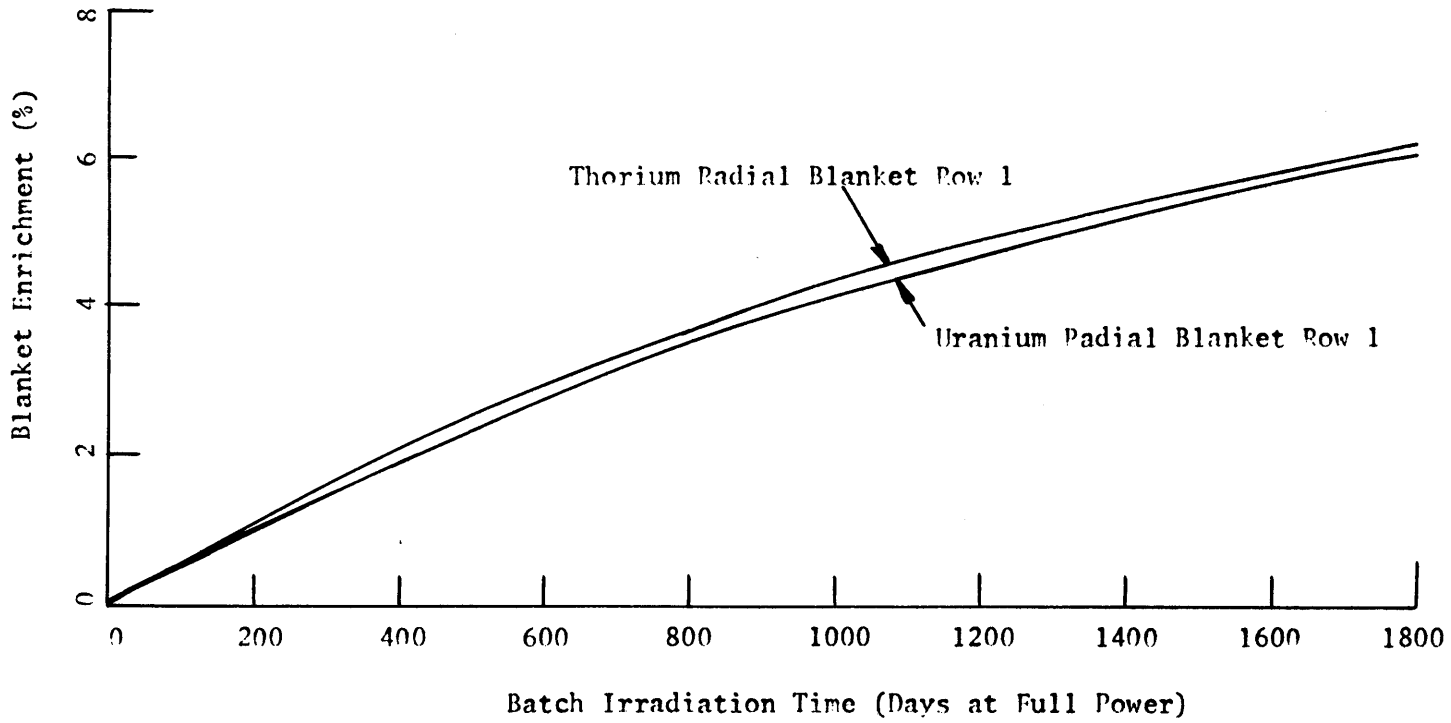

performance is shown to be superior. This apparent anomaly is a result of a combination of two factors. First, the density of pure thorium dioxide is less than that of pure uranium dioxide (10.01 g/cc for ThO_2 vs. 10.97 g/cc for UO_2). This fact means that for the same constraints on fuel volume fraction and allowable percentage of theoretical density, less thorium can be loaded into the blanket. The second factor is that over most of the neutron energy range, the capture cross section of thorium is larger than that of uranium. Table 4.10 shows a comparison of thorium and uranium resonance self-shielded cross sections. This table shows that at all neutron energies above about 21 keV the capture cross section of thorium is larger than that of uranium.

Next consider the relative performance of thorium and uranium axial blankets. Figures 4.16 and 4.17 show fissile inventories in the entire radial and axial blankets for uranium and thorium blankets, respectively. As shown, in both cases the axial blanket produces only about 70% as much fissile material as the radial blanket. In actual fact, however, on a pound fissile per pound fertile material basis, more fissile material is produced in the axial blankets than in the radial blankets. This is true because the axial blankets have only about 30% as much fertile material as the radial blanket. It should be noted here that neither the axial height nor the number of rows of radial blanket has been optimized. This topic is treated in more detail by Spitzer and O'Dell (S2).

A comparison showing the relative breeding performance of uranium and thorium axial blankets is presented in Figs. 4.18 and 4.19. These figures show that the breeding performance of a thorium axial blanket is slightly superior to that of a uranium axial blanket. This is true whether

TABLE 4.10 Comparison of Radial Blanket Region Resonance Self-Shielded Capture Cross Sections (from 1DX, (H2)).

Group	Upper Energy (eV)	σ_c (barns) Th-232	σ_c (barns) U-238	Th-232/U-238
1	10.5×10^6	0.01	0.00	–
2	6.5×10^6	0.02	0.01	2.00
3	4.0×10^6	0.04	0.02	2.00
4	2.5×10^6	0.08	0.06	1.33
5	1.4×10^6	0.14	0.13	1.08
6	0.8×10^6	0.17	0.13	1.31
7	0.4×10^6	0.19	0.14	1.36
8	0.2×10^6	0.27	0.17	1.59
9	0.1×10^6	0.42	0.26	1.62
10	46.5×10^3	0.5537	0.4919	1.13
11	21.5×10^3	0.7124	0.7247	0.98
12	10.0×10^3	1.1898	0.7024	1.69
13	4.65×10^3	1.6370	0.9548	1.71
14	2.15×10^3	1.6283	1.0499	1.55
15	1.00×10^3	1.5802	1.2366	1.28
16	465	2.1909	0.9847	2.22
17	215	2.3505	1.4499	1.62
18	100	1.7115	0.9127	1.88
19	46.5	2.8619	2.0707	1.38
20	21.5	0.9136	3.0300	0.30
21	10.0	0.46	8.2362	0.056
22	4.65	0.67	0.54	1.24
23	2.15	0.99	0.47	2.11
24	1.00	1.45	0.58	2.50
25	0.465	2.11	0.90	2.34
26	0.215	7.56	2.71	2.79
	0.0252			

Fig. 4.16 Comparison of Uranium Radial and Axial Blanket Fissile Inventories, Batch Irradiation, Cycle 1

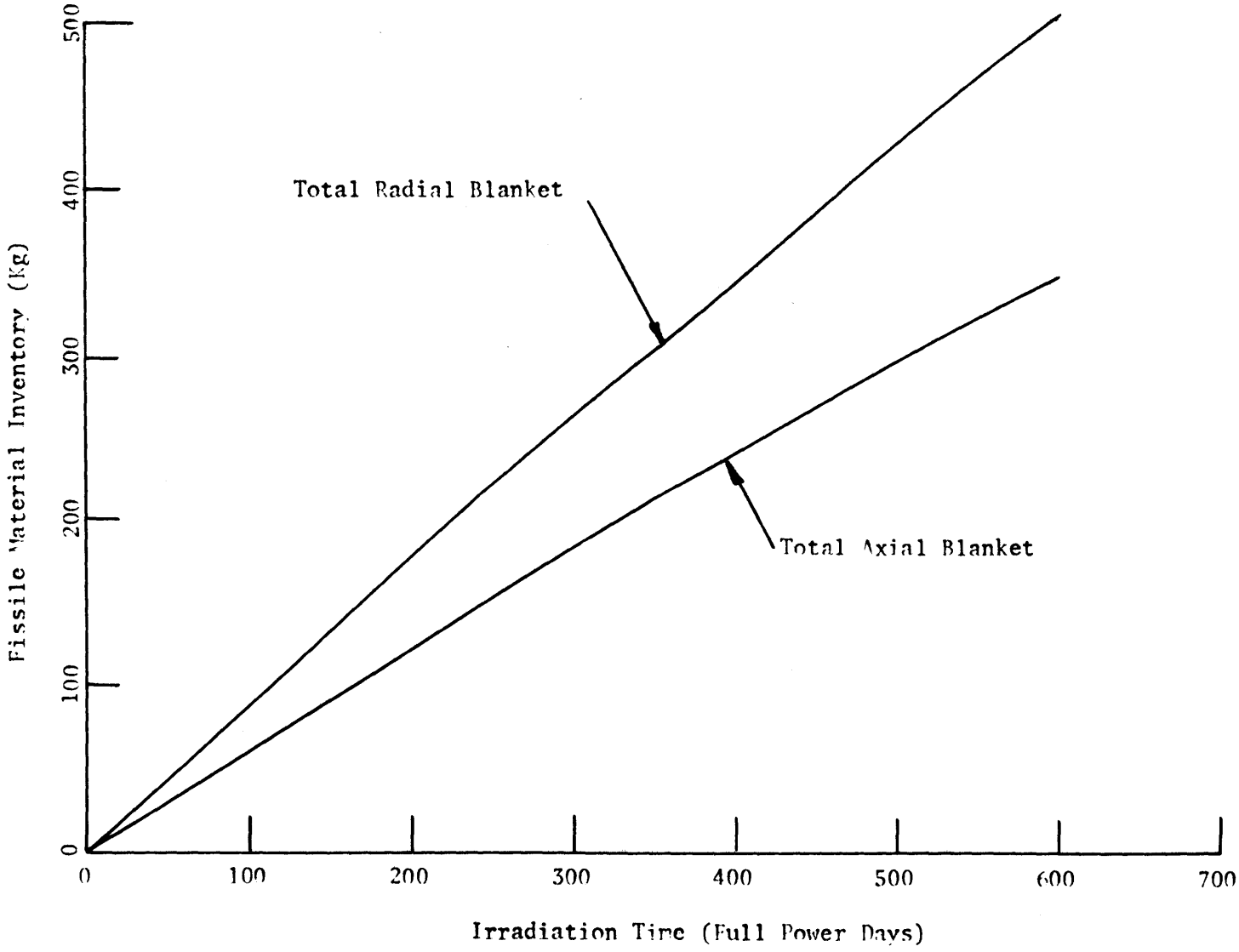

Fig. 4.17 Comparison of Thorium Radial and Axial Blanket Fissile Inventories, Batch Irradiation, Cycle 1

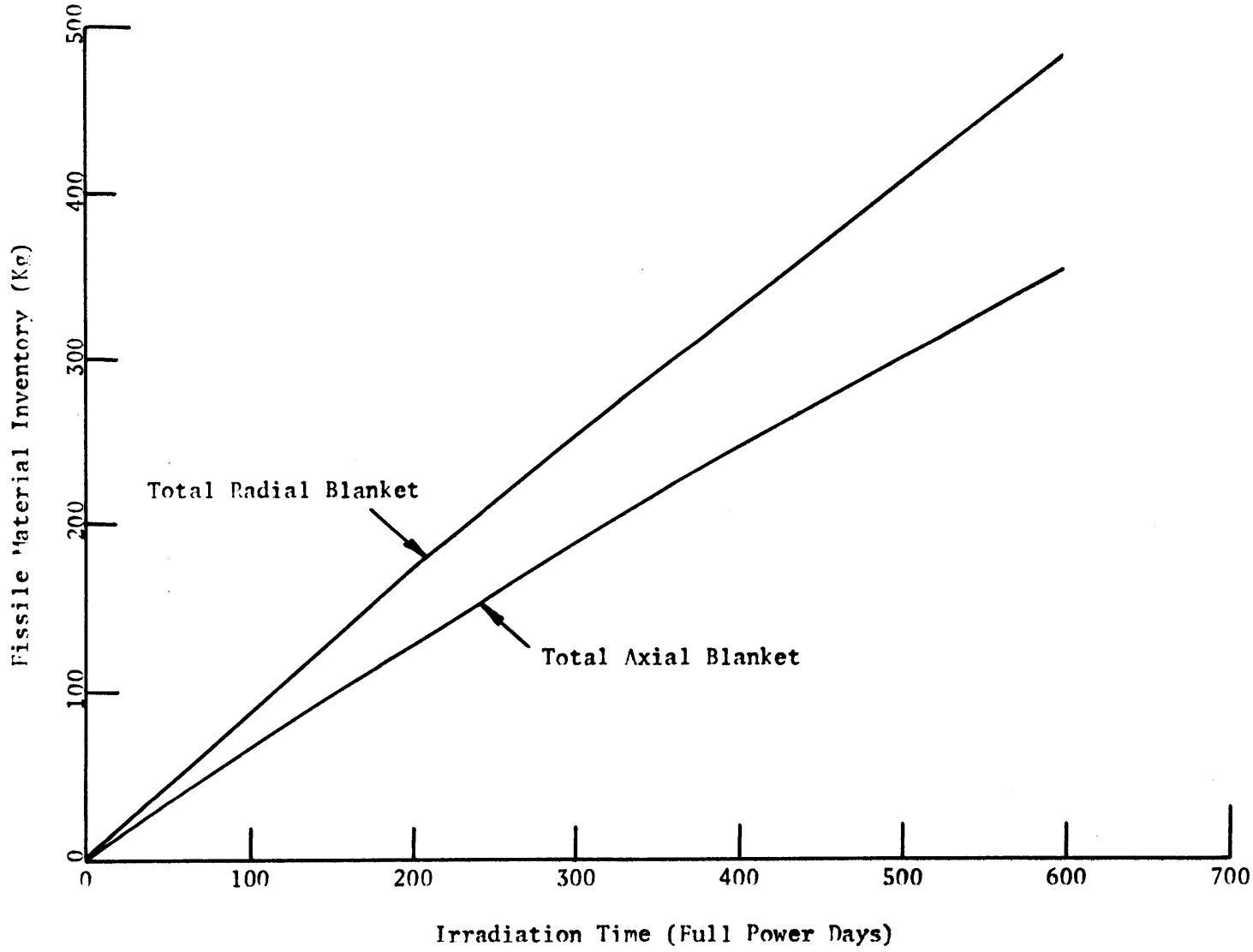

Fig. 4.18 Comparison of Axial Blanket Breeding Performance (Inventory) Under Batch Irradiation Conditions

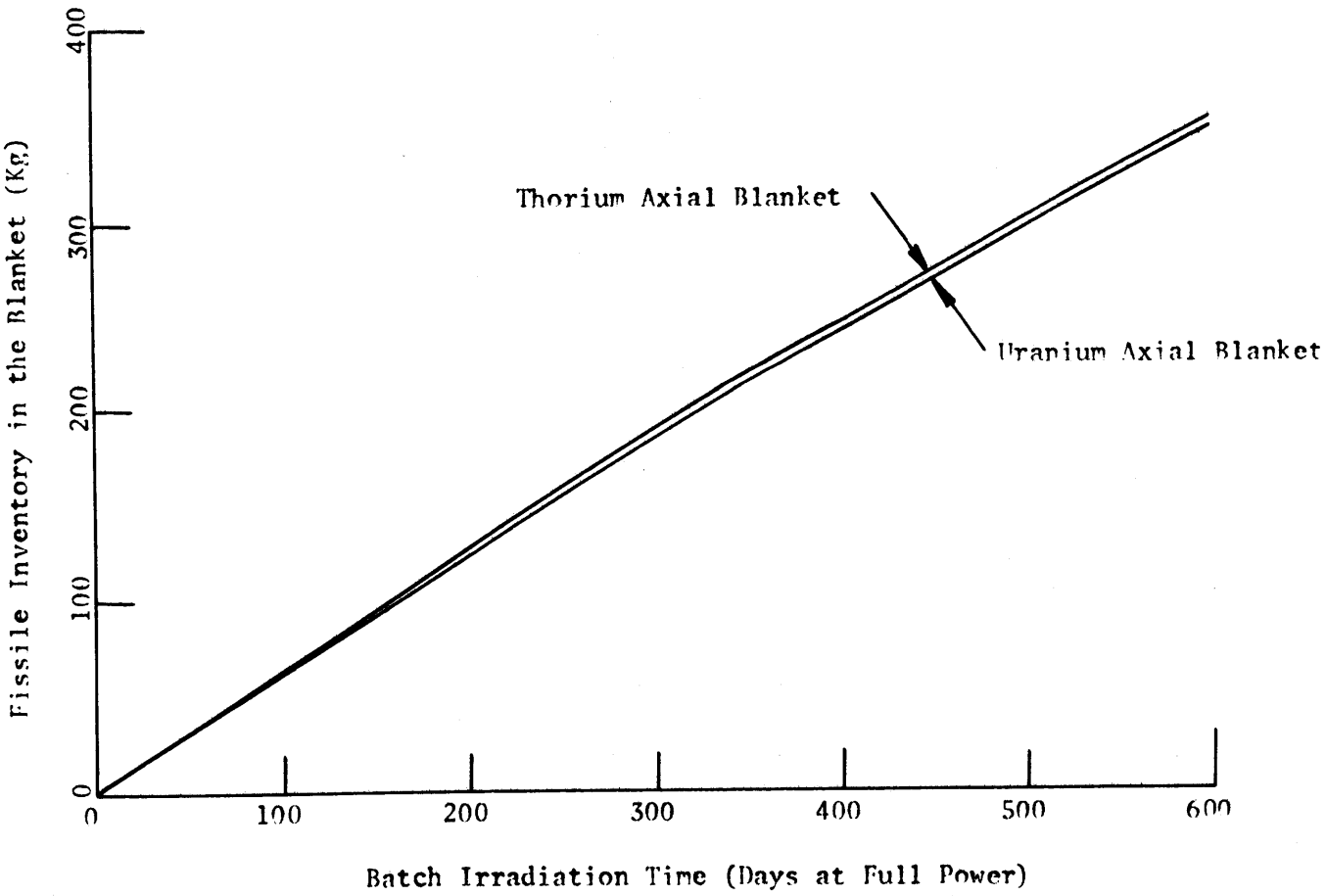

Fig. 4.19 Comparison of Axial Blanket Breeding Performance Under Batch Irradiation Conditions

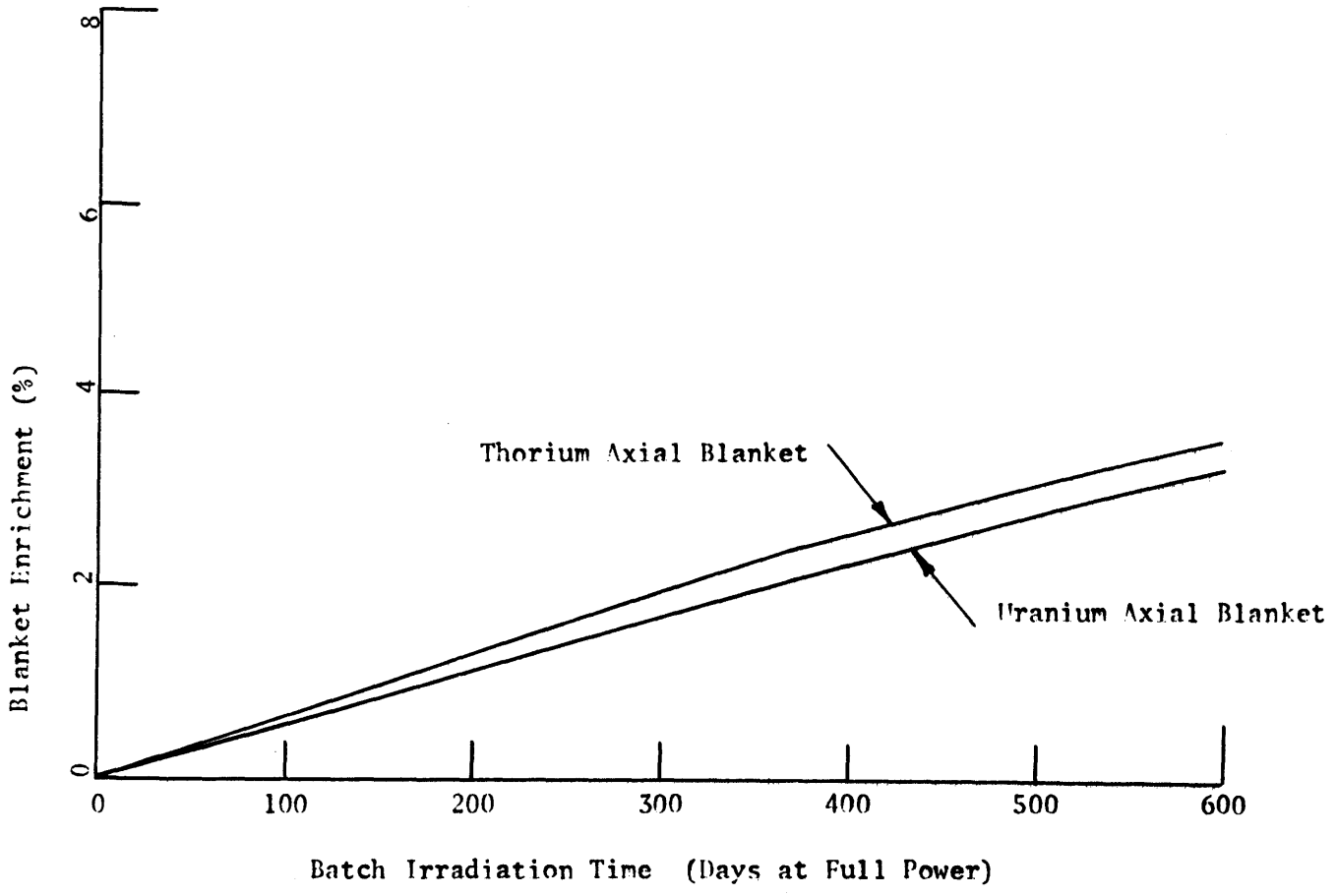

performance is measured in terms of blanket enrichment or in terms of blanket fissile inventory. Table 4.11 shows that again in the axial blanket the thorium capture cross sections are larger than those for uranium over most of the neutron energy range.

Figures 4.20 and 4.21 summarize the relative performance of uranium and thorium blankets under batch irradiation conditions. Figure 4.20 shows that, in general, the performance of a thorium radial blanket relative to that of a uranium blanket degrades both with longer irradiation times, and at distances further from the core interface. Figure 4.21 shows that again the thorium blankets (both radial and axial) perform more poorly relative to uranium blankets as the irradiation time is increased. In addition, this figure shows that thorium outperforms uranium in the axial blanket and underperforms uranium in the radial blanket.

An effect which is approximately the same for the two systems under consideration is the effect of axial blanket poison concentration on breeding performance. To evaluate this effect, two thorium blanketed cases were analyzed using 2DB (L10). The two cases were identical except that in one the average axial blanket B-10 concentration evaluated in section 4.2.3 was used, while in the other no poison was assumed to be in the axial blanket. These studies showed that the assumed poison concentration in the axial blanket reduced the fissile breeding rate in the axial blanket by about 12% while the overall system breeding ratio was reduced by about 3%. Thus the effect of axial blanket poison is significant in determining system breeding capabilities.

TABLE 4.11 Comparison of Axial Blanket Region Resonance Self-Shielded Capture Cross Sections (from 1DX, (H2)).

Group	Upper Energy (eV)	σ_c (barns) Th-232	σ_c (barns) U-238	Th-232/U-238
1	10.5×10^6	0.01	0.00	–
2	6.5×10^6	0.02	0.01	2.00
3	4.0×10^6	0.04	0.02	2.00
4	2.5×10^6	0.08	0.06	1.33
5	1.4×10^6	0.14	0.13	1.08
6	0.8×10^6	0.17	0.13	1.31
7	0.4×10^6	0.19	0.14	1.36
8	0.2×10^6	0.27	0.17	1.59
9	0.1×10^6	0.42	0.26	1.62
10	46.5×10^3	0.5570	0.4941	1.13
11	21.5×10^3	0.7262	0.7351	0.99
12	10.0×10^3	1.2507	0.7264	1.72
13	4.65×10^3	1.8208	1.0583	1.72
14	2.15×10^3	1.9128	1.2244	1.56
15	1.00×10^3	1.9528	1.4380	1.36
16	465	2.6428	1.1845	2.23
17	215	2.8371	1.7257	1.64
18	100	2.0535	1.1000	1.87
19	46.5	3.4419	2.3998	1.43
20	21.5	1.1198	3.6230	0.31
21	10.0	0.46	9.7168	0.047
22	4.65	0.67	0.54	1.24
23	2.15	0.99	0.47	2.11
24	1.00	1.45	0.58	2.50
25	0.465	2.11	0.90	2.34
26	0.215	7.56	2.71	2.79
	0.0252			

Fig. 4.20 Relative Breeding Performance of Uranium and Thorium Radial Blankets, Batch Irradiation

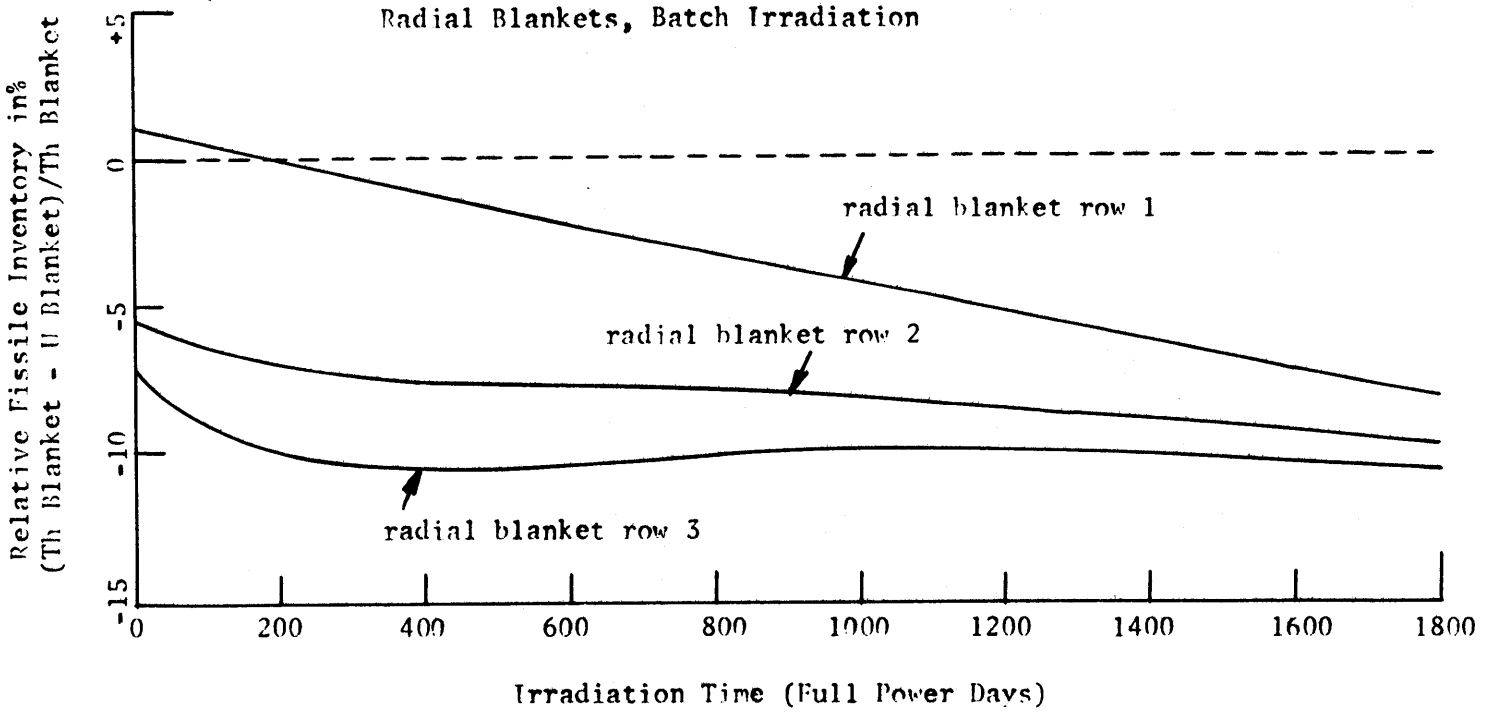

Fig. 4.21 Relative Breeding Performance of Uranium and Thorium Blankets, Batch Irradiation

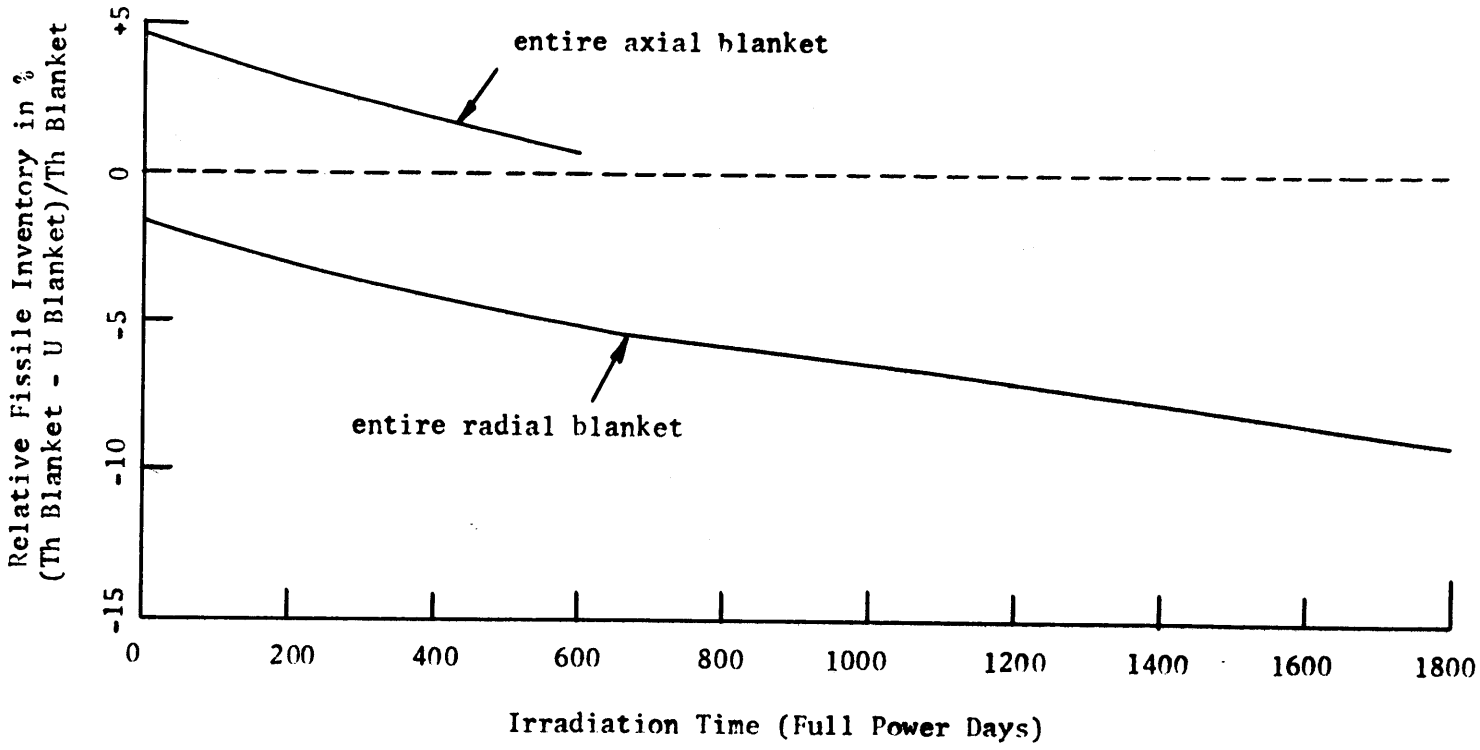

4.4.2.3 U-232 Production

Attention should be given at this point to the production of the contaminant U-232 in the thorium radial and axial blankets. Because both initiating reactions in the production of U-232 are high energy threshold reactions (see sec. 2.5.3.4), the production rate of U-232 would be expected to decrease sharply with increasing distance from the core interface. This would result from the strong spectral softening with increasing distance from the core interface. Figures 4.22 and 4.23 show that the burnup results corroborate the intuitive deduction. Cross comparison of the information presented in these two figures shows that the buildup rate of U-232 (relative to the buildup rate of U-233) in the segment nearest the core interface is nearly the same for the radial and axial blankets. However, at greater distances from the core interface, the relative production rate of U-232 in the radial blanket is greater than that in the axial blanket. In section 5.3 the economic effect of mixing radial blanket rows (having different U-232 concentrations) in the fuel reprocessing step will be evaluated. There it will be shown that a small economic penalty will be incurred if all radial blanket rows are processed together.

4.4.2.4 Core and Blanket Burnup

Another basis on which the two blankets should be compared is burnup. The units of burnup used in this work are megawatt days per metric ton of heavy metal, abbreviated MWD/MTM. Figures 4.24 and 4.25 show the core burnup profiles for the batch blanket irradiation for the uranium and thorium blanketed systems, respectively. As might be expected from the fact that the beginning-of-life thorium blanket fission

Fig. 4.22 U-232 Concentration in the Thorium Radial Blanket, Batch Irradiation

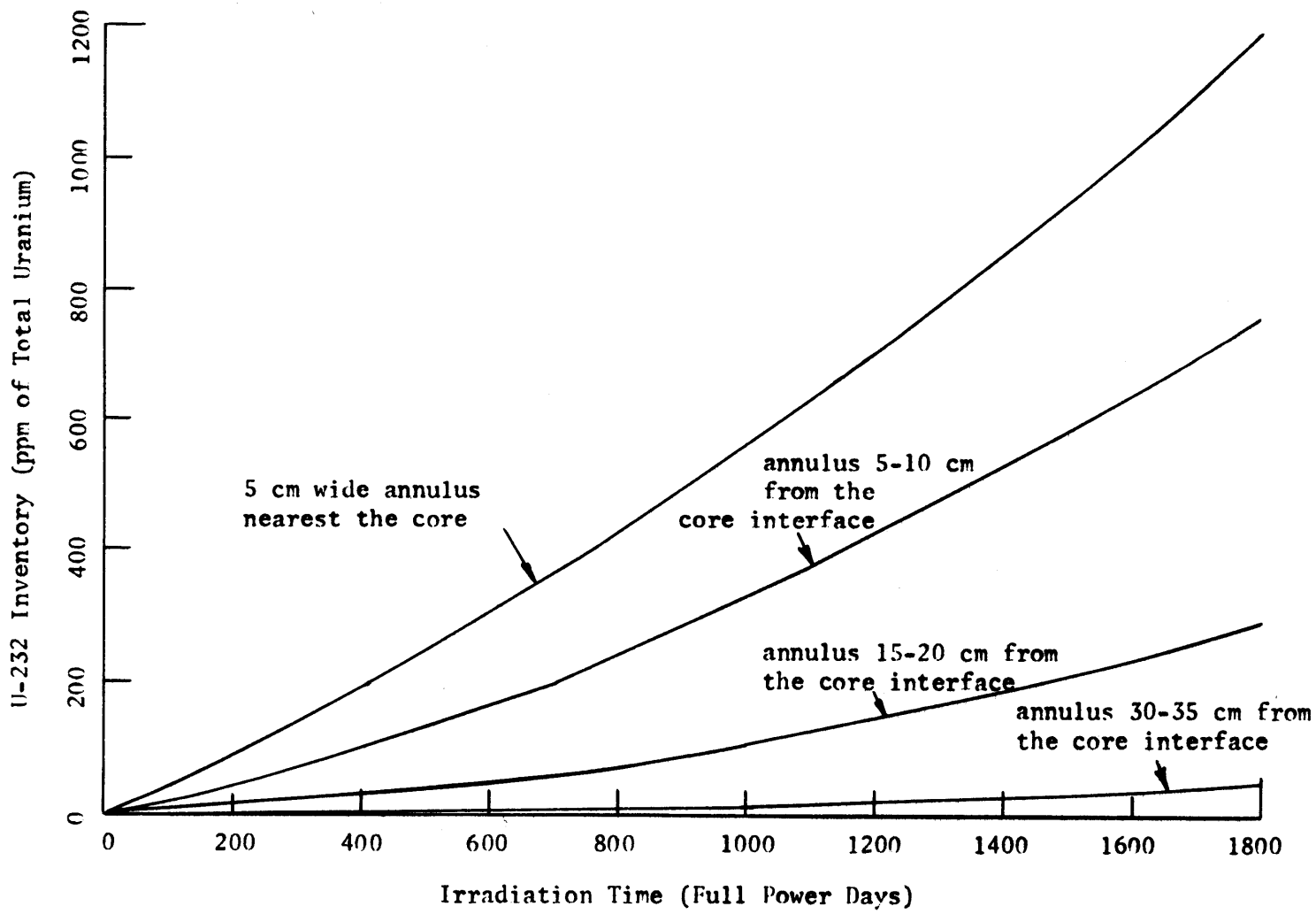

Fig. 4.23 U-232 Concentration in the Thorium Axial Blanket, Batch Irradiation, Cycle 1

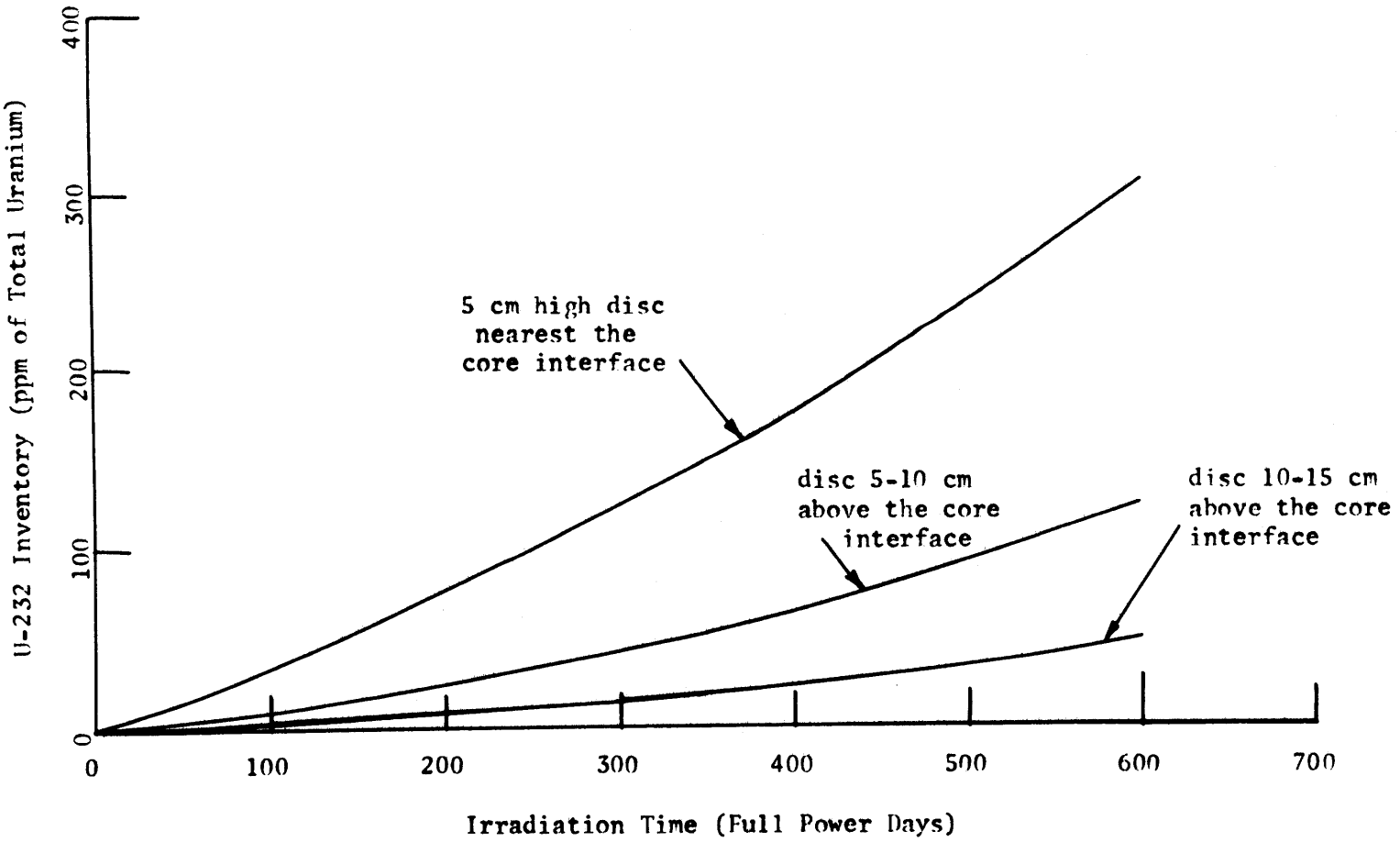

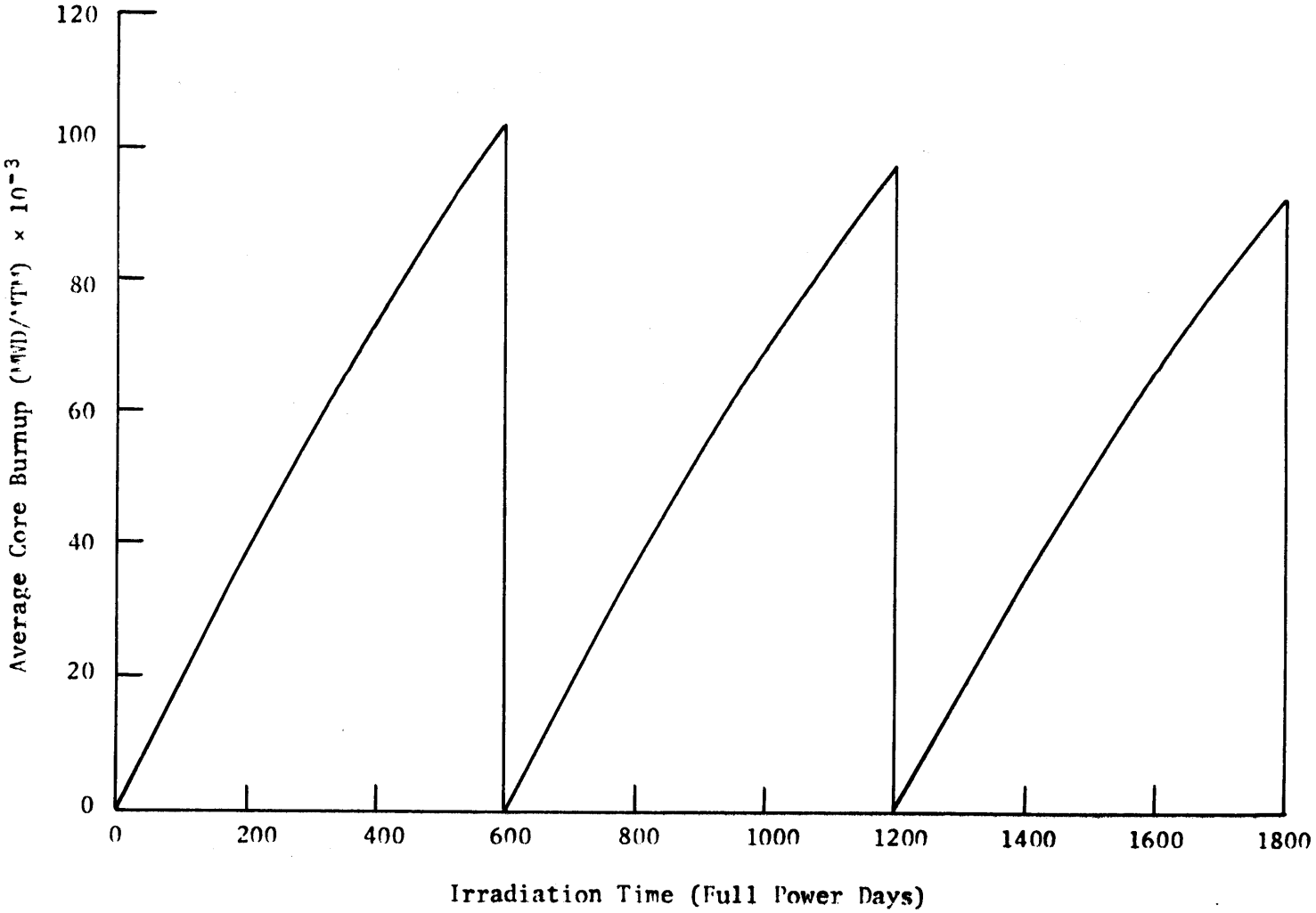

Fig. 4.24 Average Core Burnup for the Uranium Blanket System, Batch Blanket Management

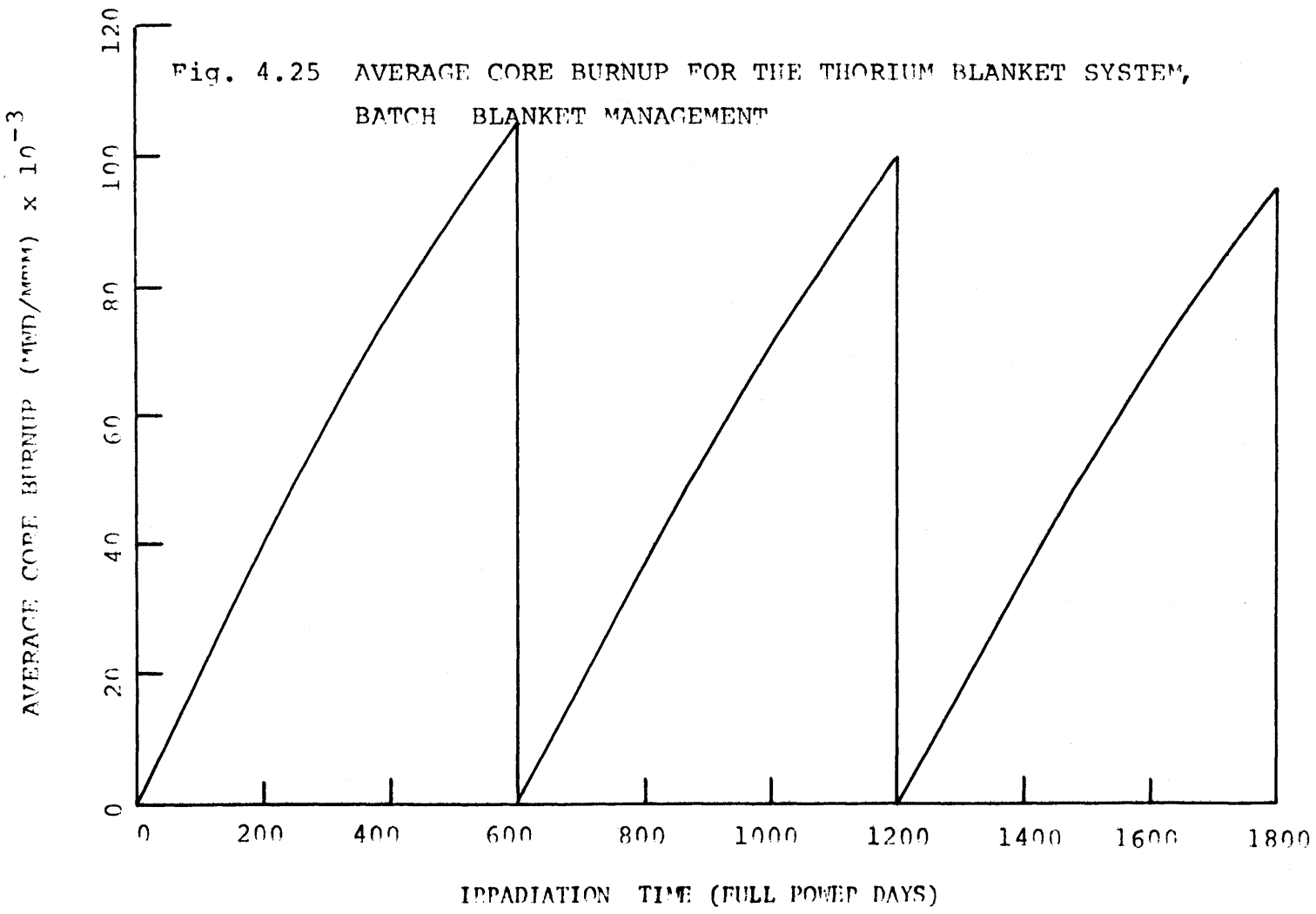

Fig. 4.25 AVERAGE CORE BURNUP FOR THE THORIUM BLANKET SYSTEM, BATCH BLANKET MANAGEMENT

rate is substantially less than that for the uranium blankets, the average core burnup at the end of cycle 1 is higher for the thorium blanketed system than for the uranium blanketed system. Table 4.12 shows the average core burnups at the end of the three cycles for the uranium and thorium blanketed systems. As shown, in all cases the thorium blanketed system requires a slightly higher core burnup. The difference between the two systems, however, never exceeds about 2% in core burnup.

TABLE 4.12 Average End-of-Life Core Burnups for the Batch Blanket Management Case.

Cycle Number	Average Core Burnups (MWD/MTM), EOL	
	Th Blanket System	U Blanket System
1	105.8×10^3	103.7×10^3
2	99.3×10^3	97.8×10^3
3	94.1×10^3	92.5×10^3

Consider next the peak burnup in the radial blankets. Figures 4.26 and 4.27 show the peak radial blanket burnups as functions of irradiation time. These peak burnups were derived by linear extrapolation (near the core interface) and interpolation (between blanket rows) of the blanket burnup near the core axial center plane. These extrapolated values were then corrected for axial peaking using the appropriate beginning-of-life axial peaking factors. Cross comparison between the two blanket types indicates that the peak burnups for the uranium radial blanket rows exceeds that for the thorium blanket initially, but that later

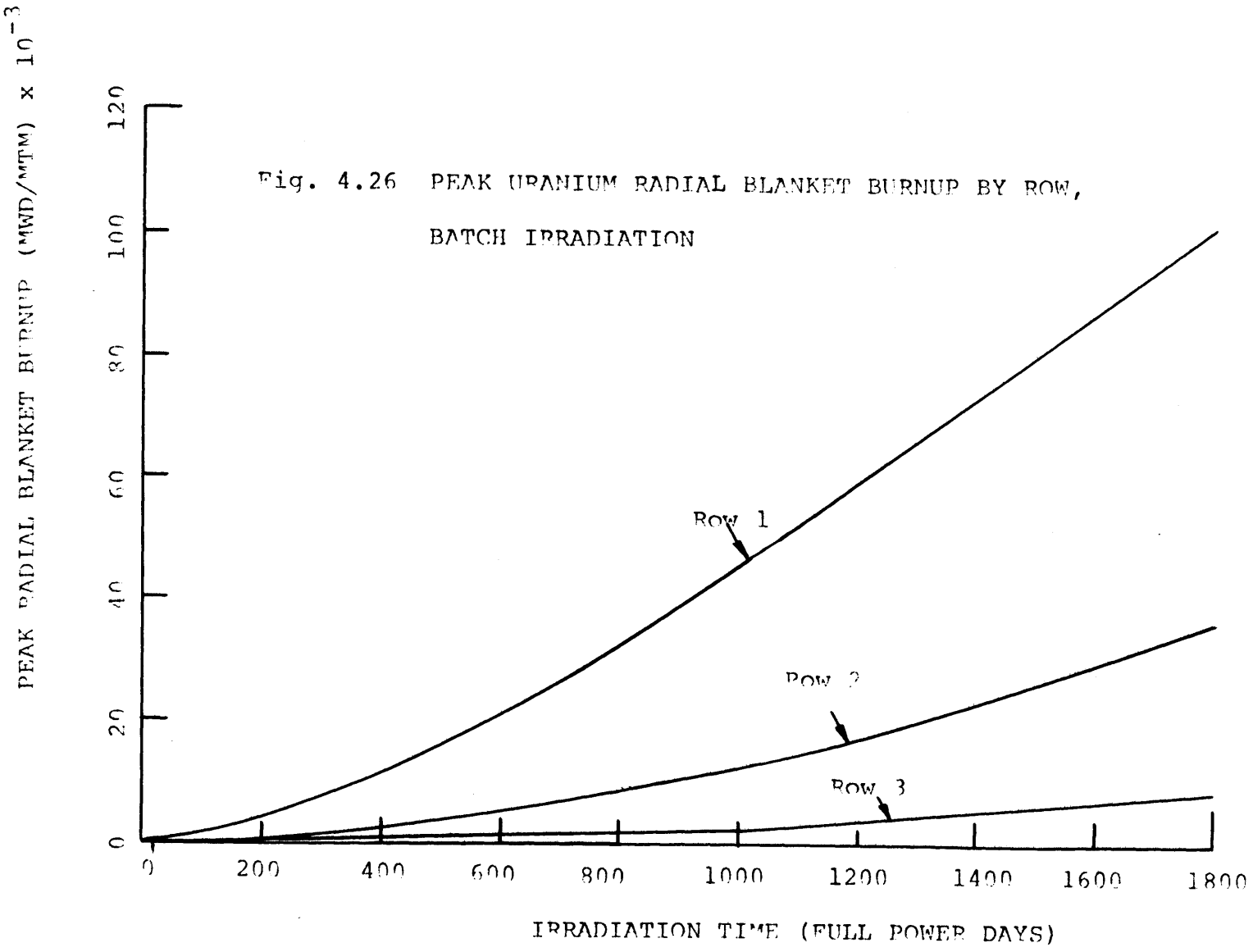

Fig. 4.26 PEAK URANIUM RADIAL BLANKET BURNUP BY ROW, BATCH IRRADIATION

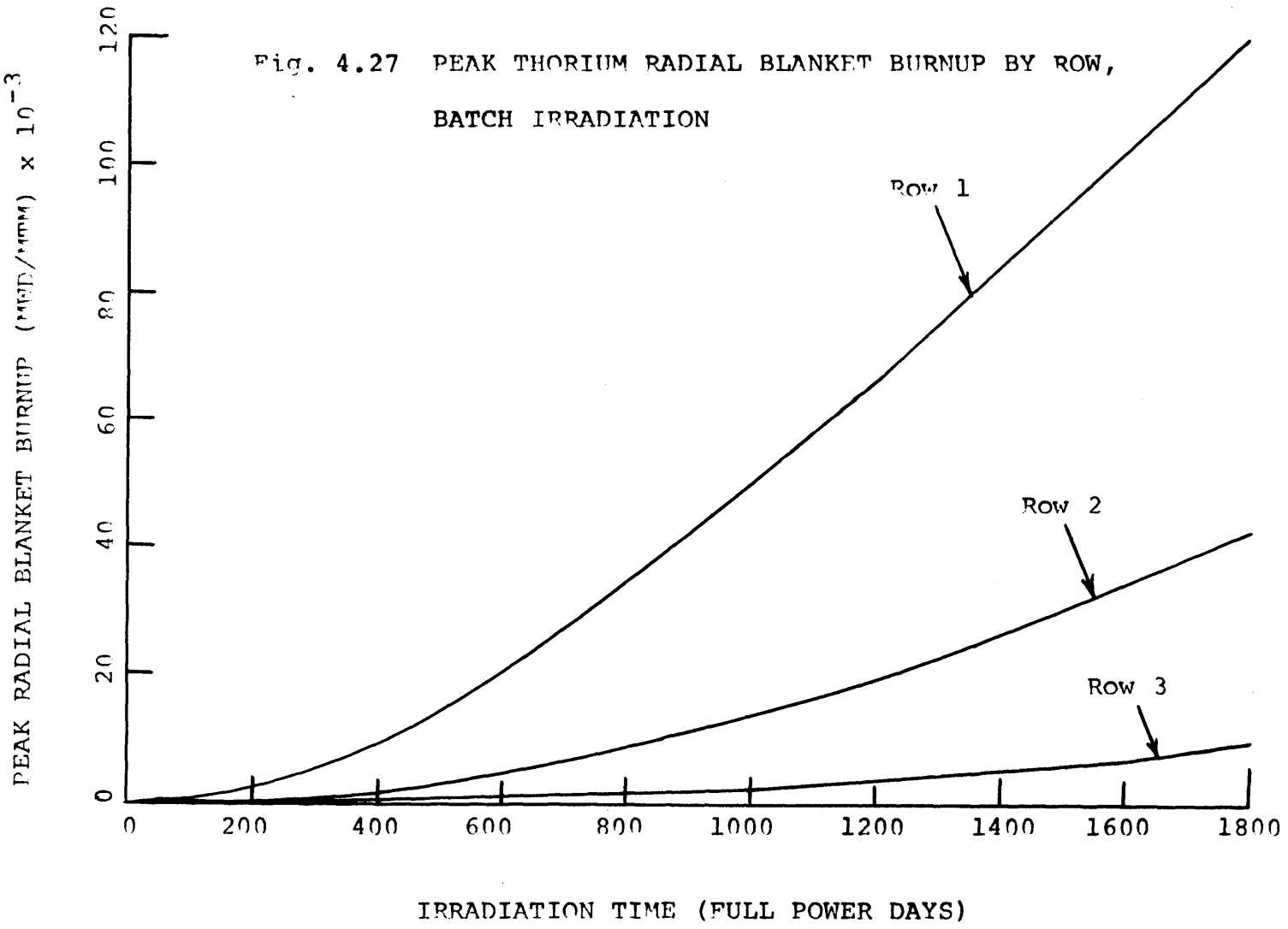

Fig. 4.27 PEAK THORIUM RADIAL BLANKET BURNUP BY ROW, BATCH IRRADIATION

during the burnup, the thorium blanket peak burnups surpass those for the uranium blanket. This observation would indicate that one might expect a larger power swing over the same irradiation interval for a thorium radial blanket if the irradiation time is sufficiently long. This topic will be discussed in more detail in section 6.3, where it will be shown that thorium blankets do experience larger temporal power variations.

4.4.2.5 Breeding Ratio

The last topics to be discussed in this section are the breeding ratio and doubling times calculated for the two systems of interest. Figure 4.28 shows the breeding ratio as calculated by 2DB as a function of irradiation time for the two systems. This breeding ratio is really a ratio of fissile absorption rate to fertile capture rate at a particular point in the irradiation cycle. It is necessary to define breeding ratio in this manner because a different fissile isotope is being produced in the thorium blanket (U-233) than is being burned in the reactor core (fissile plutonium). The values of breeding ratio for the uranium blanketed system are in reasonable agreement with that reported by Wolfe (W2), 1.26, for a 1000-MW_e LMFBR. As shown, the pointwise breeding ratio increases slightly with irradiation time for both systems. Also shown is the fact that the uranium blanket system has a breeding ratio somewhat larger than that for the thorium blanket system.

Evaluation of the system doubling times was done as follows. Fissile inventories in both systems were evaluated at the beginning of the irradiation cycles and at the end of 600 full power days. The initial

Fig. 4.28 BREEDING RATIO AS A FUNCTION OF IRRADIATION TIME FOR THORIUM AND URANIUM BLANKET SYSTEMS

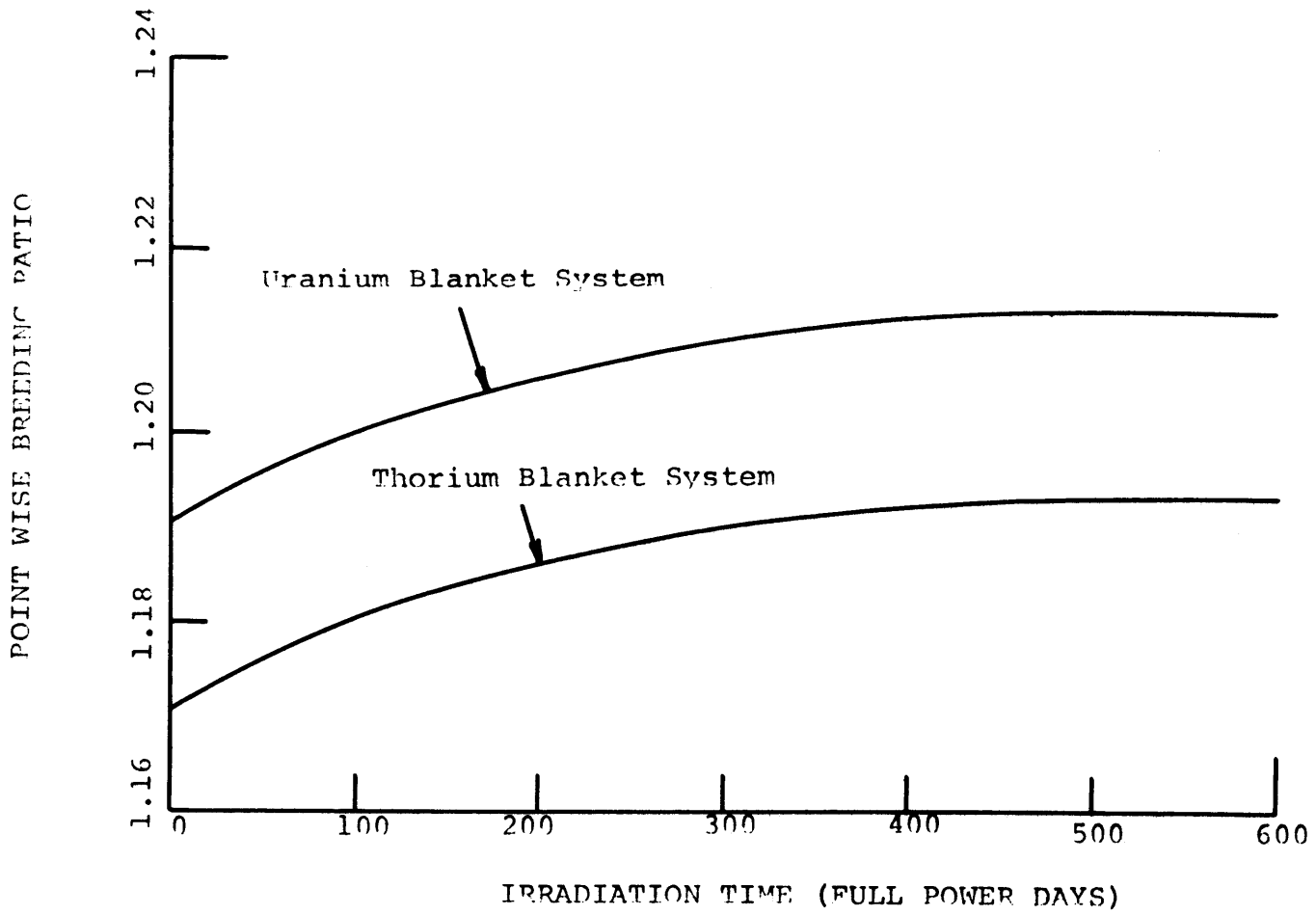

fissile inventory was then subtracted from the final inventory, and the initial inventory was divided by this difference. To obtain the doubling time, this last ratio was multiplied by two years (600 full power days corresponds to two years of operation at an availability of 82%). The result of this analysis was a doubling time of 8.1 years for the uranium blanketed system and 9.9 years for the thorium blanketed system. Clearly the advantage in both breeding ratio and doubling time goes to the uranium blanketed system. The relative advantages of the thorium blanketed system must await the economic analysis to be clarified.

4.4.3 Evaluation of Simplified Method

For this study the decision was made to use the 2DB code to evaluate fissile isotope concentrations in the blankets. Since Brewer (B3) has shown that a simplified approach to performing burnup calculations was reasonably accurate, some consideration should be given here to a discussion of the simplified model. This model, called by Brewer the semi-analytic depletion method (SAM), basically relied on a beginning-of-life snapshot physics calculation using 2DB to determine the total fluxes and one-group cross sections in the various zones of the core and blankets. These data were then assumed to be constant throughout the lifetime of the blankets, and, coupled with the depletion equations for all the isotopes of interest, were used to generate material inventories as functions of irradiation time for batch blanket burnup. The assumption inherent in this analysis was that the product of the flux times the cross sections of interest remained constant throughout lifetime. As a check on this assumption, the product of the flux times the cross section was plotted as a function of irradiation time for the reactions of

interest in the analysis of uranium and thorium radial blankets. Figure 4.29 shows the product of the flux times the U-238 capture cross section as a function of irradiation time for several positions in the radial blanket. (Reference should be made to Fig. 2.2 for the significance of the zones referred to in these figures.) Figure 4.30 shows the same information for the Pu-239 absorption cross section. As shown in these two curves the product of flux times cross section is very nearly constant in the zone nearest the core interface, while this product varies significantly (by as much as a factor of 2.0) in regions more remote from the core interface.

Figure 4.31 shows the product of the flux times the Th-232 capture cross section as a function of irradiation time for several positions in the radial blanket. Figure 4.32 shows this same information for the product of flux times U-233 absorption cross section. As shown, the assumption of constant product of flux times cross section is again not unreasonable for a thorium radial blanket zone near the core interface. However, again the assumption breaks down in regions further removed from the core interface.

This discussion leads one to conclude that the semi-analytic depletion method (SAM) will do a reasonable job of predicting fissile inventories in the first row of the radial blanket. In this row, the largest part of the blanket breeding is achieved, and the most significant negative contribution to the fuel cycle cost is made. However, if good predictions of fissile inventories are desired in radial blanket rows 2 and 3, a burnup method which takes into account the effect of flux and cross section changes with irradiation must be used. For this reason,

Fig. 4.29 Expected One Group Reaction Parameter in a U-238 Radial Blanket, U-238 Capture

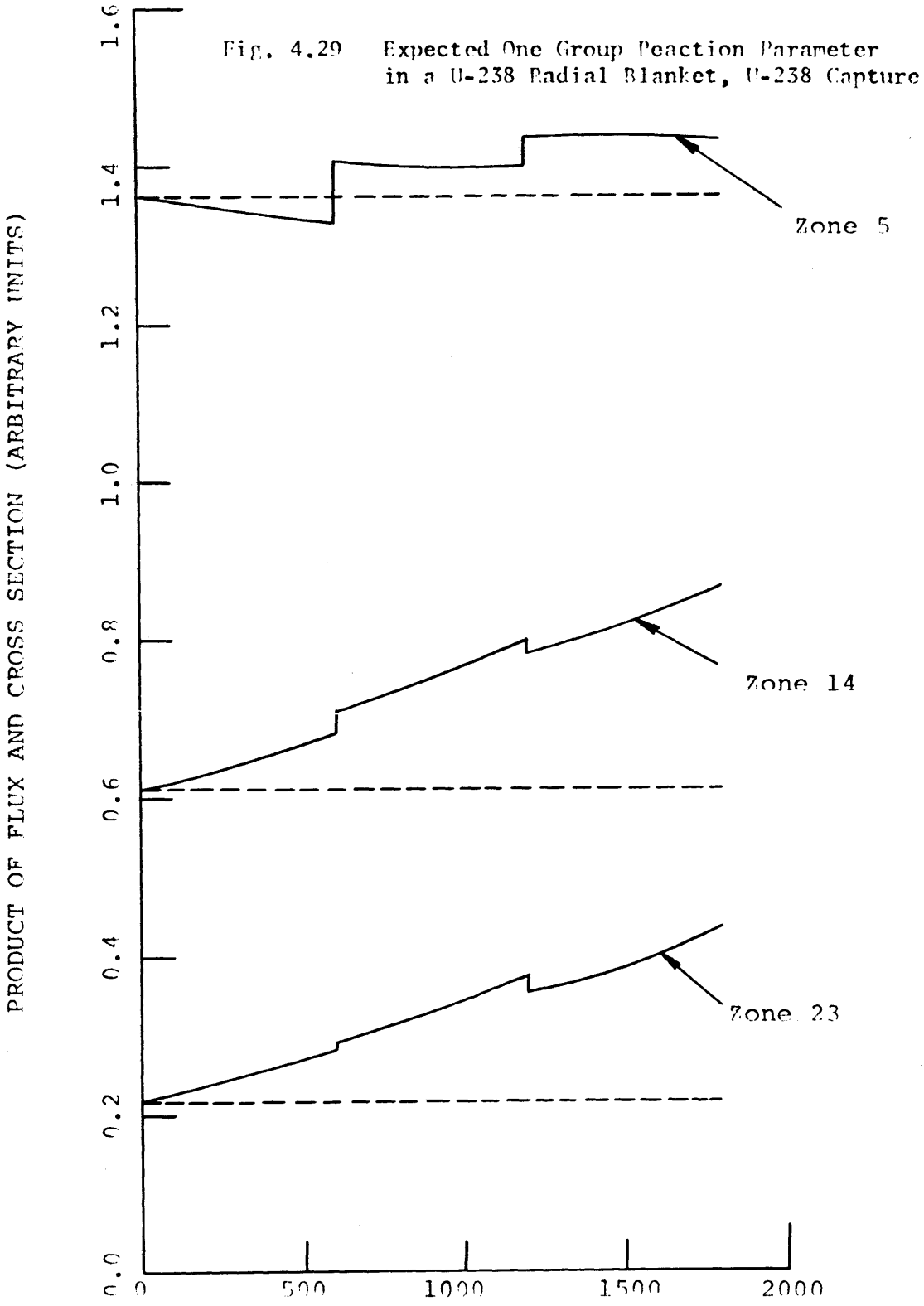

Fig. 4.30 EXPECTED ONE GROUP REACTION PARAMETER IN A U-238 RADIAL BLANKET, PU-239 ABSORPTION

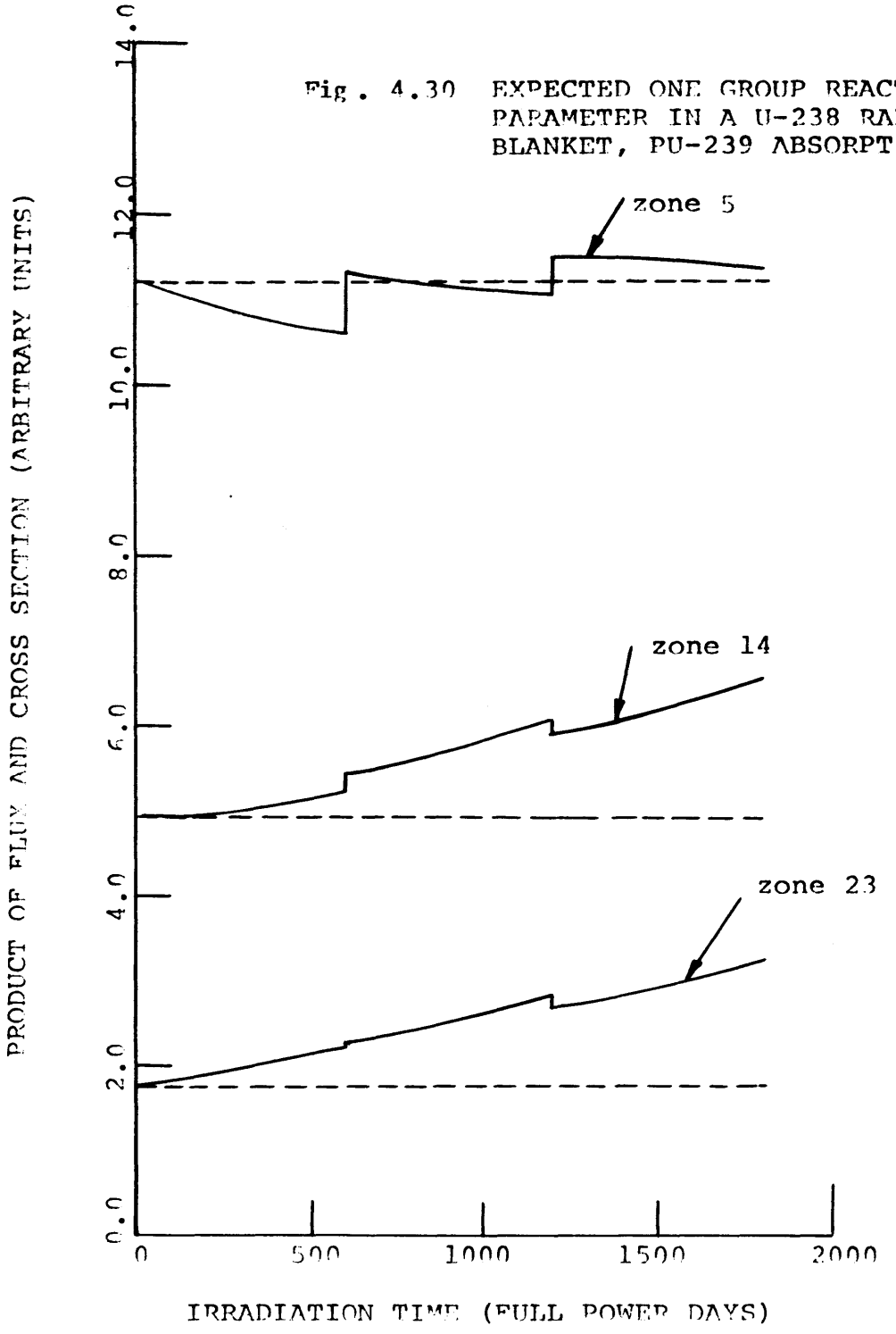

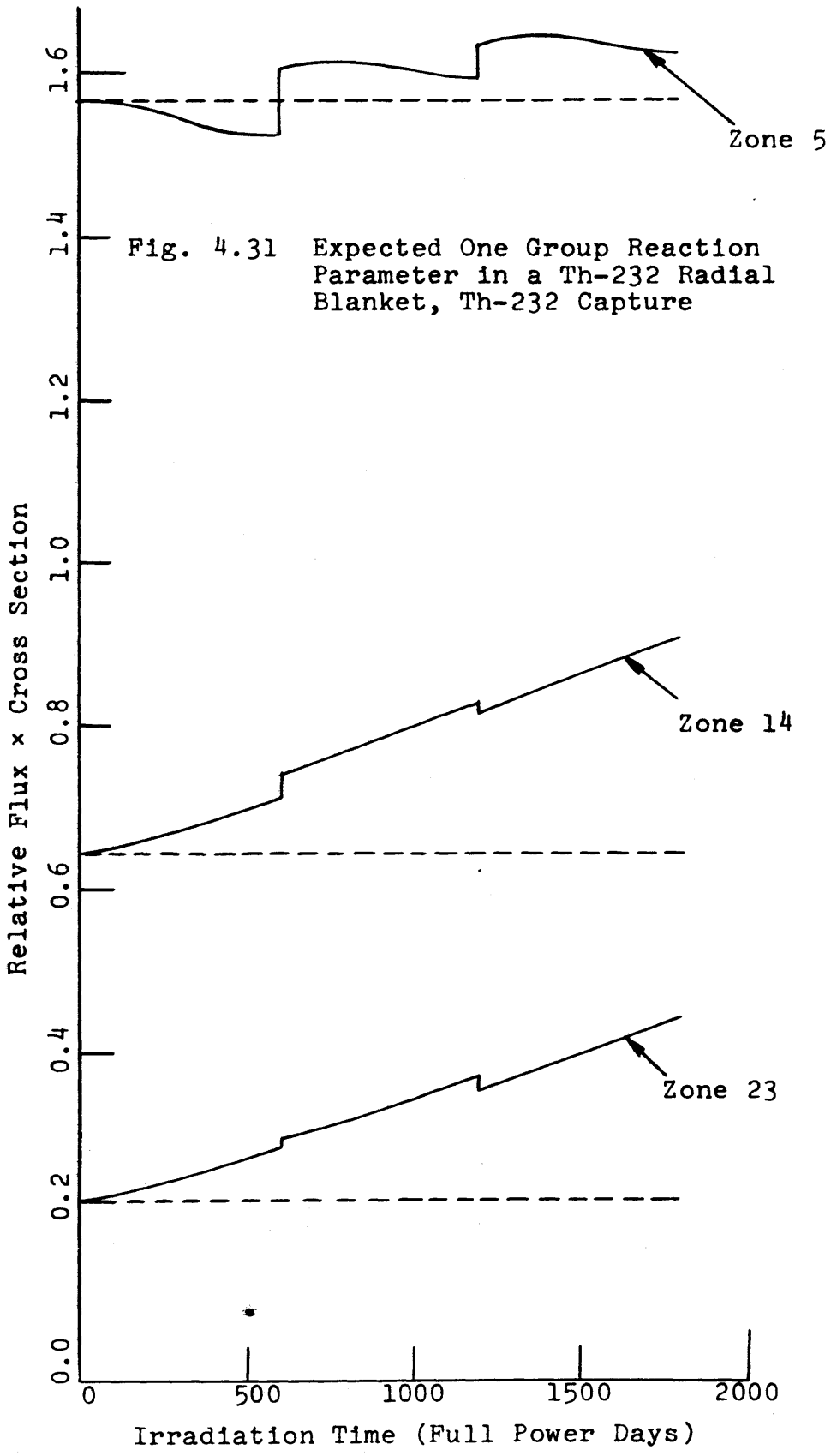

Fig. 4.31 Expected One Group Reaction Parameter in a Th-232 Radial Blanket, Th-232 Capture

Fig. 4.32 Expected One Group Reaction Parameter in a Th-232 Radial Blanket, U-233 Absorption

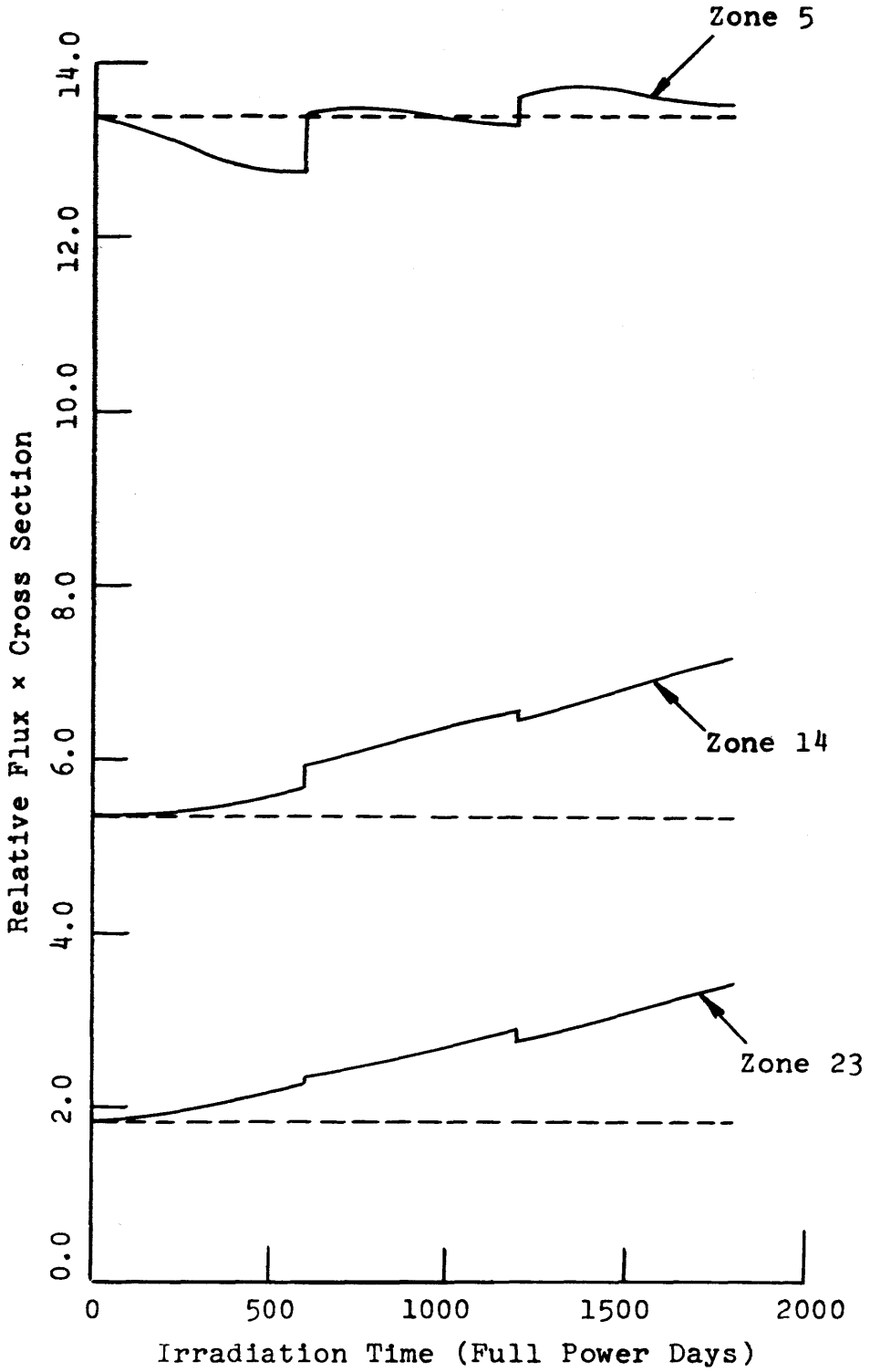

together with the fact that the SAM method does not allow the blanket to be managed conveniently, the decision was made to use the 2DB burnup analysis in this work.

4.5 ZONE SCATTER BLANKET MANAGEMENT

4.5.1 Introduction

In the previous section (4.4), a discussion was presented of the results of a burnup analysis in which the radial blanket was batch-irradiated for 1800 days while the core and axial blanket were replaced every 600 days. This section will treat a first level refinement to batch blanket management. The scheme discussed here, called zone scatter management, treats the axial blanket and the core in the same manner as was used in the batch blanket irradiation analysis. The difference in this analysis is that the row 1 radial blanket is assumed to be irradiated until its economic optimum is reached, at which time it is replaced with unirradiated material. The optimum irradiation time for the row 1 radial blanket was established by using the material inventories from the batch irradiation case together with a standard set of economic parameters (see sec. 5.2) in an economic optimization. The economic analysis was performed using the cash flow method (CFM) presented by Brewer (B3). A detailed discussion of the economic analysis is presented in section 2.6, in Appendix C, and in Chapter 5. For the present purposes, two results of this analysis are needed to proceed: the optimum irradiation time for the thorium row 1 radial blanket was 600 days, and the optimum irradiation time for the uranium row 1 radial blanket was 1000 days.

By using these two optimum times, it was possible to develop a core and blanket management scheme in which only rows 2 and 3 of the radial blanket were batch-irradiated. Table 4.13 shows the significant replacement events in the core and blanket management scheme used here. In the remainder of this section the inventories, burnups, and U-232 concentrations derived using this management method will be presented and compared to similar results from the batch irradiation case.

TABLE 4.13 Core and Blanket Management Schemes for the Simplified Zone Scatter Management of the Radial Blanket.

Thorium Blanket System		Uranium Blanket System	
Irradiation Time (Full power days)	Components Replaced	Irradiation Time (Full power days)	Components Replaced
600	Core, axial blanket, and radial blanket, row 1	600	Core and axial blanket
1200		1000	Row 1 radial blanket
1800		1200	Core and axial blanket
		1800	Core and axial blanket
		2000	Row 1 radial blanket

4.5.2 Comparison of Blankets

4.5.2.1 System k_{eff}

To allow intercomparison between the batch blanket irradiation and the zone scatter management discussed in this section, the same beginning-of-life fissile enrichments and poison concentrations were used for both (see Tables 4.4, 4.5, and 4.6). Since the first refueling operation in which the radial blanket is disturbed occurs after 600 days of irradiation, the burnup performance of the uranium and thorium blanket systems is the same for both batch managed and zone scatter managed blankets during the first 600 days. For this reason, only the system performance characteristics after 600 days of irradiation will be discussed in this section. For the performance during the first 600 days, refer to section 4.4.

As for the batch management case, the system effective multiplication factor, k_{eff}, will be used as a measure of the consistency of the burnup analysis. Figure 4.33 shows the variation of this parameter as a function of irradiation time from 600 days (2 full power years at 82% availability) to 2400 days (8 years). As shown, the differences in replacement cycle for the row 1 radial blanket between the uranium and thorium blanket systems have led to some deviations in k_{eff} behavior with burnup. As expected, replacement of an irradiated radial blanket row 1 with fresh material causes the system k_{eff} to decrease. These decreases can be seen most clearly for the uranium radial blanket after 1000 and 2000 days of irradiation. Since the thorium radial blanket row 1 was replaced at the same time as the core and axial blanket, the dependence of k_{eff} on row 1 enrichment is obscured in this graph.

Fig. 4.33 System Effective Multiplication Factor as a Function of Irradiation Time, Row 1 Radial Blanket Zone Scatter Managed

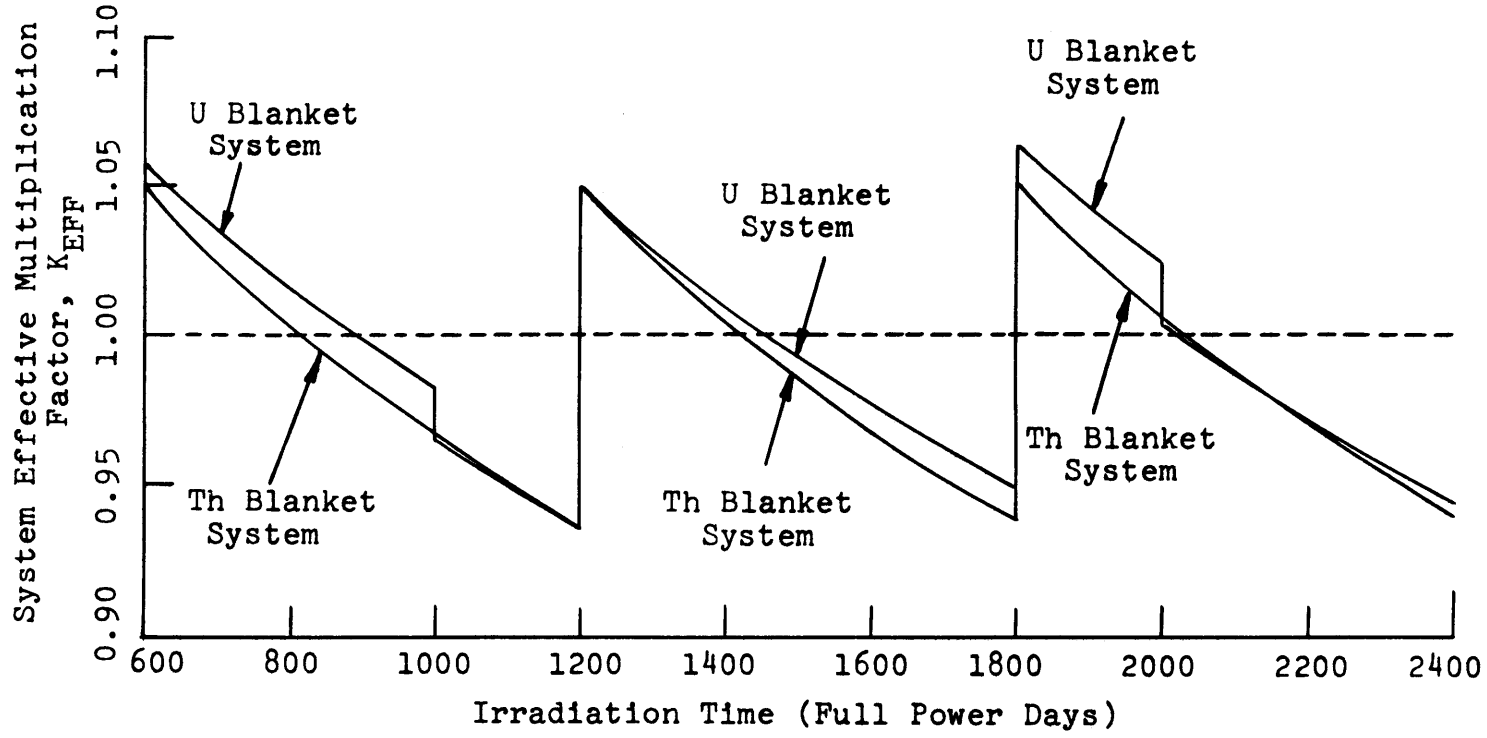

Cross-comparison between Figs. 4.11 and 4.33 will show this effect. For convenience, the system k_{eff} at refueling intervals for the thorium blanketed system are shown in Table 4.14.

TABLE 4.14 Comparison of System k_{eff} for Different Management Schemes.

Irradiation Time (days)	System k_{eff} After Refueling			
	Thorium Blanket System		Uranium Blanket System	
	Batch	Managed	Batch	Managed
0	1.0483	1.0483	1.0420	1.0420
600	1.0618	1.0493	1.0564	1.0564
1000	0.9791	0.9657	0.9821	0.9649
1200	1.0729	1.0501	1.0685	1.0489
1800	0.9615	1.0508	0.9687	1.0635
2000		1.0050		1.0032

As shown, the row 1 thorium radial blanket irradiated for 600 full power days appears to contribute slightly over 1.2% to the system k_{eff}, while the row 1 uranium radial blanket irradiated for 1000 full power days appears to contribute approximately 1.7% to the system k_{eff}.

The final observation to be made from Fig. 4.33 is that the k_{eff} for the two different blanket systems are not dramatically different over most of the burnup interval. Consequently, we will proceed to make other comparisons between these systems and the corresponding batch managed systems.

4.5.2.2 Blanket Inventories

In this section consideration will be given to the effect of radial blanket row 1 management on the breeding performance of the other radial blanket rows and of the axial blanket. It would be expected that replacing row 1 with fresh assemblies periodically might have two effects. First, the reduction in the average row 1 fission rate resulting from blanket management would be expected to cause a reduction in the flux in rows 2 and 3, leading to a reduction in the fissile inventory production in those rows. Second, periodic replacement of row 1 would be expected to change the balance between average fissile fission rate and average fertile capture rate. This change should have the effect of increasing the time average fissile production rate in row 1. Figures 4.34 and 4.35 show that, as expected, the fissile production rate in rows 2 and 3 is reduced when row 1 management is introduced. This occurs in both the uranium radial blanket (Fig. 4.34) and the thorium radial blanket (Fig. 4.35). The point in time at which the departure from batch irradiation predictions occurs is, as expected, that time when row 1 is replaced.

Figures 4.36 and 4.37 show that for the axial blanket in both systems, the fissile production rate is slightly greater for the managed case than for the batch irradiated case. A priori, it was not apparent what effect radial blanket management would have on fissile production rate in the axial blanket. Two competing factors must enter into the qualitative argument. The origin of the two factors is the same: the replacement of row 1 forces the core to contribute a larger fraction of the system fission events (the burnup is performed at constant system power). Because the core enrichment was not changed during the

Fig. 4.34 The Effect of Radial Blanket Row 1 Management on Row 2 and Row 3 Fissile Inventories, U-238 Blanket System

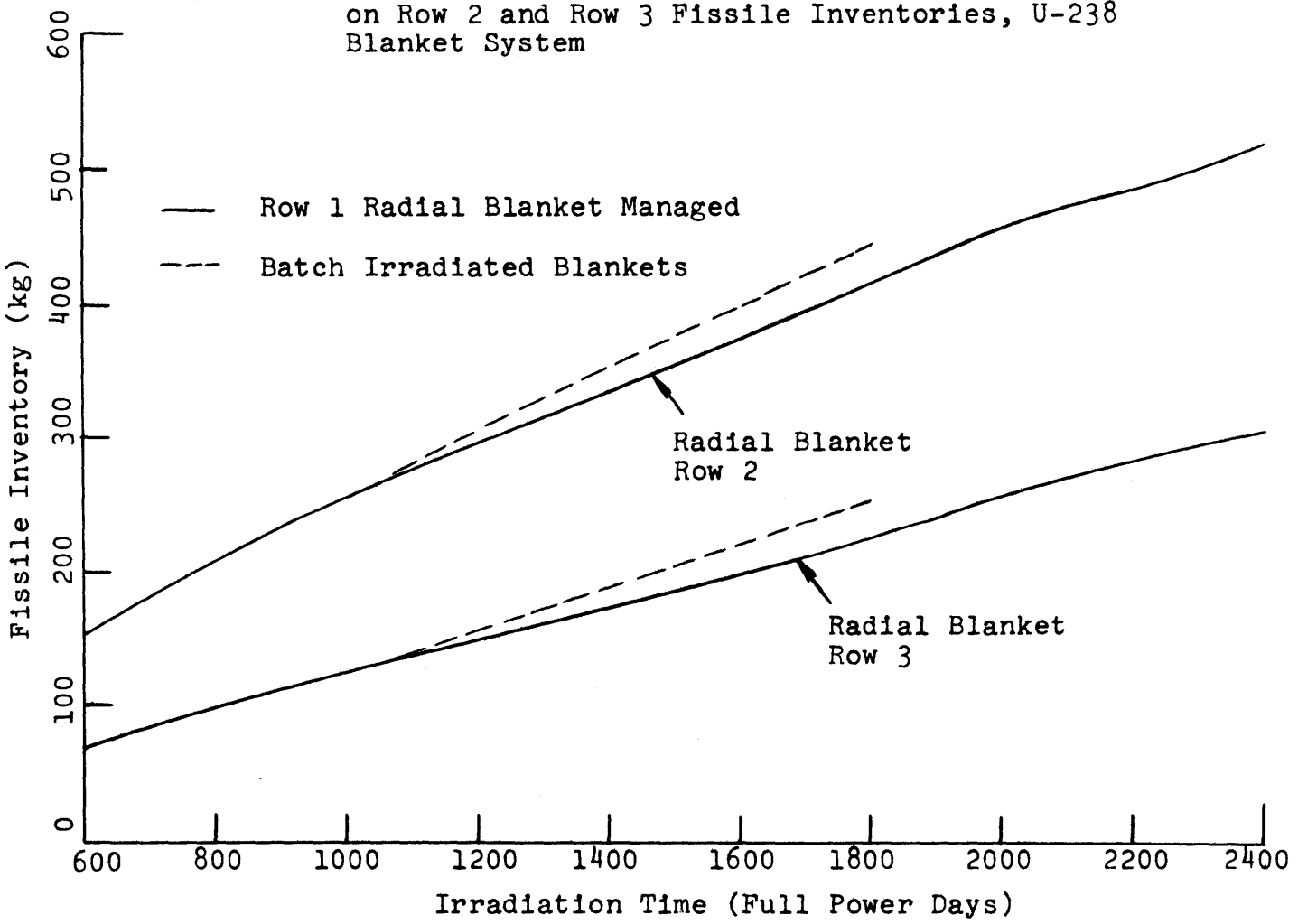

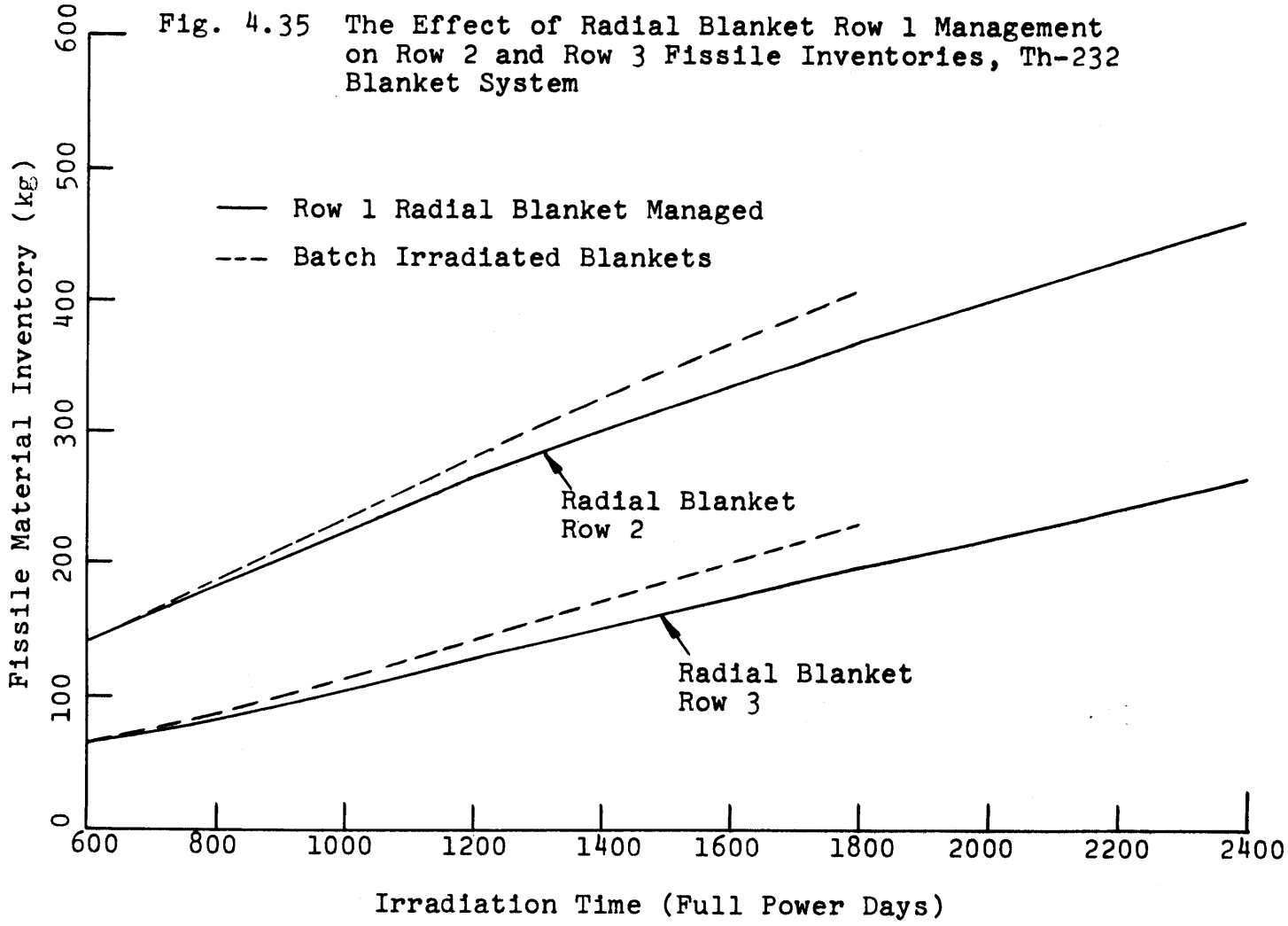
Fig. 4.35 The Effect of Radial Blanket Row 1 Management on Row 2 and Row 3 Fissile Inventories, Th-232 Blanket System
Row 1 Radial Blanket Managed
Batch Irradiated Blankets
Radial Blanket Row 2
Radial Blanket Row 3
Fissile Material Inventory (kg)
0
100
200
300
400
500
600
600
800
1000
1200
1400
1600
1800
2000
2200
2400
Irradiation Time (Full Power Days)

Fig. 4.36 The Effect of Radial Blanket Row 1 Management on Axial Blanket Fissile Inventories, U-238 Blanket System

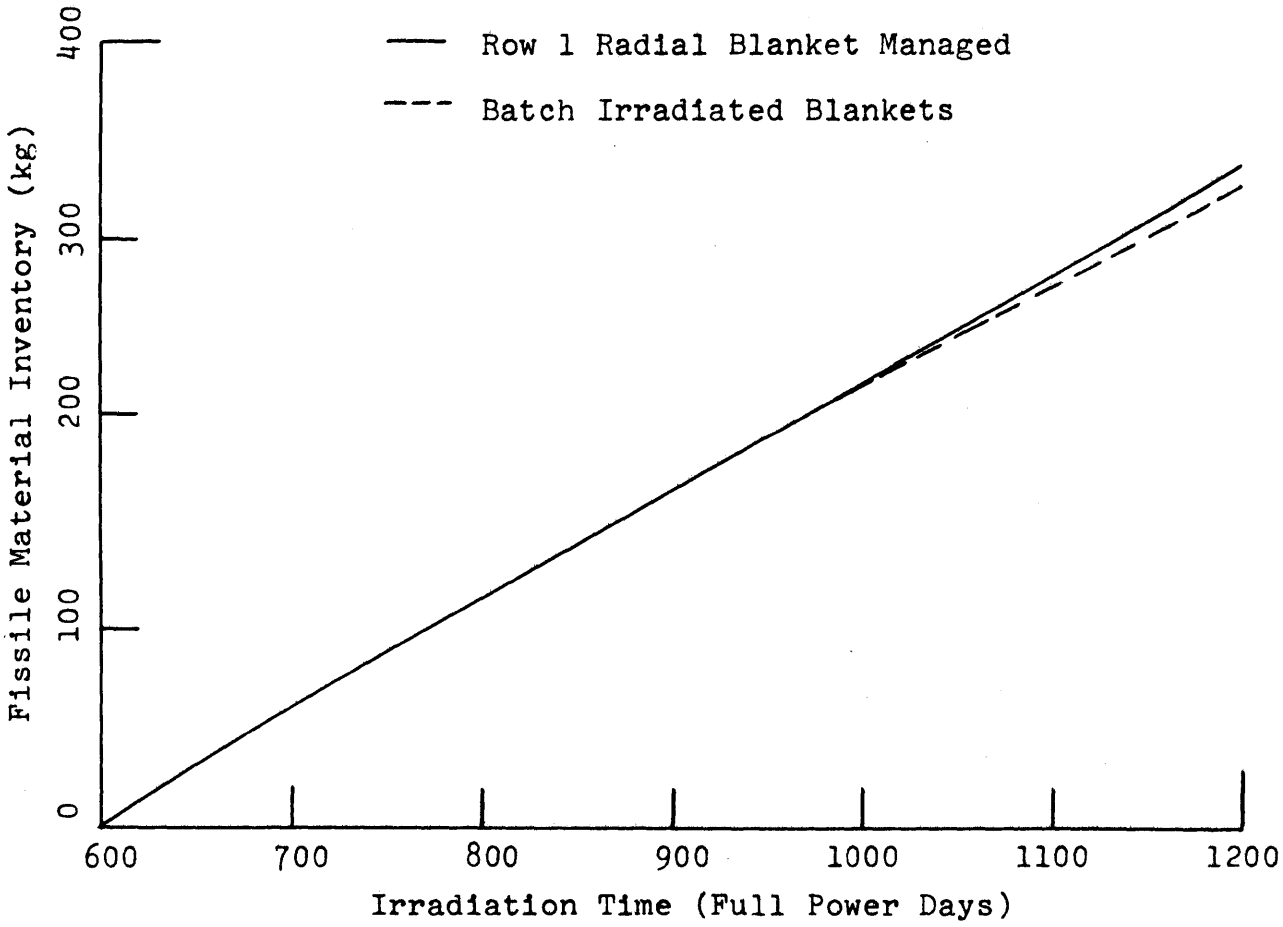

Fig. 4.37 The Effect of Radial Blanket Row 1 Management on Axial Blanket Fissile Inventory, Th-232 Blanket System

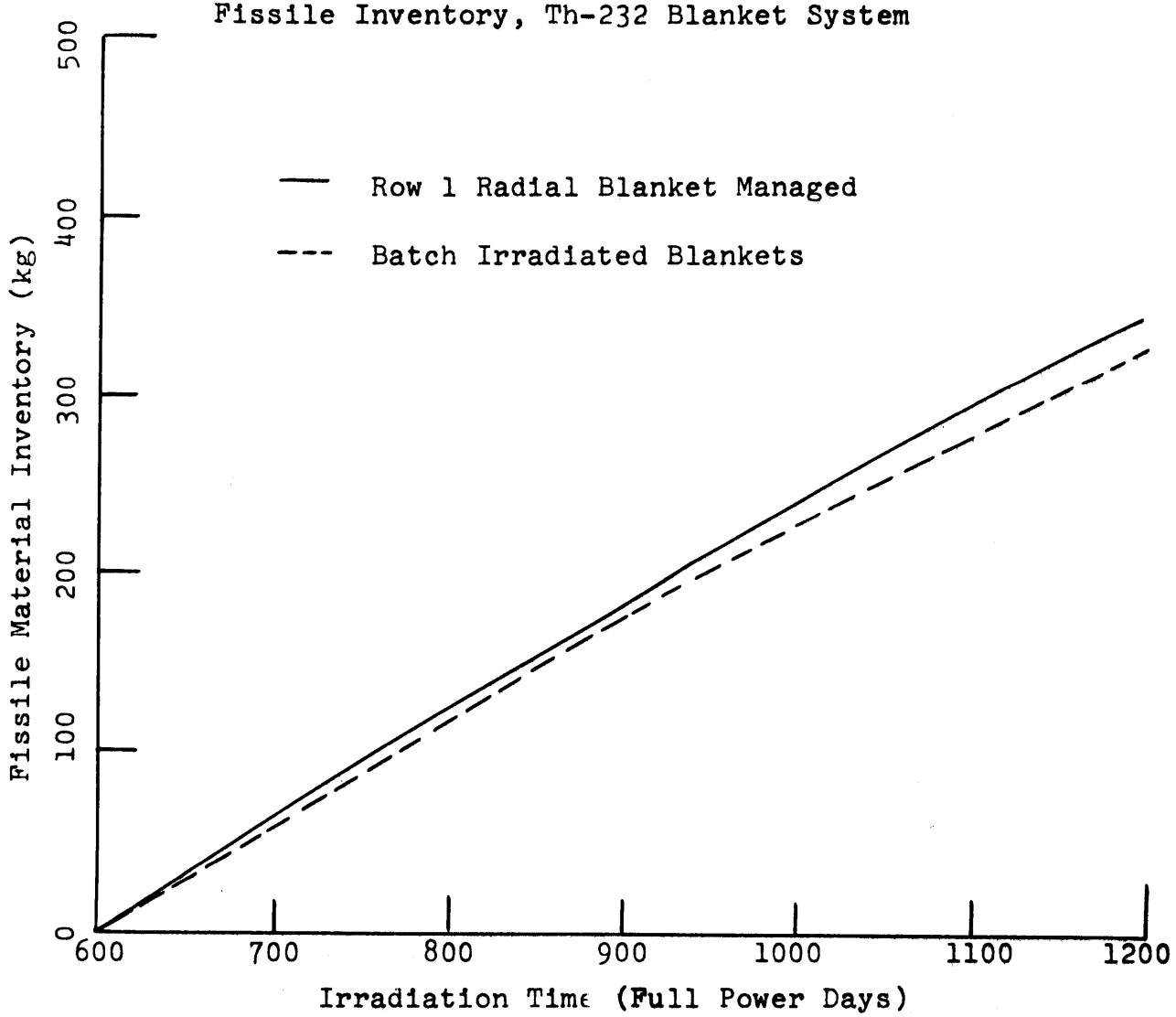

blanket management, a higher flux must exist in the core to produce more core power. This higher flux leads to the two factors mentioned earlier: the blanket flux must increase, causing the fissile fission rate in the axial blanket to increase correspondingly, and the same flux increase causes the fertile capture rate to increase. The net effect of these two competing factors is to increase slightly the fissile production rate, as shown in Figs. 4.36 (uranium blanket) and 4.37 (thorium blanket).

Consider next the effect of management on the fissile production rate in row 1. Figures 4.38 and 4.39 show, for uranium and thorium blanket systems, the integrated row 1 fissile inventory as a function of irradiation time. (These figures differ from those presented earlier in that they show the integrated fissile product generated in row 1 rather than the row 1 inventory at a specific time. This same distinction will be made later when in-out shuffle management is discussed in sec. 4.6.) As expected, replacement of row 1 with fresh material at its economic optimum resulted in a larger integrated mass of fissile material produced in row 1 than the corresponding batch irradiation case. This holds true for both uranium (Fig. 4.38) and thorium (Fig. 4.39) blanketed systems. It is now desirable to determine the effect of blanket row 1 management on the total mass of fissile material produced in the radial blanket. Figures 4.40 and 4.41 show that the net effect of managing row 1 is to increase the total fissile inventory produced in the radial blanket. Again this statement holds true for both uranium (Fig. 4.40) and thorium (Fig. 4.41) blanketed systems.

Fig. 4.38 The Effect of Radial Blanket Row 1 Management on the Total Fissile Material Produced in Row 1, U-238 Blanket System

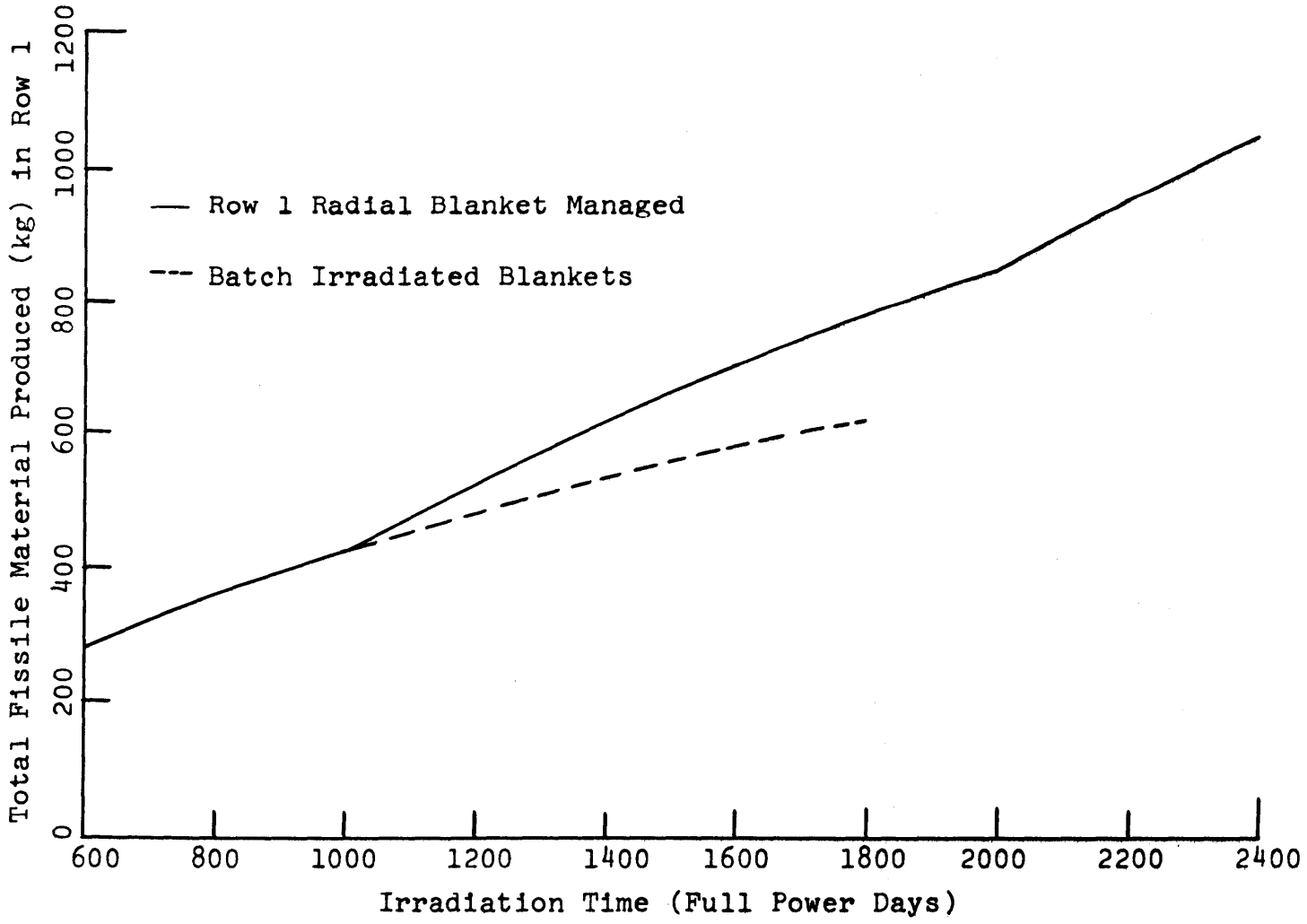

Fig. 4.39 The Effect of Radial Blanket Row 1 Management on the Total Fissile Material Produced in Row 1, Th-232 Blanket System

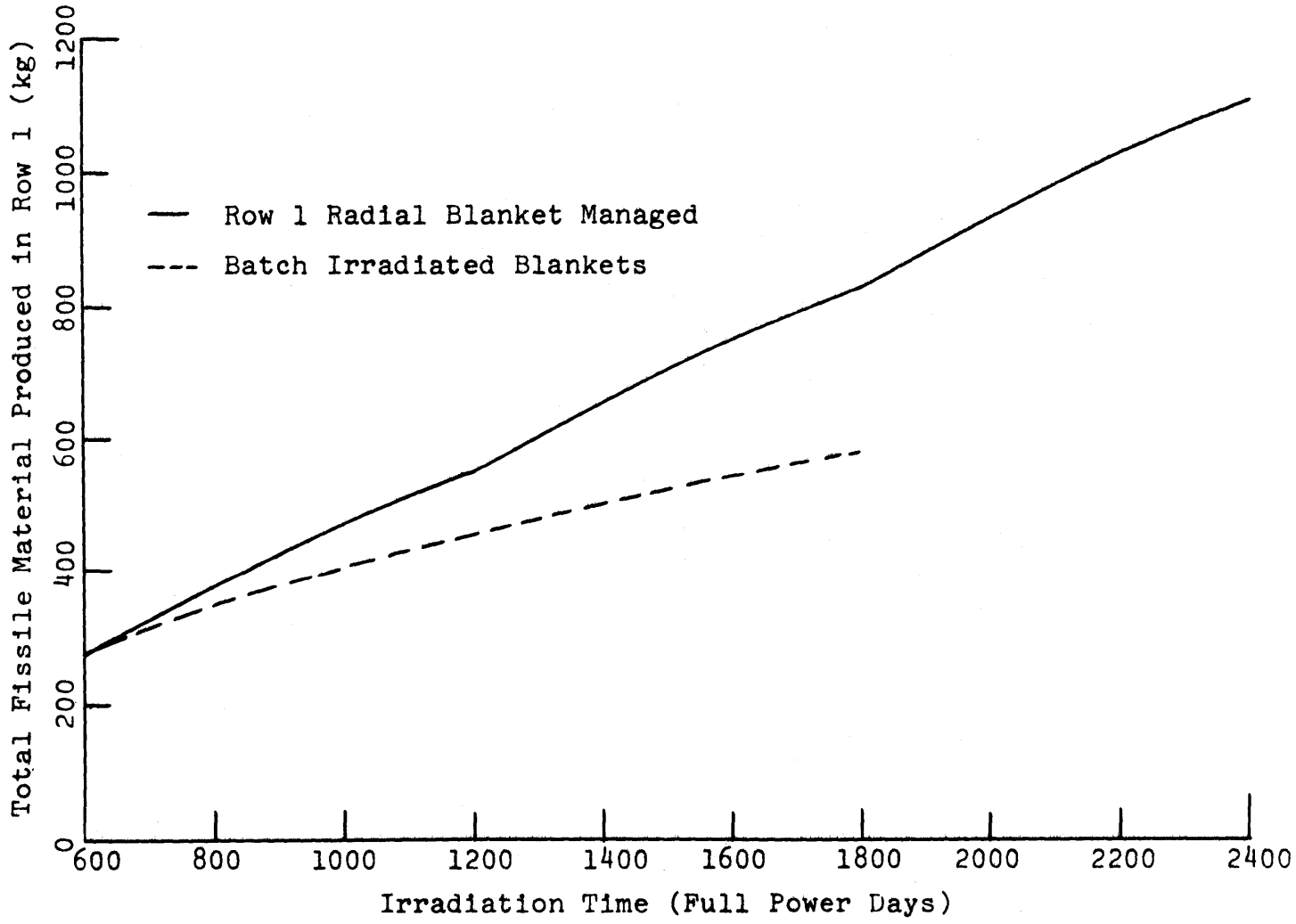

Fig. 4.40 The Effect of Radial Blanket Row 1 Management on the Total Fissile Material Produced in the Radial Blanket, U-238 Blanket System

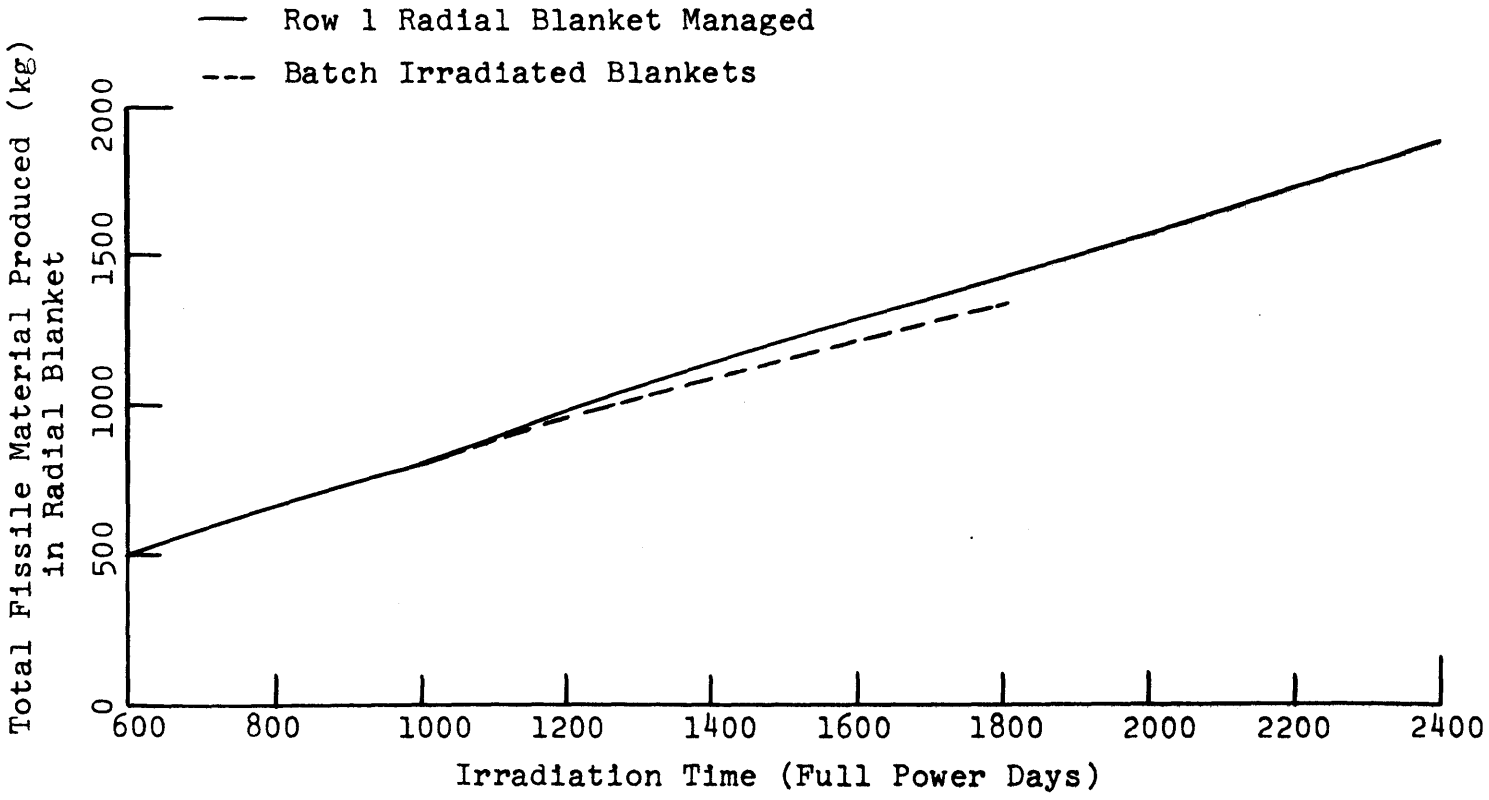

Fig. 4.41 The Effect of Radial Blanket Row 1 Management on the Total Fissile Material Produced in the Radial Blanket, Th-232 Blanket System

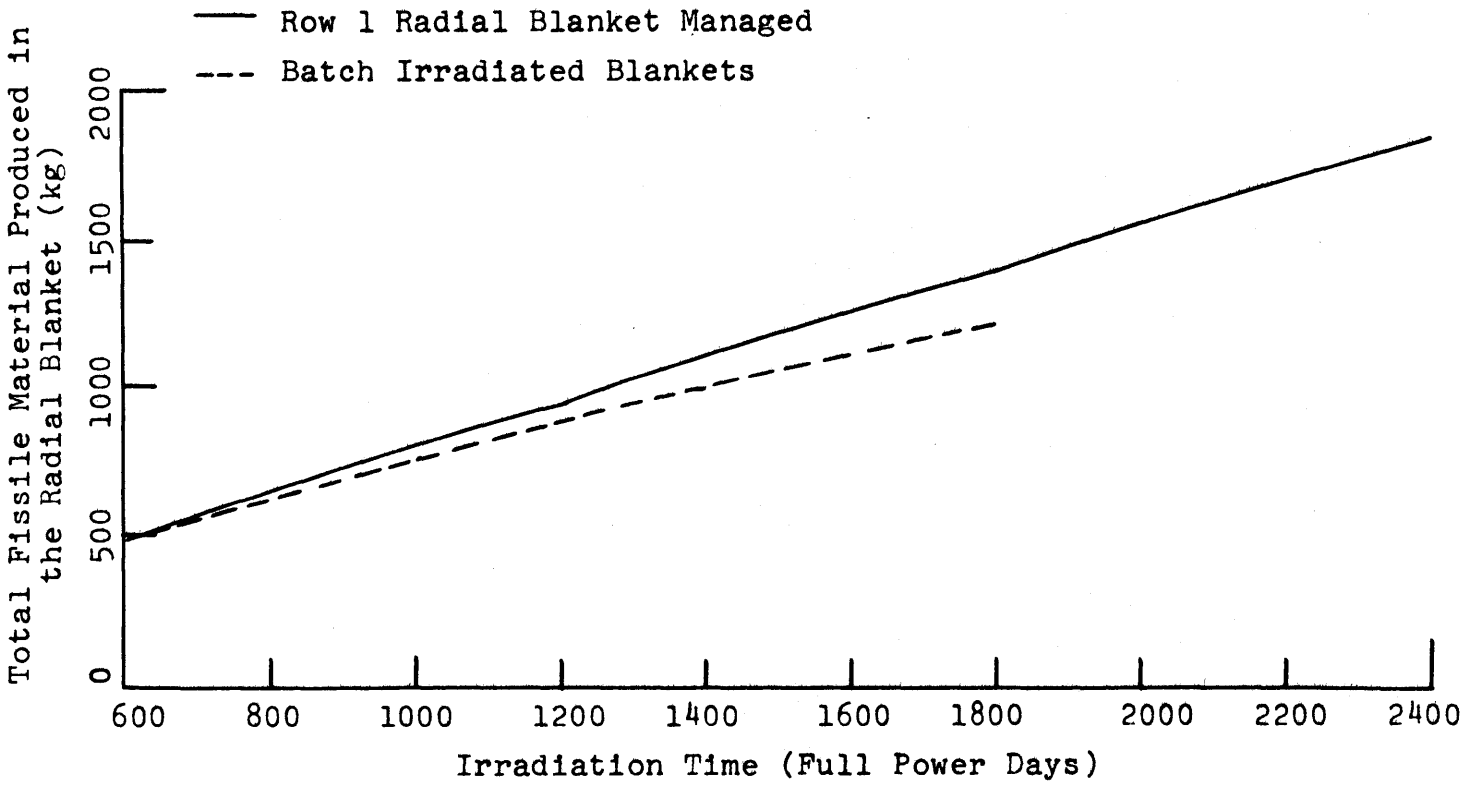

The next question which should be addressed is how radial blanket row 1 management affects the relative breeding performance of the entire thorium and uranium radial blankets. Figure 4.42 shows that management of row 1 has the effect of improving the performance of thorium radial blankets with respect to uranium radial blankets. This appears to be primarily a result of the shorter optimum irradiation time for the thorium blanket, leading to a more frequent change of the blanket, with resulting smaller fissile material loss to blanket fissions.

Since the bulk of the economic analysis reported in Chapter 5 has been based on the batch blanket irradiation cases, it is important to emphasize here the relative effect of radial blanket row 1 management on total blanket breeding performance. Examination of Figs. 4.36, 4.37, and 4.42 reveals that in both the radial and axial blankets, zone scatter management of radial blanket row 1 has the effect of improving the breeding performance of thorium blankets relative to uranium blankets. This fact bears on the comparative economic analysis to be reported in Chapter 5. Because this analysis was based on batch irradiation material inventories, it will present a relative thorium blanket economic performance slightly inferior to that which would be obtained if blanket management schemes were introduced. This is discussed further in section 5.6.

4.5.2.3 U-232 Buildup

Zone scatter management of radial blanket row 1 has been shown in the previous section to reduce the fissile inventory production rate in rows 2 and 3. This was attributed to the reduction in flux associated with the lower average fission rate (arising from a lower average fissile

Fig. 4.42 Comparison of the Effect of Radial Blanket Row 1 Management on Fissile Inventory Production for Uranium and Thorium Radial Blankets

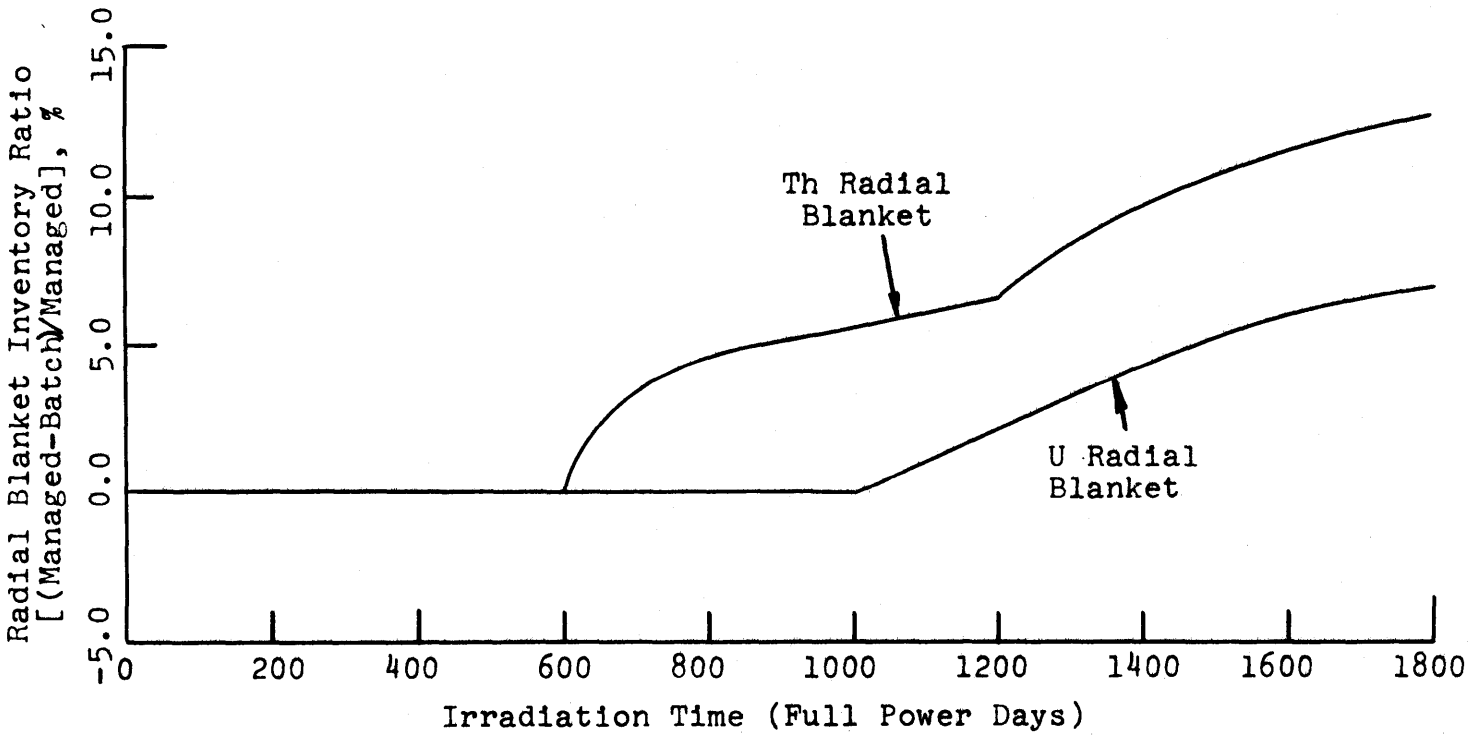

enrichment) in row 1. This same mechanism would be expected to cause a reduction in the buildup rate of the contaminant U-232 in rows 2 and 3. This logical argument is corroborated in Fig. 4.43. This figure shows the U-232 inventory (in ppm of total uranium) as a function of irradiation time for rows 1 and 2 under both the managed and batch irradiation conditions. This observation will again make thorium blankets appear slightly less than their best with respect to uranium blankets when the economic analysis is performed using material inventories derived from batch irradiation rather than those from some management scheme.

4.5.2.4 Burnup Performance

As discussed in the previous sections, radial blanket row 1 zone scatter management is expected to increase the relative contribution to total system fission rate of the core. This results from the periodic removal of large quantities of fissile materials from the blanket region near the core interface when row 1 is replaced. Table 4.15 shows the average core burnup values for the two systems being studied for both batch blanket management and radial blanket row 1 zone scatter management. The increased contribution of the core to total system power is manifested by the fact that the average core burnups for both types of systems are higher for the managed system than for the batch blanket management scheme. Accompanying the increased core burnups are decreases in the peak burnups achieved in the radial blanket. For example, in the zone scatter management scheme radial blanket row 1 is removed when its peak burnup is approximately 45,000 MWD/MTM for the uranium blanket after 1000 days, and approximately 20,000 MWD/MTM for the thorium blanket after 600 days at power

Fig. 4.43 The Effect of Radial Blanket Row 1 Management on U-232 Concentration in Rows 2 and 3, Th Blanket System

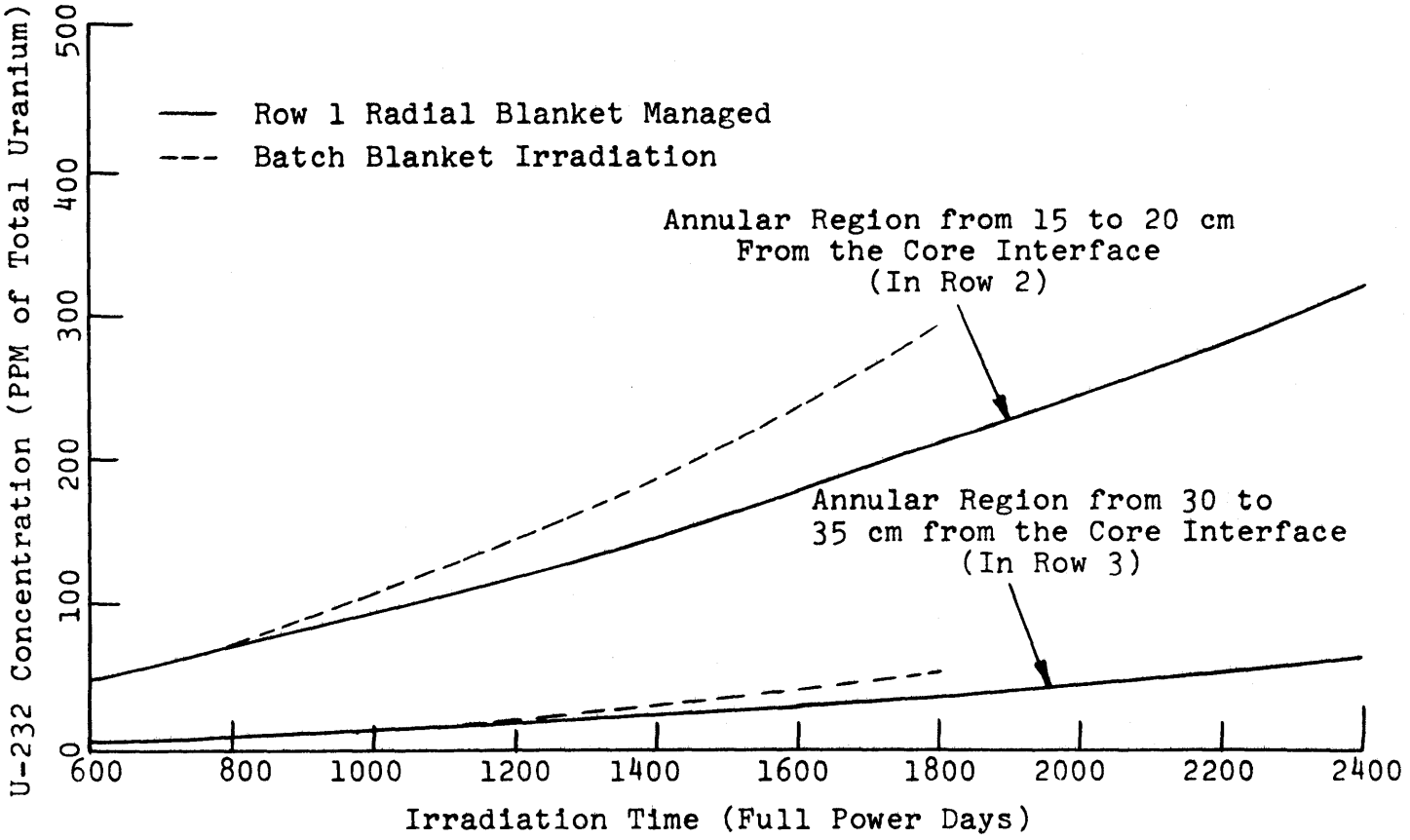

TABLE 4.15 Average Core Burnups, Managed Blanket vs. Batch Irradiated Blanket.

600-Day Cycle Number	Average Core End-of-Life Burnup (MWD/MTM) $\times 10^{-3}$			
	Uranium Blanket System		Thorium Blanket System	
	Batch	Managed	Batch	Managed
1	103.7	103.7	105.8	105.8
2	97.8	100.4	99.3	104.4
3	92.5	99.3	94.1	103.1
4		98.7		101.9

(see Figs. 4.26 and 4.27 for the source of these numbers). These burnups correspond to 101,000 and 120,000 MWD/MTM for an 1800-day batch irradiation of uranium and thorium blankets, respectively. Also resulting from the row 1 management scheme is a reduction in the average burnup values reached in radial blanket rows 2 and 3. Figures 4.44 and 4.45 show the effect of row 1 management on average burnup in the row 2 blanket zone nearest row 1. As shown, row 1 management results in a reduction in average burnup in the uranium blanket (Fig. 4.44) of approximately 15% and in the thorium blanket of approximately 20% after 1800 days of irradiation.

4.5.3 Evaluation of Simplified Method

In section 4.4.3 brief consideration was given to the fundamental assumption behind the semi-analytic depletion model (SAM) of Brewer (B3): namely, the constancy of flux times cross section with irradiation. It was shown that significant variations in the product of the flux times

Fig. 4.44 The Effect of Radial Blanket Row 1 Management on the Average Burnup Experienced in the 5 cm Wide Annular Region in Row 2 Nearest the Row 1 Interface, U-238 Blanket System

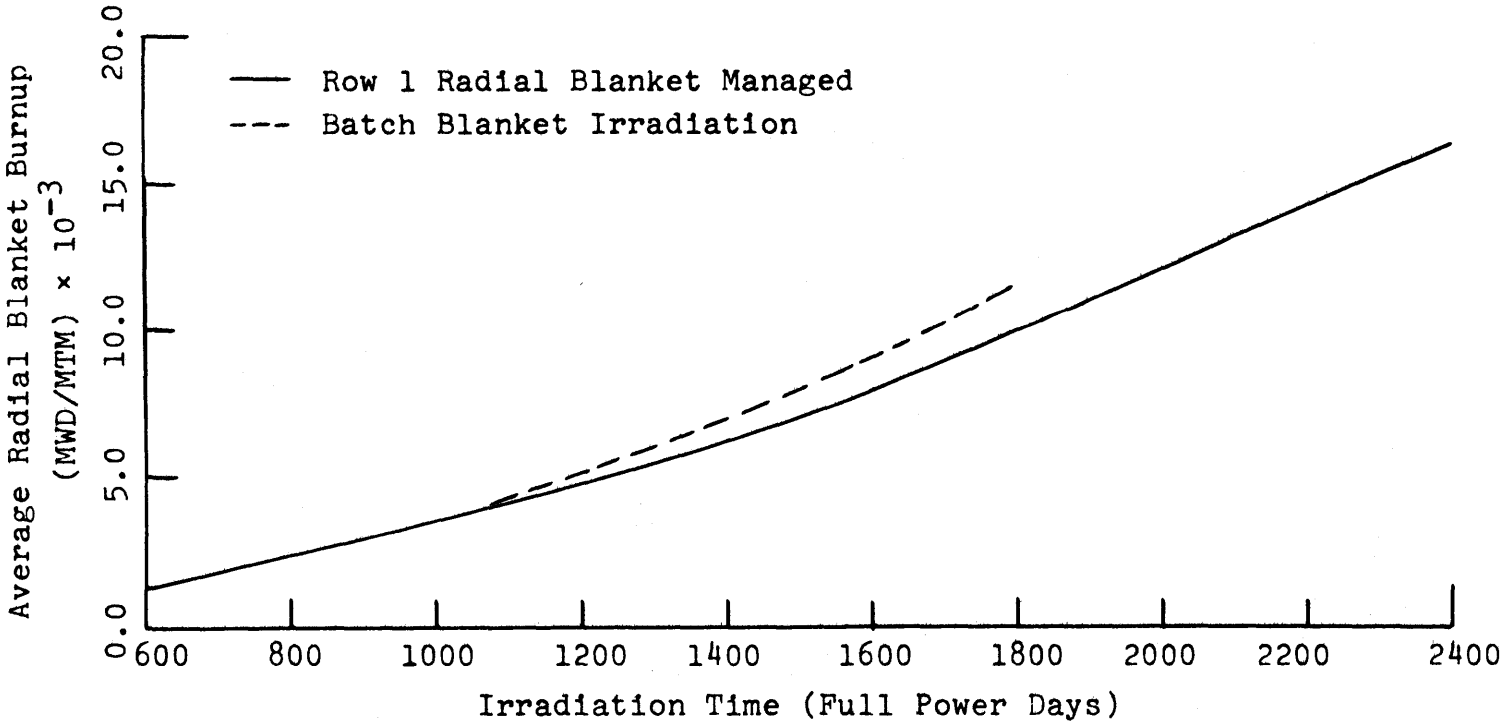

Fig. 4.45 The Effect of Radial Blanket Row 1 Management on the Average Burnup of Row 2, Thorium Blanket System

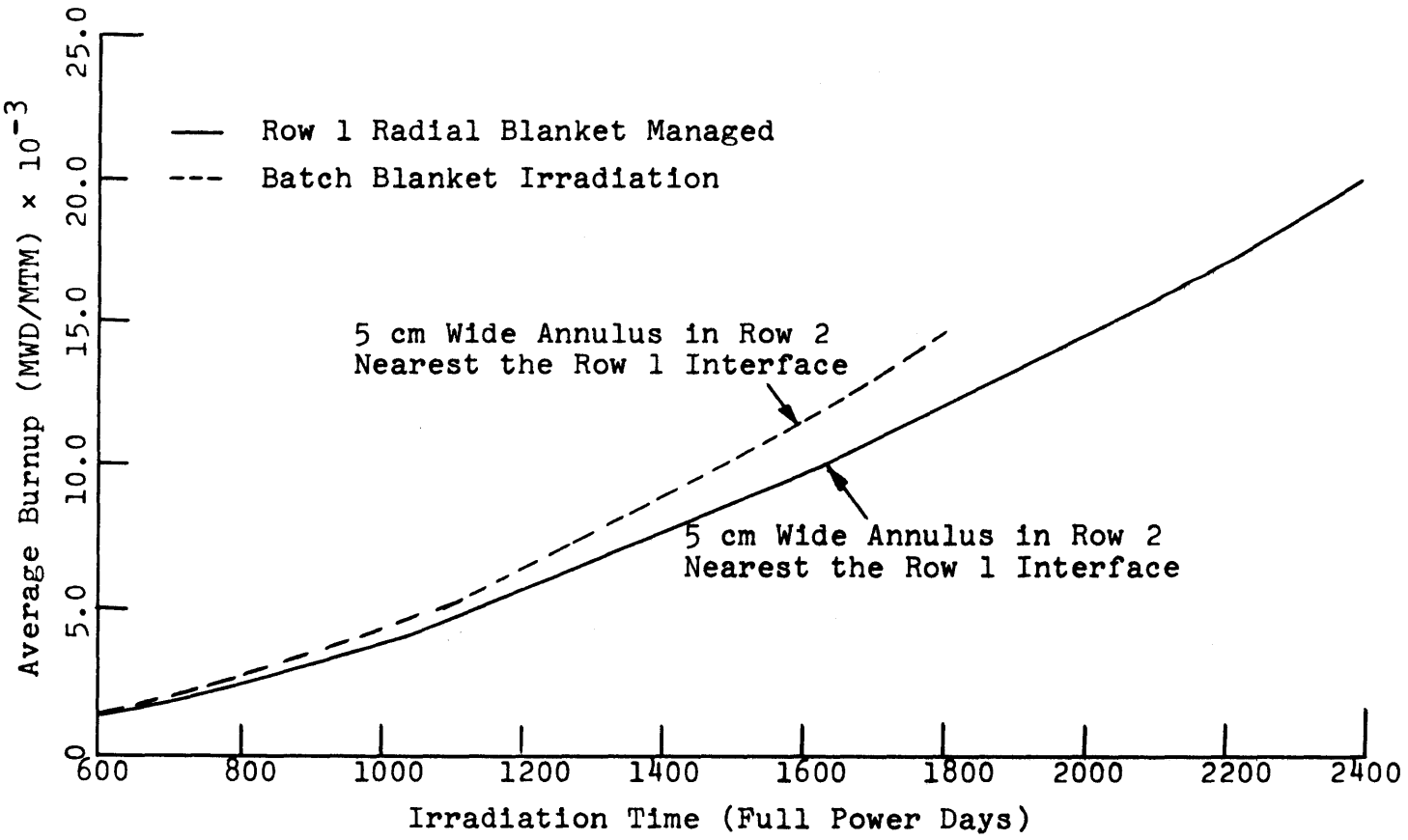

various cross sections of interest occurred in the radial blankets. These variations were shown to be more pronounced at greater distances from the core interface. The data presented earlier were, however, for batch blanket irradiation. It might be expected that zone scatter management of row 1 would lead to more constant flux in all regions, and thus improve the accuracy of the SAM method. Figures 4.46 and 4.47 show the product of the flux and the cross section for three zones in the radial blanket. Figure 4.46 is for U-233 absorption reactions while Fig. 4.47 is for Th-232 capture reactions. Comparison of these curves with Figs. 4.31 and 4.32 (for the batch irradiation) show that indeed row 1 management has improved the constancy of the flux times cross section products of interest. Variations in this product are, however, still significant. Consequently, local predictions using the SAM method, especially in blanket regions far removed from the core interface, should be undertaken with caution. This argument again corroborates the use of the burnup code 2DB to generate more precise material inventories for this study.

4.6 IN-OUT SHUFFLE BLANKET MANAGEMENT

4.6.1 Introduction

A more complicated radial blanket management scheme than the region scatter method discussed in the previous section is in-out shuffle. In this scheme, currently being considered by Westinghouse for use in the LMFBR demonstration plant, the blanket is managed by placing unirradiated assemblies in radial blanket row 1, and moving the irradiated row 1 and row 2 assemblies into rows 2 and 3,

Fig. 4.46 The Effect of Irradiation with Row 1 Radial Blanket Management on the One Group Reaction Parameter, Th-232 Blanket System, U-233 Absorption Reaction

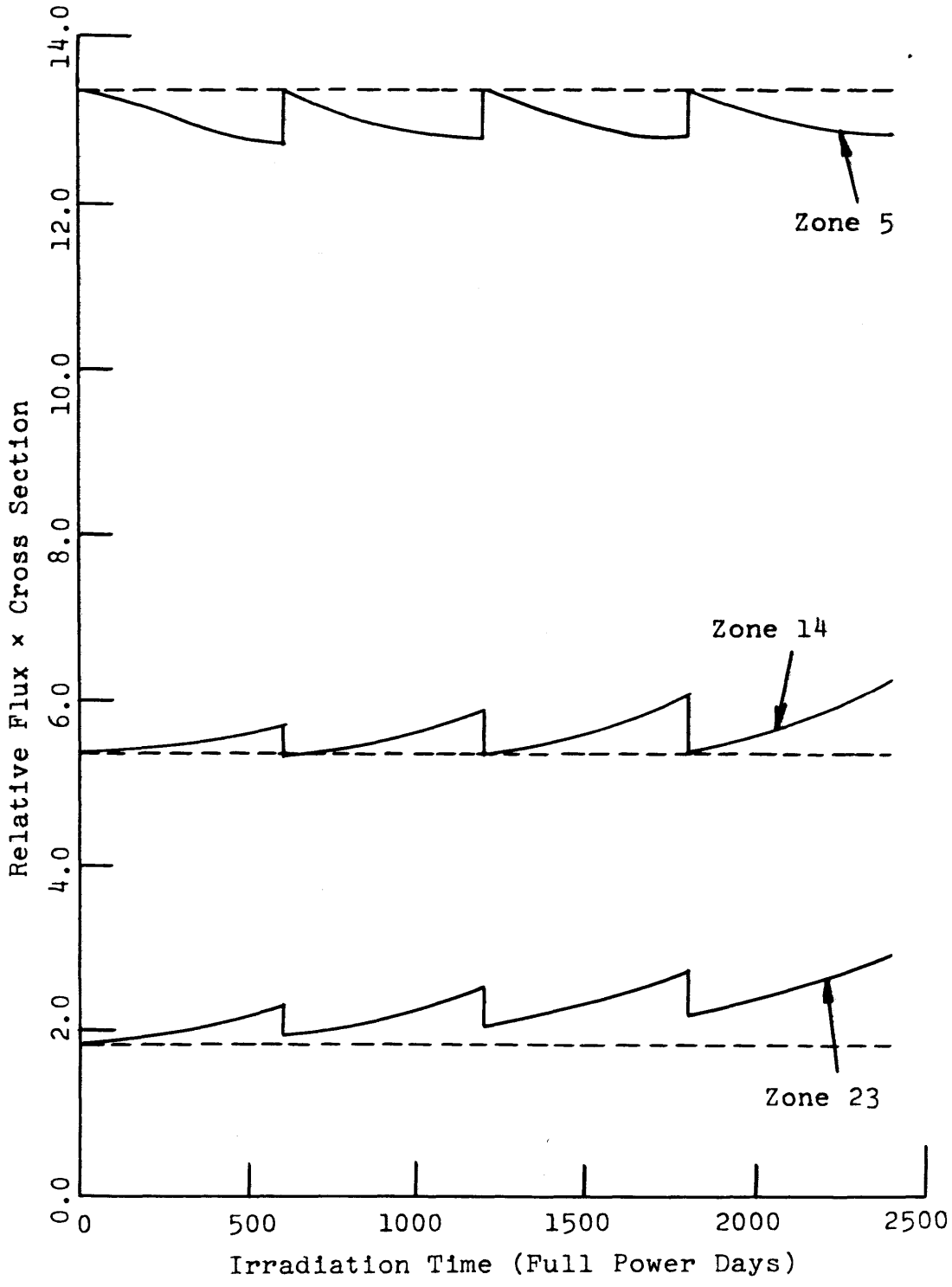

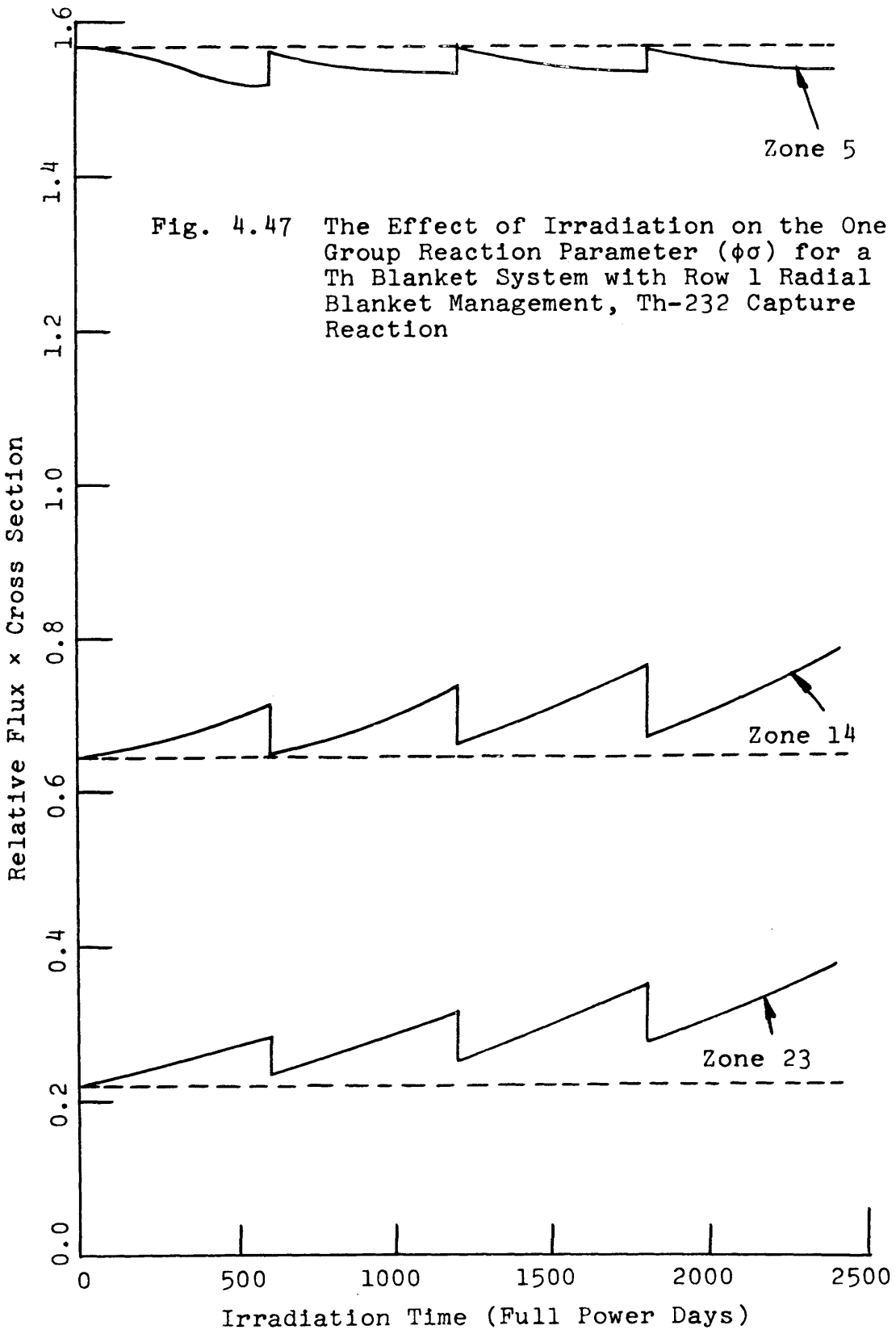

Fig. 4.47 The Effect of Irradiation on the One Group Reaction Parameter ($\phi\sigma$) for a Th Blanket System with Row 1 Radial Blanket Management, Th-232 Capture Reaction

respectively. This operation is performed at some predesignated irradiation interval. Qualitatively, the chief advantage of this scheme appears to be that the fissile inventory in the radial blanket is distributed such that the outer rows, where the flux is lower, have higher fissile concentrations. This leads to a condition in which the radial power distribution is flatter than for a batch managed or region scatter managed blanket. Because the power distribution is flatter, the blanket assembly duct wall temperature gradients are smaller, and the design problems related to the core restraint system are less severe. Another effect which will tend to reduce the core restraint system design problems is the reduced flux gradient across the radial blanket leading to a reduction in the contribution of duct wall irradiation induced swelling to radial blanket deformation.

The major possible disadvantage of in-out shuffle blanket management appears to be economic. If we neglect the possible effect of power and flux flattening on increased blanket assembly lifetime, the following economic variables must be considered in evaluating in-out shuffle management:

1. Possible reduction in the radial blanket maximum power swing will lead to an improvement in the system thermodynamic efficiency, an economic asset (B5);
2. It is claimed that increased average radial blanket fissile inventory will lead to an increase in the fissile carrying charge, an economic detriment (H6);
4. The increase in the number of times a blanket assembly must be handled in a shuffle management scheme will decrease plant availability, and have a corresponding negative impact on system economics (V1).

These economic parameters will be discussed in more detail in section 5.3.5. As a preview of that section, it can be mentioned here that the summation of all effects which differentiate batch management economics from in-out shuffle economics tend to cancel one another. Thus, with the possible exception of the effect of extending assembly lifetime and simplifying core restraint design, in-out shuffle blanket management appears to have no clear associated economic incentive or penalty. The primary purpose of the next section is to discuss the breeding performance of a system in which in-out shuffle management is practiced.

4.6.2 Comparison: In-Out Shuffle vs. Batch Management

A first estimate of the effect of in-out shuffle management on breeding performance was obtained in the following manner. Material inventories from the batch irradiation case were used with the standard economic environment for a private utility (see Table 5.1) to determine the economic optimum irradiation time for the entire radial blanket. (For this analysis the uranium blanketed system was considered because the deviation from linearity of the row 1 fissile inventory vs. irradiation time curve was greater than for the thorium blanketed system (see Figs. 4.12 and 4.13). This optimum time was determined to be approximately 1800 days. Because the radial blanket was composed of three rows, the shuffle cycle was determined to be 600 days or one third of 1800 days. Next a burnup calculation was performed using 2DB. In this calculation the core, axial blanket, and row 1 radial blanket were replaced every 600 full power days. Also, at 600-day intervals the radial blanket was shuffle managed. This consisted of moving the material inventories from rows 1 and 2 into rows 2 and 3, respectively.

This refueling and shuffle operation was carried out until an equilibrium condition was achieved in the radial blanket. This required four cycles. Figure 4.48 shows the inventories in the radial blanket for both the batch irradiation case and for the equilibrium in-out shuffle management case. As shown, if it is assumed that each assembly is irradiated for a total of 1800 days, the power swing (as indicated by the variation in fissile inventory) is smaller both for any individual row and for the blanket as a whole for the in-out shuffle management case.

The data in Fig. 4.48 can be replotted to show the total inventory contained within the radial blanket at any time during the irradiation cycle. Figure 4.49 shows this information. As expected, the average blanket fissile inventory over the irradiation interval being considered is significantly higher for the shuffle management scheme than for the batch irradiation scheme.

It is interesting to compare the relative breeding performance of each radial blanket row for the batch irradiation and shuffle management cases. Figure 4.50 shows the total fissile inventory produced in each row of the radial blanket up to a given time in the irradiation cycle. As shown, row 1 contributes relatively more to the total fissile inventory produced in the shuffle management scheme than in the batch irradiation, while the converse is true in rows 2 and 3. This might be expected because the shuffle management scheme removes the fissile material produced in row 1 to row 2, where the flux is lower, at fairly frequent intervals, thus reducing the amount of fissile material burned out of row 1. The fissile inventories produced in rows 2 and 3 are less in the shuffle management scheme than in the batch irradiation, both because the flux in those regions is lower and because more fissile

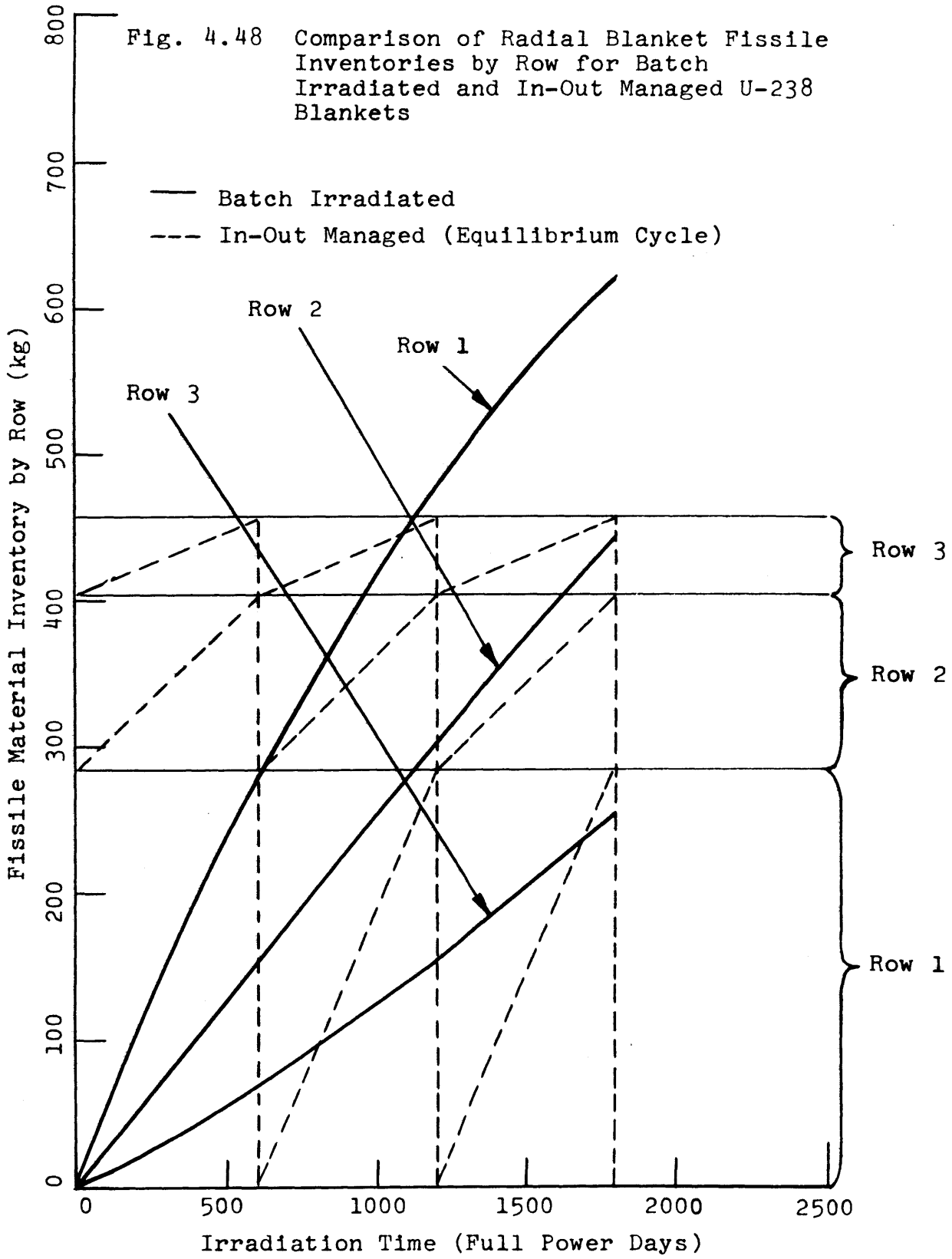

Fig. 4.48 Comparison of Radial Blanket Fissile Inventories by Row for Batch Irradiated and In-Out Managed U-238 Blankets

Fig. 4.49 Comparison of Total Radial Blanket Fissile Inventories for Batch Irradiation and In-Out Shuffle Management (Equilibrium Cycle)

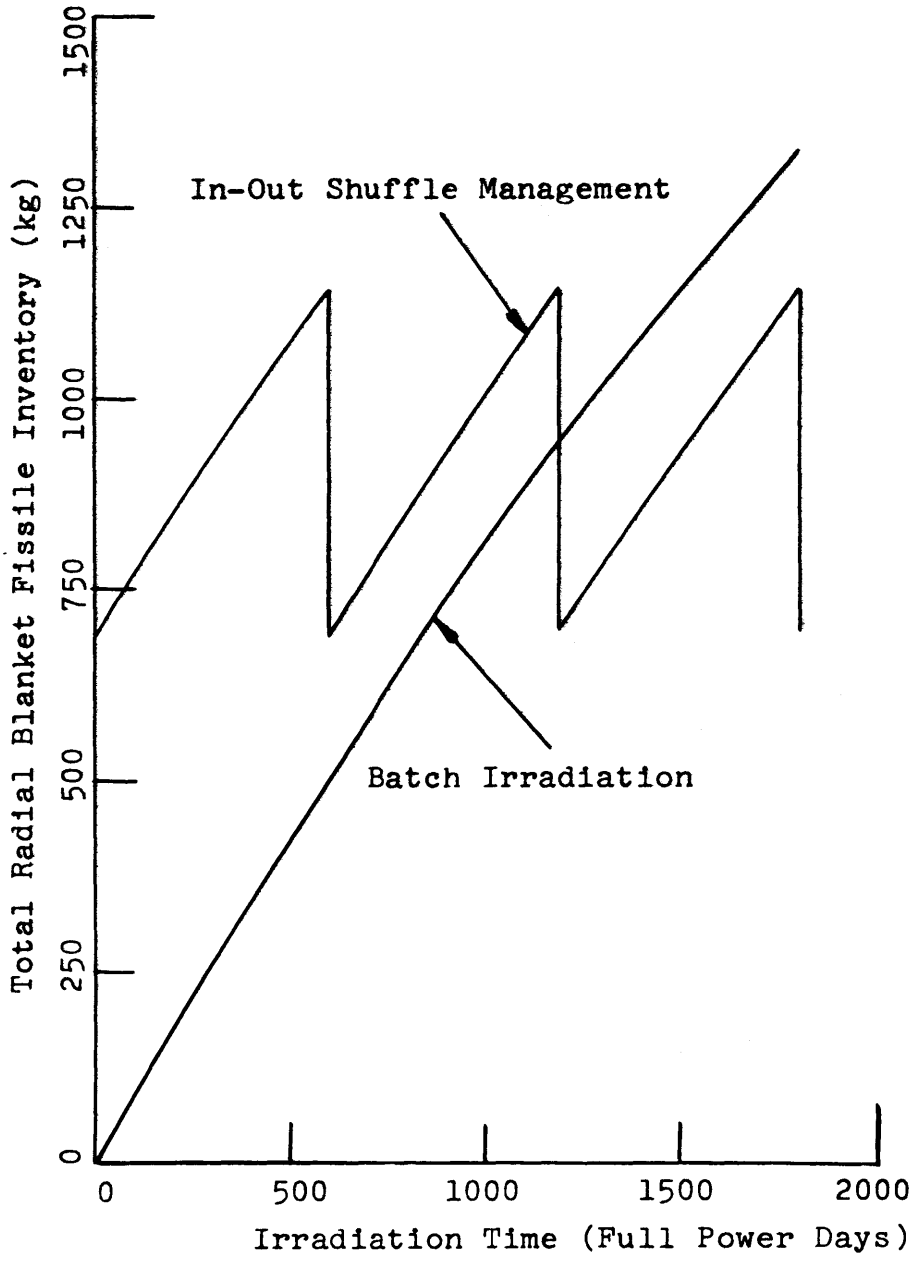

Fig. 4.50 Comparison of the Total Mass of Fissile Material Produced in the Radial Blanket for Batch and In-Out Shuffle Management of a Uranium Blanket

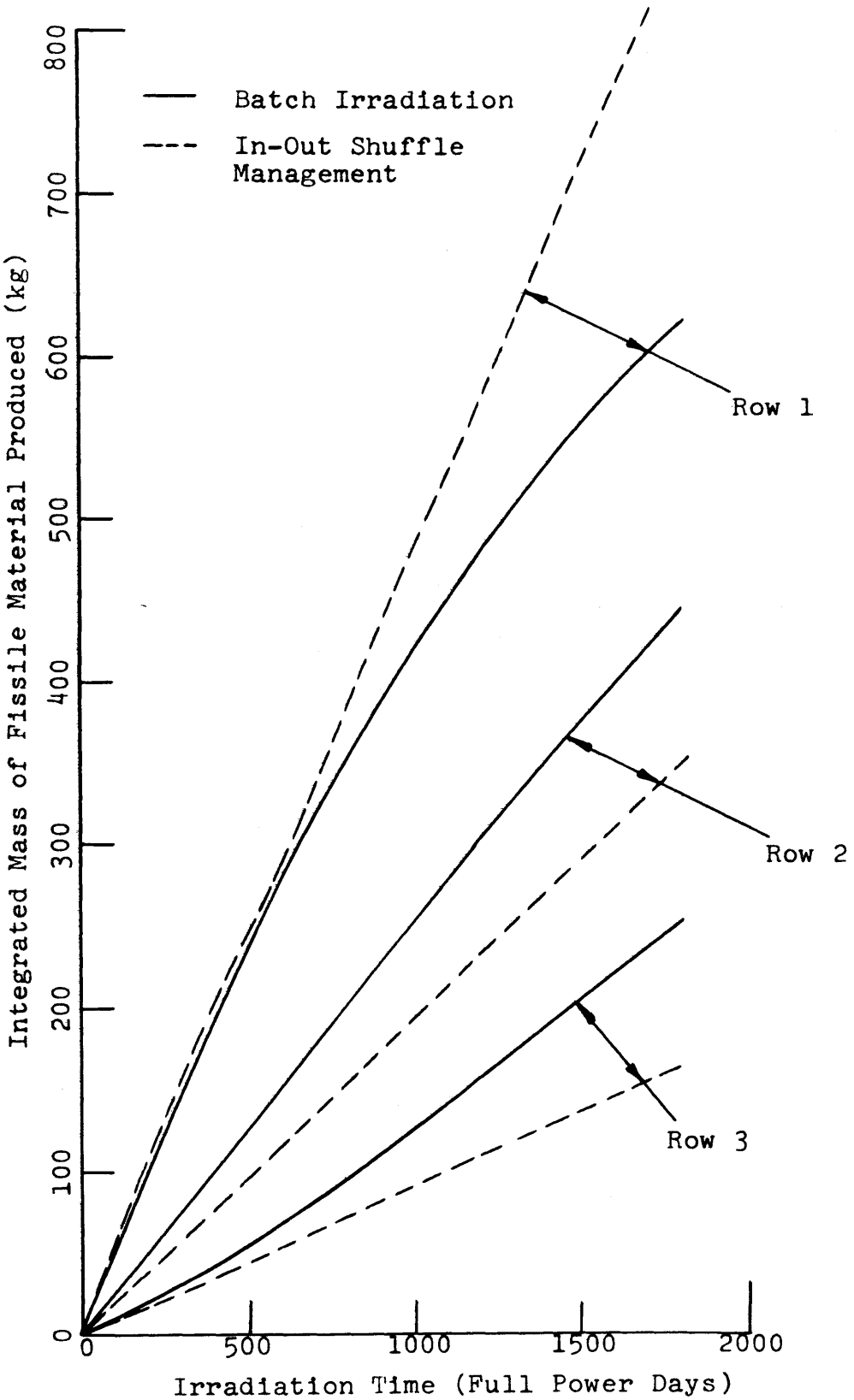

material is burned up per fertile capture. This results from the fact that the average concentration of fissile material in row 1 is lower than in the batch case, while that in rows 2 and 3 is higher than in the batch case. It should be noted that because of the changes in blanket performance resulting from consideration of shuffle management, the economics of row 3 would be expected to be less attractive from two points of view. First, the use of a three-row blanket causes fissile material created in rows 1 and 2 to reside in the system longer, thus increasing the carrying charges. Second, the breeding performance of row 3 is degraded when shuffle rather than batch blanket management is used.

Finally, consideration should be given to the total blanket breeding performance. Figure 4.51 shows the total fissile inventory produced in the entire radial blanket integrated to a given time in the irradiation cycle. As shown, the breeding performance of the entire radial blanket is virtually the same for managed and batch cases. The difference in total fissile inventory produced is only about 47 kg out of the approximately 1350 kg produced, or about 3.5%. A further discussion of management schemes will be presented in section 5.3.5 where it will be shown that, within the limitations of this study, no significant differences exist among the different management schemes from an economic point of view.

4.7 U-233/Th-232 CORE AND BLANKET SYSTEM

4.7.1 Introduction

Because the previous studies which considered the use of the U-233/Th-232 cycle for LMFBR's (A1, H1, L4, L5, O1, S1) were conducted in the early 1960's (see sec. 1.2), it was decided to take a

Fig. 4.51 Total Radial Blanket Fissile Inventory Produced for Batch Irradiation and In-Out Shuffle Management of a Uranium Blanket

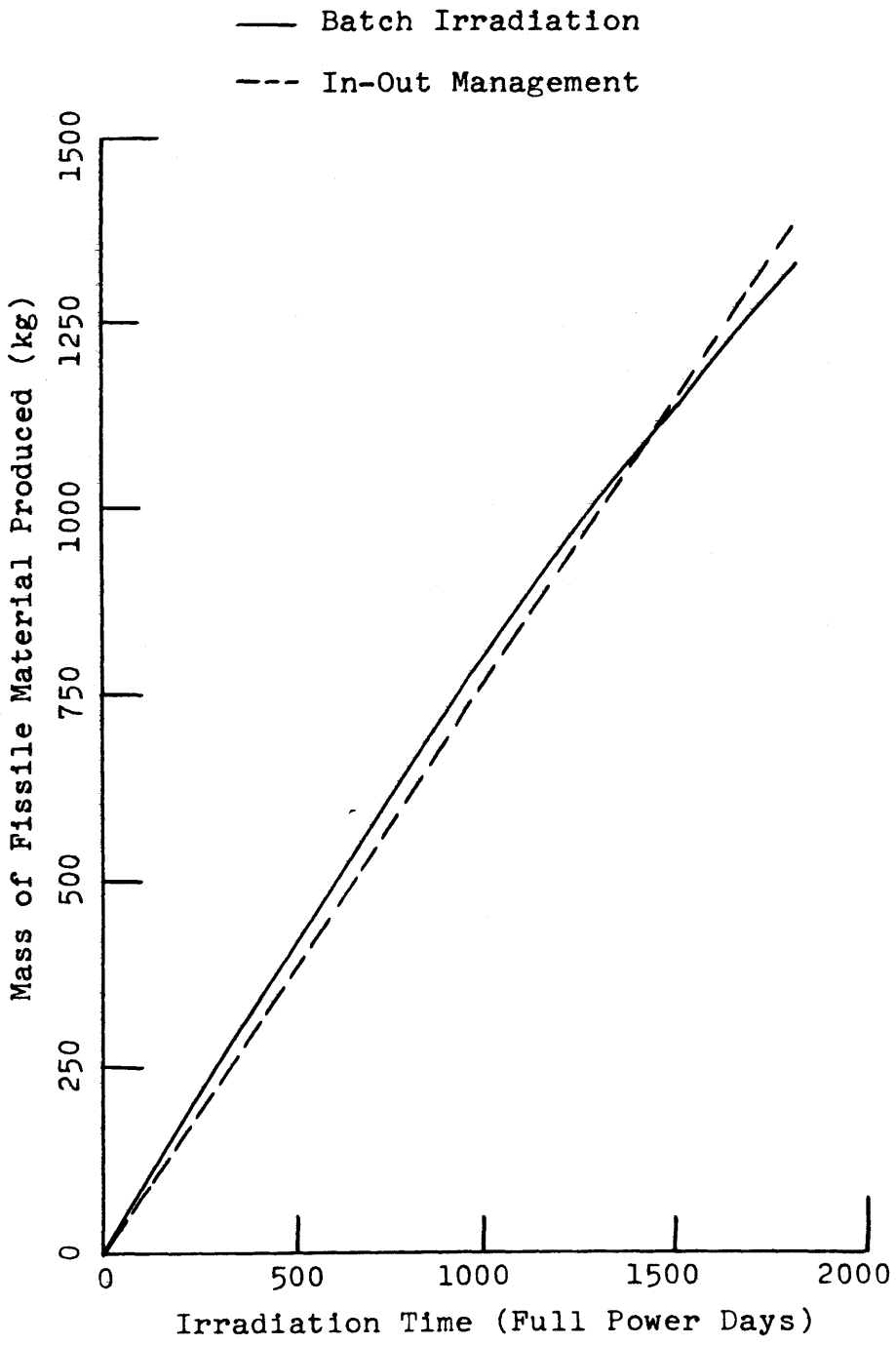

cursory look at this system. The analysis performed in this study is different from previous work in three critical areas:

1. Only oxide cores have been considered here;
2. The ABBN cross section set has been used here, in conjunction with the 1DX code which was employed to perform resonance self-shielding analysis;
3. The discovery of stainless steel swelling in the late 1960's led to an important LMFBR design change: the reduction of the volume fraction of fuel in the core from as high as 50% to approximately 30%.

Because of the impact of these three factors on LMFBR system performance, it was felt that a new look at the U-233/Th-232 system was justified.

4.7.2 Burnup Studies

4.7.2.1 System Definition

The same techniques as discussed earlier (see sec. 4.2) were used in this analysis to develop cross sections and to define system fissile enrichment and poison concentration. In summary, the procedure was the following:

1. Generate resonance self-shielded cross sections from the modified ABBN cross section set (N1) using 1DX (H2);
2. Collapse the 26-group self-shielded cross sections to 4 groups using ANISN (E1);
3. Define the dependence of the system k_{eff} on irradiation, initial fissile concentration in the core, and poison concentration using 2DB (L10);
4. Specify core fissile loading and poison concentration to allow the burnup to be performed in a manner consistent with those reported earlier.

Figures 4.52 and 4.53 show the system k_{eff} dependence on fissile loading (Fig. 4.52) and on poison concentration (Fig. 4.53). Comparison of Fig. 4.52 with Figs. 4.1 and 4.2 reveals that system k_{eff} has nearly the same dependence on core fissile loading for all three systems being analyzed here. Following the procedures outlined in section 2.5 to define system composition led to the characteristics presented in Table 4.16.

TABLE 4.16 Initial Characteristics for a U-233 Fueled LMFBR System

Region	Fissile Enrichment (%)	B-10 Concentration (atoms/barn-cm)
Core Zone I	17.47	2.1×10^{-4}
Core Zone II	27.00	2.1×10^{-4}
Axial Blanket	0.0	4.83×10^{-4}

	Number Densities (atoms/barn-cm)	
Material Name	Core Zone I	Core Zone II
U-233	0.001091	0.001685
Th-232	0.004807	0.004252
Oxygen	0.01179	0.01187

Comparison of Table 4.16 with Table 4.6 shows that the required core enrichment for the U-233 system to meet the same burnup objectives as a plutonium fueled and uranium blanketed system is 37% greater than for the Pu/U system. This significant increase in the required core fissile inventory would be expected to dramatically degrade the economic performance of the U-233/Th-232 system with respect to the Pu/U-238 system. This expectation will be verified in section 5.3.6.

Fig. 4.52 The Effect of Core Loading on System K_{EFF} for a U-233 Fueled LMFBR

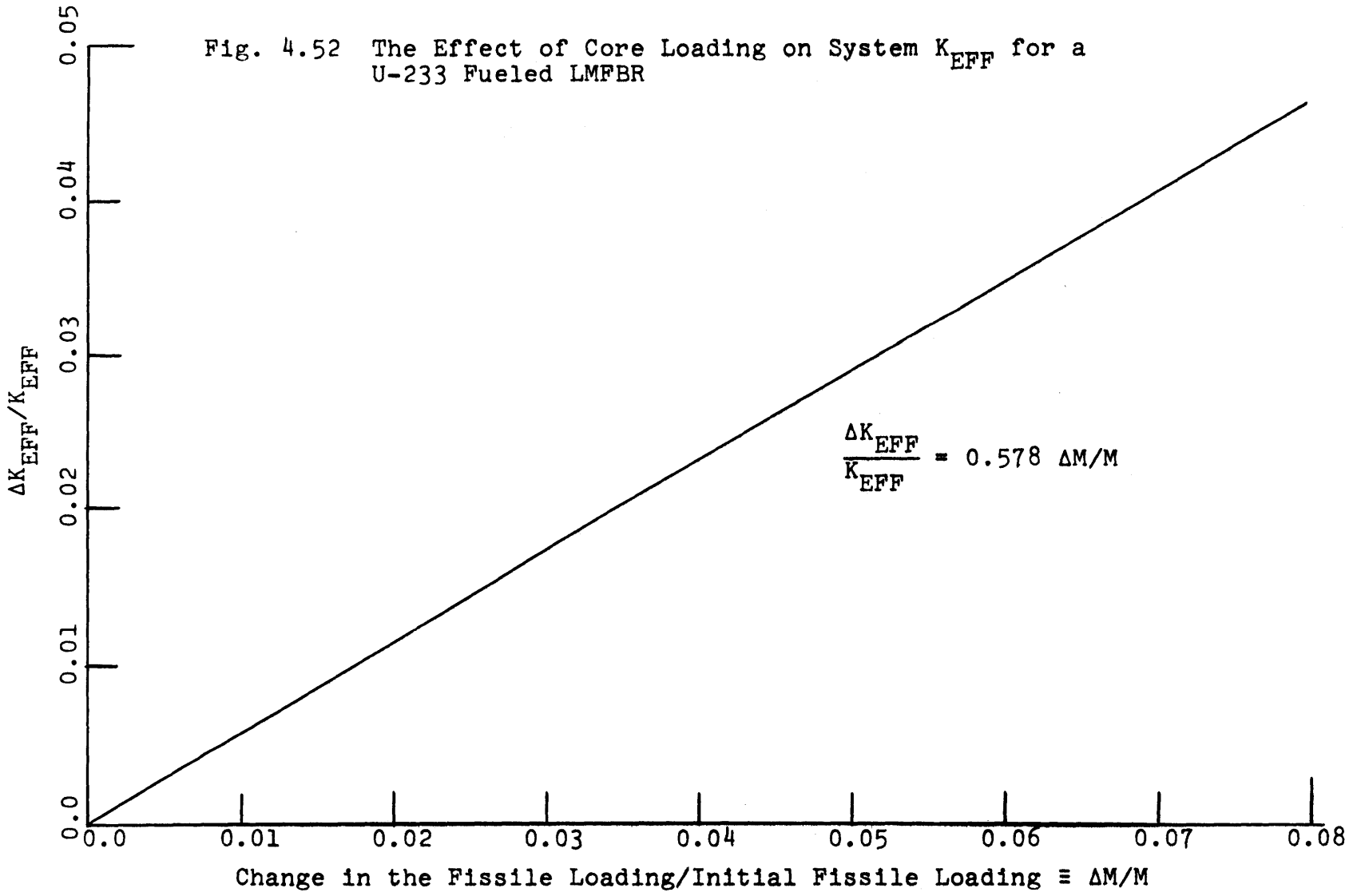

Fig. 4.53 The Effect of Poison Concentration in the Core on System K_{EFF}, U-233 Fueled System

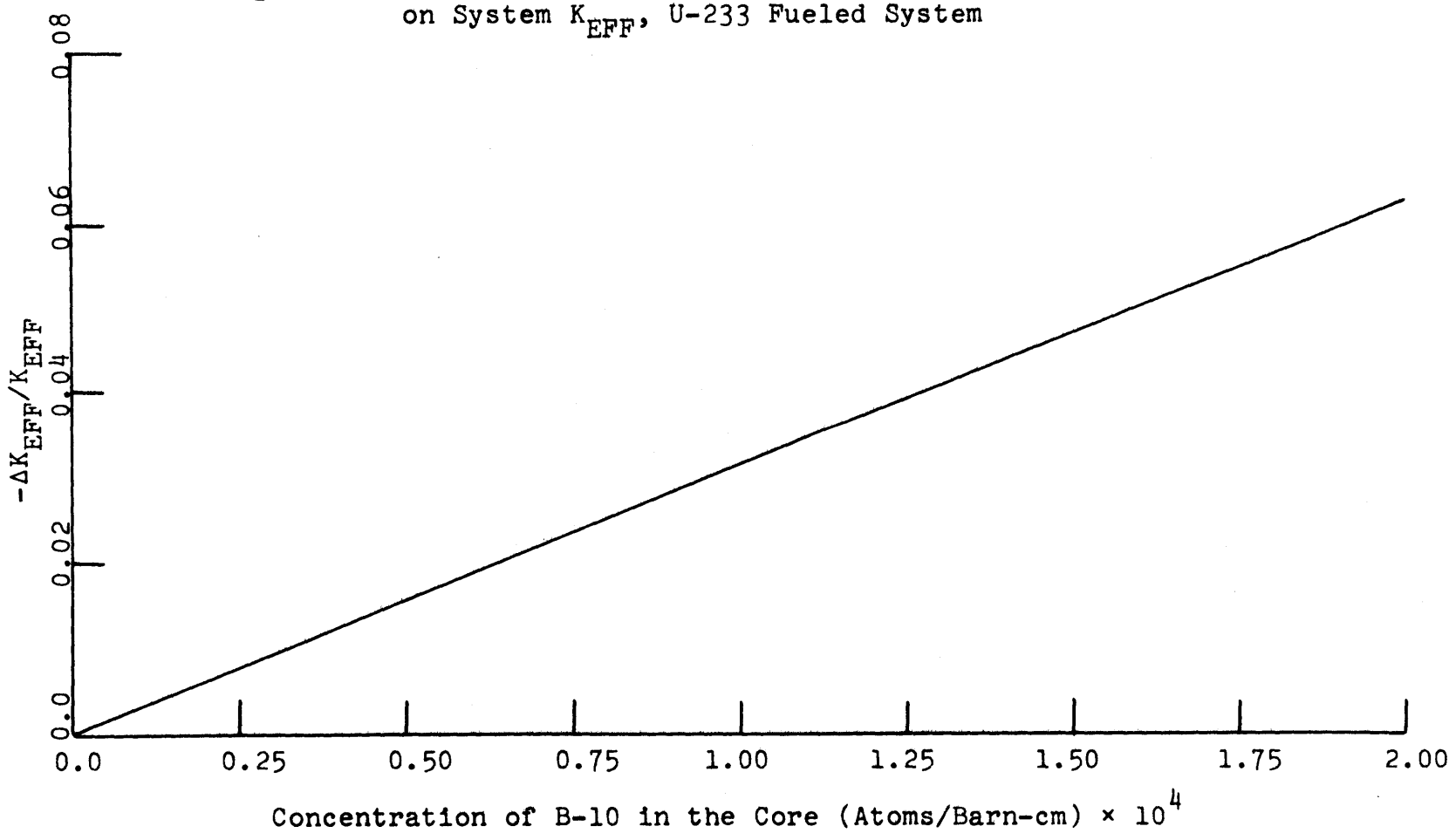

4.7.2.2 System Breeding Performance

To show the consistency between the burnup of the U-233 system and those discussed earlier, consider Fig. 4.54. This figure shows that the system k_{eff} for the U-233 core is as nearly as possible the same as for the plutonium core, given that the core is batch irradiated in both cases for 600 full power days.

The comparative breeding performance for the blankets of this system and those of the plutonium/uranium system being used as a basis of comparison is shown in Fig. 4.55. As shown, a substantial difference exists between the blanket breeding performance for the two systems with the plutonium/uranium system exhibiting superior characteristics for both blankets. Figure 4.56 shows the average U-232 concentration in the core of the U-233 fueled system. Comparison of this curve with those presented in Figs. 4.22 and 4.23 shows that, as expected, the average concentration of the U-232 contaminant in the core is nearly twice the maximum concentration in either blanket after 600 days. This factor, resulting from the large fast flux in the core, will again lead to a degradation of the U-233 fueled system economic performance with respect to that of the plutonium fueled systems.

The final comparison to be made is between average core burnups. Because of the poorer relative blanket breeding performance of the U-233 fueled system, one might expect the core to contribute a significantly larger fraction of the total fission rate in this system than in the plutonium fueled system. Figure 4.57 shows a comparison between average core burnups for the U-233 and the plutonium fueled systems. As shown, the qualitative argument has correctly predicted

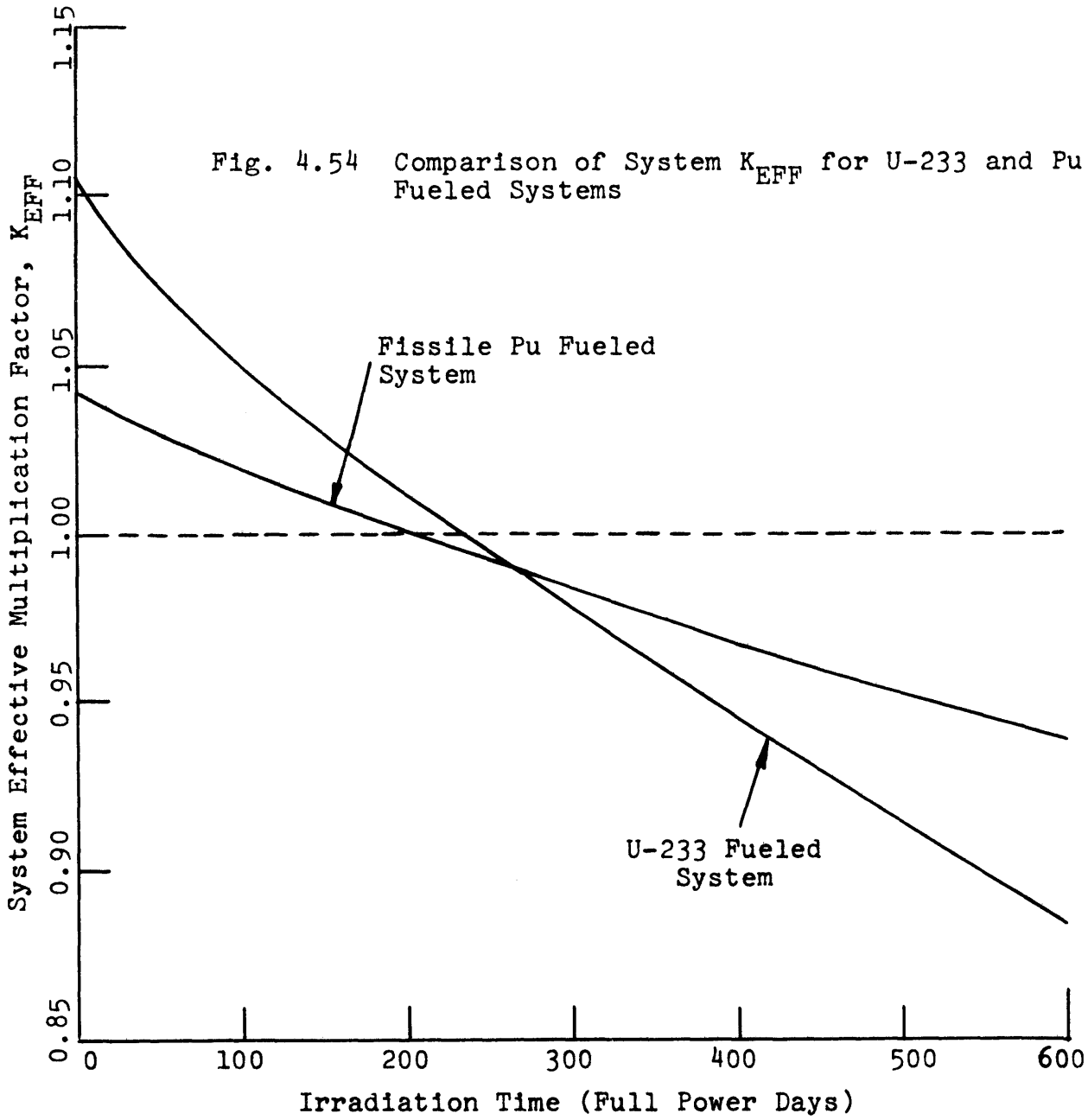

Fig. 4.54 Comparison of System K_{EFF} for U-233 and Pu Fueled Systems

Fig. 4.55 Radial and Axial Blanket Breeding Performance

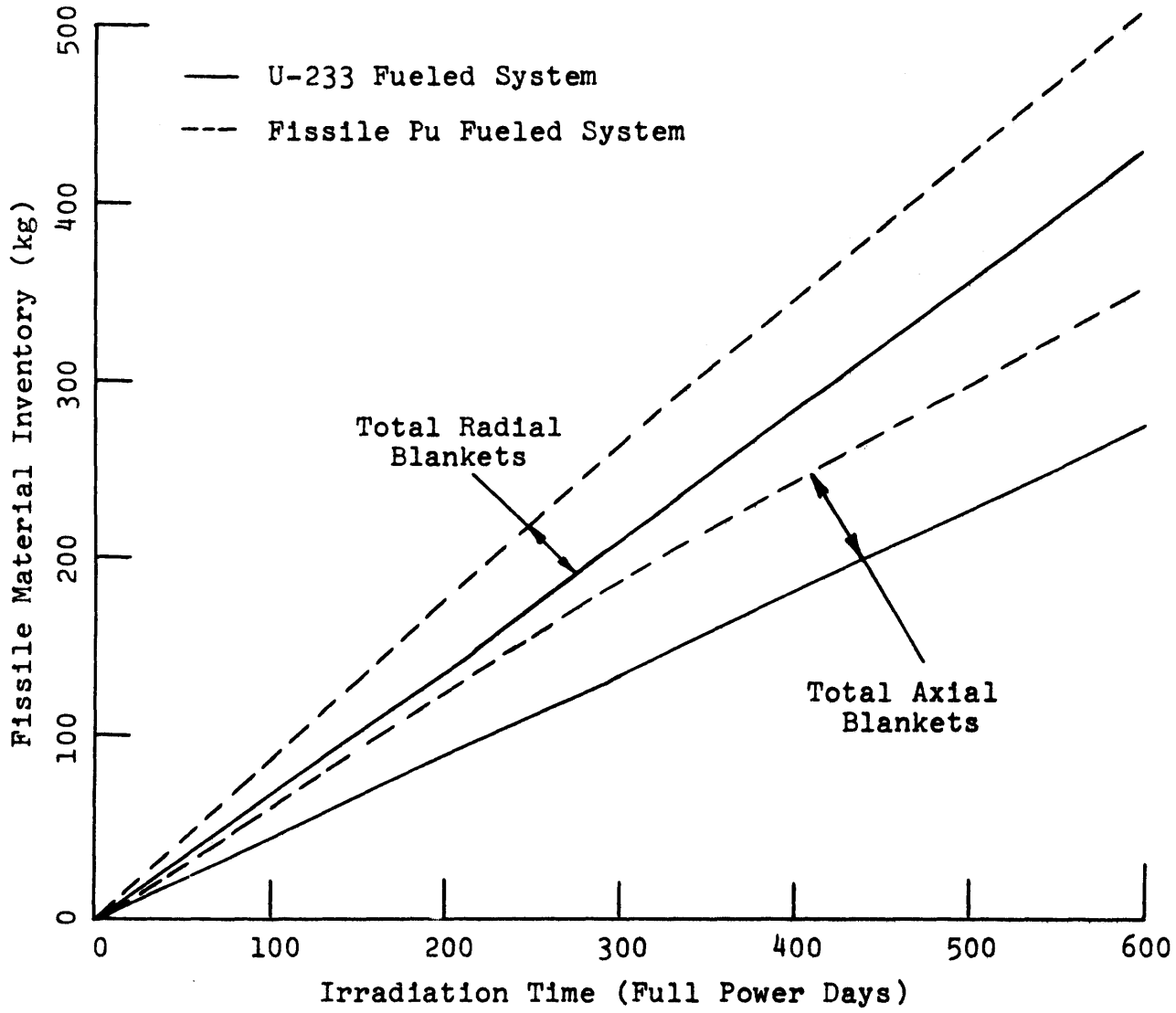

Fig. 4.56 Average Core U-232 Concentration for a U-233 Fueled System

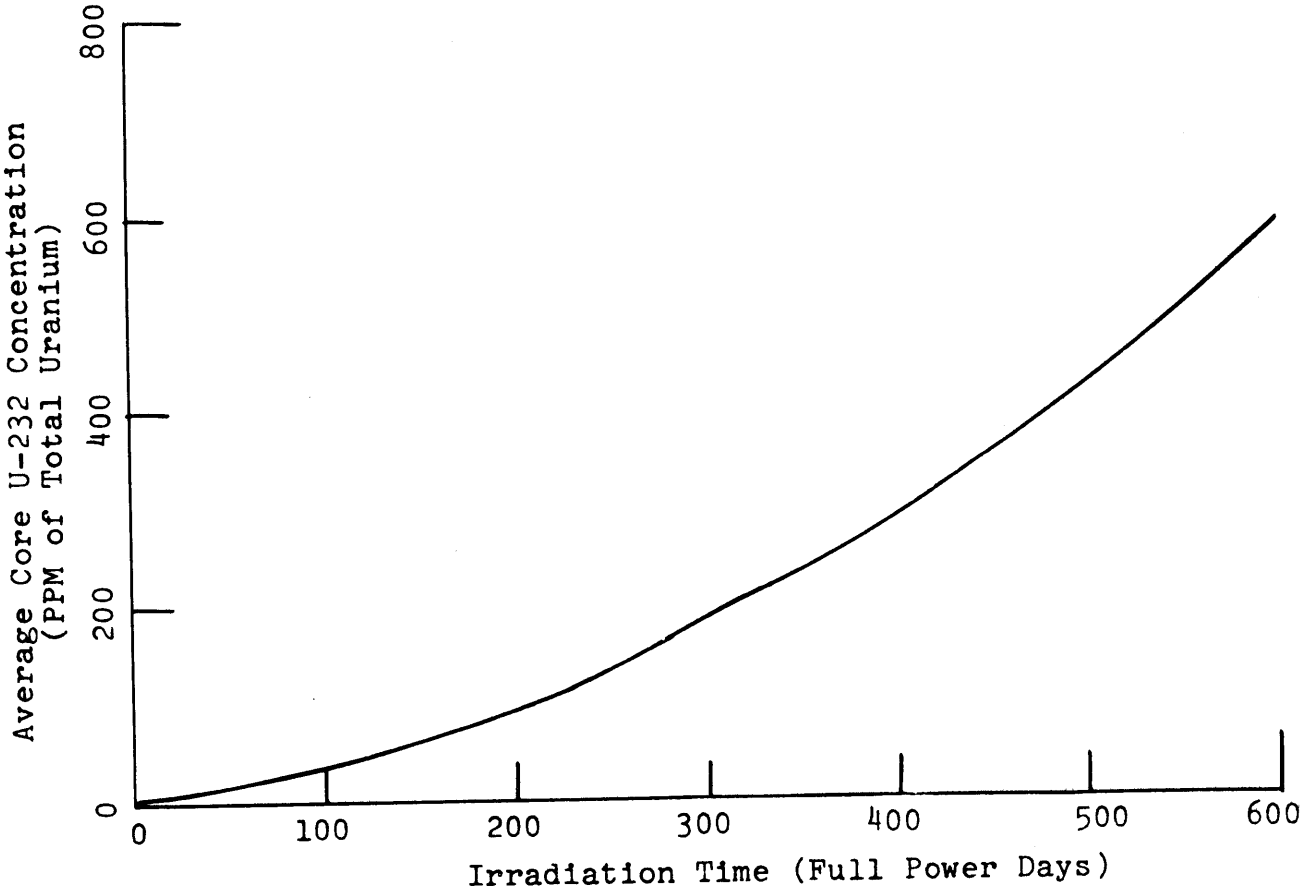

Fig. 4.57 Comparison of Average Core Burnups for U-233 and Pu Fueled Systems

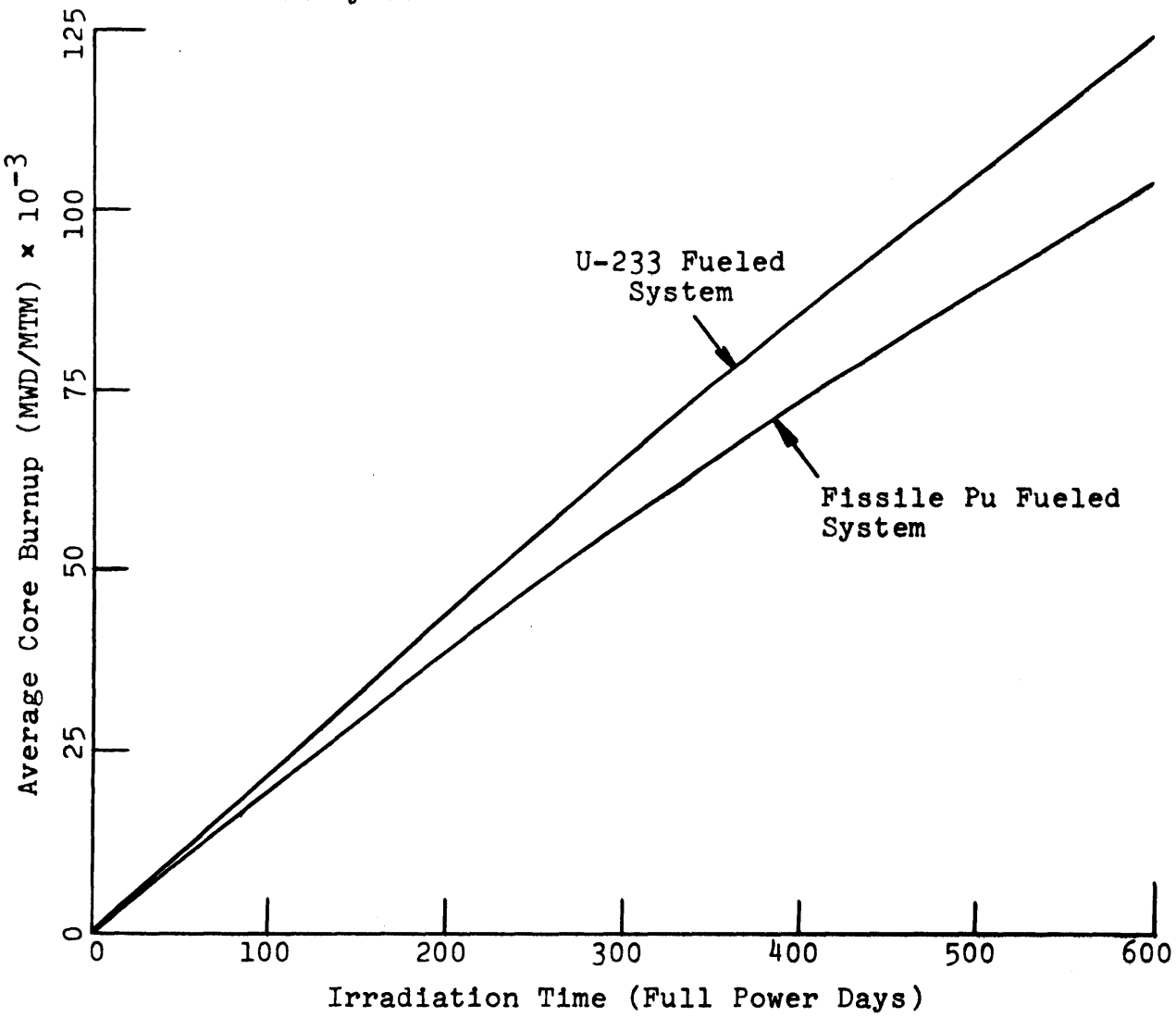

that the average burnup in the U-233 fueled system is larger than that in the plutonium fueled system.

4.7.2.3 Summary

It has been shown in this section that an LMFBR operating on the U-233/Th-232 cycle performs less effectively than a comparable system using the Pu/U-238 cycle in the following respects:

1. Higher core inventory is required in the U-233 fueled system;
2. Inferior blanket breeding characteristics are experienced with the U-233 fueled system;
3. A higher average core burnup and a larger reactivity swing results for the same total power produced with a U-233 fueled system;
4. The contaminant U-232 is produced in significant quantities in the core of the U-233 fueled system.

All these factors are expected to contribute to make the economic performance of the U-233 fueled system significantly poorer than that of a comparable plutonium fueled system. This economic analysis will be presented in section 5.3.6.

4.8 SUMMARY AND CONCLUSIONS

This chapter has considered the methods used in evaluating the burnup characteristics of three systems. These systems were

1. a plutonium fueled system with natural uranium blankets,
2. a plutonium fueled system with thorium blankets,
3. a U-233 fueled system with thorium blankets.

The geometry of the calculational model used for the analysis of all three cases was the three-row radial blanket system proposed by

Brewer (B3). The analysis was performed by using the modified ABBN cross section set (N1), in conjunction with the computer code 1DX (H2) which was used to generate a 26-group set of resonance self-shielded cross sections. These cross sections were then collapsed to 4 groups using the ANISN (E1) code. The region collapsed cross sections were then used in the 2DB (L10) code to predict the breeding performance of the systems of interest.

Results derived in this section fall into three categories, depending how the radial blanket was managed. In the batch irradiation case, the breeding performance of the uranium blanket system was superior to that of the thorium blanket system in the radial blanket, while the reverse was true in the axial blanket. In the case in which the row 1 radial blanket was replaced at its economic optimum, the same general ranking of performance prevailed. However, the relative performance of the thorium blanket system with respect to the uranium blanket system improved when blanket zone scatter management was used. Other major effects of blanket zone scatter management were to increase very slightly the fissile isotope production rate in the blankets, and to increase somewhat the average core burnup experienced in a batch core burnup of 600 full power days. The same general trends were observed for in-out shuffle management as for zone scatter management.

The performance of the U-233 fueled system was shown to be inferior to that of either of the plutonium fueled systems in required core inventory, blanket breeding characteristics, and core average burnup.

Chapter 5

ECONOMIC ANALYSIS

5.1 INTRODUCTION

As discussed in Chapter 1, the chief motivation for assessing the performance of thorium as a blanket material for LMFBR's is an economic one. It has been estimated by several investigators that the value of U-233 will exceed that of fissile plutonium for some time into the future. If these estimates are correct, producing U-233 in LMFBR blankets may be economically more attractive than producing fissile plutonium even if a lesser quantity is produced.

The purpose of this chapter is to quantify the relative economic performance of the two blanket systems using the physics depletion information presented in Chapter 4. The format of this chapter is as follows. First, the reference economic environment will be presented. Next, the results of the economic analysis of the three reference systems (plutonium core with uranium and thorium blankets, and U-233 core with thorium blankets) will be discussed, followed by a development of the ratio of the value of U-233 to that of fissile plutonium (parity ratio) above which it is economical to use thorium blankets for LMFBR's. Following the parity ratio discussion, a generalized model for predicting the optimum irradiation time for radial blanket rows will be developed and verified by economic parametric analysis. Lastly, the effect of uncertainties in the analytical methods and the blanket system physical performance on relative blanket economic performance will be discussed.

The calculational tool used to perform the economic analysis was a modified version of Brewer's code SPP1A (B3). The modifications made to the code are discussed in section 2.6. Appendix C contains a listing, input description, and sample problem for the modified code, hereafter referred to as BRECON. The two primary modifications made to the code were: first to eliminate the physics depletion section (SAM) and to provide for input of material inventories from an external source (the 2DB code in this analysis), and second to include the cost terms and penalties associated with U-233, Th-232, and U-232. The modified code, BRECON, generates the same economic data as did the original, SPP1A. These data are the contribution to the total cost of power (in mills per kilowatt hour, and other units) at each specified point in the irradiation cycle for any particular annular region of interest. The advantage of the cash flow method (CFM) used by Brewer is that it allows evaluation of the contribution to the total cost of power produced by a reactor system of any physically distinct region in the reactor. Thus a single row of the radial blanket can be evaluated independent of the remainder of the system. If the power cost contribution at its economic optimum or its irradiation limit is negative, then it is desirable to include that row in the system design. Care must be taken, however, in using the results of the code to make design decisions. Consideration must always be given to the impact of the decision related to part of the system on the economics of the remainder of the system. For example, the power cost contribution of the reactor core might be reduced somewhat by replacing row 1 of the radial blanket with a row of inconel reflector assemblies. However, a large penalty would be incurred by eliminating the fissile material bred in row 1. Thus the entire system

economics must be considered in any comparison of alternative designs. This procedure was followed in all comparative economics presented in this report.

In this chapter the primary emphasis will be on comparisons between systems in which the fuel is plutonium and either thorium or uranium blankets are used. (A brief discussion of the U-233 fueled system appears in sec. 5.3.4.) Because the present plans for the head end reprocessing of LMFBR fuel assemblies include either whole bundle or individual pin shearing prior to dissolution (A4, F5, F6), no significant penalty would be incurred by using a plutonium fueled core with a thorium axial blanket. Rather good separation of the core material from the axial blanket material could be achieved prior to reprocessing if whole bundle shearing is used, and excellent separation could be achieved if single pin shearing is used (U2). For this work, no penalty was assumed to be associated with separation of core and axial blanket material prior to reprocessing. In actual practice, losses could be limited to a few percent because the assemblies are expected to be sheared into 1-inch-long segments, and the axial blanket is approximately 16 inches long. This question is taken up again in the discussion of errors presented in section 5.6.

5.2 THE ECONOMIC ENVIRONMENT

The reference economic environment used in this study is that presented by Brewer (Ref. B3, Table 4.2). These conditions, summarized in Table 5.1, were developed by extensive review of the relevant literature, and are within the range projected for the mature U.S. nuclear fuel cycle economy (D7). A single modification to the earlier proposed

TABLE 5.1 Reference Economic Environment

Operation	Unit Fuel Processing Costs, $/kg		
	Core	Axial Blanket	Radial Blanket
Fabrication	314	80	69
Reprocessing	50	50	50

Isotope	Isotope Market Value, $/kg
U-238	0
Pu-239	10,000
Pu-240	0
Pu-241	10,000
Pu-242	0
Th-232	0
U-233	16,700

Financial Parameter	Value of Parameter	
	Private Utility	TVA
Income tax rate, τ	0.5	0.0
Capital structure		
Bond (debt) fraction, f_b	0.5	1.0
Stock (equity) fraction, f_s	0.5	0.0
Rates of return		
Bonds, r_b	0.07	0.075
Stocks, r_s	0.125	0.0
Discount rate, X*	0.08	0.075

* $X = (1-\tau)r_b f_b + r_s f_s$

environment is that the reprocessing cost estimate was revised upward to 50 $/kg (B4). The additions to the table include the values of Th-232 and U-233, and the financial parameters relevant to economic analysis of a publicly-owned utility such as TVA. The TVA financial parameters were obtained from Brewer (B6), and the U-233 value was derived from a study of the relative economic worth of U-233 and highly enriched U-235 as fuels for HTGR's (A2). The other important assumptions in the reference economic analysis were,

1. The time prior to the beginning of the irradiation at which the fabrication and material purchase cash flows occur, and the time after the end of irradiation at which the reprocessing and material credit cash flows occur were all assumed to be 0.5 years.
2. The penalty associated with the presence of U-232 contaminant in the U-233 produced in the blankets was that given in Table 2.12 (U1).

Because the incentive for using thorium rather than uranium as the blanket material for LMFBR's is primarily an economic one, it is important to present the current best estimates of the relative values of fissile plutonium and uncontaminated U-233. Table 5.2 shows the values of these isotopes as estimated by a number of investigators. By using this table consistently, it is possible to derive the parity ratio between U-233 and fissile plutonium. This information is presented in Table 5.3. The data for the light water reactors were developed for spectrum hardened LWR's. Any other LWR in which more efficient use is made of U-233, such as the Light Water Breeder Reactor under development by The Naval Reactors Division of the AEC, should be able to pay more for U-233 than indicated here. As shown in Table 5.3, in both LWR's

TABLE 5.2 Estimated Value of Fissile Isotopes

Isotope	Value ($/g)	Source	Reactor Type[1]
Fissile Pu	7.50	(B7)	LWR
U-235 (93% enriched)	14.33	(B8)	–
U-235 (3% enriched)	9.81	(B8)	–
U-235 (93% enriched)	12.00	(A2)	HTGR
U-233 (pure)	16.70	(A2)	HTGR
Fissile Pu (1980)	11.00	(K1)	HTGR
U-233 (1980)	16.20	(K1)	HTGR
Fissile Pu	10.00	(G1)[3]	HTGR
U-235 (93.5% enriched)	11.00	(G1)[3]	HTGR
Fissile Pu	7.416	(J1)	LWR
Fissile Pu	8.0	(L2)	LWR[2]
U-233	15.0	(L2)	LWR[2]
Fissile Pu (1975)	7.50	(D8)	LWR[2]
Fissile Pu (1985)	8.40	(D8)	LWR[2]

[1] LWR = light water reactor,
HTGR = high temperature gas cooled reactor.

[2] Spectral hardened LWR.

[3] Work performed at Gulf General Atomic under sponsorship of the Edison Electric Institute.

TABLE 5.3 U-233 to Fissile Plutonium Parity Ratio

Source References	Parity Ratio U-233/Pu	Reactor Type
(A2) and (G1)	1.53	HTGR
(L2)	1.88	LWR

and HTGR's the value of U-233 is quite high relative to the value of fissile plutonium. These parity ratios will be referenced later in the analysis used to obtain a break-even parity ratio for the production of U-233 vs. fissile plutonium in LMFBR blankets (see sec. 5.4).

Because of the relatively large uncertainties associated with the values of the economic parameters, studies were performed in which the economic environment was varied. Since Brewer has performed extensive economic parametric analyses in his work (B3), the number of variations examined here will be limited. Instead, a generalized correlation will be presented which has the effect of normalizing out variations in the economic environment (see sec. 5.5). This correlation relates the optimum irradiation time or the blanket enrichment at the optimum time, and an optimum economic parameter which includes all the significant economic variables.

5.3 CORE AND BLANKET ECONOMICS

5.3.1 Introduction

In the previous chapter the breeding characteristics of thorium and uranium radial blankets were presented for a number of blanket management schemes. The purpose of this section is to use the fissile inventories developed earlier to make economic comparisons between the various systems and management schemes. Because most of the economic comparisons will be based upon batch blanket irradiations, we will first address expected economic differences among management schemes. The format of this section will be to consider the system economic variations related to the following effects:

1. Core management
2. Batch blanket burnup
3. Zone scatter management
4. In-out management

The final topic to be discussed will be the economics of a U-233/Th-232 core and blanket system.

5.3.2 Effect of Core Management

Earlier, in section 4.3, a comparison was made between radial blanket breeding performance for systems in which the core was replaced at 600-day and 300-day intervals. In that earlier section it was shown that the differences in management schemes led to approximately a 0.6% improvement in breeding performance in the radial blanket when the core was replaced at more frequent intervals. The same more frequent core replacement led to a degradation of the axial blanket breeding performance by as much as 4.5%. It was noted that this last

difference was somewhat less meaningful than the radial blanket comparison because the physical design of the system requires that the axial blankets and core be managed together.

Figure 5.1 shows the effect on blanket economics of managing the core. (Note that 0.005 mills/kw-hr represents about 36,000 $/year for this reactor.) As shown, both the uranium and thorium blankets are affected in the same manner by variations in core management scheme. This is significant to note because the economic analysis presented here will concentrate on a comparison of the economic performance of uranium and thorium blanket systems. Another significant factor is that the difference in blanket economics resulting from differences in core management scheme peak shortly after the refueling. Thus lengthening the irradiation interval after the refueling would result in a smaller economic effect. It should be noted that, as expected, the difference in blanket economic performance resulting from more frequent refueling is larger for the axial blanket than for the radial blanket. Figure 5.1 also shows that more frequent core refueling leads to a smaller cost contribution from the radial blanket and a larger cost contribution from the axial blanket. In summary, more frequent refueling of the core affects thorium and uranium blankets in the same manner and the effect tends to make the thorium blanket appear slightly less economically attractive when compared to the uranium blanket. See section 5.6 for a further discussion of this effect on blanket economics.

Fig. 5.1 The Effect of Core Management on the Cost of Power Contributed by the Radial and Axial Blankets

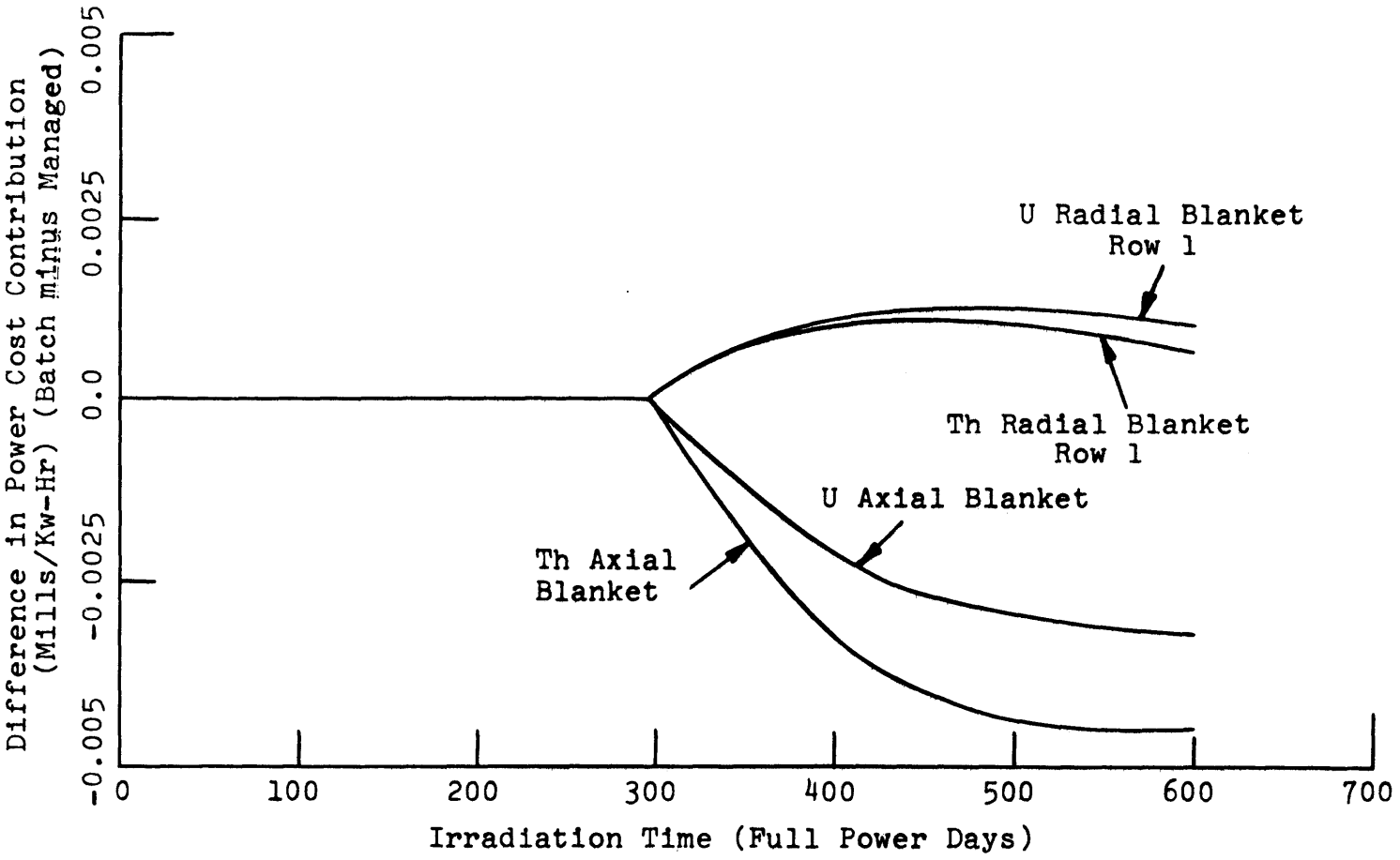

5.3.3 Batch Blanket Burnup

5.3.3.1 General Considerations

In performing the economic analyses reported in this section, number densities from 2DB were converted into material inventories for each burnup zone. These material inventories were then used directly as input to the economic analysis. One difficulty that arose in the economic analysis was how to treat the economic penalty associated with U-232. This was a problem because it was desirable to separate the cost contributions from the various rows of the radial blanket, yet the differences in U-232 concentration from row to row assured that the U-232 economic penalty would vary through the blanket. Hence, analyzing each row separately would product realistic cost contributions only if each row were reprocessed separately. In reality, the chemical processing would likely be done on the entire radial blanket as a batch, and the U-232 penalty would be that associated with the average U-232 concentration. This mixing of materials with high and low U-232 concentrations represented a thermodynamic inefficiency which could be directly related to an economic inefficiency. In an attempt to evaluate the magnitude of this inefficiency, economic analyses were performed on the various burnup regions of the radial blanket as well as on the blanket as a whole. A comparison was then made between the power cost contribution from the mixed blanket and the sum of the power cost contributions from each of separate burnup regions. These analyses were denoted as "mixed reprocessing" and "differential reprocessing," respectively. Figure 5.2 shows the results of this comparison. As shown, the maximum difference between the two schemes was approximately 0.006 mills/kw-hr. Because of the small magnitude of the U-232

Fig. 5.2 Difference in Radial Blanket Power Cost Contribution Between Mixed Reprocessing and Differential Reprocessing, Thorium Blanket

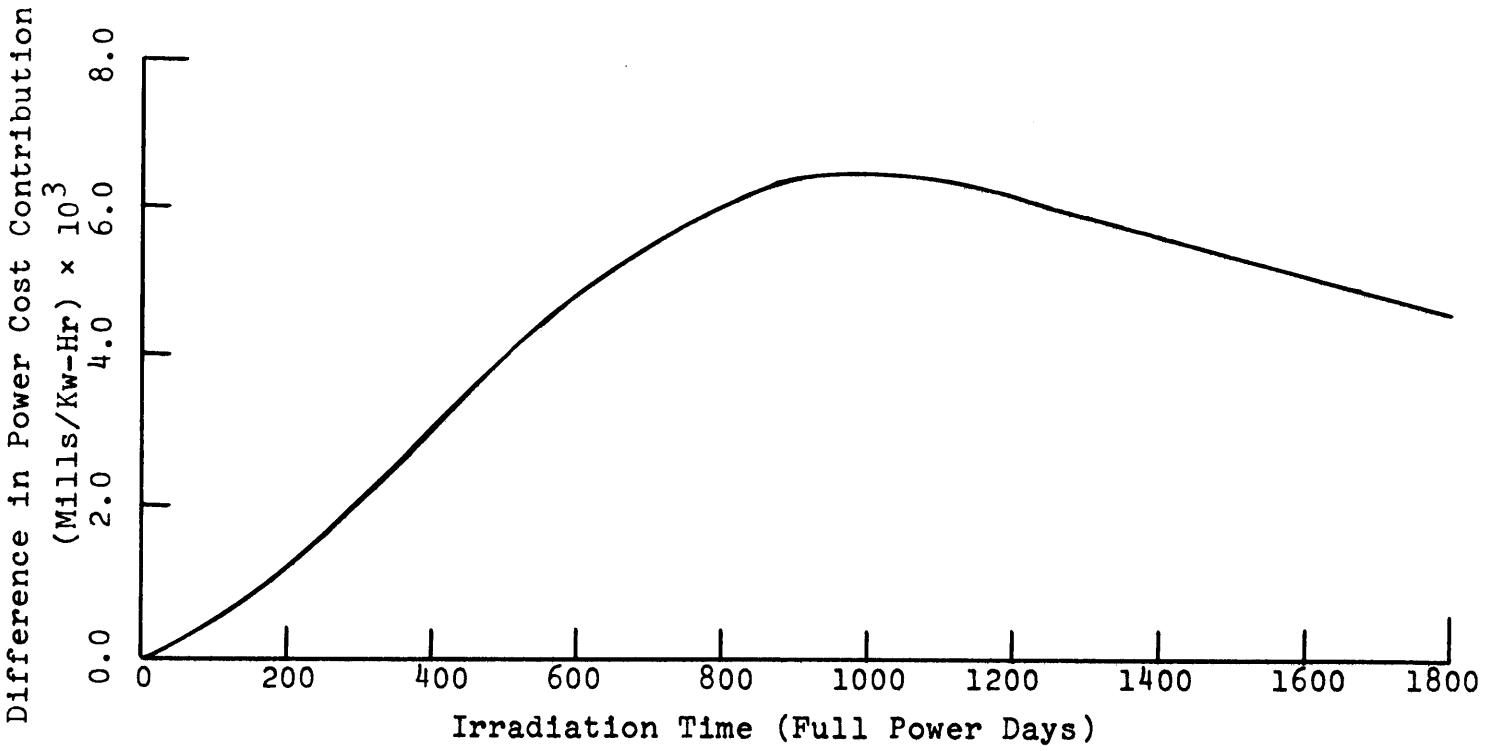

mixing effect, it was decided that comparisons of uranium and thorium blanket economic performance could be done on a row-by-row basis, and the small resulting error neglected.

5.3.3.2 Core and Axial Blankets

The comparative economic analysis of thorium and uranium blanketed systems, to be presented in section 5.4, requires, as input, economic information not only on the radial blanket performance, but also on the core and axial blanket performance. Because the management of these two regions was established as a groundrule in this study (average core burnup limit of approximately 105,000 MWD/MTM) the economic analysis will be presented separate from that for the radial blanket.

As discussed in sections 4.2.3 and 4.2.4, the lower albedo of the thorium blanket requires that the initial core fissile inventory for that system be approximately 4% greater than for the uranium blanketed system. This increase in required fissile loading would be expected to lead to a higher core power cost contribution for the thorium blanketed system than for the uranium blanketed system. Figure 5.3 shows this effect. (In all information presented in this chapter, assume that the economic parameters are those shown in Table 5.1 for a private utility unless otherwise specified.) As shown, the 4% difference in fissile inventory resulted in approximately a 0.05 mill/kw-hr difference in the core power cost contribution after 600 days at full power. This translates into a yearly difference in power cost of approximately 360,000 dollars.

To illustrate the effect of fissile material value on axial blanket economic performance, consider Figs. 5.4 and 5.5. These two figures show that the axial blanket power cost contribution is fairly significantly

Fig. 5.3 Core Power Cost Contribution for Thorium and Uranium Blanket Systems, Reference Economic Environment, Private Utility

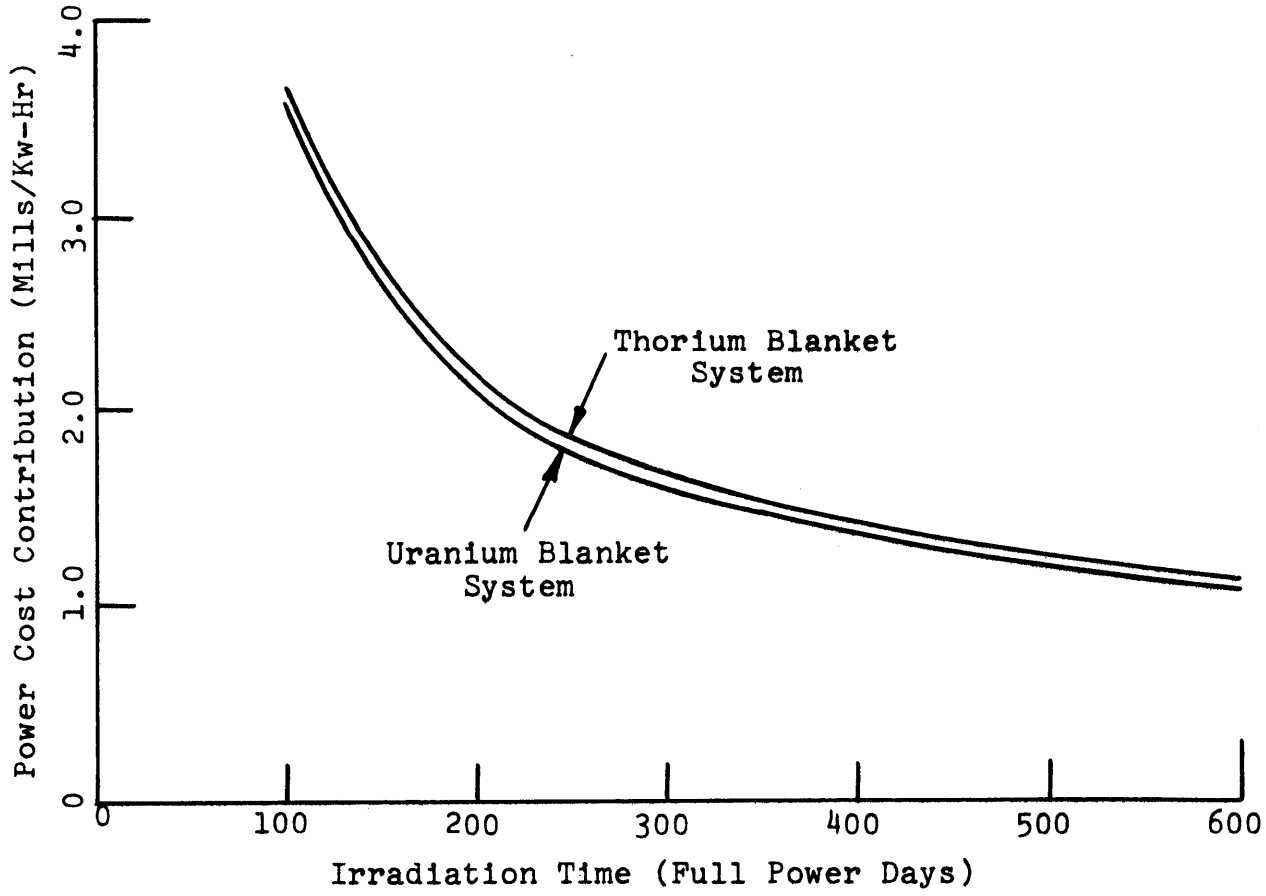

Fig. 5.4 Axial Blanket Power Cost Contribution for Uranium Blanket System, Reference Economic Environment (Except Fissile Value)

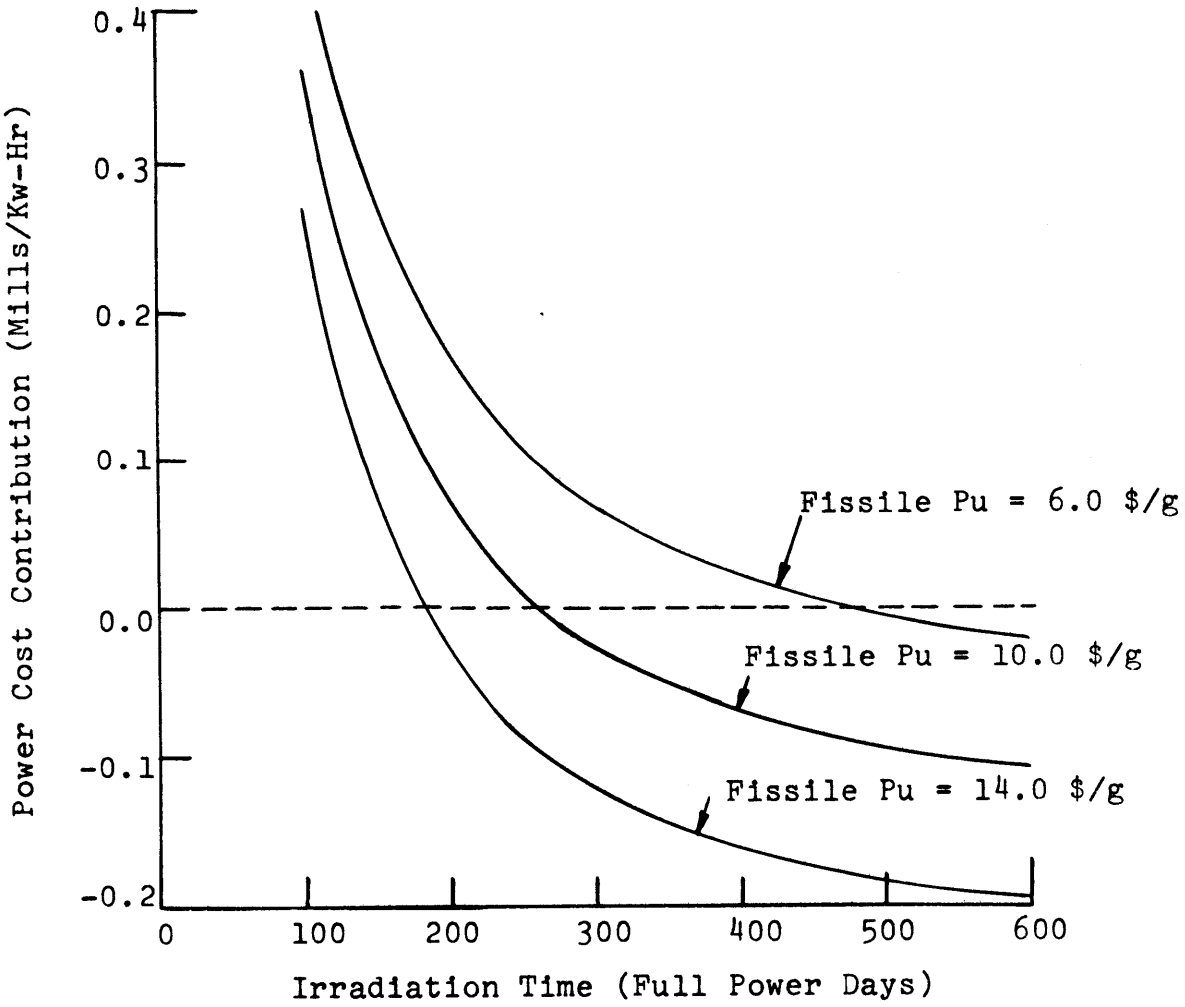

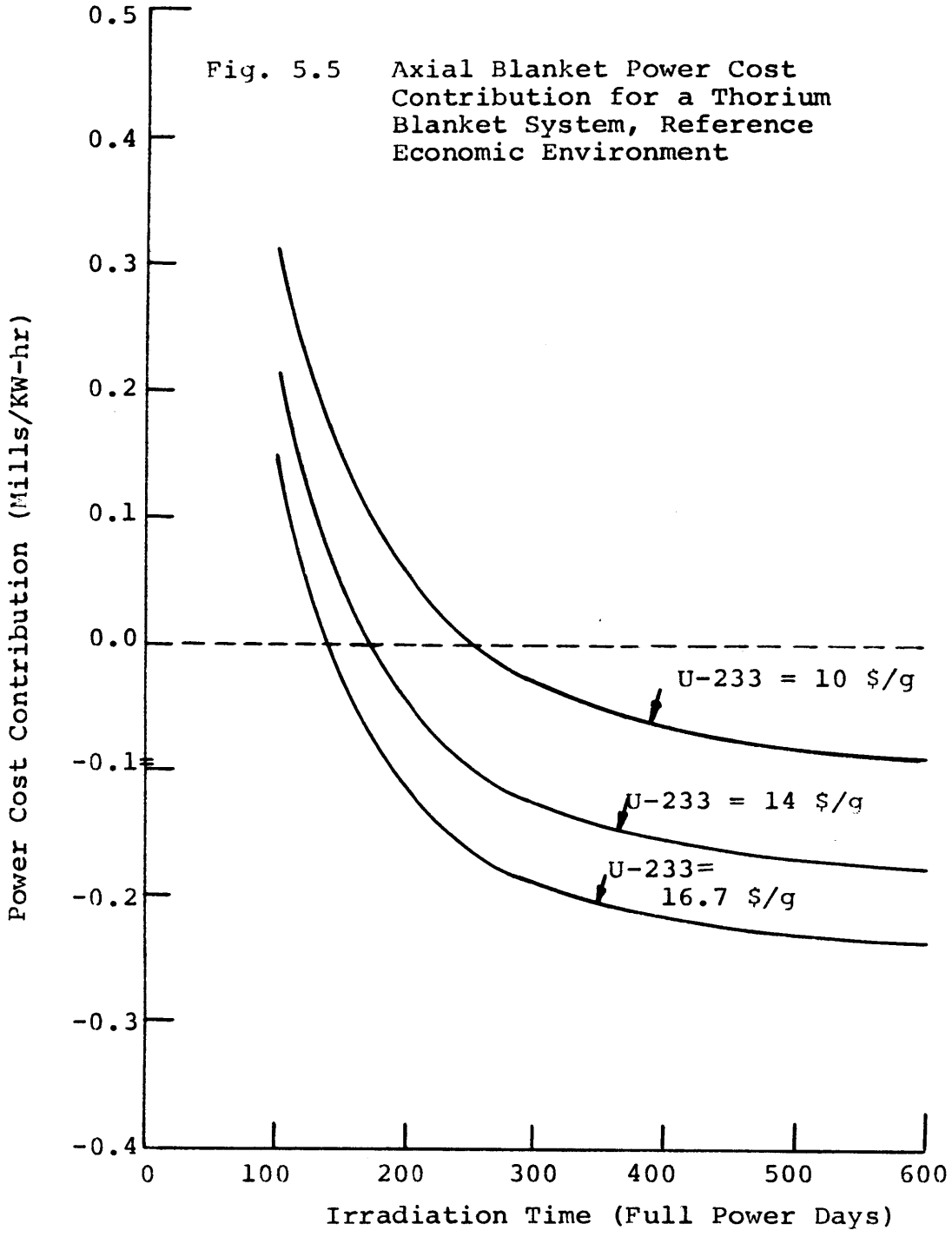

Fig. 5.5 Axial Blanket Power Cost Contribution for a Thorium Blanket System, Reference Economic Environment

affected by fissile material value. At the reference economic condition of 10 $/g for fissile plutonium, the uranium axial blanket power cost contribution is approximately -0.108 mills/kw-hr after 600 days of irradiation. Consideration of Fig. 5.5 shows that, if U-233 were worth 10 $/g, the thorium axial blanket power cost contribution would be about -0.09 mills/kw-hr after 600 days. The difference between these two axial blanket power cost contributions at the same fissile isotope value illustrates the economic effect of the U-232 contaminant in the thorium axial blanket. Despite the fact that more fissile material is produced in the thorium axial blanket (see sec. 4.4.2.2), the uranium axial blanket power cost contribution is 0.018 mills/kw-hr less than that for the thorium blanket. The last feature to note in Figs. 5.4 and 5.5 is that the blanket power cost contribution has begun to level out at 600 days. Although no optimum was reached within this time span, the power cost contribution at the optimum would not be expected to be too much more negative than that at 600 days. For comparative purposes the power cost contributions of the two axial blankets in the reference economic environment are shown in Fig. 5.6. This figure shows that the difference in axial blanket performance alone is sufficient to compensate for the economic effects associated with the extra enrichment required for the thorium blanket case.

5.3.3.3 Radial Blanket Comparison

The purpose of the radial blanket economic evaluation presented here is to serve as a basis for three later analyses:

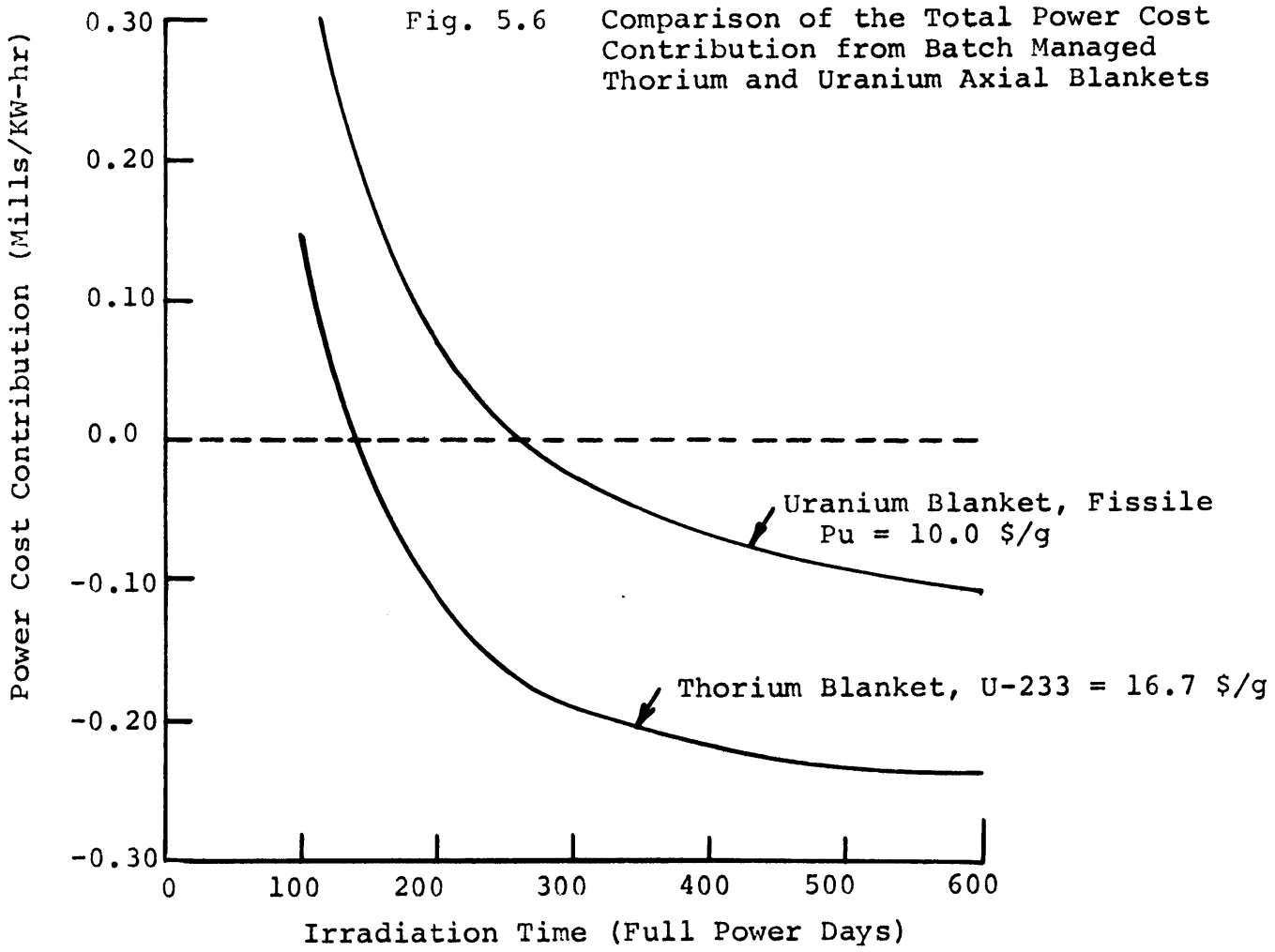

Fig. 5.6 Comparison of the Total Power Cost Contribution from Batch Managed Thorium and Uranium Axial Blankets

1. Comparison of management schemes,
2. Comparison of blanket economic performance,
3. Development of a generalized optimum correlation.

In accord with this goal, several parametric comparisons will be presented here. Figure 5.7 shows the effect of fissile plutonium value on the economic performance of a batch irradiated row 1 uranium radial blanket. As shown, increasing the fissile plutonium value has two effects. First, the minimum in the power cost contribution of row 1 is made more negative, and second, the optimum irradiation time is reduced. This second effect is somewhat difficult to observe because of the very large radius of curvature near the optimum time. The broad flat minimum allows nearly the same power cost contribution to be derived from irradiation over a wide range of times. This important characteristic will be demonstrated more clearly in section 5.5. Figure 5.8 compares the economic performance of rows 1, 2 and 3 of a batch irradiated uranium radial blanket in the reference economic environment. As shown, the reduced fissile production associated with regions farther removed from the core causes the rows nearer the core to have more negative power cost contributions and shorter optimum irradiation times. An interesting fact to note is that under the economic conditions assumed, neither rows 2 or 3 reached its optimum during the 1800-day irradiation. From this observation, it might be expected that in some economic environments an engineering limit (e.g., clad embrittlement, accumulated clad strain, or duct deformation) might be reached by outer blanket rows prior to their attaining an economic optimum. Since the scope of this work does not include definition of engineering limits, it will be assumed during

Fig. 5.7 Power Cost Contributions from Row 1 of a Batch Managed U-238 Radial Blanket

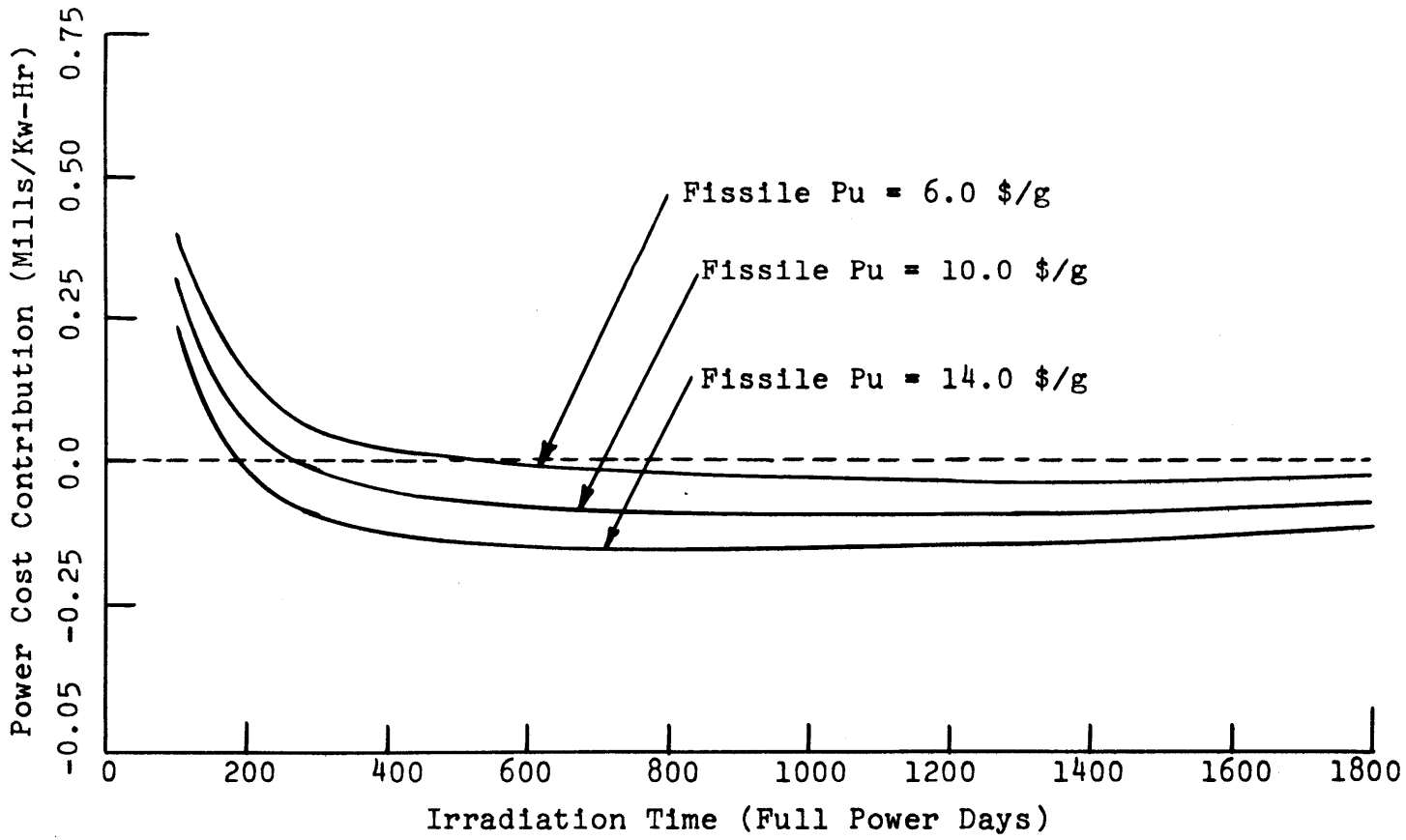

Fig. 5.8 Power Cost Contributions from Rows 1, 2, and 3 of a Batch Managed U-238 Radial Blanket, Fissile Pu = 10.0 $/g

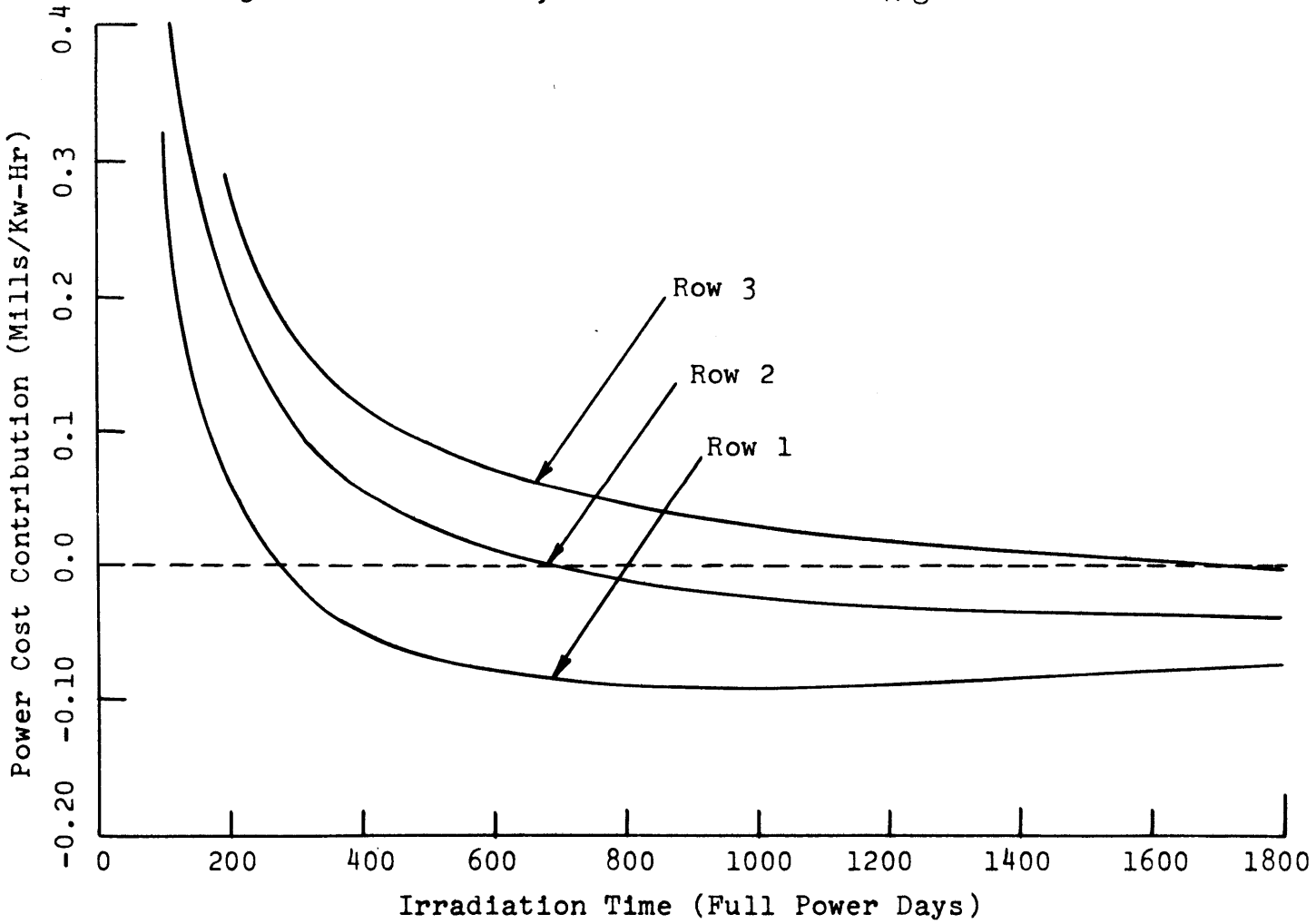

most of the analysis that an 1800-day irradiation time is the maximum allowed for both row 2 and row 3 radial blanket assemblies.

Figure 5.9 shows the same information as Fig. 5.8 for a batch irradiated thorium radial blanket. Comparison of Figs. 5.8 and 5.9 reveals several interesting features. First the difference in economic performance between row 1 and row 2 is greater in the thorium blanket than in the uranium blanket. This might be expected because of the higher value of the U-233 produced in the thorium blanket relative to the fissile plutonium produced in the uranium blanket; and because of the degraded breeding performance of the thorium blanket relative to the uranium blanket at greater distances from the core interface (see section 4.4.2.2). The second difference is that the thorium blanket reached its optimum, with a more negative power cost contribution, at an earlier time than the uranium blanket. Again this would be expected from the difference in fissile product value for the two blankets. This achievement of an earlier optimum may allow the thorium blanket to be replaced (or managed) on a shorter cycle, thus reducing the power swing in the radial blanket. (See sec. 6.3 for further discussion of this point.) The break-even point for row 3 of the thorium blanket occurs at about 1000 full power days as opposed to the nearly 1800 days in the uranium blanket system. Last, it should be noted that the optimum irradiation time for row 1 of the thorium blanket is 600 days while that for a row 1 uranium blanket is approximately 1000 days.

Figure 5.10 shows a comparison of the total power cost contribution from batch managed thorium and uranium radial blankets. As shown, the thorium blanket achieves an earlier optimum, and that optimum occurs at a more negative total power cost contribution than

Fig. 5.9 Power Cost Contribution from Rows 1, 2, and 3 of a Batch Managed Th-232 Blanket System U-233 = 16.7 $/g

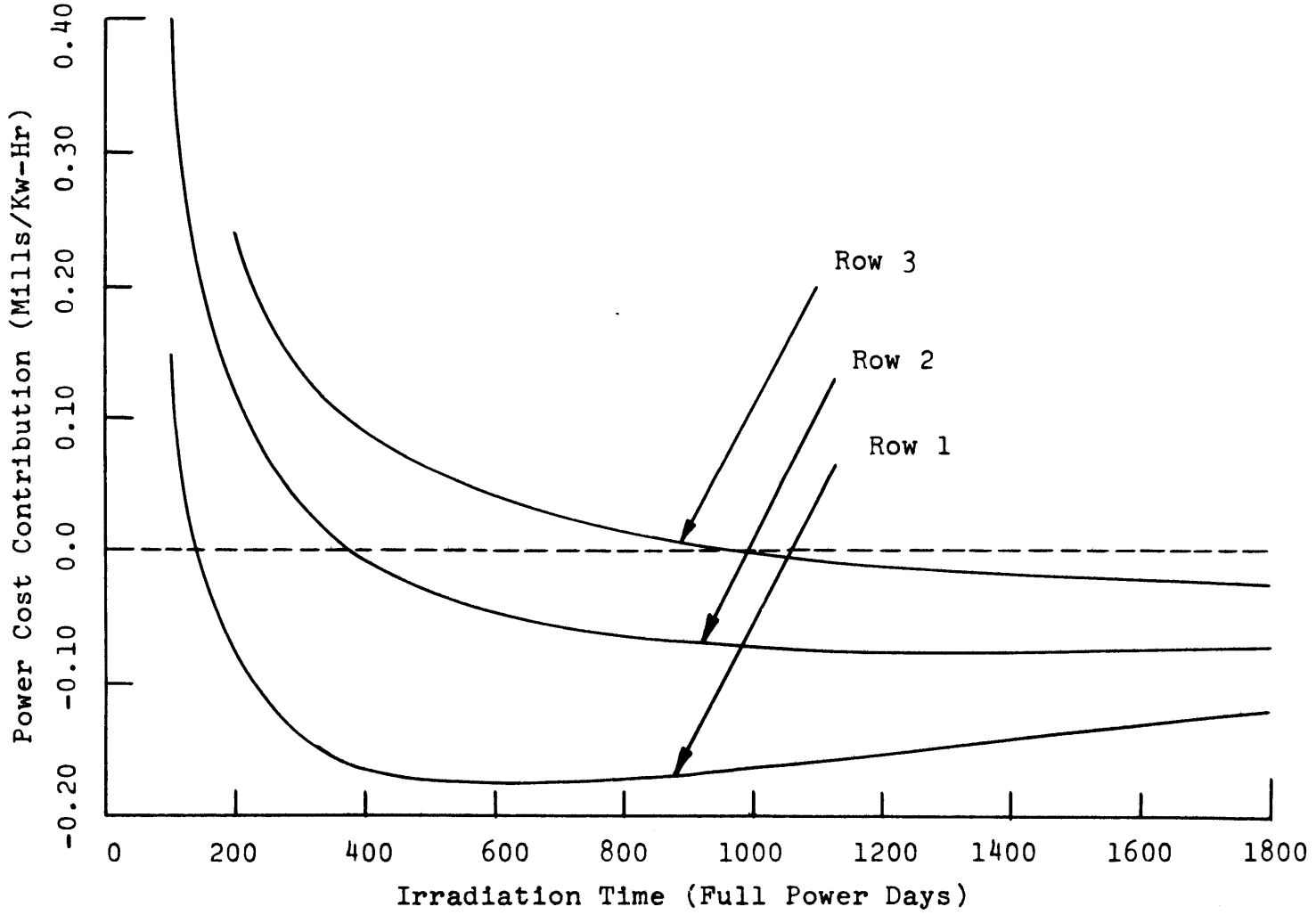

Fig. 5.10 Comparison of the Total Power Cost Contributions from Batch Managed Thorium and Uranium Radial Blankets

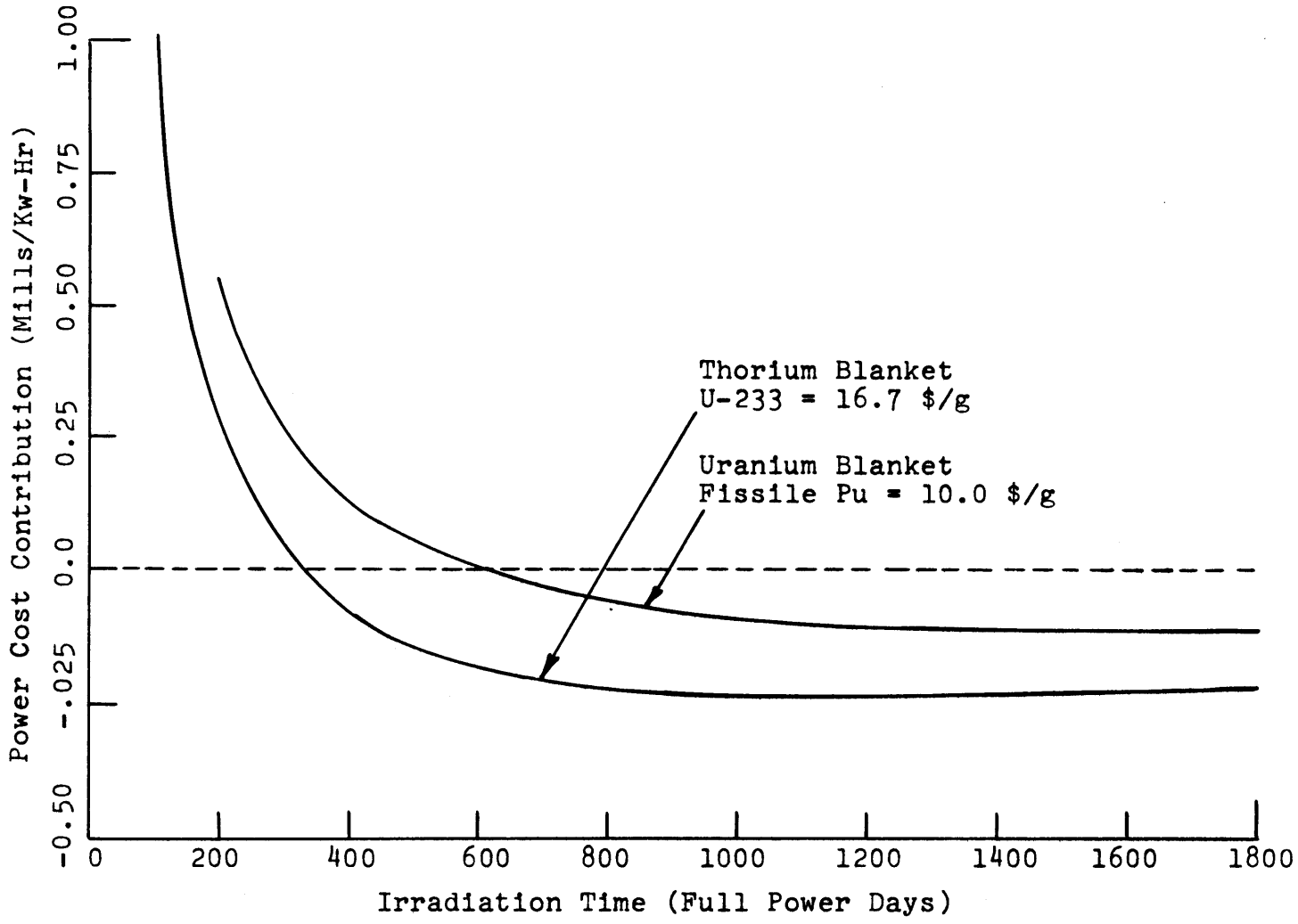

for the uranium blanket.

Analyses similar to those presented above have been performed for a large number of economic environments. The results of these studies will be presented in sections 5.4 and 5.5.

5.3.3.4 U-232 Penalty

Figures 5.11 and 5.12 show the economic penalty associated with the presence of the U-232 contaminant in axial and radial blankets. As shown, the maximum penalty is in the range \$1.30 to \$1.70 per gram of total uranium. Since the most significant fraction of the uranium present is U-233, these penalties can be viewed as being subtracted directly from the value of the U-233 produced in the blankets. In the reference economic environment, this value is \$16.70 per gram. Hence the U-232 penalty represents approximately an 8 percent to 10 percent reduction in the effective U-233 value.

5.3.3.5 Public vs. Private Utility

In Table 5.1 at the beginning of this chapter, the reference economic environment was presented. Two sets of financial parameters were shown in this table: one set for a typical private utility and one set for a typical public utility (e.g., TVA). For the sake of comparison, power cost contributions in both public and private utility economic environments for the core and two rows of the radial blanket are shown in Figs. 5.13 and 5.14. As shown, a rather small difference exists between the power cost contributions in the two environments for the radial blanket, whereas the core economic performance is significantly different. The large difference between core power cost contributions

Fig. 5.11 Economic Penalty in the Thorium Axial Blanket Associated with Production of the Contaminant U-232

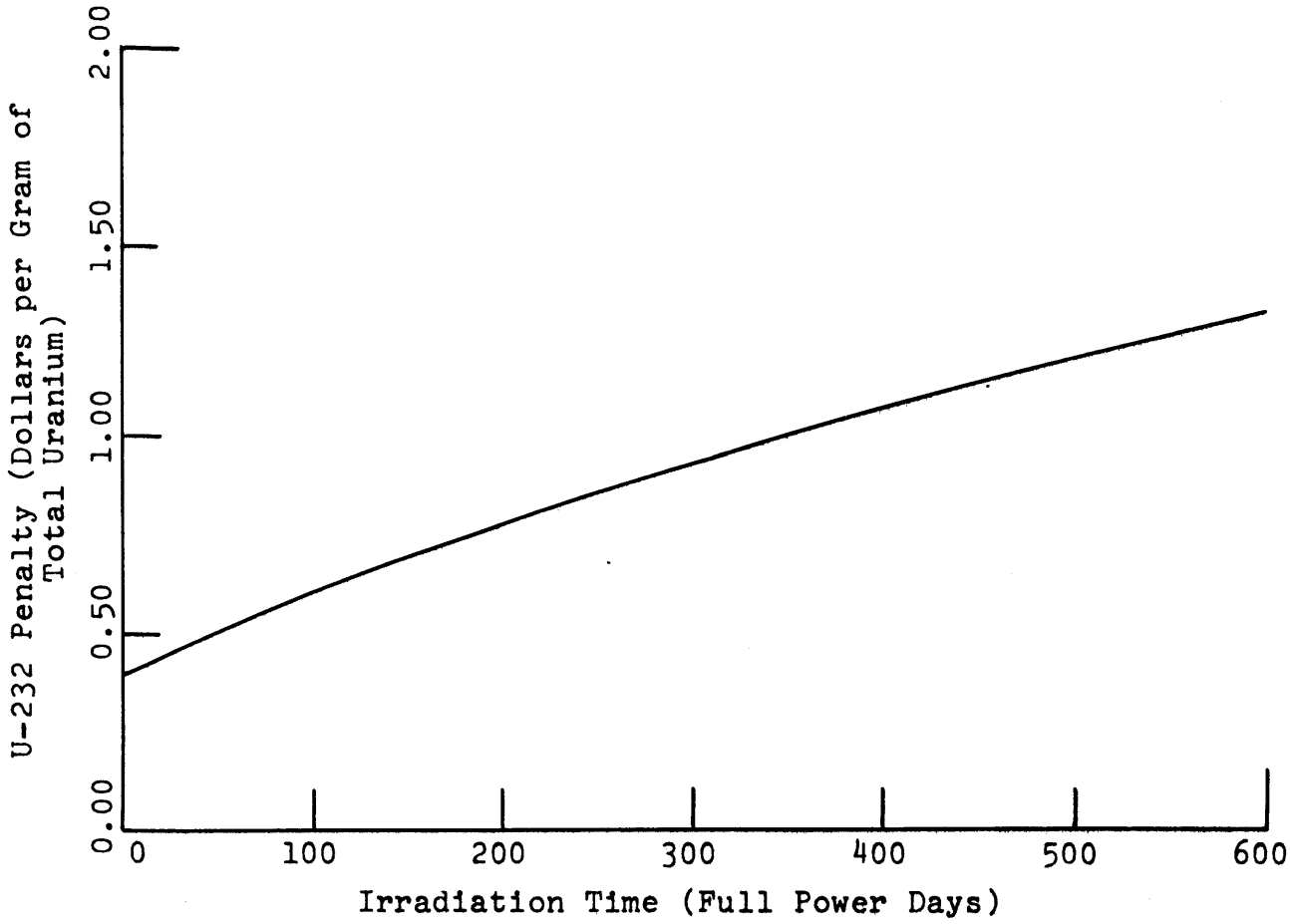

Fig. 5.12 Economic Penalty in the Thorium Radial Blanket Associated with Production of the Contaminant U-232

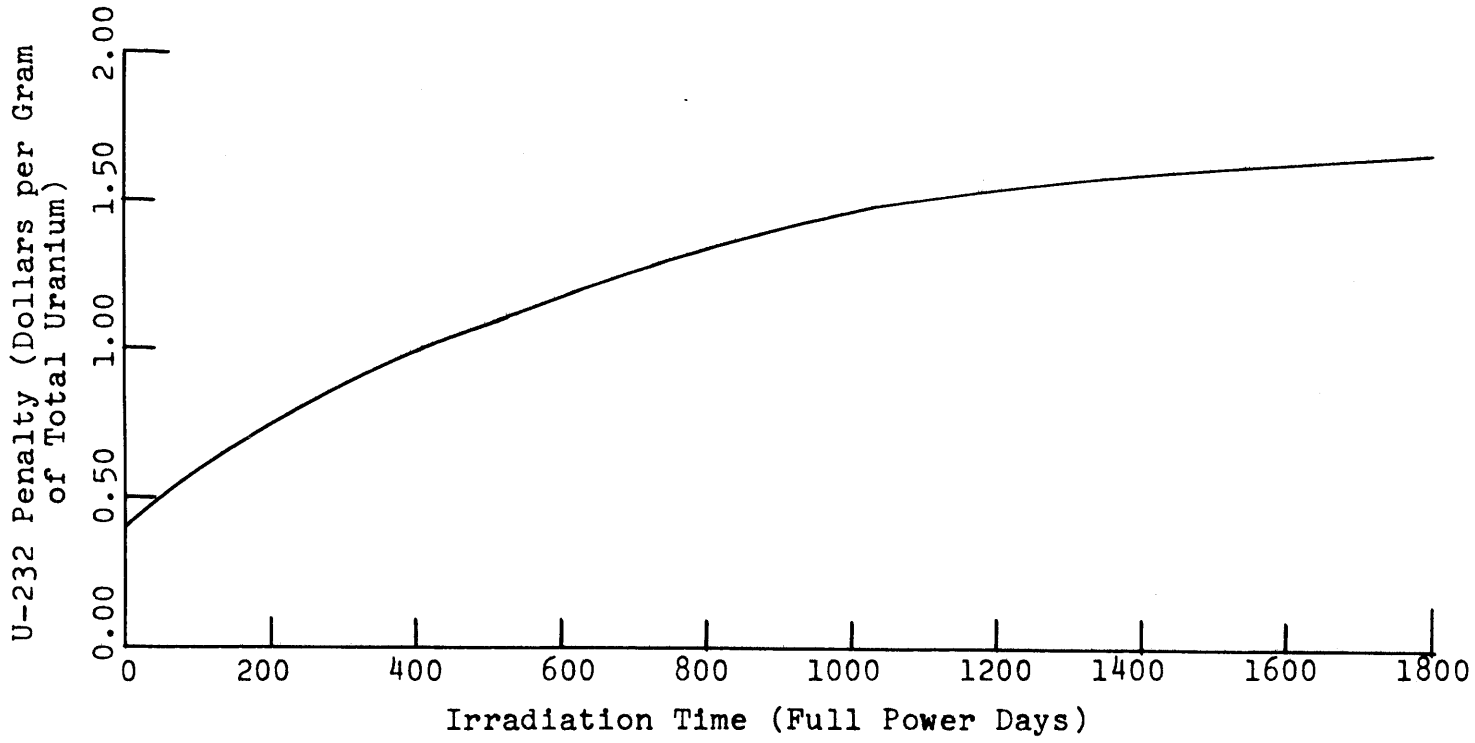

Fig. 5.13 Comparison of Core Power Cost Contribution for Typical Private and Public Utility Environments, Pu = 10.0 $/g

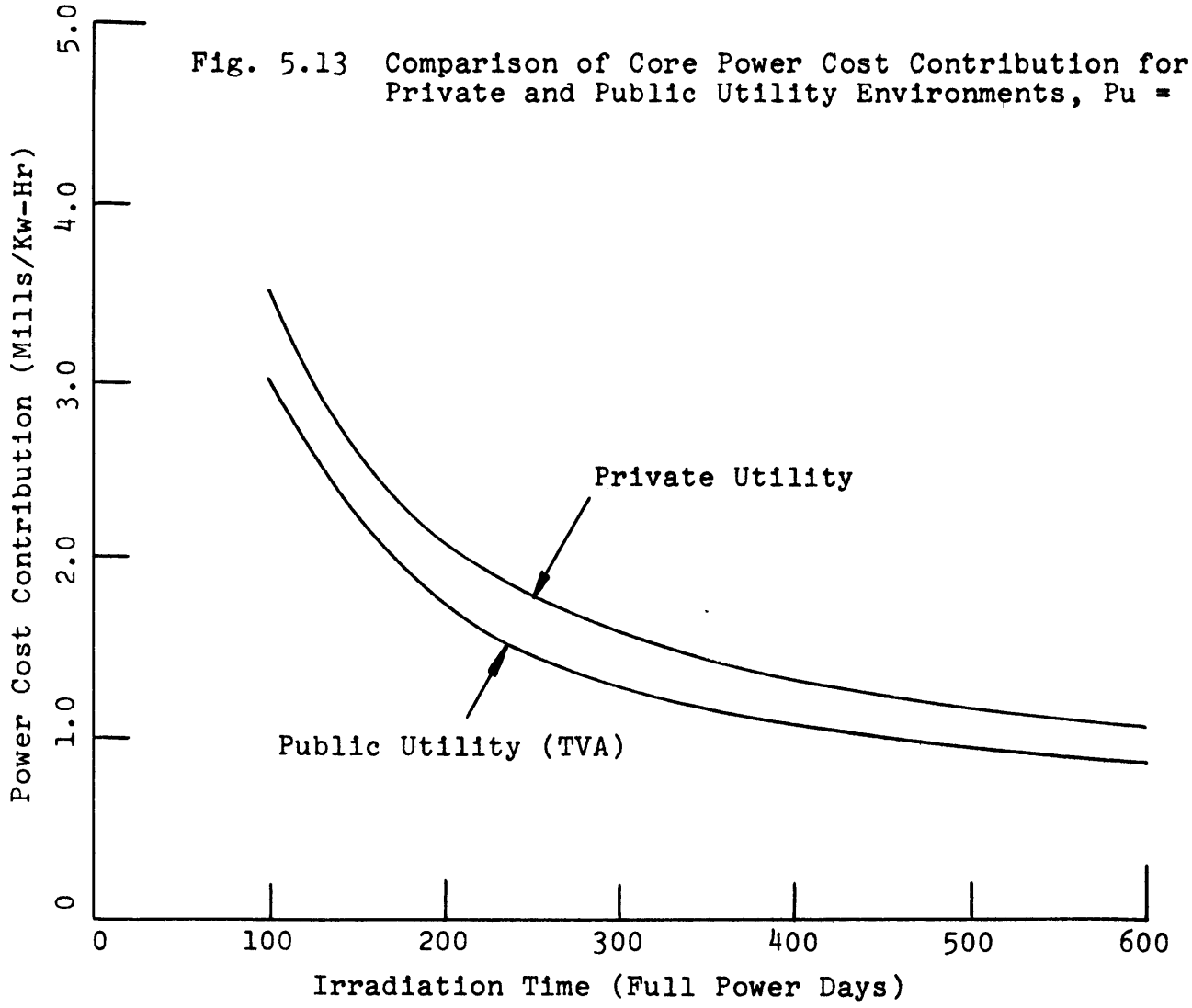

Fig. 5.14 Comparison of the Power Cost Contributions from Rows 1 and 2 of a Uranium Blanket System for Public and Private Utility Financial Parameter Sets, Fissile Pu = 10.0 $/g (See Table 5.1)

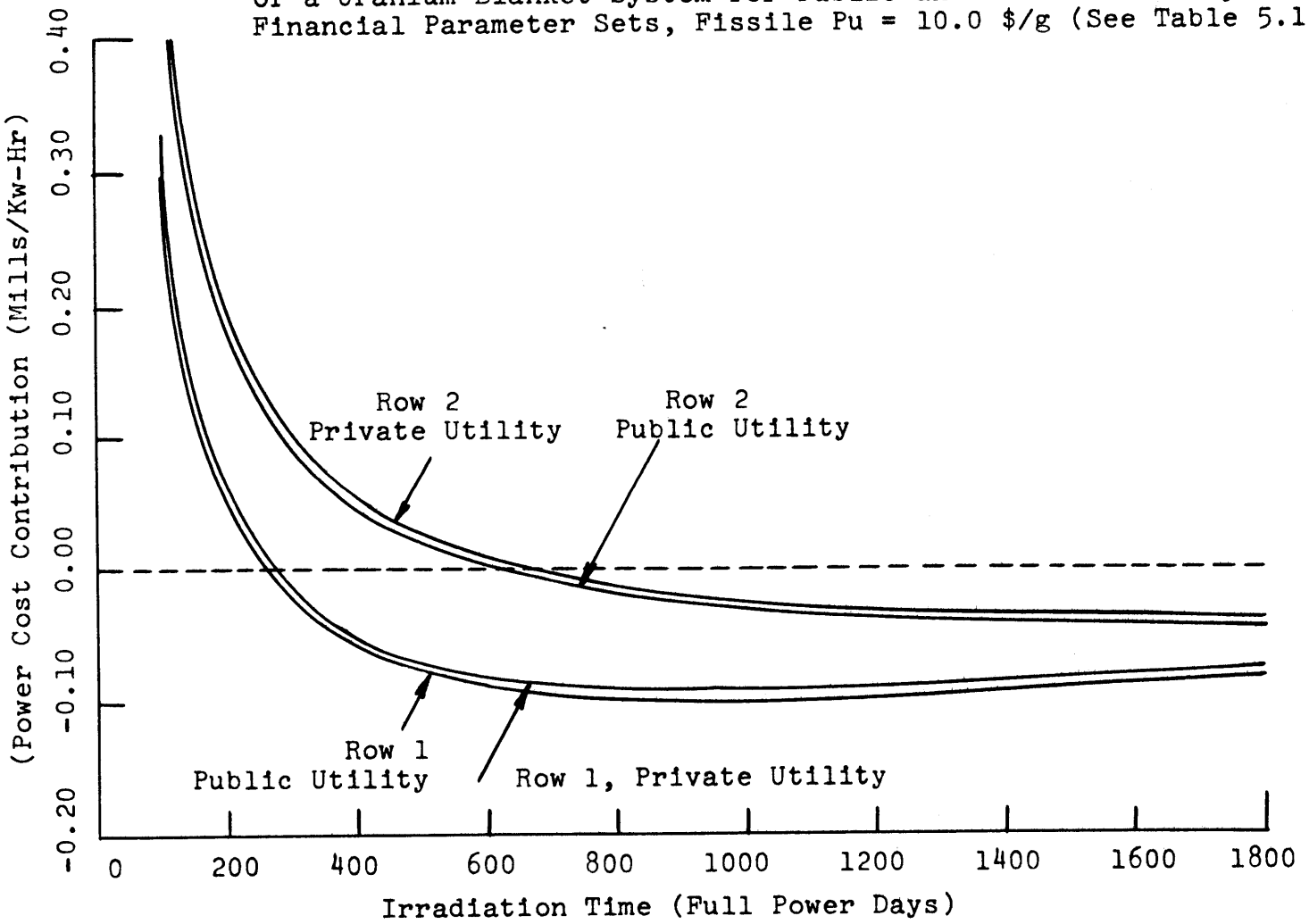

evaluated in two economic environments can be attributed to the higher core fabrication charge, the large core material purchase charge, and the fact that these charges are amplified in their effect on power cost contribution by the tax rate reduction from 0.5 to zero for the public utility. In section 5.5 a correlation will be presented in which the effect of the economic environment will be normalized out of the determination of the optimum irradiation time and the corresponding enrichment.

5.3.4 Zone Scatter Blanket Management

The first logical departure from batch blanket irradiation is zone scatter management. Under this management scheme, blanket assemblies would be irradiated to their economic optimum, removed from the reactor, and replaced by fresh assemblies. For the purpose of this analysis, the inventory data from the batch irradiation was used in conjunction with the standard economic parameters to define the optimum irradiation time of row 1 of the radial blanket. As mentioned in section 5.3.3.3, these optimum times were 600 days for the thorium blanket and 1000 days for the uranium blanket. Because the replacement cycle of row 1 had an impact on the breeding and, consequently, on the economic performance of rows 2 and 3, the analysis reported here considered only the zone scatter management of row 1. This approach allowed the determination (to a first order) of the economic optimum irradiation time of row 2 of the radial blanket.

Figures 5.15 and 5.16 show comparisons of the relative economic performance of radial blanket row 2 for the batch irradiation and first

Fig. 5.15 Comparison of Power Cost Contribution for Row 2 of a Uranium Radial Blanket for Row 1 Batch Irradiated and Zone Scatter Managed, Fissile Pu = 10.0 $/g

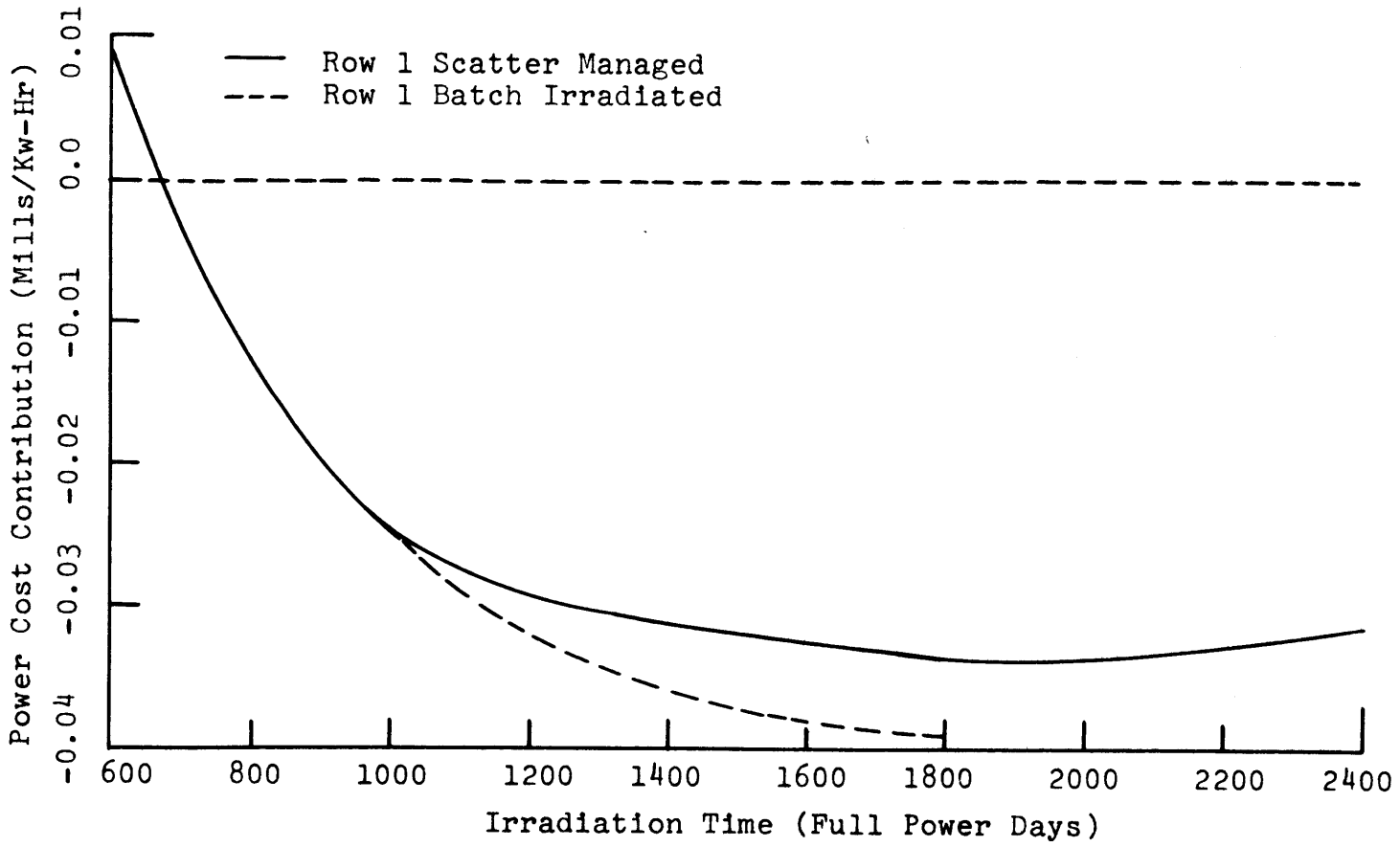

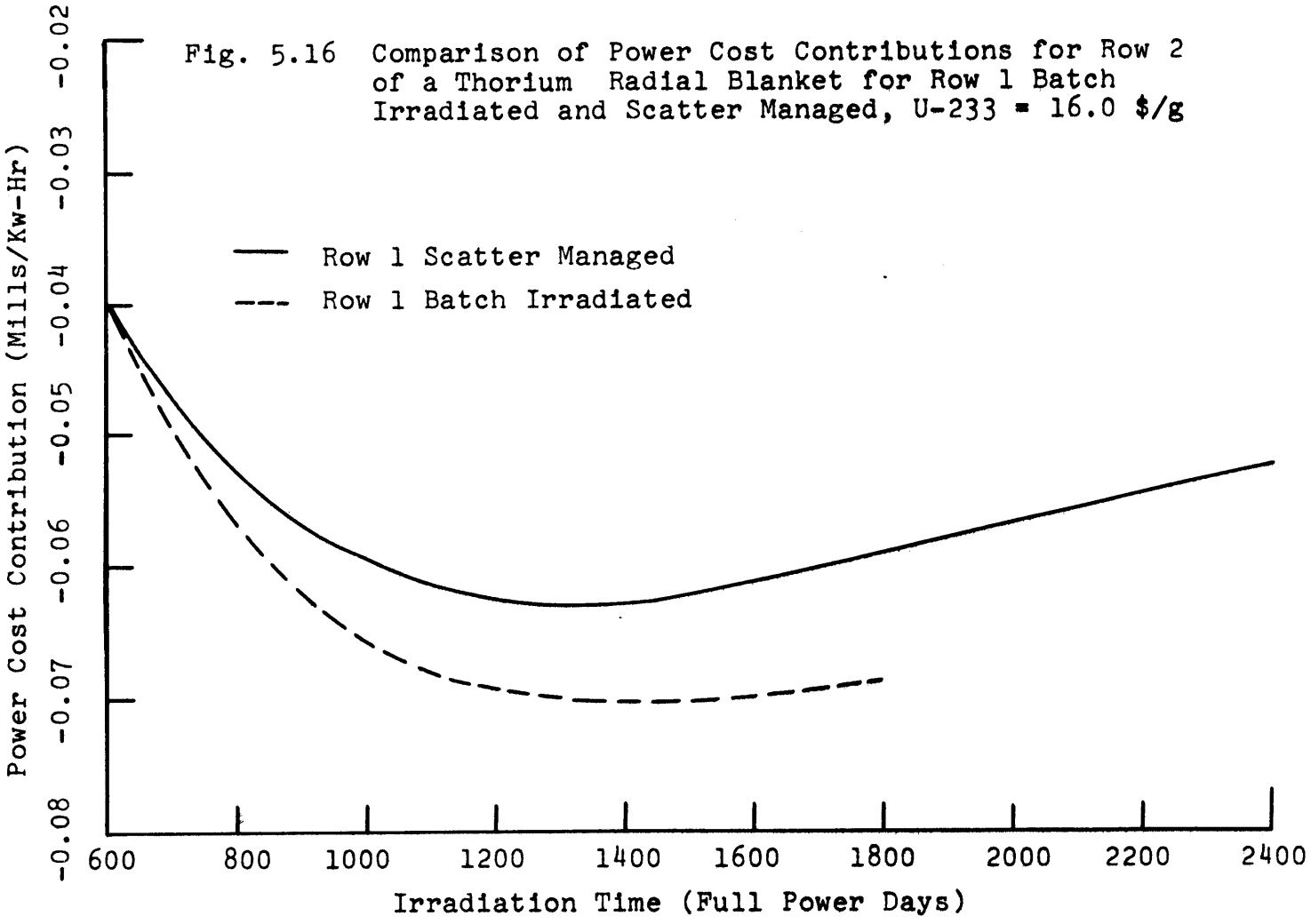

Fig. 5.16 Comparison of Power Cost Contributions for Row 2 of a Thorium Radial Blanket for Row 1 Batch Irradiated and Scatter Managed, U-233 = 16.0 $/g

row zone scatter management cases. Figure 5.15 is for the uranium blanket system and Fig. 5.16 is for the thorium blanket system. As expected from the discussion presented in section 4.5, the reduced fissile material inventory buildup rate in row 2 following replacement of row 1 has the effect of making the power cost contribution of row 2 less negative in the zone scatter managed case than in the batch irradiation case. Figure 5.16 also shows that the reduced rate of buildup of fissile inventory in row 2 has the effect of causing the economic optimum to be reached earlier than in the batch irradiation case.

Using the economic data developed to this point, a system economics comparison between the blanket batch irradiation case and the row 1 zone scatter management case can be made. The numbers for this analysis were developed using the power cost contribution at the economic optimum for radial blanket rows 1, 2 and 3, where an optimum was reached in less than 1800 days. For rows in which the optimum was not reached by 1800 days, the power cost contributions at 1800 days were used. This is equivalent to assuming that the blanket engineering design limit was not reached prior to the attainment of the economic optimum; and, where no optimum was attained, that the engineering design limit was reached at 1800 days. Other assumptions included in this analysis were

1. Typical "equilibrium cycle" performance of a zone scatter managed blanket is the same as the first cycle;
2. The economic performance of row 3 is unaffected by the management of row 2; or, equivalently, the contribution to the cost of power from row 3 is insignificant compared to the contribution from rows 1 and 2.

The effect of the staggered blanket assembly replacement schedule can be accounted for in the cash flow method simply by applying a discount factor to the contribution from each row to adjust its cost contribution to a point in the irradiation which is common for all three rows. Since for the batch irradiation, the point from which time is measured is the middle of the irradiation cycle, this same point will be used in this analysis as the basis for discounting power costs. Figure 5.17 shows the refueling schedule used as a basis in applying discount factors to correct the power cost contributions for variations in irradiation cycle length.

Table 5.4 shows the results of the comparison between the batch irradiation case and the zone scatter management case. As shown in the table, the power cost contribution for the region scatter management case is more negative than that for the batch irradiation case for both the thorium and uranium blanket cases. In the uranium blanket the power cost reduction is 0.00976 mills/kw-hr, or an approximate yearly savings of 70,000 dollars. For the thorium blanket the power cost reduction is 0.0315 mills/kw-hr, or an approximate yearly savings of 225,000 dollars. Thus it has been shown that the effect of using zone scatter management is to reduce the power cost contribution for the radial blanket relative to that for batch management. It has also been shown that this reduction is more significant for the thorium blanket than for the uranium blanket case. One cost contribution which has been neglected in this analysis is the effect of management on system availability. Obviously, when blanket assemblies are replaced more frequently, the reactor must be shut down for refueling longer, and an

Fig. 5.17 Refueling Scheme for Zone Scatter and Batch Blanket Management Schemes

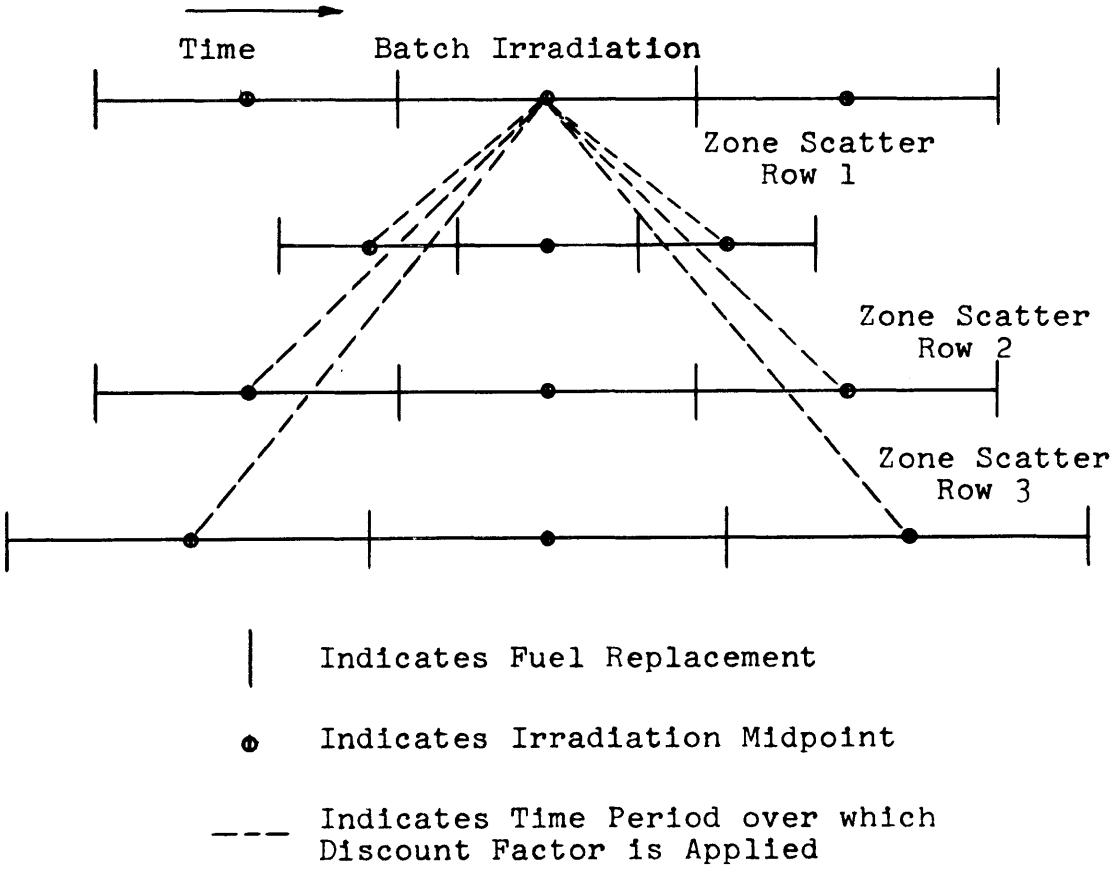

TABLE 5.4 Contributions to Fuel Cycle Cost from Batch Irradiated and Zone Scatter Managed Radial Blankets.

Blanket Type	Row Considered	Optimum Irradiation Time (days)	Type Management	Fuel Cycle Cost Contribution (mills/kw-hr)
Uranium	1, 2, and 3	1800	Batch	-0.11449
Uranium	1	1000	Zone scatter	-0.09195
Uranium	2	1800	Zone scatter	-0.03610
Uranium	3	1800	Zone scatter	+0.00380
Uranium	1, 2, and 3 (summation)	--	Zone scatter	-0.12425
Thorium	1, 2, and 3	1200	Batch	-0.23090
Thorium	1	600	Zone scatter	-0.17516
Thorium	2	1200	Zone scatter	-0.07019
Thorium	3	1800	Zone scatter	-0.01705
Thorium	1, 2, and 3 (summation)	--	Zone scatter	-0.26240

economic penalty must be paid in system availability. It has been estimated that the cost of down time for a 1000-MW_e LMFBR is approximately 10^5 dollars per day (T2). A reasonable estimate of the time required to replace or relocate a blanket or fuel assembly is about one hour (V1). By using the optimum irradiation times tabulated in Table 5.4, together with an estimate of the number of assemblies in each row, an estimate of the number of assemblies handled per 1800-day (6-year) period can be made. Consideration of the volumes in each blanket region (see Fig. 2.2), in light of the fact that consecutive rows in a hexagonal array differ in number of assemblies by 6, shows that there are 53, 59, and 65 assemblies in radial blanket rows 1, 2 and 3, respectively. Using this information, the numbers in Table 5.5 were

TABLE 5.5 Economic Effect of Blanket Management on System Availability and Power Costs.

Blanket Type	Management Scheme	Assemblies Handled Per 1800 Days	Power Cost Penalty from Refueling Down-Time
Uranium	Batch	177	123,000. ($/yr)
Uranium	Zone scatter	219	152,000. ($/yr)
Thorium	Batch	265	184,000. ($/yr)
Thorium	Zone scatter	312	217,000. ($/yr)

developed. As shown, the penalty associated with refueling time for zone scatter managed systems is approximately 40,000 dollars per year for the uranium blanket and approximately 35,000 dollars per year for the thorium blanket system.

Numbers presented above indicate that there is a net economic benefit associated with zone scatter blanket management of approximately 30,000 dollars per year for the uranium blanket system and approximately 190,000 dollars per year for the thorium blanket system. It is clear from these numbers that the economic incentive to perform zone scatter management is small. Other factors must be considered, however. For example, the question of engineering design limits in the blanket may force replacement of blanket assemblies at more frequent intervals than considered here. Consequently, it is likely that other limits than those imposed by economic considerations will require that zone scatter or some other management scheme be used. Certainly the constraints imposed by batch management on assembly engineering performance are much more stringent than those imposed by zone scatter.

5.3.5 In-Out Shuffle Management

A somewhat more complex management scheme than either batch irradiation or zone scatter is the in-out shuffle scheme proposed by Westinghouse for use in the LMFBR demonstration plant. This scheme was discussed briefly in section 4.6. The purpose of this section is to review the economic performance of a blanket which is in-out shuffle managed. For this study the uranium blanket system was chosen as the reference. Because the economic optimum for the entire radial blanket under batch irradiation conditions was approximately 1800 days (6 years), it was decided to shuffle the radial blanket every 600 days (2 years). This allowed the same total number of radial blanket assemblies to be purchased and removed from the reactor during every 1800-day period.

The economic analysis was performed by considering as a single batch one row of radial blanket assemblies as they were moved through the radial blanket from row 1 outward to row 3. Figure 5.18 shows the fissile inventory curve for this batch of fuel. The economic analysis of this batch was used as a source of information on the power cost contribution resulting from material credit. Information on the power cost contribution from fabrication and reprocessing was derived from a separate economic analysis in which the mass of uranium initially loaded into the blanket was that associated with row 2 of the radial blanket. This was valid because in the in-out shuffle management scheme, the number of assemblies purchased and reprocessed each refueling period would be, on the average, the number of assemblies in row 2. With the above information the power cost contribution for a single batch was evaluated.

Fig. 5.18 Fissile Inventory in a Single Batch of Radial Blanket Material for a Uranium Blanket with In-Out Shuffle Management

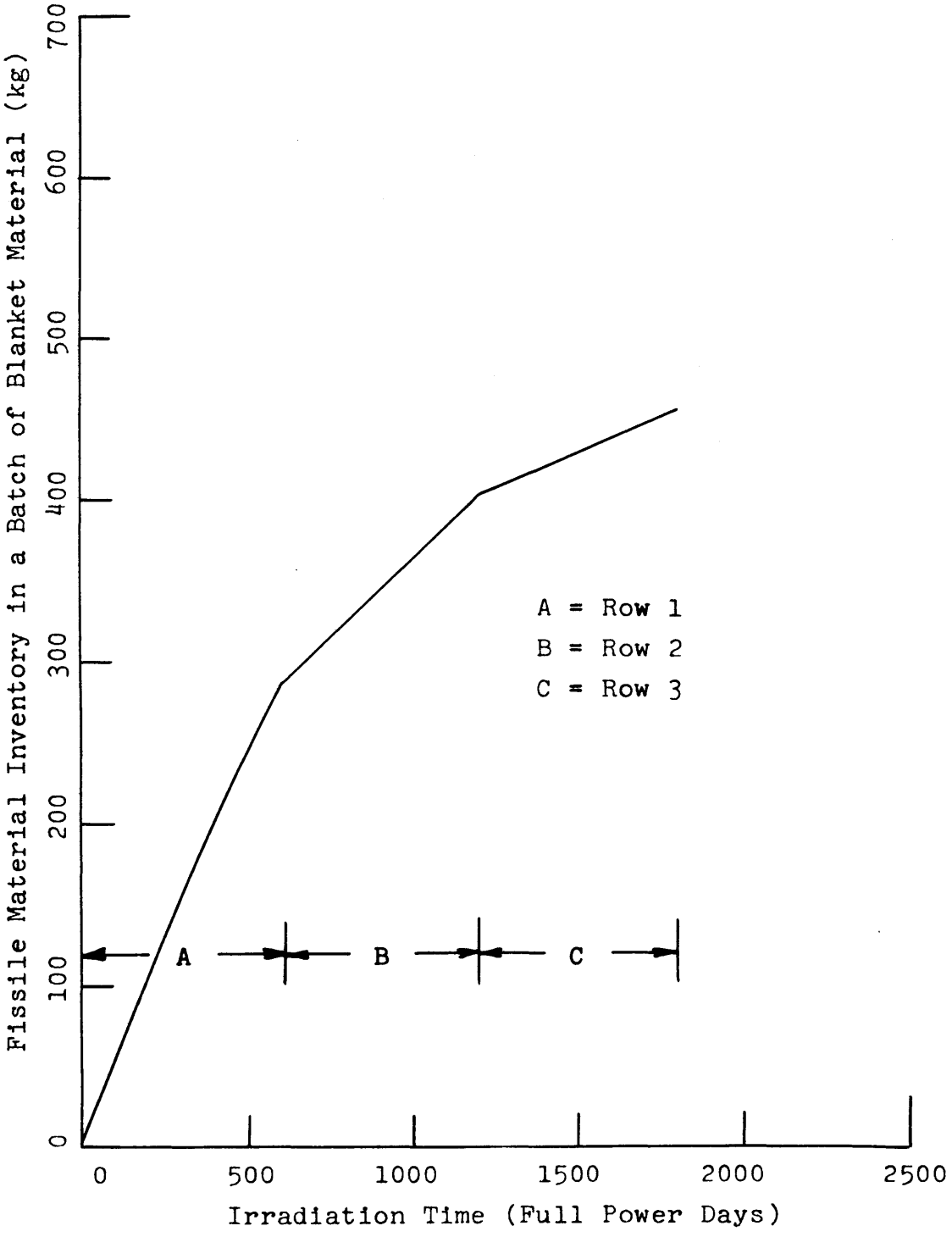

Since in a given cycle three batches would be loaded and discharged, three batches were considered in developing the radial blanket power cost contribution for the in-out shuffle management scheme. Figure 5.19 shows how the discount factors were applied in evaluating the blanket power cost contribution. The power cost contribution from each batch was the same, but the point in time to which those power cost contributions had been adjusted was the midpoint of the irradiation cycle for any given batch. Figure 5.19 shows that those midpoints did not coincide. Consequently, to evaluate the correct fuel cycle cost contribution from the radial blanket, the cost contributions of the batches whose irradiation midpoints led and lagged the middle batch were discounted to the irradiation midpoint of the middle batch (batch 2). The discount correction factor described above was less than 1% of the power cost.

Table 5.6 summarizes the results of this analysis. As shown, the power cost contribution for in-out shuffle management lies between the batch irradiation and the zone scatter management. Again consideration must be given to the effect of assembly replacement and relocation

TABLE 5.6 Blanket Economic Performance with Management

Blanket Type	Management Scheme	Fuel Cycle Cost Contribution (mills/kw-hr)
Uranium	Batch	-0.11449
Uranium	Zone scatter	-0.12425
Uranium	In-out shuffle	-0.12354
Thorium	Batch	-0.23090
Thorium	Zone scatter	-0.26240

Fig. 5.19 Irradiation and Discount Schedule for Batch Irradiation and In-Out Shuffle Management

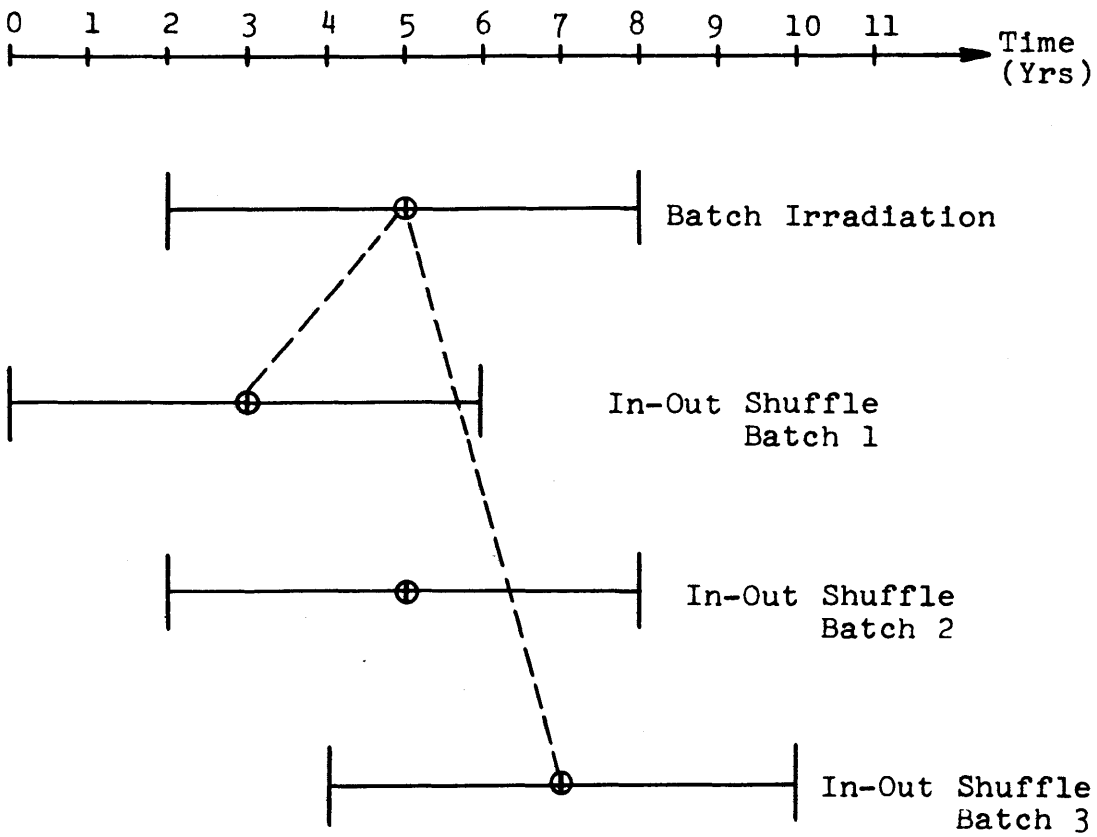

Ⓘ Irradiation Midpoint

| Replacement of Batch

--- Indicates Time Period over which Discount Factor is Applied

on the system availability and, consequently, on the system economic performance. Using the same approach as was used in the previous section, the information in Table 5.7 was developed for a uranium blanketed system.

TABLE 5.7 Economic Effect of Blanket Management on System Power Cost: In-Out Shuffle Management.

Management Scheme	Assemblies Replaced Per 1800 Days	Power Cost Penalty from Down-Time ($/yr)
Batch	177	123,000.
Zone scatter	219	152,000.
In-out shuffle	354	246,000.

(It should be noted that in the in-out shuffle management scheme it was assumed that shuffling two assemblies required the same time as replacing one assembly. This is consistent, since replacing an assembly requires handling of two assemblies.) Table 5.7 shows that the economic penalty associated with system down time for fuel management is approximately 94,000 dollars per year greater for the in-out shuffle management scheme than for the zone scatter management. Thus, from an economic point of view batch, zone scatter, and in-out shuffle management schemes are very nearly the same for a uranium blanket system. The in-out shuffle scheme is the least attractive of the three, with batch next, and zone scatter the best. If the performance of the in-out shuffle scheme had been considered for the first few refueling cycles rather than for the equilibrium cycle, it would have appeared even less economically attractive because assemblies would have been

removed from the system with much less than equilibrium cycle plutonium concentrations. This could, of course, be avoided, but only by very complex blanket management patterns during the first few cycles.

Again it should be mentioned that the analysis performed here takes no account of lifetime limits imposed by engineering considerations. It might well be that the reduction in flux and power gradients through the radial blanket for the in-out shuffle management scheme would allow the assemblies to be irradiated to much nearer their economic optimum than is possible in either batch or region scatter management. Thus the questions related to engineering design limits must be addressed prior to definition of a truely optimum irradiation scheme for the radial blanket. Some further discussion of engineering considerations will be presented in section 6.3. In addition, the cost of overcooling of the blanket assemblies has been neglected here (B5), since the degree of overcooling can be defined only after assembly lifetime limits have been established. The relative effect of overcooling on the economics of the two systems would be expected to be small.

5.3.6 U-233/Th-232 System Economics

In section 4.7 a discussion was presented of the breeding characteristics of a U-233/Th-232 core and blanket system. Several features of this system arose from that analysis:

1. The required U-233 fissile inventory to meet the same burnup objectives as a plutonium fueled and uranium blanketed system was 37% greater than for the Pu/U system,

2. The blanket breeding performance for the U-233 fueled system was inferior to that for the plutonium fueled system,
3. A significant penalty was expected in the value of U-233 from burned core assemblies due to the presence of the contaminant U-232.

In view of these factors and considering that the U-233 has a higher value, thus contributing to larger core carrying charges, one would expect the economic performance of a U-233 LMFBR to be significantly inferior to that of a comparable plutonium fueled system.

Table 5.8 shows an economic comparison (in the standard economic environment) between U-233 fueled and fissile plutonium fueled systems. As expected, the cost contribution associated with the U-233 core is so much greater than the corresponding cost for the plutonium core, that no benefits derived from the use of thorium blankets can compensate. Thus at the present time it still appears that the plutonium fueled LMFBR core is the superior system.

TABLE 5.8 Economic Comparison Between U-233 and Plutonium Fueled Systems.

System Region	Fuel Cycle Cost Contribution (mills/kw-hr) After 600 Days	
	U-233 Core, Thorium Blankets	Plutonium Core, Uranium Blankets
Core	2.38860	1.07743
Axial blanket	-0.16219	-0.10788
Radial blanket row 1	-0.14168	-0.07977
Radial blanket row 2	-0.03454	0.00937
Radial blanket row 3	0.04332	0.07108
TOTAL	2.05019	0.89915

5.4 COMPARATIVE BLANKET ECONOMICS

One of the primary purposes of this work is to compare the economic performance of LMFBR systems in which the blankets are composed of either thorium or uranium. This section will finalize this comparison. The end product of this analysis will be a graphical relationship showing the ratio of the price of U-233 to the price of fissile plutonium necessary for a thorium blanket to perform as economically as a uranium blanket. This ratio, called the break-even parity ratio, will be presented as a function of the price of fissile plutonium.

In the analysis presented here, fuel cycle cost contributions were generated using the fissile inventories from the batch irradiation case. (A comparison of the economics of batch irradiation versus zone scatter management was presented in the previous section.) Economics data were derived in the following manner. First a series of economic analyses was performed using the batch irradiation material inventories for both the thorium and the uranium blanketed systems. The variable in these economic analyses was the price of the fissile isotope: U-233 or plutonium. Core and axial blanket power cost contributions were then evaluated at 600 days (two full power years, or one core batch). Next radial blanket cost contributions were assessed. This was done by treating each row of the radial blanket separately. The power cost contribution for a given row was determined to be the contribution at the economic optimum irradiation time for that row or at 1800 days, whichever came first. Finally, a table was prepared which showed the total fuel cycle cost (including core, axial blankets, and radial blankets)

for thorium and uranium blanket systems as a function of the value of fissile plutonium and U-233. Figure 5.20 shows these results. This figure shows that for a fixed price of U-233, increasing the value of fissile plutonium has a more pronounced effect on the thorium blanketed system fuel cycle cost than on the uranium blanketed system. This is because in the uranium blanketed system, increasing the value of plutonium increases the charges related to the core, but at the same time makes the contribution to the total fuel cycle cost of the radial and axial blankets more negative. The two effects counterbalance each other to some extent. In the thorium blanketed system at constant U-233 value, however, increases in the price of fissile plutonium have only the effect of increasing the cost contribution from the core.

Because all the relationships shown on Fig. 5.20 are linear, it was possible to develop two equations which expressed the total system fuel cycle cost for uranium and thorium blanketed systems as functions of fissile isotope values. These relationships are:

U-238 Blanketed System

$$C = 0.02173\ P^{49} + 0.6203 \qquad (5.1)$$

Th-232 Blanketed System

$$C = 0.07613\ P^{49} - 0.04793\ P^{23} + 0.6648 \qquad (5.2)$$

where C = the total fuel cycle cost (mills/kw-hr)

P^{49} = value of fissile plutonium ($/g)

P^{23} = value of U-233 ($/g).

Because of the simplicity of the form of these relationships, future studies comparing the economics of two similar systems can be performed using only a small number of parametric analyses.

Fig. 5.20 Economic Comparison of Th and U Blanket Systems

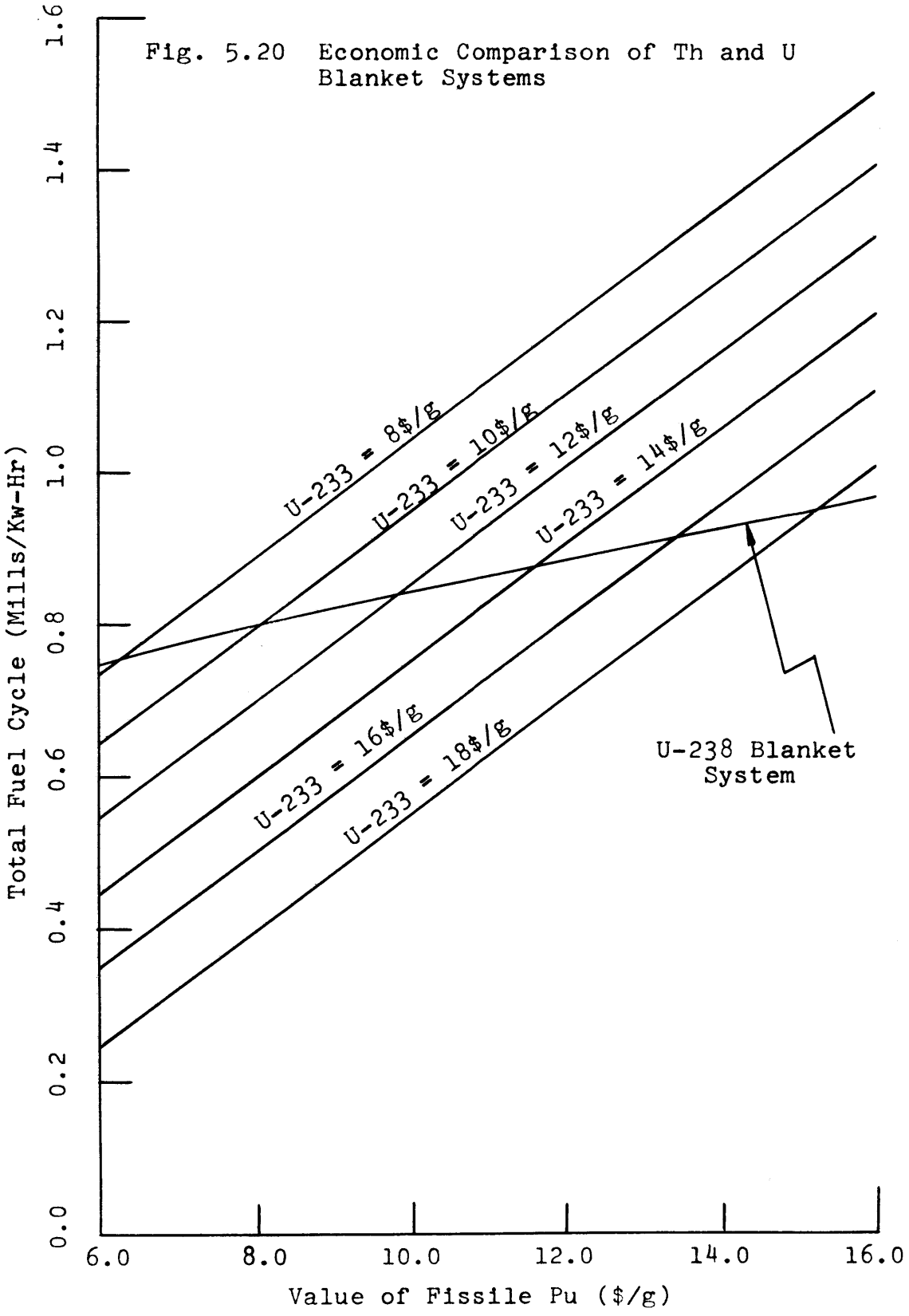

Each intersection point on Fig. 5.20 represents a point at which the cost contribution from the two systems (thorium and uranium blankets) are the same. If the ratio between the value of U-233 and the value of fissile plutonium is taken at each intersection point, then the break-even parity ratio can be plotted. Figure 5.21 shows the parity ratio as a function of the value of fissile plutonium. As shown, the value of U-233 always has to be higher than the value of fissile plutonium for the thorium blanketed system to perform as well as the uranium blanketed system. This observation results from a combination of two factors. First the thorium blankets do not produce quite as much fissile material as the uranium blankets, and second, the contamination of the product U-233 with U-232 in the thorium blanket reduces the effective value of the product by as much as $1.70 per gram (see sec. 5.3.3).

In considering Fig. 5.21, it is informative to refer back to Table 5.3 in which the expected parity ratios between U-233 and fissile plutonium are presented for both High Temperature Gas Cooled Reactors (HTGR's), and Light Water Reactors (LWR's). This table reveals that, for both prospective recycle systems, the parity ratio of interest is significantly higher than any of the break-even values shown in Fig. 5.21. This leads to the same conclusion as expressed by other investigators (F1, K1, L2), that an economically attractive fuel utilization strategy would be to use the "dirty" plutonium produced in LWR's as fuel for LMFBR's and use the blanket regions of LMFBR's to convert thorium to U-233 for use as fuel in LWR's and HTGR's.

Fig. 5.21 Break-Even Parity Ratio: Ratio of the Values of U-233 and Fissile Pu vs. Value of Fissile Plutonium

NOTE: Estimated Parity Ratio from Table 5.3
Range: 1.53 to 1.88

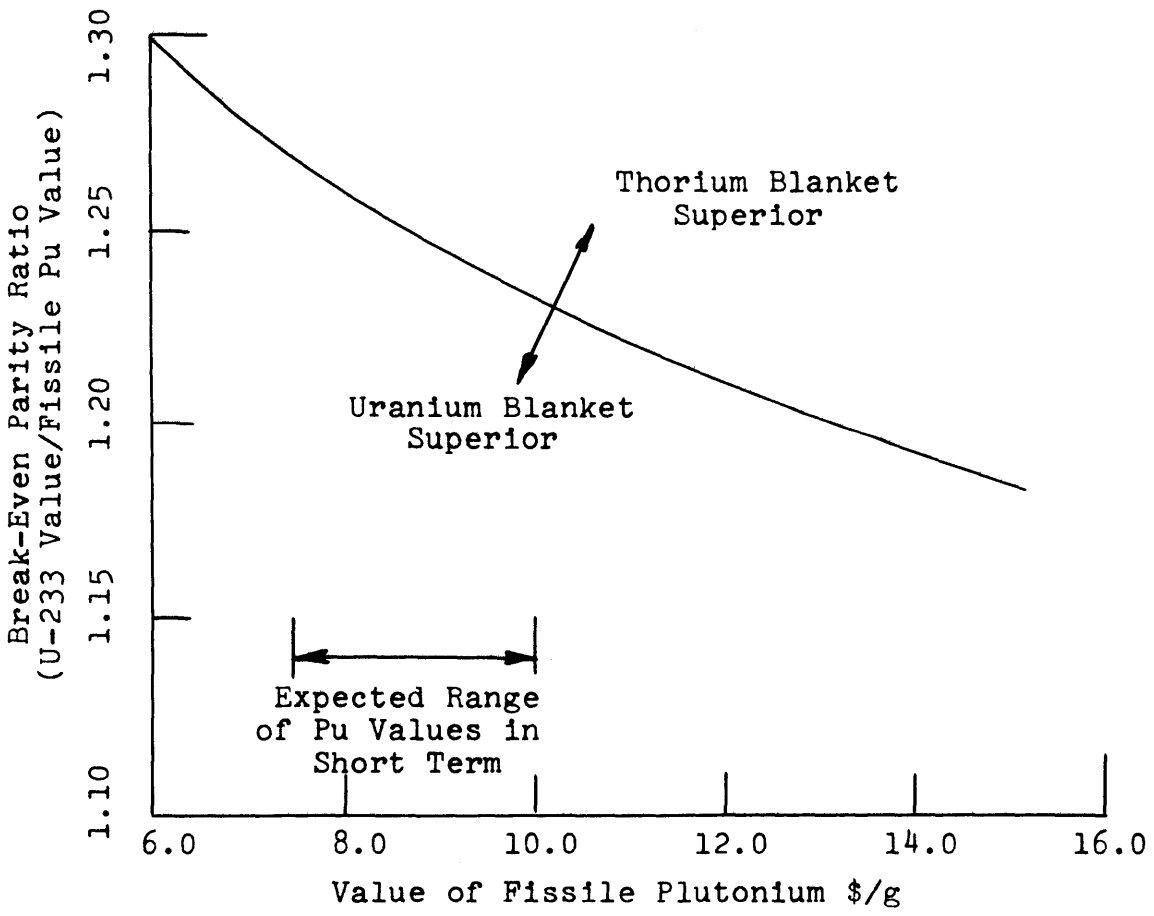

The last information presented in this section is Fig. 5.22 in which the net savings to the LMFBR system (in dollars per year) resulting from using a thorium blanket is plotted against the value of fissile plutonium. The assumed value of U-233 in this figure is 16.70 $/g. If the HTGR parity ratio value is used to derive the fissile plutonium value, the net savings is approximately 1.2 million dollars per year. If the LWR parity ratio is used, the savings is approximately 2.0 million dollars per year.

5.5 CORRELATION OF ECONOMIC OPTIMA

5.5.1 Development

In an earlier economic analysis (B3) of LMFBR radial blankets, variations in blanket economic performance with changes in the economic environment were demonstrated by presenting a large number of parametric curves for each blanket region of interest. Because changes in the economic environment can occur fairly frequently, it is desirable to develop a correlation which will predict the economic optimum irradiation time for radial blanket rows as a function of some generalized economic parameter. It is desirable to account for all the possible significant variations in environment with just one correlating parameter. It is the purpose of this section to develop such a parameter from the generalized fuel cycle cost equation presented by Brewer (B3), and to test how well the optimum irradiation time and blanket fissile enrichment at the optimum time can be correlated.

Let us begin with a modification of the local fuel cost contribution equation presented by Brewer (ref. B3, p. 89). (See also Appendix C.1.)

Fig. 5.22 Net Savings Associated with Using Th Blankets in a 1000 MWe LMFBR as a Function of Fissile Pu Value (16.70 $/g Assumed Value of U-233)

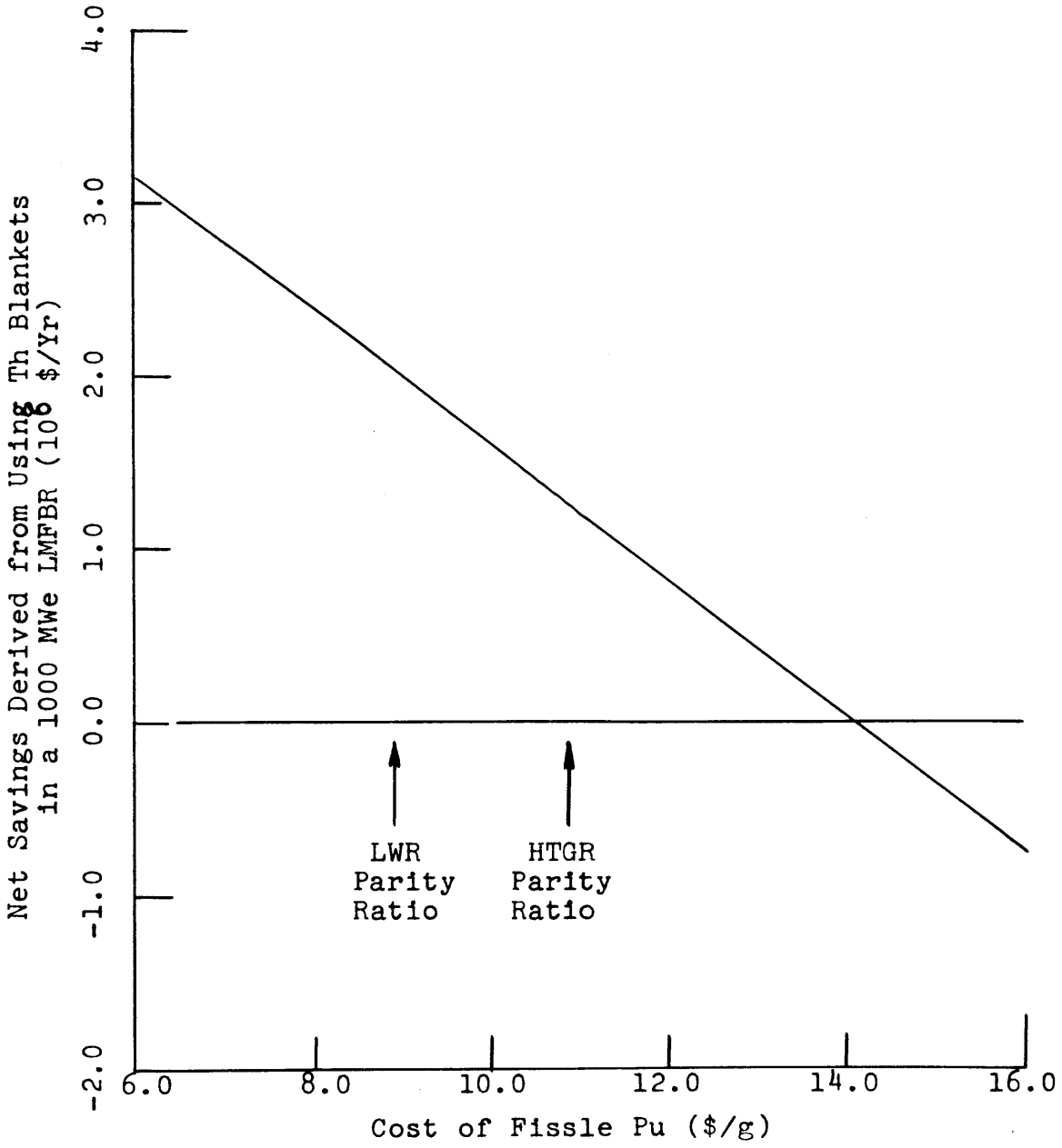

$$e \propto \frac{C_1F_1(-T_1) + C_2F_2(-T_2) - C_3F_3(-T_3)E(T)}{T} \qquad (5.3)$$

where e is the fuel cycle cost contribution

C_i are cost components ($/kg) for operation i

$F_i(-T_i)$ are carrying charge factors for operation i, occurring at time T_i measured from the irradiation midpoint

E(T) is the fissile enrichment at time, T

T is the length of the irradiation

Subscript 1 refers to fabrication

Subscript 2 refers to reprocessing

Subscript 3 refers to material credit.

In this equation the multiplicative constants have been omitted as have been the material inventories in each of the cost terms. This is justified because the parameter which is desired should be dimensionless and dependent only on parameters from the economic environment. Also assumed in this relationship is that the material purchase is either negligible or included in the fabrication charges. Because a correlation for the optimum irradiation time is desired, the next step in the development is to set the time derivative of the fuel cycle cost contribution equal to zero.

$$\frac{de}{dT} = 0 \qquad (5.4)$$

or

$$0 = TC_1 \frac{dF_1(-T_1)}{dT} - C_1F_1(-T_1) + TC_2 \frac{dF_2(-T_2)}{dT} - C_2F_2(-T_2)$$

$$- TC_3\left\{E(T) \frac{dF_3(-T_3)}{dT} + F_3(-T_3) \frac{dE(T)}{dT}\right\} + C_3E(T)F_3(-T_3) \qquad (5.5)$$

From Reference (B3), page 81, expressions for the carrying charge factors were obtained.

$$F_1(-T_1) = \frac{1}{1-\tau}\left[(1+X)^{T_1} - \tau\right] \qquad (5.6)$$

$$F_2(-T_2) = (1+X)^{T_2} \qquad (5.7)$$

$$F_3(-T_3) = (1+X)^{T_3} \qquad (5.8)$$

where τ is the tax rate

X is the discount factor.

Next, time derivatives were taken of the carrying charge factors. In these operations, series expansions were used where necessary to obtain simple expressions. First, consider $F_1(-T_1)$.

$$F_1(-T_1) = \frac{1}{1-\tau}\left[(1+X)^{T_1} - \tau\right] \cong 1 + \left(\frac{X}{1-\tau}\right) T_1 \qquad (5.9)$$

Consider only tax rates of 0.5.

$$F_1(-T_1) \cong 1 + 2XT_1 \cong (1+2X)^{T_1} \qquad (5.10)$$

$$\frac{dF_1(-T_1)}{dT} \cong F_1(-T_1)\ \ln(1+2X)\ \left(\frac{1}{2}\right) \cong F_1(-T_1)X \qquad (5.11)$$

To proceed with this development, the definitions for T_1, T_2, and T_3 must be introduced.

$$T_1 = \Delta T_1 + T/2 \tag{5.12}$$

$$T_2 = -\Delta T_2 - T/2 \tag{5.13}$$

$$T_3 = -\Delta T_3 - T/2 \tag{5.14}$$

where T is the time of the irradiation,

ΔT_1 is the length of time from the fabrication cash flow to the beginning of the irradiation,

ΔT_2 is the length of time from the end of the irradiation to the reprocessing cash flow,

ΔT_3 is the length of time from the end of the irradiation to the material credit cash flow.

Taking derivatives of Eqs. 5.12, 5.13 and 5.14 yields

$$dT_1/dT = 1/2 \tag{5.15}$$

$$dT_2/dT = -1/2 \tag{5.16}$$

$$dT_3/dT = -1/2 \tag{5.17}$$

Combining Eqs. 5.10, 5.11 and 5.12 yields

$$\frac{dF_1(-T_1)}{dT} \cong X(1+2X)^{\Delta T_1}(1+2X)^{T/2} \cong XF_1(-\Delta T_1)(1+XT) \tag{5.18}$$

Consider next the time derivatives of $F_2(-T_2)$ and $F_3(-T_3)$.

$$\frac{dF_2(-T_2)}{dT} = (1+X)^{T_2} \ln(1+X) \frac{dT_2}{dT} \tag{5.19}$$

Using Eq. 5.16 and expanding the logarithmic term yields

$$\frac{dF_2(-T_2)}{dT} \cong -\frac{X}{2} F_2(-T_2) \tag{5.20}$$

Combining Eqs. 5.20 and 5.13 gives

$$\frac{dF_2(-T_2)}{dT} = -\frac{X}{2} F_2(\Delta T_2)(1+X)^{-T/2} ; \tag{5.21}$$

expanding the last term produces

$$\frac{dF_2(-T_2)}{dT} = -\frac{X}{2} F_2(\Delta T_2)(1-X/2\ T); \tag{5.22}$$

similarly

$$\frac{dF_3(-T_3)}{dT} = -\frac{X}{2} F_3(\Delta T_3)(1-X/2\ T). \tag{5.23}$$

Equations 5.18, 5.22 and 5.23 can now be substituted into Eq. 5.5 and the carrying charge factors in the resulting expression can be approximated using the following relationships:

$$F_1(-T_1) \cong F_1(-\Delta T_1)(1+X/2\ T) \tag{5.24}$$

$$F_2(-T_2) \cong F_2(\Delta T_2)(1-X/2\ T) \tag{5.25}$$

$$F_3(-T_3) \cong F_3(\Delta T_3)(1-X/2\ T) \tag{5.26}$$

When the terms are collected in the relationship resulting from the above manipulations, the following expression is arrived at:

$$0 = T^2\left\{C_1X^2F_1(-\Delta T_1) + C_2\left(\frac{X}{2}\right)^2 F_2(\Delta T_2) + C_3\frac{E(T)}{T}\left(\frac{X}{2}\right)F_3(\Delta T_3)\right\}$$
$$- C_1F_1(-\Delta T_1) - C_2F_2(\Delta T_2) - T^2C_3E(T)\left(\frac{X}{2}\right)^2 F_3(\Delta T_3) \tag{5.27}$$

If it is now assumed that the fissile material builds up linearly in the radial blanket, Eq. 5.27 can be rewritten (neglecting the resulting T^3 term for simplicity):

$$T^2\left\{C_1X^2F_1(-\Delta T_1)+C_2\left(\frac{X}{2}\right)^2F_2(\Delta T_2)+C_3R\left(\frac{X}{2}\right)F_3(\Delta T_3)\right\}$$
$$= C_1F_1(-\Delta T_1) - C_2F_2(\Delta T_2) \qquad (5.28)$$

where the fissile enrichment has been approximated by

$$E(T) = RT \qquad (5.29)$$

Rearrangement of Eq. 5.28, with recognition of the fact that the time (T) in the resulting equation is the optimum irradiation time T_{opt}, yields the following expression:

$$T_{opt} = \frac{1}{X}\left[\frac{C_1F_1(-\Delta T_1) + C_2F_2(\Delta T_2)}{C_1F_1(-\Delta T_1)+\frac{1}{4}C_2F_2(\Delta T_2)+\frac{1}{2}C_3\left(\frac{R}{X}\right)F_3(\Delta T_3)}\right]^{1/2} \qquad (5.30)$$

Because of the low cost of fabrication and reprocessing relative to that of fissile material value, the first two terms in the denominator can be neglected with respect to the last term. The expression resulting from this analysis is

$$T_{opt} \cong \sqrt{\frac{2}{R}}\left[\frac{C_1F_1(-\Delta T_1)+C_2F_2(\Delta T_2)}{C_3F_3(\Delta T_3)(X)}\right]^{1/2} \qquad (5.31)$$

The corresponding expression for the enrichment at the optimum irradiation time is

$$E_{opt} = \sqrt{2R}\left[\frac{C_1F_1(-\Delta T_1)+C_2F_2(\Delta T_2)}{C_3F_3(\Delta T_3)X}\right]^{1/2} \qquad (5.32)$$

Because of the large number of assumptions and omissions used in developing Eq. 5.32, the actual equation would not be expected to apply. However, all of the most important economic parameters are included within the brackets in both Eqs. 5.31 and 5.32. As a result,

one might expect that the optimum irradiation time and the enrichment at the optimum irradiation time would correlate against the optimum economic parameter:

$$N_E = \left[\frac{C_1 F_1(-\Delta T_1) + C_2 F_2(\Delta T_2)}{C_3 F_3(\Delta T_3) X} \right]$$

To summarize the definitions of the terms in the optimum economic parameter, N_E, the following relationships are presented

$$F_1(-\Delta T_1) = \frac{1}{1-\tau} \left[(1+X)^{\Delta T_1} - \tau \right] \tag{5.33}$$

$$F_2(\Delta T_2) = (1+X)^{-\Delta T_2} \tag{5.34}$$

$$F_3(\Delta T_3) = (1+X)^{-\Delta T_3} \tag{5.35}$$

$$X = (1-\tau) r_b f_b + r_s f_s \tag{5.36}$$

where the terms are defined in Appendix A. Because of the form of Eq. 5.32, this correlation might also be expected to be linear when plotted on log-log graph paper. The next section will address the question of how well the economic data can be correlated with the optimum economic parameter given above.

5.5.2 Optimum Model

5.5.2.1 Parametric Variations

In the previous section an optimum economic parameter was developed. The purpose of this section is to show how well optimum irradiation time and enrichment at the optimum time can be correlated

against this parameter. The source of data for this correlation was a series of parametric studies in which the economic variables shown in Table 5.9 were used. As shown, nearly all variables in the optimum economic parameter were perturbed by at least a factor of 2 from their minimum to their maximum values. The only variable which was not varied through as significant a range was the discount rate.

TABLE 5.9 Range of Variation of Economic Parameters

Parameter	Units	Range of Variation
Value of fissile Pu	\$/g	6.0 to 16.0
Value of U-233	\$/g	8.0 to 18.0
Fabrication charges	\$/kg	69. to 140.
Reprocessing charges	\$/kg	50. to 100.
Discount rate (X)	$Year^{-1}$	0.075 to 0.085

A 1967 survey of worldwide economic parameters appropriate for use in analyzing nuclear power economics (N3) shows that interest rates in most European countries were within about a percent of those in the United States, so the small range of variation of the discount rate is acceptable.

The indicated variation in the discount rate was obtained by changing the tax rate (τ) from 0.5 to 0.35 in the otherwise standard private utility economic environment. A series of economic analyses was also made using the financial parameters appropriate for a typical public utility such as TVA. The parametric studies were made using the material inventory data from the batch irradiation and zone scatter

management cases for both the uranium and thorium radial blankets.

5.5.2.2 Batch Blanket Irradiation

To determine how well the optimum economic parameter discussed earlier correlated economic optimum data, a series of parametric analyses was performed using the inventory data from the batch blanket irradiation cases. Economic optimum irradiation times for all cases were determined by fitting a parabola through the three points where the cost contribution from a given row of the radial blanket was near its minimum. This equation for the power cost contribution was then differentiated with respect to irradiation time, and the derivative was set to zero. Solution of this equation gave the irradiation time at which the power cost contribution was a minimum. The blanket row average enrichment at the optimum time was then determined by linear interpolation between the enrichments calculated by 2DB on either side of the optimum irradiation time. The optimum irradiation times and the blanket row average enrichments were then plotted against the optimum economic parameter for all of the cases analyzed. An example of how the optimum points were derived is presented in Table 5.10.

Figure 5.23 shows the optimum irradiation time for a batch managed row 1 uranium radial blanket as a function of the optimum economic parameter. As expected, this plot – on log-log paper – yielded a straight line with very little scatter in the data about the line. For row 1 of this radial blanket, it appears that the optimum irradiation time is proportional to the economic parameter raised to the 0.62 power. This is not in bad agreement, considering the assumptions involved in developing the parameter, with the predicted value of 0.5.

TABLE 5.10 Optimum Irradiation Time Evaluation

Input Data to the Economics Model

Blanket type: Uranium radial blanket row 1

Irradiation: Batch irradiation for 1800 full power days

Economic environment: Standard (see Table 5.1)

Output Data from the Economics Model

Irradiation Time (Full Power Days)	Power Cost Contribution (mills/kw-hr)	Fissile Enrichment at the Time (%)
900	-0.089898	3.770
1000	-0.089968	4.086
1100	-0.089256	4.387

Economic Optimum Data

(Optimum time determined using a quadratic fit to the economics data above)

Optimum irradiation time = 959 days

Minimum power cost = -0.090034 mills/kw-hr

Enrichment at the optimum = 3.956% (from linear interpolation)

Optimum economic parameter = N_E = 0.1592

For C_1 = 69 $F_1(-0.5)$ = 1.07846

C_2 = 50 $F_2(0.5)$ = 0.96225

C_3 = 10,000 $F_3(0.5)$ = 0.96225

X = 0.08

Fig. 5.23 Linear Approximation to the Effect of Changes in Economic Environment on the Optimum Irradiation Time for a Pow 1 Uranium Radial Blanket under Batch Irradiation

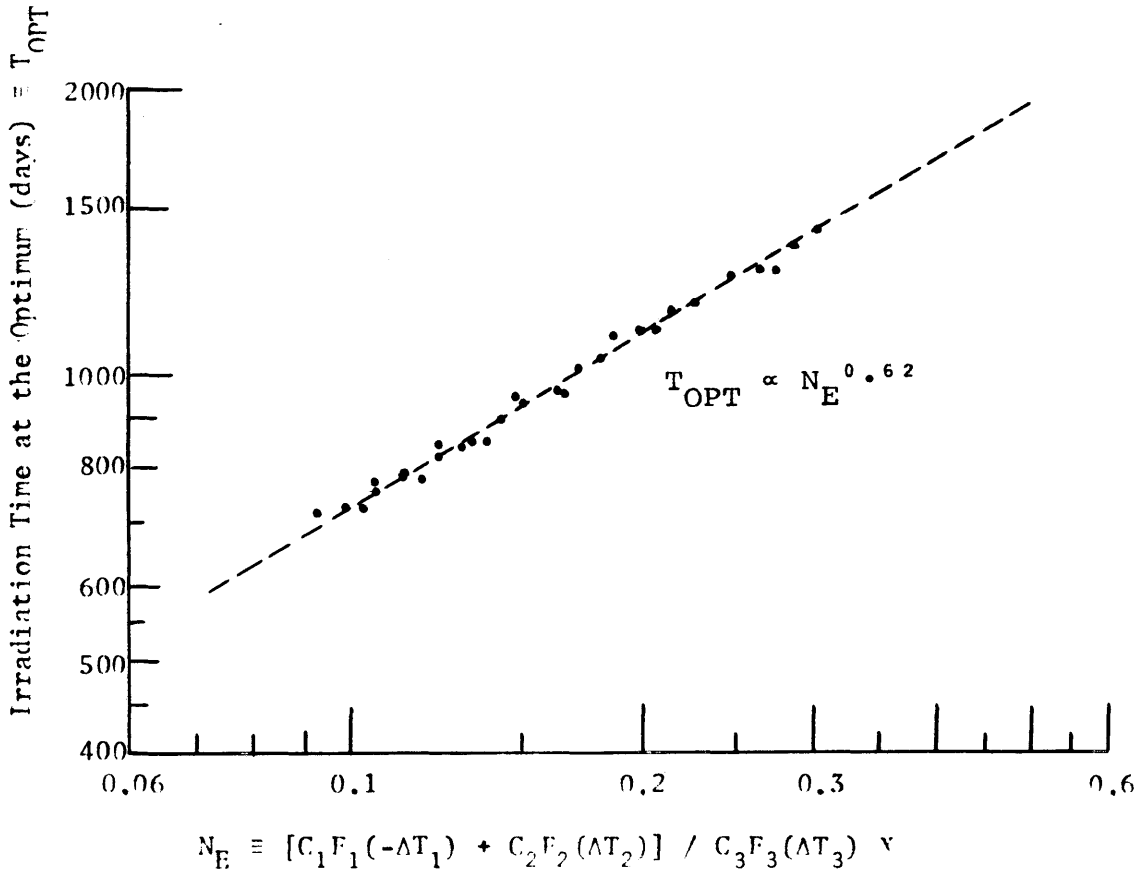

Figure 5.24 shows the correlation of the enrichment at the optimum irradiation time with the optimum economic parameter. Again the predicted linearity on log-log paper is observed, and the observed slope of 0.46 is in good agreement with the predicted value of 0.5.

Both of the two previous figures showed some scatter in the data about the correlation lines. To assess the impact of this scatter on the power cost contribution from row 1 of the radial blanket, assuming the correlation was used to select an optimum irradiation time, a sensitivity study was performed. This sensitivity analysis made use of the parabolic correlation between power cost contribution and irradiation time near the optimum which was discussed earlier. Using this correlation for each economic case analyzed, the irradiation times and enrichments corresponding to a power cost contribution 0.001 mills/kw-hr greater than the minimum were calculated. Figures 5.25 and 5.26 show the variation in the irradiation time and corresponding end point enrichment about the optimum values which can be accommodated with an economic penalty of only 0.001 mills/kw-hr. As shown, a very small economic penalty would be paid (0.001 mills/kw-hr corresponds to 7000 dollars per year for the LMFBR treated here) if row 1 of the radial blanket were removed from the reactor 100 days on either side of the optimum irradiation time. This conclusion might have been expected based on the observation earlier that curves of power cost contribution versus irradiation time were very flat near their economic optimum.

Consideration should now be given to the performance of the batch irradiated thorium radial blanket row 1. Figures 5.27 and 5.28 show the optimum irradiation time and the average enrichment at that time

Fig. 5.24 The Linear Approximation to the Effect of Changes in Economic Environment on the Enrichment in a Uranium Radial Blanket Row 1 at the Optimum Irradiation Time, Batch Irradiation

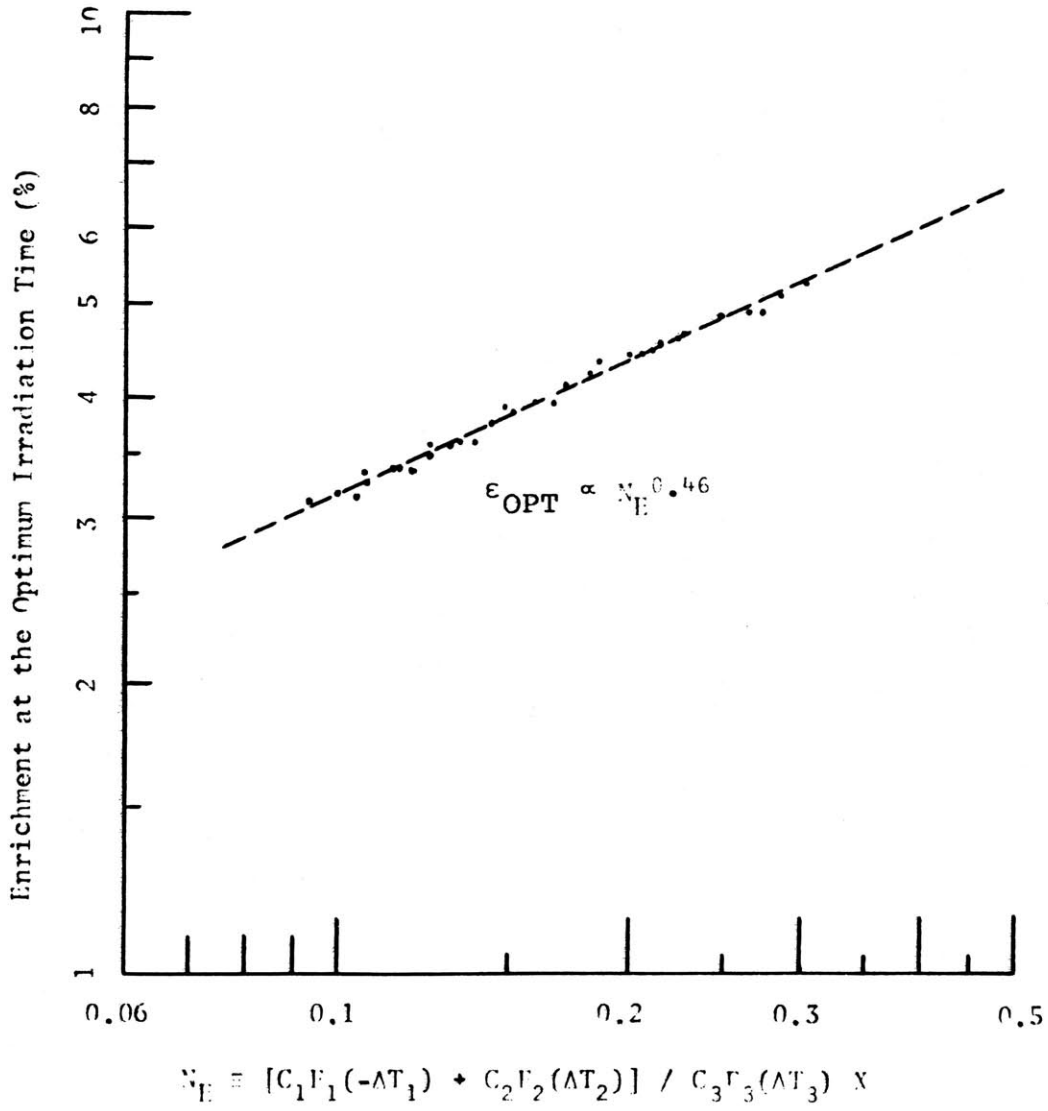

Fig. 5.25 The Sensitivity of the Uranium Radial Blanket Pow 1 Optimum Irradiation Time to Variations in the Power Cost Contribution about the Optimum

(Dashed lines indicate the range of irradiation times which would produce a power cost penalty of 0.001 mills/KW-hr)

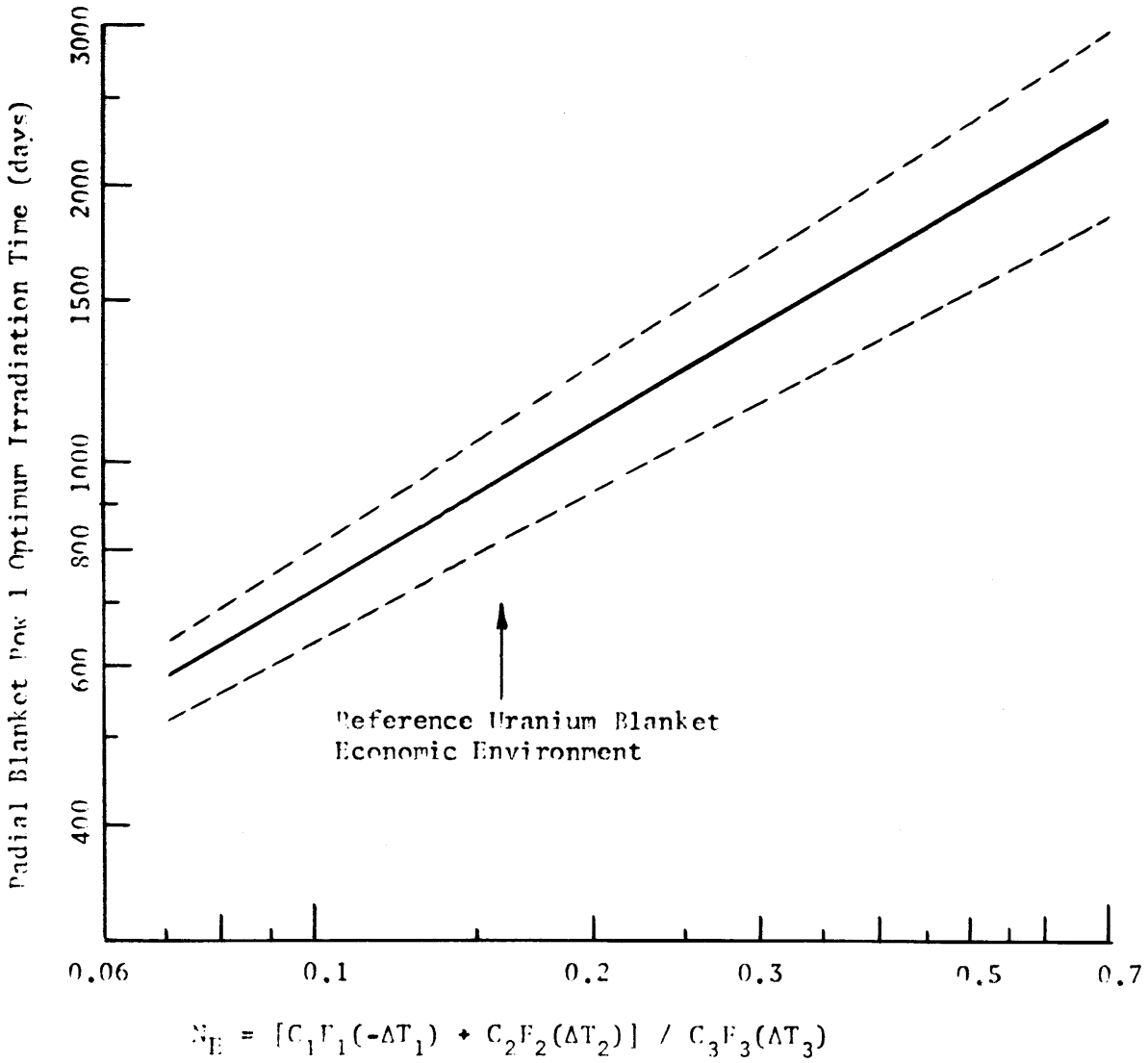

Fig. 5.26 The Sensitivity of the Uranium Row 1 Radial Blanket Optimum Enrichment to Variations in the Power Cost Contribution about the Optimum

(Dashed lines indicate the range of end point enrichments which would produce a power cost penalty of 0.001 mills/ KW-hr)

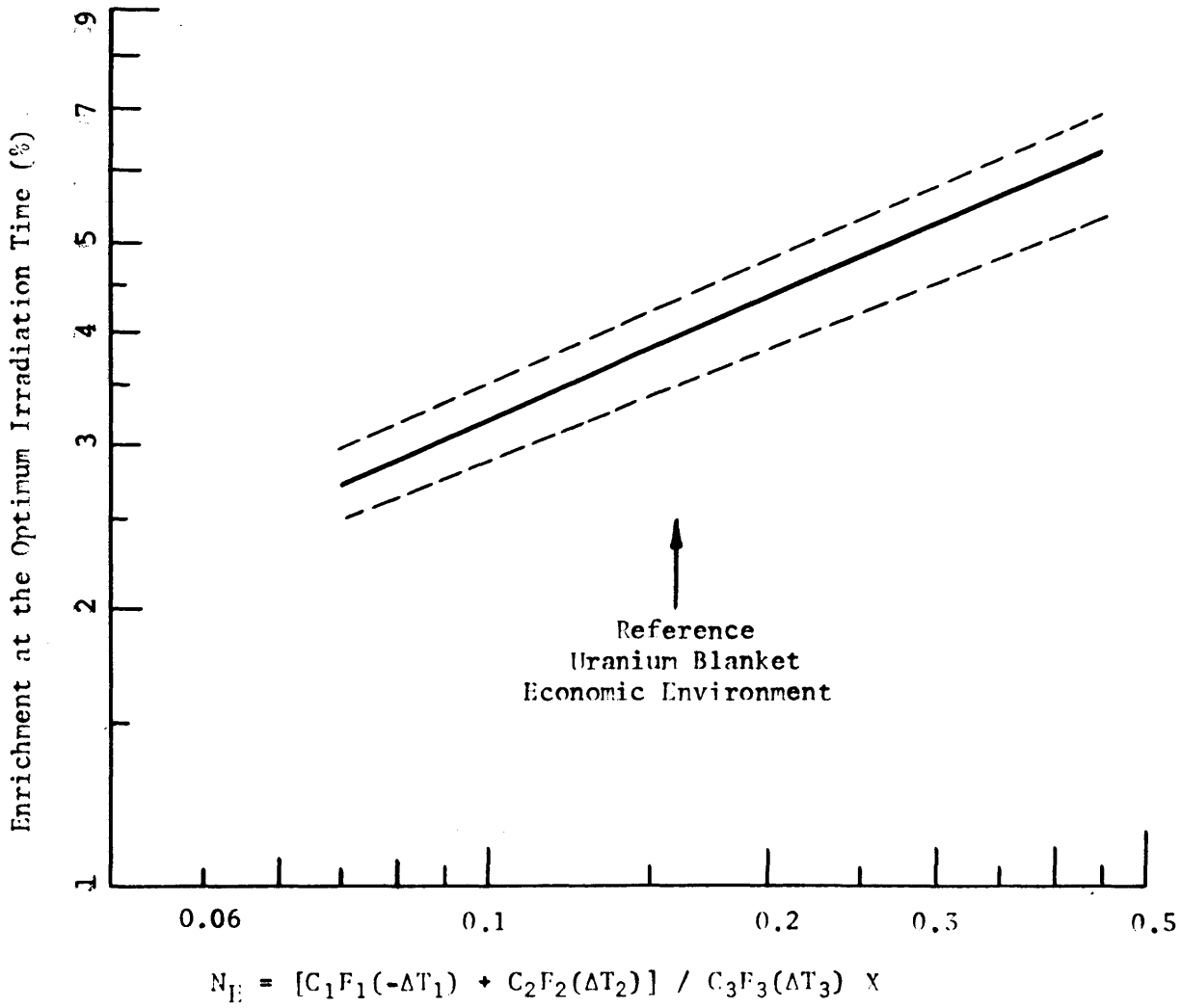

Fig. 5.27 Comparison of Radial Blanket Row 1 Optimum Irradiated Time for Batch Irradiated Thorium and Uranium Blankets

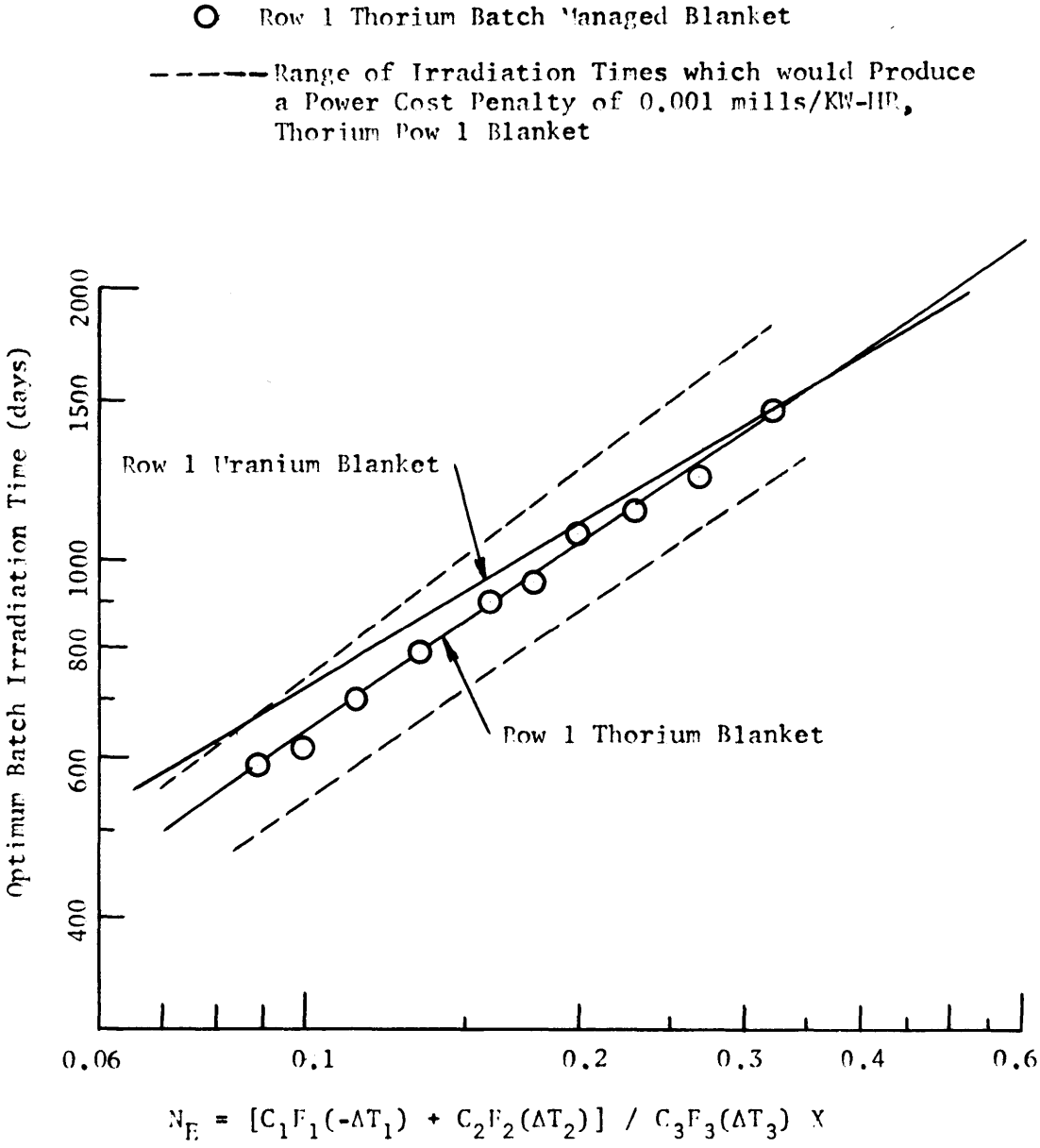

Fig. 5.28 Comparison of Radial Blanket Row 1 Optimum Enrichment for Batch Irradiated Thorium and Uranium Blankets

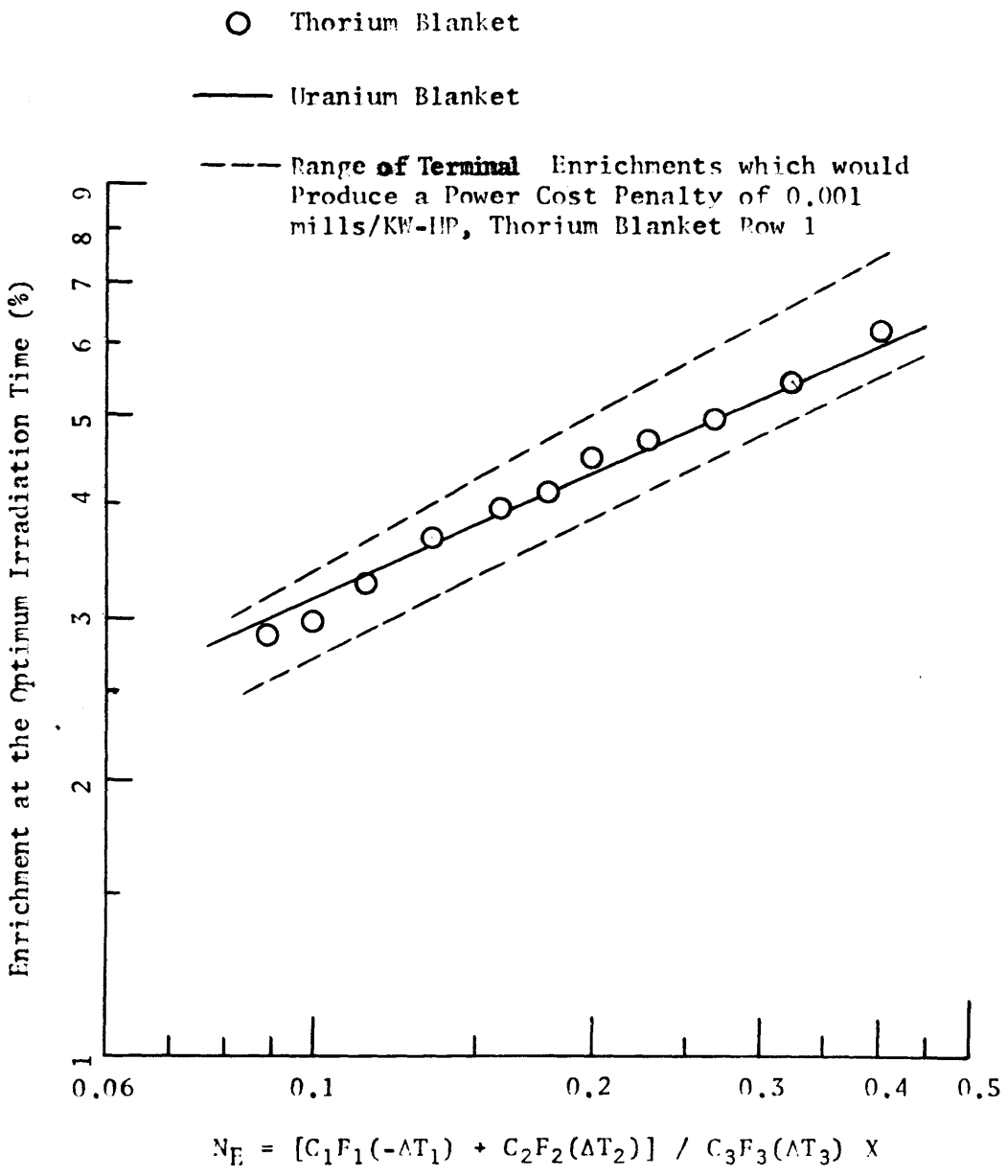

as functions of the economic parameter. As shown, not only are the thorium blanket optimum times and enrichments linear functions of the economic parameter, but the thorium blanket characteristics closely correspond to those for the uranium blanket. Two features should be noted in Fig. 5.27. First, the optimum batch irradiation time for the thorium blanket row 1 is less than that for the uranium blanket at small values of the economic parameter, and second, the slope of the correlation for the thorium blanket is greater than that for the uranium blanket. Both features can be understood in light of the fact that the contaminant U-232 builds up in the thorium blanket with an associated economic penalty. This penalty can be viewed as effectively decreasing the value of the fissile material, U-233, produced in that blanket. Thus, for small values of the economic parameter, corresponding to large values of the fissile isotope, it is desirable to remove the fissile product before the economic penalty associated with the U-232 becomes too high. Next consider the relative slopes of the two curves. The effect of U-232 buildup is to reduce the effective value of the U-233 product. As the U-232 concentration increases, which it does with irradiation time, the effective U-233 value decreases. Thus, for a given value of the economic parameter, the effective U-233 value is less than the fissile plutonium value (given a specified economic environment which is the same for both blankets). As the value of the economic parameter increases, corresponding to a decrease in fissile material value, the difference in the effective values of U-233 and fissile plutonium increases due to the longer irradiation times required to achieve equilibrium. Thus as the economic parameter

increases in value, the effective value of the parameter (corrected for U-232 penalty) increases at a more rapid rate for the thorium blanket than for the uranium blanket. Hence, the slope of the optimum irradiation time versus economic parameter plot should be steeper for the thorium blanket than for the uranium blanket. Figure 5.28 shows that the row 1 radial blanket enrichment at the optimum irradiation time is nearly the same, within the indicated sensitivity limits, as that for the uranium blanket.

Because of the slow buildup of fissile material in radial blanket row 2 relative to row 1, the economic optimum for row 2 is achieved much later in the irradiation cycle than that for row 1. Figures 5.29 and 5.30 show optimum irradiation times and enrichments at the optimum for row 2 thorium and uranium radial blankets. Again, because of the U-232 buildup, the thorium blanket achieves its economic optimum before the uranium blanket. It is also interesting to note that the apparent slopes of the correlations in Figs. 5.29 and 5.30 are nearly the same for row 2 of the uranium and thorium blankets as for row 1 of the uranium blanket. Also, the thorium and uranium blankets are the same within the sensitivity limits indicated.

Now that the optimum economic parameter has been shown to correlate the optimum irradiation times and the corresponding enrichments quite well, the question of what practical use can be made of these correlations should be addressed. Once burnup analyses have been performed to determine the breeding characteristics of a given radial blanket configuration, economic analyses are necessary to define how the blanket should be managed in a given economic environment. Because features of the economic environment (such as fissile

Fig. 5.29 The Effect of Economic Environment on the Optimum Irradiation Time of Row 2 Radial Blanket

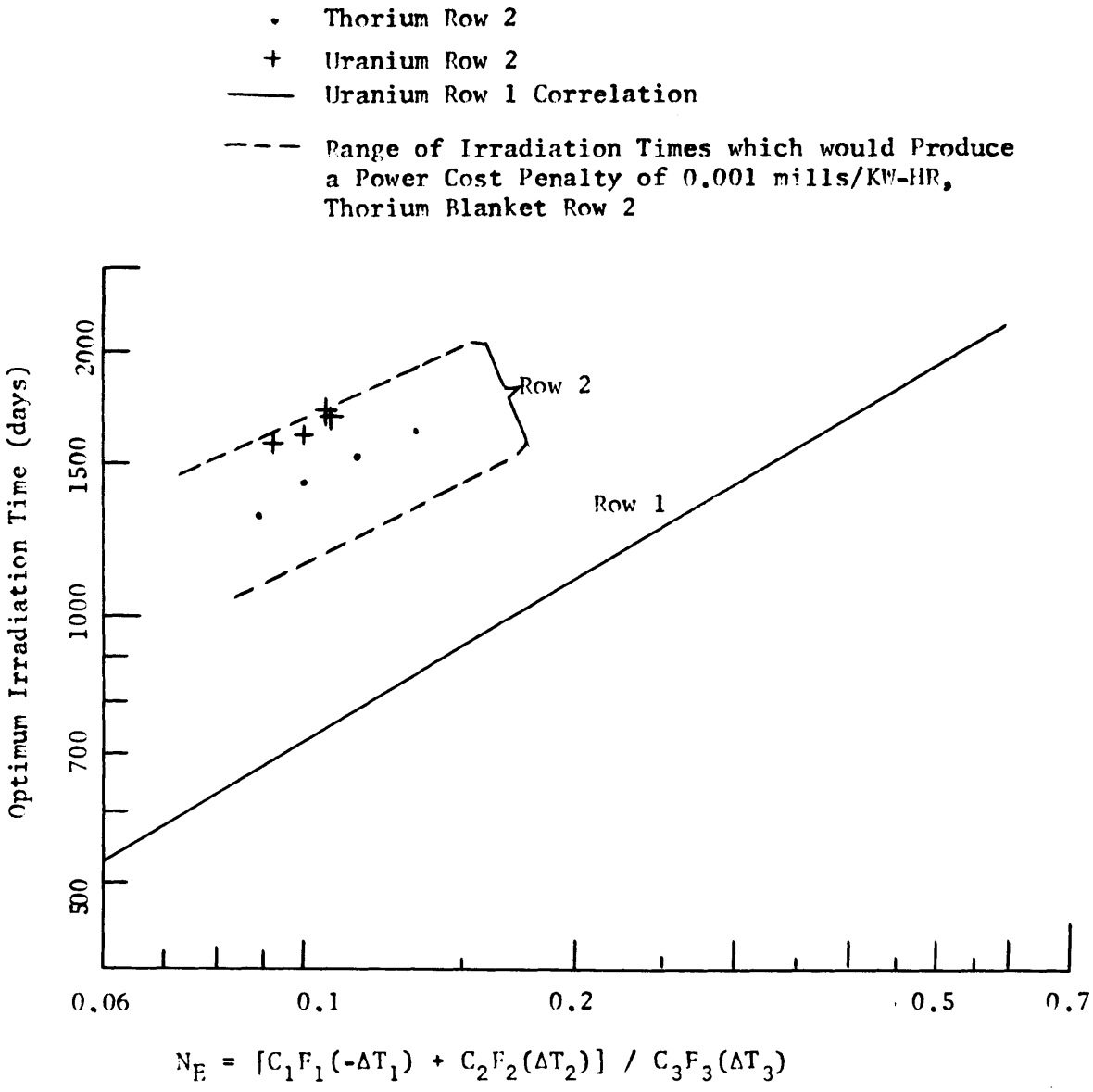

Fig. 5.30 The Effect of Economic Environment on the Radial Blanket Row 2 Enrichment at the Optimum

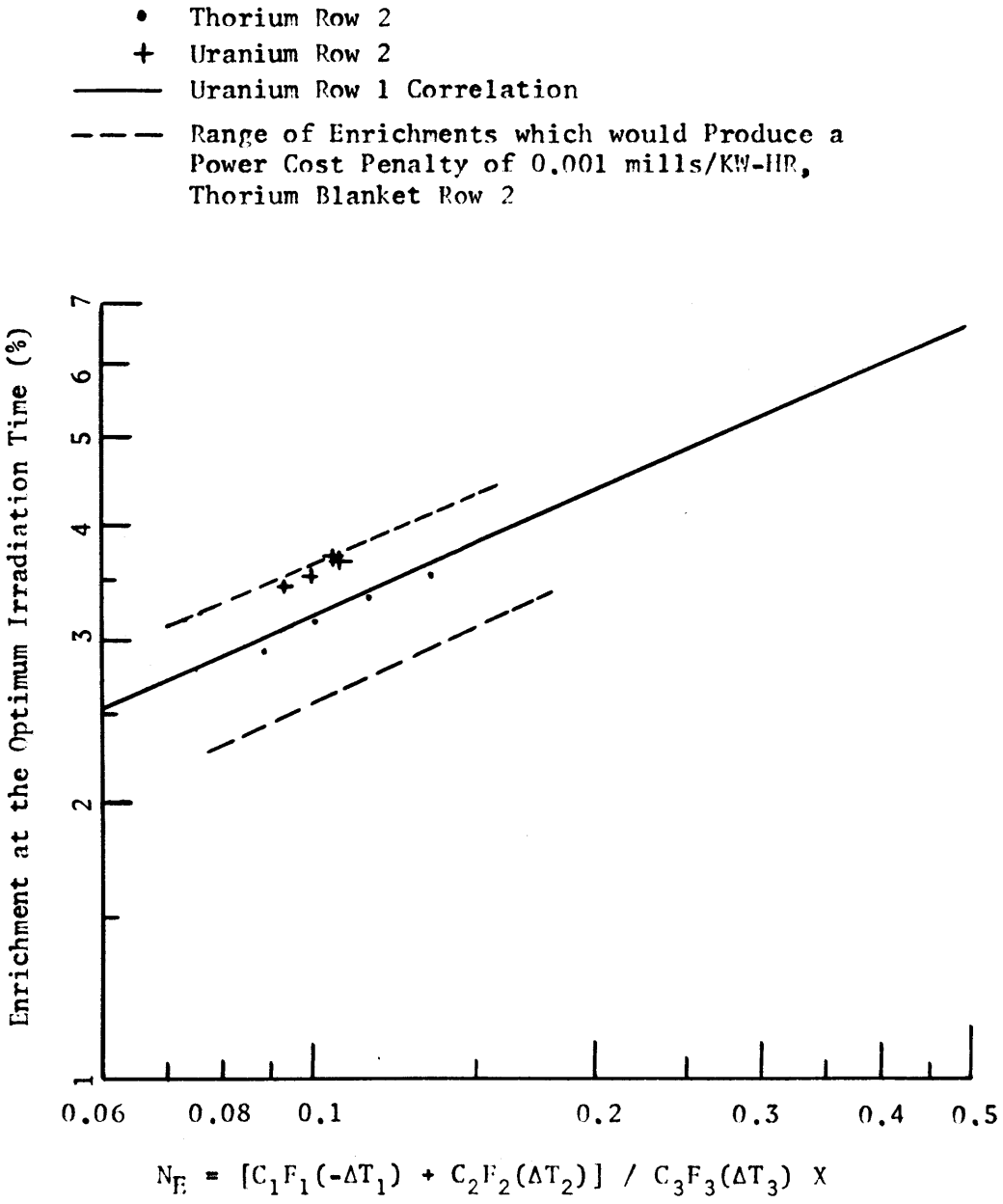

isotope value and fabrication or reprocessing costs) may change while a system is in operation, it is desirable to redefine blanket management procedures without repeating the entire economic analysis. This redefinition can be accomplished simply if the initial economic analysis included at least two sets of economic parameters in determination of the optimum irradiation times. Using the correlation line established by these two points on the curve of either optimum irradiation time or optimum enrichment versus the optimum economic parameter, the optimum irradiation times for a whole range of economic parameters can be specified. Thus, given a change in the economic environment, an operator can refer to a general curve to determine the action he should take to continue optimum management of the radial blanket.

It should be mentioned that the correlations developed in this work are specific to the reactor being analyzed. If the blanket design were to change (e.g., a reduction in the height of the fertile region in radial blanket assemblies) or the core were to change in such a way that the leakage or blanket spectrum would be affected, then a new optimum economic correlation would need to be established for the new system design. The general form of the correlation, however, should be appropriate for analysis of any radial blanket system. It may even be that further generalizations will be forthcoming: it is speculated that the slope of the correlation lines may not be as sensitive to design variations as the amplitude.

5.5.2.3 Managed Blankets

The economic optimum performance of radial blanket row 1 would be unaffected if zone scatter management were used rather than batch irradiation. However, as was shown in section 4.5, the breeding performance of radial blanket row 2 is affected by the zone scatter management of row 1. In this section the effect of blanket management on row 2 economics will be presented using the same format as in the previous section. Figures 5.31 and 5.32 show optimum irradiation time and enrichment at that time as functions of the optimum economic parameter. As shown, the radial blanket row 2 data for the case in which row 1 is zone scatter managed are more scattered than for the batch irradiation case. This might be expected from the shape of the row 2 fissile inventory versus irradiation time curves. In the batch irradiation case, these curves were smooth for all three rows. However, for the zone scatter managed case, a change of slope in the row 2 inventory curve occurred every time row 1 assemblies were replaced (see sec. 4.5). Despite the greater scatter of the data for these cases, the data all fall on a single line within the sensitivity brackets established for a variation of 0.001 mills/kw-hr in power cost contribution. Again both thorium and uranium blankets are the same within the sensitivity limits.

Figure 5.33 is a cross plot of enrichment at the optimum versus optimum irradiation time. As expected, the data all fall on straight lines. The correlations for row 1 of the uranium and thorium radial blankets have nearly identical slopes, and the optima are within a few days of each other. All of the available data for row 2 of the uranium and thorium radial blankets with row 1 zone scatter managed fall on

Fig. 5.31 The Effect of Radial Blanket Zone Scatter Management on the Optimum Irradiation Time of Radial Blanket Row 2, for a Variety of Economic Environments

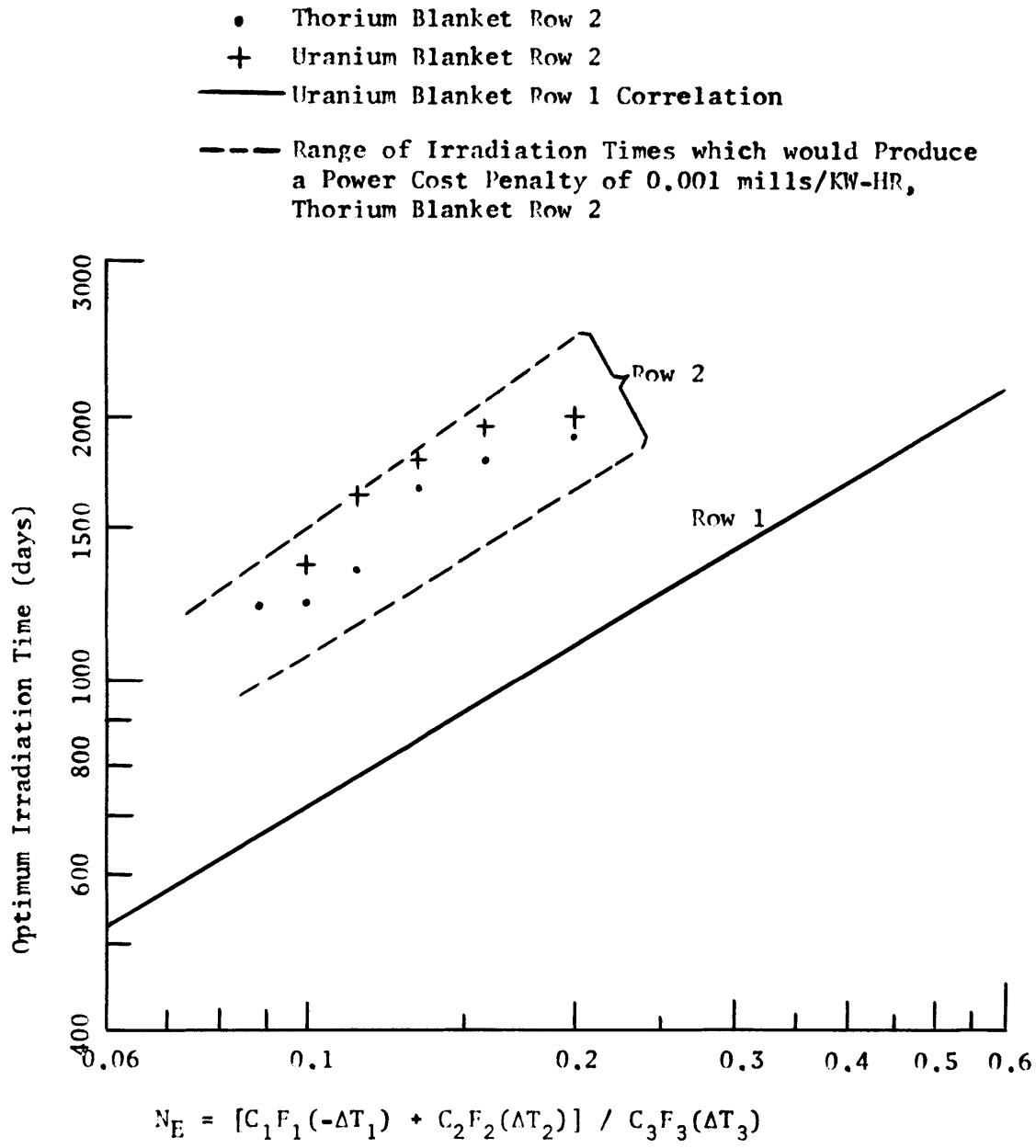

Fig. 5.32 The Effect of Radial Blanket Zone Scatter Management on Optimum Enrichment of Radial Blanket Row 2, for a Variety of Economic Environments

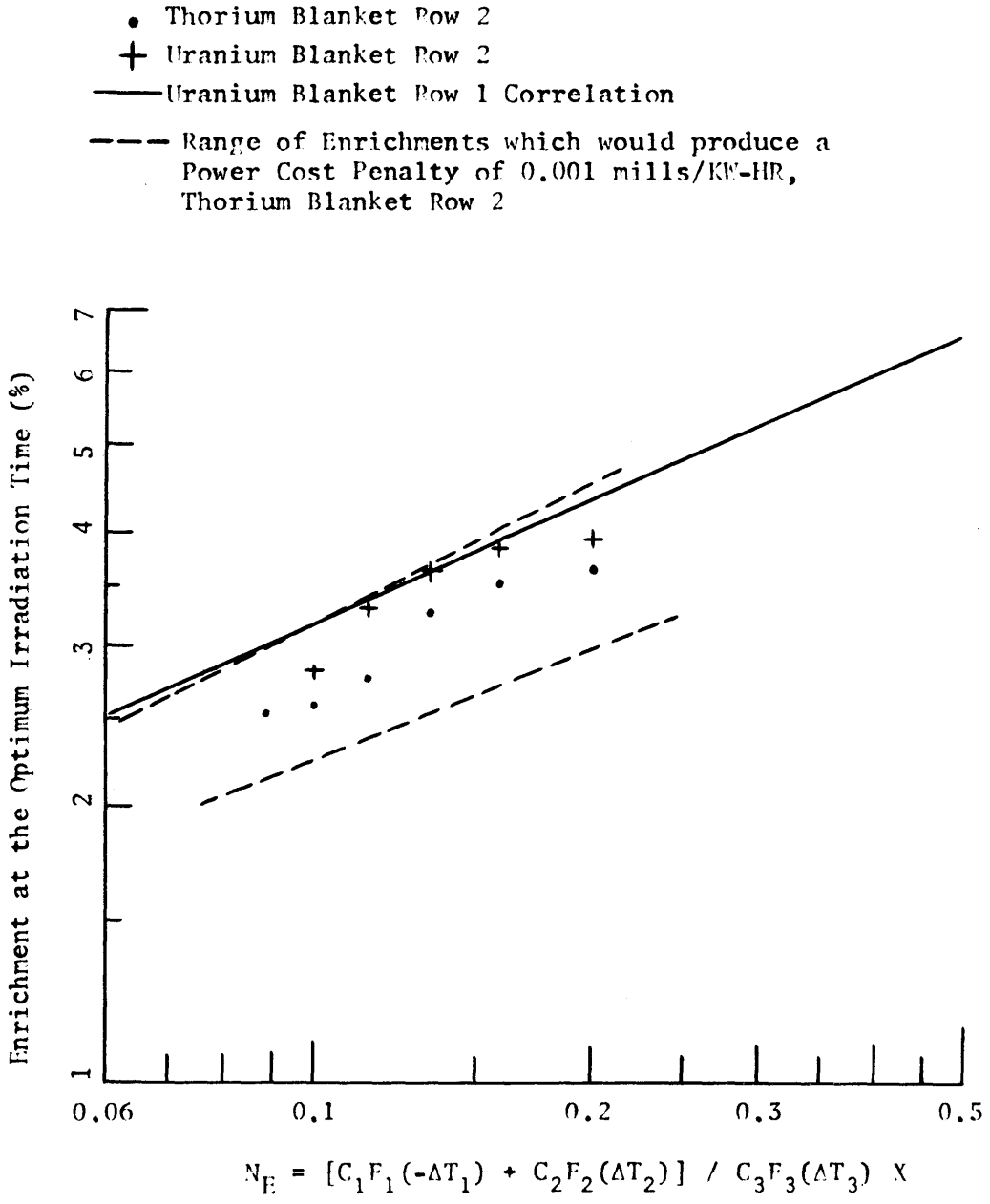

Fig. 5.33 Irradiation Time at the Optimum versus Optimum Enrichment for both Managed (Zone Scatter) and Batch Irradiated Blankets

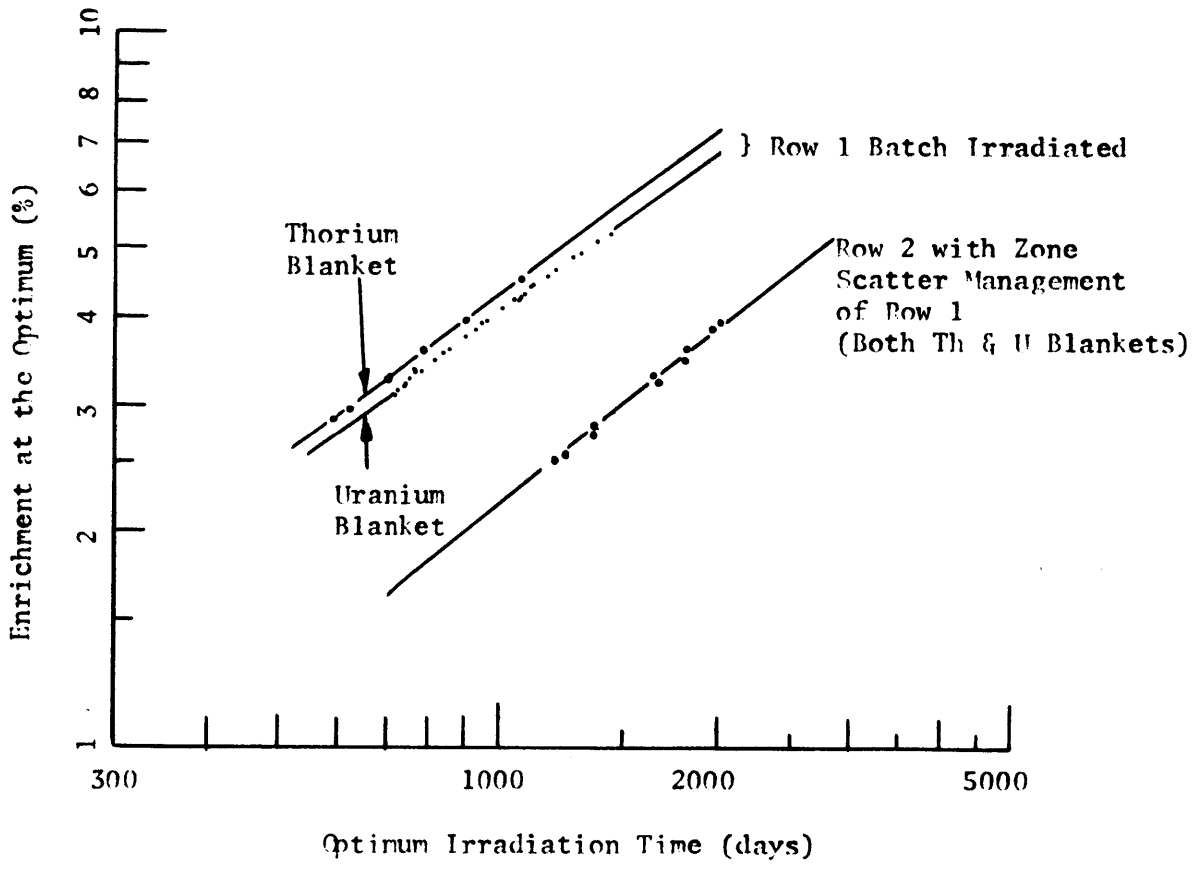

the same curve. This curve has approximately the same slope as those for the row 1 assemblies. The fact that the data in Fig. 5.33 are on a straight line implies that if fissile enrichment for a given radial blanket region were plotted against irradiation time on log-log paper, these data would fall on a straight line. The fact that the slopes of the curves shown in Fig. 5.33 are nearly 1.0 implies that the fissile isotope inventory in these regions of the radial blanket varies nearly linearly with irradiation time.

5.5.3 Break-Even Model

Because the optimum economic parameter was effective in correlating the optimum irradiation times and corresponding enrichments, the same parameter was used in an attempt to correlate the irradiation time and enrichment at the break-even point. For the purpose of this discussion, the break-even point is defined as the time when the contribution to the total system power cost from a given radial blanket row is zero. As an example, refer to Fig. 5.8. This figure shows that the break-even irradiation time for row 1 of a uranium radial blanket in the reference economic environment is approximately 265 days. The break-even points for all the uranium blanket cases are presented in Figs. 5.34 and 5.35. These figures show that the break-even irradiation times are very nearly linear when plotted on log-log paper against the optimum economic parameter. Also, the break-even irradiation time increases significantly for blanket regions farther removed from the core interface. This latter point would be expected because of the lower fissile production rate in outer rows of the radial blanket. Figure 5.35 shows that when the enrichment at the break-even

Fig. 5.34 Irradiation Time at the Break-Even Point for a U-238 Blanket

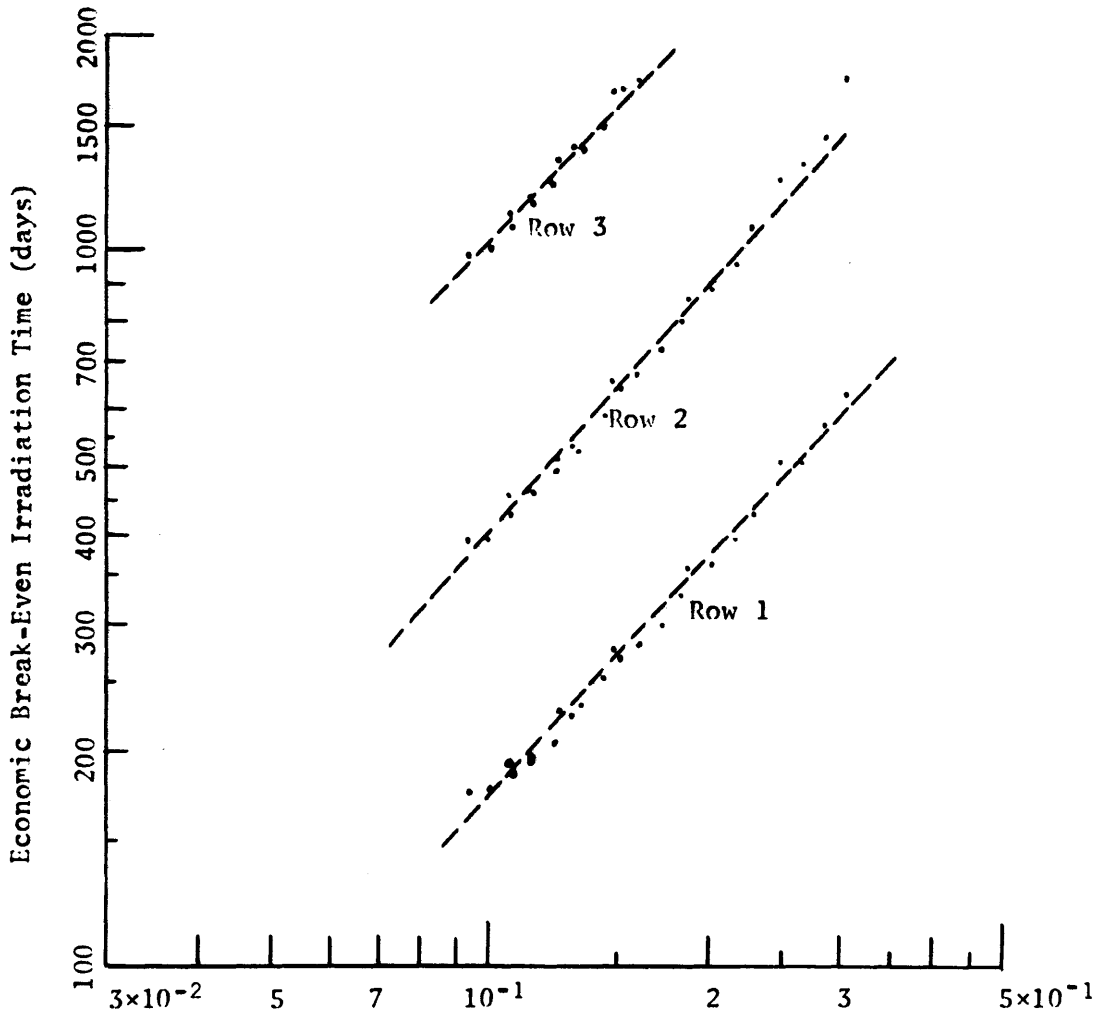

$$N_E = [C_1F_1(-\Delta T_1) + C_2F_2(\Delta T_2)] \; / \; [C_3F_3(\Delta T_3)Y]$$

Fig. 5.35 Enrichment at the Break-Even Point for a U-238 Blanket System

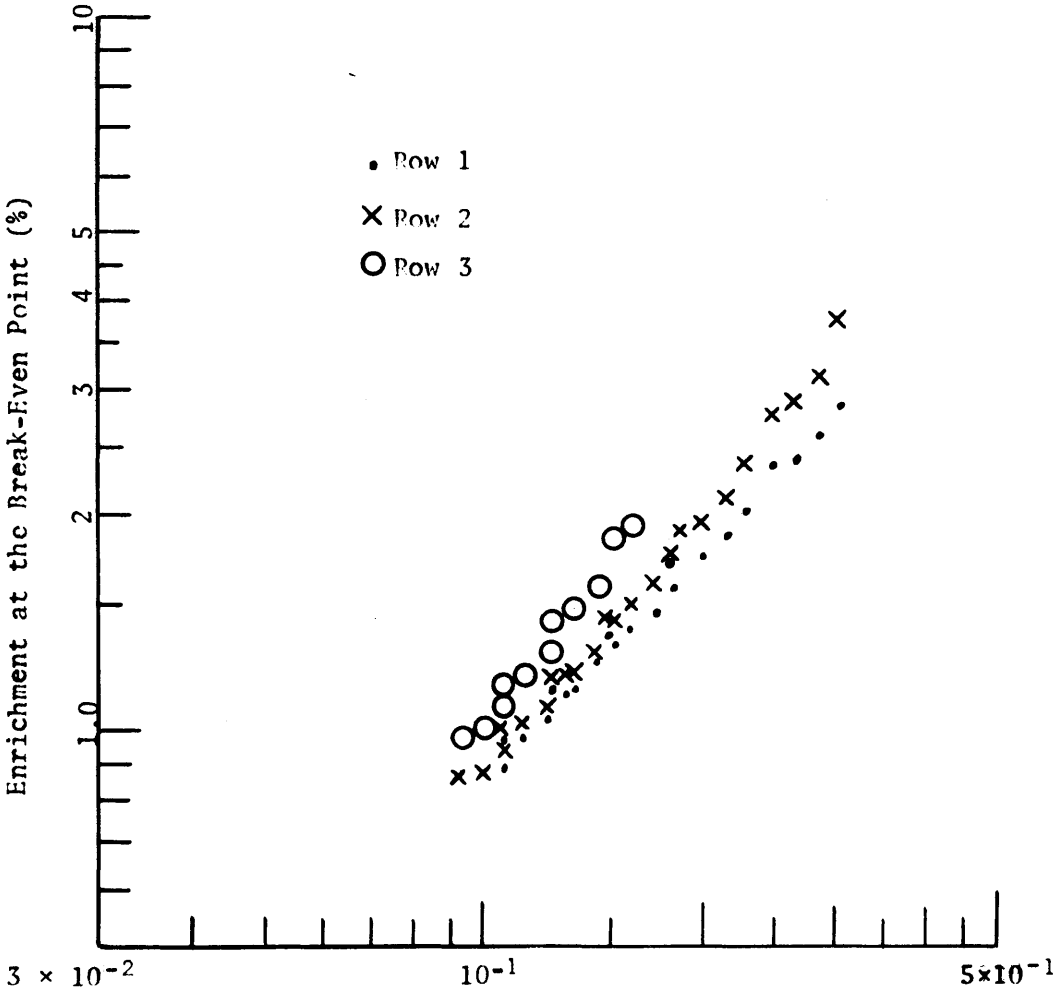

$$N_E = \frac{C_1F_1(-\Delta T_1) + C_2F_2(\Delta T_2)}{C_3F_3(\Delta T_3)X}$$

point is plotted against the optimum economic parameter, the relationship is again nearly linear on log-log paper. Also shown on that figure is the fact that the enrichment at the break-even irradiation time is a much less sensitive function of radial position in the blanket than is break-even irradiation time. As expected from the fact that both the optimum and break-even irradiation times vary nearly linearly on log-log paper when plotted against the optimum economic parameter, a log-log plot of break-even versus optimum irradiation times is nearly linear. This is shown in Fig. 5.36.

5.6 EFFECT OF UNCERTAINTIES

5.6.1 Introduction

The economic analysis which has been presented in this chapter has several sources of error and uncertainty associated with it. These errors have been discussed in the text of previous chapters and sections. In this section an attempt will be made to consolidate all the sources of error and to discuss quantitatively the effect that these errors will have in the comparative economic analysis presented earlier. This section will group the errors into three general categories: physical, analytical, and experimental. The chief source of the so-called physical error is in the separation of the core from the axial blanket for the thorium blanket case. The analytical error will be defined to include such effects as core and blanket management, and the method of physics analysis, on blanket economic analysis. Finally, the experimental error will be analyzed. This last category is something of a misnomer since what will actually be discussed is the effect of cross section

Fig. 5.36 Correlation Between Optimum and Break-Even Irradiation Times for a U-238 Blanket

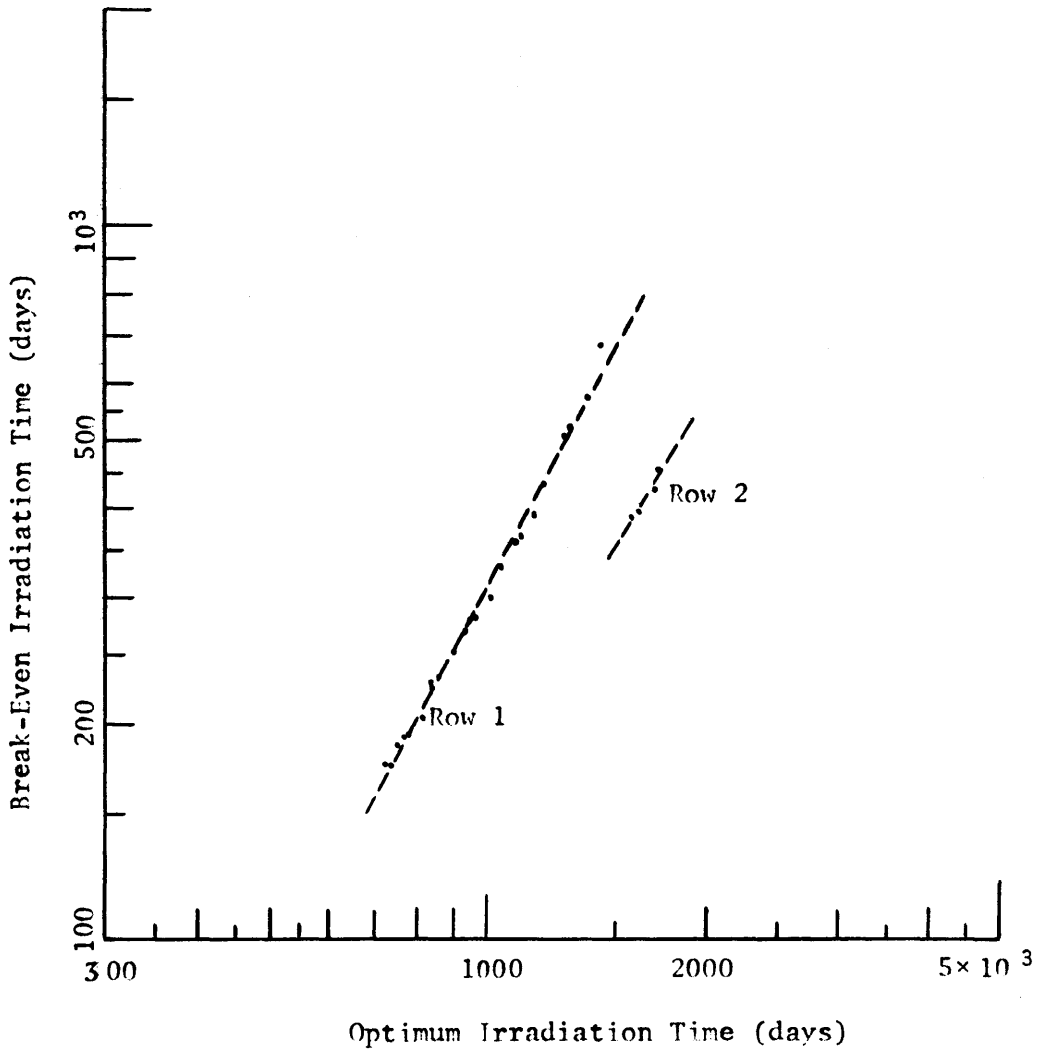

uncertainties as defined by the experiments discussed in Chapter 3 on blanket economic comparisons made in this chapter. To be consistent with the remainder of this report, errors will always be discussed as relative errors in uranium versus thorium blanket economics rather than as absolute errors.

5.6.2 Physical Errors

The primary difference between the two blanket systems which might lead to "physical errors" in the economic analysis is that the thorium axial blanket would have to be reprocessed separate from the core while the uranium axial blanket could be batch reprocessed with the core. As mentioned earlier, the head end processing of LMFBR fuel assemblies includes a shearing process (A4, F5, F6, U2) in which either the entire assembly or individual rods are sheared into 1-inch-long segments. If thorium were to be used for the axial blanket of a plutonium fueled reactor, then the physical separation between axial blanket and core would most likely lead to losses of fissile material. For the purpose of this analysis, it has been assumed that in the separation of core and axial blanket, the inch-long segment of axial blanket just above and below the core are mixed with material from the core in the head end processing, and thus the associated material credits are lost. Figure 5.37 shows the normalized beginning-of-life capture rate in the axial blanket as a function of distance from the core interface. This curve was developed using a one-dimensional ANISN analysis. Because the fissile material fission rate near the core interface is greater than in regions farther removed from the core, the net fissile production rate distribution would be expected to be

Fig. 5.37 Estimate of Fissile Production in the Thorium Axial Blanket

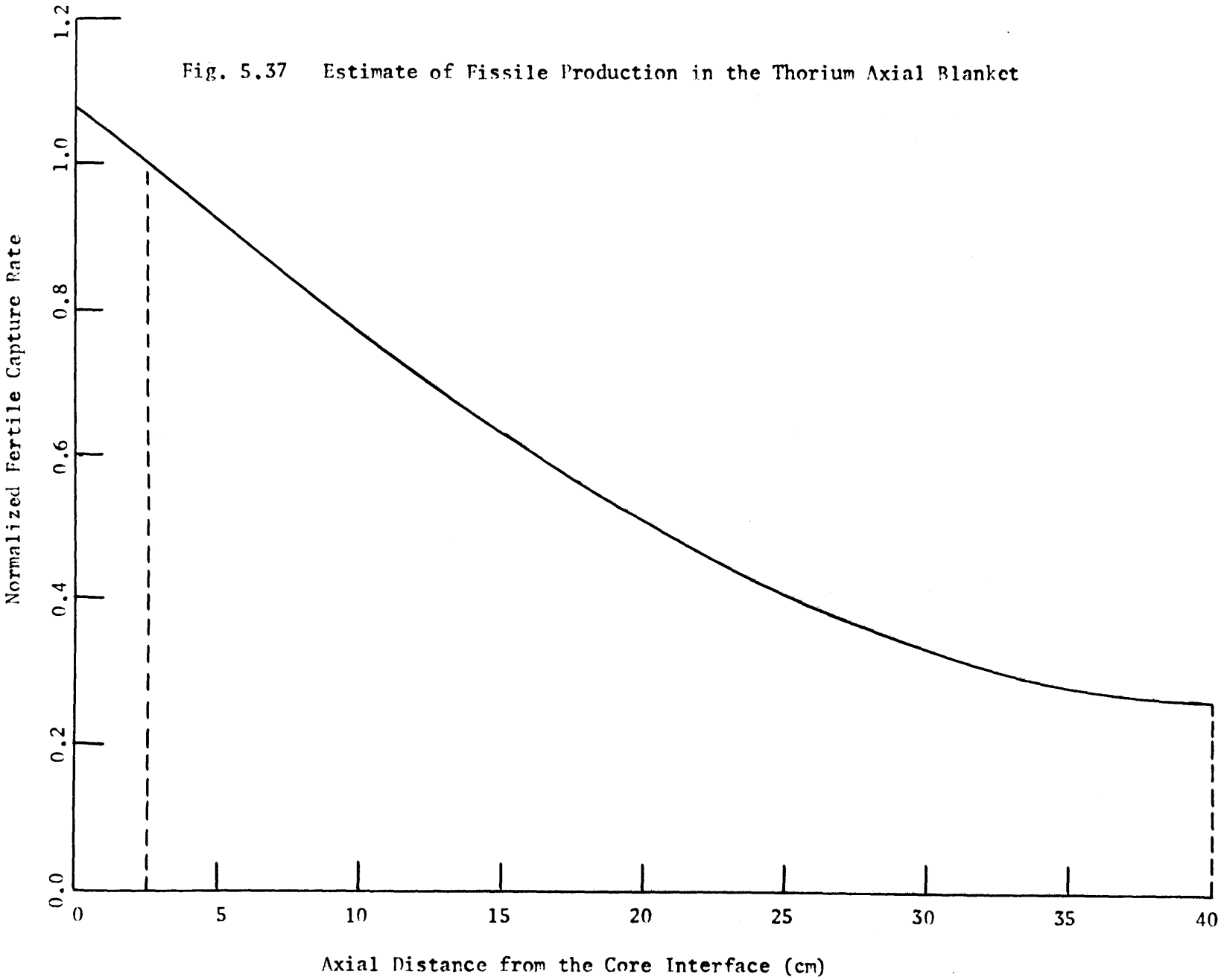

flatter than the production rate shown in Fig. 5.37 as the irradiation proceeds. Thus, it would be expected that the fissile inventory distribution calculated by use of Fig. 5.37 would show more material near the core interface than would be predicted from a burnup analysis. Consequently, when Fig. 5.37 was used to predict head end losses, a conservatively high penalty was derived. If the curve in Fig. 5.37 is integrated from the core interface to one inch from the interface, and that integral is divided by the integral over the entire axial blanket, the resulting ratio is the fraction of the fissile material produced in the axial blanket which is lost in head end processing. This analysis showed that a maximum of 11.4% of the fissile material might be lost through inexact shearing operations. This 11.4% loss represents an increase in the fuel cycle cost contribution from the axial blanket of 0.03815 mills/kw-hr in the reference economic environment, or a yearly penalty of approximately 275,000 dollars. Although this is a significant penalty, it represents only about 17% of the gross economic benefit associated with using thorium rather than uranium blankets in the standard economic environment. The complementary problem involving the presence of U-233 and U-232 in the core region should not present significant difficulties since both would appear in quite low concentrations; however, a chemical analysis of the reprocessed fuel material would need to be performed to assure that the reprocessed fuel's nuclear characteristics were as well known as possible.

A more thorough appraisal needs to be performed of the potential problems associated with a thorium axial blanket on a uranium/plutonium fuel assembly. Potential problems may arise in:

1) ascertaining the location of the axial blanket-core interface prior to the head-end shearing operation, 2) chemical separation of the core plutonium from a mixture of uranium and a small quantity of thorium. The severity of both of these problems could be reduced with a small cost penalty in breeding performance by using a 1- or 2-inch barrier of inert oxide material between the core and the axial blanket. A likely candidate for this use would be nickel oxide or some other non-contaminating, high-stability oxide.

A one-dimensional study using ANISN (E1) of the effect of a 5-cm-thick axial moat of nickel oxide between the core and the thorium axial blanket has shown that:

1) the moat causes a reduction in core critical mass of about 1.8%,
2) the fertile capture in the reduced thickness axial blanket is approximately 14% less than in the pure thorium blanket.

Based on these preliminary estimates, it appears that a NiO moat should be considered for use with a thorium axial blanket.

5.6.3 Analytical Errors

Included in the category "analytical errors" are a number of factors related to the calculations used to characterize the nuclear performance of the uranium and thorium blanketed systems. Included among these factors are,

1. The effect of core management,
2. The effect of blanket management,
3. The effect of U-232 economic losses resulting from batch blanket reprocessing.

This section will emphasize differences in the economic performance of uranium and thorium blanketed systems resulting from differences in the factors listed above.

The economic effects of core management on blanket performance were discussed in section 5.3.2. In this section, the core batch refueling interval was shown to have a small effect on blanket performance. Table 5.11 summarizes this effect on blanket performance.

TABLE 5.11 The Economic Effect of Core Batch Refueling Interval.

Region	Thorium Blanket Economic Penalty from Core Management ($/yr)
Axial blanket	9400.
Radial row 1	2200.
Radial row 2	--
Radial row 3	--
TOTAL	11600.

As shown, core management makes the uranium blanket appear only slightly better relative to the thorium blanket in its economic performance. Again the contribution of core management to relative blanket performance is insignificant with respect to the gross economic benefit associated with using a thorium blanket.

The effect of blanket management on relative economic performance was summarized in Tables 5.5, 5.6 and 5.7. These data are repeated in Table 5.12 in somewhat different form. As shown in Table 5.12, the most economical management scheme by a small margin is zone scatter. Use of this scheme would make the thorium

TABLE 5.12 Effect of Blanket Management on Economic Performance

Blanket Type	Management Scheme	Relative Economic Penalty ($/yr) Associated with Management*
Uranium	Batch	0.0
Uranium	Zone scatter	-41,000
Uranium	In-out shuffle	58,000
Thorium	Batch	0.0
Thorium	Zone scatter	-193,000

*Basis is batch management scheme.

blanket system economic performance improve relative to that for the uranium blanket system by approximately 152,000 dollars per year. This number takes into account the increase in handling associated with the zone scatter management scheme.

The last factor to be discussed here is the effect of the analytical treatment of the U-232 penalty on relative blanket performance. This problem was discussed in more detail in section 5.3.3.1. Figure 5.2 presented in that section showed that the effect of mixing all the radial blanket assemblies in the reprocessing stage would result in a penalty for the thorium blanket of approximately 0.0065 mills/kw-hr or 46,000 dollars per year. Again, this is a small penalty in view of the economic benefits associated with use of thorium blankets.

5.6.4 Reprocessing Considerations

5.6.4.1 General Discussion

A major objection which might be raised to the use of thorium blankets for LMFBR's is that special chemical reprocessing and fabrication facilities might be required to handle the blanket assemblies. Although these questions will require more detailed study prior to the actual use of thorium blankets for LMFBR's, several relevant points can be made. First, during the early years following the introduction of LMFBR's, the reprocessing and fabrication facilities for any type of assembly will be small and will suffer an economic penalty because of their size. Consequently, the penalty associated with small thorium blanket reprocessing facilities will be insignificant relative to that for uranium blanket reprocessing facilities. An estimate of this difference has been included in this analysis in the form of an economic penalty associated with the U-232 contaminant in irradiated thorium blankets. Second, fairly extensive experimental work has been done on reprocessing and fabrication of thorium assemblies at both Oak Ridge National Laboratory (N2, W4) and at the Babcock and Wilcox Company (M2, K6). This work has shown that the U-233 product can be separated from fuel assemblies with losses of less than 1% (M2). (These losses can, of course, be further reduced if the value of the recovered U-233 is sufficiently high.) The same studies have shown (M2) that thorium can be separated from a mixture of uranium and plutonium in a reasonable number of partition stages using the THOREX process. Third, the expected design lifetime of a reprocessing plant is approximately 15 years (M2); thus, separation facilities designed to process

thorium blankets have lives on the same order as the time during which thorium blankets are expected to be economically attractive. Finally, the head-end processing involved in the processing of thorium blankets is the same as for uranium blanket processing, and the chemical separation is the same as required for oxide HTGR fuels. Thus, a thorium blanket reprocessing operation might be associated with either a uranium blanket reprocessing facility or an HTGR fuel reprocessing facility, whichever is economically more attractive. In fact, a plant operated by Nuclear Fuels Services (R4) has the capability to reprocess either thorium or uranium base fuel. Thus, a firm technological basis exists for thorium fuel reprocessing, and, by proper location of the reprocessing facilities, cost differentials between thorium and uranium reprocessing and fabrications can be minimized.

5.6.4.2 Reprocessing Losses and Delays

An economic analysis was performed to evaluate the effect of reprocessing losses and delays in reprocessing time on blanket economics. Table 5.13 summarizes the results of those analyses. As shown in the table, both reprocessing delays and losses are more costly for a thorium than for a uranium blanket. However, there is no reason to expect that a thorium blanket will have either greater reprocessing losses or a longer delay from the end of irradiation to reprocessing than a uranium blanket. If a 6-month delay time is allowed between the end of irradiation and the chemical reprocessing, the undecayed Pa-233 represents only about 0.04% of the total blanket fissile product. Thus the penalty associated with Pa-233 loss is

TABLE 5.13 The Economic Effect of Reprocessing Losses and Delays

Type Blanket	Blanket Region	Economic Penalties (mills/kw-hr) for 1% Reprocessing Loss	Economic Penalties (mills/kw-hr) for 1-Month Delay in Reprocessing
Uranium	Radial row 1	0.00149	0.00095
Uranium	Radial row 2	0.00079	0.00050
Uranium	Radial row 3	0.00045	0.00029
Uranium	Radial Total	0.00273	0.00174
Uranium	Axial Total	0.00216	0.00138
Thorium	Radial row 1	0.00264	0.00165
Thorium	Radial row 2	0.00123	0.00076
Thorium	Radial row 3	0.00066	0.00042
Thorium	Radial Total	0.00453	0.00283
Thorium	Axial Total	0.00346	0.00214

insignificantly small. It should also be noted that neither the 1% reprocessing loss nor the 1-month delay in reprocessing had the effect of changing the economic optimum irradiation time when that time was evaluated to the nearest 100 days.

5.6.5 Errors in the Analysis

In Chapter 3 of this report, results from experiments in which thorium and uranium foils were irradiated in the M.I.T. Blanket Test Facility, Blanket Mockup No. 4 were discussed. The purpose of those experiments was to allow a comparison of experimental capture and fission rate data with predictions made using the same methods as have been used in the remainder of this study. The major conclusion reached in Chapter 3 was that the inexact treatment of the elastic downscattering, inherent in the ABN-FTR-200 cross section set, made interpretation of experimental results quite difficult. Two methods were presented to correct the original 26-group cross section set for this defect. If the method which resulted in the best comparison between experimental data and analytical predictions is assumed to be "correct," then the following conclusions are reached:

1. The blanket spectrum-averaged infinitely dilute thorium capture cross section was determined to be "correct" relative to those for manganese and gold within the expected uncertainty in the cross section data.

2. The blanket spectrum-averaged self-shielded uranium capture cross sections used in this study are somewhat lower than has been shown experimentally. This effect can be understood in terms of the reduction in effective uranium resonance self-shielding near the reflector interface, and the accompanying hardening of the blanket spectrum. These phenomena are expected to have the effect of increasing the fissile breeding performance near the reflector interface of both thorium and uranium blankets over that predicted in this chapter. This improved breeding performance will be similar for both thorium and uranium blankets, but will have little impact on blanket economics because it occurs in a region of low fissile production capability.

3. No firm conclusion can be drawn regarding the blanket spectrum-averaged, self-shielded thorium capture cross section, since experiments in a thorium blanket would be required to evaluate the adequacy of the self-shielding prescriptions used for thorium in this study.

Because no evaluation of the thorium self-shielding prescription was possible, it is impossible to determine the accuracy of the relative thorium and uranium blanket breeding performance predictions made in Chapter 4 of this report. However, several questions arising from Chapter 3 regarding the validity of the analysis presented here can be addressed. First, the effect of the inaccurate downscatter treatment arising from use of the ABN-FTR-200 cross section set on relative thorium and uranium blanket breeding performance will be addressed. Reference to Fig. 3.13 shows that the principal effect resulting from correction of the elastic downscatter cross sections is a hardening of the predicted neutron spectrum. Figure 3.8 has shown that neutron capture events in a thorium blanket occur, on the average, at higher neutron energies than capture events in a uranium blanket. Thus, when the predicted spectrum is hardened, the breeding performance in a thorium blanket will improve slightly relative to that in a uranium blanket, and the breeding performance of the uranium blanket will be degraded by only about 10%.

Second, the effect of a reduction in the neutron capture cross section for thorium in a thorium blanket on breeding performance will be discussed. Figure 5.38 shows the normalized neutron capture rate distribution in a thorium radial blanket predicted using the ANISN code (E1) with both the nominal resonance self-shielded thorium capture

Fig. 5.38 Comparison of BOL Capture Rates for a Thorium Radial Blanket Predicted using Thorium Capture Cross Sections 1.0 and 0.8 Times Nominal

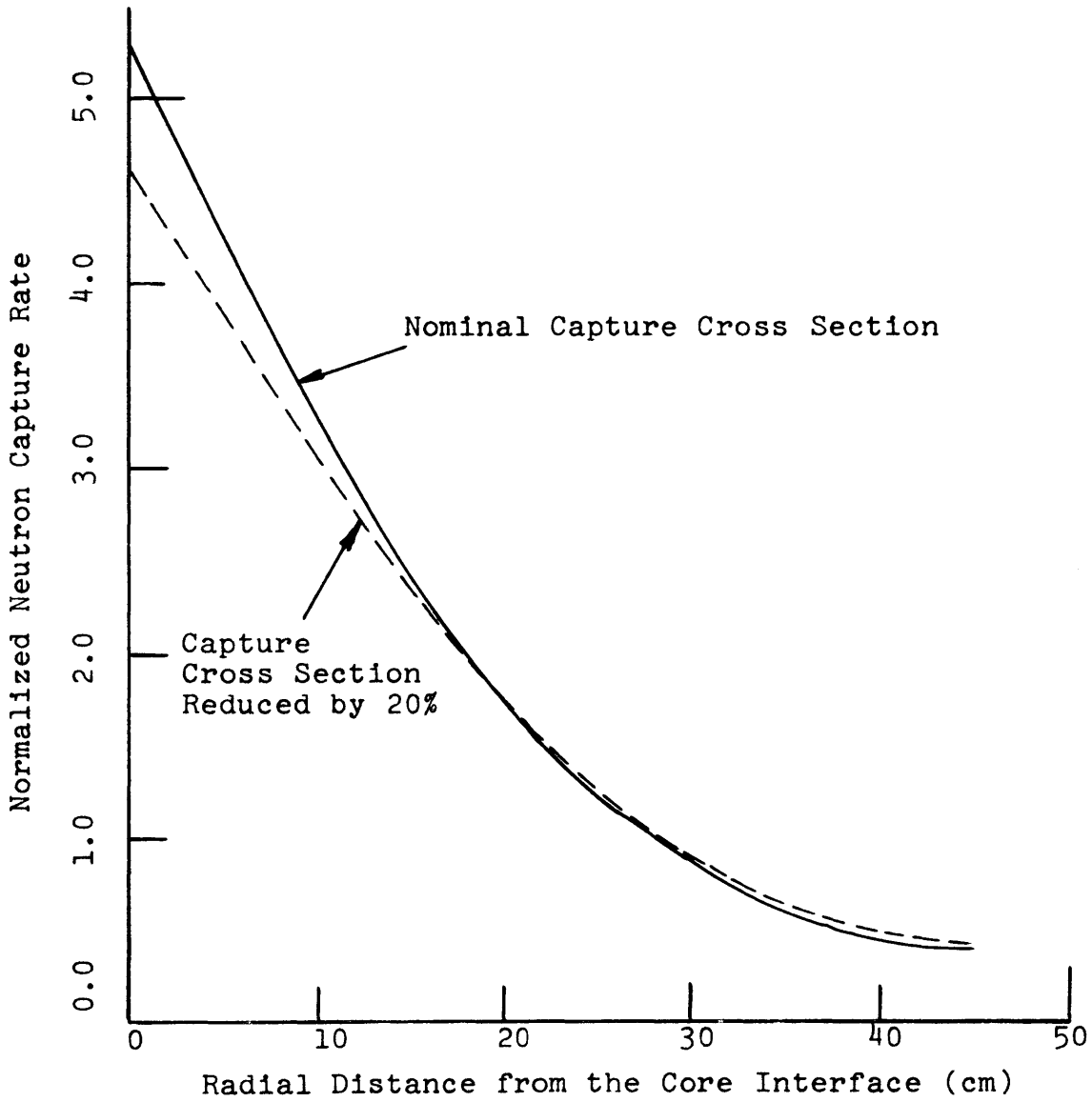

cross sections and thorium capture cross sections reduced from the nominal by 20%. As shown, the reduction in the capture cross section has resulted in a redistribution of the thorium capture rate, with a lower capture rate resulting at the core interface, and a higher capture rate resulting at the reflector interface. This redistribution results from the deeper penetration of neutrons into the blanket caused by a lower effective thorium capture cross section. The net effect of the redistribution of thorium capture events is to reduce the total radial blanket fissile production rate by approximately 4.4% for the case in which the thorium capture cross section for all energy groups was reduced by 20%. This reduction would translate to an economic penalty in a batch managed thorium radial blanket of approximately 0.032 mills/kw-hr or 228,000 dollars per year. Since reasonably good agreement was obtained between analytically and experimentally determined thorium and uranium capture rates in a fission spectrum, any error in the relative thorium capture cross section would be expected below about 10 keV (in the resonance region). When all thorium capture cross sections below 10 keV were arbitrarily reduced by 20%, the radial blanket fissile production rate was reduced by only about 0.64%, resulting in an economic penalty of 0.0047 mills/kw-hr or 33,000 dollars per year. Although the 20% capture cross section reduction in all energy groups carries a significant penalty, it is still a small fraction of the net economic advantage expected to be realized through the use of thorium blankets with LMFBR's. It should be pointed out, however, that no experimental evidence exists at the present time that any significant discrepancy exists between the relative blanket

spectrum-averaged resonance self-shielded capture cross sections for thorium in a thorium blanket and uranium in a uranium blanket. The example above has been presented only to point out the insensitivity of blanket breeding performance to changes in the fertile capture cross section.

5.7 SUMMARY AND CONCLUSIONS

The purpose of this chapter has been to utilize the fissile inventory histories generated in the burnup analysis of Chapter 4 to evaluate the relative economic performance of uranium and thorium blanketed LMFBR systems. The most significant conclusion reached in this chapter is that, due to the high value of U-233 relative to that of fissile plutonium as a fuel for LWR's and HTGR's, there is a significant economic incentive to utilize thorium blankets for LMFBR's during the twenty or so years following LMFBR commercialization. This economic incentive could be of sufficient magnitude to contribute to early widespread acceptance of LMFBR systems.

A second important conclusion presented in this study is that, aside from engineering design considerations which were beyond the scope of this work, the differences in economic performance arising from differences in blanket management technique were quite small. This conclusion is strongly dependent on the assumptions made in the economic analysis. In the Cash Flow Method (B3) used for this study, material credits were assumed to be taxable revenue. Consequently, the fissile inventory history within a given assembly was inconsequential, and only the fissile inventory at end-of-life was utilized in the economic analysis.

This method and the conclusions derived therefrom are in agreement with analysis presented by Barthold (B11), but in apparent disagreement with the results of a Westinghouse study of blanket shuffling alternatives (M3), in which a carrying charge penalty was presumably assigned the in-out shuffle management scheme because most of the fissile material is produced early in life. Development of a consistent economic basis having common consensus for evaluating various blanket management alternatives is clearly necessary.

Because of uncertainties and variations in the economic environment in which an LMFBR might operate, an optimum economic parameter was developed which has been shown to correlate blanket optimum irradiation time and enrichment at the optimum. These correlations allow determination of the effect of changes in blanket fabrication and reprocessing charges, fissile material value, and discount rate on the optimum time and the corresponding optimum enrichment, within the constraints imposed by a specific system design.

Finally, the effects of uncertainties in the analysis have been related to their impact on the economic data presented in the early parts of this chapter. The four major sources of deviation from the blanket comparative economic evaluation presented in section 5.4 are:

1. Potential losses in axial blanket produced U-233 in the head-end processing operation – these losses could result in a 0.038 mill/kw-hr power cost penalty for the thorium axial blanket;
2. Blanket management economic differences – these could result in an economic asset of 0.021 mills/kw-hr for the thorium blanketed system;

3. Errors in the relative spectrum-averaged capture cross sections for thorium and uranium – these could lead to a power cost penalty of 0.0047 mills/kw-hr for the thorium blanketed system if relative thorium capture cross sections (in the resonance region) used in this study were shown to be 20% too high. No clear evidence exists for this supposition at the present time; and

4. Errors in the total mass of fissile material produced in the blankets resulting from the use of the ABN-FTR-200 cross section set with its erroneous downscatter cross sections. Correction of these errors has been estimated to result in approximately a 10% reduction in fissile product for both thorium and uranium blankets. This reduction in fissile mass produced results in an economic penalty relative to the uranium system of approximately 0.031 mills/kw-hr for the thorium blanketed system under the reference economic environment.

The errors above are relatively small compared to the expected net economic advantage of approximately 0.286 mills/kw-hr associated with thorium blankets.

Chapter 6

COMPARISON OF SYSTEM PERFORMANCE

6.1 INTRODUCTION

In the two preceding chapters the nuclear breeding and economic characteristics of thorium and uranium blanketed systems were compared. It was shown that thorium axial blankets breed slightly more fissile material, and thorium radial blankets slightly less than comparable uranium blankets. However, the thorium blanket economic performance was shown to be significantly better because of the higher economic value of U-233 resulting from its superior nuclear characteristics. Because the fuel cycle cost calculations for the thorium blanketed system have been shown to be so favorable compared to the uranium blanketed system, it is now necessary to evaluate other system characteristics which may have an impact on the cost of thorium blanketed systems. This chapter will evaluate the two systems under study from an engineering and physics point of view.

This chapter has been subdivided into three major areas: shielding characteristics, thermal design related properties, and reactor dynamics characteristics. In the section on shielding characteristics, a direct comparison of the fast neutron shielding capabilities of thorium and uranium axial blankets will be made. Several topics will be discussed in the section on thermal design related properties, including:

1. Differences in the thermal characteristics of thoria and urania;
2. Contributions to the total heating rate in the blanket from fission, gamma heating, and neutron heating;
3. Blanket power variations with burnup;
4. Post-shutdown heating in the radial blanket.

The discussion on reactor dynamics characteristics will center on the nuclear properties of the thorium and uranium blanketed systems which are important in safety studies, including the sodium void reactivity, the isothermal Doppler coefficient, the power coefficient of reactivity, and the prompt neutron lifetime.

The purpose of all the discussions presented in this chapter is to quantity the positive and negative features of thorium blanketed systems so that an objective evaluation of the potential for their use in LMFBR blankets can be made. The final section will summarize the preceding intercomparisons and assess the practicality of interchanging thorium and uranium blankets in an operational LMFBR.

6.2 SHIELDING COMPARISON

One of the more important properties of an axial blanket, in addition to its breeding capability, is its ability to serve as a shield to protect the upper and lower core support structures from damage by fast neutrons. To allow an assessment of the relative neutron shielding characteristics of thorium and uranium blankets, the ANISN code (E1) was used to analyze the spherical reactor with an axial type blanket which was discussed in section 2.4.2. As in the earlier analysis, the S_{16} angular quadrature approximation was used for both thorium and

uranium blanketed systems. Table 6.1 summarizes the results from this analysis. As shown, use of the thorium blanket has reduced the

TABLE 6.1 Comparison of Axial Blanket Shielding Characteristics

Group Number	Upper Energy (MeV)	Ratio of Fluxes at the Edge of the Blanket (Th/U)	
		Group Flux	Integral Flux (from E to E_{max})
1	10.5	0.7620	0.7620
2	6.5	0.6568	0.6756
3	4.0	0.6443	0.6539
4	2.5	0.8394	0.7694
5	1.4	0.9148	0.8433
6	0.8	0.9691	0.9285
7	0.4	1.0041	0.9758
8	0.2	1.0245	0.9994
9	0.1	0.9665	0.9868
10	0.0465	0.9350	0.9719
11	0.0215	0.9395	0.9635
12	0.0100	0.8988	0.9552

neutron flux at the interface between the blanket and the axial shield in all groups above 0.4 MeV. Also shown is the fact that the integral flux, $E \rightarrow \infty$, is lower above a thorium axial blanket than above a uranium blanket. If only the flux above 0.1 MeV is considered, little difference exists in the shielding characteristics of the two systems. However, if neutrons with energies above 10 keV are assumed to cause damage to

structural materials in proportion to the square of the flux, the thorium blanket is approximately 8% better than the uranium blanket as a neutron shield. The general properties of thoria as a gamma shield will be discussed in section 6.3.2.

6.3 THERMAL DESIGN CHARACTERISTICS

6.3.1 General Thermophysical Properties

Although the properties of thorium dioxide are not as well characterized as those of uranium dioxide, a great deal of information has been accumulated because of its nuclear and non-nuclear utility. Irradiation experience has been gained for mixtures of thoria and urania in the thermal spectrum reactors: Indian Point 1 and Elk River. In Indian Point 1 the mixed-oxide thoria base fuel was irradiated to a peak burnup of 39,000 MWD/MTM (W4), which is somewhat higher than the peak burnup achieved in a thorium blanket of an LMFBR using zone scatter blanket management.

Among the most noteworthy of the physical properties of thorium are its relatively high melting point (5970° F versus 4980° F for UO_2 [E2, p. 182]) and its high degree of stability to both oxidation and reduction (P2). The first of these characteristics makes thorium dioxide particularly valuable as a nuclear fuel in an environment in which one of the major design limits is fuel pin centerline melt. The second of these properties assures that thorium will be compatible with typical cladding materials used on nuclear reactor fuel pins.

Care must be taken in deriving thermophysical properties of ThO_2 from the open literature because of the sensitivity of these properties to

fabrication history and impurity content (P2). Table 6.2 shows values of UO_2 and ThO_2 thermal conductivity extracted from literature relevant to the nuclear reactor field:

TABLE 6.2 Comparison of UO_2 and ThO_2 Thermal Conductivities

	Thermal Conductivity (E2) (BTU/hr-ft-°F)			Thermal Conductivity (P2) (BTU/hr-ft-°F)	
T (°F)	UO_2	ThO_2	T (°F)	UO_2	ThO_2
200	4.5	7.29	212	6.07	5.95
400	3.5	5.34	392	4.71	4.97
600	2.8	4.03	752	3.41	3.47
800	2.5	3.21	1112	2.61	2.54
1000	2.2	2.68	1472	2.17	1.97
1200	2.0	2.30	1832	2.03	1.79
1400	1.6	2.07	2192		1.45
1600	1.5	1.90			
1800	1.4	1.80			
2000	1.3	1.70			
2200	1.2	1.69			
2400	1.1	1.68			

As shown, significant variations exist in the thermal conductivity values presented by different writers. The important point to note in Table 6.2 is that the thermal conductivities of UO_2 and ThO_2 are not dramatically different, and some observations indicate that ThO_2 may actually have a higher conductivity than UO_2 if its fabrication and impurity levels are

properly controlled. Table 6.3 shows representative values of the heat capacity of UO_2 and ThO_2 (P2). Again this parameter is not substantially different for the two materials, although slightly higher values are associated with the UO_2.

TABLE 6.3 Comparison of UO_2 and ThO_2 Specific Heats

	Heat Capacity (cal/mole-°C)	
T (°C)	UO_2	ThO_2
500	18.76	16.96
1000	20.65	18.61
1500	21.99	19.66
2000	23.26	20.61
2500	24.49	21.53

Brief consideration of relative oxide densities is appropriate at this point. The theoretical density of UO_2 is about 10% higher than that of ThO_2 (10.96 g/cc for UO_2 vs. 10.0 g/cc for ThO_2). Since engineering and metallurgical considerations have been used to define both the maximum volume fraction of fertile material and the maximum percent of theoretical density which can be used for fertile material in the blankets, the fact that ThO_2 has a lower density than UO_2 implies that less fertile material can be loaded into a thorium blanket. This circumstance was shown in Chapter 4 to cause a net reduction in the amount of fissile material produced in thorium blankets relative to uranium blankets.

Finally, note should be taken of the fact that all the properties presented in this section have been for unirradiated materials. Before detailed design of either a thorium or a uranium blanket system can be undertaken, the effects of fast neutron irradiation, time at temperature, cracking of pellets, and the presence of both fissile material and fission products on the thermophysical properties of UO_2 and ThO_2 would need to be reviewed. The post operational examination of the Indian Point 1 fuel should provide initial data toward this end.

6.3.2 Blanket Heating Rate Contributions

6.3.2.1 Preface

Perhaps the most critical engineering design problem of the radial blankets in LMFBR's is the variation of the heating rate both with radial position (spatial) and with time (temporal). Because the radial blanket behaves primarily as a parasite, feeding on neutrons generated in the core, it is found that the flux in the radial blanket decreases rapidly with increased distance from the core interface. This spatial variation of the flux produces a large radial power gradient at any time during irradiation. Another consequence of the high flux gradient in the radial blanket is that the buildup of fissile material occurs much more rapidly in regions near the core interface than in regions far removed from the core. This effect alone would cause the initial gradient to become steeper with irradiation time during any subcycle in which the blanket assemblies are not replaced or shuffled. Offsetting this factor, however, is the flux buildup in the outer blanket which will be shown later to cause a net reduction in radial gradient with irradiation.

The large power and flux gradients mentioned above lead to two related problems. First, the power gradients are necessarily accompanied by fluid temperature gradients from subchannel to subchannel within the radial blanket assemblies. These fuel, coolant, and duct walltemperature gradients cause the assemblies to bow and thus complicate the problem of providing radial restraint for the core. The second problem arises because the flux gradient in the radial blanket contributes to non-uniform swelling in the walls of the ducts surrounding the blanket pins. This non-uniform swelling also contributes to assembly deformation and makes the core radial restraint problem more difficult.

The second characteristic of radial blankets which leads to engineering design problems is the large variation of local blanket power during irradiation. This forces the sodium coolant flow rate to any given assembly to be based on the highest power which that assembly is expected to generate throughout its residence time in a given position. Consequently, during the initial phase of irradiation of a radial blanket assembly it is significantly overcooled. This overcooling leads to thermodynamic inefficiencies in the performance of the entire system, which have been shown by Brown (B5) to result in a quantifiable economic penalty. Another disadvantage of overcooling radial blanket assemblies is the resulting large temperature variation among fluid streams entering the reactor outlet plenum. These large temperature variations may lead to thermal cycling of components in the outlet plenum (causing fatigue failure of these components) if great care is not taken in the arrangement of this region.

To date, several approaches have been tried to reduce radial blanket thermal gradients and temporal power variations. Froelich (F7) has evaluated the effect of assembly rotation and in-out shuffle management on single row power peaking factors and on temporal power variations of assemblies in individual positions within the radial blanket. He has shown that the use of blanket assembly rotation can reduce the row 1 rod power peaking factor (peak rod power/average rod power) from about 2.5 to about 2.2. In-out shuffle management was shown to reduce the ratio of end-of-cycle average rod power to beginning-of-cycle average rod power in a given position in the blanket by a factor of 2.1 to 2.9. In this analysis no account was taken of engineering design limits on the blanket assemblies or of the effect of management on system availability and the related economic consequences.

Another Westinghouse study (W3) has evaluated the use of perforated ducts surrounding radial blanket pin bundles. This study has shown that interassembly flow exchange using the perforated duct concept can reduce temperature gradients across outer subassemblies in the radial blanket by as much as 80° F (from ~160°F to ~80°F). In a study in progress at M.I.T. (B9), Brown is evaluating the use of high albedo reflectors and assembly preenrichment on power flattening in the radial blanket. This study will take into account the economic penalties associated with preenrichment and trade these off against the increased system thermodynamic efficiency achieved if overcooling of blanket assemblies can be reduced.

The purpose of this section (6.3.2) is to evaluate the contributions to the total blanket heating rate of fission, gamma, and neutron heating.

This information will then be used to assess the magnitude of beginning-of-life power gradients. In the next section (6.3.3) blanket power variations with burnup will be discussed for the three management schemes presented in Chapter 4. Finally, in section 6.3.4 the relative effect of post shutdown heating in thorium and uranium blankets will be evaluated.

6.3.2.2 Fission and Neutron Heating

To allow as complete as possible a definition of the total energy deposition rate in the radial blanket, three mechanisms were considered: fission heating (comprised of fission product kinetic energy, as well as prompt and delayed beta energy, excluding neutrino energy), gamma heating (comprised of prompt fission gammas, delayed fission product gammas, decay gammas, annihilation radiation and de-excitation gammas following neutron/nucleus inelastic scatter interactions), and neutron heating. In this section neutron heating rates will be evaluated and compared to the heating contribution from radial blanket fissions. Here neutron heating is considered to involve the after effects of elastic scatter, inelastic scatter, nuclear recoil following neutron capture, and nuclear recoil following capture gamma emission. Despite the fact that neutron heating is the least important of the three mechanisms, it will be discussed first with fission heating because the two analyses were performed together using the same general methods.

The general procedure followed was to use the neutron cross sections from the ABN-FTR-200 set (B1, N1) to generate energy absorption cross sections for the processes of interest. In addition,

calculations utilizing conservation of momentum were necessary to define energy deposition resulting from nuclear recoil following neutron capture, inelastic scatter, and capture gamma emission.

The first and most important contribution to the total neutron heating rate in the blanket is elastic scatter. The contribution of elastic scatter to the total heating rate is defined as

$$Q'''_{ES_k} = \sum_j \phi_{jk} \left[\sum_i N_{ik} \left(\sigma^e_{ij} \, \Delta\bar{E}_{ij} \right) \right] , \tag{6.1}$$

where

Q'''_{ES_k} is the volumetric heating rate from elastic scatter at a particular mesh interval k

ϕ_{jk} is the neutron flux in the group j at the mesh interval k

N_{ik} is the number density of material i in mesh interval k

σ^e_{ij} is the elastic scatter cross section for the material i in the energy group j

$\Delta\bar{E}_{ij}$ is the average energy lost in an elastic collision between a neutron in the energy group j and the material i.

The average energy lost per elastic collision can be defined as (L1, p. 175):

$$\Delta\bar{E}_{ij} = \bar{E}_j(1-e^{-\xi}), \tag{6.2}$$

where

$$\bar{E}_j = (E_j - E_{j+1})/\ln(E_j/E_{j+1})$$

$$\xi = 1 + [\alpha/(1-\alpha)] \ln \alpha$$

$$\alpha = [(A-1)/(A+1)]^2 ,$$

A is the nuclear mass of the nucleus i

E_j is the upper energy bound for group j

E_{j+1} is the lower energy bound for group j.

In the equations above, $\bar{E}_j$ is the average energy in group j for a 1/E intragroup spectrum. In the ABBN-FTR cross section set, cross sections for all but the top three groups have been generated using a 1/E weighting spectrum. The cross sections in the three highest energy groups, where elastic scattering contributes a very small amount to neutron slowing down, were averaged over a fission neutron spectrum. For the purpose of this analysis the $\bar{E}_j$ defined above has been used for all energy groups. This introduces a very small error in the resulting energy loss per elastic collision. As will be shown later, neutron heating is a very small fraction of the total heating rate even in the radial blanket, so this assumption will have an insignificant impact on the total blanket heating rate. The quantity in brackets [ ] in Eq. 6.1 is an elastic scatter energy deposition cross section which can be evaluated for each neutron energy group in any region of the reactor.

Consider next inelastic scatter. The heating rate resulting from inelastic scatter has two components: energy associated with the nuclear recoil when the compound nucleus is formed and the nuclear recoil energy following breakup of the compound nucleus (i.e., neutron emission). Conservation of momentum in these two processes gives the following recoil energies:

$$E_{RI} = \left[\frac{1}{A+1}\right] \bar{E}_i \tag{6.3}$$

$$E_{RF} = \left[\frac{1}{A}\right] \bar{E}_j \ , \tag{6.4}$$

where

E_{RI} is the nuclear recoil energy on formation of the compound nucleus

E_{RF} is the nuclear recoil energy on disintegration of the compound nucleus

A is the atomic weight of the initial nucleus

$\bar{E}_i$ is the incident neutron energy

$\bar{E}_j$ is neutron energy on departure from the nucleus.

The microscopic cross sections associated with these processes were available in the ABN-FTR-200 set in the form of an inelastic downscatter matrix. This form allowed separation of the two components of inelastic scatter neutron heating. An equation similar to Eq. 6.1 can be written to describe neutron heating in the inelastic scatter process:

$$Q'''_{INS_k} = \left[\sum_j \phi_{jk} \sum_i N_{ik}\left(\sigma^{IN}_{ij} E_{RI}\right)\right] + \sum_j \phi_{jk}\left[\sum_i N_{ik}\left\{\left(\sum_n \sigma^{IN}_{i(n\to j)}\right) E_{RF}\right\}\right] \tag{6.5}$$

where

Q'''_{INS_k} is the volumetric heating rate from inelastic scatter at a particular mesh interval, k

σ^{IN}_{ij} is the total inelastic scatter cross section of isotope i in group j

and

$\sigma^{IN}_{i(n\rightarrow j)}$ is the inelastic scatter cross section for material i for events in which the initial neutron is in group n and the final neutron is in group j.

Again the quantities in brackets [ ] can be thought of as inelastic energy absorption cross sections by neutron energy group for any particular region in the reactor.

In a neutron capture event, energy is deposited locally by the recoil of the product nucleus following the capture event. The recoil energy following a capture event can be written in the same form as that following the compound nucleus formation in inelastic scatter, as in Eq. 6.3. The capture recoil heating rate can therefore be written:

$$Q'''_{C_k} = \sum_j \phi_{jk} \left[\sum_i N_{ik} \left(\sigma^C_{ij} E_{RI} \right) \right], \tag{6.6}$$

where

Q'''_{C_k} is the heating rate resulting from nuclear recoil following neutron capture

σ^C_{ij} is the microscopic capture cross section for material i in energy group j.

The quantity in brackets is the energy deposition cross section for nuclear recoil following neutron capture. This quantity can be computed for each neutron energy group in any region within the reactor.

The last and least important of the energy deposition mechanisms associated here with the general topic of neutron heating is the nuclear recoil following decay gamma emission of an isotope formed by neutron capture. (Szilard and Chalmers [E3] have shown that the nuclear recoil following gamma emission is sufficient to break chemical bonds and that

this process can then be used to enrich radioactive isotopes.) Again conservation of momentum calculations can be performed to develop the following expression for the nuclear recoil following gamma emission.

$$E_{R\gamma} = \frac{1}{A}\left[E_{\gamma}^{2}/2m_{o}c^{2}\right], \tag{6.7}$$

where

$E_{R\gamma}$ is the nuclear recoil energy following gamma emission

E_{γ} is the energy of the emitted gamma

c is the speed of light

A is the atomic mass of the nucleus

m_{o} is the mass of one nucleon.

An estimate of the total heating rate resulting from nuclear recoil following gamma emission can be made by making the following assumptions:

1. The decay energy of a nucleus formed in neutron capture can be estimated as the binding energy of the last nucleon. This quantity can be calculated using the semiempirical mass formula (E3, p. 298).
2. All the decay energy is assumed to be associated with one single gamma photon emitted from the nucleus, a very conservative assumption.
3. The gamma photon is assumed to be emitted immediately following neutron capture (or alternatively, the capture and decay rate are assumed equal, corresponding to the case of infinite operating time).

These assumptions will lead to a high estimate of the contribution of nuclear recoil following gamma emission to the total heating rate.

A formulation similar to that in Eq. 6.6 has been used to estimate this contribution.

6.3.2.3 Results of the Fission and Neutron Heating Analysis

A simple computer program was developed for use in generating the total neutron heating cross sections (designated earlier in brackets) as well as their component parts from the unshielded ABN-FTR-200 cross section set. Use of unshielded cross sections will result in an overprediction of the neutron heating rate. These cross sections were then used in conjunction with neutron fluxes calculated using ANISN (E1) for two specific blanket configurations to evaluate the neutron heating rate. For the purpose of comparison, the fission heating rate in the two standard blankets (depleted uranium and thorium) was also evaluated. Figure 6.1 shows the beginning-of-life fission heating rate for the blankets. As shown, the fission heating rate in the depleted (0.2%) uranium blanket is significantly higher than that in the thorium blanket. Figure 6.2 shows that the relative contribution to the total fission heating rate in the depleted uranium blanket of U-235 fissions increases deeper into the blanket. This observation is expected because of the spectral softening which occurs deeper in the blanket. Figure 6.3 shows the calculated neutron heating rate in the uranium and thorium blankets. Neutron heating in the uranium blanket is slightly higher in the thorium blanket because of the extra source of neutrons from fission in the uranium blanket. A measure of the relative effect of neutron heating in the core and blanket is shown in Figs. 6.4 and 6.5. In these figures the ratio of the neutron to fission volumetric heating rates is

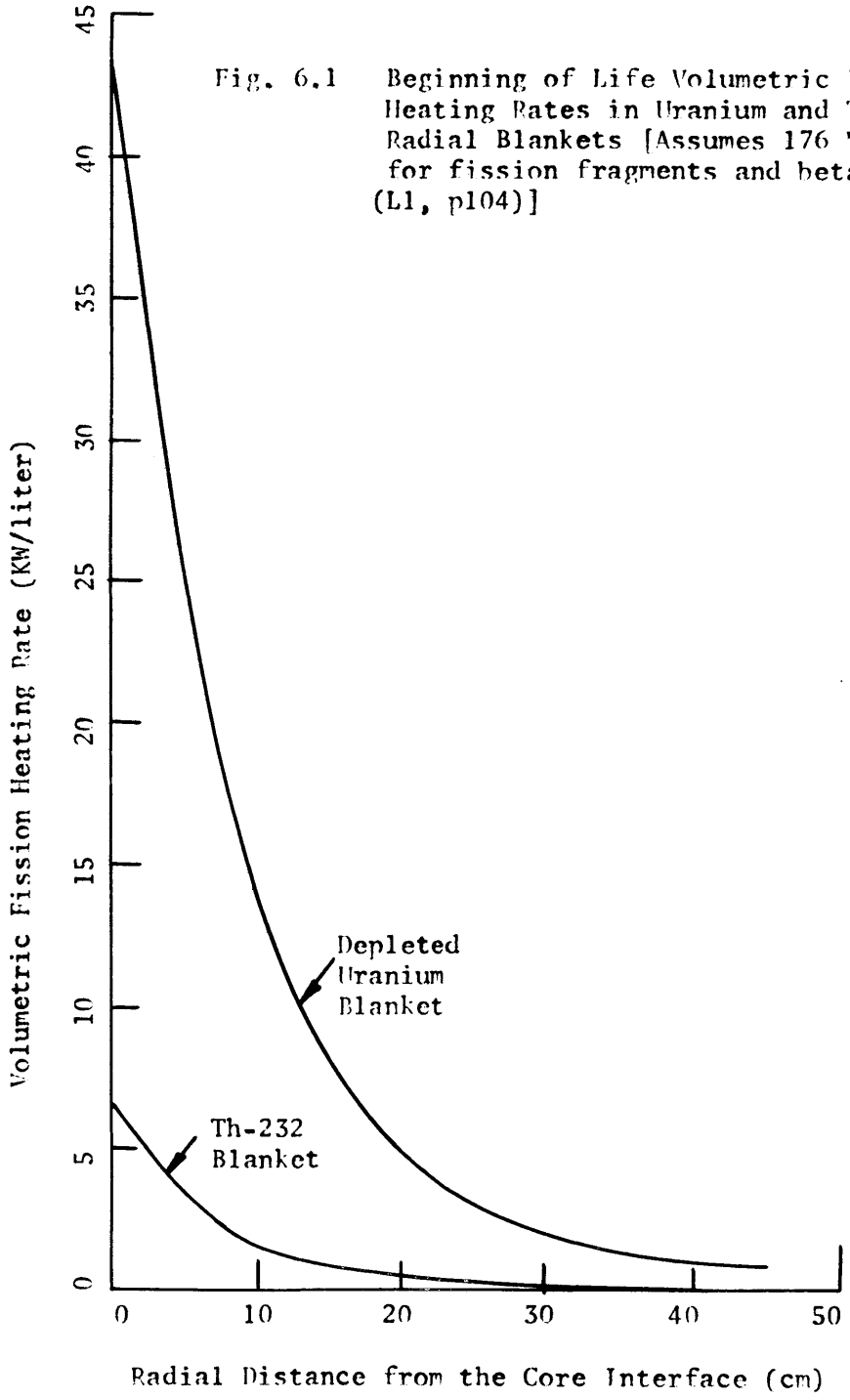

Fig. 6.1 Beginning of Life Volumetric Fission Heating Rates in Uranium and Thorium Radial Blankets [Assumes 176 MEV/Fission for fission fragments and beta rays (L1, p104)]

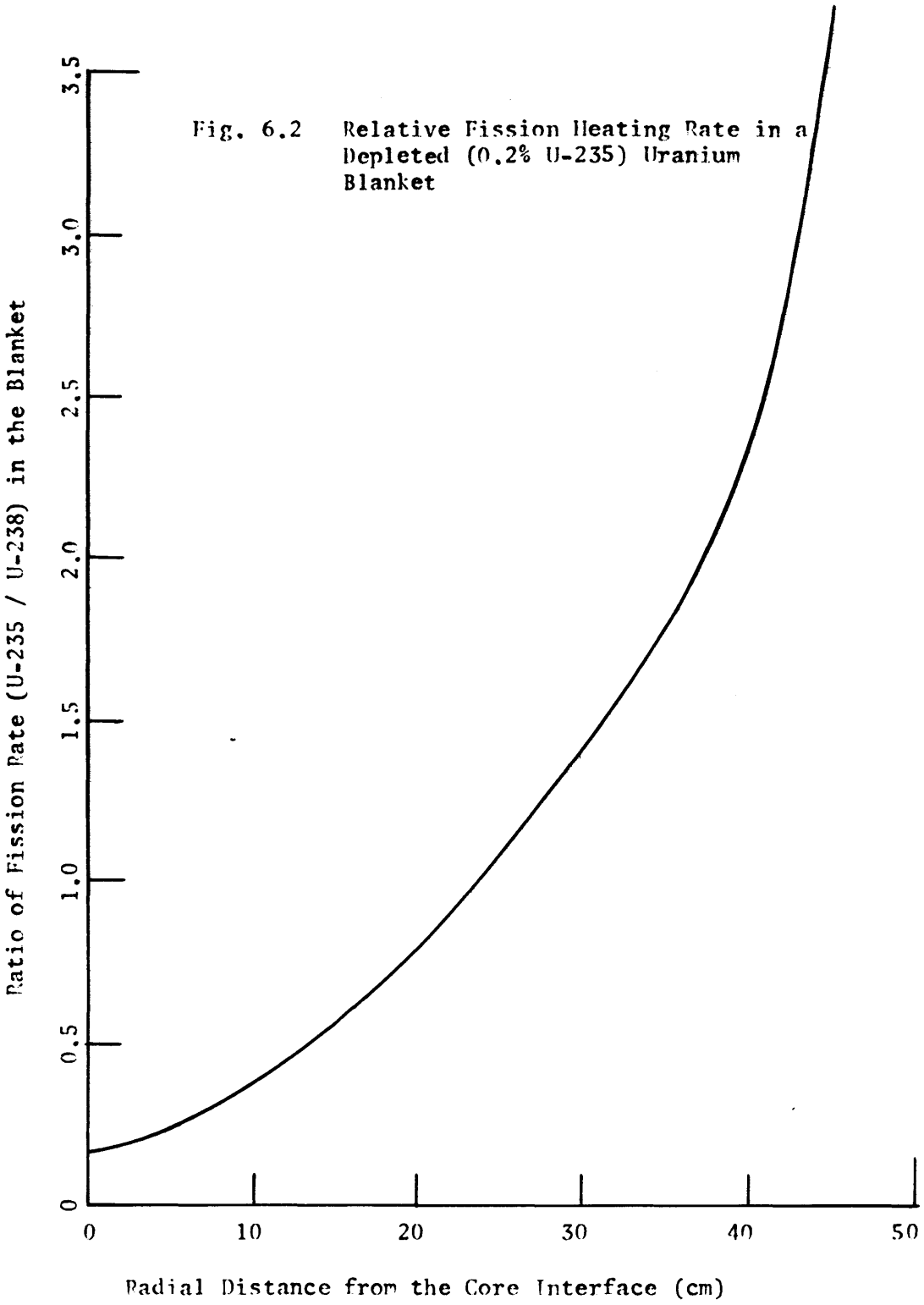

Fig. 6.2 Relative Fission Heating Rate in a Depleted (0.2% U-235) Uranium Blanket

Fig. 6.3 Comparison of Beginning of Life Neutron Heating Rate in Thorium and Uranium Radial Blankets

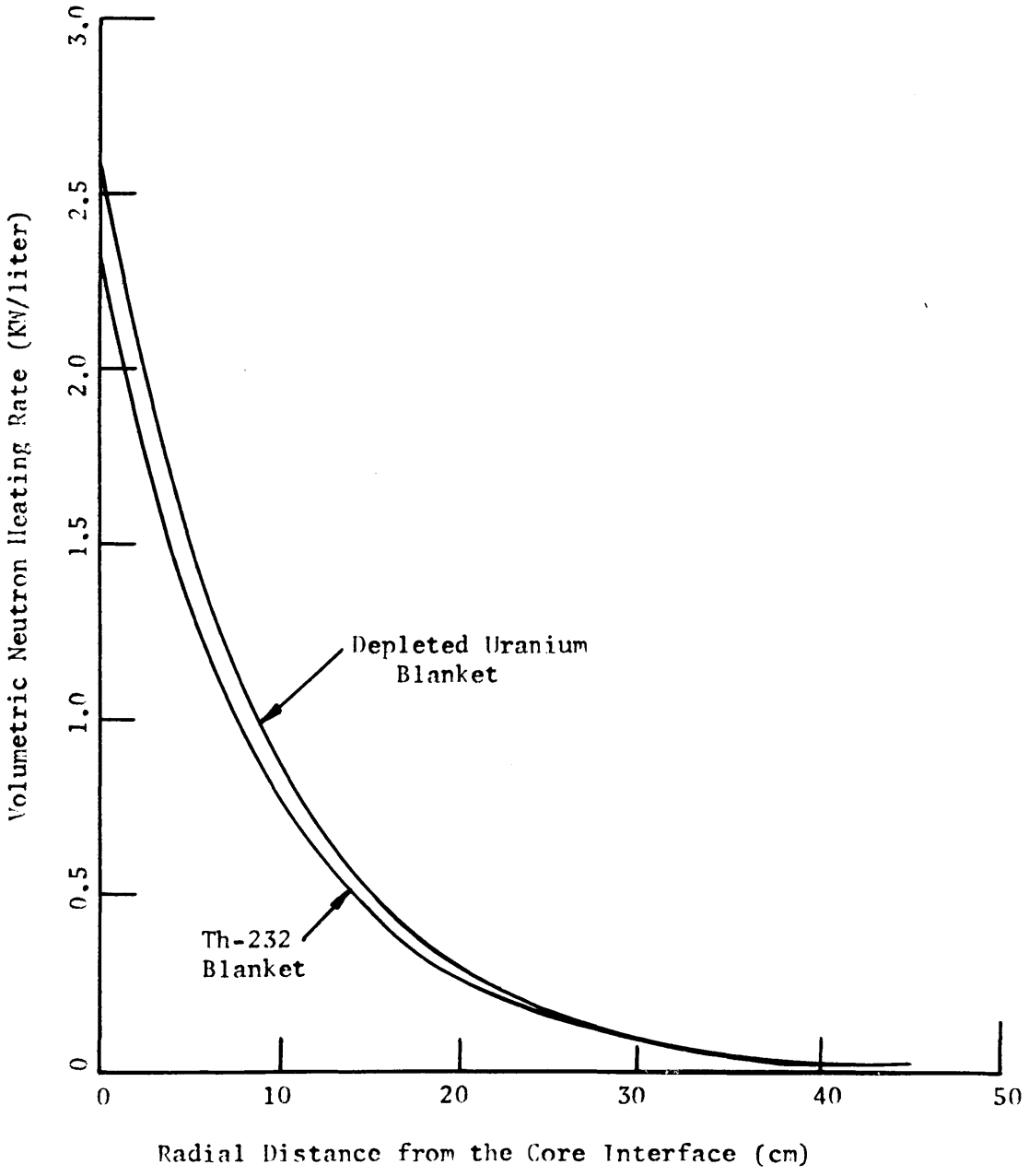

Fig. 6.4 The Ratio of Neutron to Fission Heating Rate in a Typical 1000 MW_e LMFBR with a Thorium Radial Blanket [Assumes 176 Mev/Fission (L1, p104)]

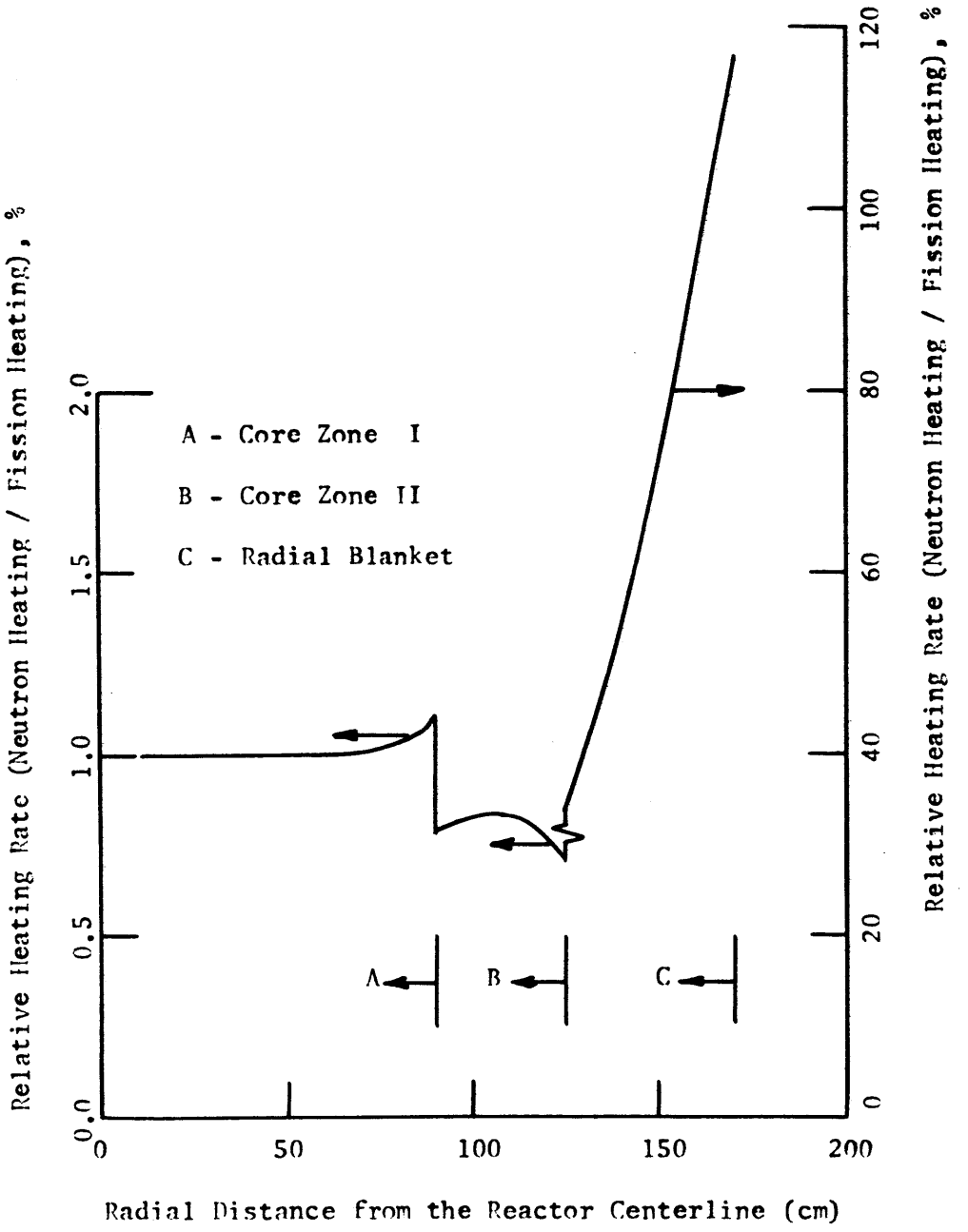

Fig. 6.5 The Ratio of Neutron to Fission Heating Rate in a Typical 1000 MW_e LMFBR with a Uranium Radial Blanket
[Assumes 176 Mev/Fission (L1,p104)]

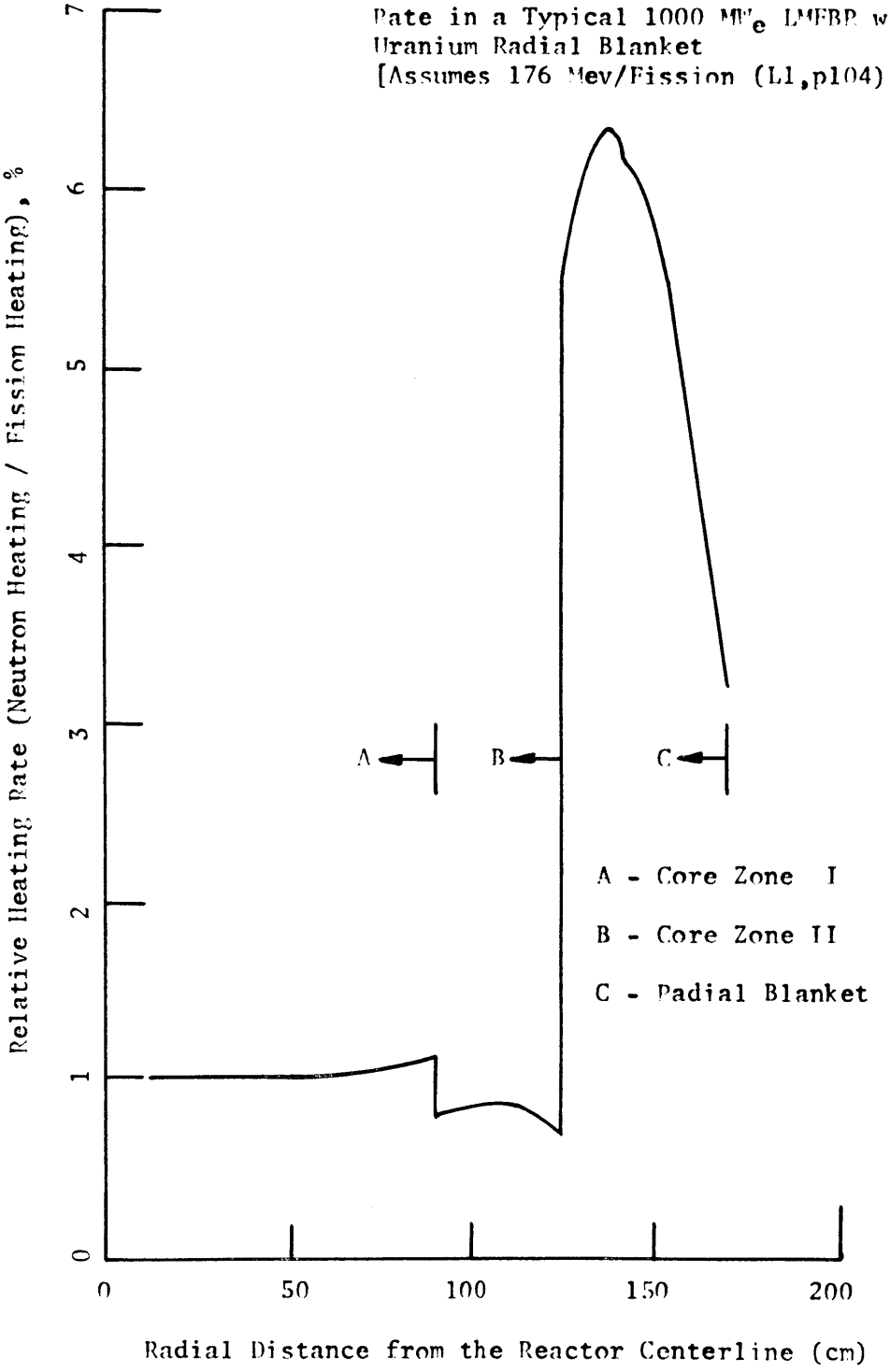

plotted for both thorium and uranium blankets. As shown, the blanket neutron heating rate becomes an increasingly important part of the total heating rate deeper in the thorium blanket, while the relative neutron heating rate peaks near the center of the uranium blanket. This difference can be attributed to the fissions in U-235 induced by low energy neutrons in the uranium blanket. No low energy fissions can occur in the thorium blanket because of the high fission threshold (~2 MeV) of thorium. Another interesting feature shown in Figs. 6.4 and 6.5 is that the neutron heating rate is only about 1.1% of the total heating rate in the core. In a thermal reactor this value would be expected to be about 2.5%. The difference in these two numbers can be attributed to three features of an LMFBR which differ from their counterparts in thermal reactors. First, the neutron leakage from the core of LMFBR's might be as high as 30%, while corresponding water reactor leakages are much smaller. Second, the spectrum in an LMFBR core has a very much higher average neutron energy, and thus neutrons are either absorbed within, or leak out of, the core before they can deposit their energy through slowing down collisions. Last, more inelastic moderation exists in an LMFBR, in which neutron energy is transformed into gamma photons.

To allow an evaluation of the relative contribution of the different components entering into the neutron heating calculation, Table 6.4 has been included. This table clearly shows that the largest contributing factor to the neutron heating rate is elastic scatter.

Finally, neutron heating rates in the radial shield were evaluated for both thorium and uranium blanketed systems. Figure 6.6 shows

TABLE 6.4 Neutron Heating Rate Contributions in a Thorium Blanket

Mean Radial Distance from the Core Interface (cm)	Heating Rate Contributions (kw/liter)				
	Elastic Scatter	Inelastic Scatter	Capture Recoil	Gamma Recoil	Total
2.5	1.682	0.070	0.004	0.001	1.757
7.5	0.984	0.035	0.002	0.000	1.021
12.5	0.584	0.018	0.001	0.000	0.603
17.5	0.343	0.009	0.001	0.000	0.353
22.5	0.202	0.005	0.000	0.000	0.207
27.5	0.118	0.003	0.000	0.000	0.121
32.5	0.069	0.001	0.000	0.000	0.070
37.5	0.041	0.001	0.000	0.000	0.042
42.5	0.025	0.000	0.000	0.000	0.025

Fig. 6.6 Neutron Heating Rates in the Reflectors of Uranium and Thorium Blanket Systems

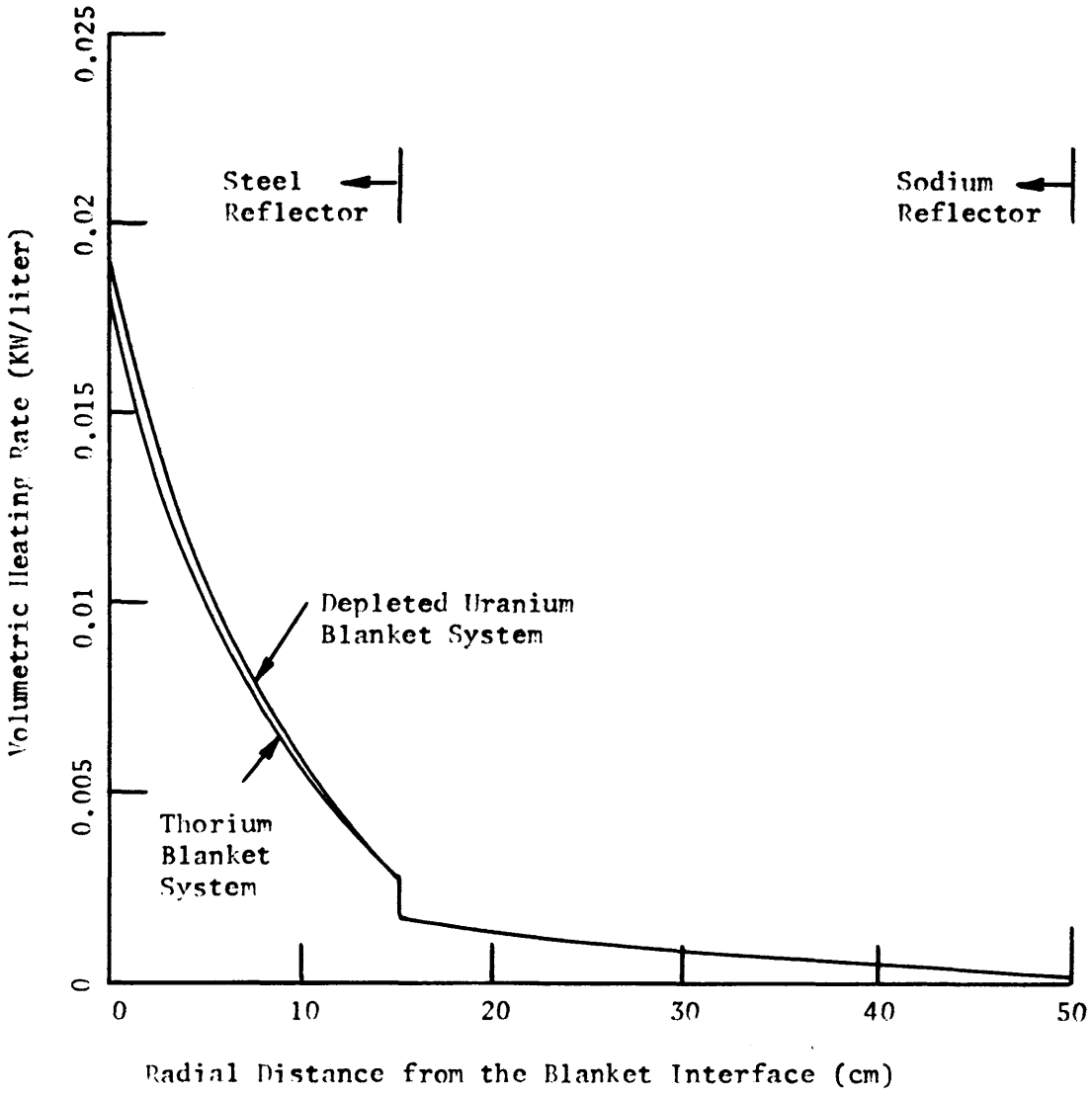

that no significant differences exist in shield neutron heating rates between the two blanket cases. The sodium reflector is shown to be somewhat less effective as a neutron shield than the steel reflector by the discontinuity in neutron heating rate at the interface between the two.

6.3.2.4 Gamma Heating Analysis

The next major component of the heating rate in the radial blanket to be evaluated was heating by gamma photons. For this analysis, a 40-group coupled neutron and gamma cross section set developed at Oak Ridge National Laboratory (ORNL) was used (M1, S3). Since cross sections for thorium were not available in the ORNL set, an analysis was performed to generate these cross sections. This development is discussed in Appendix B. The 40-group cross section set accounted for the production of gamma photons resulting from fission, fission product decay, capture product decay, inelastic scatter, and annihilation of beta particles. Gamma production is incorporated in the cross section set by use of downscatter cross sections from neutron groups into gamma groups. Gamma heating rates in the core, radial blanket, and reflectors were determined using the one-dimensional transport code ANISN (E1) in conjunction with the 40-group cross section set. The following procedure was used. First, the microscopic energy absorption cross sections (in units of MeV-barns) from the 40-group set were used to generate macroscopic energy absorption cross sections (in units of MeV/cm) for each region of interest. Next, ANISN was used to analyze the problem of interest using the 40-group cross

section set, P_1 spherical harmonics approximation (B9), and the S_8 discrete ordinate method (L11). The fluxes generated in the ANISN analysis (in units of photons/cm^2-sec) were then multiplied times the macroscopic energy absorption cross sections and summed over all energy groups. These summations were the volumetric energy deposition rates (in units of MeV/cc-sec) in the regions of interest.

The results of the gamma heating calculations for the uranium radial blanket system are shown in Figs. 6.7 and 6.8. The heating rates presented in these curves are the axial average values plotted against radial position. Figure 6.7 shows the ratio of the gamma heating rate to the corresponding fission heating rate. As shown, the gamma heating rate in the core is from 13 to 17 percent of the fission heating rate. In the radial blanket, however, the gamma heating rate is from 80 to 250 percent of the fission heating rate. This might be expected because of the greatly reduced fission rate in the radial blanket at increased distances from the core interface and from the large relative increase in the fertile capture rate compared to the fission rate at increased distance from the core interface. It should be noted that the relative heating rates in Fig. 6.7 are for beginning-of-life conditions. As fissile material builds in, the contribution of gamma heating to the total heating rate will be greatly reduced. Figure 6.8 shows axially averaged beginning-of-life (BOL) gamma heating rates in the radial blanket and in the two reflector regions for a uranium blanketed system. As shown, the gamma heating rate in the radial blanket decreases by a factor of about 4 from the core interface to the reflector interface. It should also be noted that the blanket heating

Fig. 6.7 The Relative Fission and Gamma Heating Rates in a Uranium Blanketed System, Beginning of Life, 176 Mev/Fission Assumed

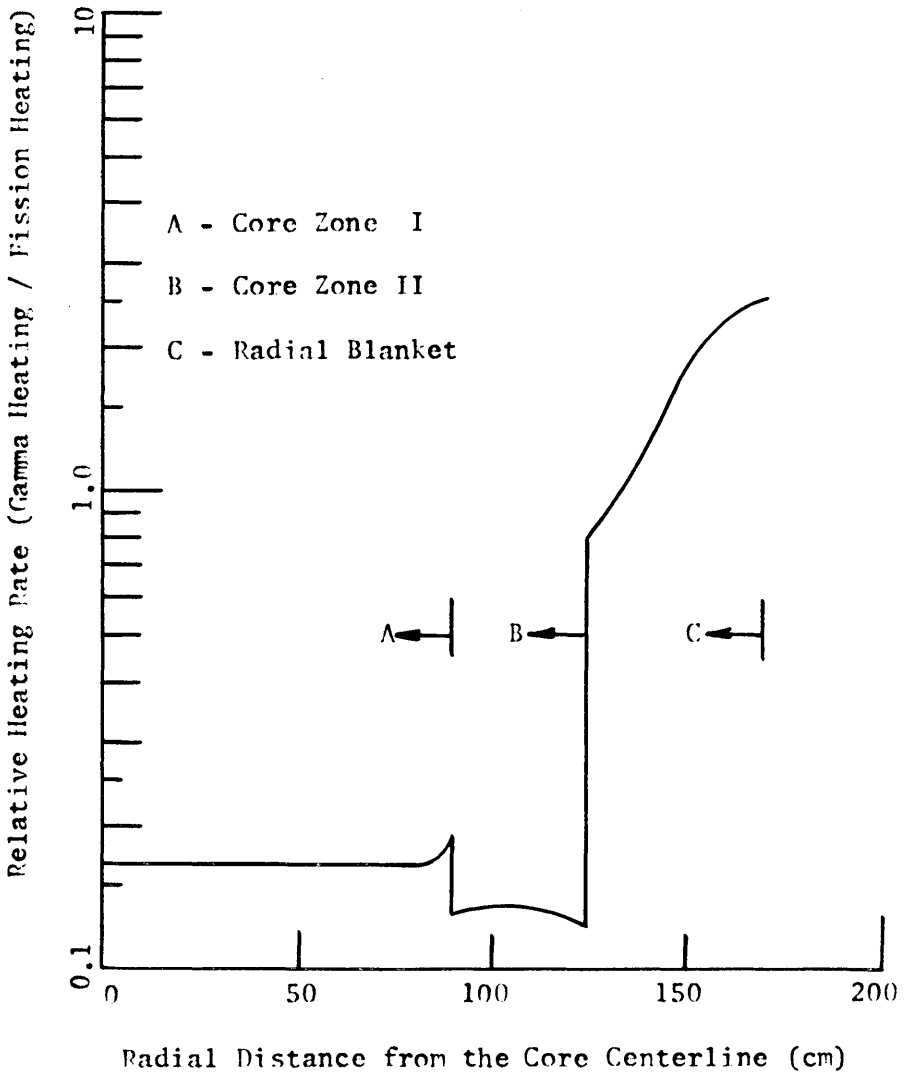

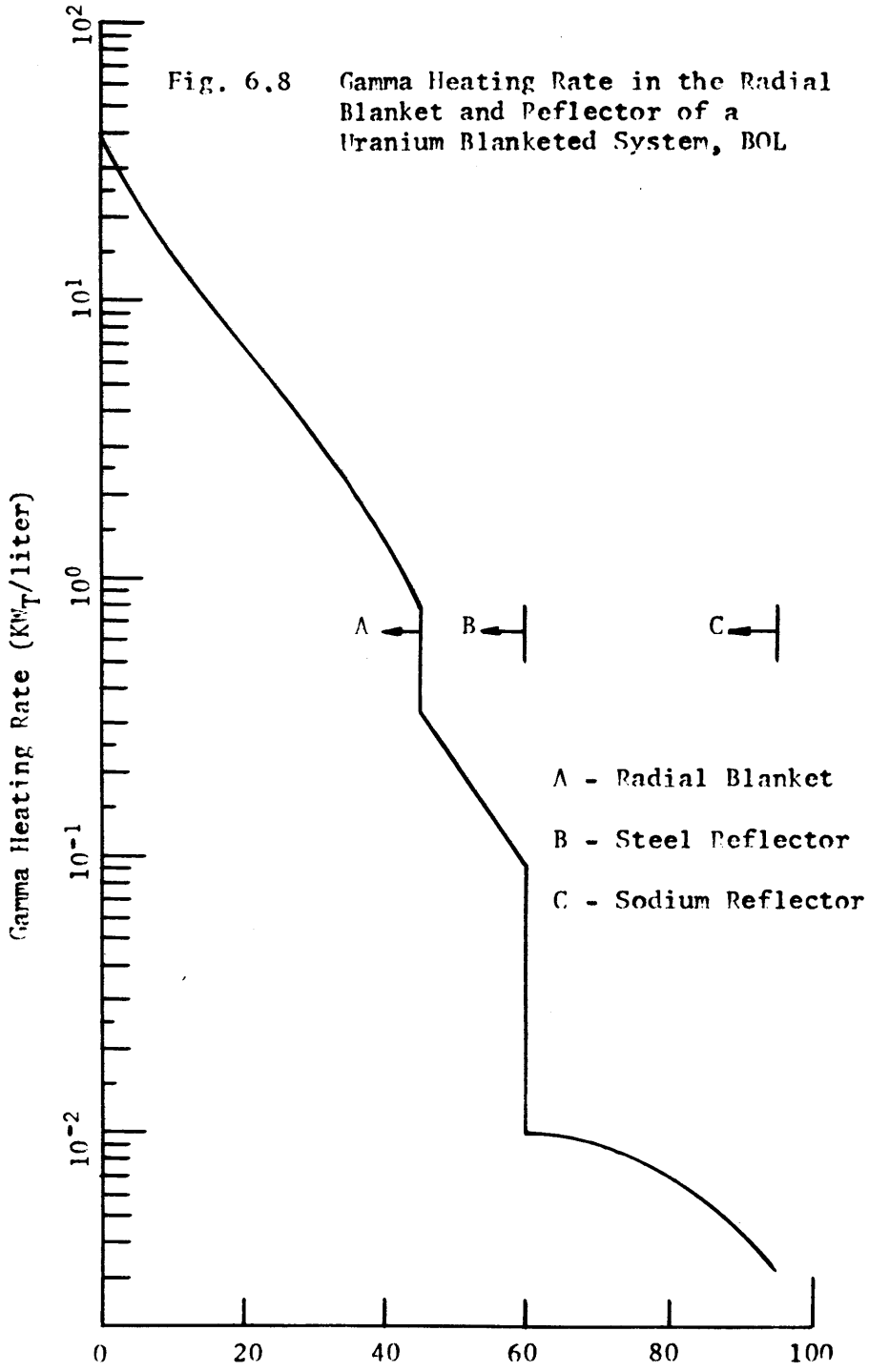

Fig. 6.8 Gamma Heating Rate in the Radial Blanket and Reflector of a Uranium Blanketed System, BOL

rate at the core interface is only about 8% of the average core heating rate (500 kw_t/liter). Since the gamma heating rate is a good measure of the gamma shielding characteristics, the steel reflector is confirmed to be a much better gamma shield than the sodium reflector.

Information on gamma heating rates in the thorium blanketed system is shown in Figs. 6.9 and 6.10. Again the information presented is for the BOL condition. Figure 6.9 shows that the relative core heating rate (gamma/fission) is substantially the same as for the uranium blanket system. As expected, the gamma heating rate is much larger relative to the fission heating rate in the thorium radial blanket than it was in the uranium blanket. When actual heating rates are considered, as in Fig. 6.10, gamma heating rates in the thorium blanket are shown to be slightly less than those in the uranium blanket. It should again be pointed out that the gamma heating rates evaluated here are for BOL conditions. As fissile material builds in, the relative contribution of gamma heating to the total energy deposition rate will be reduced. One may also conclude from these results that the thorium blanket is a slightly less efficient gamma shield than the uranium blanket, the BOL gamma dose at the blanket/reflector interface being roughly 25% higher than for a uranium blanket.

6.3.2.5 Temporal Variations of Neutron and Gamma Heating Rates

To allow definition of the variations of neutron and gamma heating rates in the radial blanket as fissile material is built in, an analysis was performed using the fissile plutonium distribution in a uranium blanket which would result after 1200 full power days of batch irradiation. Figure 6.11 shows the results of that analysis. As shown, the

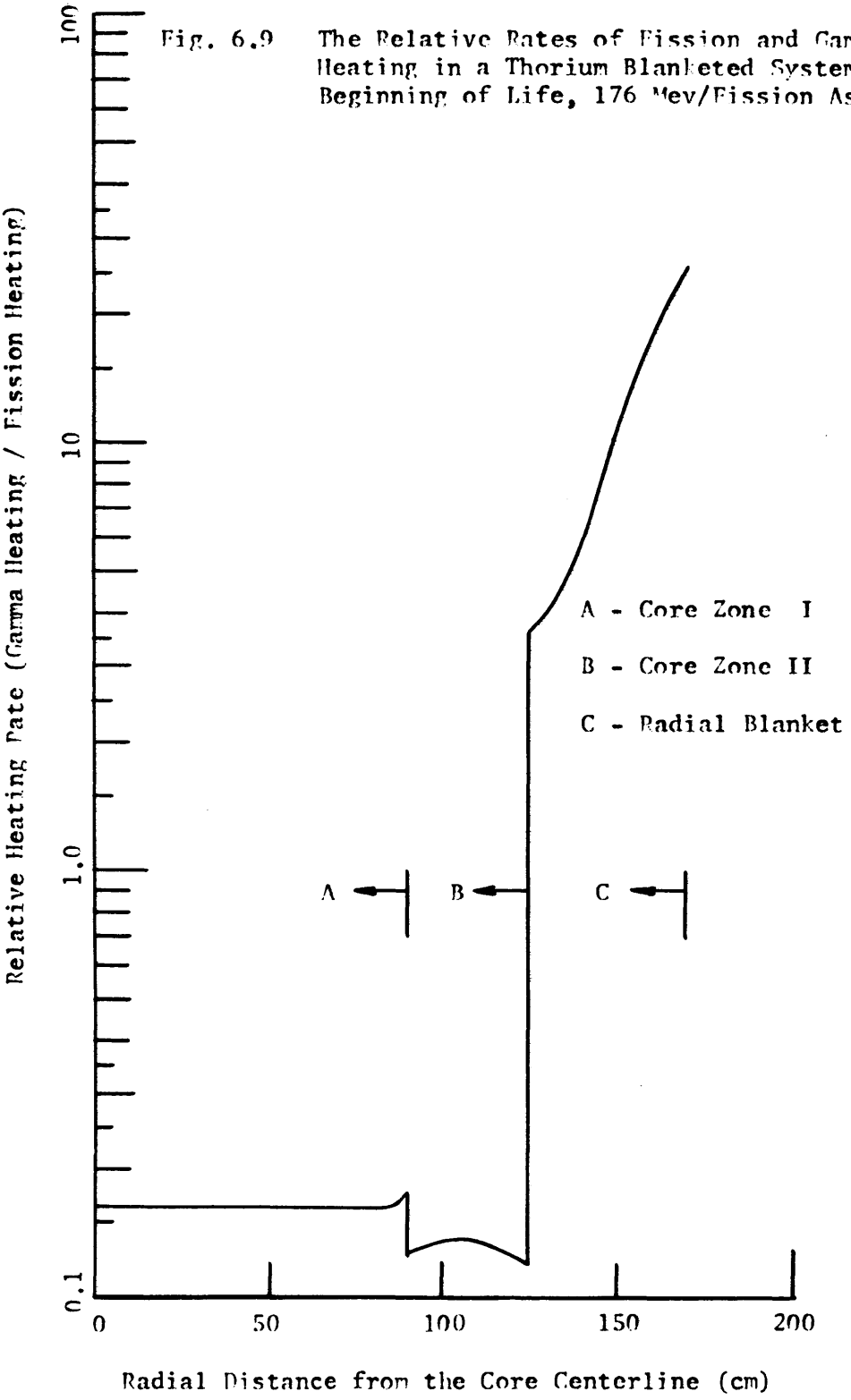

Fig. 6.9 The Relative Rates of Fission and Gamma Heating in a Thorium Blanketed System, Beginning of Life, 176 Mev/Fission Assumed

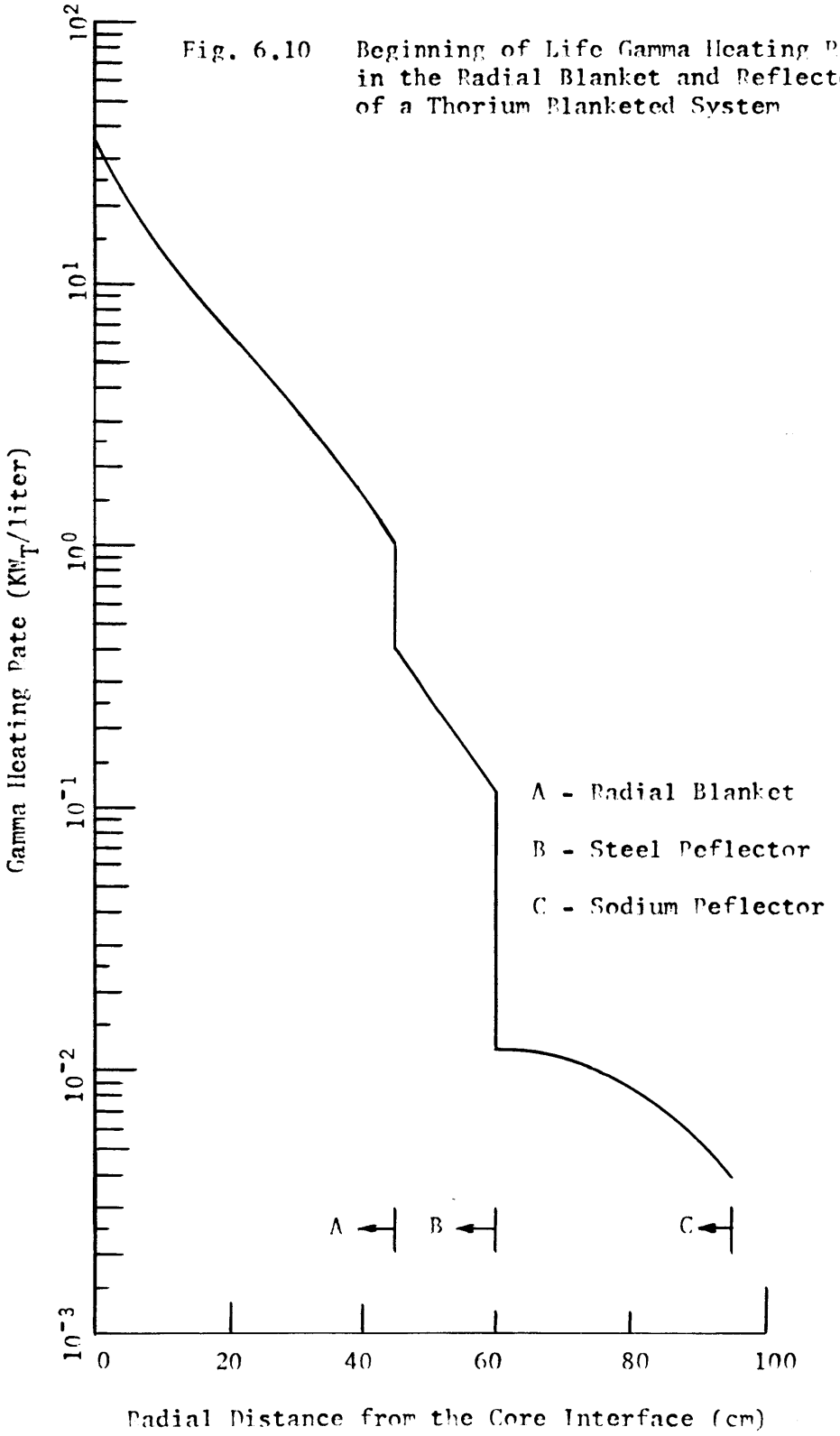

Fig. 6.10 Beginning of Life Gamma Heating Rate in the Radial Blanket and Reflector of a Thorium Blanketed System

Fig. 6.11 Comparison of Uranium Blanket Heating Rates from Gamma and Neutron Heating at the Beginning of Life and After 1200 days of Irradiation

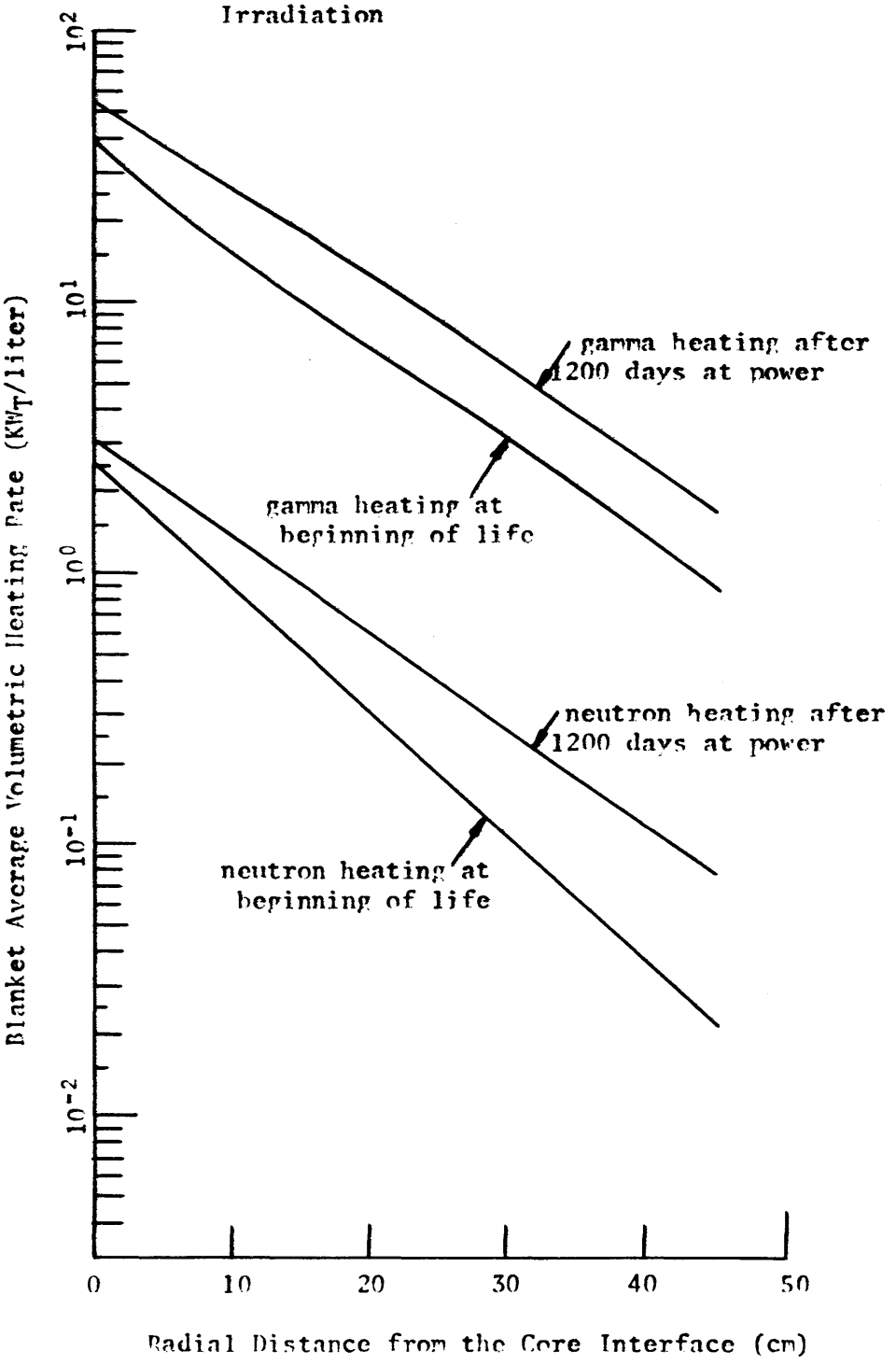

neutron heating rate after 1200 days at full power has increased by as much as a factor of 4 over the BOL values at the reflector interface. This factor is unimportant, however, in light of the extremely low heating rate contribution to the total from neutron heating. The gamma heating rate contribution has increased by as little as 35% at the core interface and by as much as 100% at the reflector interface. These increases seem significant until note is taken of the fact (to be demonstrated in section 6.3.3.2) that the fission heating rate, which is initially about twice as large as the gamma heating rate at the core interface, increases by a factor of nearly 6 at the core interface and by a much larger factor at the reflector interface. Thus, the contention to be made later, that fission heating is the dominant effect in the radial blanket after long irradiation times, has been verified here.

6.3.3 Blanket Power Shape and Its Variation with Time

6.3.3.1 Preface

As discussed earlier, two of the most important engineering considerations related to the design of a radial blanket are the power shape and the variation of blanket assembly power with burnup. In this section a comparison of radial blanket power shapes and their temporal variations will be presented. The effect of blanket management on these parameters will also be evaluated. The 2DB burnup analyses have been used as a source of the data presented in this section. Consequently, all heating rates presented are those resulting from fission heating only. Since it has been shown in the previous section that fission heating is the dominant term at EOL, examining only fission heating rates will

allow a reasonable evaluation of blanket temporal power variations. In section 6.3.3.6, the effect of gamma and neutron heating on blanket power peaking will be discussed.

6.3.3.2 Batch Irradiation

As one might expect, the largest temporal power variations in the radial blanket are experienced when the blanket is batch managed. Figures 6.12 and 6.13 show the peak blanket power density for uranium and thorium blankets as functions of batch irradiation time. Several features are important to note in these figures. First, the beginning-of-life peak power density in the thorium blanket is significantly less than that in the uranium blanket. This is a result of the small fission cross section of thorium compared to depleted uranium. As fissile material builds up in the radial blanket, the peak power density in the thorium blanket increases and actually surpasses that in the uranium blanket after 1800 days of irradiation. The second feature to note is that as irradiation time increases, the rate of change of peak power density decreases in row 1 while it increases in row 3. This would be expected from the shape of the fissile inventory curves presented in section 4.4. It will be recalled that fissile inventory in row 1 for the batch irradiation case increased at an ever slower rate (the inventory vs. time curve was concave) while that in row 3 increased at a more rapid rate (the inventory vs. time curve was convex) with increased irradiation time. A third feature to note in Figs. 6.12 and 6.13 is that the peak power density in the thorium radial blanket row 3 never achieves as high a value as that in row 3 of the uranium blanket.

Fig. 6.12 Variation of Peak Fission Power Density in a Uranium Radial Blanket with Batch Irradiation Time

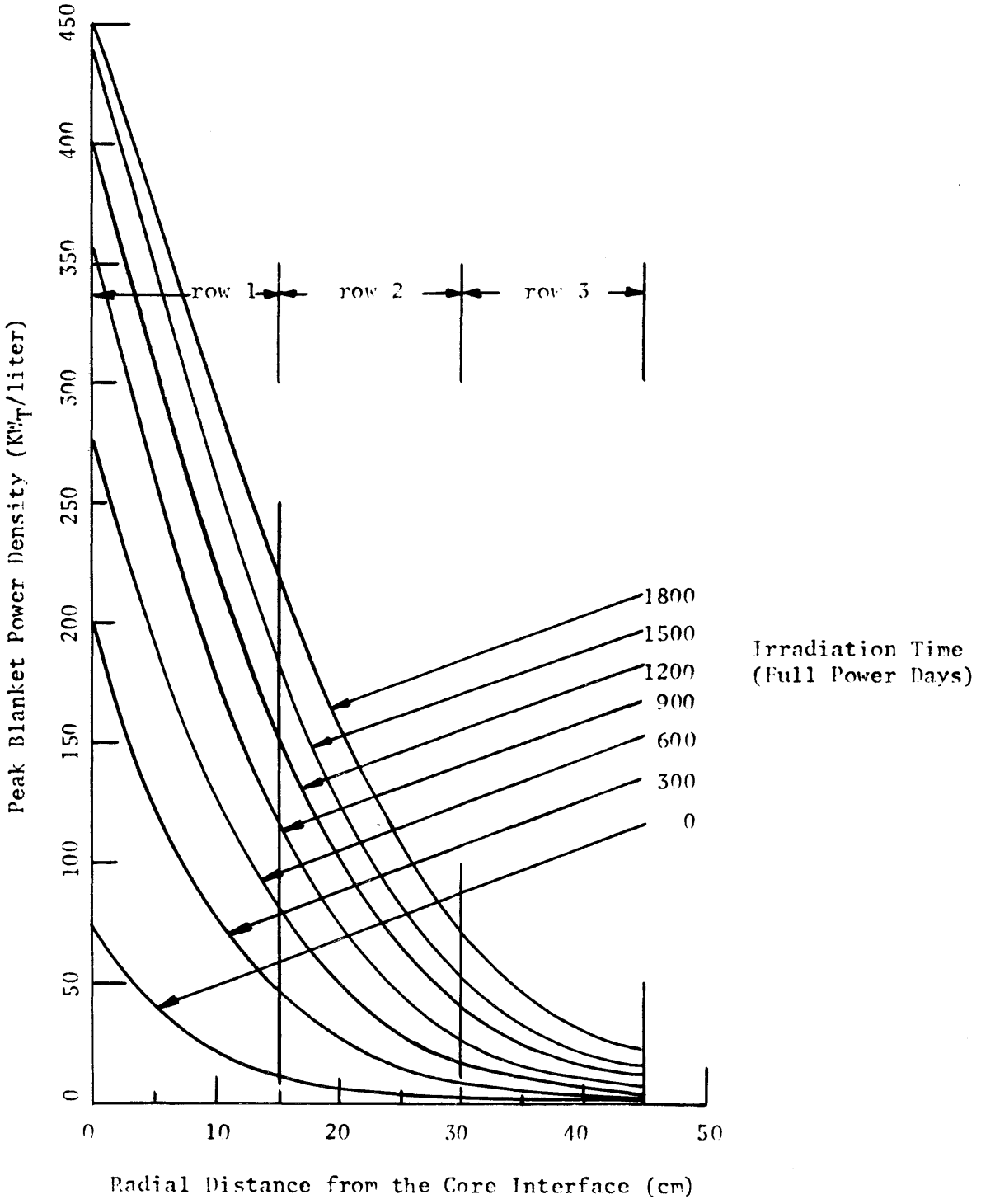

Fig. 6.13 Variation of the Peak Fission Power Density in a Thorium Radial Blanket with Batch Irradiation Time

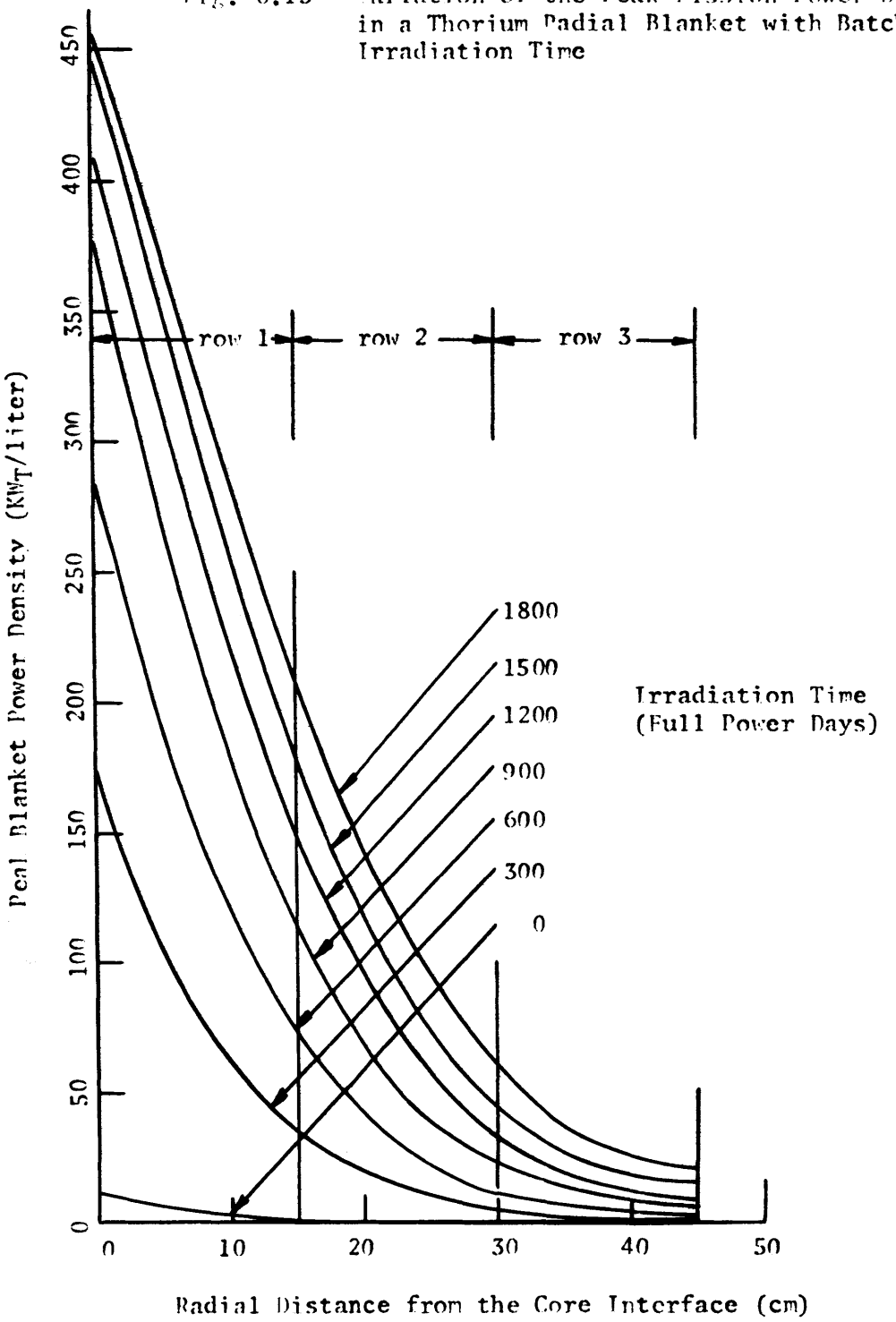

Again, this would be expected from the fact (shown in section 4.4.2.2) that the breeding performance of the thorium blanket relative to the uranium blanket degrades with increasing distance from the core interface. Finally, it should be noted that the economic optimum for batch irradiation was achieved after 1800 full power days for the uranium blanket, while it occured after only 1200 days for the thorium blanket. This means that the peak blanket power density for the thorium blanket is about 10% less than that for the uranium blanket at their respective economic optima. Later it will be shown that this 10% difference is of the same magnitude as the gamma heating contribution.

6.3.3.3 Zone Scatter Management

It was noted earlier (see section 4.5) that the major effect of zone scatter management of row 1 was to increase the total fissile product generated in row 1 while decreasing that produced in rows 2 and 3. This was caused by the reduction in average flux in rows 2 and 3 when row 1 was replaced periodically. Thus it would be expected that the zone scatter (periodic replacement) management of blanket row 1 would reduce the peak power density achieved in row 1 while at the same time reducing the peak power in rows 2 and 3. Figures 6.14 and 6.15 show the peak power densities calculated for the uranium and thorium blankets, respectively. As shown, the reasoning based on fissile production rate is substantiated. The axial peak power densities in row 1 are the same as for a batch irradiation case in which the row 1 irradiation times were the same. The peak power densities in rows 2 and 3 are, as expected, less than for the batch irradiation case at the

Fig. 6.14 Variation of Peak Fission Power Density in a Uranium Radial Blanket with Irradiation Time (Row 1 replaced every 1000 days, rows 2 and 3 batch irradiated)

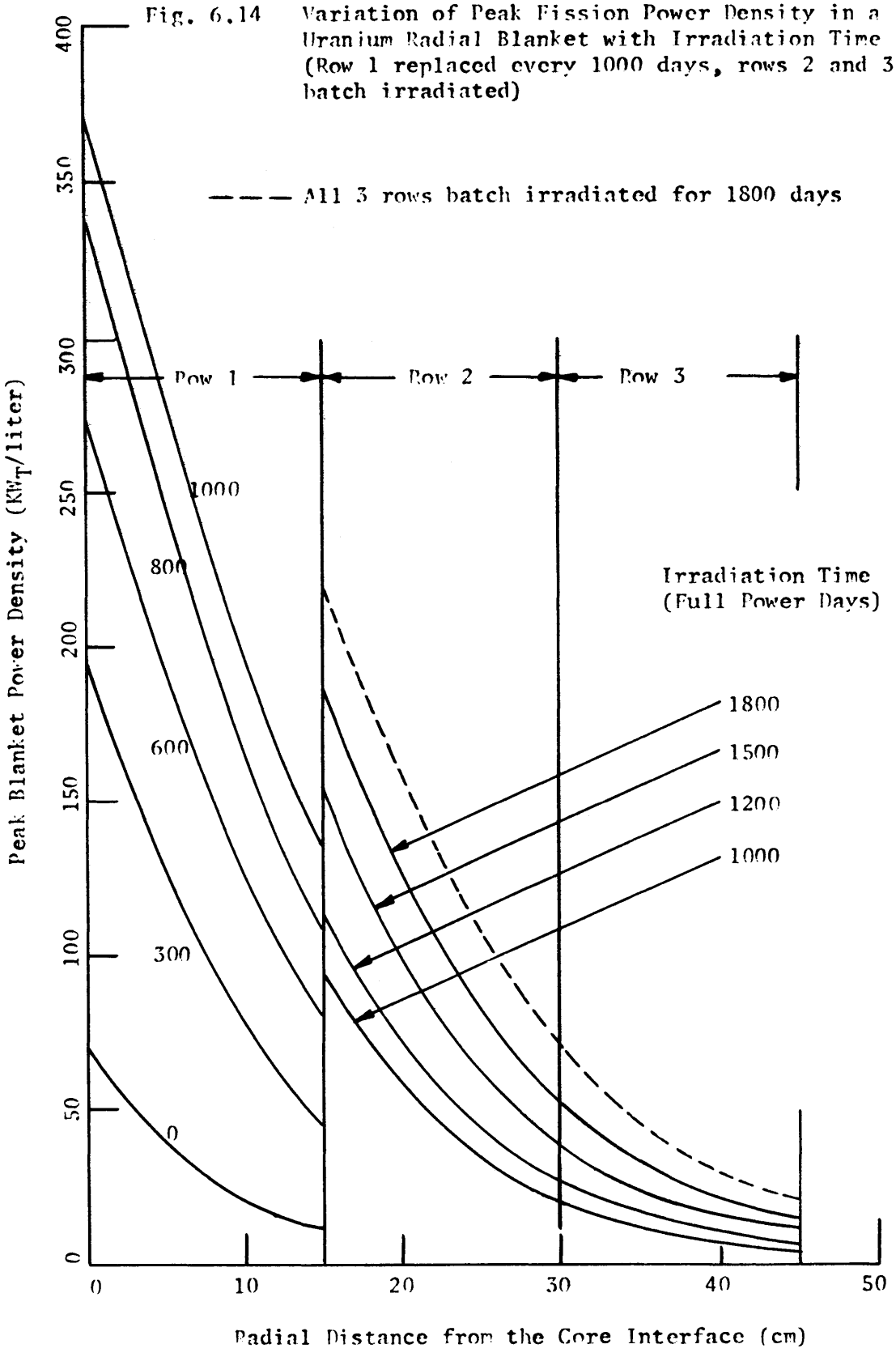

Fig. 6.15 Variation of Peak Fission Power Density in a Thorium Radial Blanket with Irradiation Time (Row 1 replaced every 600 days, rows 2 and 3 batch irradiated)

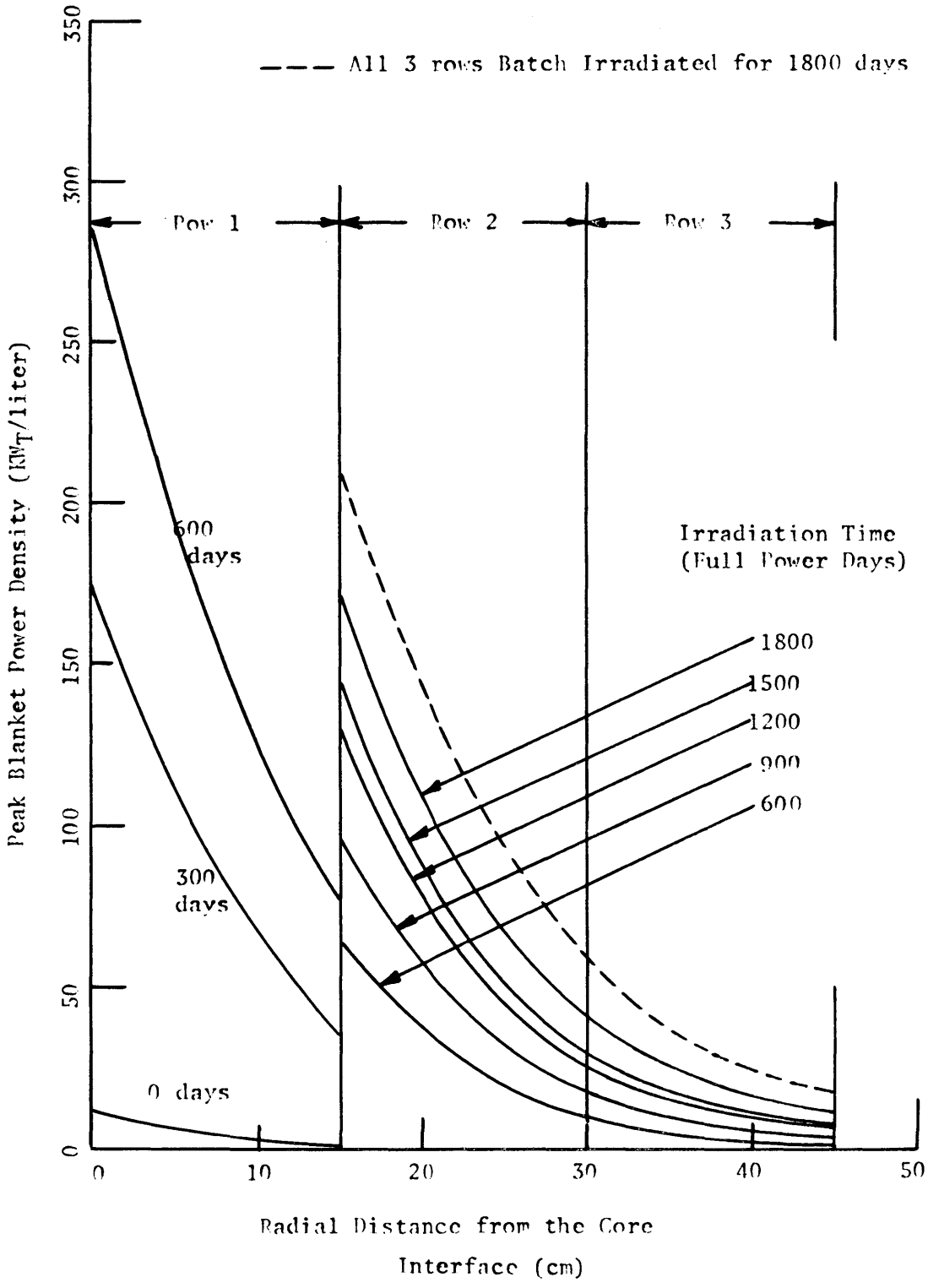

same exposure time. This can easily be seen by comparing the power densities at 1800 days for the row 1 zone scatter case with those at 1800 days for the batch irradiation case (shown as a dashed line). The information shown in Figs. 6.14 and 6.15 will be summarized later, in section 6.3.3.5.

6.3.3.4 In-Out Shuffle Management

To reduce the severity of the engineering problems associated with spatial and temporal power variations in the radial blanket, shuffle management schemes (in which blanket fuel resides for part of its life in several different blanket locations) are being considered. The scheme currently being evaluated by Westinghouse for use in the LMFBR Demonstration Plant is in-out shuffle management (B10). This scheme has been discussed previously in sections 4.6 and 5.3.5. Figure 6.16 shows the peak power density for a uranium radial blanket which was in-out shuffle managed at 600-day invervals. As shown, the effect of moving fissile material produced near the core into more remote regions of the blanket is to reduce significantly the radial power variations by increasing the outer row power production rates. This same conclusion was reached by Barthold (B11) in his comparison of in-out and out-in shuffle schemes. Cross comparison of Figs. 6.14 and 6.16 shows that the shuffle management also has the effect of reducing the maximum to minimum peak power density ratio in all rows of the radial blanket.

Since all power density comparisons have been made using the "peak" power density (the value at the core axial midplane), some discussion of the validity of these comparisons should be presented.

Fig. 6.16 Variation of Peak Fission Power Density in a Uranium Radial Blanket which is In-Out Shuffle Managed (Equilibrium Cycle)

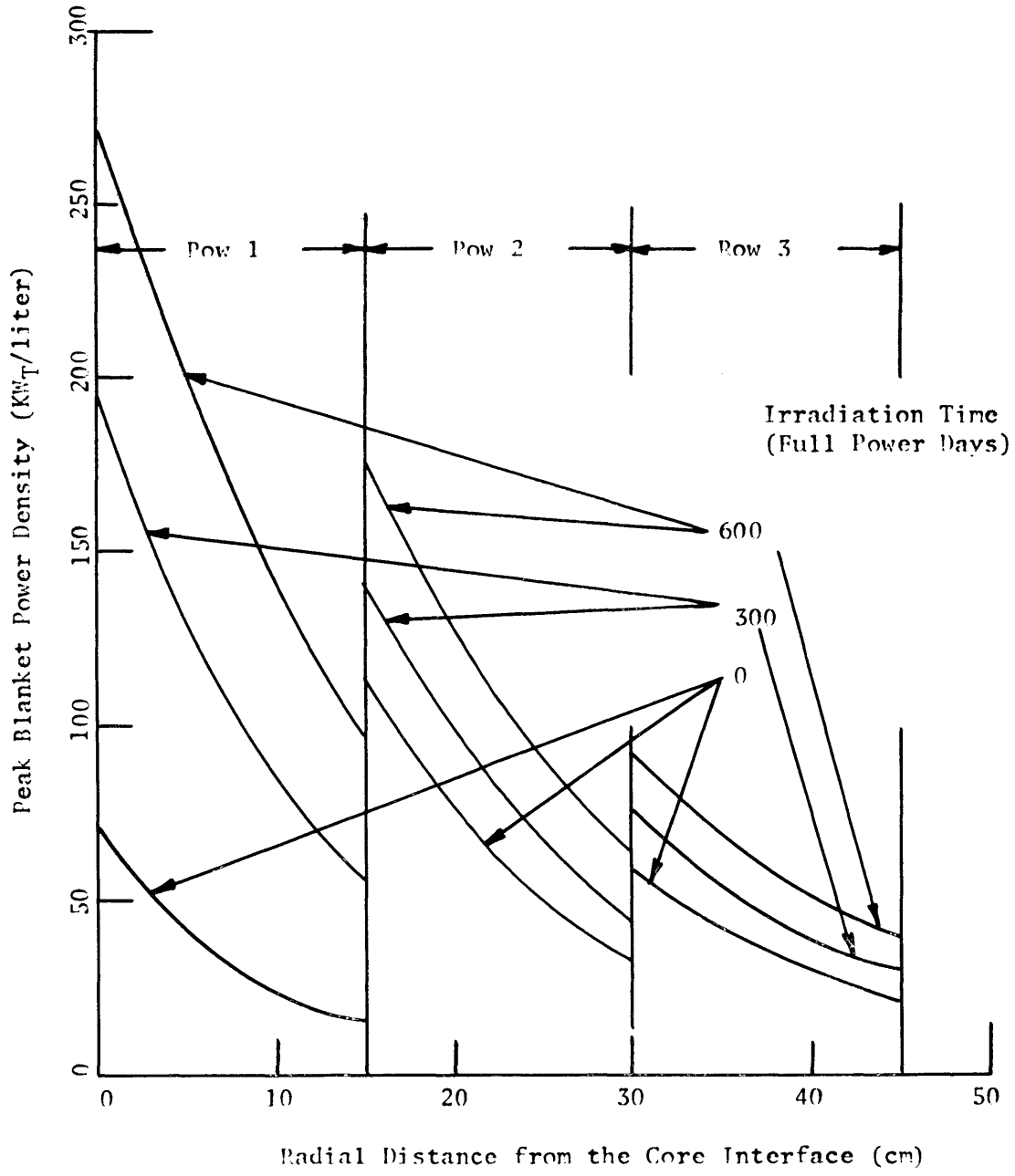

Figure 6.17 shows the variation of power density in the axial direction as a function of radial position (Fig. 6.17A) and of time (Fig. 6.17B). These curves show that the shape of the axial profile is nearly the same at all radial positions and for all irradiation times considered. Thus the peak power density values presented in this section can be considered as representative of the general trends of the average power densities in the radial blanket, and hence also of the integral channel power.

6.3.3.5 Comparison of Management Schemes

The intent of this subsection is to summarize the information presented in Figs. 6.12 through 6.16 and to show the relevance of this information to blanket engineering design. All discussion presented in this section applies to the fission heating rate only. Section 6.3.2.2 showed that neutron heating makes a small contribution to the beginning-of-life (BOL) power density in the uranium blanket, and is nearly equal to the BOL fission power density in the thorium blanket. Because of the significant increase in fission heating rate with burnup, neutron heating, which remains very nearly the same, can be safely neglected over most of the burnup interval for both thorium and uranium blankets. Gamma heating, however, is a more significant contributor to the total blanket heating rate (see sec. 6.3.2.3). Its major effect will be to increase the effective heating rates in both uranium and thorium blankets above those predicted for fission heating alone. It would also tend to increase slightly the radial power peaking factors for the radial blanket. The net result of these effects would be to make the thorium blanket appear more favorable relative to uranium than reported in this

Fig. 6.17 Variation in Axial Blanket Fission Power Shape in a Batch Irradiated Uranium Blanket

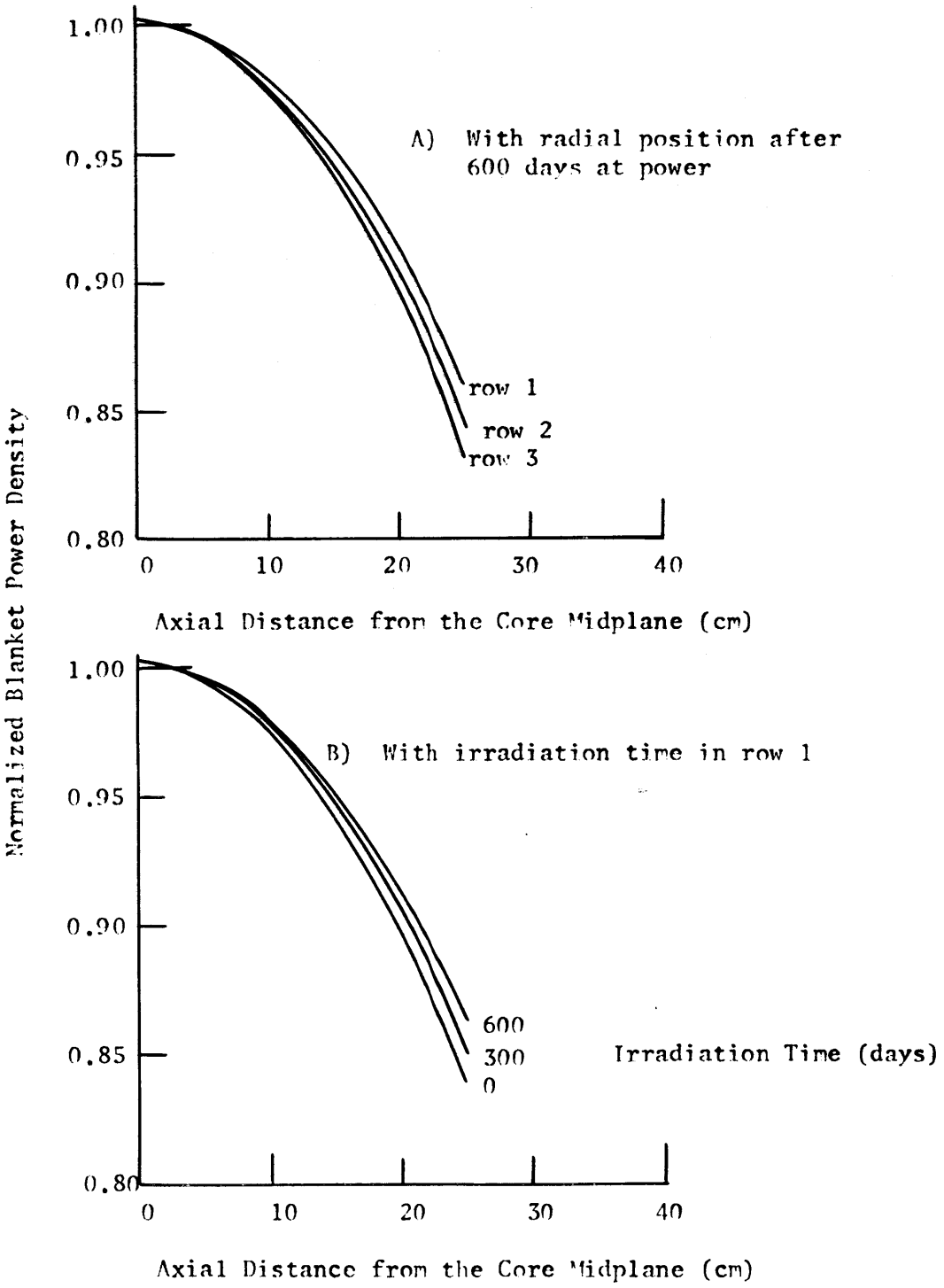

subsection. An attempt to take gamma heating effects into account in deriving the peaking factors will be made in section 6.3.3.6.

Two of the parameters of greatest interest in blanket engineering design, spatial and temporal power variations, will be treated separately here. Table 6.5 shows the ratio of the maximum to minimum heating rate in individual rows of uranium and thorium radial blankets for all management schemes considered. These ratios are shown at the time just prior to removal of the blanket as well as after 600 days of irradiation. One feature shown in Table 6.5 which should be noted is that the maximum power gradient in a given blanket row does not necessarily occur at the end of the irradiation interval. In fact, in each case shown, the peaking factors in all three rows are higher after 600 days of irradiation than at the end of their irradiation interval. Actually, the highest values of the peaking factors in all three rows occurred at the beginning of the irradiation interval. This case is of little interest to designers, however, because the blanket would be so highly overcooled at BOL conditions that no significant temperature gradients would exist in blanket assemblies at that time. The next feature to note is that the lowest power gradients after 600 days of irradiation are attained with the in-out shuffle management scheme. The EOL power gradients in rows 2 and 3 are also lower for the in-out shuffle scheme than for either of the other schemes. The smallest reported EOL power gradients in row 1 were observed for the batch managed case. This is because the net fissile isotope production near the core interface in row 1 increases less rapidly with increased irradiation than deeper in the blanket. This point was discussed previously in

TABLE 6.5 Ratio of Radial Maximum to Minimum Fission Heating Rate by Row in Thorium and Uranium Blankets with Different Management Schemes.

Blanket Type	Management Scheme	Blanket Row Number	Ratio: Maximum to Minimum Radial Heating Rate		Irradiation Time (Days)
Uranium	Batch	1	2.0	(3.5)[1]	1800
Uranium	Batch	2	3.3	(5.1)	1800
Uranium	Batch	3	3.4	(4.0)	1800
Uranium	Zone scatter	1	2.7	(3.5)	1000
Uranium	Zone scatter	2	3.6	(5.1)	1800
Uranium	Zone scatter	3	3.4	(4.0)	1800
Uranium	In-out shuffle	1	2.9	(2.9)	600
Uranium	In-out shuffle	2	2.9	(2.9)	600
Uranium	In-out shuffle	3	2.6	(2.6)	600
Thorium	Batch	1	2.9	(4.1)	1200
Thorium	Batch	2	4.7	(6.4)	1200
Thorium	Batch	3	3.9	(4.5)	1200
Thorium	Zone scatter	1	4.1	(4.1)	600
Thorium	Zone scatter	2	5.0	(6.4)	1200
Thorium	Zone scatter	3	3.5	(4.5)	1800

(1) The numbers in parentheses are the values of this ratio after 600 days of irradiation.

section 4.4. Finally, it should be noted that the peaking factors in the thorium blanket are larger than those in the uranium blanket for all management schemes under consideration. This arises because the fissile production rate in a thorium blanket relative to that in a uranium blanket decreases with increasing distance from the core interface (see sec. 4.4.2.2).

Consideration will now be given to temporal variations in blanket power generation rate. Table 6.6 shows the ratio of the end-of-life (EOL) to the beginning-of-life (BOL) heat generation rates in all rows of both thorium and uranium blankets for the management schemes considered here. This table shows that, as expected, the in-out shuffle management scheme is clearly superior to either of the other two schemes when minimum time variation of blanket assembly heating rate is desired. The variation in row 1, in which unirradiated blanket material is loaded is, however, fairly large for all management techniques considered. Table 6.6 clearly shows that the thorium blanket has a much larger fission power variation with time than a uranium blanket. This is a result of the extremely low fission rate in thorium relative to that in U-238. The significance of the large differences in EOL/BOL heating rates between thorium and uranium blankets can be more easily understood by considering the estimated BOL coolant temperature rise shown in the last column in Table 6.6. These temperature rises were derived by assuming that the blanket assembly flow rate was selected to achieve a mixed mean outlet temperature at EOL conditions in any given row of 300° F. The flow rate through any row of assemblies was assumed not to vary during irradiation. As shown for

TABLE 6.6 Temporal Variations of Average Blanket Row Fission Heating Rate at the Core Mid-Plane.

Blanket Type	Management Scheme	Blanket Row Number	Irradiation Time Interval (Days)	Heating Rate Ratio[1] EOL/BOL	BOL[2] Coolant ΔT (°F)
Uranium	Batch	1	0 - 1800	10.1	29.7
Uranium	Batch	2	0 - 1800	23.0	13.0
Uranium	Batch	3	0 - 1800	27.8	11.2
Uranium	Zone scatter	1	0 - 1000	7.6	39.7
Uranium	Zone scatter	2	0 - 1800	18.2	16.5
Uranium	Zone scatter	3	0 - 1800	20.1	14.9
Uranium	In-out shuffle	1	0 - 600	5.0	60.0
Uranium	In-out shuffle	2	0 - 600	1.7	176.2
Uranium	In-out shuffle	3	0 - 600	1.7	178.9
Thorium	Batch	1	0 - 1200	58.9	5.1
Thorium	Batch	2	0 - 1200	150.6	2.0
Thorium	Batch	3	0 - 1200	275.5	1.1
Thorium	Zone scatter	1	0 - 600	35.6	8.4
Thorium	Zone scatter	2	0 - 1200	124.7	2.4
Thorium	Zone scatter	3	0 - 1800	355.7	0.8

(1) BOL = Beginning of life.
EOL = End of life.

(2) Assumes coolant flow rate sized to give a mixed ΔT at EOL of 300°F, this number is a mixed mean value.

both the batch and zone scatter management case, the BOL coolant ΔT for the uranium blanket is never more than about 30°F higher than that for the thorium blanket. Reference back to section 6.3.3 shows that this small difference in mixed coolant ΔT would be expected to be reduced to only a few degrees after 300 full power days of irradiation. (Gamma heating contributions will also tend to reduce this value by about half.) Thus the consequences of the large difference between the temporal power variations in thorium and uranium blankets would be expected to make a relatively small difference in the relative operating characteristics of the two systems. This will have an important beneficial consequence in terms of subassembly interchangeability to be discussed in section 6.5.

6.3.3.6 The Effect of Gamma and Neutron Heating

The spatial and temporal power variations discussed in the previous section were those arising from fission events only. Figures 6.18 and 6.19 show the components of the beginning-of-life heating rate in the radial blanket for both uranium and thorium blankets. As shown, gamma and fission heating make nearly equal contributions to the total heating rate in the uranium radial blanket, while gamma heating is clearly dominant in the thorium blanket. In both cases the neutron heating contribution is quite small. If it is assumed that the gamma and neutron heating contributions do not change during blanket irradiation (a relatively good first-order approximation, see sec. 6.3.2.5), then the heating rates in the radial blanket can be defined as a function of burnup in a particularly simple manner. Figure 6.20 shows the total

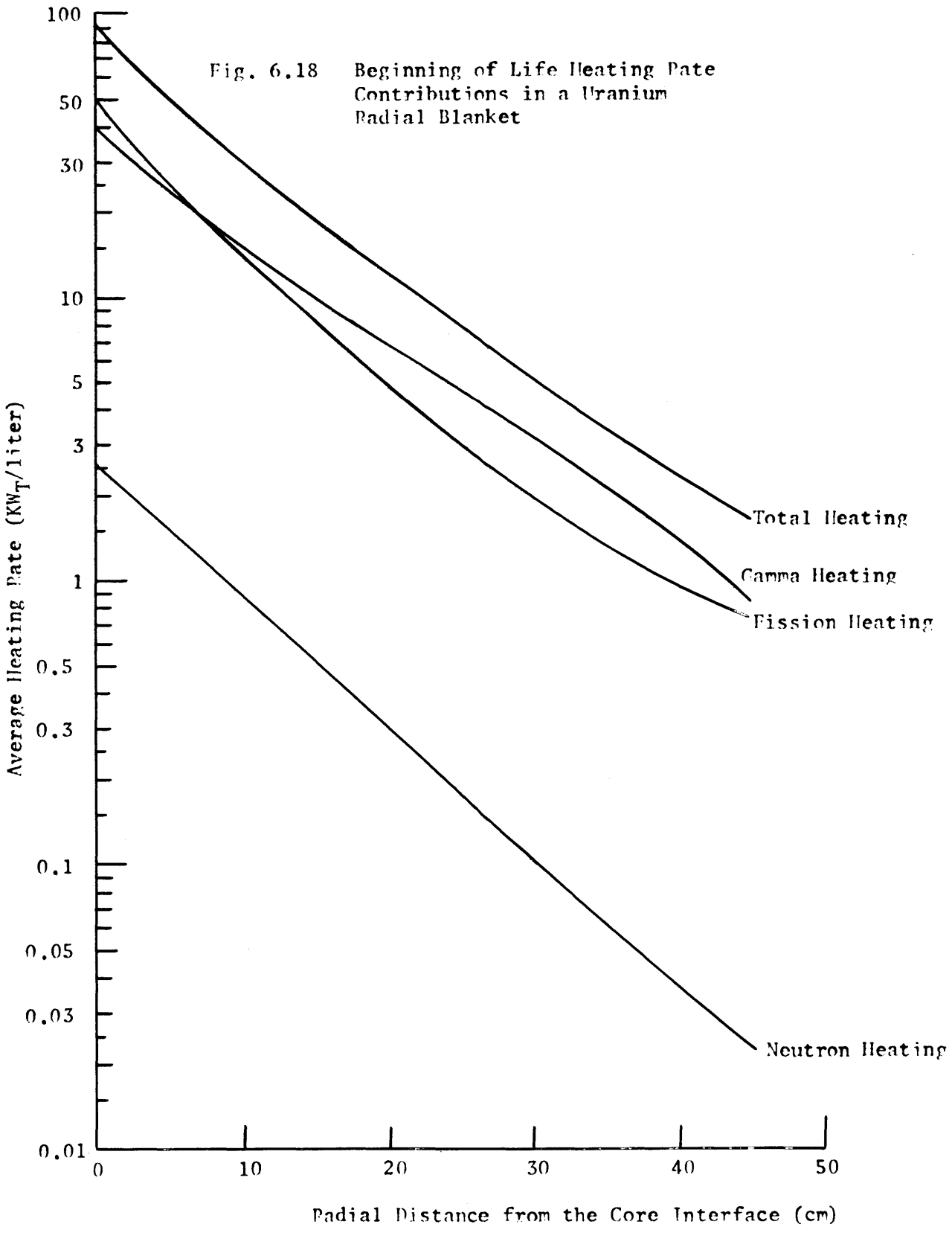

Fig. 6.18 Beginning of Life Heating Rate Contributions in a Uranium Radial Blanket

Fig. 6.19 Beginning of Life Heating Rate Contributions in a Thorium Radial Blanket

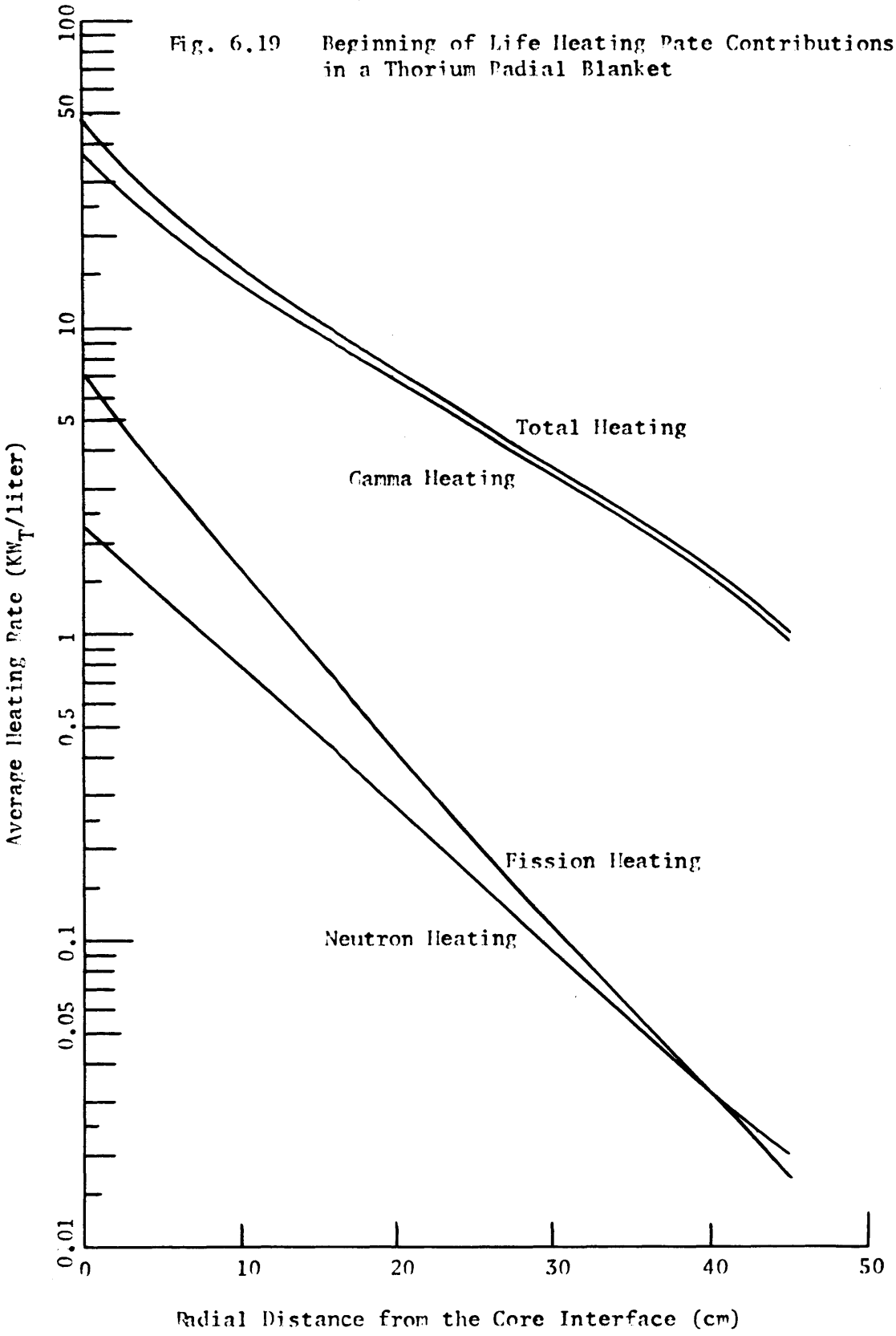

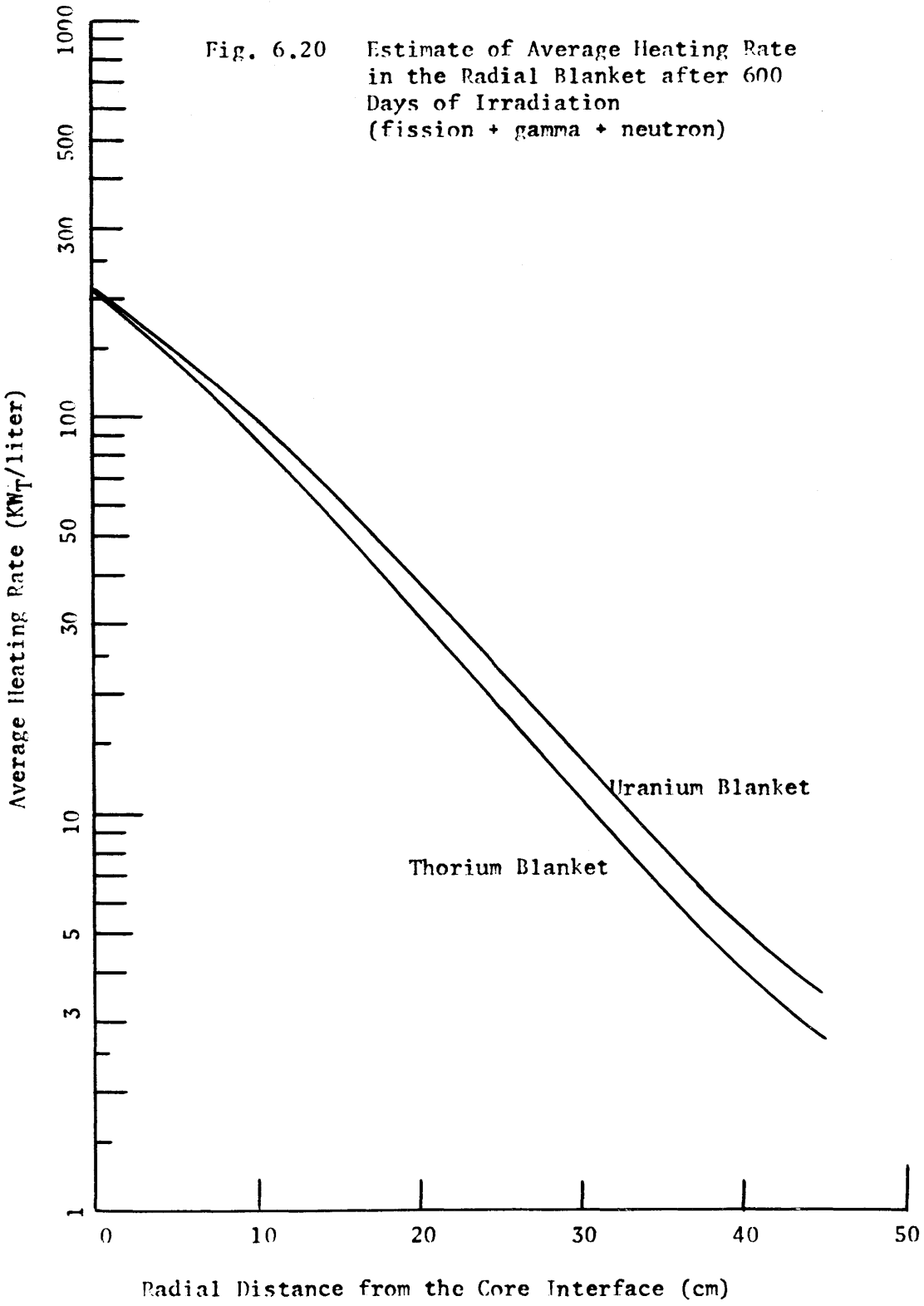

Fig. 6.20 Estimate of Average Heating Rate in the Radial Blanket after 600 Days of Irradiation (fission + gamma + neutron)

heating rate in uranium and thorium radial blankets after 600 full power days of irradiation. As shown, the heating rate at the core interface is nearly the same for both blankets, while the thorium blanket has a somewhat lower heating rate at the reflector interface. The results shown in Figs. 6.18, 6.19, and 6.20 are summarized in Table 6.7.

TABLE 6.7 Radial Blanket Total Power Peaking Factors

Blanket Row Number	Power Peaking Ratio (Maximum/Minimum)			
	Uranium Blanket		Thorium Blanket	
	BOL	600 Days	BOL	600 Days
1	4.8	3.4	4.3	4.0
2	3.7	4.5	3.1	4.9
3	3.2	3.9	3.4	4.0

Comparison between Tables 6.5 and 6.7 reveals that the inclusion of gamma and neutron heating rates in developing the power peaking ratios after 600 days of batch irradiation reduces these ratios for both thorium and uranium blankets. Also apparent from these two tables is the fact that thorium blanket peaking factors are much closer to those for the uranium blanket for the case in which all heating rate contributions are included (Table 6.7) than for the case in which only fission heating is considered (Table 6.5).

6.3.4 Post-Shutdown Heating

6.3.4.1 General Discussion

Another potential difference between thorium and uranium blanketed systems might be expected in the post-shutdown heating rate in the blanket. A qualitative comparison can be made between the post-shutdown heating rates in thorium and uranium blankets by considering fission product decay heating and the heating rate associated with beta decay of the intermediate isotopes Pa-233 and Np-239. First, consider fission product heating. The component of the post-shutdown heating rate in the radial blanket associated with fission product decay is a function of the fission rate history of the blanket (Ref. L1, p. 94). Reference to section 6.3.3 shows that after about the first 300 days of irradiation the fission heating rates in the uranium and thorium blankets are virtually the same. Thus, to a first approximation, the radial blanket post-shutdown heating rate contribution from fission product decay is the same for both uranium and thorium blankets if the shutdown occurs after more than 300 days of irradiation. (This approximation is not an unreasonable one since the fission product distribution for fission of U-233 is nearly the same as that for fission of Pu-239 [Ref. E2, Table 3-16].) For shorter irradiation times, the thorium blanket would have a smaller heating rate because of its lower fission rate early in life.

The second factor contributing to decay heating in the radial blanket is the beta emission associated with the decay of the intermediate isotopes Pa-233 and Np-239 to the fissile isotopes U-233 and Pu-239. The decay of Th-233 and U-239 to Pa-233 and Np-239, respectively, can

be neglected because the short half lives for these reactions (about 20 to 25 minutes) preclude a significant buildup of these isotopes in the blanket. Comparison of the fissile inventories in thorium and uranium radial blankets presented in Chapter 4 reveals that the rate of production of fissile material is very nearly the same in both types of blanket. This observation leads to the conclusion that the intermediate isotope decay rate in both blankets is very nearly the same. Because of the longer half life of Pa-233 (27.4 days compared to 2.35 days for Np-239), its equilibrium concentration in the thorium blanket will be significantly higher than that of Np-239 in the uranium blanket. A simple analysis shows that the ratio of concentrations must be

$$\text{Pa-233/Np-239} = \lambda^{239}/\lambda^{233} = 11.7,$$

(where λ^{239} is the decay constant for Np-239 $= \ln 2/T_{1/2}^{239}$

and λ^{233} is the decay constant for Pa-233 $= \ln 2/T_{1/2}^{233}$).

for the formation rate of Pu-239 in the uranium blanket to be equal to that for U-233 in the thorium blanket.

Because the intermediate isotope decay rates are the same in both blankets during operation, they must be the same immediately following shutdown. Thus the ratio of heating rates resulting from intermediate material beta decay in the two blankets must be, to first order, the ratio of the decay energies associated with these two reactions. This ratio is

$$E^{233}/E^{239} \cong 0.79,$$

where E^{233} is the energy (average β plus γ) from radioactive decay of Pa-233

and E^{239} is the energy (average β plus γ) from radioactive decay of Np-239.

Thus the peak radioactive decay heating contribution would be about 21% lower in a thorium blanket than in a uranium blanket. It should be pointed out, however, that because of the longer half life of Pa-233, the heating rate contribution from radioactive decay after shutdown will decrease at a much slower rate in the thorium blanket than in the uranium blanket.

6.3.4.2 Thorium Blanket Decay Heating

Attention can now be given to values of the heating rates in a thorium radial blanket resulting from decay of Pa-233 and from fission product heating. First, let us consider fission product decay heating. An expression for the average energy emitted per second in the form of beta particles and gamma photons at t seconds after one fission event has been developed (Ref. L1, p. 94):

$$E_D(t) = 2.66\, t^{-1.2} \text{ MeV/sec} \tag{6.8}$$

where

E_D is the decay energy released t seconds after one fission event.

This expression can be used in conjunction with the method outlined by West (E4, p.7-15) to generate expressions for the decay heating rate. This method involves performing the following integration:

$$P_D = \int_0^{T_o} R[\, 2.66(T+t)^{-1.2}\,]\, dT \tag{6.9}$$

where P_D is the decay power in MeV/sec

R is the fission rate in fissions/sec

T_o is the time at power, sec

t is the time after shutdown, sec.

When the fission rate is assumed constant during the time interval from 0 to T_o, the following expression is derived for the fission product decay power:

$$P_D = 13.3R\{t^{-0.2} - (T_o+t)^{-0.2}\} \text{ MeV/sec} \qquad (6.10)$$

If the fission rate is assumed to vary linearly from zero at time zero to R at time T_o, the following expression for the decay heating rate is derived:

$$P_D = 2.66R\{1.25(T_o+t)^{0.8} + 5.0t(T_o+t)^{-0.2} - 6.25t^{0.8}\} \text{ MeV/sec} \qquad (6.11)$$

Application of Eqs. 6.10 and 6.11 can be made to approximate any variation of fission heating rate in the radial blanket. For example, Fig. 6.21 shows the fission heating rate in a region of the thorium blanket near the core interface. Also shown is an approximate fission heating rate which can be used with Eqs. 6.10 and 6.11 to generate decay heating rates following reactor shutdown. Figure 6.22 shows the resulting value of the fission product decay heating in the thorium radial blanket region near the core interface. Also shown in Fig. 6.22 is the heating rate resulting from the decay of Pa-233 in the same radial blanket region. This curve was generated by assuming that the concentration of Pa-233 in the radial blanket region of interest had reached its equilibrium value and that the energy released for each decay event (0.568 MeV) was deposited locally in the blanket. Comparison of the two decay heating curves presented in Fig. 6.22 reveals that fission product decay heating represents the larger heating rate term prior to about 50 minutes after shutdown, at which time the Pa-233 decay

Fig. 6.21 Comparison of Actual Fission Heating Rate and Fission Heating Rate Assumed in Evaluating Fission Product Decay Heating in a Thorium Radial Blanket Near the Core Interface

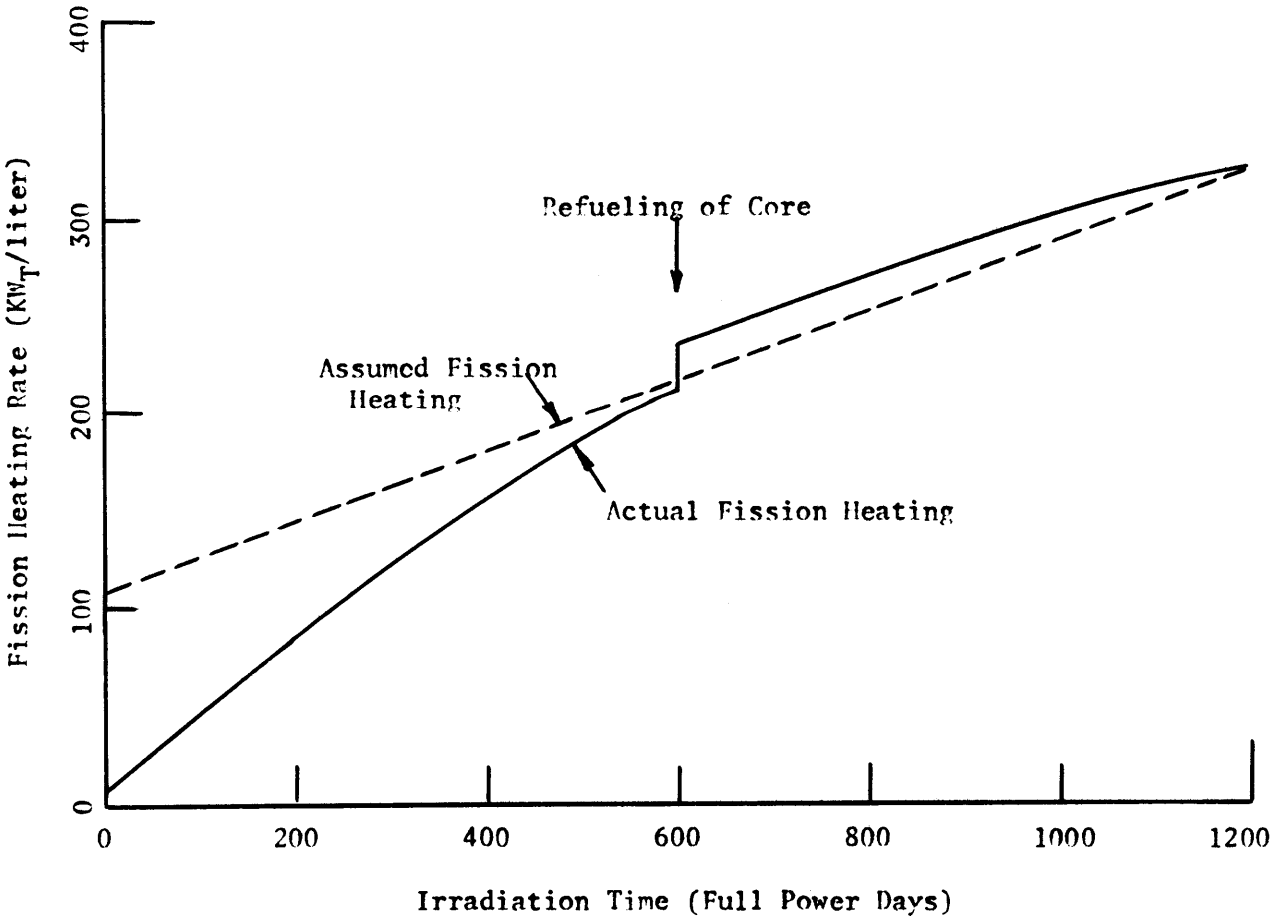

Fig. 6.22 Comparison of Heating Rates from Capture Product Decay and Fission Product Decay in a Thorium Radial Blanket near the Core Interface; Blanket was Irradiated for 1200 Days Prior to Reactor Shutdown

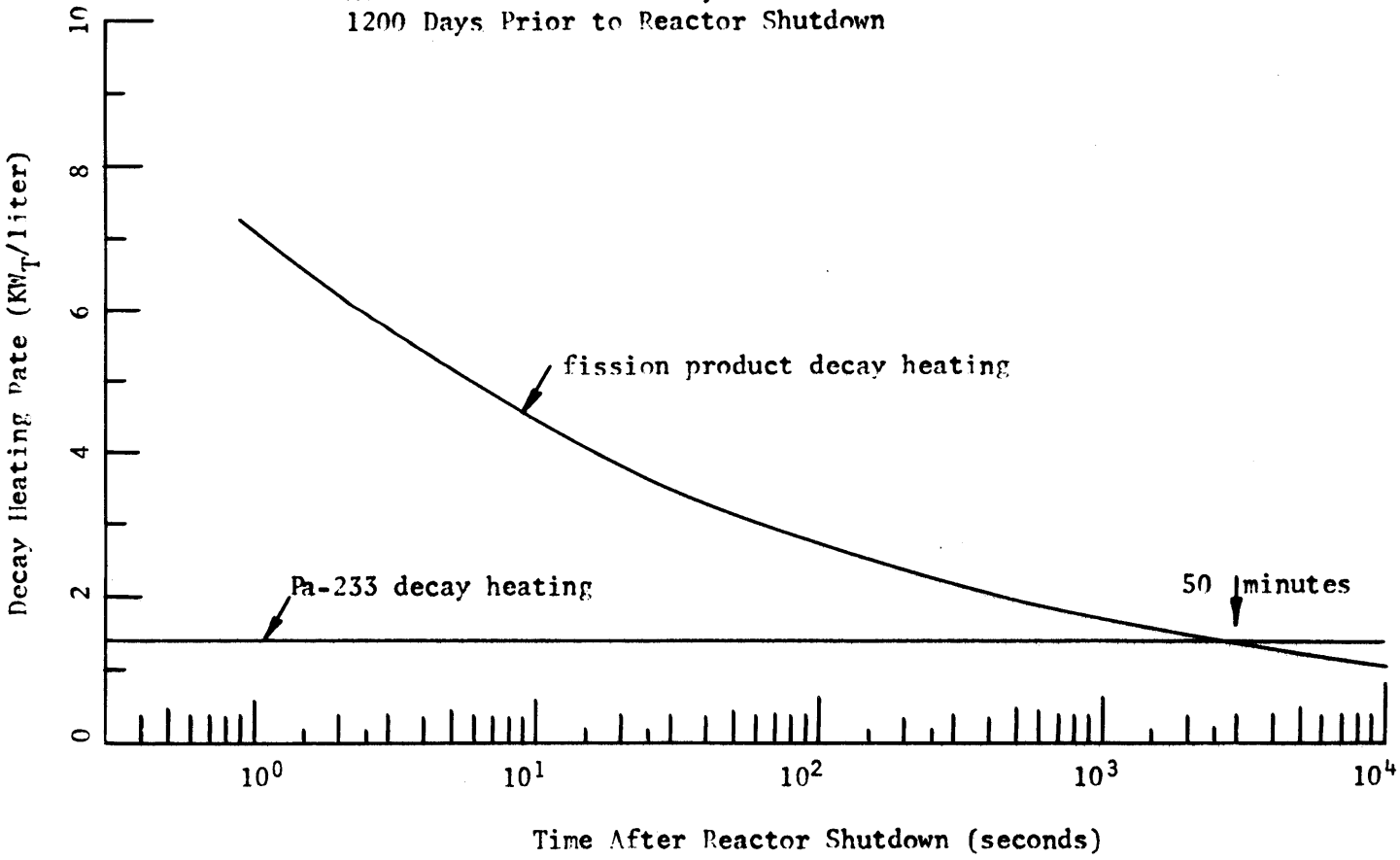

heating becomes larger. For the purpose of information, Fig. 6.23 is shown. In this figure the fission product decay power is presented as a percent of full power following shutdown after operation for 600 full power days at some fixed power level. As shown, at 1 second after reactor shutdown, the fission product decay power has fallen to about 6.4% of the initial power level.

If it is assumed that a reactor shutdown occurs at the exact time when the maximum design power level is reached in the radial blanket, an estimate can be made of the minimum allowable flow rate which must be provided to the reactor to assure that the peak operating temperatures are not exceeded after shutdown. One further assumption and one observation are needed to proceed:

1. The pumps coast down to their shutdown flow rate in 10 seconds.
2. The sum of the fission product decay heating rate in the radial blanket and the Pa-233 decay heating rate just prior to shutdown is 325 kw/liter.

Using this information, it can be determined that the blanket decay heating rate at 10 seconds after shutdown is ~1.7% of its full power value, and the core fission product decay power is ~3.9% of its full power value. Thus a minimum flow rate of about 4% of full flow must be provided to the system after shutdown, and the decay power in the core is the controlling variable. All this analysis assumes that the flow split between the core and the radial blanket remains the same after shutdown as at full flow. It has been shown here that use of a thorium radial blanket will impose no more requirements on minimum shutdown flow rate to the reactor than are imposed by the reactor core.

Fig. 6.23 Core Decay Power Following Shutdown
(Reactor had operated for 600 full power days prior to shutdown)

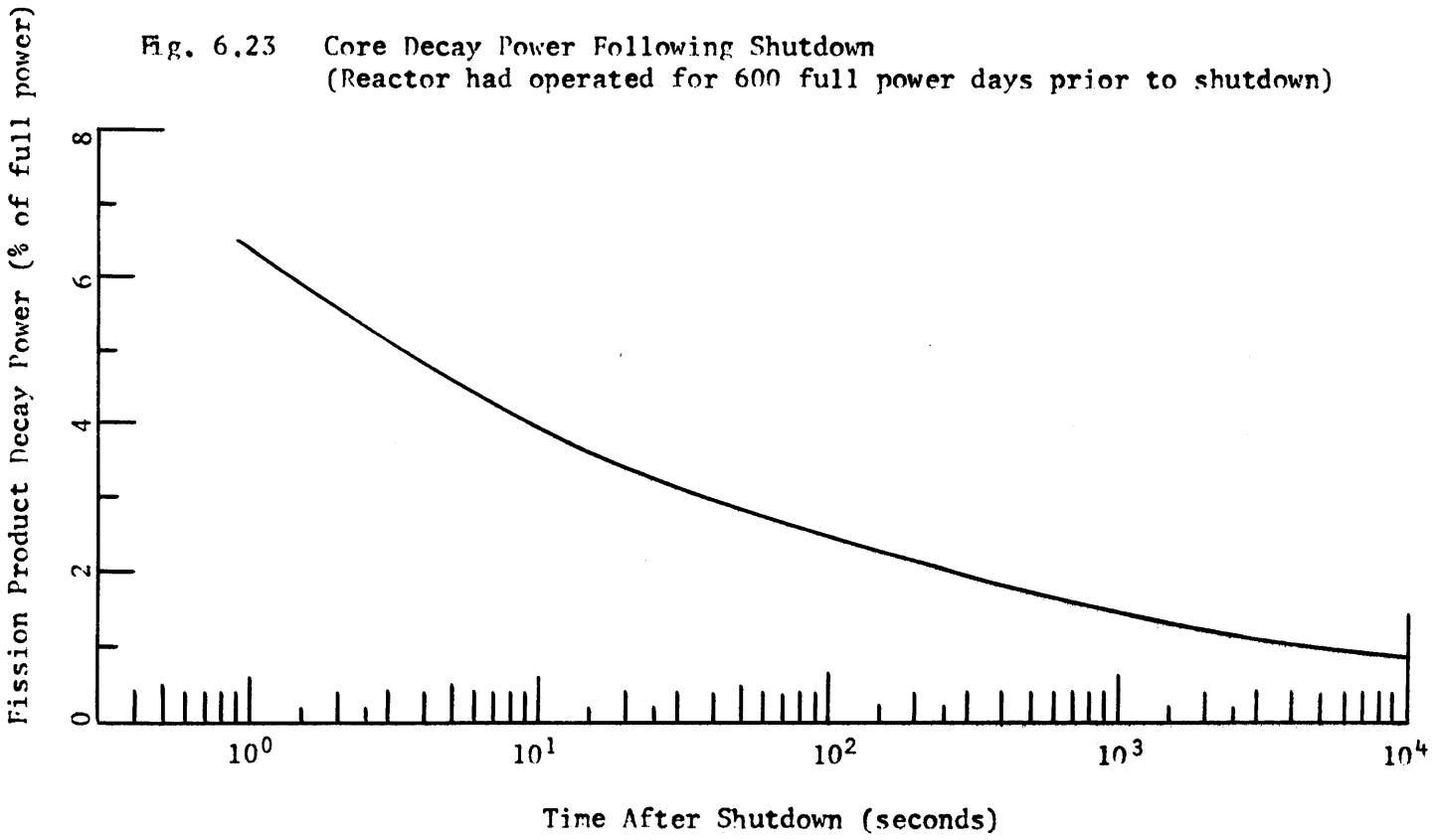

6.3.5 Sodium Activation

Because of the lower BOL fission rate in the thorium radial blanket, one would expect that the sodium activation rate in the thorium blanket system might be lower than that in the uranium blanket system. This factor might be significant because of the difficulty associated with performing repairs on the radioactive sodium primary system. Table 6.8 shows a comparison of the sodium activation rates in the thorium and uranium blanketed systems at BOL conditions. As shown, the total activation rate is about 9% less in the thorium blanketed system than in the uranium blanketed system. The largest part of this difference is in the

TABLE 6.8 Comparison of Beginning-of-Life Sodium Activation Rates

Region	Activation Rate (Normalized to U Blanket System Total)	
	Uranium Blanket System	Thorium Blanket System
Core	0.6245	0.6130
Radial blanket	0.1022	0.0760
Axial blanket	0.1641	0.1317
Reflectors	0.1092	0.0932
Total	1.0000	0.9139

radial and axial blankets, where it would be expected to be. It should be noted, however, that even the core of the thorium blanketed system contributes less to the sodium activation rate. This is a result of the lower required core flux associated with the higher core enrichment in the thorium blanketed system at the beginning-of-life. If similar sodium activation rate comparisons were made throughout the life of

the blanket, it would be expected that increased irradiation exposure would lead to smaller differences in the sodium activation rate between the two systems. This would result from higher blanket fission rates later in life as well as from the fact that the core would be depleted more rapidly for the thorium blanketed system than for the uranium blanketed system.

6.4 REACTOR DYNAMICS COMPARISON

6.4.1 Preface

The use of thorium in the blanket of an LMFBR might be expected to have a second order effect on parameters related to the dynamic characteristics of the reactor. This would result from two major differences between thorium and uranium blanketed systems. First, the use of a thorium blanket requires a slightly higher core fissile enrichment than would be necessary with a uranium blanket. Second, the fission rate at beginning-of-life in the thorium radial blanket is much less than that in the uranium radial blanket. Thus the contribution of fertile fissions to the total fission rate is reduced, and consequently the system-average delayed neutron fraction decreases because fertile fissions have larger associated delayed neutron yields than do fissions in fissile materials. It should be noted here that as burnup proceeds and the concentration of U-233 in the blanket is increased, the effective system delayed neutron fraction will increase for the thorium blanket case relative to the uranium blanket case. This would result because the effective delayed neutron fraction (β) is higher for U-233 than for Pu-239 (0.0026 for U-233 versus 0.0020 for Pu-239 [L1, p. 101]). Thus analysis of the

beginning-of-life condition would give the largest difference between the β_{eff} of thorium and uranium blanketed systems.

In the remainder of this section (6.4) comparisons will be made between thorium and uranium blanketed systems in terms of the following parameters:

1. Sodium void reactivity,
2. Isothermal Doppler coefficient,
3. Power coefficient of reactivity,
4. Adiabatic Doppler coefficient,
5. Delayed neutron fraction,
6. Prompt neutron lifetime,
7. Control requirements.

Because of the inexactness of the methods used in evaluating these parameters, only their relative values for the two blanket systems will have relevance. Finally, the results presented in this section should be viewed in the light of the projected accuracies required in the prediction of physics parameters. Table 6.9 shows the current and target accuracies with which certain kinetics-related parameters can be or should be able to be predicted. Another way of looking at the target uncertainties is that they constitute an operating band of variations with which designers are prepared to cope within a given system.

TABLE 6.9 Estimates of Prediction Accuracies for Dynamics Parameters

Parameter	SEFOR Experiments	Current Uncertainties		Target Uncertainties	
	Ref.(K4)	Ref.(K4)	Ref.(G4)	Ref.(K4)	Ref.(G4)
Isothermal Doppler	±5%	–	±15%	–	±7%
Power coefficient	±9%	±20%	–	±10-20%	–
Sodium void coefficient	–	±20-30%	±1.5$	±15-20%	±0.3$

6.4.2 Sodium Void Reactivity

In an attempt to assess the effect of blanket material on the sodium void reactivity, ANISN (E1) was used to evaluate both thorium and uranium blanketed systems. The sodium void reactivity change was determined by calculating the system effective multiplication factor for the standard radial geometry and for the same geometry with the sodium removed from core zone 1. This procedure produced the results shown below:

TABLE 6.10 Central Core Sodium Void Reactivity Comparison

Type of Radial Blanket	Central Region Na Void Reactivity ($\Delta k/k$)
U-238	0.00668
Th-232	0.00687

This table shows that use of a thorium radial blanket produces on the order of a 2.8% increase in the sodium void reactivity. This is well within the expected limits of analytical and experimental accuracy shown in Table 6.9.

6.4.3 Doppler and Power Coefficients

6.4.3.1 Isothermal Doppler Coefficient

The isothermal Doppler coefficient, defined as the change in k_{eff} per degree change in system temperature, is important in reactor analysis because it allows definition of the reactivity swing between cold and hot operating conditions. For this analysis, the formulation

presented by Siep (S4) was used to evaluate the isothermal Doppler coefficient.

$$\frac{1}{k}\frac{\partial k}{\partial T} = \frac{\int dV \left\{ \sum_i \left[\nu_i \frac{\partial \Sigma_{fi}}{\partial T} \right] - \sum_i \left[\frac{\partial \Sigma_{ai}}{\partial T} \right] \right\} \phi\phi^*}{\int dV \sum_i [\nu_i \Sigma_{fi}] \phi\phi^*} \qquad (6.12)$$

where

- k is the effective multiplication factor
- T is the temperature
- V is the volume
- Σ_{fi} is the macroscopic fission cross section of nuclide i
- Σ_{ai} is the macroscopic absorption cross section of nuclide i
- ϕ is the neutron flux
- ϕ^* is the adjoint flux
- ν_i is the yield of fission neutrons produced per fission in nuclide k

The isothermal Doppler coefficient was evaluated using Eq. 6.12 for uranium and thorium blanketed systems. Fluxes and adjoints were obtained from BOL 2DB (L10) calculations. Values for average neutron yields per fission were obtained from Ref. D6. Cross sections collapsed to one group as functions of temperature were obtained from analyses performed with 1DX (H2) at 300°K and at 1100°K using the modified 26-group ABBN cross section set (N1). When these data were substituted into Eq. 6.12, the results shown in Table 6.11 were obtained. For the purpose of comparison, the isothermal Doppler coefficient obtained using the 1DX code to calculate k_{eff} for the

TABLE 6.11 Isothermal Doppler Coefficient Comparison

Blanket Type	Isothermal Doppler, $\Delta k/k\ \Delta T$, $°K^{-1}$	
	Equation 6.12	1DX
U-238	-1.607×10^{-5}	-1.545×10^{-5}
Th-232	-1.463×10^{-5}	-1.421×10^{-5}
[(Th-U)/U]	-0.0896	-0.0803

isothermal system temperatures of 300°K and 1100°K is also presented in Table 6.11. As shown, good agreement between the two methods was achieved. Also shown is the fact that the isothermal Doppler is 8 to 9 percent less for the thorium than for the uranium blanketed system. This result implies that the reactivity loss associated with heating up the system from room temperature to operating temperature is less for the thorium blanketed system than for the uranium blanketed system. However, reference to Table 6.9 reveals that the projected analytical accuracy for evaluating the isothermal Doppler coefficient is only approximately ±7%. Thus again the difference between the two systems is less than the expected error associated with a good calculation of the coefficient.

Finally, the isothermal Doppler coefficient presented in Table 6.11 as calculated using 1DX to analyze a uranium blanketed system was used to calculate the Doppler constant. This constant is defined as

$$C = -\frac{\overline{T}}{k}\frac{\partial k}{\partial T} \tag{6.13}$$

where $\overline{T}$ is the average temperature (in degrees Kelvin) used in the evaluation of the adiabatic Doppler coefficient. This value was

determined to be 0.0108 which is somewhat higher than those reported in the literature, about 0.0077 (K7).

6.4.3.2 Power Coefficient of Reactivity

A quantity which is more relevant to the operation, stability, and safety of LMFBR's is the power coefficient, defined here as being the change in system reactivity for a given change in system power. An expression for this quantity can be developed from Eq. 6.12 as follows.

$$\frac{1}{k}\frac{\partial k}{\partial P_{total}} \cong \left(\frac{1}{k}\frac{\partial k}{\partial T}\right)\left(\frac{dT_{local}}{dP_{total}}\right) \tag{6.14}$$

where

P_{total} is the total system power

T_{local} is the local temperature

Several assumptions were made to evaluate Eq. 6.14.

1. The local fuel temperature was assumed to vary as

$$T_{LF} = T_C + \frac{r^2}{4k_{TH}} q'''_L \tag{6.15}$$

where

T_{LF} is the local fuel temperature at the centerline

T_C is the local coolant temperature

r is the radius of the fuel pin

k_{TH} is the fuel thermal conductivity

q'''_L is the local volumetric heating rate

2. The average fuel temperature was assumed to change half as much as the peak temperature (valid for a parabolic temperature profile), leading to the following expression:

$$\frac{d\bar{T}_{LF}}{dq'''} = \frac{r^2}{8k_{TH}}, \tag{6.16}$$

where $\bar{T}_{LF}$ is the radial average local fuel temperature.

3. The power shape was assumed to be the same throughout system lifetime

$$\frac{dq'''}{dP_{total}} = \frac{q'''_L}{P_{total}} \tag{6.17}$$

4. All fuel heating was assumed to be proportional to the fission rate

$$q'''_L = C\Sigma_f\phi \tag{6.18}$$

where C is the constant of proportionality.

Substitution of Eq. 6.12 and Eqs. 6.15 through 6.18 into Eq. 6.14 yields

$$\frac{1}{k}\frac{\partial k}{\partial P_T} \cong \frac{r^2 \int dV \left\{\sum_i \left[\nu_i \frac{\partial \Sigma_{fi}}{\partial T}\right] - \sum_i \left[\frac{\partial \Sigma_{ai}}{\partial T}\right]\right\} \sum_i [\Sigma_{fi}\phi]\,\phi\phi^*}{8k_{TH} \int dV \sum_i (\nu_i\Sigma_{fi})\phi\phi^* \cdot \int dV \sum_i (\Sigma_{fi}\phi)} \tag{6.19}$$

Using the thermal conductivities shown in Table 6.12, the power coefficients shown in Table 6.13 were developed.

TABLE 6.12 Thermal Conductivities of Fuel Oxides (E2, p. 182)

Temperature (°F)	Thermal Conductivity (watts/cm-°C)		Regions Used
	ThO_2	UO_2	
1600	0.0329	0.0260	Radial blanket
2000	0.0294	0.0225	Core and axial blanket

TABLE 6.13 Comparison of Power Coefficients of Reactivity

Blanket Type	System Power Coefficient, $\Delta k/k\ \Delta P_T$	
	MW_T^{-1}	$¢/MW_T$ *
U-238	-8.006×10^{-6}	-0.211
Th-232	-7.509×10^{-6}	-0.202
[(Th-U)/U]	-0.0621	-0.0427

*This value depends on the effective delayed neutron fraction which will be discussed later, in section 6.4.4.

Table 6.13 shows that the uranium and thorium blanketed system power coefficients calculated from Eq. 6.19 are the same within 4 to 6 percent, depending on whether the effective delayed neutron fraction is included in the definition. It should also be noted that the actual values of the power coefficients are within a factor of 1.5 of typical values calculated for large LMFBR's (~ -0.13 $¢/MW_T$). Again reference to Table 6.9 shows that the difference between the two systems considered here is less than the 10 to 20 percent target uncertainty reported by Küsters (K4).

6.4.3.3 Adiabatic Power Coefficient

A quantity which is of considerable interest in accident analysis is the adiabatic power coefficient, defined as the fractional change in k_{eff} for a given change in reactor power under the condition of adiabatic fuel pins. An expression for the adiabatic power coefficient can be derived from Eq. 6.12 as follows:

$$\left(\frac{1}{k}\frac{\partial k}{\partial P}\right)_{\text{adiabatic}} = \left(\frac{1}{k}\frac{\partial k}{\partial T}\right)\left(\frac{\partial T_{\text{local}}}{\partial P_{\text{total}}}\right)_{\text{adiabatic}} \tag{6.20}$$

The fuel temperature during an adiabatic excursion of period τ can be written as:

$$T_f = T_o + \frac{1}{\rho C_p}\int_0^t q'''_{c_o} e^{t/\tau} v_f \, dt \tag{6.21}$$

where

T_f is the fuel temperature at time t,

T_o is the initial fuel temperature,

q'''_{c_o} is the initial core averaged volumetric heating rate,

v_f is the volume fraction of the fuel in the core,

ρ is the oxide fuel density,

C_p is the oxide fuel heat capacity,

t is the time at which the fuel temperature is being evaluated.

When the integral in Eq. 6.21 is carried out and the resulting exponential is expanded to include only first order terms, the following expression results:

$$T_f \cong T_o + \frac{q'''_{c_o}}{\rho C_p} t \, v_f, \tag{6.22}$$

where again t is the time at which the fuel temperature is being evaluated. Differentiating Eq. 6.22 and using the assumption of constant power shape (Eq. 6.17) yields:

$$\left(\frac{dT_{\text{local}}}{dP_{\text{total}}}\right)_{\text{adiabatic}} = \left(\frac{t\,v_f}{\rho C_p}\right)\left(\frac{q'''_{\text{local}}}{P_{\text{total}}}\right) \tag{6.23}$$

Again using Eq. 6.18 for the local volumetric heating rate produces:

$$\left(\frac{dT_{local}}{dP_{total}}\right)_{adiabatic} = \left(\frac{t\,v_f}{\rho C_p}\right) \frac{\Sigma_f \phi}{\int dV\, \Sigma_f \phi} \tag{6.24}$$

Substitution of Eq. 6.24 into Eqs. 6.12 and 6.20 yields the relationship of interest:

$$\left(\frac{1}{k}\frac{\partial k}{\partial P_{total}}\right)_{adiabatic} = \frac{t \int dV \left\{\sum_i \left[\nu_i \frac{\partial \Sigma_{fi}}{\partial T}\right] - \sum_i \left[\frac{\partial \Sigma_{ai}}{\partial T}\right]\right\} \sum_i [\Sigma_{fi}\phi]\, \phi\phi^* v_f}{\rho C_p \int dV \sum_i [\nu_i \Sigma_{fi}]\, \phi\phi^* \cdot \int dV \sum_i [\Sigma_{fi}\phi]} \tag{6.25}$$

Equation 6.25 was used to generate adiabatic Doppler coefficients after 1 second of an excursion of longer duration. This analysis showed that the adiabatic Doppler coefficient was about 4% less negative for the thorium blanketed system than for the uranium blanketed system. Again the difference between the thorium and uranium blanketed systems is less than the expected accuracy of the calculation.

6.4.3.4 Core and Blanket Components

The final question addressed in this section concerns how much of the difference between the thorium and uranium blanketed systems' Doppler and power coefficients can be attributed to the core and how much is a result of differences in the blankets. Table 6.14 shows values of these parameters for the whole system and for the core only. As expected, the major contribution to the Doppler and power coefficients is from the core. Also shown in Table 6.14 is that the largest part of the difference between the uranium and thorium blanketed systems arises from differences in the extra initial core enrichment required with the thorium blanket.

TABLE 6.14 Core Contribution to Doppler and Power Coefficient Differences.

Blanket Type	Isothermal Doppler Coefficient ($°K^{-1}$)		Power Coefficient (MW_T^{-1})	
	System	Core	System	Core
U-238	-1.607×10^{-5}	-1.397×10^{-5}	-8.006×10^{-6}	-8.026×10^{-6}
Th-232	-1.463×10^{-5}	-1.294×10^{-5}	-7.509×10^{-6}	-7.513×10^{-6}
[(Th-U)/U]	-0.090	-0.074	-0.062	-0.064

6.4.4 Neutron Lifetime and Delayed Neutron Fraction

The equations presented by Hardie and Little (H7), which were similar to those presented earlier by Long et al. (L12), were used to evaluate the prompt neutron lifetime (Λ) and the effective delayed neutron fraction (β_{eff}). These equations, as used in this analysis, are presented below.

$$\beta_{eff} = \frac{\int dV \sum_i \beta_i \nu_i \Sigma_{fi} \phi\phi^*}{\int dV \sum_i \nu_i \Sigma_{fi} \phi\phi^*} \qquad (6.26)$$

where

$\int dV$ is an integral over the system volume

ν_i is the fission neutron yield for isotope i

Σ_{fi} is the macroscopic fission cross section of isotope i

ϕ is the neutron flux

ϕ^* is the adjoint flux

β_i is the delayed neutron fraction for material i

$$\Lambda = \frac{\int dV \frac{\phi\phi^*}{v}}{\int dV \sum_i \nu_i \Sigma_{fi} \phi \phi^*} \qquad (6.27)$$

where

Λ is the prompt neutron lifetime or, more properly, the neutron generation time, and

v is the average neutron velocity.

The variables required as input to Eqs. 6.26 and 6.27 were obtained as follows. Fluxes, adjoint fluxes, and macroscopic fission cross sections were generated using 2DB; fission neutron yields and delayed neutron fractions were obtained from reference (D6); average neutron velocities in each region were generated by flux and volume weighting the average group neutron velocities using flux information generated by 2DB. When these data were used in conjunction with Eq. 6.26 and Eq. 6.27, the delayed neutron fractions and prompt neutron lifetimes shown in Table 6.15 resulted. As shown, a very small difference, 1.9%, exists between the effective delayed neutron fraction for thorium and uranium

TABLE 6.15 Comparison of Prompt Neutron Lifetime and Effective Delayed Neutron Fraction.

Blanket Type	Delayed Neutron Fraction		Prompt Neutron Lifetime (sec)	
	System	Core Only	System	Core Only
U-238	3.789×10^{-3}	3.720×10^{-3}	9.319×10^{-7}	8.013×10^{-7}
Th-232	3.715×10^{-3}	3.703×10^{-3}	8.282×10^{-7}	7.483×10^{-7}
[(Th-U)/U]	-0.019	-0.004	-0.111	-0.066

blanketed systems. As discussed earlier, this means that as U-233 is generated in the blankets of the thorium blanketed system, and the relative blanket fission rate begins to increase, the delayed neutron fraction for this system will likely become greater than for a similar uranium blanketed system after the same irradiation time. This will result from the higher delayed neutron fraction of U-233 relative to Pu-239. Also shown in Table 6.15 is the fact that the prompt neutron lifetime of the uranium blanketed system is approximately 11% greater than for the thorium blanketed system. About half of this effect is caused by the extra core enrichment and half by the different blankets. Although this difference between the two systems is the largest encountered in this discussion, it is still small with respect to the expected uncertainties in most system dynamics related properties shown in Table 6.9. Also a simplified analysis by Komata (K5) has shown that the energy release associated with a disassembly transient following a ramp reactivity insertion is proportional to the prompt neutron lifetime raised to the 0.75 power. Thus when the 11% difference between system prompt neutron lifetimes is considered in light of its consequences in a disassembly transient, only about an 8% difference in energy release would result. This is certainly small compared with the uncertainty on the total energy release in a disassembly transient.

6.4.5 Control Requirements

Three factors will have an impact on system control requirements: the first is the reactivity swing during a single burnup cycle, the second is the effect of poison concentration on the system effective multiplication

factor, and the last is the control requirements for cold to hot startup. It was shown previously (sec. 4.4.2.1) that the thorium blanketed system has a larger reactivity swing during one refueling cycle than a uranium blanketed system. During the first 600 days of a batch blanket irradiation the uranium blanketed system Δk was 0.1027, while that for the thorium blanketed system was 0.1153. This represents about a 12.3% difference in reactivity swing. The second, smaller source of differences in control requirements is shown in Fig. 6.24. As shown, to achieve the same reactivity change, the thorium blanketed system requires somewhat more B-10 poison. When these two factors are taken together, the thorium blanketed system requires about 12.5% more control material than does a comparable uranium blanketed system. The analysis leading to this 12.5% difference has considered the operating condition (i.e., startup of the core with a fresh blanket, and batch burnup of both core and blanket for 600 days) which would make the thorium blanketed system appear most unfavorable. If a realistic core and blanket management scheme were chosen and analyzed for an equilibrium cycle, the difference in control requirements between the thorium and uranium blanketed systems would be expected to be reduced. This question deserves further consideration prior to use of thorium blankets with LMFBR's.

The final consideration relative to control requirements is the difference in reactivity swing from cold to hot operating conditions. This difference was shown in section 6.4.3.1 to be about 0.1% in k_{eff}, with the thorium blanketed system having a smaller reactivity swing. This difference translates to a difference of about 3.2% in control

Fig. 6.24 The Effect of Core Poison Concentration on System K_{eff}

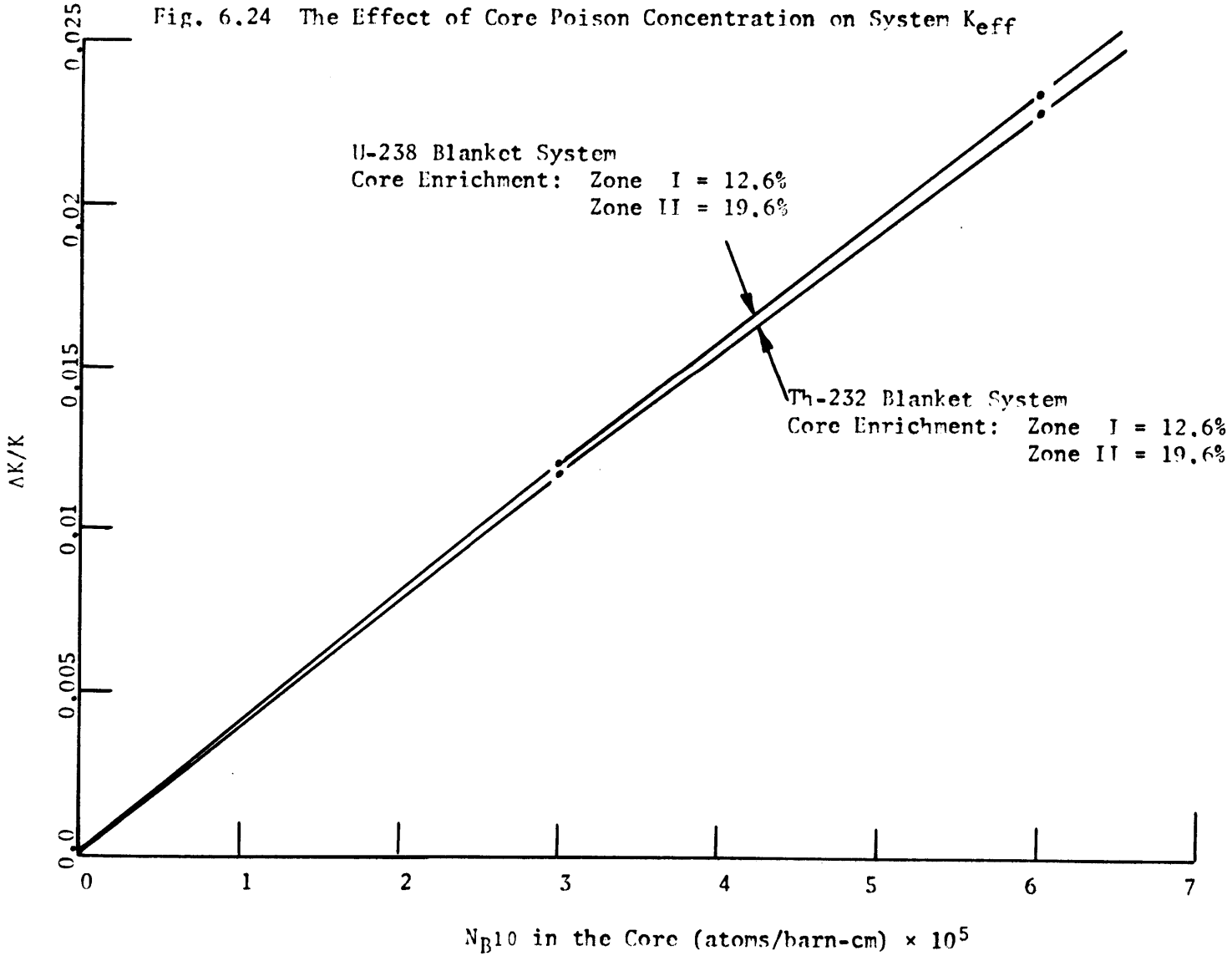

poison requirements. Thus the final difference in poison requirements between the thorium and uranium blanketed systems is about 9.3%, with the thorium blanketed system requiring more control poison.

6.4.6 Effect of Protactinium Decay

One of the safety problems associated with reactors which use thorium in the core is that the decay of Pa-233 following shutdown causes the shutdown margin to decrease or, alternately, causes the core reactivity to increase. This would not be expected to be much of a problem in a thorium blanketed LMFBR, but, nevertheless, a cursory evaluation of the problem will be made in this section. The equilibrium inventory of Pa-233 in all blanket regions of a thorium blanketed LMFBR is approximately 34 kg. In section 4.5.2.1 it was shown that removal of row 1 of a thorium radial blanket after 600 days of exposure caused the system k_{eff} to change by about 1.2%. The fissile material contained in row 1 of the radial blanket after 600 days at power is approximately 274 kg. If it is assumed that all U-233 in the blankets has the same worth as that in radial blanket row 1, then the decay of 34 kg of Pa-233 to U-233 would result in a change in system k_{eff} of approximately 0.15%. When it is recognized that this change will occur with a time constant of approximately 40 days, the 0.15% (~40 cents) in Δk appears to be a rather small contribution.

6.5 SUMMARY AND DISCUSSION OF BLANKET INTERCHANGEABILITY

As was discussed in Chapter 1, the major motivation for considering the use of thorium as the blanket material for LMFBR's is that in the early years following introduction of the LMFBR, there is expected to be a surplus of water reactor produced plutonium. This would lead to a depressed price for plutonium. During the same time period there would be a large demand for fissile material for use as fuel in thermal spectrum reactors such as Light Water Reactors and High Temperature Gas Cooled Reactors. Of the possible isotopes which could be used to meet this demand, U-233 is the most desirable, followed by enriched U-235 and finally by fissile plutonium. Thus, if early LMFBR's were designed for use with thorium rather than with uranium blankets, considerable economic benefit could be realized from the production and sale of the product U-233.

Chapter 5 of this study has addressed the question of what fissile isotope market conditions would favor the use of thorium rather than uranium blankets for LMFBR's. It was also shown in that chapter that, as expected, under anticipated market conditions prior to about the year 2000 there is an economic incentive to equip LMFBR's with thorium blankets. The purpose of this section is to review the information presented in this chapter with the objective of summarizing the possible problems associated with changing from thorium to uranium blankets or vice versa.

The first factor to be considered is whether or not physical property limitations would require different design limits for the two systems. As discussed earlier in this chapter, the chemical stability

of thoria (ThO_2) is greater than that for urania (UO_2), and the melting point of thoria is approximately 1000°F higher than that for urania. Both of these factors imply that thorium blanket design limits might be even less restrictive than those for a uranium blanket. Although discrepancies exist in the literature on the relative thermal conductivity and heat capacity of thoria and urania, it appears that the two materials are quite similar in this respect. Two areas in which some uncertainties may exist in the properties of thoria which will require assessment prior to detailed thorium blanket design are,

1. Irradiation swelling at intermediate to high burnups, Indian Point 1 has produced fuel with burnups as high as 39,000 MWD/MTM;
2. Thermo-physical property variations with changes in the U-233 content of the thoria, again some data from Indian Point 1 and Elk River fuel development programs exist in these areas.

The next factors which should be considered are the design limits related to the spatial and temporal heating rate variation in thorium and uranium radial blankets. In section 6.3.3.6 it was shown that when all the contributions to the total heating rate are taken into account, the thorium radial blanket heating rate is about half of that for a similar uranium radial blanket at beginning-of-life (BOL) conditions. After 600 full power days, however, the heating rates in the two blankets were shown to be nearly identical. A slightly larger radial power gradient was shown to exist in the thorium blanket throughout its life. This factor might have some significance in the design of the core restraint system, but analysis of this question is beyond the scope of

this work, and this point should be evaluated in more detail. The fact that the BOL heating rate in a thorium radial blanket is about half that in a uranium blanket and that the EOL heating rates are very similar implies that the mixed outlet temperature from a thorium blanket assembly would vary more during irradiation than that for a comparable uranium blanket assembly irradiated for the same time. Two factors mitigate against this problem. First, because of the extremely small mixed mean assembly temperature rise expected at BOL, a factor of two difference in the blanket heating rate would result in only a few degrees difference in mixed outlet temperature. Second, because the economic optimum irradiation time of a thorium blanket assembly is shorter than that for a uranium blanket, thorium blanket assemblies will be replaced more frequently, and a corresponding reduction in EOL heating rate (of approximately 10%) could be achieved. The shorter economic optimum irradiation time for a thorium blanket may be a significant advantage. This advantage would arise from the smaller degree of environmental damage which would be suffered by the thorium blanket assembly. In fact, once the engineering limits on maximum environmental damage to radial blanket assemblies have been established, they may require removal of uranium blanket assemblies prior to attainment of their economic optimum. In this event, thorium blanket economic performance would improve relative to that for uranium blankets.

Earlier in this chapter it was shown that, despite its lower density, the thorium axial blanket had fast neutron shielding characteristics which were somewhat superior to those of a uranium axial blanket.

Thus, from the shielding point of view, thorium axial blankets could be substituted for uranium blankets with the possibility of a net gain in core support structure design lifetime.

Finally, consideration should be given to system dynamics related questions. Table 6.16 summarizes differences between the two systems with respect to these effects.

TABLE 6.16 Summary of System Dynamics Differences

System Characteristic	Relative Characteristics, BOL Thorium System/Uranium System
Core fissile loading	1.041
Central core sodium void coefficient	1.028
Delayed neutron fraction	0.981
Mean neutron lifetime	0.889
Isothermal Doppler coefficient	0.910
Doppler power coefficient	0.938
Adiabatic power coefficient	0.958
Control requirements	1.093

As shown in Table 6.16, the thorium blanketed system has a small possible advantage over the uranium blanketed system only in its smaller isothermal Doppler coefficient. This leads to a smaller reactivity swing from cold to hot conditions. In all other comparisons made in Table 6.16, the uranium blanketed system has a small advantage. It should be noted that the difference between the two systems for all characteristics except core fissile loading and control

requirements are within the limits of accuracy with which these values can be calculated.

Two features in Table 6.16 deserve special attention: the core fissile loading and the control requirements. Clearly, if an LMFBR system were designed to accommodate thorium blankets, no difficulties would be encountered in the change over to uranium blankets. Because of the expected market conditions for U-233 and fissile plutonium, this sequence is the most likely to occur. However, if it were desirable to make the change from a uranium to a thorium blanketed system, consideration would have to be given to the adequacy of the control system to accommodate reactivity variations associated with use of the latter system.

One further difference between the thorium and uranium blanketed systems should be mentioned. That is the difference in average core burnup achieved after 600 full power days. It was shown in Chapter 4 (Table 4.12) that the average required core burnup for a thorium blanketed system is larger than that for a uranium blanketed system for the same total system power. For a batch irradiated radial blanket this difference was approximately 1.8%. This difference can also be viewed as a difference in average core power density during the batch irradiation. Because of the difference in blanket albedo between the thorium and uranium blanketed systems, the power distribution in core zone 2 should be less flat with a thorium blanket. Thus the 1.8% difference in average core power density might be compensated for by appropriate control system programming so that the peak power density

in the two systems would be no different. If this were impossible, a 1.8% power penalty would be assigned to the thorium blanket during the change over from a uranium to a thorium blanketed system.

Chapter 7

SUMMARY AND CONCLUSIONS

7.1 INTRODUCTION

The primary function of the radial and axial blankets of Liquid Metal Cooled Fast Breeder Reactors (LMFBR) is to utilize effectively core leakage neutrons for the conversion of fertile material (U-238 or Th-232) into fissile material (Pu-239 or U-233). Most design studies published to date (A6) have considered only U-238 as the blanket fertile material. This study has evaluated the use of thorium for this same application, both from the economic and from the system performance points of view.

The primary reason for considering thorium in LMFBR blanket applications is, as a number of recent studies (D3, K1) have suggested, its high value as a fuel in thermal reactor systems; U-233 is an economically more desirable product than fissile plutonium. Thus, during the early years following commercial introduction of the LMFBR, lower fuel cycle costs should be achievable if plutonium produced in Light Water Reactors (LWR) is used as fuel for LMFBR's, and fast breeder reactor blankets are used to produce the more economically desirable fuel, U-233, through neutron capture in thorium (L2, L8, L9, W1). The reason that an LMFBR system operating completely on the U-233/thorium cycle in both core and blankets has not been given serious consideration in this study is that earlier investigators (A1, H1, L4, L5, O1, S1) have shown that it is inferior to a plutonium fueled system

in fuel cycle cost, achievable core power density, doubling time, and required fissile loading.

Work presented in this summary will include sections discussing:

1. Physics-depletion analyses, in which comparisons will be made between thorium and uranium blanket breeding performance for a number of blanket management schemes. The implications of experimental studies performed using the M.I.T. Blanket Test Facility, Blanket Mockup No. 4 on the analytical work will also be discussed in this section,
2. Economic analyses, in which the economic performance of thorium and uranium blanketed systems will be compared for various blanket management schemes. A model which allows correlation of economic optimum irradiation time and the corresponding fissile enrichment against an economic parameter will also be discussed in this section, and
3. Engineering and physics aspects of uranium and thorium blanketed systems, in which the thermal and physics characteristics of the two systems will be compared with a view to the interchangeability of uranium and thorium blankets in a system originally designed to accommodate only one type of blanket.

Finally, recommendations will be made for additional work needed to complete the proposed implementation of the use of thorium blankets in LMFBR systems.

7.2 PHYSICS-DEPLETION ANALYSIS

7.2.1 Comparison of Blanket Breeding Performance

Studies of the breeding performance of thorium and uranium blanketed systems were carried out using a representative two-zone core, 1000 MW_e LMFBR (B3). A schematic diagram of the reactor is shown in Fig. 7.1. Cross sections for this work were derived from the 26-group ABN-FTR-200 set (N1), self-shielded using the shield-factor method implemented in the code 1DX (H2), and regionwise collapsed to 4 groups using the one-dimensional transport theory code ANISN (E1). The regionwise collapsed 4-group cross section sets were then used with the two-dimensional burnup code 2DB (L10) to evaluate the breeding performance of the systems under consideration. The primary features of the burnup analysis were the following:

1. Batch core and axial blanket burnup for two full power years (~105,000 MWD/MTM) was assumed for all analyses, and
2. Constant core and axial blanket poison concentration at the time-average values expected in these regions was used.

These assumptions have been shown here and elsewhere (H5) to have little impact on blanket economic performance. Consistency of analysis between thorium and uranium blanketed systems has been maintained by assuring that variations in system effective multiplication factor were, as nearly as possible, the same for all cases analyzed.

Consideration has been given in this study to three radial blanket management schemes: batch irradiation, zone scatter management, and in-out shuffle management. Batch irradiation involves, as the

Fig. 7.1 Schematic of Reference Reactor Design, 1000 MW_e LMFBR (B3)

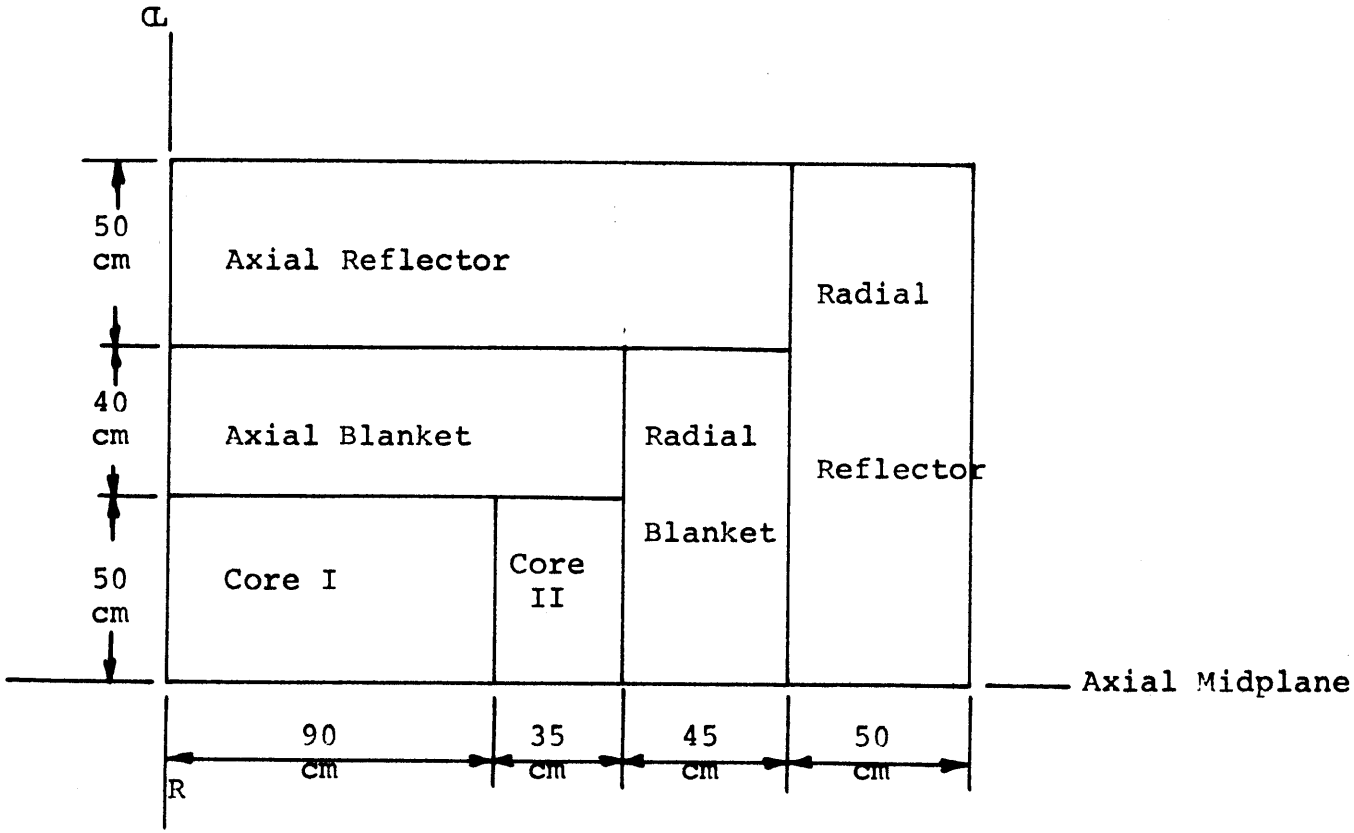

name implies, simply loading, irradiating, and removing all three rows of the radial blanket simultaneously. In zone-scatter management, blanket assemblies in any given row are irradiated to their economic optimum, and then replaced with fresh assemblies. The most complex of the three schemes is in-out shuffle management. In this management technique, irradiated assemblies are removed only from the outermost row – in our case, row 3. When row 3 assemblies are removed, row 2 assemblies are shuffled into row 3 positions, row 1 assemblies replace the old row 2 assemblies, and fresh blanket fuel is loaded into position 1 nearest the core.

Figure 7.2 shows uranium blanket fissile inventories for the batch managed case, while Fig. 7.3 shows the difference between total thorium and uranium blanket fissile product for axial and radial blankets, again for the batch managed case. As shown, more fissile material is produced in the radial blanket than in the axial blanket (as defined in Fig. 7.1). Also, Fig. 7.3 shows that the uranium radial blanket produces significantly (roughly 8%) more fissile material than the corresponding thorium blanket, while the thorium axial blanket produces marginally more fissile material than the uranium axial blanket.

The inventories shown in Figs. 7.2 and 7.3 have been used to evaluate equilibrium cycle breeding ratios, which are 1.19 and 1.21 for thorium and uranium blanketed systems, respectively. These values are in good agreement with those reported by Wolfe et al. (W2) of 1.26 for a 1000 MW_e LMFBR.

Figures 7.4 and 7.5 show that, for a uranium blanketed system,

Fig. 7.2 Fissile Material Inventory in Batch Managed Uranium Radial and Axial Blankets

Fig. 7.3 Difference in Total Fissile Product Between Thorium and Uranium Blankets

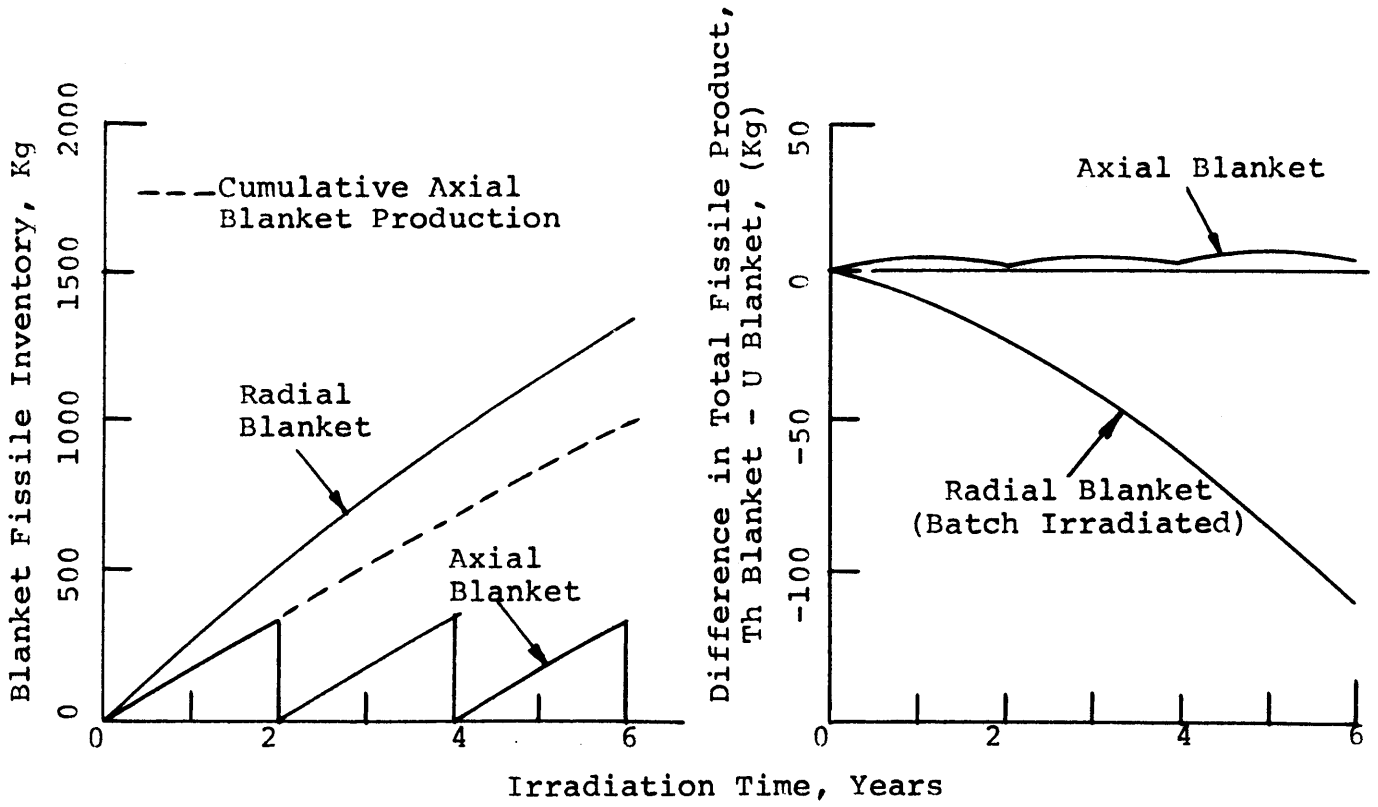

Fig. 7.4 Comparison of Uranium Radial Blanket Fissile Inventories for Various Management Schemes

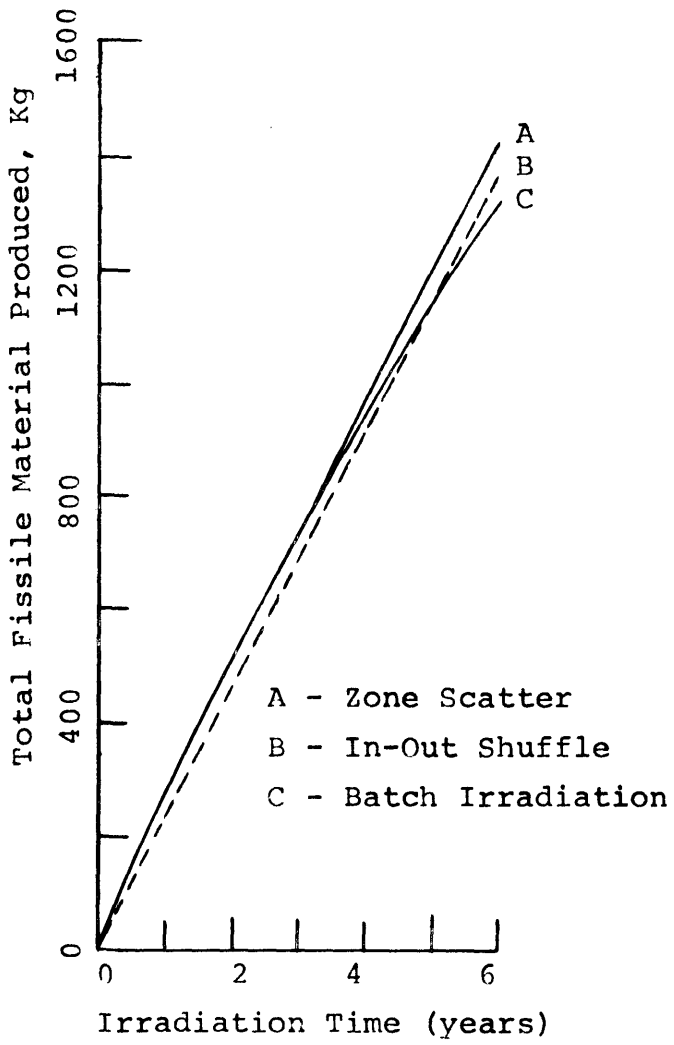

Fig. 7.5 Comparison of Thorium Radial Blanket Fissile Inventories for Batch Management and Zone Scatter Management

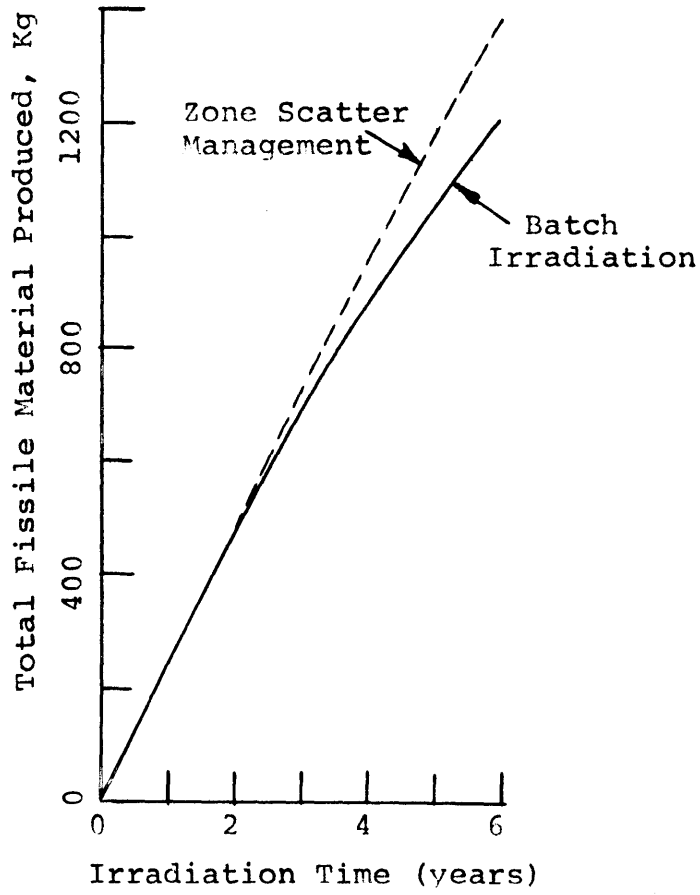

little difference exists between the total amount of fissile material produced in the radial blanket for the three management schemes considered, while, for a thorium radial blanket, the difference between the mass of fissile material produced in a batch irradiated blanket and a zone-scatter managed blanket is nearly twice as large as for a comparable uranium blanketed system. These differences among management schemes for the two types of blankets can be traced to the frequency of replacement of row 1 of the radial blanket (every 3-1/3 years for a uranium blanket and every 2 years for a thorium blanket), which, in turn, is dictated by the time required for the blanket to reach its economic optimum residence time.

In section 7.3, economic comparisons will be presented between batch irradiated thorium and uranium blanketed systems. The feature revealed by Figs. 7.4 and 7.5 which is relevant to this comparison is that consideration of managed rather than batch irradiated radial blankets would lead to improved relative performance for the thorium blanketed system.

7.2.2 Experimental Studies

A series of experiments has been performed which allowed comparison between the experimentally determined capture and fission rates for thorium and uranium foils irradiated in a spectrum typical of an LMFBR demonstration reactor blanket (M.I.T. Blanket Test Facility, Blanket Mockup No. 4) and the corresponding analytical predictions made using the same methods and cross sections as employed in the remainder of this study. Figure 7.6 shows that the comparison

Fig. 7.6 Comparison of Calculated and Experimental Fission Rates for Thorium and Uranium Foil Traverses in BTF 4, Cross Sections from ABBN-FTR-200 Set (N1)

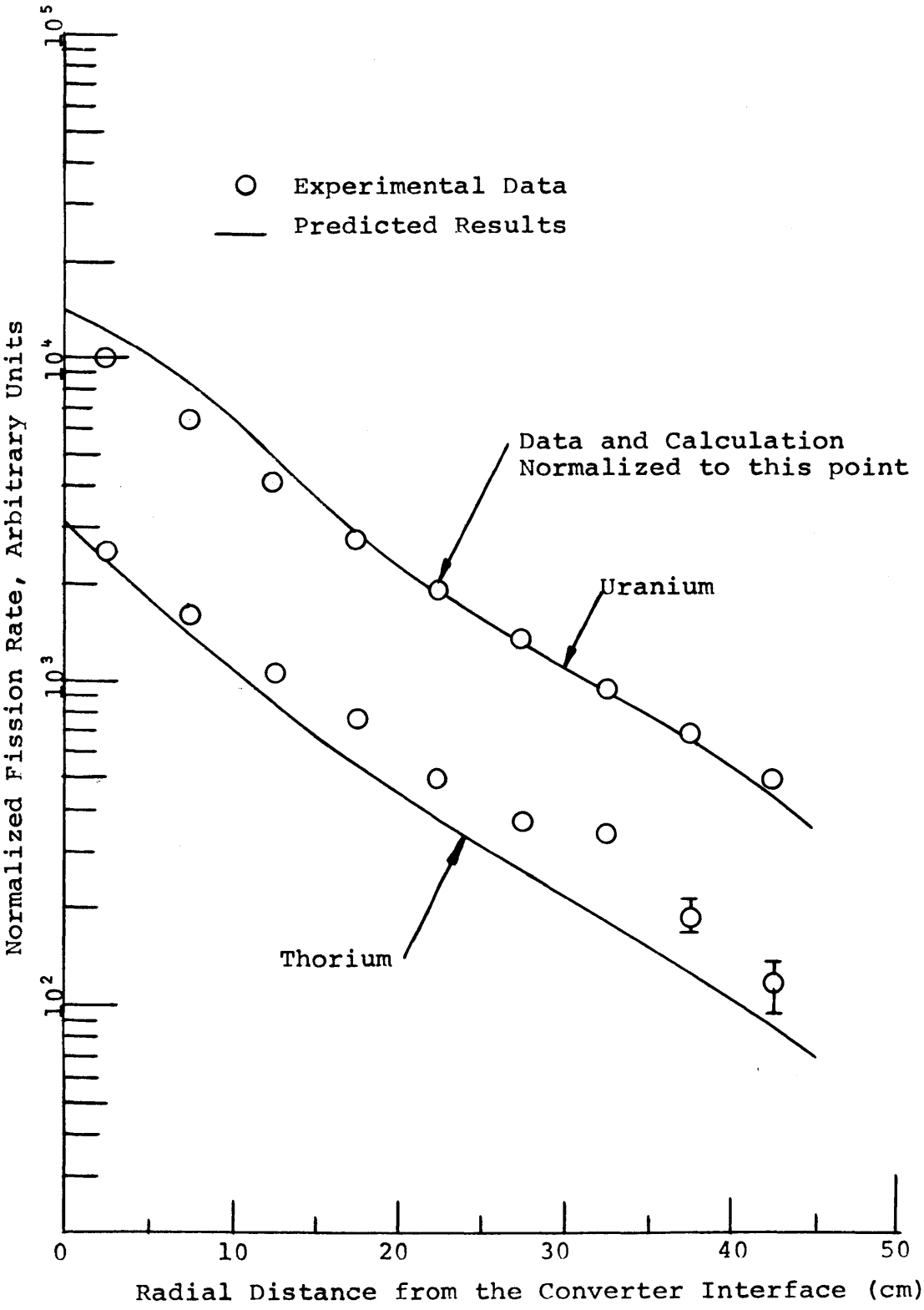

between experimental and analytically determined fission rates for thorium and uranium is reasonably good. A similar comparison, however, shows that significant discrepancy existed between experimental and analytically determined capture rates in thorium and uranium foils. This observed discrepancy has been attributed to errors in the elastic downscatter cross section in the ABN-FTR-200 set arising from the fact that this cross section set was generated using a 1/E weighting spectrum. These errors lead to a softer predicted spectrum than observed, which, as shown in Fig. 7.7, would cause the predicted capture rate in a thorium foil irradiated in a uranium blanket to be higher, relative to the uranium capture rate in the same environment, than observed experimentally. Other investigators (K9) have confirmed that this discrepancy in the elastic downscatter can be corrected by use of a technique involving iterating on the spectrum. In this study the erroneous downscatter cross section was compensated for by expanding the initial 26-group cross section set into 106 groups. Figure 7.8 shows that the agreement between experimental capture rates and those predicted using the 106-group cross section set is much better than when the unmodified 26-group set was used for the prediction. However, the modified analysis has predicted a much steeper slope of the capture rate distribution in uranium foils than was observed experimentally.

A series of diagnostic experiments in which gold and manganese foils were used as secondary standards has suggested that at least part of the discrepancy between the experimental data and the 106-group predictions can be attributed to overestimation of the resonance

Fig. 7.7 Comparison of Differential Capture Rates in Radial Blanket

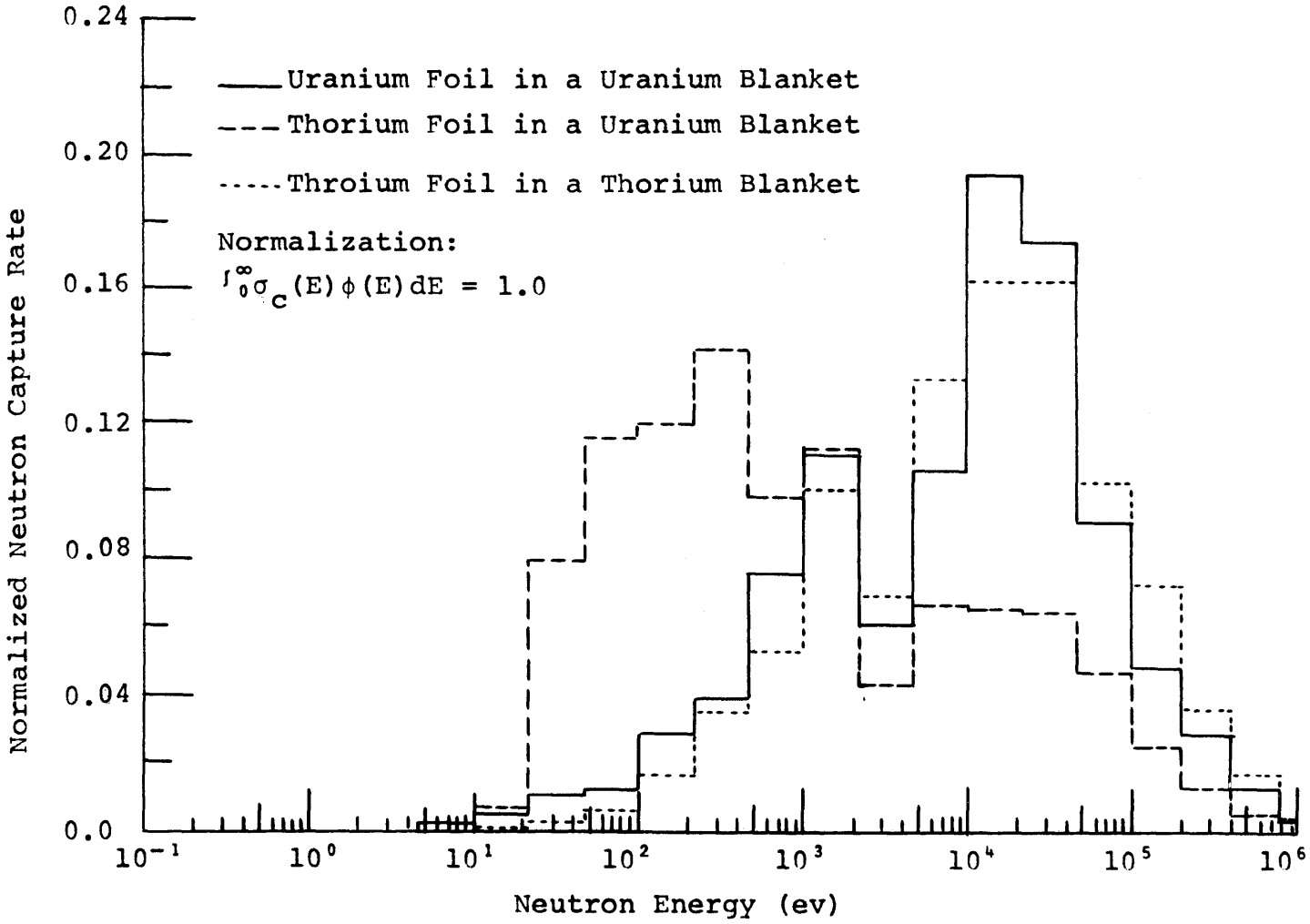

Fig. 7.8 Comparison of Calculated and Experimental Capture Rates in Thorium and Uranium Foils; Predictions were made using the 106 Group Modified ABBN Cross Section Set

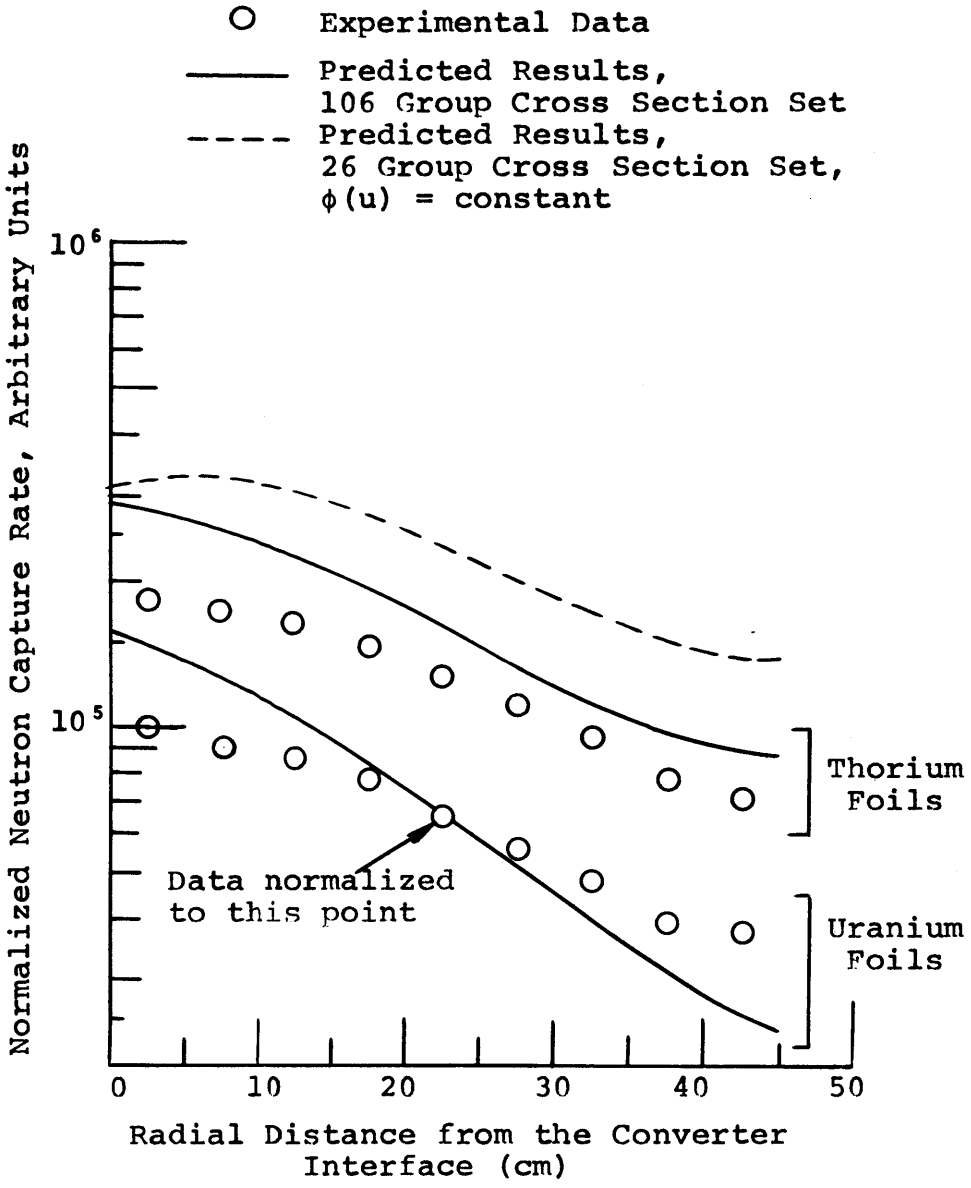

self-shielding used for uranium. It would be expected that at the very least, reduced self-shielding is required near the blanket-reflector interface because uranium blanket pins in that region are not surrounded by an effectively infinite sea of other uranium pins. Additional experiments have shown that, within experimental accuracy, the relative capture rates for thorium and uranium are the same as predicted in a fission spectrum (where uranium resonance self-shielding is not a factor), while the experimentally observed thorium capture rate is approximately 30% low relative to uranium in the mid-blanket spectrum, and approximately 10% high relative to uranium in the softer spectrum of the reflector (again where uranium resonance self-shielding is not a factor).

The impact of these experimental observations on the burnup analyses discussed earlier is difficult to characterize because, as shown in Fig. 7.7, significant differences exist between the energy-dependent capture rate distribution for neutron capture in thorium foils irradiated in a thorium and a uranium blanket. First, consider the effect of the softer predicted blanket spectrum arising from the erroneous downscatter cross section. Analysis of the energy distribution of fertile neutron capture events in thorium and uranium blankets reveals that a higher percentage of thorium capture events occurs in the high energy end of the spectrum. Thus, if the analysis were corrected to compensate for the faulty downscatter, hardening the spectrum, then the breeding performance of the thorium blanketed system would undoubtedly improve relative to the uranium blanketed system. (Calculations have shown that the downscatter correction will

lead to a decrease in the total uranium blanket Pu production by as much as 10%.) The net effect of the reduction in effective resonance self-shielding of the fertile material near the reflector interface is also difficult to characterize. Qualitatively, this effect will be very similar in both thorium and uranium blankets: consequently, little difference in relative blanket performance would be expected. This is a reasonable conclusion in view of the small contribution to total radial blanket fissile production from regions near the reflector. The general topic of resonance self-shielding near interfaces deserves considerably more attention than it has been given here because of the impact that it may have on the blanket power production near the end-of-life.

Finally, although no conclusive experimental evidence exists to indicate that there are large discrepancies between the relative spectrum-averaged self-shielded cross sections of thorium and uranium, it is interesting to note that a 20% decrease in the thorium capture cross section in the unresolved resonance region (~10 to 10^4 eV), which appears to be the most plausible consequence inferable from the data, was shown to produce less than a 1% decrease in the breeding capability of a thorium radial blanket. This is readily understandable, since once neutrons are slowed below about 1 keV, they will be absorbed by fertile material regardless of the degree of self-shielding. The product of the absorption cross section times the flux tends to be fixed by the available source and if the absorption cross section is reduced, the flux will increase to maintain the same product.

7.3 ECONOMIC ANALYSIS

7.3.1 Comparative Blanket Economics

Because the superiority of the thorium blanketed system was expected to lie in its economic performance rather than in its breeding performance, the burnup data discussed in section 7.2.1 were subjected to an economic analysis. For this analysis the cash flow method (CFM) discussed by Brewer (B3) was selected. A major advantage of this method is that it allows separate economic analysis of each reactor region, and definition of the contribution of that region to the total power cost. Figure 7.9 shows the power cost contributions from rows 1, 2, and 3 of a batch irradiated thorium radial blanket developed using the CFM. The parameters used in this analysis, hereafter called the reference economic environment (B3), are presented in Table 7.1. The curves presented in Fig. 7.9 show that all three rows of the radial blanket make a negative contribution to the total fuel cycle cost after some irradiation time. This "break-even irradiation time" is greater for assemblies irradiated at larger distances from the core interface. Figure 7.9 also shows that the assembly power cost contribution is quite insensitive to variations in the end-point of irradiation near the optimum irradiation time. Figures 7.10 and 7.11 show economic comparisons of uranium and thorium blankets for the reference economic environment. Figure 7.10 shows radial blanket performance, while Fig. 7.11 shows axial blanket performance. As expected from the fact that the value of U-233 in the standard economic environment exceeds that of fissile plutonium, the power cost contributions for thorium radial and axial blankets are significantly below those for uranium

Fig. 7.9 Power Cost Contributions from Rows 1, 2, & 3 of a Batch Managed Th-232 Blanketed System for U-233 at 16.7 $/g

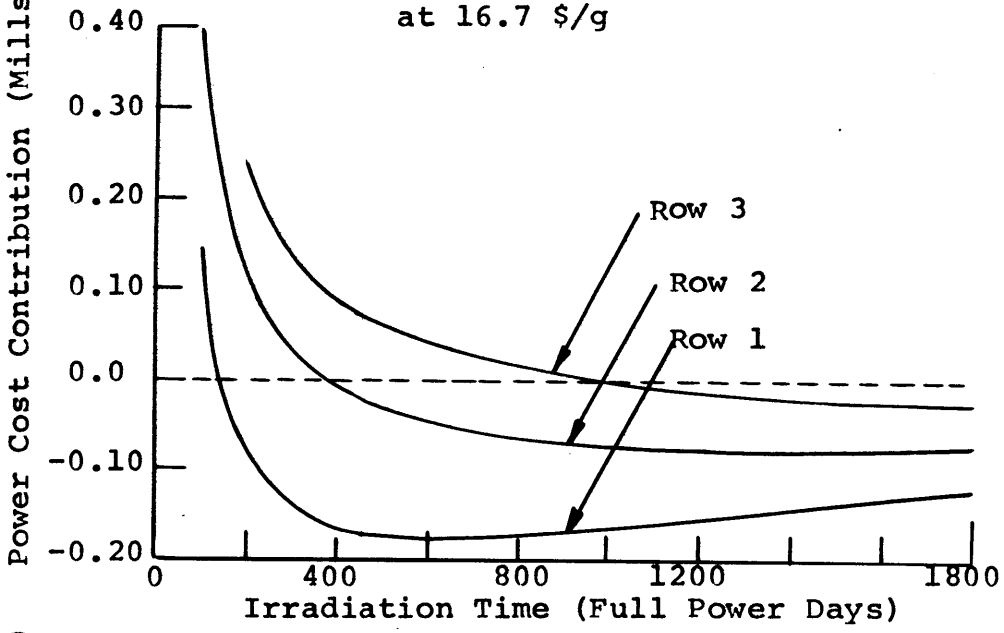

Fig. 7.10 Comparison of the Total Power Cost Contributions from Batch Managed Thorium and Uranium Radial Blankets

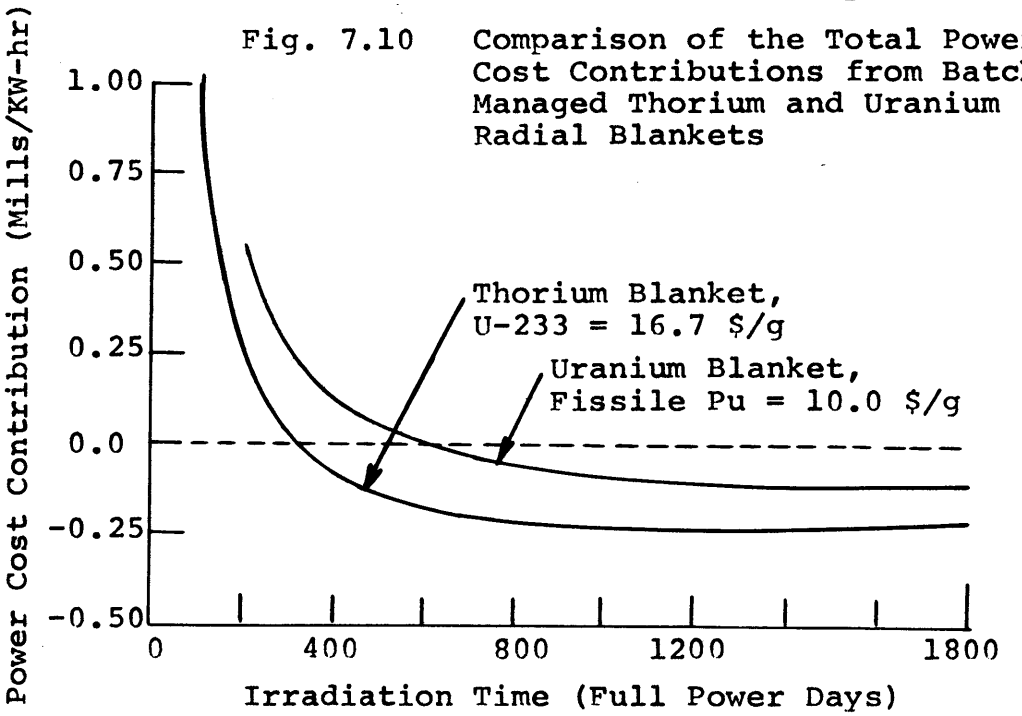

TABLE 7.1 Reference Economic Environment

Unit Fuel Processing Costs, $/kg

Operation	Core	Axial Blanket	Radial Blanket
Fabrication	314	80	69
Reprocessing	50	50	50

Isotope	Isotope Market Value, $/kg
U-238	0
Pu-239	10,000
Pu-240	0
Pu-241	10,000
Pu-242	0
Th-232	0
U-233	16,700

	Value of Parameter	
Financial Paremeter	Private Utility	TVA
Income tax rate, τ	0.5	0.0
Capital structure		
Bond (debt) fraction, f_b	0.5	1.0
Stock (equity) fraction, f_s	0.5	0.0
Rates of return		
Bonds, r_b	0.07	0.075
Stocks, r_s	0.125	0.0
Discount rate, X^*	0.08	0.075

* $X = (1-\tau)r_b f_b + r_s f_s$

Fig. 7.11 Comparison of the Total Power Cost Contribution from Batch Managed Thorium and Uranium Axial Blankets

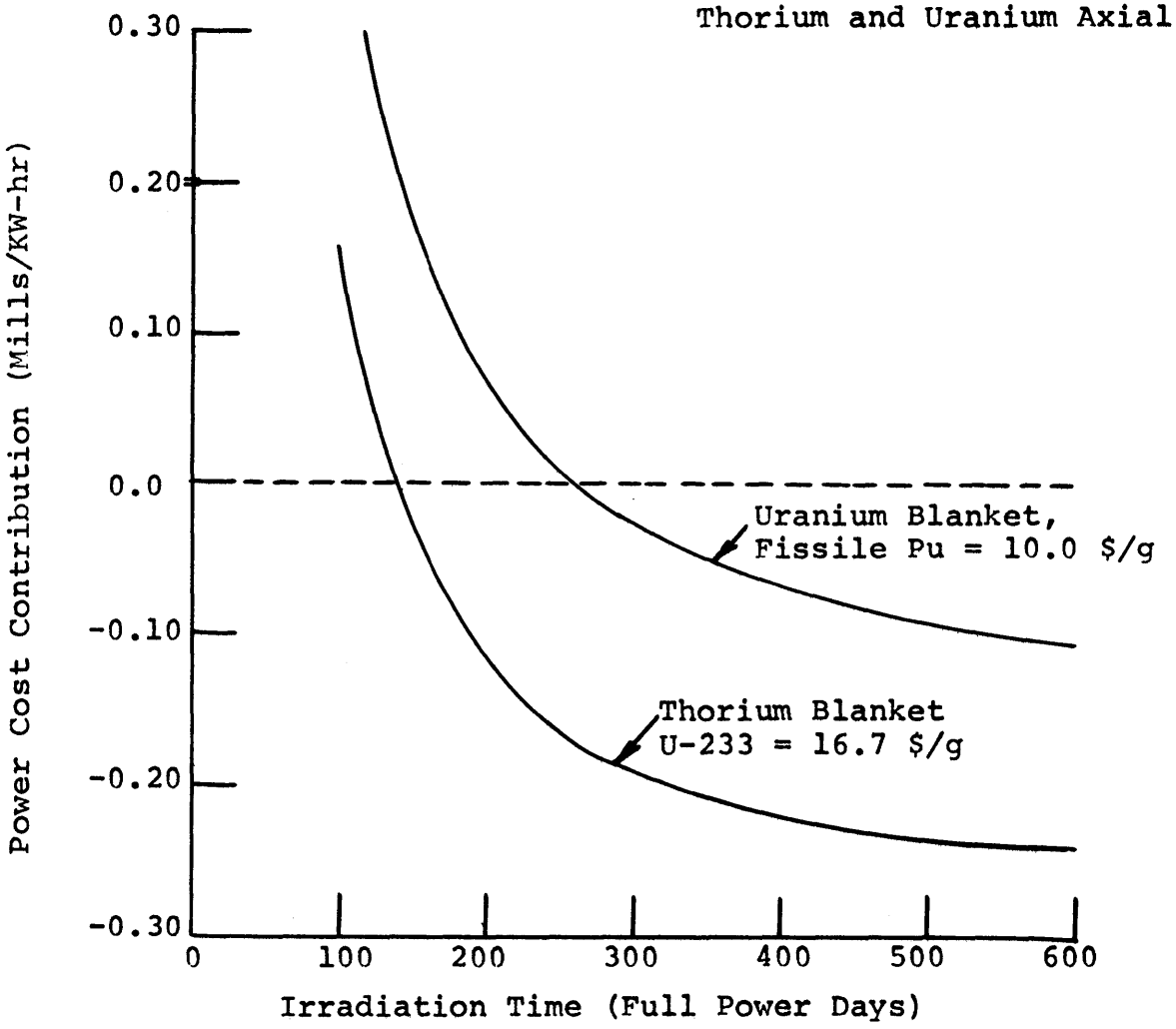

blankets. Also shown is the fact that the differences between optimum radial blanket cost contributions for uranium and thorium blankets is only slightly greater than the corresponding difference for axial blankets at the end of their useful life (assumed to be 600 full power days, the same as for the core).

Data similar to those shown in Figs. 7.9, 7.10, and 7.11 were developed, using the batch irradiation inventory data, for the core, radial blanket, and axial blanket of both the thorium and the uranium blanketed systems. From this information, economic optimum irradiation times and power cost contributions were developed for a wide range of assumed fissile isotope values. The results of these calculations are shown in Fig. 7.12, which shows the fuel cycle contribution to the cost of power as a function of the price of U-233 and fissile plutonium. It is clear that thorium blanketed systems are substantially superior under the current economic environment, which presumes an excess of LWR produced plutonium and a premium market for U-233 in the HTGR or advanced LWR's. Because of the linearity of the relationships presented in Fig. 7.12, a simple empirical expression, Eqs. 7.1 and 7.2, can be developed to summarize these data:

U-238 Blanketed System

$$C = 0.02173\ P^{49} + 0.6203 \qquad (7.1)$$

Th-232 Blanketed System

$$C = 0.07613\ P^{49} - 0.04793\ P^{23} + 0.6648 \qquad (7.2)$$

where C = the total fuel cycle cost (mills/kw-hr),
P^{49} = price of fissile plutonium ($/g), and
P^{23} = price of U-233 ($/g).

Fig. 7.12 Economic Comparison of Thorium and Uranium Blankets for 1000 MWE LMFBR

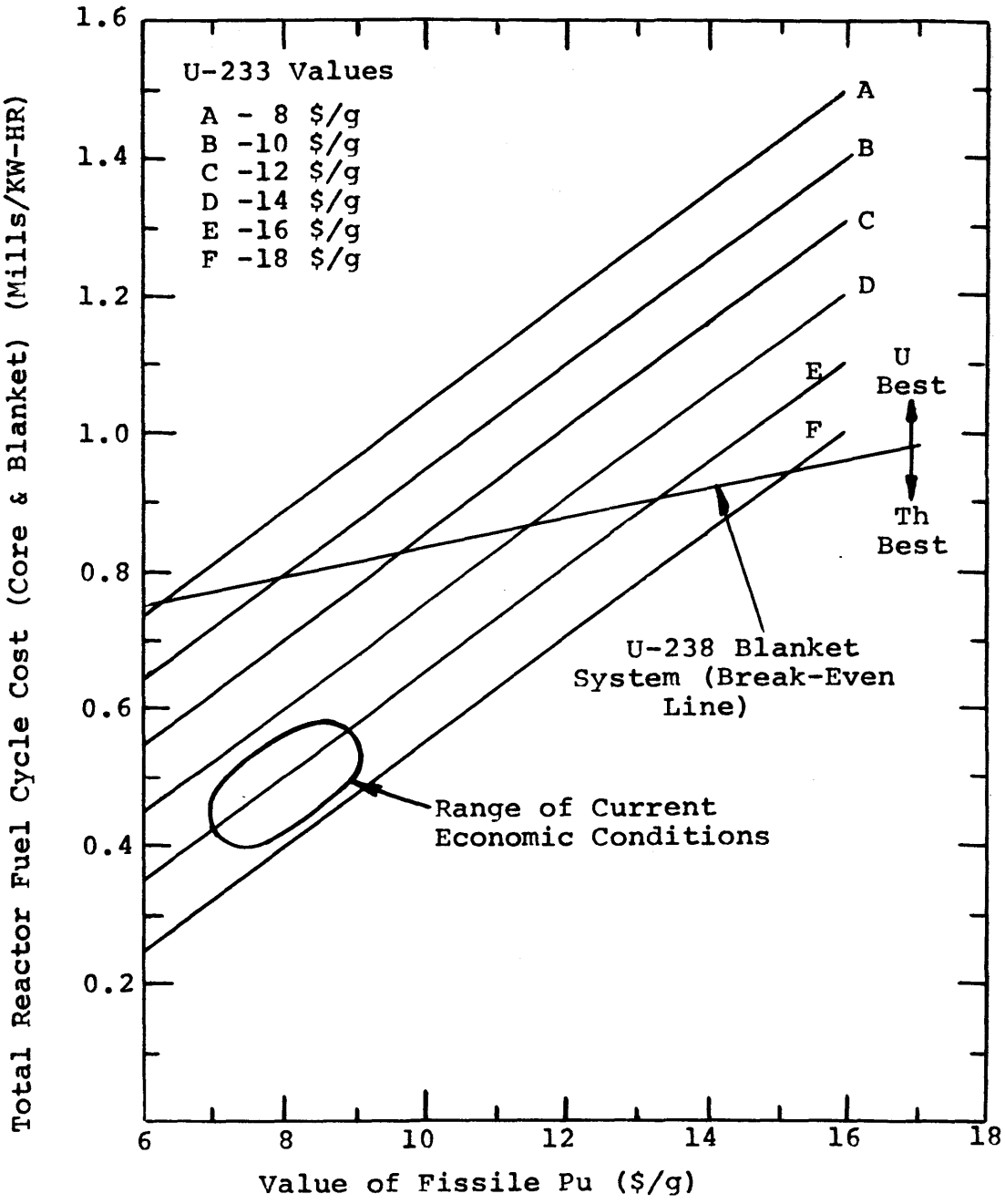

Because of the simplicity of the form of these relationships, future studies comparing the economics of two similar systems can be performed using only a small number of parametric analyses. The data in Fig. 7.12 can be summarized in one other form: the break-even parity ratio, defined as the ratio of the price of U-233 to that of fissile Pu above which a thorium blanketed system is economically superior. Figure 7.13 shows this ratio as a function of the price of fissile Pu. As shown, current estimates of the parity ratio, which range from about 1.5 to about 1.9 (A2, G1, L2), are significantly above the break-even value for any reasonable near term price of fissile Pu.

7.3.2 Comparison of Management Schemes

Fissile inventory data for the three blanket management schemes discussed earlier were analyzed using the CFM to determine their relative economic performance. Because both zone scatter and in-out shuffle management would require more blanket assembly handling than batch, an economic penalty in the form of an availability decrease (1 hour per assembly replacement [V1] , at 100,000 $/day [T2]) was assessed for assembly handling. Table 7.2 shows the final comparison among the different management schemes. As shown, the zone scatter management is economically superior, followed by batch and in-out shuffle management. The differences among the management schemes are, however, relatively small when compared to the penalty associated with a several-day loss in system availability.

This conclusion has been corroborated by one other investigator (B11), and apparently contradicted by a second investigation (M3).

Fig. 7.13 Break-Even Parity Ratio: Ratio of Value of U-233 to that of Fissile Pu versus Value of Fissile Plutonium

Note: Estimated Parity Ratio from Table 5.3, Range: 1.53 to 1.88

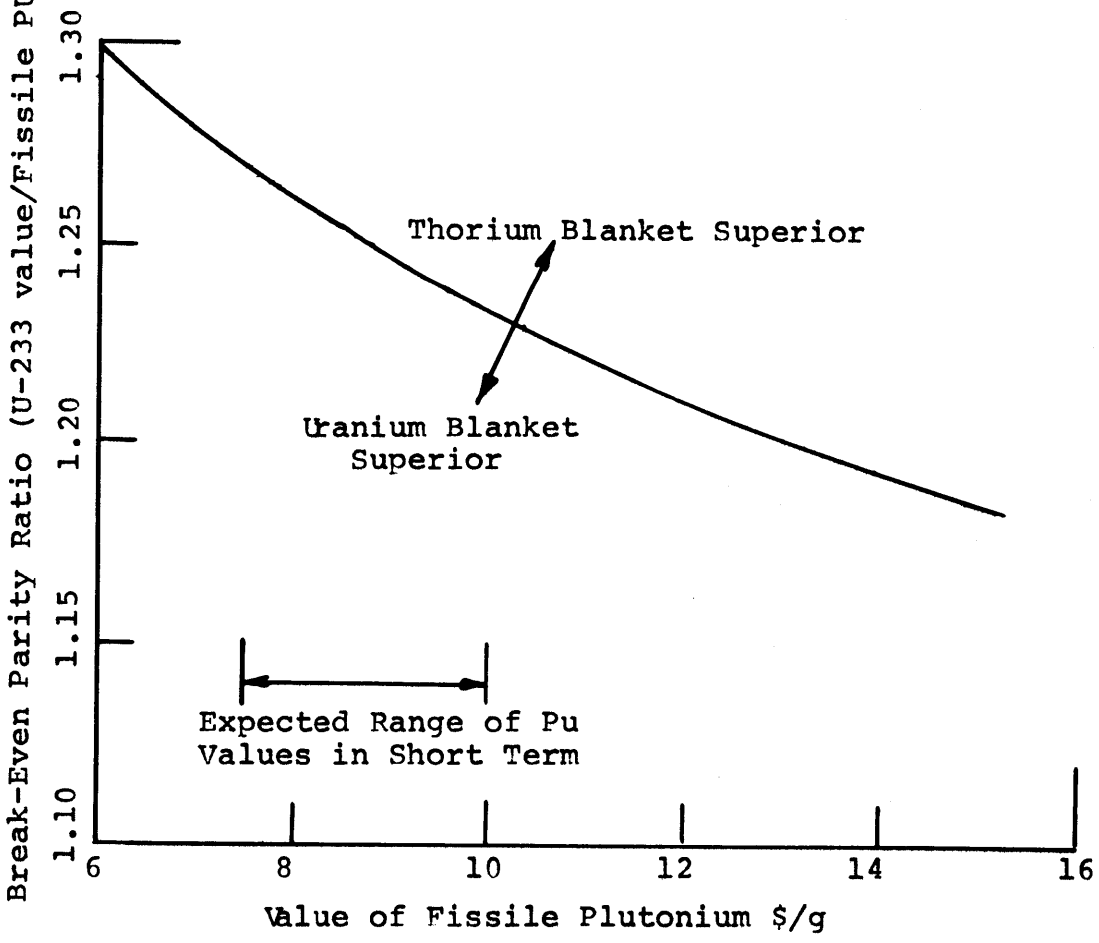

TABLE 7.2 Comparison of Radial Blanket Power Cost Contributions for Various Management Schemes.

Radial Blanket Type	Blanket Management Scheme	Power Cost Contribution (mills/kw-hr)	Economic Penalty for Management Scheme ($/yr)
Uranium	Batch	-0.097	0 (1)
Uranium	Zone scatter	-0.103	-41,000
Uranium	In-out shuffle	-0.089	58,000
Thorium	Batch	-0.205	0 (1)
Thorium	Zone scatter	-0.232	-193,000

(1) Basis: Batch irradiation case.

The discrepancy among these analyses appears to be in the method used to treat carrying charges for fissile material produced in the blanket. In the method used here, only the total irradiation time of a batch of material and the final fissile content are important in determining the carrying charges. It would appear that the contradictory results were derived assuming that carrying charges were in some way related to the time-dependent shape of the fissile inventory history curves for a given subassembly. This apparent disparity in the evaluation of the relative economics of various management schemes requires resolution before the true benefits of blanket management can be assessed.

Finally, it should be noted that engineering lifetime limits for the blanket assemblies, the effect of orificing on outlet temperature variations, and the impact of blanket assembly management either on these limits or on system (e.g., core restraint) design and economics have not been considered in developing the relative economics for the three management schemes. These considerations might easily swing the

scale in favor of in-out shuffle management over the other seemingly more economically attractive schemes. Other engineering considerations such as pellet-clad gap closure following movement of blanket assemblies into regions of higher or lower flux must also be weighed prior to final selection of a blanket management scheme.

7.3.3 Economic Model

In an attempt of develop a generalized approach to correlating variations in the economic environment against corresponding variations in the blanket optimum irradiation time and fissile enrichment at the optimum, an economic parameter was developed by linearizing Brewer's (B3) fuel cycle cost equations and solving the resulting approximate expression for the optimum irradiation time. This approach led to the economic parameter defined below:

$$N_E \equiv \left[\frac{C_1 F_1 (-\Delta T_1) + C_2 F_2 (\Delta T_2)}{C_3 F_3 (\Delta T_3) X} \right] \tag{7.3}$$

where C_1 = fabrication charge, \$/kg heavy metal,

C_2 = reprocessing charge, \$/kg heavy metal,

C_3 = fissile value, \$/kg fissile,

F_1 = the present worth factor in fabrication charges for

ΔT_1 = the time span between fabrication and loading,

F_2 = the present worth factor on reprocessing charges for

ΔT_2 = the time span between discharge and reprocessing,

F_3 = the present worth factor on material credit for

ΔT_3 = the time span between discharge and sale, and

X = the discount factor.

The exact economic model (B3) was next used to develop fuel cycle cost data over a wide range of parameters characterizing the economic environment (see Table 7.3). The results were then correlated as a

TABLE 7.3 Range of Variation of Economic Parameters

Parameter	Units	Range of Variation
Value of fissile Pu	\$/g	6.0 to 16.0
Value of U-233	\$/g	8.0 to 18.0
Fabricating charges	\$/kg	69 to 140
Reprocessing charges	\$/kg	50 to 100
Discount rate (X)	$Years^{-1}$	0.075 to 0.085

function of the economic parameter, N_E. Typical results are shown in Figs. 7.14 and 7.15. As can be seen, linear relationships result on a log-log plot, and these relationships are very similar for both uranium and thorium batch-managed row 1 radial blankets. The dashed lines shown on these figures represent the range of optimum irradiation times and optimum fissile enrichments within which a power cost penalty of only 0.001 mills/kw-hr would be suffered.

Development of these correlations will greatly simplify future economic analyses: one need only compute two cases to completely characterize system economic performance for each system design of interest.

Fig. 7.14 Comparison of Radial Blanket Row 1 Optimum Irradiation Time for Batch Irradiated Thorium and Uranium Blankets

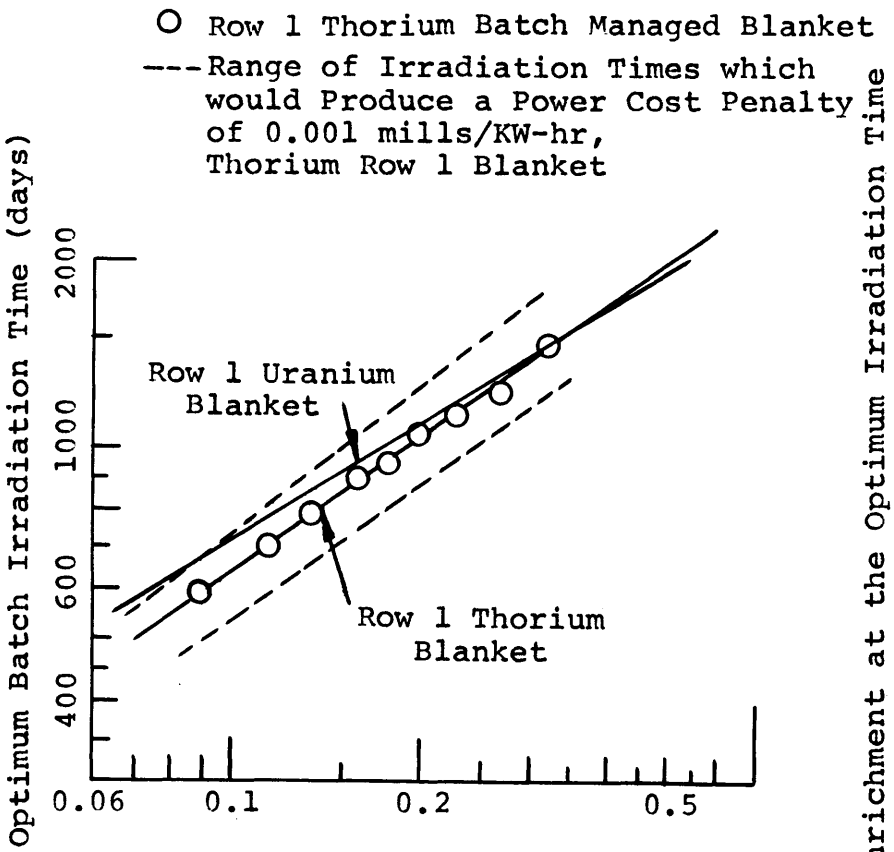

Fig. 7.15 Comparison of Radial Blanket Row 1 Optimum Enrichment for Batch Irradiated Thorium and Uranium Blankets

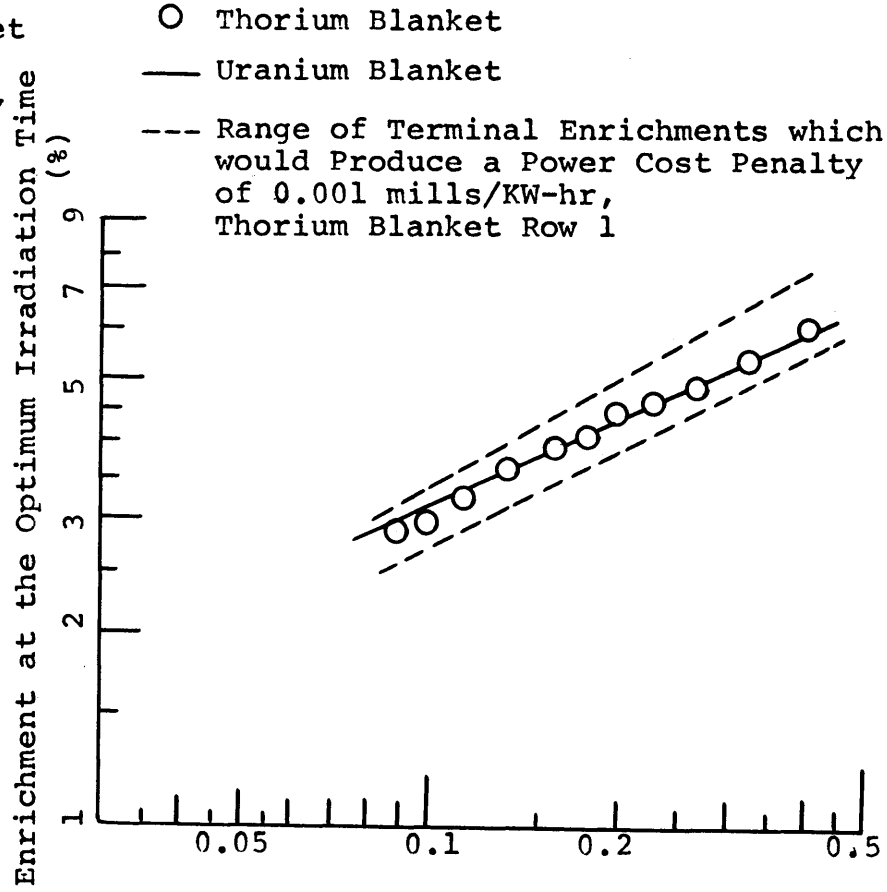

Both "X" Axes have the same label, $N_E = [C_1F_1(-\Delta T_1) + C_2F_2(\Delta T_2)] / C_3F_3(\Delta T_3)$ X

7.3.4 Effect of Uncertainties

The comparative blanket economic analysis presented in section 7.3.1 was for a batch managed blanket in which all the fissile material produced was assumed to be sold under some specified set of market conditions. Several features of that analysis, both methods and assumptions, will have an impact on the conclusions developed earlier. Table 7.4 summarizes these features. As shown, the maximum impact

TABLE 7.4 Effect of Methods and Assumptions on Thorium Blanket Relative Economic Performance.

Parameter	Net Economic Penalty Assessed Against the Thorium Blanketed System (mills/kw-hr)
Axial blanket head-end losses	0.038
Erroneous downscatter cross sections	0.031
Blanket management	-0.021
U-232 mixing in reprocessing	0.006
Erroneous thorium resonance cross sections	0.005
Reprocessing losses (1%)	0.003
Reprocessing delay (per month)	0.002
Core management variations	0.002
Total (excluding reprocessing delays)	0.064

which the parameters in that table might have on the blanket comparative economic analysis is approximately 0.064 mills/kw-hr. This penalty on the thorium blanket economics should be weighed against the earlier anticipated benefit associated with the use of a thorium blanketed system: approximately 0.286 mills/kw-hr. Thus, even when all reasonable sources of error are considered, the thorium blanketed

LMFBR still shows a net economic advantage of approximately 0.222 mills/kw-hr when compared with a uranium blanketed system.

7.4 ENGINEERING AND PHYSICS COMPARISONS

7.4.1 Blanket Heating Characteristics

Among the most troublesome engineering problems related to the design of radial blankets is the variation of the assembly heat generation rate both in space (from the core interface to the reflector interface) and in time (from beginning to end of life). Because of the differences in fertile material fission cross section and in the fissile production rate distribution between thorium and uranium radial blankets, it was necessary to evaluate space and time dependent heating rates. In this analysis the three major mechanisms for energy deposition in the blanket were considered: fission product heating, gamma heating, and neutron heating. Figure 7.16 shows the axial average beginning-of-life (BOL) heating rates in the radial blankets and reflectors of thorium and uranium blanketed systems. As shown, the BOL heating rate in the uranium blanket is nearly twice that in the thorium blanket. Nearly all of the BOL heating in the thorium blanket arises from gamma heating, while approximately half of that in the uranium blanket can be attributed to fission product heating. In neither case does neutron heating contribute significantly to the total heating rate.

Figure 7.17 shows uranium and thorium blanket heating rates in batch irradiated systems after 2 years at power. As shown, the peak heating rate is nearly the same for the two systems, while the heating

Fig. 7.16 Comparison of BOL Heating Rates External to the Core

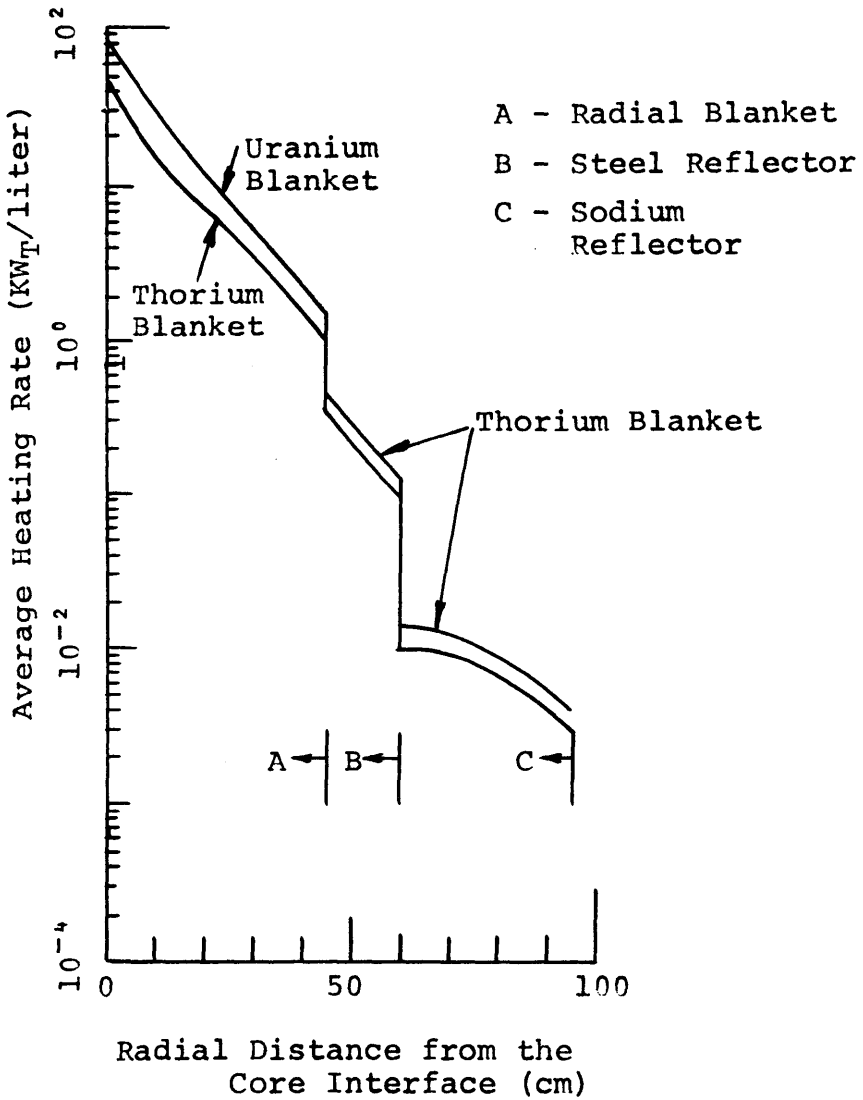

Fig. 7.17 Comparison of Uranium and Thorium Radial Blanket Heating Rates after 600 Days (2 years) of Irradiation

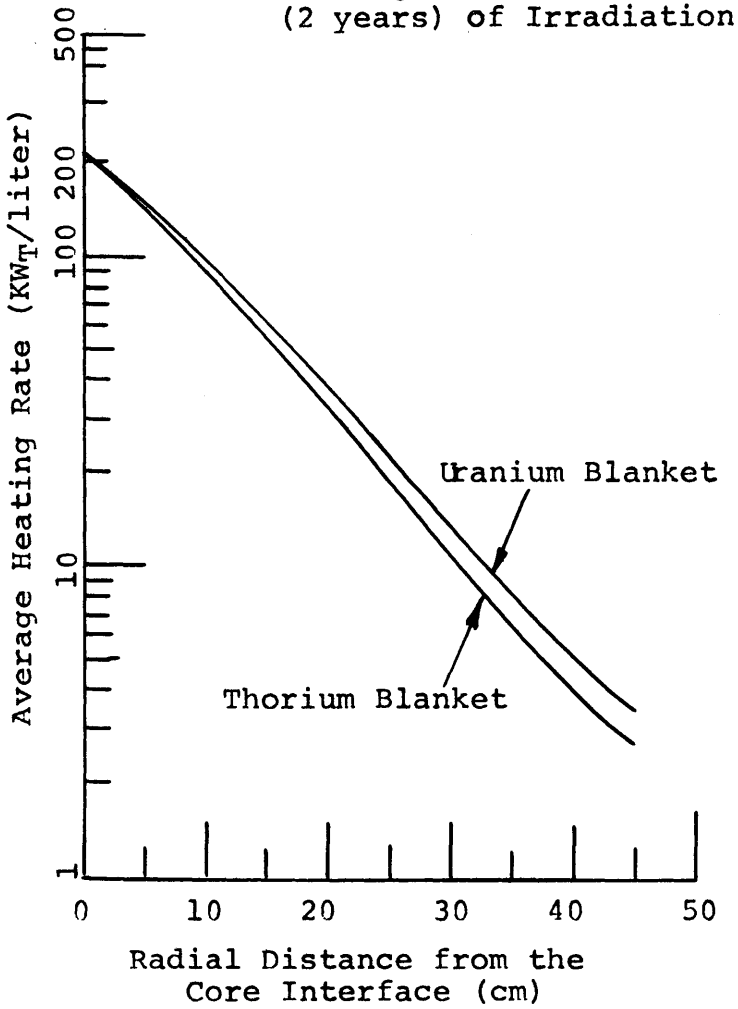

rate gradient in the thorium blanket is somewhat steeper. Cross comparison between Figs. 7.16 and 7.17 shows that during the two-year irradiation, the peak heating rate in the uranium blanket more than doubled while that in the thorium blanket reached over four times its BOL value. Analysis has shown that nearly all of the increase in blanket heating rate can be attributed to fission product heating. The main conclusion to be drawn from Figs. 7.16 and 7.17 is that the use of a thorium radial blanket somewhat complicates design problems (e.g., orificing and core restraint) related to temporal and spatial heating rate variations in the blanket. An evaluation of the effect of blanket management scheme on power variations has shown that

1. In-out shuffle management is superior to the other schemes in minimizing both spatial and temporal power variations in the blanket,
2. Both power gradients and assembly power vs. time variations are somewhat larger in a thorium blanket than in a uranium blanket.

A comparison of the post shutdown heating rates in uranium and thorium blankets has shown that the heating rate immediately after shutdown is about 80% as large in a thorium blanket as in a uranium blanket, and that the required coolant flow rate to remove the fission and capture product decay heat is dictated in both cases by the core cooling requirements.

7.4.2 Reactor Physics Characteristics

Although the differences between the dynamic characteristics of uranium and thorium blanketed systems were not expected to be great, analyses were performed to characterize these differences. Table 7.5

TABLE 7.5 Summary of Differences in System Physics Characteristics Between Uranium and Thorium Blanketed LMFBR's.

System Characteristic	Beginning-of-Life Ratio Thorium System/Uranium System
Core fissile loading	1.040
Control requirements	1.093
Central core sodium void coefficient	1.028
Isothermal Doppler coefficient	0.910
Doppler power coefficient	0.938
Adiabatic power coefficient	0.958
Delayed neutron fraction, β	0.981
Prompt neutron lifetime, Λ	0.889

is a summary of the results of those studies, including the results of static physics calculations. As shown, the two systems have very similar BOL characteristics. Of the tabulated parameters, the only one favorable to the thorium blanketed system is the smaller isothermal Doppler coefficient. However, the differences between the two systems for all the remaining parameters, with the possible exception of core fissile loading and control requirements, are smaller than the expected uncertainties associated with the calculation of the properties (G4, K4). Therefore, these variations are within the limits inside which system designers are reconciled to operate.

Account has been taken in the economic analysis, discussed earlier, of the effect of core fissile loading on system economic performance and of the effect of control poison concentration (homogeneous) on system

breeding performances. No account, however, has been taken of the cost associated with additional control rods on system economics. It is likely that a more detailed analysis of the control requirements, associated with a core management study, would show a smaller difference between the two systems relative to control requirements.

The difference between prompt neutron lifetimes shown in Table 7.5 appears significant until it is noted that a simple analysis to determine the energy release associated with a disassembly transient following a ramp reactivity insertion (K5) shows that the 11% difference in Λ results in only about an 8% difference in energy release. This is certainly small when compared with the uncertainty on the total energy release in a disassembly transient.

7.4.3 Blanket Interchangeability

Since projections of the relative values of U-233 and fissile Pu (D3, K1) show that each fuel will experience a period during which its value will be higher, a discussion of the ease with which a thorium blanket on an LMFBR can be replaced by a uranium blanket is in order. Because the thermophysical properties of thoria (ThO_2) and urania (UO_2) are substantially the same, no major design limits should apply to one system and not to the other. One possible exception to that generalization is that the melting point of thoria is about 1000°F higher than that of urania. Some differences exist between the two systems relative to the power generation shape and history, but the two systems become more similar as burnup proceeds. This can be seen by comparison of Figs. 7.16 and 7.17. One potential problem associated with

a thorium blanket is that its spatial power gradients are somewhat larger (about 30% after two years of exposure), but this problem may be significantly reduced through the use of perforated blanket ducts as suggested by Weiss et al. (W3). One important feature of a thorium blanket which will have the effect of reducing the temporal power variations is that, in the reference economic environment considered here, more frequent replacement or shuffling is dictated by the higher value of the product U-233. This shorter irradiation time will also reduce the extent of environmental damage suffered by the blanket while in the reactor.

A comparison of the static and dynamic physics characteristics for the two systems, Table 7.5, has shown that insignificant differences exist for all properties except, possibly, the required core fissile loading and the control requirements. Preliminary analysis has shown the thorium blanketed system to require approximately 4% more fissile material and approximately 9% more control poison than a comparable uranium blanketed system. In the transition from a uranium to a thorium blanketed system, therefore, a small penalty would be assessed in the form of more frequent refuelings or lower power density prior to the complete replacement of the core, and care must be taken to assure that sufficient control poison is available to accommodate the differences in burnup characteristics. Because of the differences in blanket albedo between thorium and uranium blankets, the power gradient in core zone 2 should be steeper relative to a uranium blanketed system; consequently, the thorium blanketed system power density penalty may be significantly reduced by optimum control rod programming. Other

considerations, such as shielding characteristics, sodium activation contribution, and decay heating properties are sufficiently similar for the two systems that no related problems in the transition from a thorium to a uranium blanket or vice versa should be encountered.

7.5 RECOMMENDATIONS FOR FUTURE WORK

The major areas in which additional work is needed to characterize the performance of LMFBR blankets include development of a consistent cross section set in which elastic downscatter is accommodated correctly, and evaluation of the variation in effective fertile resonance self-shielding near the blanket-reflector interface. Both of these effects must be well characterized before reliable absolute blanket breeding predictions and comparisons can be made. The M.I.T. Blanket Test Facility can be used to evaluate corrective techniques if future data taken in the facility are accompanied by normalization data from simultaneous irradiation in the thermal and fission spectrum facilities. Also, foil spectrometry can be used to generate experimental spectra for comparison with those calculated using cross sections which have been corrected for errors in downscatter and interface region resonance self-shielding.

Several aspects of the work presented here should be assessed in more detail to further define economic differences between uranium and thorium blanketed systems. Included in this category are:

1. The effect of separation between the core and thorium axial blankets using an inert buffer zone (e.g., NiO) on blanket breeding performance, required core fissile loading, and ease of core-blanket separation in head-end processing should be assessed (as shown in Table 7.4, head-end losses during reprocessing constitute the single largest penalty for a thorium system);

2. The impact of various blanket management schemes on system control requirements for thorium and uranium blanketed systems should be considered to better define control requirement differences;

3. A study of the reprocessing problems and related economics associated with thorium blankets should be performed with emphasis on the possible use of HTGR fuel reprocessing facilities in conjunction with LMFBR head-end processing units;

4. A detailed comparison of irradiation experience with thoria and urania would help to define possible differences in blanket lifetime limits between the two types of blankets. It should be noted that irradiation data from the Indian Point 1 reactor, in which thoria-urania pins have acquired peak burnups greater than those expected for thorium blankets, are available to provide quantitative insight into thorium blanket irradiation behavior;

5. Potential difficulties associated with the transition between thorium and uranium blankets, or vice versa, might be uncovered through an approach-to-equilibrium evaluation in which both core and blanket management are considered simultaneously;

6. Thorium blanket economic performance should be evaluated for use in Gas Cooled Fast Reactors, and advanced blanket fuels (e.g., ThC) should be assessed for both GCFR and LMFBR application.

Finally, because of the apparent discrepancy in the techniques used to make economic comparisons among various blanket management alternatives, a review of the methods in current use with the goal of unifying the analytical methods would be useful. Particular emphasis in this study should be given the various methods of handling carrying charges on fissile material produced in the blanket.

In conclusion, it is recommended that thorium blankets (radial at the very least) be strongly considered as the reference design for the LMFBR program in view of their demonstrated near-term economic benefits which amount to on the order of 1.1 million dollars added income per year for a 1000 MW_e system, an amount sufficient to materially enhance the attractiveness of the LMFBR relative to other competing systems. Because thorium blanketed systems appear to require slightly wider system design allowances than uranium blanketed systems, interchangeability between thorium and uranium blankets would be assured.

Appendix A Nomenclature

Chapter 1 Nomenclature

$\bar{\eta}_i$ = the average number of fission neutrons produced per neutron absorbed in isotope i

$\bar{\nu}_i$ = the average number of neutrons produced per fission for isotope i

$\bar{\sigma}_{fi}$ = the average microscopic fission cross section for isotope i, BARNS

$\bar{\sigma}_{ai}$ = the average microscopic absorption cross section for isotope i, BARNS

σ_{ci} = the microscopic capture cross section for isotope i, BARNS

Chapter 2 Nomenclature

k_{eff} = reactor system effective multiplication factor

Δk = change in k_{eff}

r = radial dimension , cm

Z = axial dimension , cm

Abreviations

FP = fission products

ID = inside diameter

OD = outside diameter

Chapter 3 Nomenclature

Normalization of Experimental Data

Thermal Spectrum

C_{TH}^{N} = the count rate of a thorium foil irradiated in the blanket, normalized to uranium foil count rate (CPM/MG),

C_{TH}^{B} = the background, weight, and self-shielding (see Eq. 3.4) corrected count rate of a thorium foil irradiated in the blanket (CPM/MG),

C_{U}^{2CH1} = the background, weight, and cadmium ratio (see Eq. 3.5) corrected count rate for a uranium foil irradiated simultaneously in the thermal spectrum facility (2CH1),

$\sigma_{C,TH}^{2CH1}$ = the thermal spectrum average capture cross section for thorium, BARNS

$\sigma_{C,U}^{2CH1}$ = the thermal spectrum average capture cross section for uranium, BARNS

Thermal Spectrum Epithermal Correction

F_{CD} = the correction factor for epithermal neutrons in the thermal facility (2CH1),

C_{B}^{j} = the background corrected count rate for a bare foil of material j in 2CH1 (CPM/MG),

C_{CD}^{j} = the background corrected count rate for a cadmium covered foil of material j in 2CH1 (CPM/MG).

Fission Spectrum

C_j^{6CH1} = the background and weight corrected count rate for a foil of material j irradiated simultaneously in the fission spectrum facility,

$\bar{\sigma}_f^j$ = the fission spectrum average fission cross section for material j, BARNS

N = the correction factor to account for the fact that the spectrum in 6CH1 is not a pure fission spectrum,

$\sigma_{f,i}^j$ = the fission cross section for material j in energy group i, BARNS

ϕ_i^k = the neutron flux in energy group i for the spectrum appropriate to spectrum, k.

Foil Self Shielding

F_T = the correction factor for foil thickness

C_5^{TH} = the background corrected count rate from the 5 mil thick foil, CPM/MG

C_{10}^{TH} = the background corrected count rate from the 10 mil thick foil, CPM/MG

Physics Parameters

$\phi(E)$ = flux per unit energy Neuts/cm^2-mev-sec

Physics Parameters Cond't

$\phi(U)$ = flux per unit lethargy

$\overline{\sigma}_{ai}$ = the average microscopic absorption cross section for isotope i BARNS

$\overline{\nu_i \sigma_{fi}}$ = the average product of the yield of fission neutrons per fission and the microscopic fission cross section for isotope i BARNS

ξ = average lethargy increase per collision

Modified 106 Group Cross Sections

X = the number of new energy groups created from each old energy group, see Eqs. 3.7 and 3.8

$\sigma_{i \to j}$ = the transfer cross section from group i to group j in the 26 group set BARNS

$\sigma^{*}_{i \to j}$ = the transfer cross section from goup i to group j in the 106 group set BARNS

Chapter 4 Nomenclature

Albedo Calculation

B^2 = the geometric buckling cm^{-2}

R = the radius of the spherical core cm

S = the reflector savings cm

β = the albedo coefficient of the blanket

Chapter 4 Nomenclature

Albedo Calculation Cond't

D_R	=	the diffusion coefficient in the reflector	cm
D_C	=	the diffusion coefficient in the core	cm
L_R	=	the diffusion length in the reflector	cm
a	=	the reflector thickness	cm

Nuclear Parameters

k_{eff}	=	system effective multiplication factor	
N_i	=	number density of material i	atoms/barn-cm
Σ_{ai}	=	macroscopic absorption cross section for isotope i	cm^{-1}
Σ_{fi}	=	macroscopic fission cross section for isotope i	cm^{-1}

Abreviations

MWD/MTM	=	burnup in units of megawatt-days/metric ton of heavy metal
BOL	=	beginning-of-life
EOL	=	end-of-life
SAM	=	semi-analytic-depletion method, described by Brewer (B3)

Chapter 5 Nomenclature

Abreviations

TVA	=	Tennessee Valley Authority
LWR	=	Light Water Reactor
HTGR	=	High Temperature Gas Cooled Reactor
LWBR	=	Light Water Breeder Reactor

Financial Parameters

x	=	discount rate
f_b	=	fraction of capital from bondholders
f_s	=	fraction of capital from stockholders
r_b	=	bondholders' rate of return
r_s	=	stockholders' rate of return
τ	=	income tax rate

Derivation of the Economic Parameter

e	=	fuel cycle cost contribution	
C_1	=	fabrication charge	\$/kg heavy metal
C_2	=	reprocessing charge	\$/kg heavy metal
C_3	=	fissile value	\$/kg fissile
F_1	=	the present worth factor on fabrication charges for	
ΔT_1	=	the times span between fabrication and loading	Years

Derivation of the Economic Parameter Cond't

F_2	=	the present worth factor on reprocessing charges for	
ΔT_2	=	the time span between discharge and reprocessing,	Years
F_3	=	the present worth factor on material credit for	
ΔT_3	=	the time span between discharge and sale	Years
X	=	the discount rate	$Years^{-1}$
E(T)	=	the fissile enrichment at time T	
T	=	the length of the irradiation	Years
T_1	=	the time from fabrication to the midpoint of the irradiation	Years
T_2	=	the time from reprocessing to the midpoint of the irradiation	Years
T_3	=	the time from material credit to the midpoint of the irradiation	Years
R	=	the rate of buildup of fissile inventory in the blanket	$Year^{-1}$
N_E	=	the universal (or optimum) economic parameter	

Correlation of Power Cost Contributions

C	=	the total fuel cycle cost (mills/kw-hr)
P^{49}	=	value of fissile plutonium ($/g)
P^{23}	=	value of U-233 ($/g).

Chapter 6 Nomenclature

Decay Heating Evaluation

λ^{233}	=	decay constant of Pa-233	$time^{-1}$
λ^{239}	=	decay constant of Np-239	$time^{-1}$
$T_{1/2}^{233}$	=	half life of Pa-233	time
$T_{1/2}^{239}$	=	half life of Np-239	time
E^{233}	=	the energy (average β plus γ) from radioactive decay of Pa-233	MEV
E^{239}	=	the energy (average β plus γ) from radioactive decay of Np-239	MEV
$E_D(t)$	=	the decay energy released t seconds after one fission event	MEV/sec
P_D	=	the decay power in MEV/SEC	
R	=	the fission rate in fissions/sec.	
T_o	=	the time at power, sec.	
t	=	the time after shutdown, sec.	

Neutron Heating Derivation

Q'''_{ES_k} = the volumetric heating rate from elastic scatter at a particular mesh interval k

ϕ_{jk} = the neturon flux in the group j at the mesh interval k

N_{ik} = the number density of material i in mesh interval k

σ^e_{ij} = the elastic scatter cross section for the material i in the energy group j

$\Delta\bar{E}_{ij}$ = the average energy lost in an elastic collision between a neutron in the energy group j and the material i

A = the nuclear mass of the nucleus i

E_j = the upper energy bound for group j

E_{j+1} = the lower energy bound for group j.

E_{RI} = the nuclear recoil energy on formation of the compound nucleus

E_{RF} = the nuclear recoil energy on disintegration of the compound nucleus

A = the atomic weight of the initial nucleus

$\bar{E}_i$ = the incident neutron energy

$\bar{E}_j$ = neutron energy on departure from the nucleus

Q'''_{INS_k} = the volumetric heating rate from inelastic scatter at a particular mesh interval, k

σ^{IN}_{ij} = the total inelastic scatter cross section of isotopes i in group j BARNS

$\sigma^{IN}_{i(n\rightarrow j)}$ = the inelastic scatter cross section for material i for events in which the initial neutron is in group n and the final neutron is in group j BARNS

Q'''_{ck} = the heating rate resulting from nuclear recoil following neutron capture

σ^{c}_{ij} = the microscopic capture cross section for material i in energy group j BARNS

$E_{R\gamma}$ = the nuclear recoil energy following gamma emission

E_{γ} = the energy of the emitted gamma

c = the speed of light

A = the atomic mass of the nucleus

M_o = the mass of one nucleon

Reactor Physics and Kinetics Parameters

Isothermal Doppler Coefficient

k = the effective multiplication factor

T = the temperature, degrees Kelvin

V = the volume Liters

Σ_{fi} = the macroscopic fission cross section of nuclide i cm^{-1}

Σ_{ai} = the macroscopic absorption cross section of nuclide i cm^{-1}

ϕ = the neutron flux

Reactor Physics and Kinetics Parameters

Isothermal Doppler Coefficient Cont'd

ϕ^* = the adjoint flux

ν_i = the yield of fission neutrons produced per fission in nuclide i

C = the doppler constant

$\overline{T}$ = the average temperature

T_{LF} = the local fuel temperature at the centerline

T_c = the local coolant temperature

r = the radius of the fuel pin

k_{TH} = the fuel thermal conductivity

q'''_i = the local volumetric heating rate

P_{TOTAL} = the total system power

T_{LOCAL} = the local temperature

$\overline{T}_{LF}$ = the radial average local fuel pin temperature

Adiabatic Power Coefficient

τ = The period of the adiabatic excursion

T_f = the fuel temperature at time t,

T_o = the initial fuel temperature,

q'''_{co} = the initial core averaged volumetric heating rate,

v_f = the volume fraction of the fuel in the core,

Adiabatic Power Coefficient Cond't

ρ = the oxide fuel density,

c_p = the oxide fuel heat capacity

t = the time at which the fuel temperature is being evaluated.

Neutron Lifetime and Delayed Neutron Fraction

Λ	=	prompt neutron lifetime	sec
β_i	=	delayed neutron fraction for isotope i	
v	=	the average neutron velocity	cm/sec
$\int dV$	=	an integral over the system volume	
ν_i	=	the fission neutron yield for isotope i	
Σ_{fi}	=	the macroscopic fission cross section of isotope i	cm^{-1}
ϕ	=	the neutron flux	
ϕ^*	=	the adjoint flux	

Chapter 7 Nomenclature

Financial Parameters

X = discount rate

f_b = fraction of capital from bondholders

f_s = fraction of capital from stockholders

r_b = bondholders' rate of return

r_s = stockholders' rate of return

τ = income tax rate

Blanket Economic Comparison

C = the total fuel cycle cost (mills/kw-hr),

P^{49} = price of fissile plutonium ($/g), and

P^{23} = price of U-233 ($/g).

Universal Economic Parameter Development

C_1 = fabrication charge, $/kg heavy metal,

C_2 = reprocessing charge, $/kg heavy metal,

C_3 = fissile value, $/kg fissile,

F_1 = the present worth factor on fabrication for

ΔT_1 = the time span between fabrication and loading,

F_2 = the present worth factor on reprocessing charges for

ΔT_2 = the time span between discharge and reprocessing,

F_3 = the present worth factor on material credit for

ΔT_3 = the time span between discharge and sale, and

X = the discount factor

N_E = the universal (or optimum) economic parameter

Section B (Appendix) Nomenclature

$\phi(E)$ = neutron flux,

C = a constant, and

E = neutron energy, MEV

Z	=	the atomic number
A	=	the atomic mass
n	=	neutron group,
g	=	gamma group,
σ_i^j	=	cross section for reaction i in isotope j,
02	=	superscript denoting thorium,
28	=	superscript denoting uranium,
f	=	subscript denoting fission, and
c	=	subscript denoting capture.

Appendix B Cross Sections

B.1 Cross Sections for Burnup Analysis

Most of the cross section data for the studies presented here have been obtained from the ABN-FTR-200 (N1) cross section set. However, several isotopes of interest were unavailable in that set, and were gathered from other sources. Table B.1 shows those cross sections together with their sources.

Table B.1 Cross Sections Unavailable in the ABN-FTR-200 Set

Material	Reaction	Source
Th-232	(n,2n)	ENDF/B (D12)
U -233	(n,2n)	ENDF/B (D12)
Pa-233	(n,γ) and (n,f)	R.B. Kidman, ETOX (S6)
Pa-231	(n,γ)	Hinkelmann (H9)
U-234	(n,γ)	Hinkelmann (H9)

The group average (n,2n) cross sections for TH-232 and U-233 were generated from the current version of the Evaluated Nuclear Data File (D12) by collapsing over the same fission spectrum as was used in the development of the ABBN (B1) cross section data:

$$\phi(E) = C \sqrt{E}\ e^{-E/1.29} \qquad (B.1)$$

Where $\phi(E)$ = neutron flux,

C = a constant, and

E = neutron energy, MEV.

The values obtained from this procedure are presented in Table B.2.

Table B.2 Group Average (n,2n) Cross Sections for Th-232 and U-233

Isotope	Lower Group Energy (MEV)	(n,2n) Cross Section, Barns
Th-232	6.5	0.85878
Th-232	4.0	0.0087323
U-233	6.5	0.36153
U-233	4.0	0.024507

The radiative capture and fission cross sections for Pa-233 were generated by R.B. Kidman, using the latest ENDF/B(D12) information, with the code ETOX(S6). These capture and fission cross sections are tabulated in Table B.3.

Finally,radiative capture cross sections for Pa-231 and U-234 were obtained from the evaluated 5-group cross section set presented by Hinkelmann (H9). These cross sections had been collapsed to the same group structure as was used in the burnup analysis reported here (see Table 2.6) except

Table B.3 Capture and Fission Cross Sections for Pa-233

Group	Lower Group Energy (EV)	Capture (Barns)	Fission (Barns)
1	6.5×10^6	0.0108	1.3396
2	4.0×10^6	0.0223	0.8387
3	2.5×10^6	0.0503	0.8316
4	1.4×10^6	0.1286	0.7197
5	0.8×10^6	0.1326	0.0664
6	0.4×10^6	0.2904	0.0008
7	0.2×10^6	0.2736	0.0
8	0.1×10^6	0.3537	0.0
9	46.5×10^3	0.5786	0.0
10	21.5×10^3	1.1958	0.0
11	10.0×10^3	2.2017	0.0
12	4.65×10^3	3.3568	0.0
13	2.15×10^3	4.8702	0.0
14	1.00×10^3	7.2575	0.0
15	465	10.882	0.0
16	215	16.324	0.0
17	100	25.386	0.0
18	46.5	36.228	0.0
19	21.5	43.840	0.0
20	10.0	71.040	0.0
21	4.65	111.87	0.0
22	2.15	117.04	0.0
23	1.00	588.22	0.0
24	0.465	20.736	0.0
25	0.215	14.216	0.0
26	0.0252	23.330	0.0

that an additional thermal group was included. Four group cross sections were developed from these 5 groups by combining the lower two groups using a spectrum appropriate to a thorium radial blanket. These collapsed group 4 cross sections were effectively the same as those in Hinklemann's group 4 because of the insignificantly small thermal flux in the blanket.

B.2 Cross Sections for Gamma Heating Analysis

Gamma heating is a significant contributing mechanism to energy deposition in the radial blanket at the beginning-of-life. To allow an evaluation of this contribution to the total heating rate in the blanket, it was necessary to perform coupled neutron-gamma transport analysis. The results of this analysis have been discussed in Section 6.3.2.4. The purpose of this section is to discuss the cross sections used in that analysis.

For the gamma heating analysis the 40 group (22 neutron groups and 18 gamma groups) coupled neutron-gamma cross section set of Morrison and Straker (M1) was selected. These cross sections were used in conjunction with the transport code ANISN (E1) to evaluate the relative contributions of gamma and fission heating rates in uranium and thorium radial blankets. Because the cross section set selected had no thorium cross sections, they were developed by systematically modifying the U-238 cross sections to account for the differences between these two materials. To provide data for these

modifications, R.B. Kidman of the Hanford Engineering Development Laboratory (HEDL) processed the ENDF/B (D12) neutron cross section data for both U-238 and Th-232 into a 22 group set with the appropriate group structure using the code ETOX (S6). A second input needed to modify the U-238 40 group cross section set to one appropriate for Th-232 were the gamma cross sections for U-238 and Th-232. These cross sections were generated by R.K. Disney of Westinghouse Advanced Reactor Division (ARD) using the GAMLEG-W code (S7).

The original 40 group cross section set for U-238 was processed in the following manner to generate a 40 group coupled cross section set for Th-232. First, using the neutron cross sections provided by Kidman, all Th-232 neutron cross sections were divided by the corresponding cross sections for U-238. These ratios were then used as multiplicative factors on the neutron cross sections in the U-238 40 group set. In this manner consistent infinitely dilute neutron cross sections were generated for thorium for these processes: absorption, fission, total, and down scatter. Second, using the gamma absorption and transport cross sections provided by Disney, thorium gamma group cross sections were divided by the appropriate uranium values. Again these ratios were used as multiplication factors to develop a consistent set of gamma absorption and transport cross sections for thorium. Third, examination of the selfscatter and downscatter gamma cross sections provided by

Disney revealed that in all cases thorium scatter cross sections were a constant multiple (0.9783) of the corresponding cross sections for uranium. This constant factor is not unreasonable when considered in light of the three dominant interaction processes which influence gamma transport (E3, page 712). These processes are shown in Table B.4 along with the expected proportionality.

Table B.4 Mass Attenuation Comparison Between Thorium and Uranium

Mechanism	Proportionality*	Ratio Th/U
Compton Scattering	Z/A	1.004
Photoelectric	$Z^{4.2}/A$	0.946
Pair Production	Z^2/A	0.985

*Z = Atomic number and A = atomic mass

Consequently, the gamma scattering cross sections for U-238 in the 40 group set were simply multiplied by 0.9783 to obtain the corresponding Th-232 cross sections.

The final manipulation which was required to convert the 40 group U-238 set to an approximate cross section set for Th-232 is somewhat more complicated. The original 40 group set accounted for prompt fission gammas, capture gammas, and delayed fission product gammas by the use of a scatter matrix in which scatter occurred between neutron and gamma

groups. The scatter matrix from neutron groups to gamma groups for Th-232 is more difficult to generate using U-238 data. For the purposes of this work the following assumptions were made to allow the conversion process to be carried out:

1. The total energy associated with prompt fission and delayed fission product gammas was taken to be 14 MEV per fission (L1, page 104) for both nuclei.
2. The total gamma energy released following neutron capture was set equal to the binding energy of the captured neutron. This value is 4.784 MEV for U-239 and 4.956 MEV for Th-233 (M4).
3. Because of the complexity of the inelastic scattering process, it was ignored in developing the scaling factors used to convert the U-238 downscatter matrix (from neutron to gamma groups) to one appropriate for Th-232. However, because, as will be shown in Table B.6, neutron inelastic scatter cross sections are very nearly the same for thorium and uranium, and because such a small percentage of the flux in the blanket is in the energy range where inelastic scattering is important, ignoring inelastic scattering in developing the scaling factors is expected to introduce a very small error into the resulting cross section set.

4. The prompt gamma spectrum following fission events was assumed to be the same as that following neutron capture for both Th-232 and U-238.

The last two assumptions might appear somewhat unrealistic upon first consideration and, consequently, will be justified later. If these assumptions are accepted for the time being, one can proceed to process the scatter cross sections (from neutron groups into gamma groups) to obtain corresponding cross sections for thorium. The following manipulation was performed to carry out this conversion:

$$\sigma^{02}_{n\to g} = \sigma^{28}_{n\to g}\left[\frac{\sigma^{28}_f}{\sigma^{28}_a}\right]\left[\frac{14.0}{(14.0)(\sigma^{28}_f/\sigma^{28}_a)+(4.784)(\sigma^{28}_c/\sigma^{28}_a)}\right]$$

$$\times \left[\frac{\sigma^{02}_f}{\sigma^{28}_f}\right]\left[\frac{14.0}{14.0}\right]$$

$$+ \sigma^{28}_{n\to g}\left[\frac{\sigma^{28}_c}{\sigma^{28}_a}\right]\left[\frac{4.784}{(14.0)(\sigma^{28}_f/\sigma^{28}_a)+(4.784)(\sigma^{28}_c/\sigma^{28}_a)}\right]$$

$$\times \left[\frac{\sigma^{02}_c}{\sigma^{28}_c}\right]\left[\frac{4.956}{4.784}\right] \qquad \text{(B.2)}$$

Where n = neutron group,

g = gamma group,

σ^j_i = cross section for reaction i in isotope j,

02 = superscript denoting thorium,

28 = superscript denoting uranium,

f = subscript denoting fission, and

c = subscript denoting capture.

As shown from this formulation, the only energy regions in which the identity of the fission gamma spectrum to the capture gamma spectrum is important are those in which neither fission nor capture events dominate.

Table B.5 shows selected neutron cross sections from the 22 group set supplied by Kidman. As shown, fission events clearly dominate in energy groups 1 through 10 for U-238 and in groups 1 through 6 for Th-232, while capture events clearly dominate in energy groups 12 through 22 for both U-238 and Th-232. Consequently, the only regions in which assumption 4 is questionable is in the energy range from about 2.0 to about 4.0 MEV (groups 7-11). Fortunatly, this energy range contains only a small fraction of the total neutron flux in the blanket, particularly at deep penetrations where gamma heating rates in thorium are of interest. Table B.6 compares the inelastic scattering cross sections for thorium and uranium. As shown, at all energies above about 2.35 MEV, thorium inelastic scatter cross sections are slightly larger than those for uranium. At neutron energies below 2.35 MEV U-238 inelastic scatter is somewhat larger. One consequence of these differences has been discussed in the section on shielding characteristics (section 6.2). The feature of

Table B.5 Selected Neutron Cross Sections from Kidman's 22 Group Set

Group	Emax(EV)	σ_f(BARNS)		σ_c(BARNS)	
		U-238	Th-232	U-238	Th-232
1	15.0×10^6	1.0815	0.3308	0.0	0.0057
2	12.2×10^6	0.9818	0.2842	0.0042	0.0071
3	10.0×10^6	0.9914	0.3036	0.0051	0.0089
4	8.18×10^6	0.9041	0.3122	0.0065	0.0116
5	6.36×10^6	0.5773	0.1464	0.0086	0.0159
6	4.96×10^6	0.5380	0.1443	0.0118	0.0212
7	4.06×10^6	0.5366	0.1370	0.0182	0.0297
8	3.01×10^6	0.5495	0.1179	0.0287	0.0419
9	2.46×10^6	0.5645	0.1125	0.0363	0.0497
10	2.35×10^6	0.5521	0.1095	0.0466	0.0616
11	1.83×10^6	0.2227	0.0506	0.0866	0.1022
12	1.11×10^6	0.0069	0.0	0.1293	0.1675
13	5.50×10^5	0.0001	0.0	0.1843	0.2373
14	1.11×10^5	0.0	0.0	0.7180	0.7074
15	3.35×10^3	0.0	0.0	2.2798	2.2987
16	5.83×10^2	0.0	0.0	11.5800	10.6271
17	1.01×10^2	0.0	0.0	45.0607	14.3524
18	29.0	0.0	0.0	62.8749	40.8007
19	10.7	0.0	0.0	104.9637	0.1788
20	3.06	0.0	0.0	0.50	0.5089
21	1.12	0.0	0.0	0.6025	1.1551
22	0.414	0.0	0.0	1.4879	3.8839

Table B.5 Selected Neutron Cross Sections from Kidman's 22 Group Set Cond't

Group	σ_c/σ_f U-238	σ_c/σ_f Th-232	Fission Neutron Spectrum
1	0.0	0.0172	0.0001568
2	0.0043	0.0250	0.0008932
3	0.0051	0.0293	0.00348
4	0.0072	0.0372	0.01392
5	0.0149	0.1086	0.03457
6	0.0219	0.1469	0.03507
7	0.0339	0.2168	0.1072
8	0.0522	0.3554	0.08898
9	0.0643	0.4418	0.02323
10	0.0844	0.5626	0.1203
11	0.3889	2.0198	0.2181
12	18.739	—	0.1983
13	1843.0	—	0.1403
14	—	—	0.0155
15	—	—	0.0
16	—	—	0.0
17	—	—	0.0
18	—	—	0.0
19	—	—	0.0
20	—	—	0.0
21	—	—	0.0
22	—	—	0.0

Table B.6 Comparison of Neutron Inelastic Scatter Cross Sections for Thorium and Uranium

Group	Emax(EV)	Inelastic Scatter Cross Section U-238	Th-232
1	15.0×10^6	1.439	2.173
2	12.2	1.896	2.528
3	10.0	1.967	2.528
4	8.18	2.134	2.555
5	6.36	2.528	2.790
6	4.96	2.611	2.828
7	4.06	2.636	2.822
8	3.01	2.670	2.772
9	2.46	2.701	2.723
10	2.35	2.754	2.632
11	1.83	2.866	2.365
12	1.11	2.051	1.921
13	5.50×10^5	1.173	1.083
14	1.11×10^5	0.062	0.073
15	3.35×10^3	0.0	0.0
16	5.83×10^2	0.0	0.0
17	1.01×10^2	0.0	0.0
18	29.0	0.0	0.0
19	10.7	0.0	0.0
20	3.06	0.0	0.0
21	1.12	0.0	0.0
22	0.414	0.0	0.0

Table B.6 to be noted here is that, in the energy range where most of the blanket neutron flux is concentrated (E < 0.55 MEV), inelastic scattering is insignificant. Therefore, ignoring inelastic scattering in the development of the scaling factors to convert U-238 scatter cross sections (from neutron to gamma groups) to appropriate Th-232 values, which is nearly equivalent to assuming that the two materials have the same inelastic cross section, will have a small effect on the magnitude of the resulting thorium cross sections.

Because the capture cross sections for neither thorium nor uranium are corrected for resonance self-shielding effects, the gamma heating rates predicted near the core interface are expected to be somewhat high, while those predicted near the reflector interface are expected to be somewhat low. This effect can be seen in the predicted capture rate distributions (using shielded and unshielded cross section sets) presented by Lenng (L 11, Fig. 4.8).

Table B.7 presents the P_0 cross sections for the 40 group coupled neutron-gamma set developed for thorium using the methods described earlier. The cross sections are tabulated in standard ANISN (E1) input format as shown in Table B.8. If future gamma heating analyses are to be performed for thorium blankets, use might be made of a code, presently under development at ORNL, which allows routine generation of coupled neutron-gamma cross section sets from information available in the ENDF/B libraries. Further

Table B.7

Thorium P_o Cross Sections for Coupled Neutron-Gamma Analysis, 40 Groups

Position	Group 1	Group 2	Group 3	Group 4
1	3.183E-01	2.796E-01	3.058E-01	3.104E-01
2	1.231E+00	9.705E-01	9.656E-01	8.859E-01
3	5.366E+00	5.596E+00	5.767E+00	6.280E+00
4	2.777E+00	2.550E+00	2.789E+00	3.369E+00
5	0.0	2.138E-02	2.183E-02	2.664E-02
6	0.0	0.0	0.0	1.343E-04
7	0.0	0.0	0.0	2.623E-03
8	0.0	0.0	0.0	0.0
9	0.0	0.0	0.0	0.0
10	0.0	0.0	0.0	0.0
11	0.0	0.0	0.0	0.0
12	0.0	0.0	0.0	0.0
13	0.0	0.0	0.0	0.0
14	0.0	0.0	0.0	0.0
15	0.0	0.0	0.0	0.0
16	0.0	0.0	0.0	0.0
17	0.0	0.0	0.0	0.0
18	0.0	0.0	0.0	0.0
19	0.0	0.0	0.0	0.0
20	0.0	0.0	0.0	0.0
21	0.0	0.0	0.0	0.0
22	0.0	0.0	0.0	0.0
23	0.0	0.0	0.0	0.0
24	0.0	0.0	0.0	0.0
25	0.0	0.0	0.0	0.0
26	0.0	0.0	0.0	0.0
27	0.0	0.0	0.0	0.0
28	0.0	0.0	0.0	0.0
29	0.0	0.0	0.0	0.0
30	0.0	0.0	0.0	0.0
31	0.0	0.0	0.0	0.0
32	0.0	0.0	0.0	0.0
33	0.0	0.0	0.0	0.0
34	0.0	0.0	0.0	0.0
35	0.0	0.0	0.0	0.0
36	0.0	0.0	0.0	0.0
37	0.0	0.0	0.0	0.0
38	0.0	0.0	0.0	0.0
39	0.0	0.0	0.0	0.0
40	0.0	0.0	0.0	0.0
41	0.0	0.0	0.0	0.0
42	0.0	0.0	0.0	0.0
43	0.0	0.0	0.0	0.0

Table B.7 continued

Position	Group 5	Group 6	Group 7	Group 8
1	1.571E-01	1.594E-01	1.594E-01	1.508E-01
2	3.866E-01	3.548E-01	3.135E-01	2.531E-01
3	7.094E+00	7.720E+00	7.786E+00	7.242E+00
4	4.369E+00	5.243E+00	5.447E+00	4.899E+00
5	3.648E-02	5.060E-02	8.838E-02	1.504E-01
6	9.042E-04	6.233E-03	3.547E-02	4.819E-02
7	1.502E-03	3.988E-03	3.872E-02	6.605E-02
8	1.898E-02	8.627E-03	2.543E-02	6.742E-02
9	0.0	4.710E-02	5.591E-02	4.065E-02
10	0.0	0.0	1.788E-01	1.005E-01
11	0.0	0.0	0.0	2.205E-01
12	0.0	0.0	0.0	0.0
13	0.0	0.0	0.0	0.0
14	0.0	0.0	0.0	0.0
15	0.0	0.0	0.0	0.0
16	0.0	0.0	0.0	0.0
17	0.0	0.0	0.0	0.0
18	0.0	0.0	0.0	0.0
19	0.0	0.0	0.0	0.0
20	0.0	0.0	0.0	0.0
21	0.0	0.0	0.0	0.0
22	0.0	0.0	0.0	0.0
23	0.0	0.0	0.0	0.0
24	0.0	0.0	0.0	0.0
25	0.0	0.0	0.0	0.0
26	0.0	0.0	0.0	0.0
27	0.0	0.0	0.0	0.0
28	0.0	0.0	0.0	0.0
29	0.0	0.0	0.0	0.0
30	0.0	0.0	0.0	0.0
31	0.0	0.0	0.0	0.0
32	0.0	0.0	0.0	0.0
33	0.0	0.0	0.0	0.0
34	0.0	0.0	0.0	0.0
35	0.0	0.0	0.0	0.0
36	0.0	0.0	0.0	0.0
37	0.0	0.0	0.0	0.0
38	0.0	0.0	0.0	0.0
39	0.0	0.0	0.0	0.0
40	0.0	0.0	0.0	0.0
41	0.0	0.0	0.0	0.0
42	0.0	0.0	0.0	0.0
43	0.0	0.0	0.0	0.0

Table B.7 continued

Position	Group 9	Group 10	Group 11	Group 12
1	1.553E-01	1.653E-01	1.565E-01	1.870E-01
2	2.402E-01	2.302E-01	1.057E-01	0.0
3	6.932E+00	6.667E+00	6.440E+00	6.886E+00
4	4.148E+00	4.776E+00	5.278E+00	6.082E+00
5	1.215E-01	5.428E-01	8.448E-01	1.081E+00
6	2.589E-02	1.291E-01	6.688E-01	9.115E-01
7	1.811E-02	1.812E-01	5.376E-01	6.674E-01
8	2.356E-02	1.496E-01	4.633E-01	8.026E-01
9	2.357E-02	1.820E-01	5.852E-01	9.447E-01
10	1.344E-02	1.757E-01	6.316E-01	1.023E+00
11	3.556E-02	1.027E-01	5.369E-01	9.878E-01
12	6.642E-02	2.747E-01	4.905E-01	8.264E-01
13	0.0	4.233E-01	9.776E-01	1.341E+00
14	0.0	0.0	1.039E+00	1.612E+00
15	0.0	0.0	0.0	8.679E-01
16	0.0	0.0	0.0	0.0
17	0.0	0.0	0.0	0.0
18	0.0	0.0	0.0	0.0
19	0.0	0.0	0.0	0.0
20	0.0	0.0	0.0	0.0
21	0.0	0.0	0.0	0.0
22	0.0	0.0	0.0	0.0
23	0.0	0.0	0.0	0.0
24	0.0	0.0	0.0	0.0
25	0.0	0.0	0.0	0.0
26	0.0	0.0	0.0	0.0
27	0.0	0.0	0.0	0.0
28	0.0	0.0	0.0	0.0
29	0.0	0.0	0.0	0.0
30	0.0	0.0	0.0	0.0
31	0.0	0.0	0.0	0.0
32	0.0	0.0	0.0	0.0
33	0.0	0.0	0.0	0.0
34	0.0	0.0	0.0	0.0
35	0.0	0.0	0.0	0.0
36	0.0	0.0	0.0	0.0
37	0.0	0.0	0.0	0.0
38	0.0	0.0	0.0	0.0
39	0.0	0.0	0.0	0.0
40	0.0	0.0	0.0	0.0
41	0.0	0.0	0.0	0.0
42	0.0	0.0	0.0	0.0
43	0.0	0.0	0.0	0.0

Table B.7 continued

Position	Group 13	Group 14	Group 15	Group 16
1	1.922E-01	5.545E-01	2.056E+00	8.396E+00
2	0.0	0.0	0.0	0.0
3	9.534E+00	1.242E+01	1.507E+01	2.124E+01
4	9.147E+00	1.183E+01	1.301E+01	1.282E+01
5	5.680E-01	1.794E-01	2.185E-02	3.528E-02
6	5.721E-01	4.094E-02	0.0	0.0
7	5.400E-01	2.904E-02	0.0	0.0
8	9.005E-01	1.559E-01	0.0	0.0
9	9.468E-01	9.196E-02	9.579E-05	0.0
10	9.554E-01	9.063E-02	1.277E-04	0.0
11	9.185E-01	8.348E-02	1.222E-04	0.0
12	8.145E-01	7.474E-02	9.718E-05	0.0
13	1.140E+00	6.295E-02	7.307E-05	0.0
14	2.018E+00	2.074E-01	7.202E-05	0.0
15	1.053E+00	9.653E-02	1.572E-04	5.204E-07
16	6.784E-01	8.380E-02	9.841E-05	2.247E-06
17	0.0	5.097E-02	8.147E-05	0.0
18	0.0	0.0	4.852E-05	0.0
19	0.0	0.0	0.0	0.0
20	0.0	0.0	0.0	0.0
21	0.0	0.0	0.0	0.0
22	0.0	0.0	0.0	0.0
23	0.0	0.0	0.0	0.0
24	0.0	0.0	0.0	0.0
25	0.0	0.0	0.0	0.0
26	0.0	0.0	0.0	0.0
27	0.0	0.0	0.0	0.0
28	0.0	0.0	0.0	0.0
29	0.0	0.0	0.0	0.0
30	0.0	0.0	0.0	0.0
31	0.0	0.0	0.0	0.0
32	0.0	0.0	0.0	0.0
33	0.0	0.0	0.0	0.0
34	0.0	0.0	0.0	0.0
35	0.0	0.0	0.0	0.0
36	0.0	0.0	0.0	0.0
37	0.0	0.0	0.0	0.0
38	0.0	0.0	0.0	0.0
39	0.0	0.0	0.0	0.0
40	0.0	0.0	0.0	0.0
41	0.0	0.0	0.0	0.0
42	0.0	0.0	0.0	0.0
43	0.0	0.0	0.0	0.0

Table B.7 continued

Position	Group 17	Group 18	Group 19	Group 20
1	8.722E+00	1.883E+01	5.559E-02	5.089E-01
2	0.0	0.0	0.0	0.0
3	2.328E+01	2.586E+01	3.739E+00	1.176E+01
4	1.432E+01	6.759E+00	6.735E+00	1.116E+01
5	5.438E-01	9.842E-03	3.260E-02	5.156E-02
6	0.0	0.0	0.0	0.0
7	0.0	0.0	0.0	0.0
8	0.0	0.0	0.0	0.0
9	0.0	0.0	0.0	0.0
10	0.0	0.0	0.0	0.0
11	0.0	0.0	0.0	0.0
12	0.0	0.0	0.0	0.0
13	0.0	0.0	0.0	0.0
14	0.0	0.0	0.0	0.0
15	0.0	0.0	0.0	0.0
16	6.431E-09	0.0	0.0	0.0
17	0.0	0.0	0.0	0.0
18	0.0	0.0	0.0	0.0
19	0.0	0.0	0.0	0.0
20	0.0	0.0	0.0	0.0
21	0.0	0.0	0.0	0.0
22	0.0	0.0	0.0	0.0
23	0.0	0.0	0.0	0.0
24	0.0	0.0	0.0	0.0
25	0.0	0.0	0.0	0.0
26	0.0	0.0	0.0	0.0
27	0.0	0.0	0.0	0.0
28	0.0	0.0	0.0	0.0
29	0.0	0.0	0.0	0.0
30	0.0	0.0	0.0	0.0
31	0.0	0.0	0.0	0.0
32	0.0	0.0	0.0	0.0
33	0.0	0.0	0.0	0.0
34	0.0	0.0	0.0	0.0
35	0.0	0.0	0.0	0.0
36	0.0	0.0	0.0	0.0
37	0.0	0.0	0.0	0.0
38	0.0	0.0	0.0	0.0
39	0.0	0.0	0.0	0.0
40	0.0	0.0	0.0	0.0
41	0.0	0.0	0.0	0.0
42	0.0	0.0	0.0	0.0
43	0.0	0.0	0.0	0.0

Table B.7 continued

Position	Group 21	Group 22	Group 23	Group 24
1	1.153E+00	6.252E+00	1.409E+02	1.028E+02
2	0.0	0.0	0.0	0.0
3	1.273E+01	2.178E+01	1.877E+01	1.776E+01
4	1.147E+01	1.594E+01	2.654E-01	3.076E-01
5	9.804E-02	9.899E-02	0.0	4.354E-01
6	0.0	0.0	0.0	0.0
7	0.0	0.0	0.0	0.0
8	0.0	0.0	0.0	0.0
9	0.0	0.0	0.0	0.0
10	0.0	0.0	0.0	0.0
11	0.0	0.0	0.0	0.0
12	0.0	0.0	0.0	0.0
13	0.0	0.0	0.0	0.0
14	0.0	0.0	8.602E-09	0.0
15	0.0	0.0	2.890E-06	1.041E-07
16	0.0	0.0	2.725E-05	3.498E-05
17	0.0	0.0	4.650E-05	3.298E-04
18	0.0	0.0	4.614E-05	5.629E-04
19	0.0	0.0	4.648E-05	5.585E-04
20	0.0	0.0	5.284E-05	5.626E-04
21	0.0	0.0	5.497E-05	6.396E-04
22	0.0	0.0	5.642E-05	6.654E-04
23	0.0	0.0	1.180E-04	6.830E-04
24	0.0	0.0	1.136E-04	1.428E-03
25	0.0	0.0	1.047E-04	1.375E-03
26	0.0	0.0	1.233E-04	1.267E-03
27	0.0	0.0	0.0	1.618E-03
28	0.0	0.0	0.0	0.0
29	0.0	0.0	0.0	0.0
30	0.0	0.0	0.0	0.0
31	0.0	0.0	0.0	0.0
32	0.0	0.0	0.0	0.0
33	0.0	0.0	0.0	0.0
34	0.0	0.0	0.0	0.0
35	0.0	0.0	0.0	0.0
36	0.0	0.0	0.0	0.0
37	0.0	0.0	0.0	0.0
38	0.0	0.0	0.0	0.0
39	0.0	0.0	0.0	0.0
40	0.0	0.0	0.0	0.0
41	0.0	0.0	0.0	0.0
42	0.0	0.0	0.0	0.0
43	0.0	0.0	0.0	0.0

Table B.7 continued

Position	Group 25	Group 26	Group 27	Group 28
1	7.438E+01	5.324E+01	3.815E+01	2.851E+01
2	0.0	0.0	0.0	0.0
3	1.710E+01	1.667E+01	1.645E+01	1.662E+01
4	4.821E-01	5.286E-01	8.583E-01	7.122E-01
5	6.699E-01	7.121E-01	1.152E+00	9.500E-01
6	4.613E-01	4.742E-01	7.569E-01	6.046E-01
7	0.0	3.424E-01	5.322E-01	4.194E-01
8	0.0	7.319E-01	4.001E-01	3.078E-01
9	0.0	1.211E-01	1.169E+00	2.382E-01
10	0.0	5.337E-02	2.102E-01	1.575E+00
11	0.0	9.105E-03	9.262E-02	2.935E-01
12	0.0	2.277E+00	2.980E-02	1.293E-01
13	0.0	4.575E-01	6.184E+00	4.721E-02
14	0.0	2.655E-01	1.997E+00	1.093E+01
15	0.0	9.218E-02	1.321E+00	3.931E+00
16	8.013E-07	3.444E-02	4.633E-01	2.629E+00
17	3.196E-04	8.441E-03	9.251E-02	9.171E-01
18	2.538E-03	1.041E-02	4.021E-02	1.918E-01
19	4.332E-03	8.203E-03	4.610E-02	5.497E-02
20	4.298E-03	1.400E-02	2.489E-02	5.163E-02
21	4.330E-03	1.389E-02	4.249E-02	2.800E-02
22	4.922E-03	1.399E-02	4.215E-02	4.778E-02
23	5.121E-03	1.591E-02	4.248E-02	4.741E-02
24	5.256E-03	1.665E-02	4.874E-02	4.827E-02
25	1.099E-02	1.819E-02	5.362E-02	5.819E-02
26	1.058E-02	3.684E-02	6.619E-02	7.402E-02
27	1.154E-02	3.463E-02	1.197E-01	1.012E-01
28	1.909E-02	7.864E-02	1.145E-01	1.503E-01
29	0.0	9.017E-02	2.377E-01	1.414E-01
30	0.0	0.0	2.129E-01	2.134E-01
31	0.0	0.0	0.0	1.954E-01
32	0.0	0.0	0.0	0.0
33	0.0	0.0	0.0	0.0
34	0.0	0.0	0.0	0.0
35	0.0	0.0	0.0	0.0
36	0.0	0.0	0.0	0.0
37	0.0	0.0	0.0	0.0
38	0.0	0.0	0.0	0.0
39	0.0	0.0	0.0	0.0
40	0.0	0.0	0.0	0.0
41	0.0	0.0	0.0	0.0
42	0.0	0.0	0.0	0.0
43	0.0	0.0	0.0	0.0

Table B.7 continued

Position	Group 29	Group 30	Group 31	Group 32
1	2.337E+01	2.015E+01	1.855E+01	1.797E+01
2	0.0	0.0	0.0	0.0
3	1.725E+01	1.855E+01	2.063E+01	2.507E+01
4	1.049E+00	1.086E+00	1.556E+00	2.492E+00
5	1.503E+00	1.520E+00	2.197E+00	3.240E+00
6	9.775E-01	1.036E+00	1.482E+00	2.191E+00
7	6.551E-01	7.088E-01	1.059E+00	1.571E+00
8	4.727E-01	4.981E-01	7.584E-01	1.185E+00
9	3.570E-01	3.715E-01	5.545E-01	8.910E-01
10	2.813E-01	2.869E-01	4.240E-01	6.763E-01
11	2.493E+00	2.292E-01	3.329E-01	5.288E-01
12	4.705E-01	2.262E+00	2.684E-01	4.207E-01
13	2.073E-01	4.249E-01	5.629E-01	3.418E-01
14	7.945E-02	1.872E-01	1.068E-01	2.491E+00
15	1.862E+01	7.050E-02	4.705E-02	4.704E-01
16	6.830E+00	1.645E+01	1.837E-02	2.073E-01
17	4.457E+00	5.994E+00	4.329E+00	7.980E-02
18	1.553E+00	3.935E+00	1.598E+00	1.867E+01
19	3.106E-01	1.371E+00	1.038E+00	6.988E+00
20	8.729E-02	2.979E-01	3.616E-01	4.449E+00
21	8.285E-02	8.184E-02	8.545E-02	1.551E+00
22	5.058E-02	7.746E-02	2.306E-02	3.851E-01
23	8.747E-02	5.833E-02	3.029E-02	1.019E-01
24	8.945E-02	1.097E-01	1.324E-01	1.039E-01
25	9.281E-02	1.151E-01	1.964E-01	2.380E-01
26	1.259E-01	1.310E-01	2.163E-01	3.394E-01
27	1.768E-01	2.015E-01	2.506E-01	3.726E-01
28	2.338E-01	2.816E-01	3.641E-01	4.252E-01
29	2.949E-01	3.392E-01	4.659E-01	5.891E-01
30	2.473E-01	3.551E-01	5.138E-01	7.162E-01
31	2.894E-01	2.608E-01	4.922E-01	7.584E-01
32	3.032E-01	2.709E-01	3.463E-01	7.792E-01
33	0.0	3.079E-01	3.453E-01	5.767E-01
34	0.0	0.0	3.957E-01	5.543E-01
35	0.0	0.0	0.0	6.419E-01
36	0.0	0.0	0.0	0.0
37	0.0	0.0	0.0	0.0
38	0.0	0.0	0.0	0.0
39	0.0	0.0	0.0	0.0
40	0.0	0.0	0.0	0.0
41	0.0	0.0	0.0	0.0
42	0.0	0.0	0.0	0.0
43	0.0	0.0	0.0	0.0

Table B.7 continued

Position	Group 33	Group 34	Group 35	Group 36
1	1.842E+01	2.032E+01	2.609E+01	3.836E+01
2	0.0	0.0	0.0	0.0
3	3.210E+01	4.311E+01	7.081E+01	1.327E+02
4	2.559E+00	4.073E+00	7.393E+00	7.652E+00
5	3.179E+00	5.109E+00	7.887E+00	7.228E+00
6	1.940E+00	3.069E+00	4.813E+00	3.802E+00
7	1.405E+00	2.062E+00	3.372E+00	2.851E+00
8	1.070E+00	1.593E+00	3.623E+00	2.268E+00
9	8.453E-01	1.272E+00	5.320E+00	1.836E+00
10	6.596E-01	1.039E+00	7.379E+00	1.547E+00
11	5.138E-01	8.306E-01	9.854E+00	1.296E+00
12	4.075E-01	6.566E-01	1.331E+01	1.084E+00
13	3.268E-01	5.244E-01	1.708E+01	8.747E-01
14	2.666E-01	4.221E-01	2.057E+01	6.915E-01
15	1.170E+00	3.448E-01	2.402E+01	5.496E-01
16	2.239E-01	2.162E+00	2.784E+01	4.396E-01
17	9.862E-02	3.967E-01	1.014E+00	3.570E-01
18	3.974E-02	1.748E-01	1.900E-01	7.001E-02
19	9.497E+00	6.023E-02	8.369E-02	1.344E-02
20	3.481E+00	1.354E+01	3.118E-02	5.921E-03
21	2.255E+00	4.519E+00	7.354E+00	2.415E-03
22	7.853E-01	2.961E+00	2.675E+00	5.728E-01
23	1.872E-01	1.032E+00	1.718E+00	2.161E-01
24	5.307E-02	2.076E-01	5.984E-01	1.340E-01
25	4.826E-01	5.362E-02	1.143E-01	4.659E-02
26	4.541E-01	4.857E-01	3.556E-01	2.275E-02
27	4.964E-01	4.859E-01	8.676E-01	3.331E-01
28	5.232E-01	5.505E-01	6.828E-01	6.264E-01
29	5.731E-01	5.769E-01	7.418E-01	4.167E-01
30	7.149E-01	6.273E-01	7.515E-01	4.270E-01
31	7.872E-01	7.765E-01	7.920E-01	4.239E-01
32	7.656E-01	8.513E-01	9.380E-01	4.389E-01
33	7.296E-01	8.313E-01	9.973E-01	5.049E-01
34	5.229E-01	8.671E-01	9.708E-01	5.250E-01
35	4.845E-01	6.552E-01	1.270E+00	5.072E-01
36	5.572E-01	6.065E-01	1.065E+00	7.361E-01
37	0.0	7.010E-01	9.781E-01	6.408E-01
38	0.0	0.0	1.114E+00	5.859E-01
39	0.0	0.0	0.0	6.589E-01
40	0.0	0.0	0.0	0.0
41	0.0	0.0	0.0	0.0
42	0.0	0.0	0.0	0.0
43	0.0	0.0	0.0	0.0

Table B.7 continued

Position	Group 37	Group 38	Group 39	Group 40
1	6.182E+01	1.284E+02	1.031E+02	4.098E+02
2	0.0	0.0	0.0	0.0
3	2.815E+02	9.476E+02	1.570E+03	1.838E+04
4	1.327E+01	3.028E+01	4.200E+01	5.348E+01
5	1.317E+01	2.075E+01	9.809E+00	5.238E+00
6	7.493E+00	9.233E+00	0.0	0.0
7	5.576E+00	3.990E+00	0.0	0.0
8	4.555E+00	1.180E+00	0.0	0.0
9	3.272E+00	1.334E-01	0.0	0.0
10	2.301E+00	0.0	0.0	0.0
11	1.740E+00	0.0	0.0	0.0
12	1.320E+00	0.0	0.0	0.0
13	1.011E+00	0.0	0.0	0.0
14	7.459E-01	0.0	0.0	0.0
15	5.428E-01	0.0	0.0	0.0
16	4.043E-01	0.0	0.0	0.0
17	3.068E-01	0.0	0.0	0.0
18	2.394E-01	0.0	0.0	0.0
19	2.092E-01	0.0	0.0	0.0
20	3.498E-02	4.475E+00	0.0	0.0
21	1.541E-02	8.341E-01	1.710E-01	0.0
22	2.982E-03	3.675E-01	2.731E-02	9.585E-01
23	6.222E-01	1.348E-01	1.203E-02	1.534E-01
24	1.598E-01	3.104E+01	1.394E-03	6.758E-02
25	9.604E-02	1.101E+01	2.326E-01	8.058E-03
26	3.341E-02	7.203E+00	1.192E-02	1.368E+00
27	4.580E-02	2.512E+00	1.950E-03	9.492E-02
28	3.427E-01	5.026E-01	6.680E-04	3.017E-02
29	6.353E-01	4.556E-01	2.947E-02	1.046E-02
30	4.167E-01	7.299E-01	1.754E-01	1.382E-01
31	4.270E-01	4.547E-01	3.203E-01	2.152E-01
32	4.239E-01	4.918E-01	1.906E-01	3.502E-01
33	4.389E-01	4.882E-01	1.832E-01	1.418E-01
34	5.049E-01	5.038E-01	1.819E-01	9.993E-02
35	5.250E-01	5.786E-01	1.892E-01	9.927E-02
36	5.072E-01	6.017E-01	2.180E-01	1.060E-01
37	7.361E-01	5.859E-01	2.267E-01	1.234E-01
38	6.408E-01	9.007E-01	2.168E-01	1.283E-01
39	5.859E-01	7.993E-01	2.912E-01	1.158E-01
40	6.589E-01	7.319E-01	2.464E-01	8.000E-02
41	0.0	8.309E-01	2.247E-01	4.302E-02
42	0.0	0.0	2.491E-01	3.732E-02
43	0.0	0.0	0.0	2.829E-02

information on this code can be obtained from Robert W. Roussin or G. Wayne Morrison at ORNL.

Table B.8 Description of Cross Sections Presented in Table B.7

Position In Table	Neutron Cross Section (Groups 1-22)		Gamma Cross Section (Groups 23-40)	
1	σ_a	(BARNS)	σ_a	(MEV-BARNS)
2	$\nu\sigma$	(BARNS)	$\nu\sigma$	(BARNS)
3	σ_T	(BARNS)	σ_T	(BARNS)
4	$\sigma_{g\to g}$	(BARNS)	$\sigma_{g\to g}$	(BARNS)
5	$\sigma_{g-1\to g}$	(BARNS)	$\sigma_{g-1\to g}$	(BARNS)
6	$\sigma_{g-2\to g}$	(BARNS)	$\sigma_{g-2\to g}$	(BARNS)
:	:		:	
43	$\sigma_{g-39\ g}$	(BARNS)	$\sigma_{g-39\ g}$	(BARNS)

Where σ_a is the microscopic absorption (neutrons or energy) cross section

ν is the number of neutrons produced per fission

σ_f is the microscopic fission cross section

σ_T is the microscopic total cross section

$\sigma_{i\to j}$ is the microscopic scatter cross section from group i to group j.

Appendix C Economic Model

C.1 Summary of Equations

The economic analysis reported here has been carried out using the Cash Flow Method (CFM) described by Brewer (B3), as implemented by a modified version of his code SPPIA. The modified code, hereafter called BRECON, requires input of fissile inventory histories developed external to the economics code (by using 2DB (L 10) in this work). BRECON also can accomodate systems in which thorium is irradiated to produce U-233 with an economic penalty being assigned to the contaminant U-232.

Input instructions for BRECON are described in section C.3; a sample problem is presented in section C.4; and a listing of the code is contained in section C.5. The purpose of this section, which has largely been extracted from Brewer's work, is simply to summarize the equations used in the CFM. Section C.2 outlines the nomenclature employed in this section.

Table C.1 summarizes the CFM fuel cycle cost equations. Based on a suggestion by Brewer (B 6), accounting method A has been employed in this work. Other deviations from Brewer's work include addition of the cost components associated with thorium and U-233, and inclusion of a penalty on material credit related to the concentration of the contaminant U-232 in the U-233 produced in a thorium blanket (see Table 2.12).

TABLE C.1 SUMMARY OF FBR FUEL COST ANALYSIS EQUATIONS (CASH FLOW METHOD)

1. Total Reactor Fuel Cost: $\bar{e}(\text{reactor}) = \sum_s (\bar{e})_s \ldots \frac{\text{mills}}{\text{KWHe}}$ $\quad s \equiv$ fuel stream index

2. Fuel Stream Cost: $(\bar{e})_s = \sum_q (\bar{e}_q)_s \ldots\ldots\ldots \frac{\text{mills}}{\text{KWHe}}$ $\quad q \equiv$ cost component index $= mp, fab, repr, mc$

3. Component Costs of a Stream: $(\bar{e}_q)_s = (\bar{e}_{q,\text{direct}})_s + (\bar{e}_{q,\text{CaChg}})_s \ldots\ldots\ldots \frac{\text{mills}}{\text{KWHe}}$

$$= 1000 \left[\frac{\sum_m^n w(t_m) z_m^q}{\sum_j^N w(j) E_j} + \frac{\sum_m^n w(t_m) z_m^q f_m^q}{\sum_j^N w(j)\, E_j} \right]_s$$

$$= 1000 \left[\frac{\sum_m^n w(t)_m z_m^q f_m^q}{\sum_j^N w(j)\, E_j} \right]_s$$

$m \equiv$ fuel lot index, stream s

TABLE C.1 - continued

4. Carrying Charge Factors:

$F_m^q = 1 + f_m^q$ = carrying charge factor, component q, fuel lot m of a given fuel stream

$= \frac{1}{1-\tau} [w(-T_m^q) - \tau]$ . . . for q capitalized

$= w(-T_m^q)$ . . . for q not capitalized (expensed cost or tax revenues)

where

$w(t) \equiv (1+x)^{-t}$ = discount factor

$x \equiv (1-\tau) r_b f_b + r_s f_s$ = discount rate

T_m^q as defined in Fig. C.1

$\tau \equiv$ tax rate

$f_b \equiv$ bond fraction

$f_s \equiv$ stock fraction

$r_b \equiv$ rate of return to bondholders

$r_s \equiv$ rate of return to stockholders

TABLE C.1 - continued

5. Tax Assumptions

Component, q	Method A	Method B
material purchase	capitalized	capitalized
fabrication	capitalized	capitalized
reprocessing	not capitalized (expensed)	capitalized
material credit	not capitalized (taxed)	capitalized

6. Direct Dollar Costs (per lot, per stream)

material purchase . . $z_m^{mp} = C_{28}M_{28}^0+C_{49}M_{49}^0 + C_{40}M_{40}^0+C_{41}M_{41}^0+C_{42}M_{42}^0+C_{02}M_{02}^0+C_{23}M_{23}^0\ldots$

... \$/LOT

fabrication . . . . . $z_m^{fab} = C_{fab}M_{HM}^0$

reprocessing. . . . . $z_m^{repr} = C_{repr}M_{HM}^0$

material credit . . . $z_m^{mc} = C_{28}M_{28}(T)+C_{49}M_{49}(T)+C_{40}M_{40}(T)+C_{41}M_{41}(T)+C_{42}M_{42}(T)+$

$+ C_{02}M_{02}(T)+C_{23}M_{23}(T)-P_{22}[M_{22}(T)+M_{23}(T)](10^3)$

TABLE C.1 - continued

7. For batch or scatter fuel management of fuel stream s:

$$(\bar{e})_s = \frac{1000}{E} M_{HM}^0 \left[\frac{C_{fissile}\,\varepsilon_o F^{mp}(T)}{T} + \frac{C_{fab} F^{fab}(T)}{T} + \frac{C_{repr} F^{repr}(T)}{T} - \frac{C_{fissile}\,\varepsilon(T) F^{mc}(T)}{T}\right]$$

$\frac{\text{mills}}{\text{KWHe}}$

[ ] = figure of merit, local fuel performance ... $\frac{\$/yr.}{\text{kg HM loaded}}$

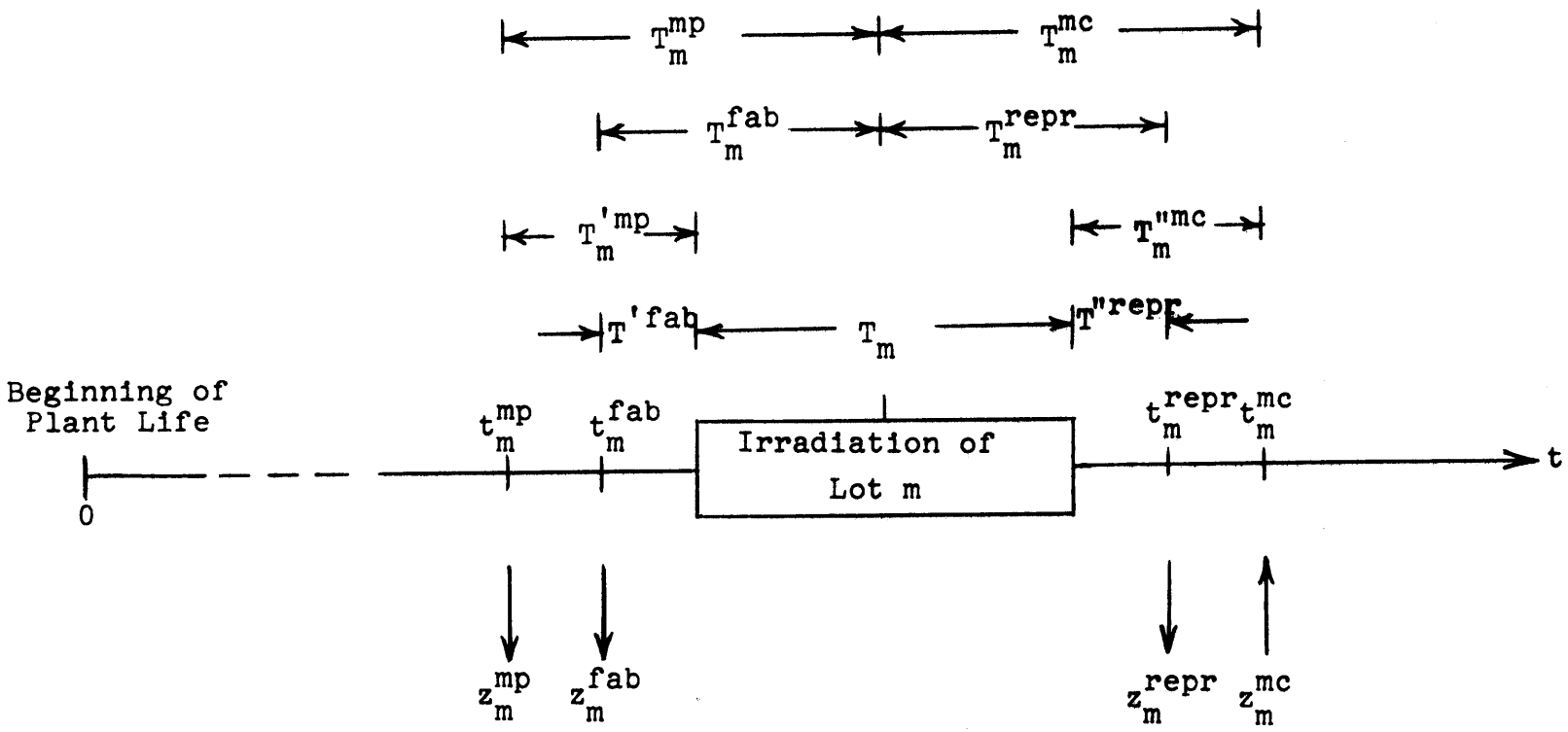

Fig. C.1 Timing of Cash Flow Associated with a Fuel Lot (See Section C.2 for Definition of Terms)

C.2 Nomenclature

Subscripts, Superscripts and Abbreviations.

q	cost component index; mp, fab, repr or mc
mp	material purchase
fab	fabrication
repr	reprocessing
mc	material credit
02	TH-232
28	U-238
49	PU-239
40	PU-240
41	PU-241
42	PU-242
23	U-232
22	U-232
HM	heavy metal (U + Pu) or (Th + U)
CFM	cash flow method

Levelized Cost (Price of Electricity

$\bar{e}$	levelized cost (price) of electricity associated with fuel. $\frac{\text{mills}}{\text{KWHe}}$

Depending on context, the symbol $\bar{e}$ denotes:

- *total reactor levelized fuel cost (sum over all fuel streams)
- *levelized fuel cost associated with a given fuel stream (sum over the cost components, q, of the fuel stream).

Unit Costs

C_{fab}	unit fabrication cost for a given type fuel	$\frac{\$}{kgHM}$
C_{repr}	unit reprocessing cost for a given type fuel	$\frac{\$}{kgHM}$
C_j	market value of isotope j	$\frac{\$}{kg}$
P_{22}	penalty associated with U-232 in fuel (see Table 2.12)	\$/g-Uranium

Annual Quantities for CFM Derivation

E_j	electrical energy generated by the plant, year j	KWHe
E	electrical energy generated by the plant during irradiation of a given batch	KWHe
w(j)	discount factor, $(1-x)^{-j}$	

Costs Associated with a Fuel Lot

z_m^q	direct cost, cost component q, fuel lot m	\$

Time

t_m^q	time from beginning of plant life to transaction q, fuel lot m	yr.
t_m	time from beginning of plant life to irradiation midpoint of fuel lot m	yr.

Time cond't

T_m	irradiation time of fuel lot m	yr.
$T_m^{'q}$	pre-irradiation time, component q, fuel lot m; time between transaction q and start of irradiation	yr.
$T_m^{"q}$	post-irradiation time, component q, fuel lot m; time between end of irradiation and transaction q	yr.
T_m^q	time between transaction q of lot m, and midpoint of irradiation	yr.

Financial Parameters

x	discount rate
f_b	fraction of capital from bondholders
f_s	fraction of capital from stockholders
r_b	bondholders' rate of return
r_s	stockholders' rate of return
τ	income tax rate
F_m^q	carrying charge factor associated with cost component q, fuel lot m
f_m^q	$F_m^q - 1$;

Fuel Composition

$M_j(T)$	Mass of nuclide j after irradiation Time, T	kg
M_j^0	Initial mass of nuclide j	kg

Fuel Composition

$\varepsilon_{(T)}$ Fissile concentration after irradiation time T,

$[M_{49}(T) + M_{41}(T)]/M^0_{HM}$ or

$[M_{23}(T)/M^0_{HM}]$

ε_0 Initial fissile concentration (enrichment),

$[M^0_{49} + M^0_{41}]/M^0_{HM}$ or

$[M^0_{23}/M^0_{HM}]$

C.3 Input Instructions

The program BRECON performs economics calculations for fast breeder reactors under any desired management scheme. Required input includes information on the economic environment under which the reactor operates, and fissile inventory histories for each region to be analyzed. The cash flow equations presented in section C.1 are used to compute local and aggregate fuel cycle cost contribution in mills/kw-hr, $/yr/kg HM, and $/kg HM as functions of irradiation time.

Fissile inventory histories may be developed using any of a number of physics depletion codes. In this study the 2DB (L 10) code was used to evaluate fissile material inventory histories for the core and for several (see Fig. 2.2) zones in the radial and axial blankets. The number density

information punched out by 2DB can be easily converted into fissile inventories, in kilograms, given data on the geometry of the system of interest.

The remainder of this section will be devoted to a tabulation of the input required to use BRECON.

BRECON INPUT

Variable	Columns	Format	Description
Card 1			
NNCAS	1-5	I5	Number of cases to be analyzed; each consists of NCASE depletion zones.
Card 2			
ID(11)	1-66	11A6	Identification card.
Card 3			
NCASE	1-6	I6	The number of depletion zones.
NVR	7-12	I6	The number of contiguous depletion zones per region, e.g. annular region. Although each zone is depleted individually, discharge compositions and economics are computed by regions which may consist of more than one zone.
NPRINT	13-18	I6	If NPRINT=0, print out of zone depletion and economics results is omitted. Only region results are printed. If NPRINT=1, both zone and region results are printed.
NDECIS	19-24	I6	If NDECIS=1, print economic results only in units of mills/kw-hr. If NDECIS=0 print economic results in $/yr/kg HM and $/kg HM as well as in mills/kw-hr.

BRECON INPUT

Variable	Columns	Format	Description
Card 4			
NTS	1-6	I6	The number of time steps. Economics results are printed out after each time step. This number includes the starting point time as a time step.
Card 5			
DT	1-12	F12.8	Duration of a time step, full power days.
Card 6			
EFF	1-12	F12.8	Net thermal efficiency.
Card 7			
F$KGHM	1-10	F10.2	Unit fabrication cost, $/KGHM
R$KGHM	11-20	F10.2	Unit reprocessing cost, $/KGHM
S$KG49	21-30	F10.2	Price of PU-239, $/KG PU-239
S$KG28	31-40	F10.2	Price of U-238, $/KG U-238
S$KG40	41-50	F10.2	Price of Pu-240, $/KG PU-240
S$KG41	51-60	F10.2	Price of PU-241, $/KG PU-241
S$KG42	61-70	F10.2	Price of PU-242, $/KG PU-242
Card 8			
S$KG23	1-10	F10.2	Price of U-233, $/KG U-233
S$KG02	11-20	F10.2	Price of TH-232, $/KG TH-232

BRECON INPUT

Variable	Columns	Format	Description
Card 9			
TAX	1-12	F12.8	Income tax rate
BDRTE	13-24	F12.8	Bondholders' rate of return
BDFRN	25-36	F12.8	Bond Fraction
SKRTE	37-48	F12.8	Stockholders' rate of return
SKFRN	49-60	F12.8	Stock fraction
Card 10			
SLF	1-12	F12.8	Plant load factor
CAPMWE	13-24	F12.8	Plant rated capacity, MWe
Card 11			
TFPRE	1-12	F12.8	Time prior to beginning of irradiation that fabrication cash flow occurs, years.
TMPPRE	13-24	F12.8	Time prior to beginning of irradiation that material purchase cash flow occurs, years.
TRPPST	25-36	F12.8	Time after end of irradiation that reprocessing cash flow occurs, years.
TMCPST	37-48	F12.8	Time after end of irradiation that material credit occurs, years.

BRECON INPUT

Variable	Columns	Format	Description
Card 12 (U-232 Penalty Factor Table, See Table 2.12)			
PPM(1)	1-12	F12.8	Lowest U-232 Concentration in PPM of total uranium.
S$DED(1)	13-24	F12.8	U-232 penalty in dollars per lowest gram of total uranium.
PPM(2)	25-36	F12.8	Second lowest U-232 concentration in PPM of total uranium.
S$DED(2)	37-48	F12.8	Second lowest U-232 penalty in dollars per gram of total uranium.
⋮			

These concentrations and penalty factors should be tabulated in the format, 6F12.8, until 12 pairs of entries (the same as in Table 2.12) are input. This will require 4 cards.

Note: The remaining cards should be tabulated for each of the NCASE depletion zones which are to be analyzed

Variable	Columns	Format	Description
Card 13			
VOL	1-12	F12.8	Zone volume, liters

BRECON INPUT

Variable	Columns	Format	Description
Card 14 (Card 14 must be repeated for each of the NTS time steps, including the initial time, being analyzed)			
U28N(I)	1-10	F10.6	U-238 Inventory at time step I, KG
P49N(I)	11-20	F10.6	Pu-239 Inventory at time step I, KG
P40N(I)	21-30	F10.6	Pu-240 Inventory at time step I, KG
P41N(I)	31-40	F10.6	Pu-241 Inventory at time step I, KG
P42N(I)	41-50	F10.6	Pu-242 Inventory at time step I, KG
TO2N(I)	51-60	F10.6	TH-232 Inventory at time step I, KG
U23N(I)	61-70	F10.6	U-233 Inventory at time step I, KG
U22N(I)	71-80	F10.6	U-232 Inventory at time step I, KG
Card 15			
EFTOT(1)	1-10	E10.4	Average burnup in zone of interest at time step 1 (beginning of the irradiation), MWD/MTM
EFTOT(2)	11-20	E10.4	Average burnup in the zone of interest at time step 2, MWD/MTM

Values of EFTOT(I) should be repeated, using the format 8E10.4, until NTS values have been entered.

Additional cases from 2 to NNCAS require that all cards from 2 through 15 be repeated for each case.

C.4 Sample Problem

This section describes a BRECON computer run in which the reference LMFBR thorium radial blanket (see Fig. 2.2) was evaluated for a 6 year (1800 full power days) batch burnup. The fissile inventories for this analysis were generated using the code 2DB. Fissile inventory histories from the 2DB analysis were condensed prior to the economic analysis into data for each of the three blanket rows. The economic evaluation will be performed using financial parameters from the reference economic environment (see Table 5.1) to analyze the economics of the entire radial blanket. Economics data for each of the three rows can be obtained by setting the control variable NPRINT equal to unity. The sample problem input deck is listed in Table C.2, while the output data at an irradiation time of 4 years and an interpretation of variable names contained therein are presented in Tables C.3 and C.4 respectively.

The key parameters to be noted in Table C.3 are on the first page of that table in lines 1 and 2 (TIMED = 1200), lines 7 and 8 (EPS = 0.02811), and line 17 (TOTALS(A) = -0.23647350). This information states that after 1200 full power days the average fissile enrichment in the radial blanket is 2.811%, and the radial blanket contribution to the fuel cycle cost is -0.2365 mills/kw-hr when the economic analysis is performed using accounting method A.

TABLE C.2 SAMPLE PROBLEM INPUT DECK

```
   1
BRECON-1, 3 ROW TH RADIAL BLKT, STD ECONOMIC ENVIRONMENT, SAMPLE
    3      3      0      0
   19
100.0
0.3906
69.00      50.00      1000.0      0.0          0.0          1000.0      0.0
16700.0    0.0
   0.5          0.07          0.5          0.125          0.5
  0.82          1000.0
   0.5          0.5           0.5          0.5
0.0          0.40          20.0          0.60          45.0          0.80
80.0         1.0           130.0         1.20          190.0         1.40
250.0        1.50          350.0         1.60          500.0         1.70
700.0        1.80          1000.0        1.90          1500.0        2.00
 2247.8081
    0.0          0.0           0.0           0.0           0.0     9395.0977      0.0          0.0
    0.0          0.0           0.0           0.0           0.0     9339.8984     53.7750      0.0015
    0.0          0.0           0.0           0.0           0.0     9285.1953    104.0210      0.0062
    0.0          0.0           0.0           0.0           0.0     9229.9961    150.9280      0.0138
    0.0          0.0           0.0           0.0           0.0     9174.3984    194.3480      0.0244
    0.0          0.0           0.0           0.0           0.0     9118.2969    235.2700      0.0379
    0.0          0.0           0.0           0.0           0.0     9064.2969    273.7959      0.0544
    0.0          0.0           0.0           0.0           0.0     9009.0977    309.4458      0.0745
    0.0          0.0           0.0           0.0           0.0     8953.2969    342.9829      0.0978
    0.0          0.0           0.0           0.0           0.0     8896.9961    374.4297      0.1242
    0.0          0.0           0.0           0.0           0.0     8842.4961    403.9299      0.1534
    0.0          0.0           0.0           0.0           0.0     8786.2969    431.6199      0.1854
    0.0          0.0           0.0           0.0           0.0     8728.7969    457.5796      0.2200
    0.0          0.0           0.0           0.0           0.0     8673.9961    480.5896      0.2569
    0.0          0.0           0.0           0.0           0.0     8620.3984    502.2795      0.2966
    0.0          0.0           0.0           0.0           0.0     8563.7969    522.6697      0.3386
    0.0          0.0           0.0           0.0           0.0     8507.9961    541.7297      0.3825
    0.0          0.0           0.0           0.0           0.0     8454.7969    559.7100      0.4287
    0.0          0.0           0.0           0.0           0.0     8399.2969    576.5999      0.4766
0.0          0.4029E+03 0.1654E+04 0.3791E+04 0.6705E+04 0.1037E+05 0.1471E+05 0.1981E+05
```

TABLE C.2 CONTINUED

0.2554E+050.3182E+050.3860E+050.4585E+050.5352E+050.6149E+050.6985E+050.7854E+05
0.8748E+050.9672E+050.1062E+06
2502.2761

0.0	0.0	0.0	0.0	0.0	10458.5977	0.0	0.0
0.0	0.0	0.0	0.0	0.0	10434.7969	23.8847	0.0001
0.0	0.0	0.0	0.0	0.0	10410.2969	47.5500	0.0004
0.0	0.0	0.0	0.0	0.0	10385.6953	71.2410	0.0009
0.0	0.0	0.0	0.0	0.0	10359.5977	94.7300	0.0018
0.0	0.0	0.0	0.0	0.0	10334.0000	118.3480	0.0030
0.0	0.0	0.0	0.0	0.0	10304.0000	142.0390	0.0047
0.0	0.0	0.0	0.0	0.0	10275.2969	165.4860	0.0070
0.0	0.0	0.0	0.0	0.0	10247.7969	188.9370	0.0098
0.0	0.0	0.0	0.0	0.0	10215.8984	212.2810	0.0134
0.0	0.0	0.0	0.0	0.0	10186.8945	235.4520	0.0177
0.0	0.0	0.0	0.0	0.0	10157.2969	258.5029	0.0228
0.0	0.0	0.0	0.0	0.0	10123.4961	281.3899	0.0288
0.0	0.0	0.0	0.0	0.0	10091.9961	302.7100	0.0355
0.0	0.0	0.0	0.0	0.0	10060.1953	323.9858	0.0432
0.0	0.0	0.0	0.0	0.0	10028.5000	345.1150	0.0519
0.0	0.0	0.0	0.0	0.0	9995.7969	365.8567	0.0616
0.0	0.0	0.0	0.0	0.0	9961.8984	386.4797	0.0725
0.0	0.0	0.0	0.0	0.0	9925.0977	406.8796	0.0846

0.0 0.6231E+02 0.2786E+03 0.6758E+03 0.1254E+04 0.2028E+04 0.3015E+04 0.4205E+04
0.5631E+040.7283E+040.9167E+040.1129E+050.1365E+050.1615E+050.1891E+050.2192E+05
0.2515E+050.2864E+050.3241E+05
2756.7451

0.0	0.0	0.0	0.0	0.0	11522.1953	0.0	0.0
0.0	0.0	0.0	0.0	0.0	11513.8984	9.6328	0.0000
0.0	0.0	0.0	0.0	0.0	11501.7969	19.5363	0.0000
0.0	0.0	0.0	0.0	0.0	11490.4961	29.9179	0.0000
0.0	0.0	0.0	0.0	0.0	11482.1992	40.6670	0.0001
0.0	0.0	0.0	0.0	0.0	11469.1992	51.9480	0.0002
0.0	0.0	0.0	0.0	0.0	11455.3984	63.7439	0.0003
0.0	0.0	0.0	0.0	0.0	11441.5977	75.8370	0.0004
0.0	0.0	0.0	0.0	0.0	11429.0937	88.3980	0.0007
0.0	0.0	0.0	0.0	0.0	11414.1992	101.3910	0.0009

TABLE C.2 CONTINUED

0.0	0.0	0.0	0.0	0.0	11398.4961	114.8220	0.0013
0.0	0.0	0.0	0.0	0.0	11383.5977	128.6797	0.0018
0.0	0.0	0.0	0.0	0.0	11365.1953	142.9200	0.0023
0.0	0.0	0.0	0.0	0.0	11348.6992	156.4860	0.0030
0.0	0.0	0.0	0.0	0.0	11331.5977	170.5220	0.0038
0.0	0.0	0.0	0.0	0.0	11316.6992	184.9510	0.0047
0.0	0.0	0.0	0.0	0.0	11297.7969	199.6821	0.0059
0.0	0.0	0.0	0.0	0.0	11278.9961	214.7860	0.0072
0.0	0.0	0.0	0.0	0.0	11259.6953	230.2660	0.0087

0.0 0.9667E+01 0.4150E+02 0.1324E+03 0.1975E+030.3315E+030.5091E+030.7352E+03
0.1016E+040.1356E+040.1760E+040.2236E+040.2789E+040.3383E+040.4063E+040.4834E+04
0.5693E+040.6659E+040.7736E+04

TABLE C.3 SAMPLE PROBLEM OUTPUT DATA

```
                                        RTIMEY          TIMEB
                                      0.0C9357e5        12[illegible]

   AFT              AEFTOT            APNUP             APERR
  0.0           0.69958E+05       0.22297E+04       0.22771E-01
   AU28M            AP49M             AP48M             AP41M             AP42M             AT02M             AU23M             AU22M
  0.0               0.0               0.0               0.0               C.C               0.302175+05       0.88189E+03       0.25110E+00
   A28MR            A49MR             A48MR             A41MR             A42MR             A02MR             A23MR             A22MR             EPS
    0.0              0.0               C.C               C.C               0.C               0.96308           0.02811           0.00001           0.02811
  CCFMP            CCFF              CCFRP             CCFMC
  0.4251881        0.4251881        -0.1753224        -0.1753224
  CCFMP            CCFF              CCFRPB            CCFMCB
  0.4251881        0.4251881        -0.3506451        -0.3506451


POWER COSTS (MILLS/KWH)
  MATPUR            FAB             REPR(A)          MATCRE(A)          TOTALS(A)          REPR(B)          MATCRE(B)          TOTALS(B)
  0.0           0.07517135       0.05447202       -0.47112811        -0.34148461        0.05447202       -0.47112811        -0.34148461        DIRECT
  0.0           0.03196157      -0.00955016        0.08259922         0.10501063       -0.01917034        0.16519868         0.17860228        CARCHG
  0.0           0.10713327       0.04492186       -0.38852888        -0.23647398        0.03530168       -0.30592942        -0.16342429        TOTALS

   MATERIAL                          PROCESSING                          TOTALS                          METHOD(A)
      DIR(BU)       -0.47112811        DIR              0.12964332        -0.34148479  DIRECT
      CARCHG(INV)    0.08259922        CARCHG           0.02241181         0.10501089  CARCHG
      TOTMAT        -0.38852888        TOTPROC          0.15205508        -0.23647389  TOTALS
   MATERIAL                          PROCESSING                          TOTALS                          METHOD(B)
      DIR(BU)       -0.47112811        DIR              0.12964332        -0.34148479  DIRECT
      CARCHG(INV)    0.16519868        CARCHG           0.01286163         0.17806029  CARCHG
      TOTMAT        -0.30592942        TOTPROC          0.14250493        -0.16342449  TOTALS
```

TABLE C.3 CONTINUED

POWER COSTS ($/YR/KGHMLOADED)

MATPUR	FAB	REPR(A)	MATCRE(A)	TOTALS(A)	REPR(B)	MATCRE(B)	TOTALS(B)	
0.0	17.21	12.47	-107.86	-78.18	12.47	-107.86	-78.18	DIRECT
0.0	7.32	-2.15	18.51	24.04	-4.37	37.82	40.77	CARCHG
0.0	24.53	10.28	-88.95	-54.14	8.10	-70.04	-37.41	TOTALS

MATERIAL		PROCESSING		TOTALS	METHOD(A)
DIR(BU)	-107.86	DIR	29.68	-78.18	DIRECT
CARCHG(INV)	18.91	CARCHG	5.13	24.04	CARCHG
TOTMAT	-88.95	TOTPROC	34.81	-54.14	TOTALS

MATERIAL		PROCESSING		TOTALS	METHOD(B)
DIR(BU)	-107.86	DIR	29.68	-78.18	DIRECT
CARCHG(INV)	37.82	CARCHG	2.54	40.77	CARCHG
TOTMAT	-70.04	TOTPROC	32.63	-37.41	TOTALS

POWER COSTS ($/KGHMLOADED)

MATPUR	FAB	REPR(A)	MATCRE(A)	TOTALS(A)	REPR(B)	MATCRE(B)	TOTALS(B)	
0.0	69.00	50.00	-432.45	-313.45	50.00	-432.45	-313.45	DIRECT
0.0	29.34	-8.77	75.82	96.39	-17.53	151.64	168.44	CARCHG
0.0	98.34	41.23	-356.63	-217.06	32.47	-280.81	-150.01	TOTALS

MATERIAL		PROCESSING		TOTALS	METHOD(A)
DIR(BU)	-432.45	DIR	119.00	-313.45	DIRECT
CARCHG(INV)	75.82	CARCHG	20.57	96.39	CARCHG
TOTMAT	-356.63	TOTPROC	139.57	-217.06	TOTALS

MATERIAL		PROCESSING		TOTALS	METHOD(B)
DIR(BU)	-432.45	DIR	119.00	-313.45	DIRECT
CARCHG(INV)	151.64	CARCHG	11.81	163.44	CARCHG
TOTMAT	-280.81	TOTPROC	130.81	-150.01	TOTALS

MATCRE/MATPUR+FAB+REPR

DIRECT	TOT(A)	TOT(B)
-3.634032	-2.555183	-2.146756

TABLE C.4

INTERPRETATION OF BRECON PRINTED OUTPUT

Variable	Description	Units
RTIMEY	Actual irradiation time	years
TIMED	Irradiation time in full power days	days
ABNUP	Burnup in the annular region	MWD/MTHM
APFRN	Fraction of total reactor power supplied by the annular region	
Nuclide Masses:		
AU28M	Mass of U-238 in annular region after irradiation	kg
AP49M	Mass of PU-239 in annular region after irradiation	kg
AP40M AP41M AP42M	Masses of PU-239, 241, 242 in annular region after irradiation	kg
AT02M	Mass of TH-232 in annular region after irradiation	kg
AU23M AU22M	Masses of U-233 and U-232 in annular region after irradiation	kg
AHMKGL	Initial mass of heavy metal (U+PU) or (TH+U)	kg
Nuclide Fractions:		
A28MR	AU28M/AHMKGL	
A49MR	AP49M/AHMKGL	
A40MR	AP49M/AHMKGL	

TABLE C.4 Cond't

Variable	Description	Units
Nuclide Fractions:		
A41MR	AP41M/AHMKGL	
A42MR	AP42M/AHMKGL	
A02MR	AT02M/AHMKGL	
A23MR	AU23M/AHMKGL	
A22MR	AU22M/AHMKGL	
EPS	Fissile Mass/Initial Mass of Heavy Metal	
MATPUR	Material Purchase Component	
FAB	Fabrication Component	
REPR(A)	Reprocessing Component (Tax Method A)	
REPR(B)	Reprocessing Component (Tax Method B)	
MATCRE(A)	Material Credit Component (Tax Method A)	
MATCRE(B)	Material Credit Component (Tax Method B)	
DIR	Direct Component	
CACHG	Carrying Charge Component	
TOTMAT	Total Material Component (Burnup+Inventory)	
TOTPROC	Total Processing Component (fabrication + reprocessing, including their carrying charges)	

C.5 BRECON Listing

This section contains a FORTRAN listing of the program BRECON.

```
C      BREW-ECON A COMPUTER PROGRAM FOR CALCULATING FAST REACTOR FUEL     BRCN   1
C               CYCLE ECONOMICS FOR BOTH CORE AND BLANKETS                BRCN   2
C      PROGRAM WAS WRITTEN BY S.T.BREWER AND MODIFIED BY P.J.WOOD         BRCN   3
C                                                                         BRCN   4
       COMMON      AU28M(30),AP49M(30),AP40M(30),AP41M(30),AP42M(30)      BRCN   5
       COMMON      AMPD(30),AFBD(30),ARPD(30),AMCD(30),ADT(30),           BRCN   6
      1            AMPCC(30),AFBCC(30),ARPCC(30),AMCCC(30),ACCT(30),      BRCN   7
      2            AMPTT(30),AFBTT(30),ARPTT(30),AMCTT(30),AT(30)         BRCN   8
       COMMON      FAMPD(30),FAFBD(30),FARPD(30),FAMCD(30),FADT(30),      BRCN   9
      1            FAMPCC(30),FAFBCC(30),FARPCC(30),FAMCCC(30),FACCT(30), BRCN  10
      2            FAMPTT(30),FAFBTT(30),FARPTT(30),FAMCTT(30),FAT(30)    BRCN  11
       COMMON      AEFTOT(30),ABNUP(30),SFTV(30),AFT(30),EFTOT(30)        BRCN  12
       COMMON       ARPCCB(30),ARPTTB(30),AMCCCB(30),AMCTTB(30),          BRCN  13
      1   ACCTB(30),ATB(30)                                               BRCN  14
       COMMON       FARPCB(30),FAMCCB(30),FACCTB(30),FARPTB(30),          BRCN  15
      1  FAMCTB(30),FATB(30)                                              BRCN  16
       COMMON      A28MR(30),A49MR(30),A40MR(30),A41MR(30),A42MR(30),     BRCN  17
      1  EPS(30)                                                          BRCN  18
       COMMON      ABU(30),AINV(30),AINVB(30),AMAT(30),AMATB(30),APRSD(30)BRCN  19
      1  ,APRSC(30),APRST(30),APRSCB(30),AAT(30),AATB(30),AADT(30),       BRCN  20
      2  AACCT(30),AACCTB(30)                                             BRCN  21
       COMMON      APRSTB(30)                                            BRCN  22
       COMMON      ID(11)                                                BRCN  23
       DOUBLE PRECISION  ID                                              BRCN  24
       COMMON     U28N(30),P49N(30),P40N(30),P41N(30),P42N(30),           BRCN  25
      1 T02N(30),U23N(30),U22N(30),PPM(20),S$DED(20)                     BRCN  26
       COMMON     AT02M(30),AU23M(30),AU22M(30),A02MR(30),A23MR(30),     BRCN  27
      1 A22MR(30)                                                       BRCN  28
C                                                                         BRCN  29
C      FORMATS FOR READ CARD INPUT                                        BRCN  30
C                                                                         BRCN  31
     1 FORMAT(4I6)                                                      BRCN  32
     2 FORMAT(4F12.8)                                                   BRCN  33
    22 FORMAT(6F12.8)                                                   BRCN  34
     3 FORMAT(F12.8)                                                    BRCN  35
     4 FORMAT(5F12.8)                                                   BRCN  36
```

```
    5 FORMAT(F12.8)                                                    BRCN  37
    6 FORMAT(I6)                                                       BRCN  38
    7 FORMAT(F12.8)                                                    BRCN  39
   21 FORMAT(2F12.8)                                                   BRCN  40
   31 FORMAT(7F10.2)                                                   BRCN  41
   41 FORMAT(5F12.8)                                                   BRCN  42
   51 FORMAT(2F12.8)                                                   BRCN  43
   61 FORMAT(4F12.8)                                                   BRCN  44
C                                                                      BRCN  45
C     READ IN AND PRINT OUT INPUT DATA                                 BRCN  46
C                                                                      BRCN  47
      NNN=0                                                            BRCN  48
      READ 1270, NNCAS                                                 BRCN  49
 1270 FORMAT(I5)                                                       BRCN  50
 1272 NNN=NNN+1                                                        BRCN  51
      IF(NNN.GT.NNCAS) GO TO 1271                                      BRCN  52
      PRINT 400                                                        BRCN  53
      READ 4444,(ID(I),I=1,11)                                         BRCN  54
 4444 FORMAT(11A6)                                                     BRCN  55
      PRINT 4445,(ID(I),I=1,11)                                        BRCN  56
 4445 FORMAT(////24H PROBLEM IDENTIFICATION:, 11A6)                    BRCN  57
      PRINT 1231                                                       BRCN  58
      PRINT 411                                                        BRCN  59
      READ 1, NCASE,NVR,NPRINT,NDECIS                                  BRCN  60
      PRINT 2010                                                       BRCN  61
 2010 FORMAT(1X,6H NCASE,3X,4H NVR,1X,7H NPRINT,1X,7H NDECIS)          BRCN  62
      PRINT 2011, NCASE,NVR,NPRINT,NDECIS                              BRCN  63
 2011 FORMAT(1X,2I6,1X,I6,1X,I6)                                       BRCN  64
      READ 6, NTS                                                      BRCN  65
      READ 7, DT                                                       BRCN  66
      READ 21,EFF                                                      BRCN  67
      READ 31,F$KGHM,R$KGHM,S$KG49,S$KG28,S$KG40,S$KG41,S$KG42         BRCN  68
      READ 31, S$KG23,S$KG02                                           BRCN  69
      READ 41,TAX,BDRTE,BDFRN,SKRTE,SKFRN                              BRCN  70
      READ 51,SLF,CAPMWE                                               BRCN  71
      READ 61,   TFPRE,TMPPRE,TRPPST,TMCPST                            BRCN  72
```

```
1201 READ 1203,(PPM(K),S$DED(K),K=1,12)                                  BRCN  73
1203 FORMAT(6F12.8)                                                      BRCN  74
     PRINT 406                                                           BRCN  75
 406 FORMAT(3X,4H NTS)                                                   BRCN  76
     PRINT 416, NTS                                                      BRCN  77
 416 FORMAT(1X,I6)                                                       BRCN  78
     PRINT 407                                                           BRCN  79
 407 FORMAT(3X,3H DT)                                                    BRCN  80
     PRINT 417,DT                                                        BRCN  81
 417 FORMAT(1X,F12.8)                                                    BRCN  82
     PRINT 500                                                           BRCN  83
 500 FORMAT(1X,19H COST ANALYSIS DATA)                                   BRCN  84
     PRINT 598                                                           BRCN  85
 598 FORMAT(4X,4H EFF)                                                   BRCN  86
     PRINT 599, EFF                                                      BRCN  87
 599 FORMAT(1X,2F12.6)                                                   BRCN  88
     PRINT 531                                                           BRCN  89
 531 FORMAT(3X,7H F$KGHM,2X,3X,7H R$KGHM,2X,3X,7H S$KG49,                BRCN  90
    1  2X,3X,7H S$KG28,2X,3X,7H S$KG40,2X,3X,7H S$KG41,2X,3X,7H S$KG42,BRCN  91
    2 5X,7H S$KG23,5X,7H S$KG02)                                         BRCN  92
     PRINT 532,F$KGHM,R$KGHM,S$KG49,S$KG28,S$KG40,S$KG41,S$KG42,         BRCN  93
    1 S$KG23,S$KG02                                                      BRCN  94
 532 FORMAT(1X,2F12.8,7F12.2)                                            BRCN  95
     PRINT 541                                                           BRCN  96
 541 FORMAT(3X,4H TAX,5X,3X,6H BDRTE,3X,3X,6H BDFRN,3X,3X,6H SKRTE,3X,   BRCN  97
    1 3X,6H SKFRN)                                                       BRCN  98
     PRINT 542, TAX,BDRTE,BDFRN,SKRTE,SKFRN                              BRCN  99
 542 FORMAT(1X,5F12.8)                                                   BRCN 100
     PRINT 551                                                           BRCN 101
 551 FORMAT(3X,4H SLF,5X,3X,7H CAPMWE)                                   BRCN 102
     PRINT 552,SLF,CAPMWE                                                BRCN 103
 552 FORMAT(1X,F12.8,F12.1)                                              BRCN 104
     PRINT 561                                                           BRCN 105
 561 FORMAT(3X,6H TFPRE,3X,2X,7H TMPPRE,3X,2X,7H TRPPST,3X,2X,           BRCN 106
    1 7H TMCPST)                                                         BRCN 107
     PRINT 562,TFPRE,TMPPRE,TRPPST,TMCPST                                BRCN 108
```

```
  562 FORMAT(1X,4F12.8)                                                  BRCN 109
C                                                                        BRCN 110
C     INITIALIZE ALL VARIABLES                                           BRCN 111
C                                                                        BRCN 112
      DO 10001  J = 1,30                                                 BRCN 113
      CALL INIT(J)                                                       BRCN 114
10001 CONTINUE                                                           BRCN 115
      NCOUNT  =  0.0                                                     BRCN 116
      AHMKGL  =  0.0                                                     BRCN 117
      ATHMLD  =  0.0                                                     BRCN 118
      AVOL  =  0.0                                                       BRCN 119
      AU28MO = 0.0                                                       BRCN 120
      AP49MO = 0.0                                                       BRCN 121
      AP40MO = 0.0                                                       BRCN 122
      AP41MO = 0.0                                                       BRCN 123
      AP42MO = 0.0                                                       BRCN 124
      AT02MO=0.0                                                         BRCN 125
      AU23MO=0.0                                                         BRCN 126
      AU22MO=0.0                                                         BRCN 127
      IAR =  0                                                           BRCN 128
C                                                                        BRCN 129
C     CASE LOOP                                                          BRCN 130
C     EACH CASE IS A REGION, ZONE, OR A "LOT" OF FUEL                    BRCN 131
C     THIS LOOP EXTENDS TO THE END OF THE MAIN PROGRAM                   BRCN 132
C                                                                        BRCN 133
      DO 10 I = 1,NCASE                                                  BRCN 134
      NCOUNT  =  NCOUNT  +  1                                            BRCN 135
C     READ CARD INPUT FOR CASE # I                                       BRCN 136
 1200 READ 5, VOL                                                        BRCN 137
      DO 1210 K=1,NTS                                                    BRCN 138
      READ 1202, U28N(K),P49N(K),P40N(K),P41N(K),P42N(K),T02N(K),        BRCN 139
     1 U23N(K),U22N(K)                                                   BRCN 140
 1210 CONTINUE                                                           BRCN 141
      READ 1212,( EFTOT(K),K=1,NTS)                                      BRCN 142
 1212 FORMAT(8E10.4)                                                     BRCN 143
 1202 FORMAT(8F10.6)                                                     BRCN 144
```

```
      PRINT 400                                                                  BRCN 145
  400 FORMAT(1H1)                                                                BRCN 146
      PRINT 401                                                                  BRCN 147
  401 FORMAT(8H CASE NO)                                                         BRCN 148
      PRINT 101,I                                                                BRCN 149
  101 FORMAT(I6///)                                                              BRCN 150
C     PRINT OUT INPUT DECK IMAGE                                                 BRCN 151
      PRINT 411                                                                  BRCN 152
  411 FORMAT(12X,17H INPUT DECK IMAGE)                                           BRCN 153
      PRINT 405                                                                  BRCN 154
  405 FORMAT(3X,4H VOL)                                                          BRCN 155
      PRINT 415,VOL                                                              BRCN 156
  415 FORMAT(1X,F12.4)                                                           BRCN 157
C     MASSES IN KG FROM 2DB                                                      BRCN 158
      U28MO=U28N(1)                                                              BRCN 159
      P49MO=P49N(1)                                                              BRCN 160
      P40MO=P40N(1)                                                              BRCN 161
      P41MO=P41N(1)                                                              BRCN 162
      P42MO=P42N(1)                                                              BRCN 163
      T02MO=T02N(1)                                                              BRCN 164
      U23MO=U23N(1)                                                              BRCN 165
      U22MO=U22N(1)                                                              BRCN 166
      HMKGLD=U28MO+P49MO+P40MO+P41MO+P42MO+T02MO+U23MO+U22MO                     BRCN 167
      FAB$L=HMKGLD*F$KGHM                                                        BRCN 168
      REPR$L=HMKGLD*R$KGHM                                                       BRCN 169
      UTOTAL=U28MO+U23MO+U22MO                                                   BRCN 170
      IF(T02MO.GT.0.0) GO TO 1250                                                BRCN 171
      YVALUE=0.0                                                                 BRCN 172
      GO TO 1206                                                                 BRCN 173
 1250 IF(UTOTAL.EQ.0.0) GO TO 1220                                               BRCN 174
      XVALUE=(1.0E+06)*(U22MO/UTOTAL)                                            BRCN 175
      GO TO 1221                                                                 BRCN 176
 1220 XVALUE=0.0                                                                 BRCN 177
 1221 CALL LININT(PPM,S$DED,XVALUE,YVALUE,12)                                    BRCN 178
      IF(YVALUE.LE.2.0) GO TO 1206                                               BRCN 179
      YVALUE=2.00                                                                BRCN 180
```

```
 1206 SMP$L=U28MO*S$KG28+P49MO*S$KG49+P40MO*S$KG40+P41MO*S$KG41+P42MO*   BRCN 181
     1 S$KG42+T02MO*S$KG02+U23MO*S$KG23-UTOTAL*YVALUE*1000.             BRCN 182
       PRINT 920                                                        BRCN 183
  920 FORMAT(4X,6H U28MO,5X,4X,6H P49MO,5X,4X,6H P40MO,5X,4X,6H P41MO,5XBRCN 184
     1  ,4X,6H P42MO,5X,4X,6H T02MO,9X,6H U23MO,9X,6H U22MO,10X,7H HMKGLBRCN 185
     2D)                                                                BRCN 186
       PRINT 921, U28MO,P49MO,P40MO,P41MO,P42MO,T02MO,U23MO,U22MO,HMKGLD BRCN 187
  921 FORMAT(1X,9F14.5)                                                 BRCN 188
       PRINT 922                                                        BRCN 189
  922 FORMAT(3X,6H SMP$L,3X,3X,6H FAB$L,3X,3X,7H REPR$L)                BRCN 190
       PRINT 923, SMP$L,FAB$L,REPR$L                                    BRCN 191
  923 FORMAT(1X,3F12.2)                                                 BRCN 192
C                                                                       BRCN 193
C      LEVELIZING PARAMETERS                                            BRCN 194
C                                                                       BRCN 195
       TAXF1 = 1.0/(1.0-TAX)                                            BRCN 196
       TAXF2 = TAX/(1.0-TAX)                                            BRCN 197
       DISRTE = (1.0-TAX)*BDRTE*BDFRN  + SKRTE*SKFRN                    BRCN 198
C      ACTUAL ANNUAL ENERGY PRODUCED BY REACTOR PLANT(KWH/YEAR)         BRCN 199
       AARPE = SLF*CAPMWE*1000.0*8760.0                                 BRCN 200
       AARPT = AARPE/EFF                                                BRCN 201
       PRINT 611                                                        BRCN 202
  611 FORMAT(//3X,7H DISRTE)                                            BRCN 203
       PRINT 612, DISRTE                                                BRCN 204
  612 FORMAT(1X,F12.8)                                                  BRCN 205
       PRINT 621                                                        BRCN 206
  621 FORMAT(//3X,6H AARPE,6X,3X,6H AARPT)                              BRCN 207
       PRINT 622, AARPE,AARPT                                           BRCN 208
  622 FORMAT(1X,2E15.5)                                                 BRCN 209
       PRINT 1231                                                       BRCN 210
 1231 FORMAT(//)                                                        BRCN 211
       PRINT 1230, YVALUE                                               BRCN 212
 1230 FORMAT(' U-232 PENALTY IS ',F10.4, ' DOLLARS PER GRAM TOTAL U ')  BRCN 213
       DO 1211 K=2,NTS                                                  BRCN 214
       L=K-1                                                            BRCN 215
       U28N(L)=U28N(K)                                                  BRCN 216
```

```
      P49N(L)=P49N(K)                                                   BRCN 217
      P40N(L)=P40N(K)                                                   BRCN 218
      P41N(L)=P41N(K)                                                   BRCN 219
      P42N(L)=P42N(K)                                                   BRCN 220
      T02N(L)=T02N(K)                                                   BRCN 221
      U23N(L)=U23N(K)                                                   BRCN 222
      U22N(L)=U22N(K)                                                   BRCN 223
      EFTOT(L)=EFTOT(K)                                                 BRCN 224
 1211 CONTINUE                                                          BRCN 225
C                                                                       BRCN 226
C     TIME LOOP                                                         BRCN 227
C                                                                       BRCN 228
      N=NTS-1                                                           BRCN 229
      DO 100  J=1,N                                                     BRCN 230
      TJ = J                                                            BRCN 231
C     EQUIVALENT FULL POWER TIME                                        BRCN 232
      TIMED = TJ*DT                                                     BRCN 233
      TIME = TIMED*86400.0                                              BRCN 234
      RTIMEY=TIMED/(365.0*SLF)                                          BRCN 235
      P49M=P49N(J)                                                      BRCN 236
      U28M=U28N(J)                                                      BRCN 237
      P40M=P40N(J)                                                      BRCN 238
      P41M=P41N(J)                                                      BRCN 239
      P42M=P42N(J)                                                      BRCN 240
      T02M=T02N(J)                                                      BRCN 241
      U23M=U23N(J)                                                      BRCN 242
      U22M=U22N(J)                                                      BRCN 243
C                                                                       BRCN 244
C     CALCULATE POWER COSTS  (MILLS/KWHE)                               BRCN 245
C     POWER COSTS, DIRECT (MILLS/KWH)                                   BRCN 246
C                                                                       BRCN 247
      TPPE = 1000.0/(AARPE*RTIMEY)                                      BRCN 248
C      MATERIAL PURCHASE                                                BRCN 249
      PCMPD = SMP$L*TPPE                                                BRCN 250
C      FAB                                                              BRCN 251
      PCFBD = FAB$L*TPPE                                                BRCN 252
```

```
C       REPROCESSING                                                          BRCN 253
        PCRPD = REPR$L*TPPE                                                   BRCN 254
C       MATERIAL CREDIT                                                       BRCN 255
        UTOTAL=U28M+U23M+U22M                                                 BRCN 256
        IF(T02M.GT.0.0) GO TO 1251                                            BRCN 257
        YVALUE=0.0                                                            BRCN 258
        GO TO 1240                                                            BRCN 259
 1251   IF(UTOTAL.EQ.0.0) GO TO 1222                                          BRCN 260
        XVALUE=(1.0E+06)*(U22M/UTOTAL)                                        BRCN 261
        GO TO 1223                                                            BRCN 262
 1222   XVALUE=0.0                                                            BRCN 263
 1223   CALL LININT(PPM,S$DED,XVALUE,YVALUE,12)                               BRCN 264
        IF(YVALUE.LE.2.0) GO TO 1240                                          BRCN 265
        YVALUE=2.00                                                           BRCN 266
 1240   PRINT 1230, YVALUE                                                    BRCN 267
        SMC$L = P49M*S$KG49 + U28M*S$KG28 + P40M*S$KG40 + P41M*S$KG41         BRCN 268
       1    + P42M*S$KG42+T02M*S$KG02+U23M*S$KG23-UTOTAL*YVALUE*1000.         BRCN 269
 1209   IF(NPRINT.LT.1)  GO TO 1403                                           BRCN 270
        PRINT 301                                                             BRCN 271
  301   FORMAT(3X,6H SMC$L)                                                   BRCN 272
        PRINT 302,SMC$L                                                       BRCN 273
  302   FORMAT(1X,F12.2)                                                      BRCN 274
        PRINT 2222                                                            BRCN 275
 1403   CONTINUE                                                              BRCN 276
        PCMCD = -SMC$L*TPPE                                                   BRCN 277
C       POWER COSTS,CARRYING CHARGES (MILLS/KWH)                              BRCN 278
C       MATERIAL PURCHASE                                                     BRCN 279
        TMP = 0.5*RTIMEY + TMPPRE                                             BRCN 280
        DISFMP = 1.0/((1.0+DISRTE)**(-TMP))                                   BRCN 281
        CCFMP = TAXF1*DISFMP  -  TAXF2  -  1.0                                BRCN 282
        PCMPCC =  (PCMPD)*(CCFMP)                                             BRCN 283
        PCMPTT =  PCMPD + PCMPCC                                              BRCN 284
C       FAB                                                                   BRCN 285
        TFB = 0.5*RTIMEY  +  TFPRE                                            BRCN 286
        DISFF = 1.0/((1.0+DISRTE)**(-TFB))                                    BRCN 287
        CCFF = TAXF1*DISFF  - TAXF2  -  1.0                                   BRCN 288
```

```
      PCFBCC = (PCFBD)*(CCFF)                                                  BRCN 289
      PCFBTT =  PCFBD + PCFBCC                                                 BRCN 290
C     REPROCESSING                                                             BRCN 291
      TRP =  -(0.5*RTIMEY + TRPPST)                                            BRCN 292
      DISFRP = 1.0/((1.0+DISRTE)**(-TRP))                                      BRCN 293
      CCFRP = DISFRP  -  1.0                                                   BRCN 294
      PCRPCC = (PCRPD)*(CCFRP)                                                 BRCN 295
      PCRPTT =  PCRPD + PCRPCC                                                 BRCN 296
      CCFRPB = TAXF1*DISFRP - TAXF2 - 1.0                                      BRCN 297
      PCRPCB = (PCRPD)*(CCFRPB)                                                BRCN 298
      PCRPTB = PCRPD + PCRPCB                                                  BRCN 299
C     MATERIAL CREDIT                                                          BRCN 300
      TMC = -(0.5*RTIMEY + TMCPST)                                             BRCN 301
      DISFMC = 1.0/((1.0+DISRTE)**(-TMC))                                      BRCN 302
      CCFMC = DISFMC - 1.0                                                     BRCN 303
      PCMCCC =  (PCMCD)*(CCFMC)                                                BRCN 304
      PCMCTT =  PCMCD + PCMCCC                                                 BRCN 305
      CCFMCB = TAXF1*DISFMC - TAXF2 - 1.0                                      BRCN 306
      PCMCCB = (PCMCD)*(CCFMCB)                                                BRCN 307
      PCMCTB = PCMCD + PCMCCB                                                  BRCN 308
C                                                                              BRCN 309
C     TOTALS                                                                   BRCN 310
C                                                                              BRCN 311
C     DIRECT                                                                   BRCN 312
      PCDT=PCMPD+PCFBD+PCRPD+PCMCD                                             BRCN 313
C     CARRYING CHARGE                                                          BRCN 314
      PCCCT=PCMPCC+PCFBCC+PCRPCC+PCMCCC                                        BRCN 315
      PCCCTB = PCMPCC + PCFBCC + PCRPCB + PCMCCB                               BRCN 316
C     GRAND TOTAL                                                              BRCN 317
      PCT=PCDT+PCCCT                                                           BRCN 318
      PCTB = PCDT + PCCCTB                                                     BRCN 319
      IF(NPRINT.LT.1)  GO TO 1404                                              BRCN 320
      PRINT 303                                                                BRCN 321
  303 FORMAT(3X,6H CCFMP,3X,3X,5H CCFF,4X,3X,6H CCFRP,3X,3X,6H CCFMC)          BRCN 322
      PRINT 304,CCFMP,CCFF,CCFRP,CCFMC                                         BRCN 323
  304 FORMAT(1X,4F12.7)                                                        BRCN 324
```

```
      PRINT 30310                                                          BRCN 325
30310 FORMAT(3X,6H CCFMP,3X,3X,5H CCFF,4X,3X,7H CCFRPB,2X,3X,7H CCFMCB)    BRCN 326
      PRINT 3041, CCFMP,CCFF,CCFRPB,CCFMCB                                 BRCN 327
 3041 FORMAT(1X,4F12.7)                                                    BRCN 328
      PRINT 800                                                            BRCN 329
  800 FORMAT(//24H POWER COSTS (MILLS/KWH))                                BRCN 330
      PRINT 804                                                            BRCN 331
      PRINT 814,PCMPD,PCFBD,PCRPD,PCMCD,PCDT,PCRPD,PCMCD,PCDT              BRCN 332
      PRINT 815,PCMPCC,PCFBCC,PCRPCC,PCMCCC,PCCCT,PCRPCB,PCMCCB,PCCCTB     BRCN 333
      PRINT 816,PCMPTT,PCFBTT,PCRPTT,PCMCTT,PCT,PCRPTB,PCMCTB,PCTB         BRCN 334
 1404 CONTINUE                                                             BRCN 335
C                                                                          BRCN 336
C     SUM OR AVERAGE OVER ZONES TO OBTAIN ANNULAR REGION RESULTS           BRCN 337
C                                                                          BRCN 338
      AU28M(J)  =  AU28M(J)  +  U28M                                       BRCN 339
      AP49M(J)  =  AP49M(J)  +  P49M                                       BRCN 340
      AP40M(J)  =  AP40M(J)  +  P40M                                       BRCN 341
      AP41M(J)  =  AP41M(J)  +  P41M                                       BRCN 342
      AP42M(J)  =  AP42M(J)  +  P42M                                       BRCN 343
      AT02M(J)=AT02M(J)+T02M                                               BRCN 344
      AU23M(J)=AU23M(J)+U23M                                               BRCN 345
      AU22M(J)=AU22M(J)+U22M                                               BRCN 346
      AMPD(J)  =  AMPD(J)  +  PCMPD                                        BRCN 347
      AMPCC(J)  =  AMPCC(J)  +  PCMPCC                                     BRCN 348
      AMPTT(J)  =  AMPTT(J)  +  PCMPTT                                     BRCN 349
      AFBD(J)  =  AFBD(J)  +  PCFBD                                        BRCN 350
      AFBCC(J)  =  AFBCC(J)  +  PCFBCC                                     BRCN 351
      AFBTT(J)  =  AFBTT(J)  +  PCFBTT                                     BRCN 352
      ARPD(J)  =  ARPD(J)  +  PCRPD                                        BRCN 353
      ARPCC(J)  =  ARPCC(J)  +  PCRPCC                                     BRCN 354
      ARPTT(J)  =  ARPTT(J)  +  PCRPTT                                     BRCN 355
      AMCD(J)  =  AMCD(J)  +  PCMCD                                        BRCN 356
      AMCCC(J)  =  AMCCC(J)  +  PCMCCC                                     BRCN 357
      AMCTT(J)  =  AMCTT(J)  +  PCMCTT                                     BRCN 358
      ADT(J)  =  ADT(J)  +  PCDT                                           BRCN 359
      ACCT(J)  =  ACCT(J)  +  PCCCT                                        BRCN 360
```

```
      AT(J)  =  AT(J)  +  PCT                                          BRCN 361
      ARPCCB(J) = ARPCCB(J) + PCRPCB                                   BRCN 362
      ARPTTB(J) = ARPTTB(J) + PCRPTB                                   BRCN 363
      AMCCCB(J) = AMCCCB(J) + PCMCCB                                   BRCN 364
      AMCTTB(J)  =  AMCTTB(J) + PCMCTB                                 BRCN 365
      ACCTB(J) = ACCTB(J) + PCCCTB                                     BRCN 366
      ATB(J) = ATB(J) + PCTB                                           BRCN 367
      SFTV(J)=0.0                                                      BRCN 368
      AEFTOT(J)  =  AEFTOT(J)  +  EFTOT(J)                             BRCN 369
  100 CONTINUE                                                         BRCN 370
      AHMKGL  =  AHMKGL  +  HMKGLD                                     BRCN 371
      ATHMLD  =  AHMKGL/ 1000.0                                        BRCN 372
      AVOL  =  AVOL  +  VOL                                            BRCN 373
      CONV1 = 1.0/AHMKGL                                               BRCN 374
      AU28MO = AU28MO + U28MO                                          BRCN 375
      AP49MO = AP49MO + P49MO                                          BRCN 376
      AP40MO = AP40MO + P40MO                                          BRCN 377
      AP41MO = AP41MO + P41MO                                          BRCN 378
      AP42MO = AP42MO + P42MO                                          BRCN 379
      AT02MO=AT02MO+T02MO                                              BRCN 380
      AU23MO=AU23MO+U23MO                                              BRCN 381
      AU22MO=AU22MO+U22MO                                              BRCN 382
      A28MRO = AU28MO*CONV1                                            BRCN 383
      A49MRO = AP49MO*CONV1                                            BRCN 384
      A40MRO = AP40MO*CONV1                                            BRCN 385
      A41MRO = AP41MO*CONV1                                            BRCN 386
      A42MRO = AP42MO*CONV1                                            BRCN 387
      A02MRO=AT02MO*CONV1                                              BRCN 388
      A23MRO=AU23MO*CONV1                                              BRCN 389
      A22MRO=AU22MO*CONV1                                              BRCN 390
      EPSO = A49MRO + A41MRO + A23MRO                                  BRCN 391
      IF(NCOUNT.LT.NVR)  GO TO 10                                      BRCN 392
      IAR  =  IAR + 1                                                  BRCN 393
      PRINT 400                                                        BRCN 394
      PRINT 1001                                                       BRCN 395
 1001 FORMAT(3X,23H ANNULAR REGION RESULTS)                            BRCN 396
```

```
      PRINT 1002                                                        BRCN 397
 1002 FORMAT(//6X,4H IAR)                                               BRCN 398
      PRINT 1003, IAR                                                   BRCN 399
 1003 FORMAT(6X,I2)                                                     BRCN 400
      PRINT 2001                                                        BRCN 401
 2001 FORMAT(//5X,5H AVOL,5X,4X,7H AHMKGL)                              BRCN 402
      PRINT 2002,  AVOL, AHMKGL                                         BRCN 403
 2002 FORMAT(1X,2E15.5)                                                 BRCN 404
      PRINT 2222                                                        BRCN 405
      PRINT 1004                                                        BRCN 406
      RTIMEY = 0.0                                                      BRCN 407
      TIMED = 0.0                                                       BRCN 408
      PRINT 1005, RTIMEY, TIMED                                         BRCN 409
      PRINT 1006                                                        BRCN 410
      PRINT 1007, AU28MO,AP49MO,AP40MO,AP41MC,AP42MC                    BRCN 411
     1,AT02MO,AU23MO,AU22MO                                             BRCN 412
      PRINT 10071                                                       BRCN 413
      PRINT 1107,A28MRO,A49MRO,A40MRO,A41MRO,A42MRO                     BRCN 414
     1 , A02MRO,A23MRO,A22MRO,EPSO                                      BRCN 415
      CONV  =  AARPE/(1000.0*AHMKGL)                                    BRCN 416
      N=NTS-1                                                           BRCN 417
      DO 10000   J=1,N                                                  BRCN 418
      FAMPD(J)  =  AMPD(J)*CONV                                         BRCN 419
      FAMPCC(J)  =  AMPCC(J)*CONV                                       BRCN 420
      FAMPTT(J)  =  AMPTT(J)*CONV                                       BRCN 421
      FAFBD(J)  =  AFBD(J)*CONV                                         BRCN 422
      FAFBCC(J)  =  AFBCC(J)*CONV                                       BRCN 423
      FAFBTT(J)  =  AFBTT(J)*CONV                                       BRCN 424
      FARPD(J)  =  ARPD(J)*CONV                                         BRCN 425
      FARPCC(J)  =  ARPCC(J)*CONV                                       BRCN 426
      FARPTT(J)  =  ARPTT(J)*CONV                                       BRCN 427
      FAMCD(J)  =  AMCD(J)*CONV                                         BRCN 428
      FAMCCC(J)  =  AMCCC(J)*CONV                                       BRCN 429
      FAMCTT(J)  =  AMCTT(J)*CONV                                       BRCN 430
      FADT(J)  =  ADT(J)*CONV                                           BRCN 431
      FACCT(J)  =  ACCT(J)*CONV                                         BRCN 432
```

```
      FAT(J)   =   AT(J)*CONV                                          BRCN 433
      FARPCB(J) = ARPCCB(J)*CONV                                       BRCN 434
      FAMCCB(J) = AMCCCB(J)*CONV                                       BRCN 435
      FACCTB(J) = ACCTB(J)*CONV                                        BRCN 436
      FATB(J) = ATB(J)*CONV                                            BRCN 437
      FARPTB(J) = ARPTTB(J)*CONV                                       BRCN 438
      FAMCTB(J) = AMCTTB(J)*CONV                                       BRCN 439
C                                                                      BRCN 440
C     OTHER GROUPINGS OF COSTS                                         BRCN 441
C                                                                      BRCN 442
      ABU(J) = AMPD(J) + AMCD(J)                                       BRCN 443
      AINV(J) = AMPCC(J) + AMCCC(J)                                    BRCN 444
      AINVB(J) = AMPCC(J) + AMCCCB(J)                                  BRCN 445
      AMAT(J) = ABU(J) + AINV(J)                                       BRCN 446
      AMATB(J) = ABU(J) + AINVB(J)                                     BRCN 447
      APRSD(J) = AFBD(J) + ARPD(J)                                     BRCN 448
      APRSC(J) = AFBCC(J) + ARPCC(J)                                   BRCN 449
      APRST(J) = APRSD(J) + APRSC(J)                                   BRCN 450
      APRSCB(J) = AFBCC(J) + ARPCCB(J)                                 BRCN 451
      APRSTB(J) = APRSD(J) + APRSCB(J)                                 BRCN 452
      AAT(J)   =  AMAT(J) + APRST(J)                                   BRCN 453
      AATB(J) = AMATB(J) + APRSTB(J)                                   BRCN 454
      AADT(J) = ABU(J) + APRSD(J)                                      BRCN 455
      AACCT(J) = AINV(J) + APRSC(J)                                    BRCN 456
      AACCTB(J) = AINVB(J) + APRSCB(J)                                 BRCN 457
      AFT(J)=0.0                                                       BRCN 458
      ABNUP(J)   =  AEFTOT(J)/ATHMLD                                   BRCN 459
      A28MR(J) = AU28M(J)*CONV1                                        BRCN 460
      A49MR(J) = AP49M(J)*CONV1                                        BRCN 461
      A40MR(J) = AP40M(J)*CONV1                                        BRCN 462
      A41MR(J) = AP41M(J)*CONV1                                        BRCN 463
      A42MR(J) = AP42M(J)*CONV1                                        BRCN 464
      A02MR(J)=AT02M(J)*CONV1                                          BRCN 465
      A23MR(J)=AU23M(J)*CONV1                                          BRCN 466
      A22MR(J)=AU22M(J)*CONV1                                          BRCN 467
      EPS(J) = A49MR(J)  +  A41MR(J) + A23MR(J)                        BRCN 468
```

```
      TJ  =  J                                                                  BRCN 469
      TIMED =  TJ*DT                                                            BRCN 470
      RTIMEY  =  TIMED/(365.0*SLF)                                              BRCN 471
      TIME  =  TIMED*86400.0                                                    BRCN 472
      PRINT 400                                                                 BRCN 473
      PRINT 1004                                                                BRCN 474
 1004 FORMAT(45X,7H RTIMEY,6X,6H TIMED)                                         BRCN 475
      PRINT 1005,  RTIMEY,TIMED                                                 BRCN 476
 1005 FORMAT(44X,F12.8,3X,F12.4)                                                BRCN 477
      TERTR = AARPT*RTIMEY/(24.0*1000.0)                                        BRCN 478
      APFRN  =  AEFTOT(J)/TERTR                                                 BRCN 479
      PRINT 2003                                                                BRCN 480
 2003 FORMAT(5X,4H AFT,6X,4X,7H AEFTOT,4X,4X,6H ABNUP,5X,                       BRCN 481
     1  4X,6H APFRN)                                                           BRCN 482
      PRINT 2004,AFT(J),AEFTOT(J),ABNUP(J),APFRN                                BRCN 483
 2004 FORMAT(1X,4E15.5)                                                         BRCN 484
      PRINT 1006                                                                BRCN 485
 1006 FORMAT(5X,6H AU28M,4X,5X,6H AP49M,4X,                                     BRCN 486
     1      5X,6H AP40M,4X,5X,6H AP41M,4X,5X,6H AP42M,9X,6H AT02M,9X,          BRCN 487
     26H AU23M,9X,6H AU22M)                                                     BRCN 488
      PRINT 1007, AU28M(J),AP49M(J),AP40M(J),AP41M(J),AP42M(J)                  BRCN 489
     1 , AT02M(J),AU23M(J),AU22M(J)                                             BRCN 490
 1007 FORMAT(1X,8E14.5)                                                         BRCN 491
      PRINT 10071                                                               BRCN 492
10071 FORMAT(4X,6H A28MR,5X,4X,6H A49MR,5X,4X,6H A40MR,5X,                      BRCN 493
     1  4X,6H A41MR,5X,4X,6H A42MR,9X,6H A02MR,9X,6H A23MR,9X,6H A22MR,         BRCN 494
     2 9X,4H EPS)                                                               BRCN 495
      PRINT 1107,A28MR(J),A49MR(J),A40MR(J),A41MR(J),A42MR(J),                  BRCN 496
     1 A02MR(J),A23MR(J),A22MR(J),EPS(J)                                        BRCN 497
 1107 FORMAT(1X,9F14.5)                                                         BRCN 498
      TMP = 0.5*RTIMEY  +  TMPPRE                                               BRCN 499
      DISFMP = 1.0/((1.0+DISRTE)**(-TMP))                                       BRCN 500
      CCFMP  =  TAXF1*DISFMP  -  TAXF2  -  1.0                                  BRCN 501
      TFB = 0.5*RTIMEY  +  TFPRE                                                BRCN 502
      DISFF = 1.0/((1.0+DISRTE)**(-TFB))                                        BRCN 503
      CCFF =  TAXF1*DISFF -TAXF2  -  1.0                                        BRCN 504
```

```
      TRP  =  -(0.5*RTIMEY  +  TRPPST)                                  BRCN 505
      DISFRP  =  1.0/((1.0+DISRTE)**(-TRP))                             BRCN 506
      CCFRP = DISFRP - 1.0                                              BRCN 507
      CCFRPB  =  TAXF1*DISFRP - TAXF2 - 1.0                             BRCN 508
      TMC = -(0.5*RTIMEY + TMCPST)                                      BRCN 509
      DISFMC = 1.0/((1.0+DISRTE)**(-TMC))                               BRCN 510
      CCFMC = DISFMC - 1.0                                              BRCN 511
      CCFMCB = TAXF1*DISFMC - TAXF2 - 1.0                               BRCN 512
      PRINT 303                                                         BRCN 513
      PRINT 304,CCFMP,CCFF,CCFRP,CCFMC                                  BRCN 514
      PRINT 30310                                                       BRCN 515
      PRINT 3041,CCFMP,CCFF,CCFRPB,CCFMCB                               BRCN 516
      PRINT 1008                                                        BRCN 517
 1008 FORMAT(//24H POWER COSTS (MILLS/KWH))                             BRCN 518
      PRINT 804                                                         BRCN 519
      PRINT 814,AMPD(J),AFBD(J),ARPD(J),AMCD(J),ADT(J),ARPD(J),AMCD(J),  BRCN 520
     1  ADT(J)                                                         BRCN 521
      PRINT 815,AMPCC(J),AFBCC(J),ARPCC(J),AMCCC(J),ACCT(J),ARPCCB(J),  BRCN 522
     1   AMCCCB(J),ACCTB(J)                                           BRCN 523
      PRINT 816,AMPTT(J),AFBTT(J),ARPTT(J),AMCTT(J),AT(J),ARPTTB(J),    BRCN 524
     1  AMCTTB(J),ATB(J)                                              BRCN 525
      PRINT 3030                                                        BRCN 526
      PRINT 3032, ABU(J),APRSD(J),AADT(J)                               BRCN 527
      PRINT 3033,AINV(J),APRSC(J),AACCT(J)                              BRCN 528
      PRINT 3034, AMAT(J),APRST(J),AAT(J)                               BRCN 529
      PRINT 3031                                                        BRCN 530
      PRINT 3032, ABU(J), APRSD(J),AADT(J)                              BRCN 531
      PRINT 3033,AINVB(J),APRSCB(J),AACCTB(J)                           BRCN 532
      PRINT 3034, AMATB(J),APRSTB(J),AATB(J)                            BRCN 533
      IF(NDECIS.EQ.1) GO TO 1225                                        BRCN 534
      PRINT 400                                                         BRCN 535
      PRINT 1013                                                        BRCN 536
 1013 FORMAT(//30H POWER COSTS ($/YR/KGHMLOADED))                       BRCN 537
      PRINT 804                                                         BRCN 538
      PRINT 1014, FAMPD(J),FAFBD(J),FARPD(J),FAMCD(J),FADT(J),          BRCN 539
     1  FARPD(J),FAMCD(J),FADT(J)                                       BRCN 540
```

```
      PRINT 1015, FAMPCC(J),FAFBCC(J),FARPCC(J),FAMCCC(J),FACCT(J),      BRCN 541
     1    FARPCB(J),FAMCCB(J),FACCTB(J)                                   BRCN 542
      PRINT 1016, FAMPTT(J),FAFBTT(J),FARPTT(J),FAMCTT(J),FAT(J),        BRCN 543
     1    FARPTB(J),FAMCTB(J),FATB(J)                                     BRCN 544
 1225 CONTINUE                                                            BRCN 545
      ABU(J) = ABU(J)*CONV                                                BRCN 546
      AINV(J) = AINV(J)*CONV                                              BRCN 547
      AINVB(J) = AINVB(J)*CONV                                            BRCN 548
      AMAT(J) = AMAT(J)*CONV                                              BRCN 549
      AMATB(J) = AMATB(J)*CONV                                            BRCN 550
      APRSD(J) = APRSD(J)*CONV                                            BRCN 551
      APRSC(J)  =  APRSC(J)*CONV                                          BRCN 552
      APRST(J) = APRST(J)*CONV                                            BRCN 553
      APRSCB(J) = APRSCB(J)*CONV                                          BRCN 554
      APRSTB(J) = APRSTB(J)*CONV                                          BRCN 555
      AAT(J) = AAT(J)*CONV                                                BRCN 556
      AATB(J) = AATB(J)*CONV                                              BRCN 557
      AADT(J) = AADT(J)*CONV                                              BRCN 558
      AACCT(J) = AACCT(J)*CONV                                            BRCN 559
      AACCTB(J) = AACCTB(J)*CONV                                          BRCN 560
      IF(NDECIS.EQ.1) GO TO 1226                                          BRCN 561
      PRINT 3030                                                          BRCN 562
      PRINT 3042, ABU(J),APRSD(J),AADT(J)                                 BRCN 563
      PRINT 3043, AINV(J),APRSC(J),AACCT(J)                               BRCN 564
      PRINT 3044, AMAT(J),APRST(J),AAT(J)                                 BRCN 565
      PRINT 3031                                                          BRCN 566
      PRINT 3042, ABU(J),APRSD(J),AADT(J)                                 BRCN 567
      PRINT 3043, AINVB(J), APRSCB(J),AACCTB(J)                           BRCN 568
      PRINT 3044, AMATB(J),APRSTB(J),AATB(J)                              BRCN 569
 1226 CONTINUE                                                            BRCN 570
 2222 FORMAT(//5X,80H METHOD(A): (MATCRE-REPR) IS TAXED.     METHOD(B): BRCN 571
     1(MATCRE-REPR) IS CAPITALIZED.)                                      BRCN 572
  804 FORMAT(2X,7H MATPUR,3X,4X,4H FAB,4X,3X,8H REPR(A),1X,2X,            BRCN 573
     1  10 H MATCRE(A),3X,4X,10H TOTALS(A),7X,8H REPR(B),1X,2X,          BRCN 574
     2   10H MATCRE(B),3X,4X,10H TOTALS(B))                              BRCN 575
  814 FORMAT(1X,4F12.8,4X,F12.8,5X,2F12.8,4X,F12.8,5X,7H DIRECT)          BRCN 576
```

```
 815 FORMAT(1X,4F12.8,4X,F12.8,5X,2F12.8 ,4X,F12.8,5X,7H CARCHG)          BRCN 577
 816 FORMAT(1X,4F12.8,4X,F12.8,5X,2F12.8,4X,F12.8,5X,7H TOTALS)          BRCN 578
1014 FORMAT(1X,4F12.2,4X,F12.2,5X,2F12.2,4X,F12.2,5X,7H DIRECT)          BRCN 579
1015 FORMAT(1X,4F12.2,4X,F12.2,5X,2F12.2,4X,F12.2,5X,7H CARCHG)          BRCN 580
1016 FORMAT(1X,4F12.2,4X,F12.2,5X,2F12.2,4X,F12.2,5X,7H TOTALS)          BRCN 581
3030 FORMAT(3X,9H MATERIAL,18X,3X,11H PROCESSING,16X,3X,7H TOTALS,20X,   BRCN 582
    1     10H METHOD(A))                                                 BRCN 583
3031 FORMAT(3X,9H MATERIAL,18X,3X,11H PROCESSING,16X,3X,7H TOTALS,20X,   BRCN 584
    1     10H METHOD(B))                                                 BRCN 585
3032 FORMAT(6X,8H DIR(BU),4X,F12.8,6X,4H DIR,8X,F12.8,6X,F12.8,          BRCN 586
    1 7H DIRECT)                                                         BRCN 587
3033 FORMAT(6X,12H CARCHG(INV),F12.8,6X,7H CARCHG,5X,F12.8,6X,F12.8,     BRCN 588
    1 7H CARCHG)                                                         BRCN 589
3034 FORMAT(6X,7H TOTMAT,5X,F12.8,6X,8H TOTPROC,4X,F12.8,6X,F12.8,       BRCN 590
    1 7H TOTALS)                                                         BRCN 591
3042 FORMAT(6X,8H DIR(BU),4X,F12.2,6X,4H DIR,8X,F12.2,6X,F12.2,          BRCN 592
    1 7H DIRECT)                                                         BRCN 593
3043 FORMAT(6X,12H CARCHG(INV),F12.2,6X,7H CARCHG,5X,F12.2,6X,F12.2,     BRCN 594
    1  7H CARCHG)                                                        BRCN 595
3044 FORMAT(6X,7H TOTMAT,5X,F12.2,6X,8H TOTPROC,4X,F12.2,6X,F12.2,       BRCN 596
    1  7H TOTALS)                                                        BRCN 597
     IF(NDECIS.EQ.1) GO TO 1227                                          BRCN 598
     PRINT 4013                                                          BRCN 599
4013 FORMAT(//27H POWER COSTS ($/KGHMLOADED))                            BRCN 600
1227 CONTINUE                                                            BRCN 601
     FAMPD(J) = FAMPD(J)      * RTIMEY                                   BRCN 602
     FAFBD(J) = FAFBD(J)      * RTIMEY                                   BRCN 603
     FARPD(J) = FARPD(J)      * RTIMEY                                   BRCN 604
     FAMCD(J) = FAMCD(J)      * RTIMEY                                   BRCN 605
     FADT(J) = FADT(J)        * RTIMEY                                   BRCN 606
     FAMPCC(J) = FAMPCC(J)    * RTIMEY                                   BRCN 607
     FAFBCC(J) = FAFBCC(J)    * RTIMEY                                   BRCN 608
     FARPCC(J) = FARPCC(J)    * RTIMEY                                   BRCN 609
     FAMCCC(J) = FAMCCC(J)    * RTIMEY                                   BRCN 610
     FACCT(J) = FACCT(J)   * RTIMEY                                      BRCN 611
     FARPCB(J)=FARPCB(J)      * RTIMEY                                   BRCN 612
```

```
      FAMCCB(J) = FAMCCB(J)    * RTIMEY                                  BRCN 613
      FACCTB(J) = FACCTB(J)    * RTIMEY                                  BRCN 614
      FAMPTT(J) = FAMPTT(J)    * RTIMEY                                  BRCN 615
      FAFBTT(J) = FAFBTT(J)    * RTIMEY                                  BRCN 616
      FARPTT(J) = FARPTT(J)    * RTIMEY                                  BRCN 617
      FAMCTT(J) = FAMCTT(J)    * RTIMEY                                  BRCN 618
      FAT(J) = FAT(J)          * RTIMEY                                  BRCN 619
      FARPTB(J) = FARPTB(J)    * RTIMEY                                  BRCN 620
      FAMCTB(J) = FAMCTB(J)    * RTIMEY                                  BRCN 621
      FATB(J) = FATB(J)        * RTIMEY                                  BRCN 622
      ABU(J) = ABU(J)          * RTIMEY                                  BRCN 623
      AINV(J) = AINV(J)*RTIMEY                                           BRCN 624
      AINVB(J) = AINVB(J)      * RTIMEY                                  BRCN 625
      AMAT(J) = AMAT(J)        * RTIMEY                                  BRCN 626
      AMATB(J) = AMATB(J)      * RTIMEY                                  BRCN 627
      APRSD(J) = APRSD(J)      * RTIMEY                                  BRCN 628
      APRSC(J) = APRSC(J)      * RTIMEY                                  BRCN 629
      APRST(J) = APRST(J)      * RTIMEY                                  BRCN 630
      APRSCB(J) = APRSCB(J)    * RTIMEY                                  BRCN 631
      APRSTB(J) = APRSTB(J)    * RTIMEY                                  BRCN 632
      AAT(J) = AAT(J)          * RTIMEY                                  BRCN 633
      AATB(J) = AATB(J)        * RTIMEY                                  BRCN 634
      AADT(J) = AADT(J)        * RTIMEY                                  BRCN 635
      AACCT(J) = AACCT(J)      * RTIMEY                                  BRCN 636
      AACCTB(J) = AACCTB(J)    * RTIMEY                                  BRCN 637
      IF(NDECIS.EQ.1) GO TO 1228                                         BRCN 638
      PRINT 804                                                          BRCN 639
      PRINT 1014, FAMPD(J),FAFBD(J),FARPD(J),FAMCD(J),FADT(J),           BRCN 640
     1  FARPD(J),FAMCD(J),FADT(J)                                        BRCN 641
      PRINT 1015, FAMPCC(J),FAFBCC(J),FARPCC(J),FAMCCC(J),FACCT(J),      BRCN 642
     1    FARPCB(J),FAMCCB(J),FACCTB(J)                                  BRCN 643
      PRINT 1016, FAMPTT(J),FAFBTT(J),FARPTT(J),FAMCTT(J),FAT(J),        BRCN 644
     1    FARPTB(J),FAMCTB(J),FATB(J)                                    BRCN 645
      PRINT 3030                                                         BRCN 646
      PRINT 3042, ABU(J),APRSD(J),AADT(J)                                BRCN 647
      PRINT 3043, AINV(J),APRSC(J),AACCT(J)                              BRCN 648
```

```
      PRINT 3044, AMAT(J),APRST(J),AAT(J)                                BRCN 649
      PRINT 3031                                                         BRCN 650
      PRINT 3042, ABU(J),APRSD(J),AADT(J)                                BRCN 651
      PRINT 3043, AINVB(J), APRSCB(J),AACCTB(J)                          BRCN 652
      PRINT 3044, AMATB(J),APRSTB(J),AATB(J)                             BRCN 653
 1228 CONTINUE                                                           BRCN 654
      RMCD  =  FAMCD(J)/(FAMPD(J)+FAFBD(J)+FARPD(J))                     BRCN 655
      RMCT = FAMCTT(J)/(FAMPTT(J)+FAFBTT(J)+FARPTT(J))                   BRCN 656
      RMCTB = FAMCTB(J)/(FAMPTT(J)+FAFBTT(J)+FARPTB(J))                  BRCN 657
      PRINT 8210                                                         BRCN 658
 8210 FORMAT(//5X,23H MATCRE/MATPUR+FAB+REPR)                            BRCN 659
      PRINT 8211                                                         BRCN 660
 8211 FORMAT(3X,7H DIRECT,2X,3X,7H TOT(A),2X,3X,7H TOT(B))               BRCN 661
      PRINT 8212, RMCD,RMCT,RMCTB                                        BRCN 662
 8212 FORMAT(1X,3F12.6)                                                  BRCN 663
      CALL INIT(J)                                                       BRCN 664
10000 CONTINUE                                                          BRCN 665
      NCOUNT  =  0.0                                                     BRCN 666
      AHMKGL  =  0.0                                                     BRCN 667
      ATHMLD  =  0.0                                                     BRCN 668
      AVOL  =  0.0                                                       BRCN 669
      AU28MO = 0.0                                                       BRCN 670
      AP49MO = 0.0                                                       BRCN 671
      AP40MO = 0.0                                                       BRCN 672
      AP41MO = 0.0                                                       BRCN 673
      AP42MO = 0.0                                                       BRCN 674
      AT02MO=0.0                                                         BRCN 675
      AU23MO=0.0                                                         BRCN 676
      AU22MO=0.0                                                         BRCN 677
      APERN = 0.0                                                        BRCN 678
   10 CONTINUE                                                           BRCN 679
      GO TO 1272                                                         BRCN 680
 1271 CONTINUE                                                           BRCN 681
      STOP                                                               BRCN 682
      END                                                                BRCN 683
```

```
      SUBROUTINE LININT(X,Y,XVALUE,YVALUE,NUM)                          BRCN 684
CC                                                                      BRCN 685
CC    LINEAR INTERPOLATION                                              BRCN 686
CC                                                                      BRCN 687
      DIMENSION X(50), Y(50)                                            BRCN 688
CC                                                                      BRCN 689
      IF(XVALUE-X(1))900,1000,1010                                      BRCN 690
  900 M1=1                                                              BRCN 691
      M2=M1+1                                                           BRCN 692
      GO TO 2000                                                        BRCN 693
 1000 YVALUE=Y(1)                                                       BRCN 694
      GO TO 9000                                                        BRCN 695
 1010 CONTINUE                                                          BRCN 696
      DO 1040 M=2,NUM                                                   BRCN 697
      IF(XVALUE-X(M)) 1050,1030,1040                                    BRCN 698
 1030 YVALUE=Y(M)                                                       BRCN 699
      GO TO 9000                                                        BRCN 700
 1040 CONTINUE                                                          BRCN 701
 1050 M1=M-1                                                            BRCN 702
      M2=M1+1                                                           BRCN 703
 2000 YVALUE=Y(M1)-((X(M1)-XVALUE)*(Y(M1)-Y(M2)))/(X(M1)-X(M2))         BRCN 704
 9000 RETURN                                                            BRCN 705
      END                                                               BRCN 706
```

```
      SUBROUTINE INIT(J)                                                BRCN 707
C                                                                       BRCN 708
C     THIS SUBROUTINE PERFORMS VARIABLE INITIALIZATION                  BRCN 709
C                                                                       BRCN 710
      COMMON      AU28M(30),AP49M(30),AP40M(30),AP41M(30),AP42M(30)     BRCN 711
      COMMON      AMPD(30),AFBD(30),ARPD(30),AMCD(30),ADT(30),          BRCN 712
     1            AMPCC(30),AFBCC(30),ARPCC(30),AMCCC(30),ACCT(30),     BRCN 713
     2            AMPTT(30),AFBTT(30),ARPTT(30),AMCTT(30),AT(30)        BRCN 714
      COMMON      FAMPD(30),FAFBD(30),FARPD(30),FAMCD(30),FADT(30),     BRCN 715
     1            FAMPCC(30),FAFBCC(30),FARPCC(30),FAMCCC(30),FACCT(30),BRCN 716
     2            FAMPTT(30),FAFBTT(30),FARPTT(30),FAMCTT(30),FAT(30)   BRCN 717
      COMMON      AEFTOT(30),ABNUP(30),SFTV(30),AFT(30),EFTOT(30)       BRCN 718
      COMMON       ARPCCB(30),ARPTTB(30),AMCCCB(30),AMCTTB(30),         BRCN 719
     1   ACCTB(30),ATB(30)                                              BRCN 720
      COMMON       FARPCB(30),FAMCCB(30),FACCTB(30),FARPTB(30),         BRCN 721
     1  FAMCTB(30),FATB(30)                                             BRCN 722
      COMMON      A28MR(30),A49MR(30),A40MR(30),A41MR(30),A42MR(30),    BRCN 723
     1  EPS(30)                                                         BRCN 724
      COMMON      ABU(30),AINV(30),AINVB(30),AMAT(30),AMATB(30),APRSD(30)BRCN 725
     1  ,APRSC(30),APRST(30),APRSCB(30),AAT(30),AATB(30),AADT(30),      BRCN 726
     2  AACCT(30),AACCTB(30)                                            BRCN 727
      COMMON      APRSTB(30)                                            BRCN 728
      COMMON      ID(11)                                                BRCN 729
      DOUBLE PRECISION  ID                                              BRCN 730
      COMMON     U28N(30),P49N(30),P40N(30),P41N(30),P42N(30),          BRCN 731
     1 T02N(30),U23N(30),U22N(30),PPM(20),S$DED(20)                     BRCN 732
      COMMON     AT02M(30),AU23M(30),AU22M(30),A02MR(30),A23MR(30),     BRCN 733
     1 A22MR(30)                                                        BRCN 734
      AU28M(J)   =   0.0                                                BRCN 735
      AP49M(J)   =   0.0                                                BRCN 736
      AP40M(J)   =   0.0                                                BRCN 737
      AP41M(J)   =   0.0                                                BRCN 738
      AP42M(J)   =   0.0                                                BRCN 739
      AT02M(J)=0.0                                                      BRCN 740
      AU23M(J)=0.0                                                      BRCN 741
      AU22M(J)=0.0                                                      BRCN 742
```

```
 AMPD(J)   =  0.0
FAMPD(J)   =  0.0
 AFBD(J)   =  0.0
FAFBD(J)   =  0.0
 ARPD(J)   =  0.0
FARPD(J)   =  0.0
 AMCD(J)   =  0.0
FAMCD(J)   =  0.0
 ADT(J)   =  0.0
FADT(J)   =  0.0
 AMPCC(J)   =  0.0
FAMPCC(J)   =  0.0
 AFBCC(J)   =  0.0
FAFBCC(J)   =  0.0
 ARPCC(J)   =  0.0
FARPCC(J)   =  0.0
 AMCCC(J)   =  0.0
FAMCCC(J)   =  0.0
 ACCT(J)   =  0.0
FACCT(J)   =  0.0
 AMPTT(J)   =  0.0
FAMPTT(J)   =  0.0
 AFBTT(J)   =  0.0
FAFBTT(J)   =  0.0
 ARPTT(J)   =  0.0
FARPTT(J)   =  0.0
 AMCTT(J)   =  0.0
FAMCTT(J)   =  0.0
 AT(J)   =  0.0
FAT(J)   =  0.0
ARPCCB(J) = 0.0
ARPTTB(J) = 0.0
AMCCCB(J) = 0.0
AMCTTB(J) = 0.0
ACCTB(J) = 0.0
ATB(J) = 0.0
```

```
BRCN 743
BRCN 744
BRCN 745
BRCN 746
BRCN 747
BRCN 748
BRCN 749
BRCN 750
BRCN 751
BRCN 752
BRCN 753
BRCN 754
BRCN 755
BRCN 756
BRCN 757
BRCN 758
BRCN 759
BRCN 760
BRCN 761
BRCN 762
BRCN 763
BRCN 764
BRCN 765
BRCN 766
BRCN 767
BRCN 768
BRCN 769
BRCN 770
BRCN 771
BRCN 772
BRCN 773
BRCN 774
BRCN 775
BRCN 776
BRCN 777
BRCN 778
```

```
      FARPCB(J) = 0.0                                                   BRCN 779
      FAMCCB(J) = 0.0                                                   BRCN 780
      FACCTB(J) = 0.0                                                   BRCN 781
      FARPTB(J) = 0.0                                                   BRCN 782
      FAMCTB(J) = 0.0                                                   BRCN 783
      FATB(J) = 0.0                                                     BRCN 784
      A28MR(J)  =  0.0                                                  BRCN 785
      A49MR(J)  =  0.0                                                  BRCN 786
      A40MR(J)  =  0.0                                                  BRCN 787
      A41MR(J)  =  0.0                                                  BRCN 788
      A42MR(J)  =  0.0                                                  BRCN 789
      A02MR(J)=0.0                                                      BRCN 790
      A23MR(J)=0.0                                                      BRCN 791
      A22MR(J)=0.0                                                      BRCN 792
      FPS(J)  =  0.0                                                    BRCN 793
      ABU(J) = 0.0                                                      BRCN 794
      AINV(J)  =  0.0                                                   BRCN 795
      AINVB(J)  =  0.0                                                  BRCN 796
      AMAT(J)  =  0.0                                                   BRCN 797
      AMATB(J)  =  0.0                                                  BRCN 798
      APRSD(J)  =  0.0                                                  BRCN 799
      APRSC(J)  =  0.0                                                  BRCN 800
      APRST(J)  =  0.0                                                  BRCN 801
      APRSCB(J)  =  0.0                                                 BRCN 802
      APRSTB(J)  =  0.0                                                 BRCN 803
      AAT(J)  =  0.0                                                    BRCN 804
      AATB(J)  =  0.0                                                   BRCN 805
      AADT(J)  =  0.0                                                   BRCN 806
      AACCT(J)  =  0.0                                                  BRCN 807
      AACCTB(J)  =  0.0                                                 BRCN 808
      AEFTOT(J)  =  0.0                                                 BRCN 809
      ABNUP(J)  =  0.0                                                  BRCN 810
      SFTV(J)  =  0.0                                                   BRCN 811
      AFT(J)  =  0.0                                                    BRCN 812
      RETURN                                                            BRCN 813
      END                                                               BRCN 814
```

Appendix D References

(A1) Allen, W.O., D.J. Stoker, and A.V. Campise, "Fast Breeder Reactors with Mixed Fuel Cycles", Proceedings of Second International Thorium Fuel Cycle Symposium, Gatlinburg, Tennessee (May, 1966).

(A2) Asmussen, K.E., and R.K. Lane, "U-233 Indifference Value for Use in HTGRS", Gulf-GA-A12204 (August, 1972).

(A3) Andersson, T.L., et al., "Experimental and Theoretical Work at the Zero Energy Fast Reactor FRO", Proceedings of the International Conference on Fast Critical Experiments and Their Analysis, ANL-7320, pp. 159-185 (October, 1966).

(A4) "Aqueous Processing of LMFBR Fuels-Technical Assessment and Experimental Program Definition", ORNL-4436, pp. 63-90 (June, 1970).

(A5) Akalin, O., "Development of a Counting Facility for Activation Analysis," S.M. Thesis, MIT (February, 1972).

(A6) Argonne National Laboratory, 1000 MWe LMFBR Follow-on Study: Evaluation Report, draft (January 16, 1970).

(B1) Bondarenko, I.I., Editor, Group Constants for Nuclear Reactor Calculations, Consultants Bureau, New York (1964).

(B2) Batyrebekov, G.A., et al., "Some Characteristics of a Fast Reactor With a Thorium Shield", Soviet Atomic Energy, Vol. 17, No. 4. (1964).

(B3) Brewer, S.T., E.A. Mason, and M.J. Driscoll, "The Economics of Fuel Depletion in Fast Breeder Reactor Blankets", COO-3060-4, MITNE-123 (November, 1972).

(B4) Brewer, S.T., USAEC-RDT, personal communication (November, 1972).

(B5) Brown, G.J., "A Study of High-Albedo Reflectors for LMFBR's", SM/Nucl. Eng. Thesis, Nuclear Engineering Department, MIT (March, 1972).

(B6) Brewer, S.T., USAEC-DRDT, Washington, D.C., personal communication (April, 9, 1973).

References Cond't

(B7) Benedict, M., Department of Nuclear Engineering, MIT, personal communication (April, 1973).

(B8) Benedict, M., Course Notes for MIT Course 22.35, "Economics of Nuclear Power", MIT (Spring, 1973).

(B9) Brown, G.J., "Evaluation of High Performance LMFBR Blanket Configurations", ScD Thesis, Department of Nuclear Engineering, MIT, FORTHCOMING.

(B10) Bishop, E.C., and P. Murray, "Radial Blanket Design and Development Quarterly Progress Report for Period Ending August 31, 1972", WARD-3045T2B-6, UC-79e (January, 1973).

(B11) Barthold, W.P., "Fuel Shuffling in LMFBR Blankets", Argonne National Laboratory, FRA-TM-40 (August, 1972).

(B12) Bell, G.I., "A Simple Treatment for Effective Resonance Absorption Cross Sections in Dense Lattices", Nucl. Sci. Eng., 5, 138 (1959).

(B13) Becker, M., et al., "Analysis and Interpretation of Anisotropic Spectrum Measurements in Depleted Uranium", Trans. Am. Nucl. Soc., 16, 1, 305 (June, 1973).

(C1) Carpenter, S.G., et al., "Dependence of the Doppler Coefficient of Reactivity for Heavy Elements on Chemical Form, Surface-to-Mass Ratio, and Neutron Spectrum", ANL-7320, pp. 334-340 (October, 1966).

(D1) DRDT, USAEC, "The Use of Thorium in Nuclear Power Reactors", WASH-1097. (June, 1969).

(D2) Driscoll, M.J., "Notes on Fast Reactor Physics", MIT Course 22.94, P. 1.9 (1968).

(D3) DRDT, USAEC, "Potential Nuclear Power Growth Patterns", WASH-1098 (November, 1969).

(D4) Dyos, M., Westinghouse Advanced Reactors Division, personal communication (September 26, 1972).

(D5) Davey, W.G., "A Critical Evaluation of Fast Fission Cross Sections", Conference on Neutron Cross Section Technology, Washington, D.C., pp. 796-804 CONF-660303, Book 2 (March, 1966).

References Cond't

(D6) Driscoll, M.J., Notes for MIT Special Summer Session Course, "The Physics of Fast Reactors", MIT (1969).

(D7) DRDT, USAEC, "Reactor Fuel Cycle Costs for Nuclear Power Evaluation, WASH-1099 (1971).

(D8) Deonigi, D.E., "The Value of Plutonium Recycle in Thermal Reactors", Nuclear Technology, 18, pp. 80-86 (May, 1973).

(D9) Driscoll, M.J., et al., "LMFBR Blanket Physics Project Progress Report No. 3", COO-3060-6, MITNE-143 (June 30, 1972).

(D10) Davletshin, A.N., et al., "Radiative Capture of Neutrons by the TH-232 Nucleus in the Energy Range 0.01-15 MEV", INDC(CCP)-20/L, FEI-234, IAEA (1971).

(D11) Deen, J.R., et al., "Measurement of the Integral Fission Cross Section of TH-232 in a CF-252 Fission Neutron Spectrum", Trans. Am. Nucl. Soc., 16, 1, 316 (June, 1973).

(D12) Drake, M.K., "Data Formats and Procedures for the ENDF Neutron Cross Section Library", BNL 50274, Vol. 1 (October, 1970).

(E1) Engle, W.W., Jr., "A Users Manual for ANISN, A One Dimensional Discrete Ordinates Transport Code with Anisotropic Scattering", K-1693 (March 30, 1967).

(E2) El-Wakil, M.M., Nuclear Power Engineering, McGraw Hill, New York, 182-184 (1962).

(E3) Evans, R.D., The Atomic Nucleus, McGraw Hill, New York (1955).

(E4) Etherington, H., Editor, Nuclear Engineering Handbook, McGraw-Hill (1958).

(F1) Fortescue, P., "A Reactor Strategy: FBR's and HTGR's", Nuclear News, 36-39 (April, 1972).

(F2) Fuller, E.L., "Reactivity Effects of Core Slumping in Fast Reactors: A Case Study", FRA-TM-35, ANL (1972).

(F3) Forbes, I.A., Lowell Technical Institute, personal communication, (October, 1972).

References Cont'd

(F4) Foell, W.K., "Resonance Absorption of Neutrons in Mixtures of Thorium-232 and Uranium-238: An Investigation of Interference Between Absorbers by Means of Reactivity Measurements in the Advanced Reactivity Measurement Facility", IDO-16986 (August, 1965).

(F5) Ferguson, D.E., et al., "Chemical Technology Division Annual Progress Report for the Period Ending March 31, 1971", ORNL-4682, P. 42 (July, 1971).

(F6) Ferguson, D.E., et al., "Chemical Technology Division Annual Progress Report for the Period Ending March 31, 1972", ORNL-4794, p. 16 (August, 1972).

(F7) Froelich, R., "Optimum Blanket Fuel Management for an LMFBR", Trans Am Nuc. Soc., 15, 1, (June, 1971).

(F8) Forbes, I.A., et al., "Design Construction and Evaluation of a Facility for the Simulation of Fast Reactor Blanket," MITNE-110, MIT-4105-2 (February 1970).

(F9) Forbes, I.A., et al., (editors), "LMFBR Blanket Physics Project Progress Report No. 1," MITNE-116, MIT-4105-3 (June 30, 1970).

(F10) Forbes, I.A., et al., (editors), "LMFBR Blanket Physics Project Progress Report No. 2" COO-3060-5, MITNE-131 (June 30, 1971).

(G1) George, C.H., Gulf General Atomic, personal communication (November, 11, 1972).

(G2) Glasstone, S., and M.C. Edlund, The Elements of Nuclear Reactor Theory, VanNostrand, p. 133(1952).

(G3) Glasstone, S., and M.C. Edlund, The Elements of Nuclear Reactor Theory, VanNostrand, p. 235 (1952).

(G4) Greebler, P., and B.A. Hutchins, "Significance of Integral Parameters in the Design and Performance of Fast Breeder Reactors", National Topical Meeting on New Developments in Reactor Physics and Shielding", pp. 928-939 (September, 1972).

(G5) Greebler, P., and B.A. Hutchins, "User Requirements for Cross Sections in the Energy Range from 100EV to 100 KEV", Conference on Neutron Cross Section Technology, CONF-660303, Book 1, pp. 357-380 (March, 1966).

References Cond't

(H1) Hankel, R., et al., "An Evaluation of U-233/ Thorium Fast Breeder Power Reactors", NDA-2164-3, United Nuclear Corporation, April (1962).

(H2) Hardie, R.W., and W.W. Little, Jr., "1DX, A One-Dimensional Diffusion Code for Generating Effective Nuclear Cross Sections", BNWL-954 (March, 1969).

(H3) Hinkelmann, B., "Evaluation of Neutron Nuclear Data for Several Actinides in the Energy Range from Thermal to 10Mev", IAEA, Nuclear Data for Reactors, Helsinki (June, 1970).

(H4) Hoover, J., and D.A. Menley, "Alternative Neutron Energy Group Collapsing Schemes Applied to Fuel Cycle Calculations", ANL-7710 (January 1971).

(H5) Hirons, T.J., and R.D. O'Dell, "Calculational Modeling Effects on Fast Breeder Fuel Cycle Analysis", LA-4187 (September, 1969).

(H6) Hasnain, S.D., and D. Okrent, "On the Design and Management of Fast Reactor Blankets", Nucl. Sci. Eng., 9, 314-322 (1961).

(H7) Hardie, R.W., and W.W. Little, Jr., "PERT-V, A Two-Dimensional Perturbation Code for Fast Reactor Analysis", BNWL-1162 (September, 1969).

(H8) Ho, S.L., "Measurement of Fast and Epithermal Neutron Spectra using Foil Activation Techniques", S.M. Thesis, MIT (January, 1970).

(H9) Hinkelmann, B., "Evaluation of Neutron Nuclear Data for Several Actinides in the Energy Range from Thermal to 10 MEV", Proceedings of the Second International Conference on Nuclear Data for Reactors, Helsinki, IAEA (June, 1970).

(J1) Johnson, E.R., excerpt from AIF Conference on Nuclear Power and the Public, AIF Background Info. (March, 1973).

(K1) Kasten, P.R., L.L. Bennett, and W.E. Thomas, "An Evaluation of Plutonium Use in High Temperature Gas Cooled Reactors", ORNL-TM-3525 (October, 1971).

References Cond't

(K2) Kidman, R.B., "Cross Section Structure Factor Interpolation Schemes", HEDL-TME-71-40 (March, 1971).

(K3) Krylov, V.I., Approximate Calculation of Integrals, The MacMillan Company, New York (1962).

(K4) Kusters, H., "Progress in Fast Reactor Physics in the Federal Republic of Germany", KFK-1632, EACRP-U-46 (1972).

(K5) Komata, M., "Qualitative Evaluation of Fast Reactor Meltdown Accidents", Nucl Sci Eng, 40, 150(1970).

(K6) Kerr, J.M., et al., Direct Fabrication of U-233 Fuel Elements", Proceedings of the Second International Thorium Fuel Cycle Symposium, Gatlinburg, Tennessee, pp. 537-545 (May, 1966).

(K7) Kidman, R.B., et al., "The Shielding Factor Method of Generating Multigroup Cross Sections for Fast Reactor Analysis", Nucl. Sci. Eng., 48, 189-201 (1972).

(K8) Kang, C.S., et al., "Use of Gamma Spectroscopy for Neutronic Analysis of LMFBR Blanket", COO-3060-2, MITNE-130 (Nov. 1971).

(K9) Kidman, R.B., et al., "The Shielding Factor Method for Generating Multigroup Cross Sections", Trans Am Nucl Soc., 16, 1, 125(June, 1973).

(L1) Lamarsh, J.R., Introduction to Nuclear Reactor Theory, Addison-Wesley, (1966).

(L2) Lang, L.W., "Power Cost Reduction by Crossed-Progeny Fueling of Thermal and Fast Reactors", Nuclear Applications, 5, 302-310 (November, 1968)

(L3) Little, W.W., Hanford Engineering Development Laboratory, personal communication at MIT (January, 1973).

(L4) Loewenstein, W.B., and D. Okrent, "The Physics of Fast Power Reactors; A Status Report", Proceedings of the Second International Conference on the Peaceful Uses of Atomic Energy, Vol. 12 (1958).

(L5) Loewenstein, W.B., and B. Blumenthal, "Mixed Fuel Cycle Fast Breeder Reactors: Nuclear, Safety, and Materials Considerations", Proceedings of the Conference on Safety, Fuels, and Core Design in Large Fast Power Reactors, ANL-7120 (October, 1965).

References Cond't

(L6) Leipunskii, A.I., O.D. Kazachkovskii, S.M. Shikhov, and V.M. Murogov, "An Investigation of the Possibility of Using Thorium in High Energy Reactors", Soviet Atomic Energy, Volume 18, No. 4 (April, 1965).

(L7) Leipunskii, A.I., et al., "Improved Physical Characteristics of Fast Plutonium Reactors by Using U-233 and Thorium", Soviet Atomic Energy, Vol. 30, No. 6 (June, 1971).

(L8) Lang, L.W., "Thorium Can Reduce Power Costs for Thermal and Fast Reactors", Trans Am Nuc Soc., 11, p. 38 (June, 1968).

(L9) Lang, L.W., "Dependence of Fast Reactor Start-Ups on the Thorium Fuel Cycle", Trans Am Nuc Soc., 12, p. 443 (December, 1969).

(L10) Little, W.W., Jr., and R.W. Hardie, "2DB User's Manual-Revision 1", BNWL-831 Rev 1 (August, 1969).

(L11) Leung, T.C. et al., "Neutronics of an LMFBR Blanket Mock-up", COO-3060-1, MITNE-127 (January, 1972).

(L12) Long, J.K., et al., "Fast Neutron Power Reactor Studies with ZPRIII", Second International Conference on the Peaceful Uses of Atomic Energy, P. 598, Geneva (1958).

(L13) Leger, R., "Semiconductor Radiation Hardness Assurance Study", E-2415, Instrumentation Laboratory, MIT (February, 1969).

(M1) Morrison, G.W., E.A. Straker, and R.H. Odegaarden, "A Coupled Neutron and Gamma Ray Multigroup Cross Section Library for Use in Shielding Calculations", Trans Am Nuc Soc., 15, 1, p. 535 (June, 1972).

(M2) Moncrief, E.C., et al., "Thorium Fuel Separation Engineering Studies", Proceedings of the Second International Thorium Fuel Cycle Symposium, Gatlinburg, Tennessee, pp. 509-535 (May, 1966).

(M3) Markley, R.A., et al., "Design Analysis of the LMFBR Radial Blanket", WARD-3045T2B-9 (March, 1973).

(M4) Mattauch, J.H.E., W. Thiele, and A.H. Wapstra, "Consistent Set of Q Values", Nuclear Physics, Vol. 67, No. 1 (1965).

Reference Cond't

(N1) Nelson, J.V., "Cross Sections for Preliminary Design of FTR, FTR Set No. 200", HEDL-TME-71-65 (1971).

(N2) Nicholson, E.L., et al., "Recent Developments in Thorium Fuel Processing", Proceedings of the Second International Thorium Fuel Cycle Symposium, Gatlinburg, Tennessee, pp. 589-615 (May, 1966).

(N3) "Nuclear Power Costs", Nuclear Engineering, p. 929 (December, 1967).

(O1) Okrent, D., K.P. Cohen, and W.B. Loewenstein, "Some Nuclear and Safety Considerations in the Design of Large Fast Power Reactors", Proceedings of the Third International Conference on the Peaceful Uses of Atomic Energy, Vol. 6 (1965).

(O2) Ortiz, N.R., et al., "Instrumental Methods for Neutron Spectroscopy in the MIT Blanket Test Facility", COO-3060-3, MITNE-129 (May 1972).

(P1) Price, W.J., Nuclear Radiation Detection, Chapter 3 McGraw Hill, (1964).

(P2) Peterson, S., R.E. Adams, and D.A. Douglas, Jr., "Properties of Thorium, Its Alloys and Its Compounds", IAEA T.R. Series No. 52, Utilization of Thorium in Power Reactors (1966).

(R1) Rocks, L, and R.P. Runyon, The Energy Crisis, Crown Publishers, Inc., New York, P. 71 (1972).

(R2) Rohan, P.E., "Comparisons of Transport and Diffusion Theory Calculations of Performance Characteristics for Large Fast Reactors", PhD Thesis, Nuclear Engineering Program, University of Illinois (1970).

(R3) Ramchandran, S., Westinghouse Advanced Reactors Division, personal communication (October, 1972).

(R4) Roberts, J.T., "Reprocessing Methods and Costs for Selected Thorium-Bearing Reactor Fuel Types", Utilization of Thorium in Power Reactors, IAEA TR-52 (1966).

(R5) Ramchandran, S., and G.H. Madden, "Analyses of the FTR-3 Critical Experiments in Support of FTR Nuclear Design", WARD-2171-19 (April, 1971).

(S1) Sofer, G.A., et al., "Economics and Safety Aspects of Large Ceramic U-TH Fast Breeder Reactors", ANL-6792 (October, 1963).

References Cond't

(S2) Spitzer, J.E., and R.D. O'Dell, "Effects of Optimal Blanket Shape on the LMFBR Fuel Cycle", Trans Am Nuc Soc., 14, 2, p. 493 (October, 1971).

(S3) Straker, E.A., and M.L. Gritzner, "Neutron and Secondary Gamma Ray Transport in Infinite Homogeneous Air", ORNL-4464 (December, 1969).

(S4) Siep, I, "Calculation of Doppler Coefficients for Fast Reactors", KFK-983, EURFNR-697, Karlsruhe Nuclear Research Center (April, 1969).

(S5) de Saussure, G., et al., "Measurement of the U-238 Capture Cross Section for Incident Neutron Energies Up to 100 KEV", ORNL-TM-4059 (February, 1973).

(S6) Schenter, R.E., J.L. Baker, and R.B. Kidman, "ETOX, A Code to Calculate Group Constants for Nuclear Reactor Calculations", BNWL-1002, Battelle Northwest Laboratory (1969).

(S7) Soltesz, R.G., R.K. Disney, and S.L. Zeigler, "Nuclear Rocket Shielding Methods, Modifications, Updating, and Input Data Preparation" Vol 3, WANL-PR-(LL)-034 (August 1970).

(T1) Tzanos, C.P., E.P. Gyftopoulos, and M.J. Driscoll, "Optimization of Material Distributions in Fast Breeder Reactors", MIT-4105-6, MITNE-128 (August, 1971).

(T2) Taylor, J.J., and N.A. Petrick, "LMFBR: Keys to Industrial Success", Nuclear News (January, 1973).

(U1) Uranium Enrichment Services Criteria and Related Matters. Hearings Before the Joint Committee on Atomic Energy, Congress of the United States, Eighty-Ninth Congress, Second Session, August 2, 3, 4, 16, and 17, pp. 411-416 (1966).

(U2) Unger, W.E., Oak Ridge National Laboratory, personal communication, (October 16, 1972).

(V1) Vendryes, G.A., "Fuel Management and Economics, "Proceedings of the 1972 International Conference on Nuclear Solutions to World Energy Problems (November, 1972).

(V2) Vlasov, M.F., et al., "Status of Neutron Cross Section Data for Reactor Radiation Experiments", INDC (NDS) - 47/L, IAEA (October, 1972).

References Cond't

(V3) Volk, W., Applied Statistics for Engineers, McGraw Hill (1958).

(W1) Wenzel, P., "Crossed Uranium-Plutonium and Thorium-Uranium Fuel Cycles for a Developing Nuclear Power System with Thermal Converters and Fast Breeder Reactors", KERNENERGIE 14, (July-August, 1971).

(W2) Wolfe, B., et al., "Towards a 1000 MWe LMFBR: The Influence of Component Development, Prototypes, and Construction Experience", Nuclear News (January, 1973).

(W3) Weiss, E., R.A. Markley, and A. Battacharyya, "Open Duct Cooling Concept for the Radial Blanket Region of a Fast Breeder Reactor", Nuclear Engineering and Design, 16, 375-386 (1971).

(W4) Weissert, L.R., and G. Schileo, Fabrication of Thorium Fuel Elements, AEC Monograph (1968).

(Y1) Yule, T.J., et al., "Neutron Spectra in an Exponential Depleted-Uranium Pile", Trans Am Nuc Soc., 16, 1, 306 (June, 1973).

(Z1) Zorzoli, G.B., "The Potential of Metallic Thorium for LWR's", Energia Nucleare, 20, 2, pp. 97-101 (February, 1973).

(Z2) Zijp, W.L., "Review of Activation Methods for the Determination of Intermediate Neutron Spectra", RCN-40, Reactor Centrum Nederlands, (October 12, 1965).